Measurement of On-Road Emission Rates by Laser Remote Sensing: Westminster Field Study

Measurement of On-Road Emission Rates by Laser Remote Sensing: Westminster Field Study

Assessment and Standards Division
Office of Transportation and Air Quality
U.S. Environmental Protection Agency

Prepared for EPA by
ERG, Eastern Research Group, Inc.
EPA Contract No. EP-C-17-011
Work Assignment 5-13

Table of Contents

Table of Contents (Continued)

Table of Contents (Continued)

List of Appendices

Appendix A : Test Vehicle EDAR Exhaust Emissions Measurements

Appendix B : Westminster Dataset and Analysis Program Locations

Appendix C : Plots for Signal Adjustment Demonstration

Appendix D : Examples of Blind Source Separation using Standard ICA

Appendix E : Examples of Blind Source Separation with Correlation Constraints (BSScov)

Appendix F : Comparing Westminster and MOVES Release Rates by Class and Age Group

List of Figures

List of Figures (Continued)

List of Figures (Continued)

Page

List of Tables

Acknowledgments

Glossary

100% Illumination Speed (100%IS) – A geometric characteristic of an RSD instrument in which a vehicle travelling at the 100%IS speed would produce a signal equivalent to the signal produced if the scan path would be illuminated once and only once by the RSD light beam.

Air Speed – The speed of a vehicle at 1 meter above the roadway with respect to the air surrounding the vehicle at a substantial distance from the vehicle.

AirSpeed Para – The scalar air speed component parallel to the direction of vehicle motion at 1 meter above the roadway surface. The sign convention is positive for air moving toward the windshield.

AirSpeed Perp – The scalar air speed component perpendicular to the direction of vehicle motion at 1 meter above the roadway surface. The sign convention is positive for air moving toward the left side of the vehicle.

Data Location Index – The scan or pixel in the data stream that corresponds to a transit event, such as the passing of the front or rear of a vehicle.

Detailed data – The raw data stream of optical mass species measurements collected by an RSD at individual pixels.

Drag Area – The product of a vehicle's aerodynamic drag coefficient and the vehicle's frontal area.

EDAR – Emissions Detection and Reporting, which is the remote sensing instrument manufactured by HEAT and used in this study.

Emission Rate (g/mile) – The distance-based rate at which a species mass is emitted from a body in a flow field.

Evaporative HC (EvapHC) – Hydrocarbon gas that is produced by release of liquid gasoline or gasoline vapor, or by the release of other hydrocarbon vapor from other vehicle materials such as paint solvents. Evaporative HC specifically does not include exhaust hydrocarbon emissions from the tailpipe.

Exhaust HC (ExhHC) – Hydrocarbon gas that is produced as a pollutant during combustion of a fossil fuel and is emitted from a vehicle's tailpipe.

Footprint – The contiguous group of RSD pixels with missing detailed data values that are produced when the outgoing RSD beam is blocked by the vehicle body.

Frontal area – The area of the silhouette of a vehicle as viewed from the front of the vehicle.

Improved data – Raw data that has been improved through processing to reduce noise, artifacts, outliers, distortion, and baseline offsets.

HEAT – Hager Environmental and Atmospheric Technology, which is the company that manufactures the EDAR remote sensing device that was used in this study.

Location (Locn) – An emission point on a body in a flow field.

Optical mass (mole/m^2) – An RSD's fundamental measured quantity that is proportional to a species' mass per cross-sectional area of the RSD light beam.

Pixel – A small location where an RSD makes a detailed optical measurement. A scan is made up of pixels.

Plume – The region in a flow field that contains a material released from a body in a flow field.

Pollutant Conversion Factor – A factor that is used to convert RSD optical values to mass, for example, molecular weight for gases, or extinction coefficient for particulate material.

Raster-scanning process – A method of spatial scanning that uses motion of a beam across a field of view.

Release Location Factor – A factor that reflects the Vortex Entrainment Time of an emission release location relative to the Vortex Entrainment Time of a release from the tailpipe.

Release Rate (g/hr) – The time-based rate at which a species mass is released from a body in a flow field.

Remote Sensing Device (RSD) – an instrument for measuring pollutants in the air around a vehicle without touching the vehicle or notifying the vehicle operator.

Remote Sensing Device (RSD) system – an RSD instrument plus associated instrumentation for defining vehicle, vehicle operation, and ambient conditions including determining vehicle license plate, road speed, and wind velocity.

Retro-reflective tape – A surface-applied tape that reflects a substantial portion of incident light back toward the source of the light regardless of the angle of incidence.

Road Direction – The direction (with respect to north) that a vehicle or traffic is moving on a road.

Road Speed – The speed of a vehicle with respect to the road surface.

RSD Signal (g) – The mass of a species reported by an RSD in the sample of a vortex that the RSD illuminates.

Scan – A sequential series of pixels produced by an RSD when its light beam is moving in one direction.

ScanSum – The sum of a pollutant's pixel values for a given scan.

Species – a material measured by an RSD including gases, mixtures of gases, and particulate material.

Stripping Rate – The rate at which species are removed from a vortex by air that is passing over the surface of the vortex.

Surface Roughness – A measure of the irregularities of the terrain in the vicinity of a roadway. Surface roughness influences the wind speed profile at different heights above a roadway.

Transit – An event in which a vehicle passes by an RSD.

Vehicle reference frame – The coordinate system in which a vehicle is stationary and all things that are moving with respect to the vehicle are not stationary.

Vortex – the low-pressure zone downstream of a body in a gaseous flow field. The vortex can act as a temporary storage region for species released from the body.

Vortex Entrainment Time (VET) – A proportionality constant that expresses the ratio of the mass (g) of a released species in the vortex to the release rate (g/hr) from a body in a flow field.

Wake – The region downstream of the vortex formed by a body in a flow field.

Weights – Spatial factors assigned to spatial coordinates in a vortex that describe the anticipated relative mass distribution of species emitted from a body in a flow field.

Wind speed and direction – The speed and direction (with respect to north) of wind as measured by an RSD system.

1.0 Executive Summary

1.1 Research Goals

The broad goal of this research was to find a method to measure on-road evaporative emissions, known as running losses, of gasoline-fueled vehicles. Running losses are hydrocarbon (HC) gaseous emissions generated primarily from unintended releases of gasoline vapor or gasoline liquid from vehicles. For many years, researchers have wanted to quantify running losses, in part to answer the question: Which on-road fleet emissions are larger, on-road exhaust hydrocarbon emissions (ExhHC) or on-road evaporative hydrocarbon emissions (EvapHC)? This report documents the recent in-depth effort to develop a remote sensing device (RSD) method to measure the running loss emissions of vehicles as they drive in traffic. But the work has importantly produced an unanticipated capability: an RSD method that can be used to measure on-road release rates (g/hr) and emission rates (g/mile) of any type of emissions (exhaust, evaporative, fugitive) for gases and particulate material.

The emission rate (g/mile) of running losses from an individual vehicle is affected by many vehicle, fuel, operational, and environmental factors including fuel tank capacity and volume, fuel tank thermal shielding, emission control system malfunctions, evaporative control canister state, canister purge schedule, fuel level, fuel volatility, fuel oxygenate content, recent driving pattern, recent soak time, ambient temperature, atmospheric pressure, and the presence of gasoline liquid and vapor leaks. Because of the numerous factors affecting running loss emission rate and because evaporative emission control systems operate in a non-linear manner, modeling running losses is challenging. And even if they could be modelled, without real-world on-road running loss data, there would not be any real-world data to validate a model.

Nevertheless, for decades running losses could be measured on vehicles in the laboratory. Using lab methods, the Environmental Protection Agency started certifying light-duty vehicles to meet a running loss specification beginning with the 1996 model year. The running loss certification uses a well-defined test condition to determine if a prototype vehicle can meet the standard of 50 mg/mile.

All of the current traditional on-road vehicle RSD technologies (University of Denver, Opus, and Hager Emissions and Atmospheric Technology) report estimates of exhaust pollutant concentrations (ppm) or mass of pollutant per mass of fuel (g/gFuel). The instruments use light beams or lasers to collect detailed optical data around a vehicle as it drives by. The RSDs process the detailed data using procedures that were developed over 30 years ago. However, vehicle emissions researchers really want mass emission rates – not concentrations or fuel-based mass rates. It was thought that release rates and emission rates could not be measured by RSDs. In this report we show that, using an alternative data processing procedure, the same detailed data that is used to calculate exhaust concentrations can be used to calculate release rates (g/hr) and emission rates (g/mile).

For this study, the Colorado Department of Public Health and Environment (CDPHE), the U.S. Environmental Protection Agency (EPA), and Eastern Research Group (ERG) collected RSD detailed data on over 30,000 transits in October 2019 in Westminster, Colorado. We embedded a convoy of electric and gasoline test vehicles in the local traffic while we metered artificial

evaporative and exhaust emissions. The RSD emission rate method was developed on the test vehicle detailed data. Then, the method was used to begin characterization of the fleet vehicle emissions.

1.2   Benefits of the RSD Instrumentation Used in this Study

We chose the Hager Environmental and Atmospheric Technology (HEAT) RSD instrument, known as Emissions Detection and Reporting (EDAR), to collect the detailed data for this study. The EDAR instrument is described in more detail in Section 2.2. EDAR has several advantages for this effort.

EDAR scans the width of a lane of traffic from above the pavement. For each vehicle transit, EDAR generates thousands of individual detailed optical measurements (pixels). The large number of individual measurements benefits the signal processing algorithms. Because EDAR scans from above the vehicle, it sees pollutants in front of, to the side of, as well as, behind the vehicle. Evaporative emissions originating under the hood are typically first seen at the side of a moving vehicle.

EDAR uses lasers as the light source. EDAR uses Differential Absorption LIDAR (DIAL) to collect high signal-to-noise (S/N) detailed optical data at each pixel for pure compounds CO_2, CO, NO, and NO_2. EDAR uses a non-DIAL technique, which has a lower S/N, to collect HC detailed data on the mixture of HC compounds present in vehicle emissions.

For each detailed data pixel measurement, EDAR reports the mass (mole/m^2) of the pollutant illuminated by the laser beam between the RSD instrument and the pavement. Thus, the combination of the laser beam scanning the full width of the lane from above and the individual detailed data measurements for all pollutant channels reported as mass provides a reasonably good optical sample of the mass of emissions released from a moving vehicle.

1.3   Dispersion of Vehicle Pollutant Releases

One key realization made the determination of release rate (g/hr) and emission rate (g/mile) from RSD detailed data possible: a practical way to quantitatively relate the mass of a pollutant in the vortex to the release rate of the pollutant from the moving vehicle.

The RSD instrument gets its signal by scanning the laser beam through the air and pollutants around the moving vehicle. RSD instrument designers have known for years that the largest RSD signals come from the first few scans behind the vehicle rear. When vehicles move through air, they create a low-pressure zone just behind the vehicle. The water mist swirling behind the trailer of an 18-wheeler driving on wet pavement is a vivid demonstration of this process. In this report, we call this ill-defined, swirling low-pressure zone the vortex.

Any current RSD gets a large part of its signal from pollutants caught up, or temporarily stored, in the vortex. When pollutants are released from anywhere on a vehicle, they have a good chance of getting into the vortex, where the RSD can measure a sample of them. Then, as surrounding air passes over the surface of the vortex, some of the pollutant in the vortex will be stripped away to be laid down in the air over the roadway.

The major conceptual problem to be resolved is the units of the measured quantities. The release rate has units of grams/hour, but the RSD-measured mass of pollutant in the vortex is in grams. We resolve this seeming units incompatibility by thinking about what happens to the emissions as they leave the release point on the vehicle. For a given vehicle moving at a constant speed and having a constant pollutant release rate, a dynamic equilibrium is set up between the release rate and the mass in the vortex. The rate of pollutant going into the vortex tends to be equal to the rate that the pollutant is stripped from the vortex by surrounding air. Thus, the pollutant mass in the vortex (g) will tend to be proportional to the pollutant release rate (g/hr). For example, if the release rate is zero, there will be zero mass in the vortex. If the release rate is high, the mass in the vortex will be high. The proportionality constant has units of time. We call it the Vortex Entrainment Time (VET) with units of hours.

In the study, we released metered flows of different gases (artificial EvapHC and artificial exhaust mixtures) at various release locations on different light-duty test vehicles while we drove them under the RSD instrument at different speeds. For each RSD transit of a test vehicle, we calculated the effective VET by simply dividing the RSD-measured Mass in Vortex (g) by the metered release rate (g/hr). The results indicated that for light-duty vehicles the VET was typically around 4 seconds. We also found that the VET was relatively well behaved. The VET was approximately proportional to the inverse square root of the vehicle's air speed in the direction of motion, to the one-third root of the vehicle drag area, and to the release location relative to the rear bumper of the vehicle. The VET is independent of pollutant.

Calculating the emission rate (g/mile) for a transit begins by determining the VET from the vehicle's air speed (from the vehicle velocity and the wind velocity) in the direction of vehicle motion, estimating the vehicle drag area, and estimating the relative front-to-back release location (under the hood = 0.3, rear tailpipe = 1). Then, the RSD-measured Mass in Vortex (g) is used with the VET and an easily calculated RSD-instrument geometry factor to produce the release rate (g/hr). Finally, the emission rate (g/mile) is calculated by dividing the release rate (g/hr) by the vehicle road speed (mile/hr).

1.4 RSD Data Signal Processing

The HEAT EDAR instrument uses the traditional RSD method to calculate its reported exhaust concentrations. The method compares a transit's detailed optical data for the pollutant of interest with the corresponding detailed optical data for CO_2 taken at the same time along the same optical path. HEAT has worked out its own signal conditioning methods to de-noise, adjust, and improve the raw optical data before the calculation of exhaust concentrations.

The new RSD emission rate method, which is described in this report, uses the same detailed optical data to produce release rates and emission rates – instead of concentrations. Also, instead of using two pollutant "channels" to calculate each pollutant result, the new method uses only the pollutant's detailed dataset from the pollutant's one channel. These differences call for the detailed optical data to be conditioned differently.

For this study we applied standard signal conditioning methods to adjust the constant-level offset, remove outliers, de-stripe via multi-tonal cancellation, perform adaptive notch filtering, and interpolate the scanning laser's optical mass measurements to a rectangular grid. See Section 7.1.

Evaporative hydrocarbon emissions (EvapHC) and exhaust hydrocarbon emissions (ExhHC) have different chemical compositions and are always released from different locations on a vehicle. To separately quantify EvapHC and ExhHC emission rates, we applied a signal processing technique generally known as Blind Source Separation (BSS) to the conditioned detailed data. The specific technique that we used for the analysis of the Westminster data is known as Independent Component Analysis[1] (ICA). We found that when the EvapHC plume and the ExhHC plume are not overlapping, as produced by EvapHC from the fuel fill door and ExhHC from the tailpipe, ICA provides very good results.

However, if plumes overlap substantially, as produced by EvapHC from the fuel tank and ExhHC from the tailpipe, ICA produces only satisfactory separations. Therefore, for this project, we began development of a new type of BSS called BSScov, which produces good separations even if plumes overlap substantially.

1.5 RSD Emission Rate Method Performance

The collection of field data for this project was designed primarily to collect EDAR detailed data on light-duty test vehicles with metered natural and artificial running losses and exhaust emissions. Using the test condition variables identified from prior staged data collection efforts, the test design was planned with wide variations in test conditions so that the test vehicle data could be used to create an RSD method that could connect metered running loss emission rates and RSD detailed data measurements. We embedded the test vehicle operation in real traffic (in Westminster) so that <u>if</u> we could actually develop a method, we could apply it to a sample of a real-world fleet.

This report documents the fundamentally sound RSD emission rate method that we developed. However, we found that our ability to fully characterize Westminster's fleet emission rates was hampered by some EDAR data characteristics that we were unaware of until we analyzed the Westminster data. We believe that during preparations for the next field data collection effort, we can work with HEAT to address these issues.

Accordingly, this report is heavy on method development and description and light on fleet emissions characteristics.

Section 9 compares the method's results for the test vehicles with their metered release rates (g/hr). Overall, the method's measured exhaust release rates for CO, NO, and CO_2 on the test vehicles had recovery rates between 66 and 87%. Recovery of artificial running losses was linear with the metered EvapHC release rates and varied between 0 and 100% depending on test vehicle and release location. The detection limit for a single RSD measurement for the RSD release rate appears to be about 75 g/hr. Turbulence of the vortex and noise in the RSD HC detailed data both contribute to this rather high detection limit. We expect that improved noise reduction techniques will be able to lower the EvapHC detection limit. We would expect that the

---

[1] Jonathon Shlens, "A Tutorial on Independent Component Analysis," https://arxiv.org/abs/1404.2986, April 14, 2014. This freely downloadable article provides an excellent, intermediate-level discussion of independent component analysis.

average release rates of major fractions of fleets could be determined with small errors if the uncertainties of individual transits are randomly distributed.

Section 10 compares the method's results with model predictions from MOVES as set up for October 2019 in Westminster. Overall, the method's exhaust release rates were in the same range as MOVES release rates for CO_2, CO, and NO, but HC release rates were high compared to MOVES values. The relative effects of vehicle age were quite similar between the method's and MOVES values. The method's low-VSP average values tended to be higher than MOVES values, and the method's high-VSP average values tended to be lower than MOVES values.

We provide an example transit of a 2001 pick-up truck that happened to drive by the EDAR at Westminster. The traditional RSD calculation indicated that the vehicle had a low ExhHC concentration. The RSD emission rate method indicated that the vehicle had massive evaporative emissions of 8.6 g/mile.

1.6   Areas for Future Development

The RSD emission rate method was developed primarily on the test vehicle EDAR data collected in Westminster. The method development and its application to the real-world data from the Westminster fleet sample has pointed out areas where the method needs improvement. Subsection 9.4 describes sixteen suggested areas to improve the RSD emission rate method in general and to extend it to medium- and heavy-duty on-road vehicles:

1. Poor Correlations among Exhaust Pollutant Detailed Data
2. RSD Signal Dependence on Laser Pathlength
3. Vortex Entrainment Time
4. Release Location Detection of Light-Duty EvapHC
5. Vortex Shape
6. RSD Signal Accuracy
7. RSD Signal Attenuation
8. Evaporative Plume Signal-to-Noise Improvement
9. Drag Area
10. Enhanced Blind Source Separation
11. Release Location Detection of Medium- and Heavy-Duty Exhaust
12. Diesel Engine Load
13. Particulate Material Pollutant Correction Factor
14. Trailer Configuration Detection
15. Emissions of Vehicles with Trailers
16. Interfering Plumes

2.0   Testing Description

2.1   Testing Location and Conditions

The testing was conducted on public roadways in Westminster, Colorado, a suburb northwest of Denver. A Google Map view of the test site is shown in Figure 2-1. The EDAR instrument was set up on the northeast-bound lane of N. Federal Parkway at approximately 39.91776 N, 105.02018 W. The 1.48 mile test loop consisted of a rectangle formed by N. Federal Parkway on the west to the EDAR instrument (0.39 mile), N. Federal Parkway on the north from the EDAR instrument to N. Zuni Street (0.26 mile), N. Zuni Street on the east (0.33 mile), and W. 120th Avenue on the south (0.50 mile).

Figure 2-1.   Roadways Used for EDAR Testing in Westminster, Colorado

As shown in the figure, speed limits were 50 mph on W. 120th Avenue and 45 mph on N. Federal Parkway. Test vehicles were driven on the loop in a clockwise direction. At the EDAR instrument, the roadway has a moderate upward grade.

Colorado routinely monitors the gasoline sold in the state. Tests of gasoline samples collected in Westminster between 10/8/2019 and 10/24/2019 had an average volatility of 12.0 psi RVP and 9.4 vol% ethanol.

Figure 2-2 shows the ambient temperatures recorded by the EDAR instrument during vehicle emissions measurements for the 6 days of testing. Snow caused wet pavement from about 6:00 pm of Wednesday, October 23 through about 11:00 am on Thursday, October 24. EDAR cannot make emissions measurements with wet pavement.

Figure 2-2. Ambient Temperature at the Test Site During Testing
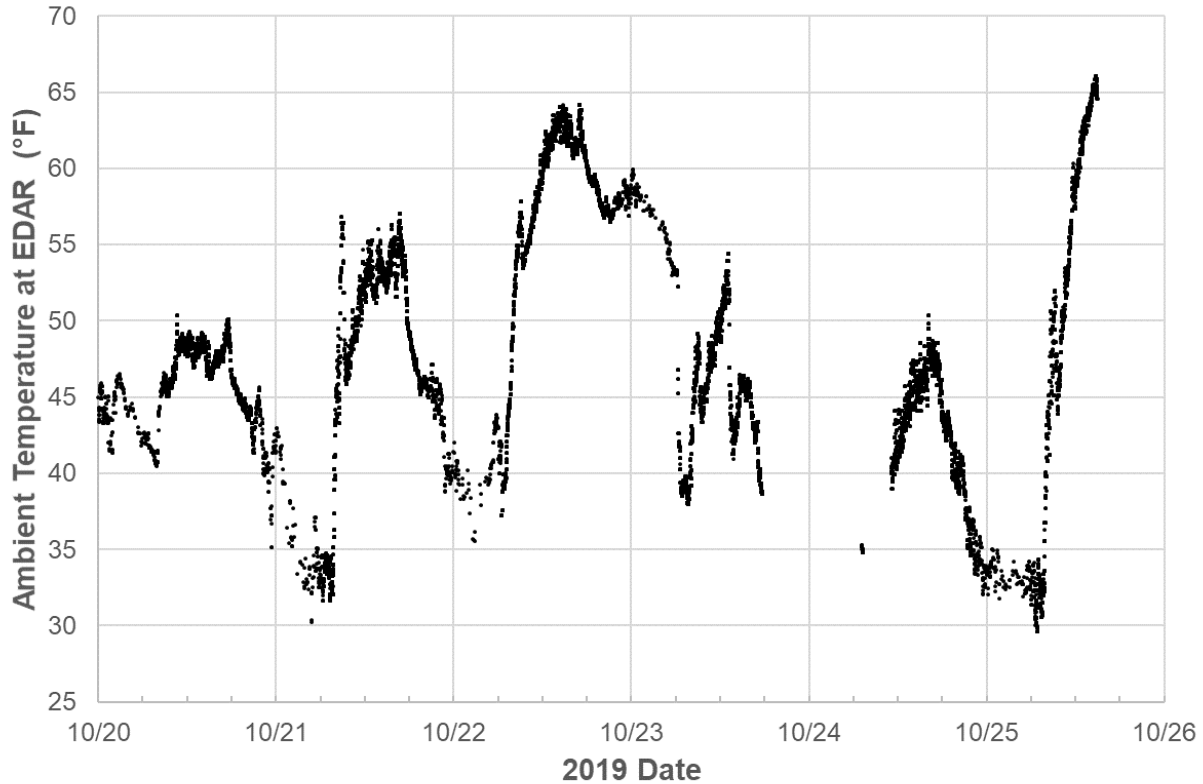
2.2   EDAR Configuration

Figure 2-3 shows the HEAT EDAR and associated instrumentation set up on N. Federal Parkway during the testing in Westminster. The EDAR laser instrument is the box hanging from the horizontal gantry boom. The approximate infrared laser scanning curtain is drawn in the figure in red. The instrument scans a 20mm diameter infrared laser at 20 scans per second onto a retro-reflective tape that is attached to the pavement perpendicular to the direction of traffic flow. The laser light returns to the instrument for analysis as gases emitted from vehicles absorb a portion of the light. The instrument used in this study provided HC, CO, NO, NO_2, and CO_2 optical mass (moles/m^2) measurements for 256 pixels across the 3.66 meter (12 feet) long tape.

The optical window at the bottom of the EDAR box was measured to be 5.3 meters directly above a point on the reflective tape 0.56 meters from the white line and 3.53 meters from the closest yellow line.

Figure 2-3. EDAR Test Set-Up (Looking West) at the Test Site
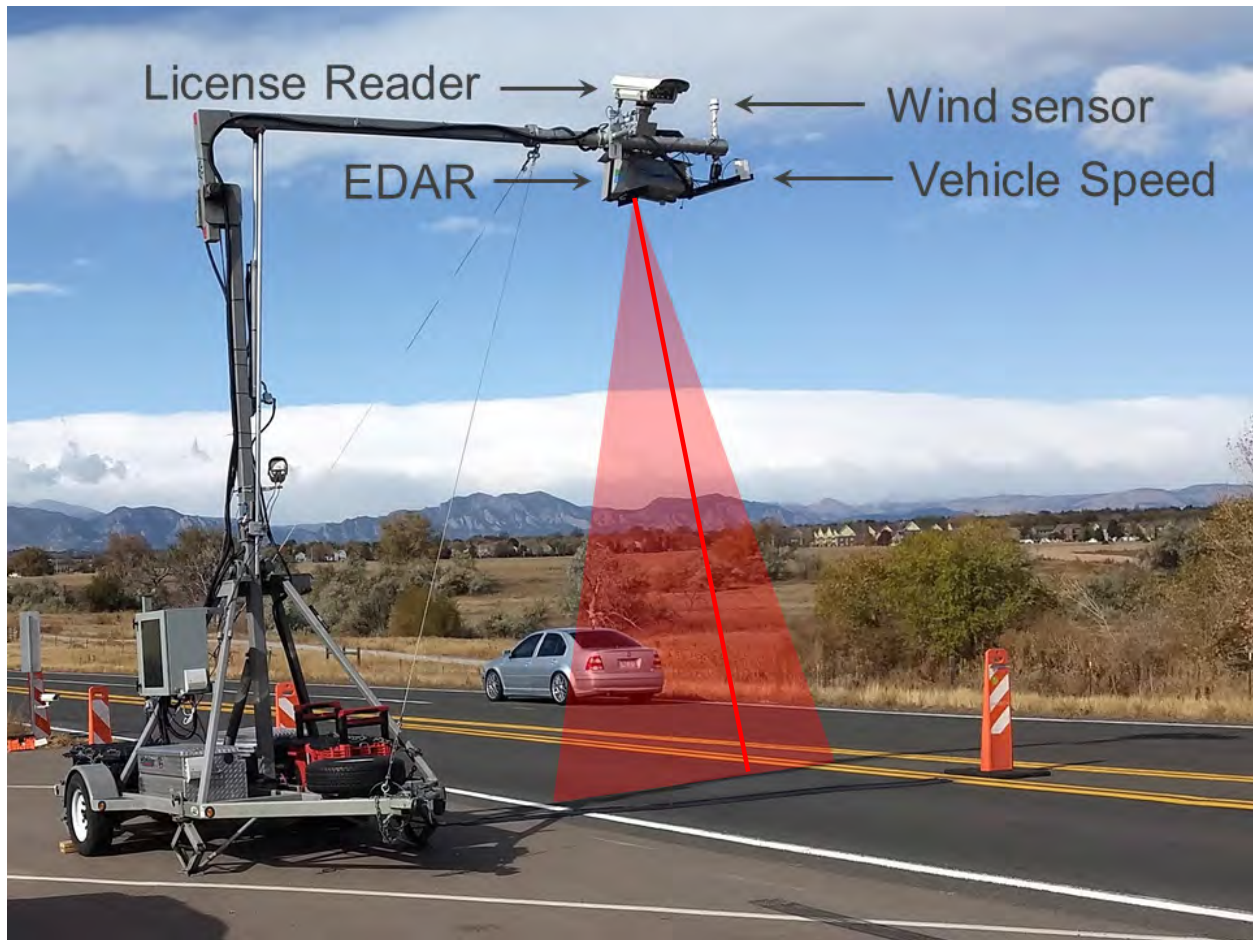
The horizontal gantry boom is also equipped with a license plate reader that can operate at night as well as during the day, a weather sensor that measures wind speed and direction, ambient temperature, relative humidity, and barometric pressure at about 6 meters above the pavement, and a sensor bar that measures vehicle speed and acceleration when a vehicle passes under the instrument. The EDAR system instruments and data storage computer were powered by a set of 12-volt deep-cycle batteries, which allowed the EDAR system to be operated unattended for 12-hour periods.

The EDAR instrument saves scanned optical mass data for a specified number of scans after the rear bumper of a target vehicle clears the laser beam. As a default, the data from 30 scans after the rear bumper is saved. If another vehicle is following the target vehicle too closely, the second vehicle will prevent any of the scans following the target vehicle to be saved. Instead, the scans behind the second vehicle would be saved. We wanted to collect most fleet vehicle data and half of the test vehicle test runs with the default 30 scans, but we also wanted to collect some data with 60 lines to explore the potential benefits of more scans behind vehicles. Figure 2-4 shows the location of orange traffic cones that we put on the sidewalk to help test vehicle drivers judge convoy test vehicle following distances.

Figure 2-4. EDAR Test Site on N. Federal Parkway, Westminster, Colorado

The minimum following distances are given in Table 2-1 for the EDAR instrument scan rate of 20 times per second, the nominal test vehicle operating speeds of 22.5 and 45 mph, and the minimum scans behind each vehicle of 30 and 60 scans. Because all distances in Table 2-1 are approximately multiples of 50 feet, we put traffic cones at the 0-, 50-, 100-, and 200-foot distances as shown in Figure 2-4. The convoy vehicle drivers were able to conveniently judge their following distances by using the traffic cones as a visual gauge. When the vehicle they were following was at the 0-foot cone, they had to be no closer than the cone whose distance is given in Table 2-1.

Table 2-1. Minimum Following Distances for Test Vehicles

		Number of After-Rear-Bumper Scan Lines Set in EDAR	
		30 scan lines	60 scan lines
Vehicle Speed (mph)	22.5	49.5 feet	99 feet
	45	99 feet	198 feet

2.3 Traffic Flow Monitoring Equipment

A camera was used for taking continuous video of cars passing through the monitoring location. The camera was set up with its focus on vehicle license plates. The camera model was a GoPro Hero 5 mounted inside a security camera housing to protect the camera and then bolted to a sign post near the roadside as shown in Figure 2-5. The camera housing can also be seen at the left margin of Figure 2-3. There was space inside the security housings for a USB battery to power both the camera and a cooling exhaust fan. The battery powered the camera for approximately 8 hours.

Batteries were charged overnight, and extra batteries were always in reserve for backup or if a battery could not be charged in time overnight. Two identical cameras and housings were available to be able to easily swap units, if needed. The GoPro camera could be controlled wirelessly within 20-30 feet of the unit using an iPad application that allowed for a live view of what the camera saw, adjustment of settings, and the starting and stopping of image storage. This application was used to confirm the correct field of view for the security camera housing when positioning it on its mount to the sign post, and to periodically check the units and ensure that they were still running and not out of storage space.

Figure 2-5. Video Camera Installed Near EDAR System

The GoPro Hero 5 model is capable of 12 MegaPixel still images and up to 4K resolution live video. For this project, live video was made using a resolution slightly below the maximum of 4K to maximize storage space and reduce the heat created by the camera when continuously run. More importantly was the frames-per-second (fps) rate of filming, which was selected at 90 fps to capture the highest number of frames possible as vehicles moved past the camera at 20 to 60 miles per hour to reduce blurring and make license plates legible. Very large 500 GB microSD storage cards were used to store the video as the selected high-resolution, high-fps format consumed considerable space for each minute recorded. About 500 GB was needed for an 8-hour period. It was discovered that if the highest possible resolution and an ever faster 120 fps speed was used then the resulting data writing operation to the storage card would overheat the camera and cause it to shut down when run continuously for multiple hours. Slightly reducing the filmed resolution and frame-acquisition rate (fps) solved this problem.

Post-processing of the videos was performed with the "DVMP Pro 7" software product to extract timestamp metadata from the video files and burn it into each frame of the video. This provided a running clock and date at the bottom of each video for reviewers to easily reference and find specific times and vehicles when needed. The DVMP Pro 7 software was relatively slow, hindered both by the technical limitations of the available computer hardware to run the software and as well simply by the nature of the process, which is to open and write a timestamp to each single frame of a high-definition, high-fps video and then write that new frame back to a new high-definition, high-fps video file, frame by individual frame. Processing all of the captured video took multiple weeks of continuously running the software. Future project work with cameras should ensure that a timestamp can be written directly to the video at the time of filming, which the GoPro Hero 5 model camera used here was not capable of doing.

2.4   Test Vehicles

The EDAR instrument was set up to collect measurements on fleet vehicles. However, at this point in the development of EDAR for measuring running loss emissions, the connection between EDAR measurements and an individual vehicle's running loss emission rate (g/mile) was unknown. Therefore, to help establish that connection, we operated a set of test vehicles with metered flows of artificial and real exhaust and/or running loss emissions in the traffic on N. Federal Parkway during the six days of remote sensing testing. The EDAR data collected on the test vehicles will be used for two purposes:

- establishing a connection between EDAR internal-instrument measurements and the metered running loss emission rate (g/mile) as modified by test conditions such as vehicle speed and wind speed and direction, and

- applying that connection to the test conditions and EDAR instrument-internal measurements taken on fleet vehicles to estimate the running loss emission rates (g/mile) of the fleet vehicles.

Table 2-2 gives descriptions of the six test vehicles used in the study. We used two all-electric vehicles and four light-duty gasoline vehicles. Because the all-electric vehicles carry no gasoline on board and have no combustion source, their inherent running loss and exhaust emissions are

zero[2]. Therefore, by metering artificial running loss and/or exhaust gases, we can know the composition, concentrations, and release rates of all emissions from these vehicles down to very low levels. Disadvantages of using all-electric test vehicles are that they are somewhat difficult to procure, must be regularly charged, which can be time-consuming, must be fitted with a fake tailpipe that can only approximate the exit position and flow rates of a real exhaust system, and simulated exhaust gases are most easily released in a dry state, which is different from combustion emissions, which contain water of combustion. The connection between EDAR internal-instrument measurements and the metered running loss emission rate (g/mile) would be developed on data obtained from the all-electric test vehicles.

Table 2-2. Descriptions of Test Vehicles

Vehicle Desc.	Plate	VIN	Certification	Fuel	Group	Evap	Equipment
Position 1: 2017 Chevrolet Bolt	Ohio J595030	1G1FW6S01H4190705	n/a	Electric	n/a	n/a	n/a
Position 2: 2017 Chevrolet Bolt	Ohio J595031	1G1FW6S03H4190771	n/a	Electric	n/a	n/a	n/a
Position 3: 2019 Subaru Outback	Colorado ABWD21	4S4BSAFC4K3376269	EPA: T3B70 LDV/LDT2 CA: SULEV30 PC/LDT2	Gasoline	KFJXJ02.5HRV 2.5L	KFJXR01485DX	TWC(2)/ WR-HO2S/ HO2S/ SFI/ EGR/ EGRC
Position 3: 2019 GMC 1500	Colorado BXS510	3GTU9DEL2KG154600	EPA: LDT / Tier3 CA: LDT / ULEV125	Gasoline	KGMXT06.2375 6.2L	KGMXR017350D	DFI/ HO2S/ TWC
Position 3: 2016 Ford F150	Colorado ZQO710	1FTFX1EG5GKF11400	EPA: T2B4 LDT4 CA: Not for sale in CA	Gasoline	GFMXT03.54JG 3.5L	GFMXR0235NBC	TWC/ DFI/ WR-HO2S/ HO2S/ TC/ CAC
Position 4: 2015 Infiniti Q50	Colorado 582ZHP	JN1BV7AR8FM415300	EPA: T2B5 LDV CA: LEV2-ULEV PC	Gasoline	FNSXV03.7GAA 3.7L	FNSXR0120MBA	2TWC(2)/ 2HO2S/ 2WR-HO2S/ SFI

---

[2] We acknowledge that off-gas evaporative emissions from vehicle materials such as elastomers, paints, and lubricants are not zero. We assume that those emissions are negligible compared to the levels of gases that we are artificially releasing from the all-electric reference vehicles.

The three gasoline test vehicles listed for Position 3 in Table 2-2 were used to overcome the disadvantages of the all-electric test vehicles, and their results can be used to evaluate algorithms that predict the running loss emissions of gasoline vehicles. That is, if the application of connections developed between EDAR internal-instrument measurements and the metered running loss emission rate (g/mile) of the all-electric test vehicles produce accurate predictions of the artificial running loss emissions from the gasoline test vehicles, then we would be even more confident that running loss estimates of fleet vehicles would be accurate.

The two electric vehicles, which were obtained in Aurora, Colorado, were rented from Mike Albert Rental (mikealbertrental.com) of Cincinnati, Ohio. The Subaru was also a rental vehicle. The GMC, Ford, and Infiniti test vehicles were personal vehicles of CDPHE staff.

2.5   Test Vehicle Exhaust Emissions Equipment

For the four gasoline test vehicles, the normal exhaust was emitted through the as-equipped exhaust system. The GMC and Infiniti had dual tailpipes exiting at the bottom edge near the ends of the rear bumper. The Subaru had a single tailpipe exiting at the left rear. The Ford F150 had a single tailpipe exiting at the right rear, but it was aimed to the side just behind the right rear wheel.

Since the EDAR instrument uses signals from the exhaust CO_2 to trace the exhaust plume and calculate exhaust emissions concentrations, we wanted to release artificial CO_2 from fake tailpipes attached to the rear of the two all-electric test vehicles. We attached short pieces of PVC tubing to the EVs at locations that might be used if those vehicles had gasoline engines. To be able to distinguish the two EVs from each other in EDAR's infrared plume images, EV-1's fake tailpipe was installed under the bumper on the left rear end, as shown in Figure 2-6, and EV-2's was installed under the right end of the rear bumper, as shown in Figure 2-7. Simulated exhaust gas was routed from a gas cylinder inside each vehicle, through the regulator, an on-off valve, and finally via ¼-inch Teflon tubing to the forward end of the PVC tubing, as shown in Figure 2-7.

We also wanted to use exhaust compositions and release rates that might be observed for gasoline combustion vehicles. We ordered 7 cylinders for each of two different stoichiometric exhaust gas mixtures – a clean mixture and a dirty mixture – that came close to satisfying this equation:

$$[CO2] \quad = \quad 150537.66 \, - \, 0.7168 * [CO] \, - \, 0.3011 * [HC] \, - \, 0.3584 * [NO]$$

where:

[CO2] is the CO_2 concentration in ppm,
[CO] is the CO concentration in ppm,
[HC] is the HC concentration in ppmC3, i.e., ppm Propane, and
[NO] is the NO concentration in ppm.

Figure 2-6. Fake Tailpipe Location on EV-1 Test Vehicle

Figure 2-7. Fake Tailpipe Installed on EV-2 Test Vehicle

The clean and dirty mixtures were ordered in aluminum cylinder size 150A using standard part numbers used by Envirotest for Colorado I/M testing. The cylinders received had the following labelled concentrations:

Clean mixture (AirGas Part Number X02NI84T15AC004 $\pm$ 2% blend tolerance):
        15.05 % CO_2, balance N_2.

Dirty mixture (AirGas Part Number X05NI84T15AC004 $\pm$ 2% blend tolerance):
        14.76% CO_2, 402 ppm C_3H_8, 5043 ppm CO, 996 ppm NO, balance N_2

The clean mixture was released from test vehicle EV-1. The dirty mixture was released from test vehicle EV-2.

2.6   Test Vehicle Running Loss Emissions Equipment

The Position 1, 2, and 3 test vehicles, which were the EV-1, the EV-2, and either the Subaru, GMC, or F150, were set up with equipment to release metered flows of 100% consumer-grade propane to simulate running loss emissions. After the propane tank and regulator, propane was routed to a series of three rotameters piped in parallel and then to a 4-way diverter valve. An example set-up is shown in Figure 2-8. The rotameters were sized for low, medium, and high flow capacities to cover the wide range of flows needed for propane releases:

        Dwyer RMA-150-SSV, 10 to 100 cc/min air (0.021 to 0.21 scfh)
        Dwyer RMA-3-SSV, 0.2 to 2.0 scfh air
        Dwyer RMA-6-SSV, 2 to 20 scfh air

Teflon tubing from the three outlets of each test vehicle's diverter valve routed the flow of metered artificial running loss propane to a location at either the fuel fill door (DOOR), the top of fuel tank (TANK), or under the hood (HOOD). Figure 2-9 shows the tubing outlet on the left quarter panel of EV-2 to simulate a fuel fill door release location on the opposite side of the vehicle from the fake tailpipe. Figure 2-6 shows the corresponding simulated fuel fill door release point for EV-1. Figure 2-10 shows the under-hood release point used for both EV-1 and EV-2. Figure 2-11 shows the top of tank release point used for the GMC test vehicle.

Figure 2-8. Rotameters and Diverter Valve for Simulated Running Loss Releases
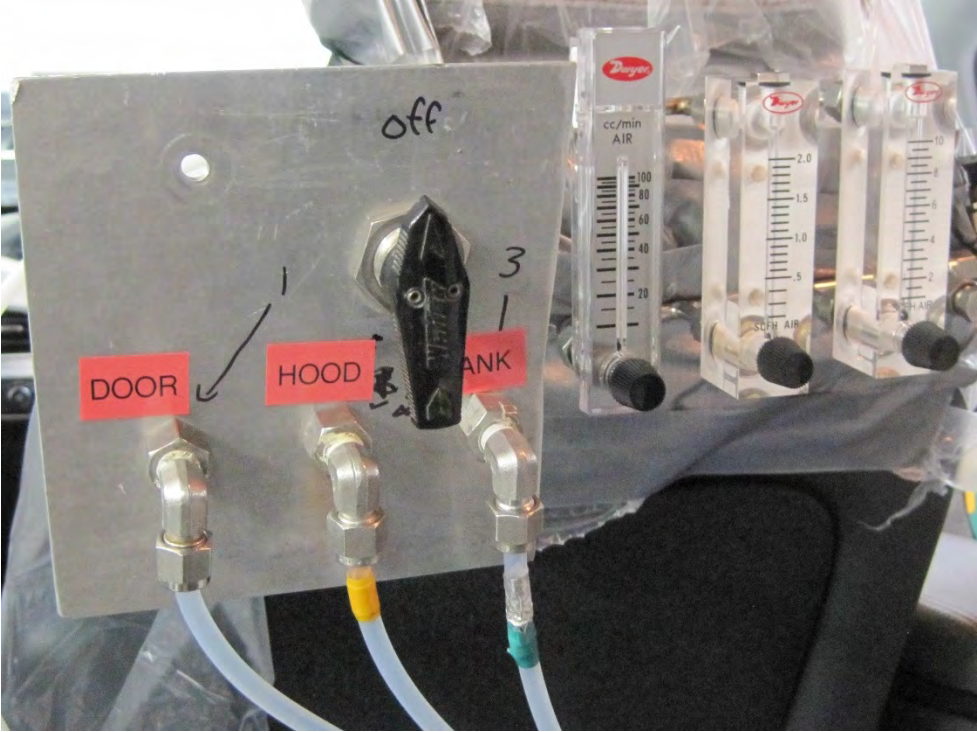
Figure 2-9. Fake Fuel Fill Door Release Point on EV-2 Test Vehicle

Figure 2-10. Under-Hood Release Point on an EV Test Vehicle
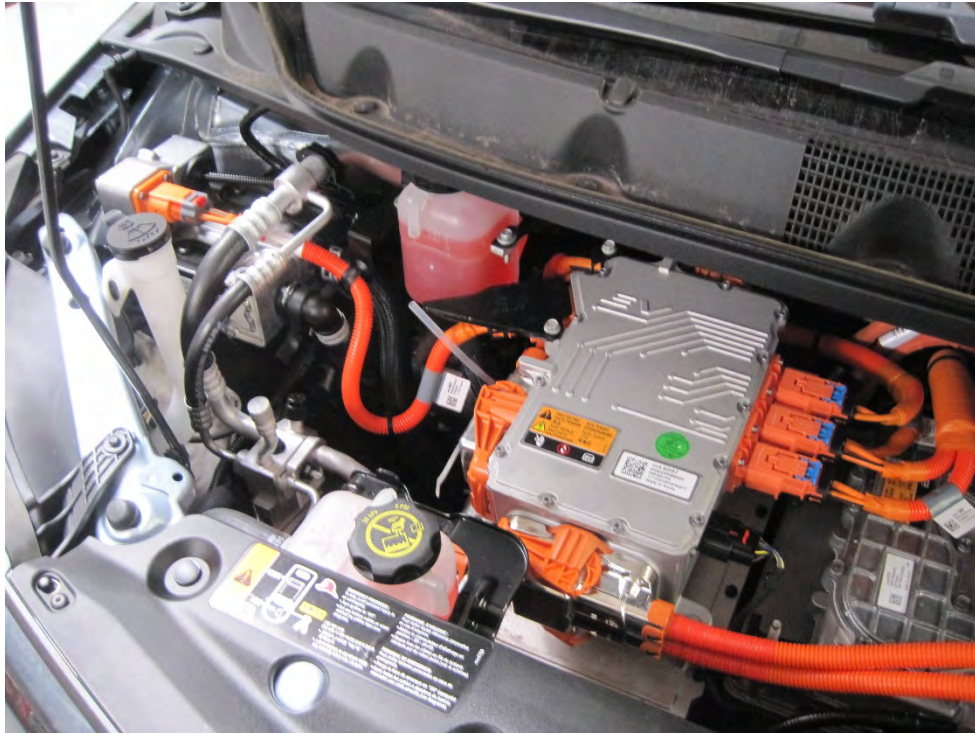
Figure 2-11. Fake Tank Release Point on GMC Test Vehicle
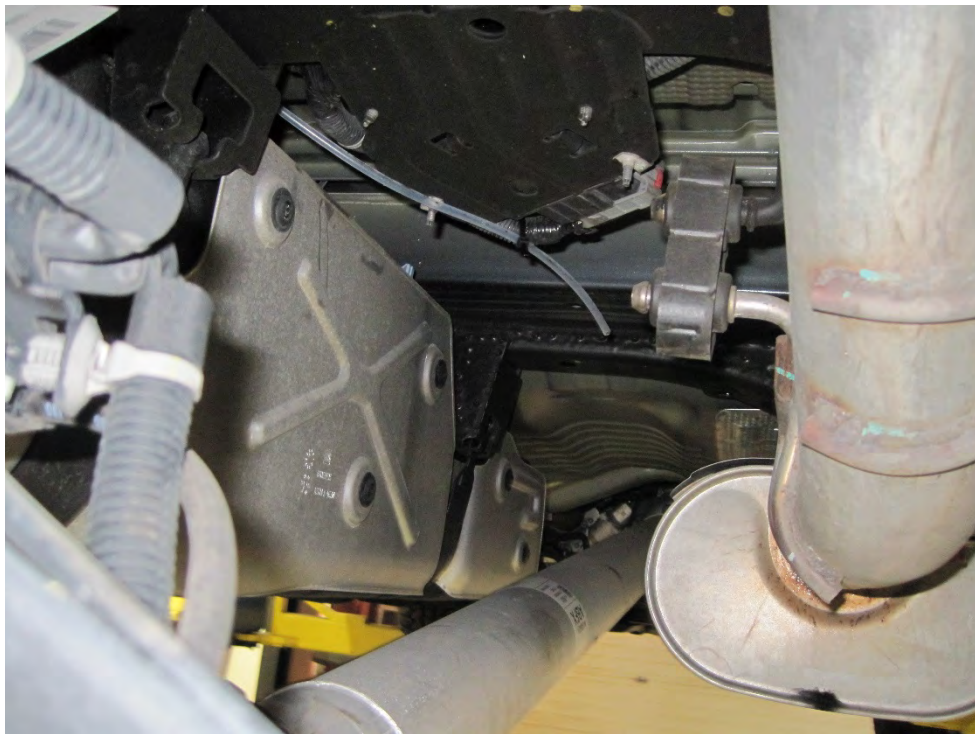
The eight propane emissions rates (mg/mile) were produced by paired combinations of two test speeds and four propane release rates (scfh), as shown in Table 2-3.

Table 2-3. Rotameter Settings Required for Designed Propane Releases

Propane Emission Rate (mg/mile)	Vehicle Speed (mph)	Propane Release Rate (scfh)	Propane Rotameter Setting (air basis)
6400	22.5	2.78	3.43 scfh
3200	45	2.78	3.43 scfh
1600	22.5	0.70	0.86 scfh
800	45	0.70	0.86 scfh
400	22.5	0.174	100 cc/min (0.214 scfh)
200	45	0.174	100 cc/min (0.214 scfh)
100	22.5	0.043	25 cc/min (0.054 scfh)
50	45	0.043	25 cc/min (0.054 scfh)

The propane emissions rate was calculated from the speed and propane release rate using this equation, with scfh defined at 70 F:

$$\frac{\text{mg Propane}}{\text{mile}} = \frac{\text{scfh Propane}}{\text{mph Speed}} * \frac{(460+32)}{(460+70)} * \frac{28.32\ \text{L}}{\text{ft3}} * \frac{1\ \text{mole Propane}}{22.4\ \text{L Propane}} * \frac{44.10\ \text{g Propane}}{1\ \text{mole Propane}} * \frac{1000\ \text{mg}}{\text{g}}$$

Additionally, each test condition had zero-propane release tests interspersed. The purpose of frequently interlacing zero running loss tests was to collect data to help distinguish non-zero running loss data streams from those of zero running loss emissions. This will especially assist the analysis of the data collected at low propane emissions rates (mg/mile) where EDAR's running loss signal may be hidden in a noisy background.

The propane release rates in the third column of Table 2-3 needed to be converted to settings for the rotameters, which are calibrated on air. The correction for the specific gravity of the gas flowing through the rotameters is given by Dwyer (https://www.dwyer-inst.com/Products/FlowmeterCurves.cfm), whose rotameters were used:

$$Q2 = Q1 * \text{SQRT}(\ 1\ /\ \text{S.G.})$$

where:

Q1	= Observed flowmeter reading
Q2	= Actual flow of test gas corrected for specific gravity of test gas
1	= Specific gravity of air, which was used to calibrate flowmeter
S.G.	= Specific gravity of test gas used in flowmeter

For example, for propane, which has a specific gravity of 1.52 (=44.1/29), a rotameter setting of 1.23 scfh would be required to produce a propane flow of 1.0 scfh.

2.7 EDAR Data Collection for Mass Emission Rate Method Development

Here we provide a brief description of how EDAR obtains optical measurements from pollutants of vehicles operating on the road. While many aspects of how EDAR works are proprietary, others have been discussed publicly by HEAT.

The EDAR instrument uses laser-based open-path infrared photometry to collect optical measurements of the gases that surround a vehicle as it passes under the instrument. EDAR scans a 12-foot-long retro-reflective tape attached to the pavement with a collimated 20mm-diameter beam of laser light. The laser beam scans the tape back and forth at 10 Hz and therefore obtains 20 scans each second. In this study, the instrument was set up to make measurements at 256 individual points (pixels) during each scan. By comparing the intensity of outgoing light with the intensity of returning light, the instrument determines the amount of light that is absorbed between the instrument and the pavement. By selecting appropriate infrared frequencies, the instrument can make measurements for a variety of gaseous compounds. The EDAR instrument used in this study collected optical data for measuring the four pure compound pollutants, CO, NO, NO_2, and CO_2, and a mixture of pure hydrocarbon (HC) compounds.

A laser technique known as differential absorption LIDAR (DIAL) can be used to get high signal-to-noise ratio (SNR) infrared absorption signals for small molecules that have small moments of inertia. Such compounds have infrared rotation-vibration spectra with many sharp absorption peaks separated by nearby zero-absorption valleys. The DIAL technique uses a single laser to rapidly oscillate between the peak frequency and the adjacent valley frequency. DIAL thereby produces a signal that is directly proportional to the amount of the pure compound present in the optical path. In addition, because the peak and valley frequencies are close, any interference or noise generally affects absorptions at both frequencies. This makes DIAL, by its nature, able to reject substantial amounts of noise.

Examples of compounds that can be measured with DIAL include CO, NO, NO_2, CO_2, methane (CH_4), ethane (C_2H_6), and ethylene (C_2H_4). However, larger molecules, like butane (C_4H_{10}) and ethanol (C_2H_5OH), have larger moments of inertia and have so many possible modes of rotations and vibrations that the infrared spectra are generally continuous with no or few distinct sharp peaks and valleys. Thus, DIAL cannot generally be used to obtain signals from larger molecules. For larger molecules, regular non-DIAL absorption techniques can be used, but the SNRs of such measurements can be hundreds of times poorer than DIAL techniques. Thus, the EDAR instrument uses the DIAL technique for CO, NO, NO_2, and CO_2, but the less sensitive standard absorption technique for the mixture of HC compounds.

The EDAR instrument uses five lasers to measure optical absorptions and store five channels of data – in this study, one channel for each of CO, NO, NO_2, CO_2, and the HC mixture. The data for each channel typically consists of an array of individual optical mass measurements at each pixel from 10 scans (0.5s) in front of the front bumper to 30 scans (1.5s) behind the rear bumper of a vehicle. The total number of scans in the array depends on the speed of the vehicle. For example, a 15-foot vehicle moving at 30 ft/s would cause the array to have an additional 5 scans. In that case, the complete array would have 45 scans made up of 10 scans before, 5 scans during, and 15 scans after the vehicle transit. Since each scan has 256 pixels, the complete array for one channel would have 11,520 optical mass measurements. The optical mass measured for each pixel is reported in units of mole/m^2, which means moles of the compound being measured per

square meter of the laser beam. It is important to recognize that the optical mass measurements are not for the entire emissions plume but only for the 20mm wide zigzag swath of the plume that the laser beam illuminates as the vehicle transits.

In usual EDAR operation while measuring specifically for exhaust emissions, EDAR does not routinely save the arrays for the five channels. EDAR just uses the data in the arrays to calculate, save, and output the exhaust emissions concentrations (ppm) or fuel-based emission rate (g/kg fuel). The arrays are not routinely saved. But for this study, we asked HEAT to save all arrays so that we could analyze them. Basically, we want to find an algorithm that uses the same array data, which is used to calculate exhaust emissions, to additionally calculate Release Rates (g/hr) and Emission Rates (g/mile) of exhaust emissions and evaporative emissions.

2.8   Field Data Handling and Storage

After the end of field data collection, HEAT provided ERG and CDPHE data for each transit that EDAR had recorded during the field deployment. The data included the variables on the left side of Table 2-4 and still photographs[3] of vehicle license plates. In addition, HEAT used their license plate transcriptions to look up variables for each Colorado-registered vehicle in a snapshot of the Colorado registration database. Those variables are shown in the top right of Table 2-4. ERG transcribed the hand-written notes from the paper data packets that were filled out by the personnel in each of the test vehicles corresponding to each of the convoy vehicle test conditions. Those variables, which are specific to the test vehicle test runs, are shown in the lower right of Table 2-4.

We then time-aligned the data provided by HEAT with the data from the transcribed data packets so that the EDAR results for each test vehicle transit could be easily found for analysis. Additional flag variables were added to the final spreadsheet[4] for sorting and analysis purposes. For analysis of the data by SAS, a CSV version of the spreadsheet was read by a SAS program[5] and merged with decoded information[6] from the ERG VIN decoder to create a final SAS dataset[7].

HEAT also provided ERG with the EDAR data arrays[8] for each transit and for each of the five EDAR pollutant channels (HC, CO, NO, NO_2, CO_2).

---

[3] P:\EDARinDenver-OCT2019\HEATphotos\All_33074_EDAR_snapshots-OCT2019/*.jpg

[4] P:\EDARinDenver-OCT2019\EDARpngs_Denver_20_24OCT2019-200120/ Westminster_OCT2019Results_200124Reprocess-200203_wReleaseRates_gph.xlsx

[5] P:\EDARinDenver-OCT2019\Analysis/ read_SS_VIN.sas

[6] P:\EDARinDenver-OCT2019\Analysis/ vin_output.csv

[7] P:\EDARinDenver-OCT2019\Analysis/ Westminster_ss_vin.sas7bdat

[8] P:\EDARinDenver-OCT2019\EDAR_CSVs\OriginalCSVs-received200124\ 7_2019102?_*_0005??_Denver_2019/ *_array.csv

Table 2-4. Reported Variables in Master Dataset

Source	Variable	Source	Variable
HEAT	EDAR Date_MTN (mm/dd/yyyy)	CO Regis	VIN
HEAT	EDAR Time_MTN (hh:mm:ss AM/PM)	CO Regis	Model Year
HEAT	EDAR License Plate Number	CO Regis	Make
HEAT	EDAR License Plate State	CO Regis	Model
HEAT	EDAR Vehicle Speed (mph)	CO Regis	Fuel Type
HEAT	EDAR Road Grade (rise/run)	CO Regis	Body Type
HEAT	EDAR Latitude (deg)	CO Regis	Vehicle Type
HEAT	EDAR Longitude (deg)	CO Regis	Emissions Expiration Date
HEAT	EDAR Ambient Temperature (F)	CO Regis	Emissions Area
HEAT	EDAR Relative Humidity (%)	CO Regis	Registration Date
HEAT	EDAR Barometric Pressure (inch Hg)	CO Regis	Registration County
HEAT	EDAR Wind Speed @ 6m (mph)		
HEAT	EDAR Wind Direction (degN)	ERG	Test Vehicle ID
HEAT	EDAR Vehicle Acceleration (mph/s)	ERG	GMC TailGate
HEAT	EDAR Vehicle Specific Power (kW/Mg)	ERG	Run No.
HEAT	EDAR Epoch Car_Time (micro s)	ERG	Evap Location
HEAT	EDAR Car_Name	ERG	Nominal Speed (mph)
HEAT	EDAR HC Mole Ratio (moleC6/moleCO2)	ERG	Nominal Propane Emission Rate (mg/mile)
HEAT	EDAR NO Mole Ratio (moleNO/moleCO2)	ERG	Measured Release Rate (g/hr)
HEAT	EDAR CO Mole Ratio (moleCO/moleCO2)	ERG	Exhaust Gas Release Volume (scf)
HEAT	EDAR HC (ppmC6)	ERG	Labeled Exhaust Cylinder HC (ppmC3)
HEAT	EDAR CO (%)	ERG	Labeled Exhaust Cylinder CO (ppm)
HEAT	EDAR NO (ppm)	ERG	Labeled Exhaust Cylinder NO (ppm)
HEAT	EDAR CO2 (%)	ERG	Labeled Exhaust Cylinder CO2 (%)
HEAT	EDAR Clean Screened?	ERG	Field Notes QC
HEAT	EDAR QC	ERG	Test Vehicle Run Quality Flag

2.9   Westminster Dataset EDAR Quality Flag

The EDAR instrument produces the EDAR QC flag, which is listed at the bottom of the left column of Table 2-4. The EDAR QC flag assigns one of four values to each vehicle transit. "Interfering plume" is assigned if the instrument detects substantial amounts of pollutants in front of the vehicle. The source for an interfering plume could be from emissions of a vehicle driving in front of the target vehicle or from a vehicle in the oncoming lane. "Low CO2" is assigned when the size of the CO_2 plume is small. This can occur if the driver takes his foot off the accelerator while passing under the EDAR instrument. "No plate" is assigned if the vehicle has no discernable license plate. Otherwise, the EDAR QC flag is set to "valid."

Table 2-5 shows the counts of the test vehicle transits that met the planned test condition criteria and for the fleet vehicles as a whole. Because the test vehicle convoy scrupulously maintained

specified minimum following distances, interfering plumes should only be generated by fleet vehicles in the oncoming lane. On the other hand, tailgating was common for fleet vehicles. Test vehicles EV-1 and EV-2 show relatively high counts of Low CO_2 flags compared to the other test vehicles. We believe that this is a consequence of the 30 scfm release rate of artificial exhaust from EV-1 and EV-2 which is low compared to the likely higher release rate of the other four test vehicles that had natural exhaust emissions releases. The fleet vehicle counts of Low CO_2 flags probably occurred when some drivers saw the RSD equipment and took pressure off the accelerator pedal.

Table 2-5. Transit Counts by EDAR QC Label and Vehicle Category

EDAR QC Label	Test Vehicles						Fleet Vehicles
	EV-1	EV-2	Subaru	F150	GMC	Infiniti	
Valid	236	282	103	86	15	290	25544
Interfering Plume	8	6	14	5	0	5	2302
Low CO2	59	19	0	0	0	2	2833
No Plate	0	2	1	0	44	2	1084
Total	*303*	*309*	*118*	*91*	*59*	*299*	*31763*

2.10 Westminster Dataset and Analysis Program Locations

Appendix B gives the locations of the Westminster datasets and analysis programs with details of the inputs and outputs of each program. This information can be used to help the analysis of future RSD data.

3.0   Field Data Collection Results

During the field event, EDAR collected data on on-road private vehicles, on the imbedded test vehicles that we drove as a convoy interspersed in normal traffic, and on weather for each EDAR vehicle transit while the emissions measurements were being taken. In the following subsections, we discuss the test vehicle test conditions, the characteristics of the weather during the study, and the optical data collected by the EDAR instrument.

3.1   Test Vehicle Test Conditions

We drove a group of study test vehicles repeatedly past the RSD instrument on each day of field testing. The test vehicles, which served as RSD measurement controls in the study, were imbedded in normal traffic flow as a four-vehicle[9] "convoy." Table 3-1 gives the purpose, characteristics, and emissions releases of the vehicles that were convoy members. The test crew drove the convoy under the EDAR instrument at the designed test conditions while trying to prevent any public vehicles from getting between the individual test vehicles. Test vehicle drivers did not allow "interlopers" to sneak in to maintain adequate following distances so that the EDAR instrument would properly "trigger" on test vehicles in Position 1, 2, and 3. Vehicle 4 was used solely as a "blocker" to prevent public vehicles from tailgating Vehicle 3. Occasionally, aggressive interlopers did force into the convoy. In those instances, the entire data collection run was aborted, all data was marked for deletion, and the test condition was repeated on the next transit.

On any given test run, all vehicles in the convoy drove past the EDAR instrument at the same nominal speed – either 22.5 or 45 mph. Vehicle 1 released "clean" artificial exhaust, while Vehicle 2 released "dirty" artificial exhaust, as shown in the table. The artificial exhaust was released at 30 scfm[10] for about 10 seconds before and during each test vehicle's transit under the EDAR instrument. The exhaust from vehicles in Positions 3 and 4 were their natural exhaust.

On any given test run, Vehicles 1, 2, and 3 released propane, as the artificial running loss emissions, at the same artificial running loss release rate and release location. Of course, since Vehicles 1 and 2 were EVs, their propane releases were their only running losses. On the other hand, since Vehicle 3 was always a gasoline-fueled vehicle, its propane releases were in addition to any natural running losses that Vehicle 3 might have.

As shown in Table 3-1, nine non-zero propane release rates (288, 144, 72, 36, 18, 9, 4.5, 2.25, and 1.125 g/hr) were used. Some tests were also performed with no propane released (0 g/hr). With the two nominal speeds (22.5 and 45 mph), these ten release rates produced nine nominal running loss emission rates (6400, 3200, 1600, 800, 400, 200, 100, 50, and 0 mg/mile).

---

[9] The third vehicle position was not filled on the 10/24/2019 test day. Therefore, the convoy had only three vehicles on that day.

[10] Standard (70°F, 760 Torr) cubic feet per minute

Table 3-1. Vehicles Used in the Test Vehicle Convoy

Vehicle Position (Test Dates) Purpose	Vehicle Description	Nominal Vehicle Speed (mile/hr)	Exhaust Mixture and Flow	Propane: Artificial Running Loss Release Rate (g/hr)	Propane: Artificial Running Loss Release Location
1 (10/20-24/2019) Clean exhaust, 0 natural running loss	EV-1: 2017 Chevrolet Bolt	22.5 mph, 45 mph	Artificial: 15.05% CO_2 balance N2 at 30 scfm (left exhaust)	Artificial only: 288, 144, 72, 36, 18, 9, 5, 3, 1, 0	Fuel Fill DOOR, Top of TANK, Under HOOD
2 (10/20-24/2019) Dirty exhaust, 0 natural running loss	EV-2: 2017 Chevrolet Bolt		Artificial: 402 ppm C3H8 5043 ppm CO 996 ppm NO 14.76% CO_2 balance N2 at 30 scfm (right exhaust)		
3 (10/20-21/2019) Natural exhaust	2019 Subaru Outback		Natural (left exhaust)	Natural + Artificial: 288, 144, 72, 36, 18, 9, 5, 3, 1, 0	
3 (10/22/2019) Natural exhaust	2019 GMC 1500		Natural (dual exhaust)		
3 (10/23/2019) Natural exhaust	2016 Ford F150		Natural (right exhaust)		
4 (10/20-24/2019) Blocker	2015 Infiniti Q50		Natural (dual exhaust)	Natural	Natural

The total 298 realized combinations of metered artificial propane release rates and nominal speeds for the test vehicle convoy are described in Table 3-2. During each transit, the propane releases of Vehicles 1, 2, and 3 were all set to the same release location and rate.

Table 3-2. Test Condition Combinations Used by the Test Vehicle Convoy[11]

Propane: Metered Artificial Running Loss Release Rate (g/hr)	Nominal Vehicle Speed (mile/hr)	Propane: Nominal Artificial Running Loss Emission Rate (mg/mile)	Number of Convoy Transits			
			Release Location: DOOR	Release Location: TANK	Release Location: HOOD	Total
288	45	6400	5	5	5	15
144	22.5	6400	5	6	5	16
144	45	3200	5	6	5	16
72	22.5	3200	5	5	5	15
72	45	1600	5	5	5	15
36	22.5	1600	5	6	5	16
36	45	800	5	6	5	16
18	22.5	800	5	5	5	15
18	45	400	5	5	5	15
9	22.5	400	5	6	5	16
9	45	200	5	5	5	15
4.5	22.5	200	5	5	5	15
4.5	45	100	5	5	5	15
2.25	22.5	100	5	6	5	16
2.25	45	50	5	6	5	16
1.125	22.5	50	5	5	5	15
0	45	0	n/a	n/a	n/a	25
0	22.5	0	n/a	n/a	n/a	26

As the table shows, during the study at least five replicates were obtained for each test condition. The convoy was driven to achieve this minimum number of replicates. That is, if some feature of a convoy run did not meet quality assurance criteria, for example, if a following distance was too short or a gas valve was not in the proper position on one vehicle, then the transit for the entire convoy for the needed test condition was repeated. In general, each of the five or six replicates was performed on a different day of the testing to reduce the risk of an imbalanced dataset as a

---

[11] C:\Documents\EPA WA3-13 (MAR20-FEB21)\8_Reports/Table_ConvoyTestConditions.xlsx

consequence of a pause in or termination of data collection caused by inclement weather or equipment malfunctions. Thus, at least one replicate of the entire set of test conditions in Table 3-2 was completed during each test day.

In addition to the 298 convoy transits described by Table 3-2, eleven more convoy transits were made with EV-1 and EV-2 not releasing either simulated exhaust gas or simulated running loss gas. These runs provided EDAR instrument-internal data that could be used to characterize instrument noise when no vehicle emissions are present. During these "blank" runs, the test vehicles in Positions 3 and 4 were operated with their natural exhaust emissions and no artificial running losses released.

3.2 Model Years and Gross Vehicle Weight Ratings of Fleet Vehicles

The characteristics of the fleet vehicles were examined[12] using the license plates, Colorado vehicle registration database, and the ERG VIN decoder. Because of various idiosyncrasies, the counts of transits and vehicles presented in this subsection should be regarded as approximate.

In general, during the October 2019 Westminster field study, the HEAT RSD instrument and its license plate reader operated day and night. 30,590 RSD transits of fleet vehicles (i.e., not test vehicle transits) were obtained by the RSD instrument. After eliminating missing license plates (N=973) and "NOREAD" plates (N=11), the license plate reader had recorded 18,547 unique plates. Because the plate reader occasionally reads plates improperly, the actual number of unique vehicles would be slightly lower.

Of those 18,547 unique plates, 17,927 vehicles had Colorado plates. We used the ERG VIN Decoder to determine the GVWRs of the vehicles, where possible. The GVWR distribution is shown in Table 3-3. We also used the ERG VIN Decoder and a snapshot of the Colorado registration database to determine, where possible, the consensus model years of the vehicles with Colorado plates. The model year distribution is shown in Table 3-4.

Table 3-3. Gross Vehicle Weight Ratings of Vehicles with Colorado Plates

GVWR Bin (pounds)	Frequency	Percent	Cumulative Frequency	Cumulative Percent
LDV	8113	45.26	8113	45.26
0-3,750	212	1.18	8325	46.44
3,751-6,000	5029	28.05	13354	74.49
6,001-8,500	2719	15.17	16073	89.66
8,501-10,000	326	1.82	16399	91.48
10,001-14,000	74	0.41	16473	91.89
14,001-19,500	5	0.03	16478	91.92
Unknown	1449	8.08	17927	100

---

[12] P:\EDARinDenver-OCT2019\Analysis_MLout\220817\Anal_MLout\FleetVehs/ OCT19_FleetStats.sas

Table 3-4. Model Years of Vehicles with Colorado Plates

Consensus Model Year	Frequency	Percent	Cumulative Frequency	Cumulative Percent
1947	1	0.01	1	0.01
1966	2	0.01	3	0.02
1967	1	0.01	4	0.03
1970	1	0.01	5	0.03
1973	2	0.01	7	0.04
1974	1	0.01	8	0.05
1978	2	0.01	10	0.06
1981	1	0.01	11	0.07
1983	1	0.01	12	0.08
1984	6	0.04	18	0.11
1985	2	0.01	20	0.13
1986	4	0.03	24	0.15
1987	6	0.04	30	0.19
1988	4	0.03	34	0.22
1989	6	0.04	40	0.25
1990	11	0.07	51	0.32
1991	21	0.13	72	0.46
1992	17	0.11	89	0.56
1993	20	0.13	109	0.69
1994	55	0.35	164	1.04
1995	62	0.39	226	1.43
1996	61	0.39	287	1.82
1997	114	0.72	401	2.54
1998	137	0.87	538	3.4
1999	204	1.29	742	4.7
2000	265	1.68	1007	6.37
2001	298	1.89	1305	8.26
2002	346	2.19	1651	10.45
2003	401	2.54	2052	12.99
2004	512	3.24	2564	16.23
2005	545	3.45	3109	19.68
2006	586	3.71	3695	23.38
2007	723	4.58	4418	27.96
2008	748	4.73	5166	32.69
2009	498	3.15	5664	35.85
2010	648	4.1	6312	39.95
2011	799	5.06	7111	45
2012	885	5.6	7996	50.6
2013	1027	6.5	9023	57.1
2014	1194	7.56	10217	64.66
2015	1395	8.83	11612	73.49
2016	1308	8.28	12920	81.77
2017	1246	7.89	14166	89.65
2018	1148	7.27	15314	96.92
2019	482	3.05	15796	99.97
2020	5	0.03	15801	100
missing	2126			

3.3   Wind Speed and Direction

Wind speed and direction measurements are important for the determination of vehicle Release Rates (g/hr) and Emission Rates (g/mile) from RSD measurements. The reason for this is that, in addition to vehicle road speed, wind speed and direction influence the dispersion of emissions from vehicles driving on the road and thereby influence the dimensions and location of the vortex behind each moving vehicle. Because RSDs get their largest signals from pollutants in the vortex, the factors that influence the vortex affect the optical pathlengths and size of emissions plumes sampled by RSDs.

The EDAR instrument was equipped with a weather sensor that measured wind speed and direction, ambient temperature, relative humidity, and barometric pressure at about 6 meters above the pavement. At each vehicle transit, the EDAR system recorded those variables. Accordingly, because of diurnal differences in traffic flow, weather measurements are frequent during the day and infrequent at night. Figure 3-1 shows a plot of the EDAR-reported wind speed and direction as measured at the 6-meter height of the weather sensor above the pavement. Each point represents a measurement taken at a vehicle transit. Figures 3-2 and 3-3 show separate wind direction and wind speed histograms of the same dataset. The winds tended to be high-speed and gusty during the week.

Figure 3-1. Wind Speed vs. Wind Direction at 6 Meters above Pavement[13]

/proj1/EDARinDenver-OCT2019/Analysis/analyze_Fleet_Wind_1.sas 06MAY20 17:28

---

[13] C:\Documents\EPA WA3-13 (MAR20-FEB21)\8_Reports/
Westminster_OCT2019Results_200124Reprocess-200203_wReleaseRates_gph.xlsx, Wind Plots tab

Figure 3-2. Wind Direction at 6 Meters above Pavement

Figure 3-2. Wind Direction at 6 Meters above Pavement

Wind Direction (degN)	FREQ	CUM. FREQ	PCT	CUM. PCT
8	326	326	1.03	1.03
15	346	672	1.09	2.12
23	375	1047	1.18	3.30
30	416	1463	1.31	4.61
38	432	1895	1.36	5.97
45	538	2433	1.69	7.66
53	1017	3450	3.20	10.86
60	552	4002	1.74	12.60
68	294	4296	0.93	13.53
75	294	4590	0.93	14.45
83	403	4993	1.27	15.72
90	348	5341	1.10	16.82
98	398	5739	1.25	18.07
105	504	6243	1.59	19.65
113	847	7090	2.67	22.32
120	893	7983	2.81	25.13
128	700	8683	2.20	27.34
135	580	9263	1.83	29.16
143	674	9937	2.12	31.28
150	657	10594	2.07	33.35
158	533	11127	1.68	35.03
165	451	11578	1.42	36.45
173	424	12002	1.33	37.79
180	466	12468	1.47	39.25
188	370	12838	1.16	40.42
195	739	13577	2.33	42.74
203	864	14441	2.72	45.46
210	863	15304	2.72	48.18
218	645	15949	2.03	50.21
225	590	16539	1.86	52.07
233	667	17206	2.10	54.17
240	847	18053	2.67	56.84
248	1312	19365	4.13	60.97
255	1754	21119	5.52	66.49
263	2187	23306	6.89	73.37
270	1699	25005	5.35	78.72
278	1229	26234	3.87	82.59
285	1183	27417	3.72	86.32
293	941	28358	2.96	89.28
300	870	29228	2.74	92.02
308	705	29933	2.22	94.24
315	614	30547	1.93	96.17
323	389	30936	1.22	97.40
330	283	31219	0.89	98.29
338	162	31381	0.51	98.80
345	147	31528	0.46	99.26
353	235	31763	0.74	100.00

FREQUENCY

Figure 3-3. Wind Speed at 6 Meters above Pavement

Wind Speed at 6m (mph)	FREQ	CUM. FREQ	PCT	CUM. PCT
1	2056	2056	6.47	6.47
2	2440	4496	7.68	14.15
3	1980	6476	6.23	20.39
4	2647	9123	8.33	28.72
5	2233	11356	7.03	35.75
6	2299	13655	7.24	42.99
7	1686	15341	5.31	48.30
8	1275	16616	4.01	52.31
9	1648	18264	5.19	57.50
10	1208	19472	3.80	61.30
11	1543	21015	4.86	66.16
12	1060	22075	3.34	69.50
13	1401	23476	4.41	73.91
14	1124	24600	3.54	77.45
15	1249	25849	3.93	81.38
16	757	26606	2.38	83.76
17	1023	27629	3.22	86.98
18	676	28305	2.13	89.11
19	735	29040	2.31	91.43
20	407	29447	1.28	92.71
21	481	29928	1.51	94.22
22	299	30227	0.94	95.16
23	341	30568	1.07	96.24
24	203	30771	0.64	96.88
25	198	30969	0.62	97.50
26	193	31162	0.61	98.11
27	118	31280	0.37	98.48
28	106	31386	0.33	98.81
29	103	31489	0.32	99.14
30	82	31571	0.26	99.40
31	47	31618	0.15	99.54
32	31	31649	0.10	99.64
33	31	31680	0.10	99.74
34	22	31702	0.07	99.81
35	15	31717	0.05	99.86
36	12	31729	0.04	99.89
37	8	31737	0.03	99.92
38	6	31743	0.02	99.94
39	5	31748	0.02	99.95
40	2	31750	0.01	99.95
41	3	31753	0.01	99.97
42	4	31757	0.01	99.98
43	3	31760	0.01	99.99
44	1	31761	0.00	99.99
45	0	31761	0.00	99.99
46	1	31762	0.00	100.00
47	0	31762	0.00	100.00
48	1	31763	0.00	100.00
49	0	31763	0.00	100.00
50	0	31763	0.00	100.00

FREQUENCY

/proj1/EDARinDenver-OCT2019/Analysis/analyze_Fleet_Wind_1.sas 06MAY20 17:28

4.0 Detailed Data Post-Processing by HEAT

During planning of the field testing, ERG anticipated using raw, unprocessed data – just as it was obtained by download from the instrument. The reason was that we expected that the signal analysis methods that we would develop for maximizing the signal-to-noise ratio for running loss emissions would be different from those used routinely by HEAT for reporting exhaust emissions. Also, we wanted to have the raw data so that any signal processing that we developed could be used to write a processing algorithm that could be installed on the instrument for in-real-time processing in future studies.

We had discussions with HEAT to identify the different post-processing actions that HEAT used to determine the actions that were acceptable. Our main concern was that we did not want to lose data or to do something that would harm or mask information in the data. On the other hand, we did want HEAT to post-process for things that we did not want to spend a substantial amount of time to "re-invent." The following paragraphs describe the raw data post-processing activities that HEAT performed before conveying the data files to ERG.

Background Corrections – HEAT routinely corrects the background of the CO_2 arrays for absorption by the ambient 400 ppm CO_2 levels. This correction amounts to about 20% of the total CO_2 absorption from vehicle exhaust. Additionally, because the EDAR pathlength varies with scan angle, the absorption varies with scan angle, as can be seen in Figure 2-3. HEAT has a proprietary method to make the correction. Therefore, we decided to have HEAT continue to make the correction to the CO_2 arrays. We believe that HEAT makes corrections only for the global ambient CO_2 and not for CO_2 or other vehicle pollutants that are above the roadway from previous vehicles driving past the instrument.

Scan Position Corrections – The EDAR instrument used in this study had 256 different scan positions along each scan. An optical measurement for each channel is taken at each scan position. For a variety of reasons, including wear on the retro-reflective strip, the recorded absorption among the scan positions can vary systematically. HEAT uses the average optical measurement for each scan position in the last several scans to adjust all of the optical measurements for the corresponding scan position for the entire transit's array. Since this is a relatively simple calculation, we judged that the risk of damaging the underlying optical measurements was low. Therefore, we agreed to have HEAT make these corrections.

Vehicle Footprint Blanking – During a vehicle transit, EDAR's outgoing beam is not reflected back to the instrument from scan positions during scans when the vehicle is covering the retro-reflective tape. Without correction, the instrument would normally calculate a 100% absorption for those pixels, even though those absorptions would not represent high pollutant concentrations. Also, when the 20mm diameter beam is partially obscured by the edge of the vehicle, the resulting measurement also does not correspond to an elevated pollutant concentration. Therefore, for both of these situations, which occur on the transit of every vehicle, HEAT must process the raw optical measurements to blank out those array pixels that completely or partially blocked by the vehicle.

To make its blanking code simple and reliable, HEAT wrote an algorithm that circumscribes a perfect rectangle around the vehicle footprint. The disadvantage of circumscribing is that the

optical measurements for some pixels – particularly near the corners of vehicles – are not output to the final processed array. This loss of data is not a problem for calculating exhaust emissions, but we did not want to lose any data – especially since the largest running loss absorptions are likely near the edges and corners of the vehicle footprint. Therefore, we asked HEAT to process the raw data without circumscribing the vehicle footprint.

Pixel Glitches and Footprint Glints – Occasionally, arrays contain isolated pixels with optical mass values that are substantially different from the values of adjacent pixels. The optical mass values are more different than can be expected from the usual background noise. If the pixels are adjacent to the vehicle footprint, the values might be caused by glints as the laser beam scans the edge of the vehicle body. Isolated, spurious optical mass values can also occur anywhere in an array. We refer to these as pixel glitches. Whether these abnormal values are glints or glitches, neither HEAT nor ERG believe that they represent good values. HEAT has methods to identify, remove, smooth, or otherwise handle such suspect optical mass values. We asked HEAT to convey all suspect values to us unchanged so that we could develop methods to identify them and prevent them from adversely influencing running loss calculations. This approach gives us multiple opportunities to develop ever-improving signal analysis techniques.

5.0 RSD Emission Rate Method: Step-by-Step Description

The measurement of pollutant emissions rates by remote sensing devices (RSDs) is based on three concepts observed in our studies:

- A portion of pollutants released from a moving vehicle become temporarily entrained in the vehicle's low-pressure zone, or vortex, which is the dominant source of RSD signals.

- Under steady-state vehicle air velocity and pollutant release rate, the pollutant Mass in Vortex (g) is relatively constant and is proportional to pollutant Release Rate (g/hr).

- The proportionality constant, which we call the Vortex Entrainment Time (hr), depends only mildly on vehicle air speed, pollutant release location, and light-duty vehicle shape.

The pollutant Mass in Vortex (g) is calculated from the RSD signal with corrections for road speed and a geometrical factor characteristic of the RSD configuration. The Vortex Entrainment Time (VET) is estimated from the vehicle air velocity, the estimated vehicle drag area, and the estimated source location on the vehicle. Then, the pollutant Release Rate (g/hr) is calculated as the Mass in Vortex (g) divided by the VET (hr). Finally, the pollutant Emission Rate (g/mile) is just the Release Rate (g/hr) divided by the vehicle Road Speed (mile/hr).

The calculations also use the discovered dependence of vortex shape on vehicle air velocity and vehicle length, as well as standard signal analysis techniques, to improve RSD signal-to-noise ratio. Finally, Blind Source Separation is used to apportion the RSD HC signal into an Exhaust HC signal and an Evaporative HC signal, from which their separate release rates and emission rates are determined.

All of the above are presented in this section using a recipe-like description of the calculations. Following sections detail the analyses for the determination of VET functionality and vortex shape functionality.

Overview of the Method's Flow of Calculations – The method for calculating vehicle Emission Rates (g/mile) and Release Rates (g/hr) from RSD measurements flows from left to right using the elements shown in Figure 5-1:

- A Remote Sensing Device (RSD), described in Section 5.1, collects measurements of the species emitted from a moving vehicle as it passes by the RSD system,

- A Pre-Processing Device (PPD), described in Section 5.2, adjusts these measurements to improve their overall quality and reduce noise effects,

- A Vortex Shape Estimation Device (VSED), described in Section 5.4, calculates Weights, which describe the vortex shape, and the Vortex Entrainment Time (VET), which is critical to the estimation of emission rates, and

- An Emission Calculation Device (ECD), described in Section 5.5, uses one or more of the outputs of the Pre-Processing Device to calculate the Release Rate and the Emission Rate of one or more emitted species from the vehicle.

An alternative method is shown in Figure 5-2. This method contains the same elements as in Figure 5-1 and adds an optional new element: a combined Separation/Estimation (SED) Device, described in Section 5.3. The calculation extracts components of the measured species signals to associate them with one or more different plume sources: exhaust plume and evaporative plume. This allows the estimation of emission rates of specific species that are associated with specific spatial locations around the vehicle.

**Figure 5-1. Flow Diagram of Methodology
without Separation/Estimation of Emission Sources**
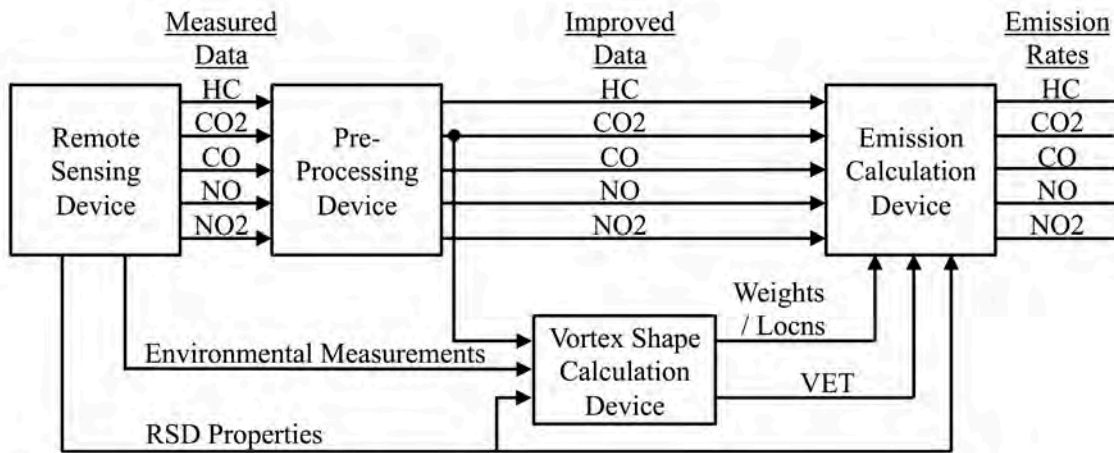
**Figure 5-2. Flow Diagram of Methodology
with Separation/Estimation of Emission Sources**
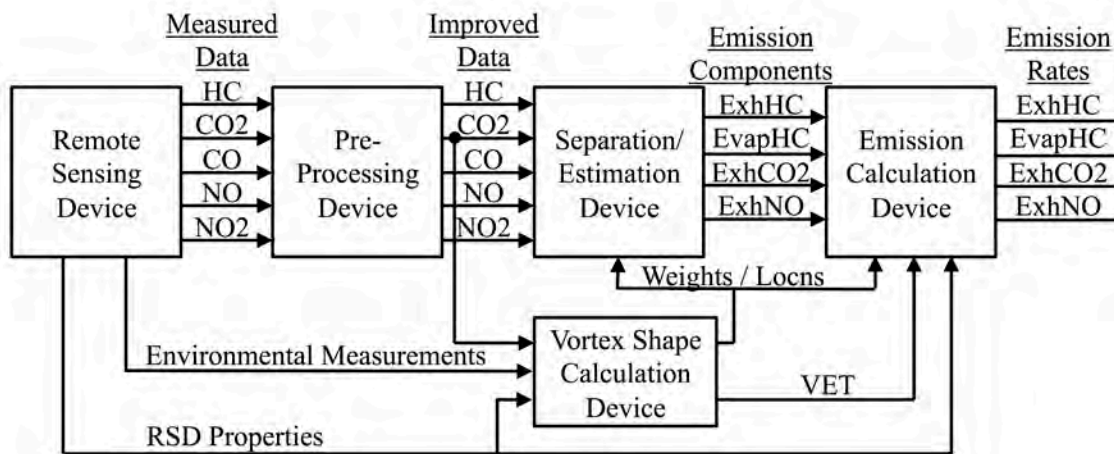
5.1   Remote Sensing Device

The Remote Sensing Device (RSD) is a system that collects spatial and/or temporal representations of one or more species that are potentially emitted from a moving vehicle as it passes by the RSD without touching the vehicle.

Figure 5-3 shows the Hager Environmental and Atmospheric Technology (HEAT) RSD and associated instrumentation that was used to collect data. The RSD laser instrument (labelled EDAR) is the box hanging from the horizontal gantry boom. The approximate location of the path of the scanning infrared laser is drawn in the figure in red. The instrument scans a 20mm diameter infrared laser beam at 20 scans per second onto a retro-reflective tape that is attached to the pavement perpendicular to the direction of traffic flow. The laser light returns to the instrument for analysis as gases emitted from vehicles absorb a portion of the light. The instrument shown provides HC, CO, NO, NO_2, and CO_2 optical mass (moles/m2) measurements for 256 pixels across the 3.66 meter (12 feet) long tape.

The horizontal gantry boom is also equipped with a license plate reader, a weather sensor that measures wind speed and direction at about 6 meters above the pavement, and a sensor that measures the road speed of each vehicle that passes under the instrument.

When a vehicle moves through the air, a low-pressure zone typically forms behind the vehicle. In this description, the low-pressure zone is called the vortex. As the vehicle drives down the road, the vortex follows the vehicle at the same speed as the vehicle. The vortex is a dynamic, swirling, mass of gases and particles with ill-defined boundaries that exchanges material with the surrounding air moving past it.

RSD instruments obtain their signals using open-path photometric measurements of pollutants. While pollutants can be anywhere around the moving vehicle, the highest levels of pollutant mass are usually found in the vortex because the vortex temporarily stores pollutants. The vortex is approximately as tall and as wide as the rear of the vehicle. In general, current RSD instruments do not have enough sensitivity to quantify emissions in the wake behind the vortex. Thus, an RSD's signal is dominated by the mass of a pollutant in the vortex.

Figure 5-4 shows a representation of a vehicle (the black square) driving to the left in the vehicle's reference frame from above the roadway. If a pollutant is released from the vehicle (the left red arrow), a portion of the mass of the release is temporarily stored in the vortex (the pink triangular area behind the vehicle). At the same time, air moving around the vehicle and the vortex strips off a portion of the pollutant mass from the vortex (the right red arrow). Under steady-state conditions, the release rate, the mass in the vortex, and the stripping rate are in a dynamic equilibrium. Consequently, on average, the release rate from the vehicle equals the stripping rate from the vortex, and the mass in the vortex tends to be constant and proportional to the release rate. So, for example, if the pollutant release rate from the vehicle is zero, the pollutant mass in the vortex will tend to be zero.

Figure 5-3. HEAT Remote Sensing Device Test Set-Up
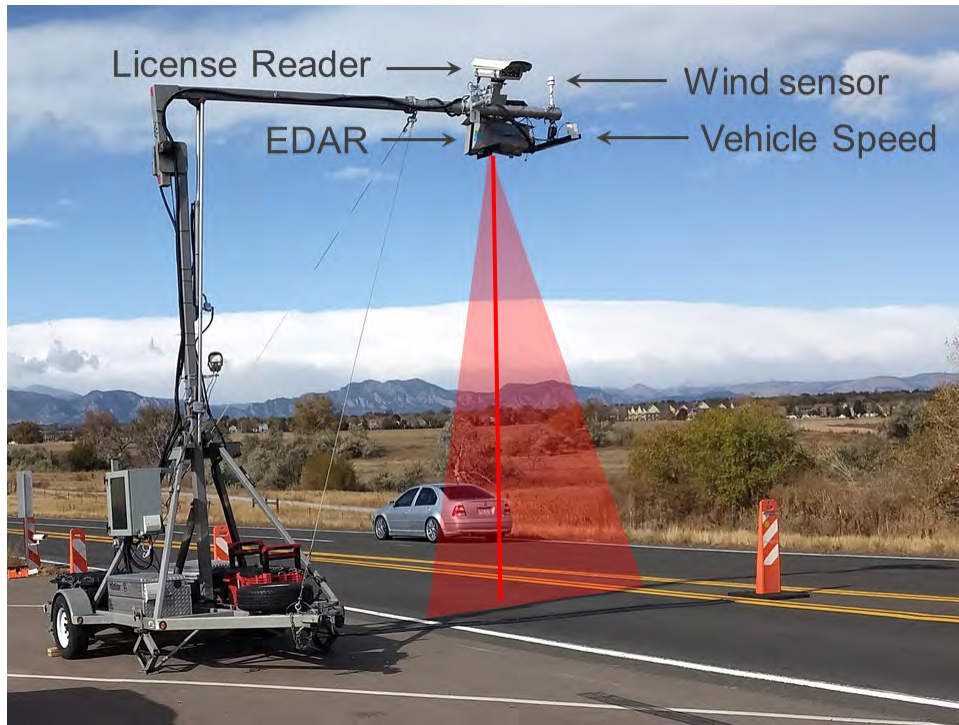
Figure 5-4. RSD ZigZag Scan Pattern on Pollutants from a Moving Vehicle
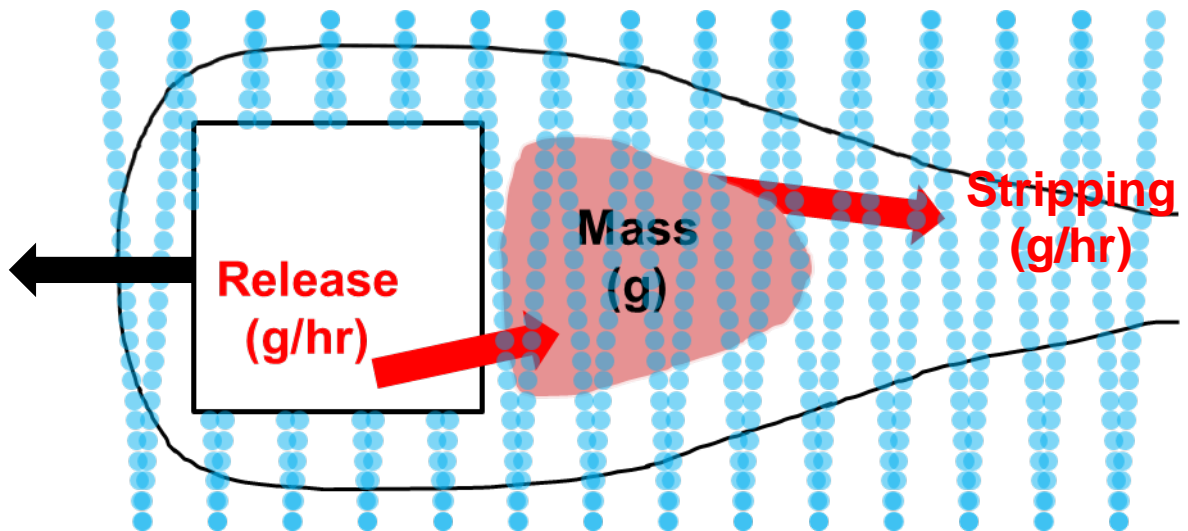
Figure 5-4 also shows a representation of the RSD's measurement collection pattern across the vehicle reference frame using blue dots. In this figure, the horizontal dimension is elapsed time, and the vertical dimension is the spatial position across the roadway. The motion of the vehicle through this scanning device causes a two-dimensional image-like measurement to be collected for each type of pollutant that is being assessed. The blue dots in Figure 5-4 show how the RSD's light beam scans the vehicle and its vortex from above as they pass under the RSD. Because the vehicle and its vortex are moving but the RSD is stationary, the light beam tends to make a zigzag in the vehicle/vortex reference frame. The blue dots represent the pixels, which are the spots where the RSD makes each detailed data measurement. At each pixel, the RSD records the optical mass (mole/m^2) of a pollutant between the instrument and the pavement.

The RSD in this study measured the masses of HC, CO, NO, NO$_2$, and CO$_2$ at each pixel. Note that the RSD does not collect any detailed data while the vehicle is covering the retro-reflective tape on the pavement. This is shown in the figure as the lack of blue dots on top of the vehicle.

Measurements collected for the vehicle emissions task are assumed to be multichannel in nature. The data for the vehicle emissions task consists of sets of multiple registered images, collected simultaneously in a raster-scanning process using a laser-based measurement system over a roadway. Each image is a collection of pixels in which the horizontal dimension represents time and the vertical dimension represents position across the roadway. As a vehicle passes through the measurement system, the system measures the amount of a particular species present in the reflection of the laser beam at the sensor system. The species being monitored by this RSD measurement system are hydrocarbons (HC), carbon dioxide (CO$_2$), carbon monoxide (CO), and nitrogen oxides (NO, NO$_2$), which are associated with five unique RSD measurement channels, respectively.

The focus of the measurement task is on understanding the hydrocarbon emissions of a moving vehicle. The location of these emissions is an important key to understanding various parameters of the vehicle's operation, including the possibility of leaks or other performance-limiting behaviors of the combustion engine system. In addition, certain emission locations, such as the vehicle's tailpipe, will emit multiple gases, and thus the spatial extent of one emission type, such as CO$_2$, may be highly correlated with that of another emission type, such as HC. For processing purposes, gases emitted from the same location typically have the same spatial signature. Moreover, due to the optical measurement process, these spatial signatures are linear and additive where the plume emissions overlap. Thus, we have the following linear model,

$$\mathbf{x}(t) = \mathbf{A}\mathbf{s}(t) + \mathbf{n}(t)$$

Equation 5-1

where

$$\mathbf{x}(t) = [x_1(t)\ x_2(t)\ x_3(t)\ x_4(t)\ x_5(t)]^T$$

denotes the vector of five measurements of HC, CO$_2$, CO, NO, and NO$_2$ collected at time t,

$$\mathbf{s}(t) = [s_1(t)\ s_2(t)\ s_3(t)]^T$$

denotes the vector of three different spatial signatures indexed by emission location at time t, and

$$\mathbf{A} \quad = \quad \begin{bmatrix} a_{11} & a_{12} & a_{13} \\ a_{21} & a_{22} & a_{23} \\ a_{31} & a_{32} & a_{33} \\ a_{41} & a_{42} & a_{43} \\ a_{51} & a_{52} & a_{53} \end{bmatrix}$$

denotes the matrix of coefficients that map the amount of each spatial signature to the resulting data channel collected by the measurement system. The coefficient a_{ij} corresponds to the proportionality constant associated with the spatial signature emitted from Location j as measured in the ith channel at measurement time t. Note that t corresponds to measurement position in the collected images, not the location where a particular gas has been emitted. Finally, there is additive noise and artifacts in each channel, which is denoted by the noise vector

$$\mathbf{n}(t) \quad = \quad [n_1(t)\ n_2(t)\ n_3(t)\ n_4(t)\ n_5(t)]^T$$

where "T" denotes the transpose of a vector. For purposes of the model, the spatial signatures have some normalization associated with their scale. For example, each signature has the same signal power or some other unit measure of area or volume, *e.g.,* the temporal average of each signature is one.

5.2   Pre-Processing Device

The Pre-Processing Device (PPD) takes the detailed data measurements collected by the RSD and adjusts these measurements to improve their overall quality and reduce noise effects. These improvements include:

- Adjusting constant-level offsets to all measurements of a single species to remove biases,

- Identifying outlier measurements and omitting them from processing,

- Filtering measurements to remove non-physical noise components such as tonal disturbances and striping artifacts, and

- Adjusting the spatial location of the measured data points to a regular rectangular grid using interpolation techniques.

Both the statistical and spatial structure of the data is used in this stage, as described below. The resulting outputs are improved versions of the original data measurements, broken out by measurement type, e.g., HC, CO_2, and NO, among possible others.

Later, Section 7.1 will demonstrate each step in the pre-processing used in the Westminster dataset by presenting examples for individual vehicle transits.

Adjusting Constant-Level Offsets: In this processing, each channel of data is treated as a statistical measurement with an assumed constant value or offset when no species is present. Thus, the measured value consists of a measured mixed signal, an additive noise signal, and a possible constant offset value. To determine the value of the constant-offset value for this channel of data, we first form a histogram of the values within the channel, denoted as $p(bin)$, where *bin* denotes the range of bin values corresponding to the overall range of values in the original measured signal, such that each $p(bin)$ value is the count of values within each bin.

Assuming that the number of measurements in the channel is large, the spatial extent of the measured mixed signal is small, and the additive noise is Gaussian-distributed, we can take the logarithm of the histogram *p*(*bin*) and plot it as a function of the bin values in *bin.* The peak of this plot will correspond to the bin value that is nearest the constant offset value. We solve for the quadratic function of *p*(*bin*) versus *bin* to determine this offset value in the range of *bin*, and then adjust all of the values in the measured signal to remove this offset value from them. This also results in an estimate of the variance of the noise in the channel using the curvature of the quadratic fit of the *p*(*bin*) versus *bin* values, which is used for outlier estimation, described next.

Outlier Removal: After Offset Adjustment, the signal may still contain large values that are non-physical in nature due to erroneous operations within the RSD. Typically, these outlier values are found near the vehicle due to erroneous light reflections (glints) caused by the vehicle's shape as it is scanned by the RSD. To identify these values, we look for large values that exceed a predetermined threshold value near the pixel positions identified by the RSD to be vehicle pixels. The logic for this detection is as follows: A pixel must exceed a threshold value. If it does, then the following conditions must also be true:

The pixel next to this pixel (either left or right) must be a vehicle pixel AND the pixel on the other side of this pixel must not exceed a threshold.

OR

Both the pixel next to this pixel AND the pixel in front of this pixel occurring earlier in measurement time must be vehicle pixels.

The threshold value for the detection is 1.96 times the noise standard deviation as determined in the Offset Adjustment step. After this step, the values in the measured signal channels are largely free of outliers due to vehicle pixel artifacts.

Filtering of Non-Physical Noise Components: As measured, the RSD signal may contain periodic disturbances due to the mechanical nature of the measurement scanning process. Such periodic disturbances are non-physical and are unrelated to the mass measurements being collected. To reduce these noise artifacts, the following processing is performed:

1. The measured data in each channel is examined as a one-dimensional signal, corresponding to the sequence of blue dots as shown in Figure 5-4.

2. The power spectrum of this signal is computed using standard frequency-domain processing whereby a) the data is divided into blocks and windowed using a Hamming window, b) the Fast Fourier Transform (FFT) of each windowed data block is computed, and c) the magnitudes of the FFT values for each frequency bin are averaged across the data blocks. A tonal noise signal will appear in the data as a peak in the power spectrum, and the frequency of this peak is determined from the frequency bin value where the peak occurs, denoted as *estfreq*. Finally, this value is then used in a two-pole, two-zero digital infinite impulse response (IIR) filter with the form:

$y[n] = x[n] + 2 \cos(estfreq * pi) \{ 0.95\, y[n-1] - 0.99\, x[n-1] \} + \{0.95^2\, x[n-2] - 0.99^2\, y[n-2] \}$

where x[n] is the measured input signal, and y[n] is the processed output signal for each measured channel. After filtering, the signal is arranged into its zigzag pattern for further processing.

Adjusting Measured Pixel Positions to a Rectangular Grid: The measured data locations as shown in Figure 5-4 are not on a regular two-dimensional grid, and thus any estimation of physical quantities based on these positions might distort the mass estimates based off of them. To reduce these distortions, the measured data is interpolated to a rectangular grid, where the blue dot positions represent the input to the interpolation process, and a corresponding set of rectangular grid points corresponding to pixel positions that are evenly spaced in time across the transit are used as output locations for the interpolation process. The interpolation is performed in the *x*-direction only, thus corresponding to a one-dimensional interpolation of the data; the *y*-direction dimension is neither adjusted nor interpolated.

After this interpolation is performed, a two-dimensional array of measurements for each channel indexed by scan position m and scan number n is obtained, where m corresponds to the position across the road and n corresponds to the passage of time along the road. We define these measurements for each measurement channel using a vector representation for position and indexed by scan number value n as

$$\mathbf{x}_n = [x_{1,n}\ x_{2,n} \cdots x_{M,n}]^T$$

where M is the number of positions measured in a single scan and the range of n corresponds to an appropriate time slot before the vehicle has arrived at the RSD instrument to an appropriate time slot after the vehicle has passed the RSD instrument. Note that this representation still corresponds to the linear model in Equation 5-1. In later portions of this description, we will allow the signal x(t) for t=1 to t=L to correspond to all of the interpolated measurements for a particular channel through an appropriate assignment from t to the pair (m,n). For example, if there are N scan numbers, this assignment is

$$\{x(1), x(2), \ldots, x(L)\} = \{x_{1,1}, x_{2,1}, \ldots, x_{M,1}, x_{1,2}, x_{2,2}, \ldots, x_{M,N}\}$$

5.3   Separation/Estimation Device

This section describes the methodology's optional Separation/Estimation Device for determining the separate emission rates of two or more different sources on a moving vehicle. If the emission rates for a vehicle is to be determined without apportionment of emissions to separate source, then this optional device is not needed as described by the flow diagram in Figure 5-1. However, if the methodology is to be used to quantify emission rates for separate sources, such as for evaporative HC emissions and exhaust HC emissions, then this optional device should be used. The integration of this device with the methodology's other devices is described in Figure 5-2.

Later, Sections 7.2, 7.3, and 7.4 will demonstrate each step in the separation and estimation used in the Westminster dataset by presenting examples for individual vehicle transits.

A flow diagram of the Separation/Estimation Device (SED) is shown in Figure 5-5. It consists of two processing stages:

Blind Source Separation (Stage 1): In this first stage of the Separation/Estimation Device, the measured data is assumed to be of the form of the linear model in Equation 5-1. Blind source separation algorithms are applied to the output of the Pre-Processing Device in Figure 5-2. The resulting outputs are in the form of spatial patterns corresponding to plumes emitted from the vehicle at different spatial locations around the vehicle. If the number of plumes identified is fewer than the number of signal channels, the additional outputs produced from this stage are labelled as noise components.

Emission Estimation (Stage 2): In this stage, those signals identified as plumes are combined with the outputs of the Noise Reduction and Signal Correction block to estimate the emission type contained in one or more identified plume patterns. For example, the plume associated with tailpipe emissions can be combined with the improved NO channel data to determine the amount of NO gas emitted from the exhaust location. As another example, the plume associated with evaporative emissions at the fuel fill door location of the vehicle can be combined with the improved HC channel data to determine the amount of HC gas emitted from the evaporative fuel fill door location.

Figure 5-5. Flow Diagram of Separation/Estimation Device
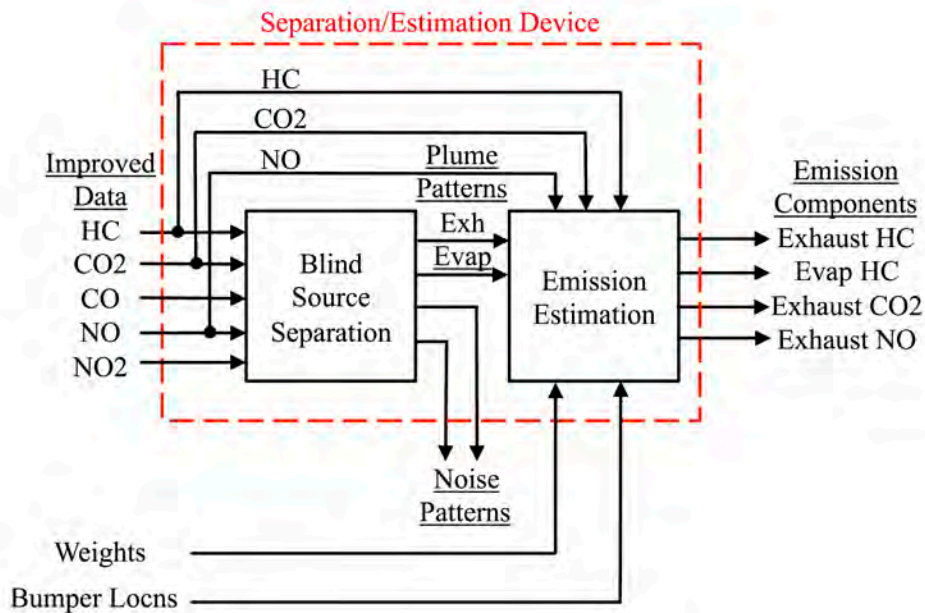
Two exemplary methods for extracting these components are described in a section below. The result of this calculation is a set of images that correspond to selected gas types as emitted from specific locations around the vehicle.

The overall goals and processing methodology for the Separation/Estimation Device is now described. The approach leverages known results and algorithms in the signal processing literature with unique design modifications and tuning for the methodology.

Given the measurement model, the overall goal of the SED is to estimate the portion of a particular gas being released from a particular location on the vehicle that is present in a particular pixel measurement. This calculation is expected to be performed on a portion of an extracted image generated from this linear model. To better understand this task, let the first measurement at one pixel position for a given time instant be modeled as

$$x_1(t) \quad = \quad x_{11}(t) + x_{12}(t) + x_{13}(t) \hspace{3cm} \textbf{Equation 5-2}$$

where $x_{11}(t)$, $x_{12}(t)$, and $x_{13}(t)$ denote the hydrocarbon emissions emitting from three different emission Locations #1, #2, and #3, respectively, where any noise $n_1(t)$ contained in the first measurement has been neglected. These locations could correspond to known point emission locations, such as a tailpipe or fuel door, or they could correspond to patterns generated from specific point locations, such as a leakage point under the vehicle hood. For the model in Equation 5-2, these emissions are given by

$$x_{11}(t) = a_{11}s_1(t), \quad x_{12}(t) = a_{12}s_2(t), \quad \text{and} \quad x_{13} = a_{13}s_3(t),$$

respectively. In this model, each $s_i(t)$ represents the spatial signature of gases emitted from the ith location on the vehicle as observed in the pixel $x_1(t)$ being analyzed. Thus, the goal is to process the measurements in $\mathbf{x}(t)$ such that estimates of each $x_{11}(t)$, $x_{12}(t)$, and $x_{13}(t)$ are generated. This problem can be broken down into two tasks:

1. Process the measurements such that the spatial signatures $s_i(t)$, i={1,2,3} are reliably extracted.

2. Use the ith spatial signature and the original measurements to estimate a specific component, such as $x_{1i}(t)$ for a particular choice of i.

From the resulting images, an estimate of the total emissions coming from the particular spatial location can be formed.

Stage 1: Blind Source Separation

Consider the Blind Source Separation stage. Assuming that the levels of additive noise and artifacts are small, a linear model can be used to extract candidate spatial signatures from three appropriately chosen channels of the five-channel measurement data as

$$\hat{s}(t) \quad = \quad \mathbf{B}\mathbf{x}(t)$$

where

$$\hat{s}(t) \quad = \quad [\hat{s}_1(t)\ \hat{s}_2(t)\ \hat{s}_3(t)]^T$$

contains the estimated spatial signatures in a desired order, and

$$\mathbf{B} \quad = \quad \begin{bmatrix} b_{11} & b_{12} & b_{13} & b_{14} & b_{15} \\ b_{21} & b_{22} & b_{23} & b_{24} & b_{25} \\ b_{31} & b_{32} & b_{33} & b_{34} & b_{35} \end{bmatrix}$$

is a matrix of separation coefficients. If there is no noise or artifacts, then, the optimal solution for the separation matrix satisfies

$$\mathbf{BA} = \mathbf{I}$$

where $\mathbf{A}$ is as defined in Equation 5-1 and $\mathbf{I}$ is an identity matrix with ones along its diagonal and zeros everywhere else.

In practice, the number of spatial signatures may not be known. In addition, some residual noise is present in the improved RSD signals. Thus, it is desirable to use an approach that can both isolate remaining noise components and identify candidate spatial signatures that can be analyzed to determine which of the signatures corresponds to significant parts of the improved RSD data for specific species.

Given the measurement model, blind source separation is a well-known approach for processing the measurements to produce candidate spatial signature signals. The FastICA algorithm[14] can be employed for this task. The FastICA algorithm describes an iterative approach for adjusting the rows of a square matrix $\mathbf{W}$ according to the following criterion,

$$\text{minimize/maximize} \quad \sum_{i=1}^{5} E\left\{C(y_i(t))\right\}$$
$$\text{such that} \quad \mathbf{W}\overline{\mathbf{R}}\mathbf{W}^T = \mathbf{\Sigma}$$
$$\text{where} \quad \overline{\mathbf{R}} = E\{\mathbf{x}(t)\mathbf{x}^T(t)\}$$

$C(y_i(t))$ is a contrast function, the matrix $\mathbf{\Sigma}$ is the identity matrix for the FastICA algorithm, $E\{\mathbf{M}(t)\}$ denotes the sample average of a matrix sequence $\mathbf{M}(t)$, and the candidate sources in the vector $\mathbf{y}(t)$ are computed as

$$\mathbf{y}(t) = \mathbf{W}\mathbf{x}(t)$$

This algorithm is appropriate for situations where the candidate plume spatial signatures do not have significant spatial overlap, such that the constraint $\mathbf{\Sigma} = \mathbf{I}$ is appropriate. For some situations, it is useful to model the overlap of the candidate plume signatures by allowing a non-diagonal constraint matrix $\mathbf{\Sigma}$ that models this overlap. An example of a non-diagonal constraint matrix that is appropriate for the separation task in the methodology is

$$\mathbf{\Sigma} = \begin{bmatrix} 1 & \rho & 0 & 0 & 0 \\ \rho & 1 & 0 & 0 & 0 \\ 0 & 0 & 1 & 0 & 0 \\ 0 & 0 & 0 & 1 & 0 \\ 0 & 0 & 0 & 0 & 1 \end{bmatrix}$$

---

[14] A. Hyvarinen, E. Oja, "Independent Component analysis: algorithms and applications, <u>Neural Networks</u>, Volume 13, Issues 4-5, June 2000, pages 411-430.

where a positive value of ρ models the normalized cross-correlation between the exhaust and evaporative spatial plume signatures. A typical value for ρ is $\rho=0.15$, although ρ values in the range $0 \leq \rho \leq 0.4$ are useful.

An iterative approach[15] for adjusting $\mathbf{W}$ to solve the separation task in this methodology is as follows:

1. Choose $f_i(y_i) = \partial C(y_i)/\partial y_i$ or another appropriate function, $e.g.$ $f_i(y_i) = y_i^3$.

2. Do for each $i = \{1, 2, \ldots, 5\}$, where $\mathbf{W} = [\mathbf{w}_1 \ \mathbf{w}_2 \ \mathbf{w}_3 \ \mathbf{w}_4 \ \mathbf{w}_5]^T$ and σ_{ii}^2 is the ith diagonal element of $\mathbf{\Sigma}$:

$$
\begin{aligned}
\overline{\mathbf{R}} &= E\{\mathbf{x}(t)\mathbf{x}^T(t)\} \\
\widetilde{\mathbf{w}}_i &= \overline{\mathbf{R}}^{-1} E\{\mathbf{x}f_i(y_i)\} - E\{f_i'(y_i)\}\mathbf{w}_i \\
\overline{\mathbf{w}}_i &= \sqrt{\frac{\sigma_{ii}^2}{\widetilde{\mathbf{w}}_i^T \overline{\mathbf{R}} \widetilde{\mathbf{w}}_i}} \widetilde{\mathbf{w}}_i
\end{aligned}
$$

3. Do for $k = 1$ to 10 or until convergence, where $\overline{\mathbf{W}} = [\overline{\mathbf{w}}_1 \ \overline{\mathbf{w}}_2 \ \overline{\mathbf{w}}_3 \ \overline{\mathbf{w}}_4 \ \overline{\mathbf{w}}_5]^T$:

$$
\overline{\mathbf{W}}_{new} = \overline{\mathbf{W}} + \frac{1}{2}\left(\mathbf{\Sigma} - \overline{\mathbf{W}}\mathbf{R}\overline{\mathbf{W}}^T\right)\overline{\mathbf{W}}
$$

4. Set $\mathbf{W}_{new} = \mathbf{P}(\mathbf{y})\overline{\mathbf{W}}_{new}$ and $\widehat{\mathbf{s}}(t) = \mathbf{P}(\mathbf{y})\mathbf{y}(t)$ and repeat the above steps until convergence.

After separation, the candidate signatures in the vector $\mathbf{y}(t)$ need to be checked to see how well they represent the improved RSD signals of one or more of the HC, CO_2, CO, NO, and/or NO_2 measurements. Knowledge of the typical plumes that can be emitted from vehicles on the road is used here. For example, since CO_2 concentrations above the ambient level are largely indicative of exhaust emissions, the normalized correlations between the CO_2 channel $x_2(t)$ and the five candidate plume signatures in $\mathbf{y}(t)$ can be computed. Let $\rho_{CO2,i}$ denote these normalized correlation values. The one with the largest absolute value of normalized correlation with index j corresponds to the exhaust plume, and its sign can be used to adjust the amplitude of the candidate exhaust plume as

$$
\widehat{s}_1(t) = \text{sgn}(\rho_{CO2,j})y_j(t).
$$

where the sign-function $\text{sgn}(\rho)$ is 1 if ρ is positive-valued, 0 if ρ is zero-valued, and -1 if ρ is negative-valued.

As an additional example, evaporative emissions, where they exist, are typically observed in the HC measurements. The normalized correlations between the improved HC signal $x_1(t)$ and the four remaining candidate plume signatures in $\mathbf{y}(t)$ can be computed as $\rho_{HC,i}$. The one with the

---

[15] S.C. Douglas, T.H. DeFries, "Blind Source Separation under Signal Covariance Constraints: Criteria and Algorithms," 2021 55th Asilomar Conference on signals, Systems, and Computers, 31 October 2021 – 3 November 2021.

largest absolute value of normalized correlation with index k corresponds to the evaporative plume, and its sign can be used to adjust the amplitude of the candidate evaporative plume as

$$\widehat{s}_2(t) = \text{sgn}(\rho_{HC,k})y_k(t).$$

In this way, candidate plume signatures can be identified with the appropriate sign according to the number of possible plumes that are observed in the improved RSD data, up to the number of RSD data channels available. If the number of possible plumes is less than the number of RSD data channels, then the identity assignment

$$\widehat{s}_i(t) = y_i(t)$$

is made for the remaining data channels, as these remaining signals are noise spatial signatures.

These assignments of $y_i(t)$ to $s\_\{hat\}_i(t)$ are also used to define the permutation matrix $\mathbf{P}(\mathbf{y})$ in the algorithm. For example, if j=2 and k=1, then

$$\mathbf{P}(\mathbf{y}) \;=\; \begin{bmatrix} 0 & \text{sgn}(\rho_{CO2,j}) & 0 & 0 & 0 \\ \text{sgn}(\rho_{HC,k}) & 0 & 0 & 0 & 0 \\ 0 & 0 & 1 & 0 & 0 \\ 0 & 0 & 0 & 1 & 0 \\ 0 & 0 & 0 & 0 & 1 \end{bmatrix}$$

Other methods to perform this assignment and sign recovery could be used as well.

Stage 2: Emission Estimation

Consider the Emission Estimation stage, which performs estimations of the portions of these spatial signatures in the original measurement data. Note that each improved RSD signal sample $x\_i(t)$ has units of mass, whereas each plume signature $s\_\{hat\}_j(t)$ are effectively unitless because of normalization during the separation process. Thus, the primary goal of the estimation task is to "recover" the mass units of each plume type for each species in an accurate way. These estimates are computed using a linear model. For example, for the first measurement signal $x_1(t)$, the estimates are

$$\begin{aligned} \widehat{x}_1(t) &= \mathbf{h}_1^T \widehat{\mathbf{s}}(t) & (15) \\ &= h_{11}\widehat{s}_1(t) + h_{12}\widehat{s}_2(t) + h_{13}\widehat{s}_3(t) & (16) \\ &= \widehat{x}_{11}(t) + \widehat{x}_{12}(t) + \widehat{x}_{13}(t) & (17) \end{aligned}$$

where the "hatted" quantities are estimates of their true values within the signal model. Thus, the estimate of hydrocarbons emitted from Location #2 on the vehicle is denoted as

$$\widehat{x}_{12}(t) \;=\; h_{12}\widehat{s}_2(t) \qquad\qquad (18)$$

These estimates are generally computed from the available signals using least-squares techniques. Any one of a number of least-squares estimation techniques could be used, including weighted least-squares and constrained weighted least-squares, amongst other methods. These estimation tasks are formulated as a minimization of a cost function $J(\mathbf{h})$ that depends on the

measured and computed signals in a particular way, some with additional constraints on the parameters in **h**. As illustrative examples, we describe two such approaches below.

Consider the weighted least-squares (LS) cost function

$$\mathcal{J}_{LS}(\mathbf{h}_i) \;=\; \frac{1}{L}\sum_{t=1}^{L} w_t(x_i(t) - \widehat{x}_i(t))^2$$

where L is the number of improved RSD signal samples corresponding to the HC RSD measurements and w_t is a weighting function across the L measurements for the improved RSD signal images. In this context, t is the signal sample number, and each t can be mapped to a particular (x,y) position in each plume image. Note that the exact mapping from t to (x,y) determines the form of the weighting function for the estimation task. This weighting function can be computed from the Weights W(v) output from the Vortex Shape Estimation Device by extending the Weights across the improved RSD signal sample dimension t according to the converse of the Weights computation. For example, if the Weight values are one-dimensional and assigned by scan number, they can be extended to a two-dimensional weighting function by replicating these Weight values across the width of the two-dimensional improved RSD signal sample datasets, after which they can be assigned a one-dimensional index t associated with the improved RSD signal samples. Other extensions of the Weights to a spatial arrangement associated with the RSD measurement device are possible depending on the operation of the RSD device.

The weighted least-squares cost function is minimized according to standard least-squares methods. The resulting weighted least squares (LS) solution can be described as

$$\mathbf{h}_{LS,i} \;=\; \mathbf{R}^{-1}\mathbf{p}_i$$

where

$$\mathbf{R} \;=\; \sum_{t=1}^{L} w_t \widehat{\mathbf{s}}_t \widehat{\mathbf{s}}_t^{T}$$

$$\mathbf{p}_i \;=\; \sum_{t=1}^{L} w_t x_i(t) \widehat{\mathbf{s}}_t$$

are the weighted autocorrelation matrix and weighted cross-correlation matrix for the improved RSD signal $x_i(t)$ being modeled. From these calculations, we can identify the estimated plume emission for the chosen species to be analyzed from the weights and signals that have been computed. For example, the evaporative HC plume samples can be identified according to the description provided as

$$\widehat{x}_{11}(t) \;=\; h_{11}\widehat{s}_1(t).$$

Other estimated plume emissions for different species can be computed similarly.

Other least-squares methods can be employed for the Emission Estimation Stage as well. Suppose instead the following constraints are desired to be imposed for each i

$$\frac{1}{L}\sum_{t=1}^{L}\sum_{n=1}^{3} h_{in}\widehat{s}_n(t) = \mathbf{h}_i^T \mathbf{s}_x = s_{d,i}$$

where the quantities $\mathbf{s}_x$, $s_{x,n}$, and $s_{d,i}$ all contain sample average values:

$$\mathbf{s}_x = \begin{bmatrix} s_{x,1} & s_{x,2} & s_{x,3} \end{bmatrix}^T$$

$$s_{x,i} = \frac{1}{L}\sum_{t=1}^{L}\widehat{s}_i(t)$$

$$s_{d,i} = \frac{1}{L}\sum_{t=1}^{L} x_i(t)$$

Then, we formulate the constrained least squares (CLS) problem

$$\text{minimize} \quad \mathcal{J}_{CLS}(\mathbf{h}_i) = \mathbf{h}_i^T \mathbf{R}\mathbf{h}_i - 2\mathbf{h}_i^T \mathbf{p}_i + \frac{1}{L}\sum_{t=1}^{L} w_t x_i^2(t)$$

$$\text{such that} \quad \mathbf{h}_i^T \mathbf{s}_x = s_{d,i}.$$

This is in the form of a quadratic linear programming problem with equality constraints. The explicit solution for $\mathbf{h}_i$ is the linear combination of two vectors $\mathbf{h}_{LS,i}$ and $\mathbf{h}_{C,i}$ as

$$\mathbf{h}_i = \mathbf{h}_{LS,i} + \lambda_i \mathbf{h}_{C,i},$$

where $\mathbf{h}_{LS,i}$ is computed as before,

$$\mathbf{h}_{C,i} = \mathbf{R}^{-1} \mathbf{s}_{x,i}$$

$$\lambda_i = \frac{s_{d,i} - \mathbf{h}_{LS,i}^T \mathbf{s}_x}{\mathbf{h}_{C,i}^T \mathbf{s}_x}.$$

It is straightforward to show that $\mathbf{h}_i^T \mathbf{s}_x = s_{d,i}$. This constrained least squares (CLS) solution works best if the constraint is highly accurate; that is, the sample means are very close to the true means.

5.4 Vortex Shape Estimation Device

The purpose of the Vortex Shape Estimation Device (VSED) is to characterize the expected shape of the vortex for each vehicle as it drives past the RSD instrument. These characteristics are needed to calculate vehicle emission rates from the RSD vortex mass measurements of emission components as shown in the flow diagrams of Figures 5-1 and 5-2.

The categories of inputs are the improved CO_2 data array, measured road speed and direction, estimated vehicle size properties, RSD instrument measurement characteristics, wind speed and direction, and estimated terrain surface roughness. The output categories are estimated for each

vehicle transit. The general output categories are identification of the data location index (RSD scan number) of the front and rear of each vehicle, weights that characterize the expected relative magnitude of emissions at locations in the vortex, and the Vehicle Entrainment Time (VET) expected for the vortex.

The flow diagram in Figure 5-6 shows the four steps that make up the Vortex Shape Estimation Device. Each of the steps is described below.

Figure 5-6. Flow Diagram of Vortex Shape Estimation Device
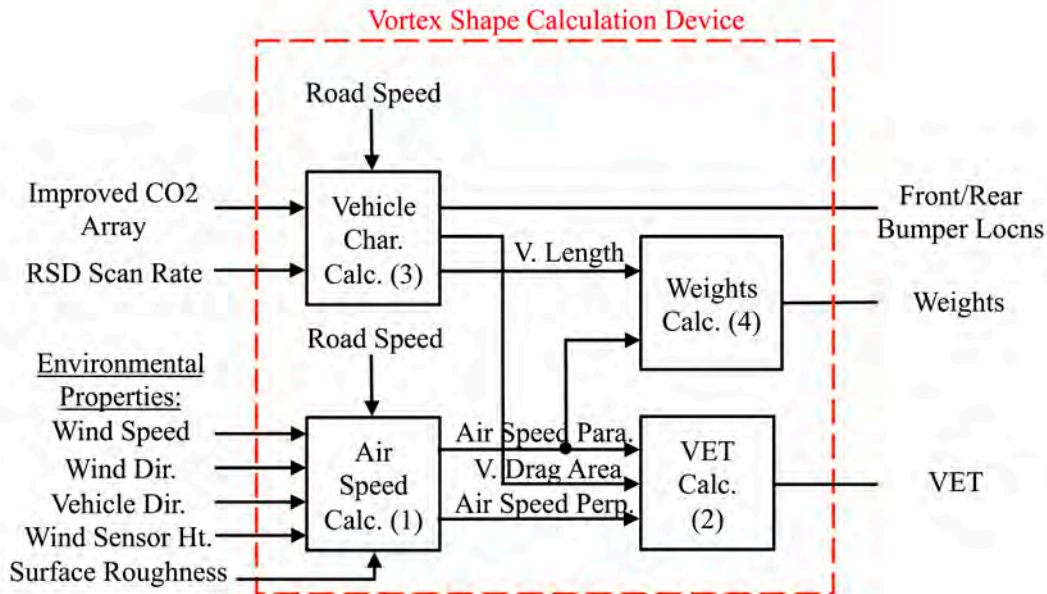
Step 1. Air Speed Calculation Device

The shape of the vortex is influenced by the vehicle air speed, that is, the speed of the air moving across the vehicle. The vehicle air speed is a function of the vehicle road speed and direction and the wind speed and direction.

RSD systems may measure the wind velocity at a height above the pavement that is different from the height that vehicles drive – typically 1 meter for light-duty vehicles. Therefore, the first step is to calculate wind velocity at 1 meter from the wind velocity at the height that RSD measures it. Then, the second step is to calculate the vehicle's air velocity at 1 meter from the vehicle's road velocity and the calculated wind velocity at 1 meter.

The Danish Wind Industry Association relationship[16] can be used to estimate the wind speed at one height from wind speed measurements made at another height:

$$v = v\_ref * \ln(z/z0) / \ln(z\_ref/z_0) \hspace{2cm} \textbf{Equation 5-3}$$

---

[16] http://xn--drmstrre-64ad.dk/wp-content/wind/miller/windpower%20web/en/tour/wres/shear.htm

where:

v = wind speed at height z (meters) above the ground
v_ref = measured wind speed at a height z_ref (meters) above the ground
z = height (meters) above the ground for the desired wind speed v
z_0 = terrain surface roughness length (meters), estimated from Table 5-1, in the current wind direction

Table 5-1. Terrain Surface Roughness Length Descriptions

z_0 Terrain Surface Roughness Length (m)	Surface Description
0.0024	Concrete runways, mowed grass.
0.03	Open agricultural area without fences and hedgerows with very scattered buildings. Soft-rounded hills.
0.055	Agricultural land with some houses and 8 m tall hedgerows about 1250 m apart.
0.1	Agricultural land with some houses and 8 m tall hedgerows about 500 m apart.
0.2	Agricultural land with many houses, shrubs and plants, or 8 m hedgerows about 250 m apart.
0.4	Villages, small towns, ag land with many or tall sheltering hedgerows, forests, and very rough and uneven terrain.
0.8	Larger cities with tall buildings.
1.6	Very large cities with tall buildings and skyscrapers.

The calculated wind direction is assumed to be the same as the measured wind direction.

The vehicle air speed vector at 1 m height is calculated from the wind speed vector at 1 m height and the vehicle's road speed vector using standard vector algebra:

$$\mathbf{AS} \;=\; \mathbf{RS} - \mathbf{WS} \qquad\qquad\qquad \textbf{Equation 5-4}$$

where

AS = Air Speed vector at 1 m elevation referenced to North heading
RS = Road Speed vector referenced to North heading
WS = Wind Speed vector at 1 m elevation referenced to North heading

Finally, the Air Speed vector at 1 m elevation is resolved into air speed components parallel and perpendicular to the direction of vehicle motion, where • denotes the dot product for vectors and $\| . \|$ denotes the length of a vector.

RP = Perpendicular vector to Road Speed vector

$$\mathbf{RP} \;=\; \begin{bmatrix} 0 & 1 \\ -1 & 0 \end{bmatrix} \mathbf{RS}$$

AirSpeed Para	=	$(\mathbf{AS} \cdot \mathbf{RS}) / \| \mathbf{RS} \|$	**Equation 5-5a**
AirSpeed Perp	=	$(\mathbf{AS} \cdot \mathbf{RP}) / \| \mathbf{RP} \|$	**Equation 5-5b**

We used the following conventions for positive air-speed components in the vehicle reference frame. Positive AirSpeed Para values represent air movement toward the windshield of the vehicle. Positive AirSpeed Perp values represent air movement toward the left side of the vehicle.

Step 3. Vehicle Characteristics Device

The purpose of the Vehicle Characteristics Device is to estimate the vehicle drag area and to use the RSD improved CO_2 measurements to identify the data location index (RSD scan number) of the front and rear of each vehicle and the length of each vehicle. The drag area is used to improve the estimate of the VET. The data location indexes of the front and rear of each vehicle are used to time-align the improved RSD data arrays with the vortex weights that characterize the expected relative magnitude of emissions at locations in the vortex. The front and rear vehicle locations are in turn used to calculate vehicle length, which also influences the vortex weights.

The inputs to the device are the measured road speed, the improved CO_2 array, and the RSD scan rate. The outputs of the device are the scan number of the last scan before the front of the vehicle, the scan number of the first scan after the rear of the vehicle, vehicle length, and vehicle drag area.

The data location indexes of the front and rear of each vehicle are determined by examining the pixels where the outgoing RSD laser beam is not reflected back to the RSD since the laser beam is occluded by the vehicle as exemplified by the missing blue dots in Figure 5-4. In that figure the Last Scan Before Vehicle Front is Scan 2, and the First Scan After Vehicle Rear is Scan 11.

The length of the vehicle is then determined by:

Length **Equation 5-6**

$$= \frac{(\text{FirstScanAfterVehicleRear} - \text{LastScanBeforeVehicleFront} - 1) \ * \ \text{Road Speed} \ * \ 5280}{\text{RSD Scan Rate} \ * \ 3600}$$

where

Length	= Vehicle length (ft)
FirstScanAfterVehicleRear	= First full scan after the vehicle rear
LastScanBeforeVehicleFront	= Last full scan before the vehicle front
Road Speed	= Vehicle road speed (mile/hour)
5280	= 5280 ft/mile
RSD Scan Rate	= Rate that RSD scans the vortex (scans/s)
3600	= 3600 s/hr

The drag area is given by:

$$\text{Drag Area (ft2)} = C_D * \text{FrontalArea} \qquad \textbf{Equation 5-7}$$

where
C_D = Coefficient of drag
FrontalArea = Frontal Area of the vehicle (ft2)

A default drag area of 10 ft2 can be used for light-duty vehicles. Optionally, to provide a more precise value for drag area, the RSD license plate reader can be used with a state vehicle registration database to look up vehicle year, make, and model, which can be used in turn to look up specific drag areas for many vehicles.

Step 2. Vortex Entrainment Time Calculation Device

Vortex Entrainment Time (VET) is key to this methodology for measuring pollutant emission rate using RSD. The Vortex Entrainment Time establishes a connection between the RSD-measured pollutant Mass in Vortex and pollutant Release Rate (g/hr) and pollutant Emission Rate (g/mile). The purpose of the Vortex Entrainment Time Calculation Device is to calculate the Vortex Entrainment Time (VET) for each vehicle RSD transit.

Section 6.4 (below) describes the analyses of the September 2016 dataset and the October 2019 dataset collected to estimate the Vortex Entrainment Time of vehicles driving on the road. The analysis of the September 2016 dataset found that the VET is a mild function of vehicle drag area. The analysis of this October 2019 Westminster data found that the VET also depends mildly on the AirSpeed Para and the emissions Release Location.

Regression analysis from the September 2016 dataset and from the October 2019 dataset shows (see Section 6.4) that VET values can be determined by considering descriptors of vehicle, vehicle operation, and environmental conditions as described by:

$$\textbf{Equation 5-8}$$

$$\text{VET (s)} = \frac{B * \text{Release Location Factor} * \text{DragArea (ft2)}^{\wedge}(1/3)}{\text{AirSpeed Para (mile/hr)}^{\wedge}(1/2)}$$

where
B = A constant determined by calibration
Release Location Factor = 1.00, if release location is known to be the tailpipe
= 0.67, if the release location is unknown
DragArea (ft2) = Vehicle drag area from Step 3
AirSpeed Para (mile/hr) = Parallel component of the AirSpeed from Step 1

For releases from the vehicle rear, such as from the tailpipe or a fuel fill door located on the rear of a quarter panel, the Release Location Factor will be near 1. If the emissions release location is known to be the tailpipe, then the Release Location Factor of 1.00 should be used in Equation 5-8. A Release Location Factor of 0.67 can be used if the actual release location is unknown. As shown in Table 6-4, the Release Location Factor will be lower for release locations more forward

on the vehicle. For example, analysis has shown that releases from under the hood have Release Location Factors around 0.34.

The B coefficient value in Equation 5-8 is specifically for the RSD used in the October 2019 dataset. The B coefficient will be different for different RSDs due to their different optical efficiencies, for example, retro-reflector efficiency, and their different optical strategies for illuminating the vortex. The value of B for alternative RSDs can be determined using the following procedure, based on currently available technology and methods:

1. Select a test vehicle of known Drag Area. Instrument the test vehicle to determine its tailpipe exhaust CO_2 Release Rate (g/hr) by either querying its CAN bus data stream or its driver instrument display for fuel economy, or by directly measuring the tailpipe CO_2 release rate with an external measurement device, such as a Portable Emissions Measurement System (PEMS) or miniPEMS.

2. Drive the test vehicle past the RSD while collecting RSD detailed CO_2 data of the vortex and data to determine the AirSpeed Para for the transit.

3. Calculate the CO_2 Mass in Vortex (g) using the collected RSD detailed CO_2 data.

4. Calculate the VET (hr) using Equation 5-16 with the measured CO_2 Mass in Vortex (g) and the measured CO_2 Release Rate (g/hr).

5. Calculate the value of B using Equation 5-8 with the calculated VET, known Drag Area, determined AirSpeed Para, and a Release Location Factor of 1.00, which is the defined value for tailpipe releases.

Step 4. Weights Calculation Device

The purpose of the Weights Calculation Device (WCD) is to provide weights that reflect the probable distribution of _relative_ emissions Mass in Vortex. The weights are used by the Emission Calculation Device as a distribution to which RSD measurements of any pollutant are fit to determine the mass of emissions in the vortex while enhancing the signal-to-noise ratio and thereby improving the method detection limit of the pollutant emission rate. The weights are also used by the Separation/Estimation Device to better assign RSD-measured pollutant mass to separately located pollutant sources.

The inputs to the Weights Calculation Device are the vehicle length, which is determined from the Vehicle Characteristics Device, and the AirSpeed Para at 1 meter, which is determined by the Air Speed Calculation Device. The output of the Weights Calculation Device is a set of weights as a function of time after the rear of the vehicle.

The weights can be expressed in terms of three factors: time after the vehicle rear, vehicle length, and AirSpeed Para:

Equation 5-9

Weight = Time-Decay Factor * Length Factor * Air-Speed Factor

The dependencies for the three factors are shown in Figures 5-7, 5-8, and 5-9.

Figure 5-7. Time-Decay Factor for Weights
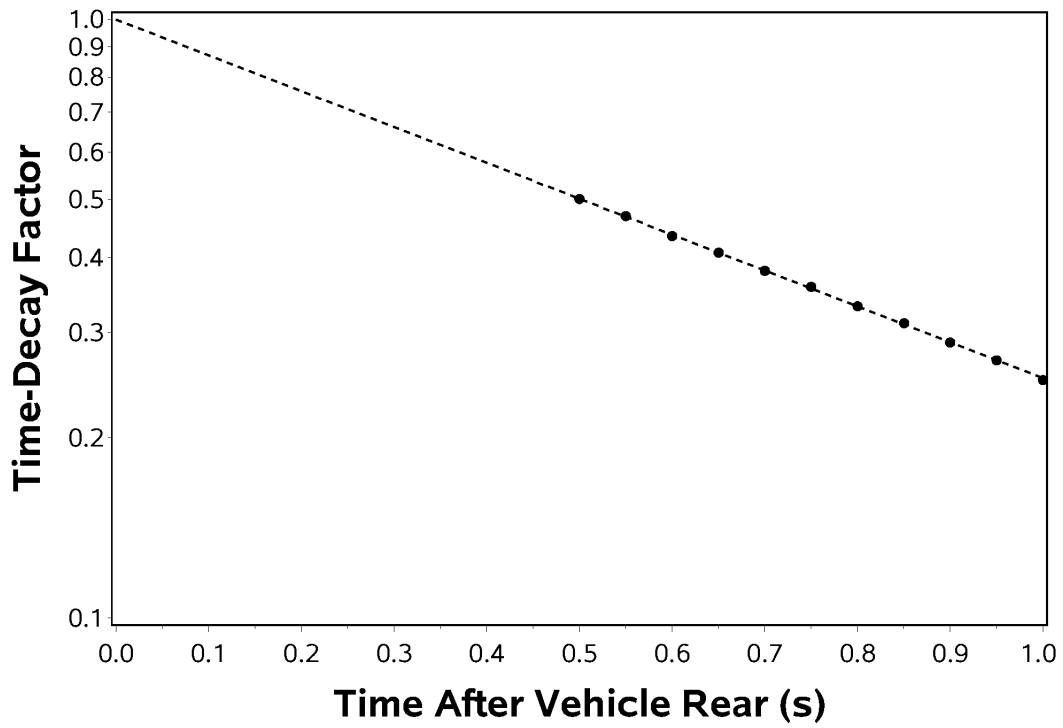
/proj1/EDARinDenver-OCT2019/Analysis_MLout/211122/Anal_MLout/OCT19_interpshapeCO2_5.sas 15JUN22 12:03

Figure 5-8. Vehicle Length Factor for Weights
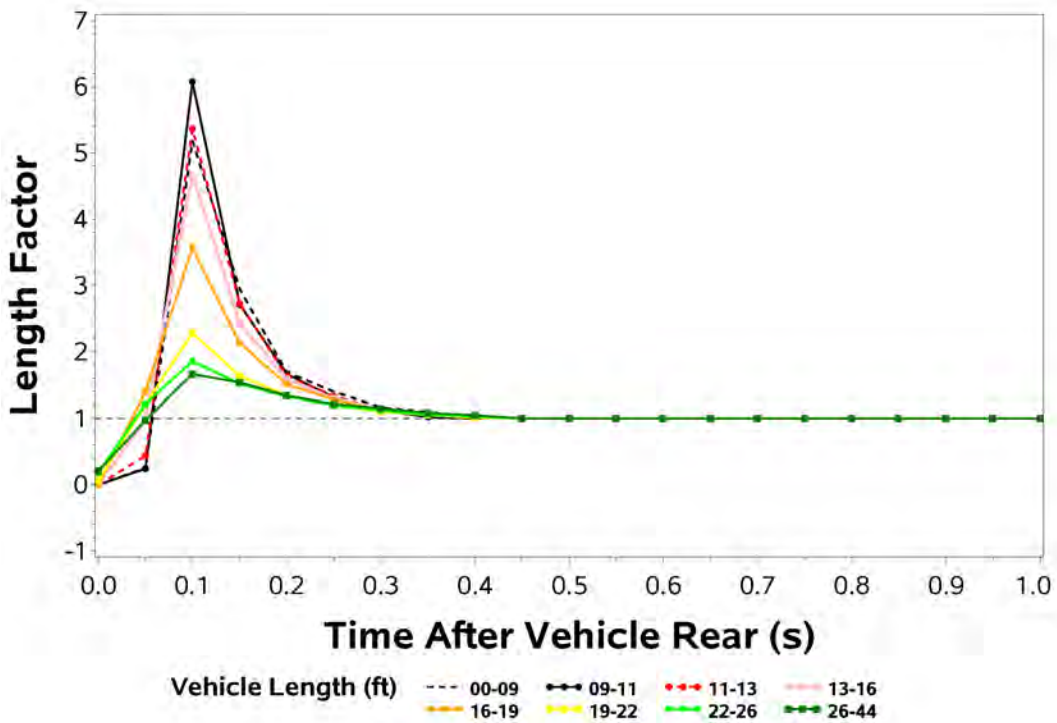
/proj1/EDARinDenver-OCT2019/Analysis_MLout/211122/Anal_MLout/OCT19_interpshapeCO2_5.sas 16JUN22 12:38

Figure 5-9. Air Speed Parallel Factor for Weights
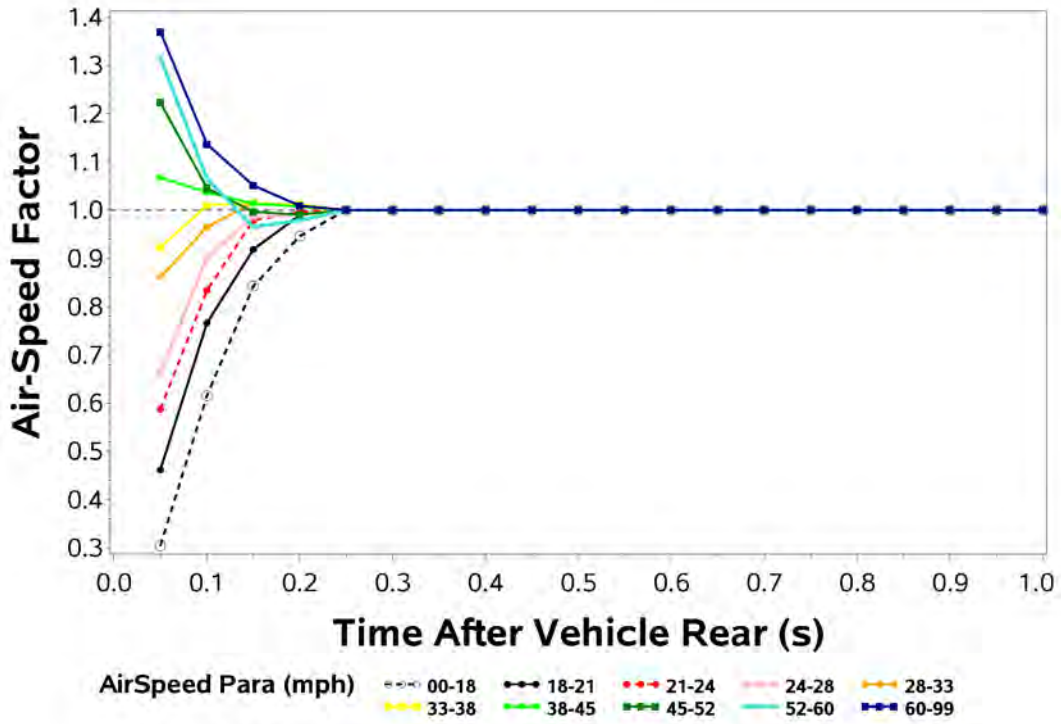
The Time-Decay Factor is shown in Figure 5-7 as a function of time after the vehicle rear. The plot shows that the time-decay factor is an almost perfect exponential decay.

The Length Factor is shown in Figure 5-8 and is a function of time after the vehicle rear and the vehicle length. The figure shows that after 0.5 seconds after the vehicle rear, the factor has a value of 1, which indicates that vehicle length has no influence after 0.5 seconds after the vehicle rear. The different curves for vehicle length indicate that the peak at 0.1 seconds is large for short vehicles and decreases and approaches 1 for longer vehicles.

The Air-Speed Factor is shown in Figure 5-9 as a function of time after the vehicle rear and AirSpeed Para. The figure shows that after 0.25 seconds after the vehicle rear, the factor has a value of 1, which indicates that AirSpeed Para has no influence after 0.25 seconds after the vehicle rear. For times shorter than 0.25 seconds, the figure shows that AirSpeed Para less than about 40 mph are associated with air-speed factors less than 1, and AirSpeed Para greater than about 40 mph are associated with air-speed factors greater than 1.

Examination of Figures 5-7, 5-8, and 5-9 indicates that after 0.5s after the vehicle rear, the product of the three factors depends almost entirely on the exponential time-decay factor shown in Figure 5-7. At shorter times after the vehicle rear, the influences of vehicle length and air speed make substantial modifications to the decay – particularly for short vehicles and for low values of AirSpeed Para.

The region at short times after the vehicle corresponds to the region close behind the vehicle rear where the vortex has the largest mass of pollutants. Accordingly, the RSD gets a large part of its signal from this region. Therefore, the weights for vehicle length and airspeed in this region are important to achieving accurate emissions rate measurements with good detection limits.

While the values for the three factors that contribute to the weight could be read from Figures 5-7, 5-8, and 5-9 one convenient set of parameterizations of the curves in those figures is given by Equations 5-10a[17], 5-10b[18], and 5-10c[19]. The parameterization covers vehicle lengths from 10 to 27 feet and AirSpeed Para values from 16 to 67 mile/hr.

---

[17] P:\EDARinDenver-OCT2019\Analysis_MLout\211122\Anal_MLout/ OCT19_interpshapeCO2_5.sas

[18] P:\EDARinDenver-OCT2019\Analysis_MLout\211122\Anal_MLout/ rat2length.xlsx/tab:Parms + pred2 rat2decay and P:\EDARinDenver-OCT2019\Analysis_MLout\211122\Anal_MLout/ OCT19_interpshapeCO2_7.sas (draft NLIN)

[19] P:\EDARinDenver-OCT2019\Analysis_MLout\211122\Anal_MLout/ OCT19_interpshapeCO2_5.sas

Time-Decay Factor $\quad = \quad$ exp (K * t) **Equation 5-10a**

where $\quad$ K $\quad = -1.38 \text{ s}^{-1}$, for high altitudes (October 2019 study)
$\quad\quad\quad\quad\quad -1.03 \text{ s}^{-1}$, for altitudes near sea level (September 2016 study)
$\quad\quad$ t $\quad = \quad$ Time after the vehicle rear (s)

Length Factor $\quad\quad = \quad$ 1 + FastDecay + RampCorr $\quad\quad$ **Equation 5-10b**

where $\quad\quad$ FastDecay $\quad = \quad$ exp (Length_Intercept + Length_Slope * t)

$\quad\quad\quad\quad\quad$ Length_Intercept $\quad = \quad$ - 0.3088 * Slope - 2.2568
$\quad\quad\quad\quad\quad$ Length_Slope $\quad\quad = \quad$ 0.5211 * Length(ft) - 23.662

$\quad\quad\quad\quad\quad\quad$ Length(ft) $\quad\quad = \quad$ 10.0, for LengthBin = 00-09
$\quad\quad\quad\quad\quad\quad\quad\quad\quad\quad\quad = \quad$ 10.0, for LengthBin = 09-11
$\quad\quad\quad\quad\quad\quad\quad\quad\quad\quad\quad = \quad$ 11.9, for LengthBin = 11-13
$\quad\quad\quad\quad\quad\quad\quad\quad\quad\quad\quad = \quad$ 14.2, for LengthBin = 13-16
$\quad\quad\quad\quad\quad\quad\quad\quad\quad\quad\quad = \quad$ 17.3, for LengthBin = 16-19
$\quad\quad\quad\quad\quad\quad\quad\quad\quad\quad\quad = \quad$ 21.5, for LengthBin = 19-22
$\quad\quad\quad\quad\quad\quad\quad\quad\quad\quad\quad = \quad$ 24.0, for LengthBin = 22-26
$\quad\quad\quad\quad\quad\quad\quad\quad\quad\quad\quad = \quad$ 27.0, for LengthBin = 26-44

where $\quad\quad$ RampCorr $\quad = \quad$ (1+ exp(Length_Intercept)) * Ramp

$\quad\quad\quad\quad$ Ramp $\quad\quad = \quad$ - 1.000, for t=0
$\quad\quad\quad\quad\quad\quad\quad\quad = \quad$ - 0.410, for t=0.05
$\quad\quad\quad\quad\quad\quad\quad\quad = \quad$ 0.030, for t=0.10
$\quad\quad\quad\quad\quad\quad\quad\quad = \quad$ 0, for t>0.0125

Air-Speed Factor $\quad = \quad$ 1 + Air_Intercept * exp(-18.8260 * t) $\quad$ **Equation 5-10c**

where $\quad\quad$ Air_Intercept $= \quad$ 2.4720 – exp(exp(0.7716 – 0.0240 * AirSpeedPara (mile/hr)))

$\quad\quad\quad\quad\quad$ AirSpeedPara (mile/hr)= $\quad$ 16.0, for AirParaBin = 00-18
$\quad\quad\quad\quad\quad\quad\quad\quad\quad\quad\quad = \quad$ 19.5, for AirParaBin = 18-21
$\quad\quad\quad\quad\quad\quad\quad\quad\quad\quad\quad = \quad$ 22.5, for AirParaBin = 21-24
$\quad\quad\quad\quad\quad\quad\quad\quad\quad\quad\quad = \quad$ 25.0, for AirParaBin = 24-28
$\quad\quad\quad\quad\quad\quad\quad\quad\quad\quad\quad = \quad$ 31.0, for AirParaBin = 28-33
$\quad\quad\quad\quad\quad\quad\quad\quad\quad\quad\quad = \quad$ 33.5, for AirParaBin = 33-38
$\quad\quad\quad\quad\quad\quad\quad\quad\quad\quad\quad = \quad$ 40.0, for AirParaBin = 38-45
$\quad\quad\quad\quad\quad\quad\quad\quad\quad\quad\quad = \quad$ 49.0, for AirParaBin = 45-52
$\quad\quad\quad\quad\quad\quad\quad\quad\quad\quad\quad = \quad$ 57.0, for AirParaBin = 52-60
$\quad\quad\quad\quad\quad\quad\quad\quad\quad\quad\quad = \quad$ 67.0, for AirParaBin = 60-99

5.5 Emission Calculation Device

The purpose of the Emission Calculation Device (ECD) is to calculate the pollutant Release Rate and Emission Rate using the calculated quantities derived earlier from the RSD system measurements and estimates of vortex properties.

The categories of inputs are the improved pollutant data arrays, RSD data location index for the vehicle rear, vortex weights, RSD instrument geometry and operating characteristics, Vortex Entrainment Time (VET), and vehicle road speed. The outputs are the time-based Release Rate (g/hr) and the distance-based Emission Rate (g/mile) for each transit and each pollutant measured by the RSD.

The Emission Calculation Device consists of Steps 5, 6, 7, and 8 as shown in Figure 5-10. These steps are described below.

Figure 5-10. Flow Diagram of Emission Calculation Device
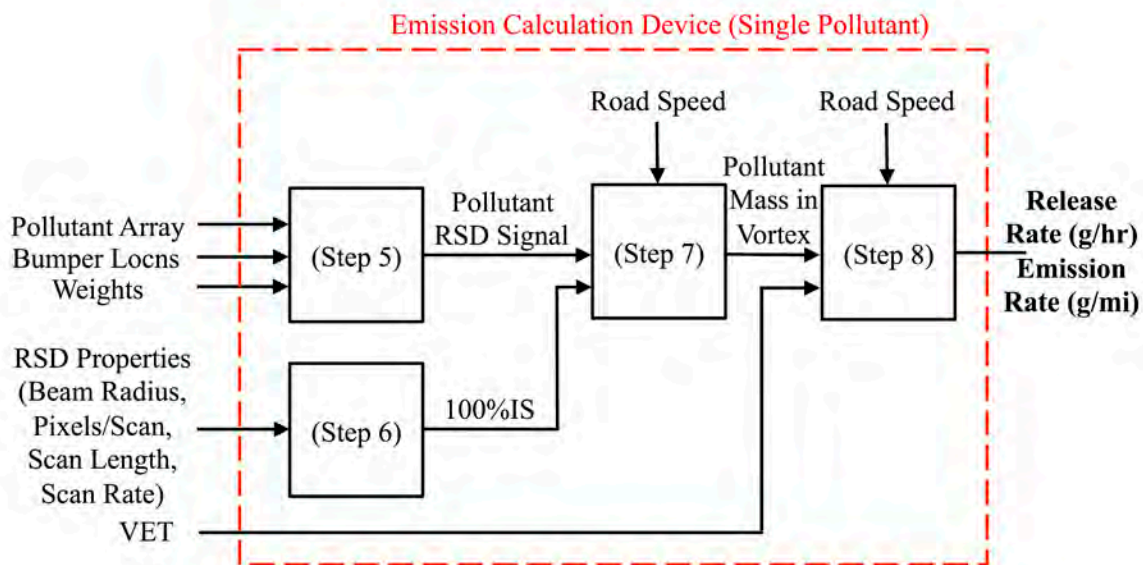
Step 5. Pollutant RSD Signal Device

The purpose of the Pollutant RSD Signal Device is to calculate the mass equivalent of a pollutant signal obtained by an RSD instrument from the vortex behind a moving vehicle.

The inputs to the device are the pollutant Improved Data array from the Pre-Processing Device or the pollutant Emission Components array from the Separation/Estimation Device (if separation is performed), Weights from the Weights Calculation Device, Vehicle Rear Scan Number from the Vehicle Characteristics Device, and a Pollutant Conversion Factor that gives the conversion between the RSD optical measurement quantity and the pollutant mass. The output of the device is Pollutant RSD Signal (g).

The device's first step is to convert the optical mass measurement of each pixel in the pollutant array into a mass value:

Pollutant Mass in Pixel (g)   **Equation 5-11**

$=$ Pixel Optical Mass (mole/m^2) $*$ Light Beam Area (m^2) $*$ Pollutant Conversion Factor

where
        Pixel Optical Mass (mole/m^2)$=$ RSD-measured pollutant optical mass in each pixel
        Light Beam Area (m^2) $=$ Cross-sectional area of the RSD light beam
        Pollutant Conversion Factor $=$ Factor that converts the RSD-measured optical mass
                                   to pollutant mass

The RSD instrument used by this study reports gaseous pollutant Pixel Optical Mass in units of mole/m^2. Therefore, in this study for pure compound gaseous pollutants (CO, NO, NO$_2$, CO$_2$), the Pollutant Conversion Factor is the Pollutant Molecular Weight (g/mole). For Exhaust HC, Evaporative HC, and their sum, Total HC, which are mixtures of pure HC compounds, the Pollutant Conversion Factor is the Pollutant Molecular Weight (g/mole) of the basis gas, propane, in which the emission rates are to be calculated. Accordingly, for all RSD channels, Equation 5-11 becomes:

Pollutant Mass in Pixel (g)   **Equation 5-11a**

$=$ Pixel Optical Mass (mole/m^2) $*$ Light Beam Area (m^2) $*$ Pollutant MW (g/mole)

The device's second step is to convert the two-dimensional RSD data location indexes referenced by scan position m and scan number n to one-dimensional data location indexes referenced to the vehicle rear so that the pollutant data array can be spatially and temporally aligned with the Weights. The data location indexes are the scan identifier values v. This process is performed in two sub-steps. In the first sub-step, the Pollutant Mass in each Scan Number is computed by summing values of the two-dimensional interpolated RSD measurements in each instrument channel indexed by scan number n across the range of scan positions m as

$$\text{Pollutant Mass in Each Scan}(n) = \sum_{m=1}^{M} x_{m,n}$$

In the second sub-step, the Pollutant Mass in Each Scan is shifted by the Scan Number of the Vehicle Rear using the conversion:

                                                             Equation 5-12
Scan Value v After Vehicle Rear $=$ Scan Number n - Scan Number of Vehicle Rear

In this way, we obtain the Pollutant Mass in Each Scan values indexed by the Scan Value v. Typical ranges of the value v are from $v=0$ to $v=20$.

The device's third sub-step is to combine the array of pollutant Mass in Each Scan values with the Weights to produce the Pollutant RSD Signal. This step can be considered as a fitting of the Weights to the array of Pollutant Mass in Each Scan values, followed by taking the area under the fit to the Pollutant Mass data array. Let W(v) be the Weights indexed by scan value v

produced by the Vortex Shape Estimation Device, denoted as W(v), v={1,2,...,20}. The Pollutant RSD Signal is computed as

$$\text{Pollutant RSD Signal} \quad = \quad \frac{\sum_{v=0}^{20} W(v) \cdot \text{Pollutant Mass in Each Scan}(v)}{\sum_{v=0}^{20} W(v)}$$

Step 6. 100% Illumination Speed Device

The purpose of this device is to calculate the RSD 100% Illumination Speed (100%IS), which is the road speed at which the vehicle/vortex would have to move to produce an RSD signal that would equal the RSD signal produced if the RSD light beam illuminated the scan path once and only once. The 100%IS is independent of other variables including vehicle, road speed, pollutant, release rate, release location, and wind.

The inputs to the 100% Illumination Speed Device are the geometrical and operating properties of the RSD instrument. For this set-up, these inputs are the RSD laser beam radius, laser beam scan rate, scan path length, and number of pixels per scan. The device output is the 100% Illumination Speed:

100% Illumination Speed (m/s)   **Equation 5-13**

$= \quad \dfrac{\text{Number of Pixels/Scan } * \text{ Effective Pixel Area (m}^2\text{/pixel) } * \text{ Scan Rate (scan/s)}}{\text{Scan Length (m)}}$

Step 7. Mass-in-Vortex Calculation Device

The Mass-in-Vortex Calculation Device calculates the mass of pollutant in the vortex. The calculation uses the pollutant RSD Signal (g), the vehicle Road Speed, and the RSD's 100% Illumination Speed.

In general, RSD instruments do not illuminate the entire vortex. They illuminate a sample of the vortex. Thus, RSD signals are proportional only to the fraction of the vortex that they illuminate. The fraction of the vortex that RSDs illuminate is related to the geometry of the RSD's light beam and its illumination of the vortex.

As the vehicle and vortex move faster, the distance between consecutive scans in the vortex gets larger, and therefore the fraction of the vortex that is illuminated decreases. Consequently, as road speed increases, the RSD signal tends to decrease. The RSD Signal (g) is just the sum of the pollutant masses measured by the RSD in all RSD scans of the vortex or in all RSD pixels of the vortex. Therefore, to determine the mass in the entire vortex, the RSD signal must be corrected for the road speed.

The purpose of the Mass-in-Vortex Calculation Device is to calculate the pollutant Mass in Vortex from the pollutant mass that was illuminated and measured by the RSD. The Mass in Vortex is given by:

Equation 5-14

$$\text{Mass in Vortex (g)} = \frac{\text{RSD Signal (g)} * \text{Road Speed (mile/hr)}}{100\% \text{ Illumination Speed (mile/hr)}}$$

where

Mass in Vortex (g)   =   Mass of the pollutant in the entire vortex

RSD Signal (g)   =   Pollutant RSD signal output by the Pollutant RSD Signal Device

Road Speed (mile/hr) =   Vehicle road speed measured by the RSD system

100% Illumination Speed (mile/hr)   =   100% illumination speed from the 100% Illumination Speed Device

Step 8. Emission Rate Calculation Device

The purpose of the Emission Rate Calculation Device is to calculate the Release Rate (g/hr) and Emission Rate (g/mile) from the calculated pollutant Mass in Vortex using the calculated value of the Vortex Entrainment Time (VET) and the measured vehicle Road Speed.

A portion of the emissions released from a vehicle is temporarily stored or entrained in the swirling vortex that follows a moving vehicle. This entrainment process is a dynamic equilibrium consisting of the emissions released from the vehicle, flow of a portion of the emissions into the vortex behind the vehicle, and the stripping of emissions from the vortex by the air passing over the vortex as the vortex moves down the road. This process is shown in the left side of Figure 5-11. For a vehicle operating under steady-state conditions, which can be defined as constant road speed, constant wind speed and direction, and constant emissions release rate, the mass of a given pollutant in the vortex will oscillate around an average value.

This steady-state entrainment process is similar to the continuously stirred tank model in chemical engineering as shown in the right side of Figure 5-11. For the stirred tank model, a stream of liquid, which contains a solute, flows into the tank, and an equivalent flow exits the bottom of the tank. Under steady-state conditions, the mass of solute in the tank is proportional to the solute release rate with a proportionality constant called the turnover time:

Mass in Tank (g)   =   Turnover Time (hr) * Release Rate (g/hr)

Equation 5-15

Under steady-state conditions, if the solute release rate is low, the mass in the tank will be low. If the release rate is high, then the mass in the tank will be high. The turnover time is characteristic of the inlet flow rate, the volume of the tank, and the mixing in the tank.

Figure 5-11. Continuously Stirred Tank Analogy
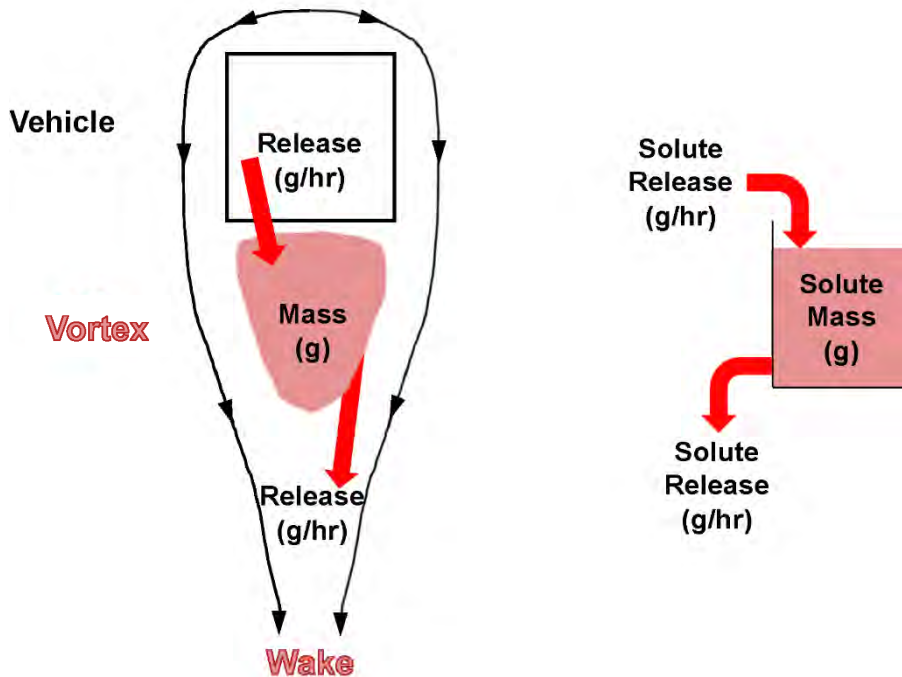
Following the stirred tank model, Equation 5-15 is expressed in terms of entrainment of released emissions into the vehicle's vortex:

Mass in Vortex (g) = VET (hr) * Release Rate (g/hr)   **Equation 5-16**

where the proportionality constant is now called the Vortex Entrainment Time (VET). From Equation 5-16, a large VET value means that the ratio of Mass in Vortex to Release Rate is large. There are two contributions to the size of VET: 1) the efficiency of entrainment of emissions released from the vehicle, and 2) the volume of the vortex.

When most of the released emissions bypass the vortex and only a small fraction becomes entrained, the VET is small. This is more likely to happen for emissions released farther up front on the vehicle and especially when there is strong sideways air movement caused by wind.

Vehicles that have large drag areas tend to have large vortexes. Large vortexes can store more pollutant mass for the same release rate than a small vortex can. Thus, large vortexes tend to produce larger RSD signals and tend to have larger VETs.

A rearrangement of Equation 5-16 provides Equation 5-17, which expresses the pollutant Release Rate based on an RSD measurement of Mass in Vortex and the VET.

Release Rate (g/hr) = $\dfrac{\text{Mass in Vortex (g)}}{\text{VET (hr)}}$ **Equation 5-17**

Then, the Emission Rate from Equation 5-17 divided by the Road Speed gives the Emission Rate:

$$\text{Emission Rate (g/mile)} = \frac{\text{Release Rate (g/hr)}}{\text{Road Speed (mile/hr)}} \qquad \textbf{Equation 5-18}$$

where

Mass in Vortex (g) = Pollutant mass in vortex calculated from the Mass-in-Vortex Calculation Device

VET (hr) = Vortex Entrainment Time calculated from the Vortex Entrainment Time Calculation Device

Road Speed (mile/hr) = Vehicle road speed as measured by the RSD system

Overall, a direct expression for the Emission Rate can be obtained by substituting the expression for the Mass in Vortex (Equation 5-14), into the expression for Release Rate (Equation 5-17), and then into the expression for Emission Rate (Equation 5-18) to produce:

Equation 5-19

$$\text{Emission Rate (g/mile)} = \frac{\text{RSD Signal (g)}}{100\% \text{ Illumination Speed (mile/hr)} * \text{VET (hr)}}$$

This fundamental expression shows that a vehicle's instantaneous emission rate (g/mile) can be determined from the RSD signal from pollutant mass in the vortex, the RSD instrument's geometry, and an estimate of the Vortex Entrainment Time of the vehicle driving past the RSD.

6.0 Quantities Needed by the RSD Emission Rate Method

6.1 Vehicle Air Speed and Direction

While the wind speeds were measured by EDAR at 6 meters above the pavement, light-duty vehicle plume dispersion is affected by wind speeds closer to the ground where the vehicles are located. We estimated the wind speeds at 1 meter above the pavement using the 6-meter wind speed measurements and a relationship[20] used by the Danish Wind Industry Association that describes wind speeds at different heights as a function of surface roughness lengths, which are described in Step 1 in Section 5.4 using Equation 5-3 and Table 5-1.

The land to the northwest of the Federal Parkway site was a dry creek bed with low grassy vegetation and a few widely spaced trees and bushes and no buildings for at least 200 m. The southeast side of the road had a tall hedgerow along the sidewalk with two-story buildings beyond. Based on the descriptions in Table 5-1 and consideration of the topography of the Westminster measurement site, we chose $z_0 = 0.1$ m. Using this value of z_0 and $z\_ref = 6$ m and Equation 5-3, the estimated wind speed at 1 meter above the surface would be 56.2% [$=\ln(1/0.1)/\ln(6/0.1)$] of the measured wind speed at 6 meters. The distribution of estimated wind speeds at 1 meter is shown in Figure 6-1. We assumed that the wind direction at 1 meter above the pavement was the same as the measured wind direction at 6 meters above the pavement.

Figure 6-1. Estimated Wind Speeds at 1 Meter above Pavement

/proj1/EDARinDenver-OCT2019/Analysis/analyze_Fleet_Wind_1.sas 06MAY20 17:28

---

[20] http://xn--drmstrre-64ad.dk/wp-content/wind/miller/windpower%20web/en/tour/wres/shear.htm

The dispersion of emissions from a moving vehicle is affected by the apparent movement of air around the vehicle, which is made up of two components in the vehicle's reference frame: 1) the wind at the height of the vehicle, which we have estimated as described above, and 2) the apparent air movement as a consequence of the forward motion of the vehicle. For example, if there is no wind, a vehicle driving on the road at 30 mph experiences an apparent air movement, in the vehicle's reference frame, of 30 mph blowing toward the front of the vehicle. For another example, if a vehicle is driving north at 20 mph, and if there is a 20 mph tail wind from the south, in the vehicle's reference frame there is zero apparent air movement. That condition is as if the vehicle were motionless on a calm, no-wind day.

Therefore, to analyze the EDAR emissions data, and because plume dispersion may be affected by the apparent air movement in the vehicle's reference frame, we need to calculate the air speed and direction from the 1m wind speed and direction and the vehicle's road speed and direction. This is a vector calculation. Figure 2-1 shows that all vehicles moved on a bearing of 72 degN (approximately ENE) and the speed measured by the EDAR instrument. Figure 6-2 shows the road speed distribution of the fleet vehicles in the study.

Figure 6-2. Distribution of Fleet Vehicle Road Speeds

Vehicle Speed (mph)	FREQ	CUM. FREQ	PCT	CUM. PCT
1	0	0	0.00	0.00
3	0	0	0.00	0.00
5	0	0	0.00	0.00
7	0	0	0.00	0.00
9	0	0	0.00	0.00
11	3	3	0.01	0.01
13	16	19	0.05	0.06
15	17	36	0.05	0.11
17	38	74	0.12	0.23
19	76	150	0.24	0.47
21	185	335	0.58	1.05
23	292	627	0.92	1.97
25	347	974	1.09	3.07
27	370	1344	1.16	4.23
29	585	1929	1.84	6.07
31	888	2817	2.80	8.87
33	1389	4206	4.37	13.24
35	1901	6107	5.98	19.23
37	2601	8708	8.19	27.42
39	3406	12114	10.72	38.14
41	4038	16152	12.71	50.85
43	4064	20216	12.79	63.65
45	3859	24075	12.15	75.80
47	3041	27116	9.57	85.37
49	2097	29213	6.60	91.97
51	1110	30323	3.49	95.47
53	646	30969	2.03	97.50
55	348	31317	1.10	98.60
57	180	31497	0.57	99.16
59	91	31588	0.29	99.45
61	44	31632	0.14	99.59
63	35	31667	0.11	99.70
65	34	31701	0.11	99.80
67	14	31715	0.04	99.85
69	12	31727	0.04	99.89
71	10	31737	0.03	99.92
73	3	31740	0.01	99.93
75	5	31745	0.02	99.94
77	8	31753	0.03	99.97
79	2	31755	0.01	99.97
81	1	31756	0.00	99.98
83	2	31758	0.01	99.98
85	0	31758	0.00	99.98
87	0	31758	0.00	99.98
89	0	31758	0.00	99.98
91	1	31759	0.00	99.99
93	0	31759	0.00	99.99
95	1	31760	0.00	99.99
97	0	31760	0.00	99.99
99	3	31763	0.01	100.00

FREQUENCY

/proj1/EDARinDenver-OCT2019/Analysis/analyze_Fleet_Wind_1.sas 06MAY20 17:28

We established a convention for the calculation of air speeds and direction in the vehicle's reference frame: Air moving directly toward the front of the vehicle has a positive speed and a direction of 0 degV, that is, 0 degrees in the Vehicle reference frame. Positive angles for air movement are expressed in a clockwise direction; negative angles in the counter-clockwise direction. For example, air movement at 10 mph directly at the driver's door would have Air

Speed = 10mphV and Air Direction = -90 degV. To serve as a check, the following are the measured quantities and the calculation results[21] for the vehicle transit on 10/20/2019 at 10:11:13 AM:
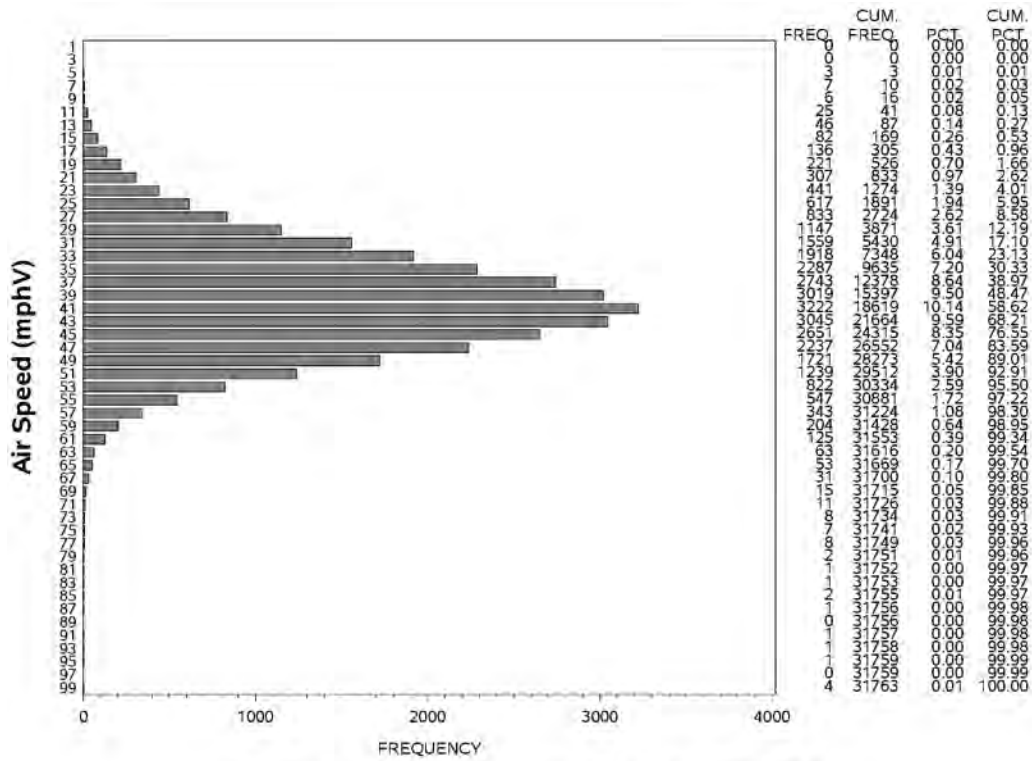
Vehicle Speed (measured)	= 44.5 mph
Vehicle Direction (measured)	= 72 degN
6m Wind Speed (measured)	= 47.6 mph
Wind Direction (measured)	= 279 degN
1m Wind Speed (calculated)	= 26.8 mph (=0.562 * 47.6 mph)
Air Speed (calculated)	= 23.8 mphV
Air Direction (calculated)	= -30 degV

Thus, in this vehicle's reference frame, air is moving toward the front left of the vehicle from 30 degrees left of the vehicle's centerline at 23.8 mph. This is the air movement resultant in the vehicle's reference frame as a consequence of driving ENE (72 degN) at 44.5 mph in a 47.6 mph wind coming from the west (279 degN) as measured at 6m above the pavement.

The air movement calculations were performed for all fleet vehicle transits of the EDAR instrument. Figures 6-3 and 6-4 show distributions of the air speed and direction in the vehicle reference frame. Figure 6-5 shows a plot of air speed vs. air direction in the vehicle's reference frame. Note that almost all air movement directions are ±20 degV with respect to directly in front of the vehicle, but the air speeds have a wide range from 10 to 80 mphV.

---

[21] P/EDARinDenver-OCT19/Analysis/Westminster_OCT19Results_200124Reprocess-200219.xlsx

Figure 6-3. Vehicle Reference Frame: Fleet Air Speed Distribution

Air Speed (mphV)	FREQ	CUM. FREQ	PCT	CUM. PCT
1	0	0	0.00	0.00
3	0	0	0.00	0.00
5	3	3	0.01	0.01
7	7	10	0.02	0.03
9	6	16	0.02	0.05
11	25	41	0.08	0.13
13	46	87	0.14	0.27
15	82	169	0.26	0.53
17	136	305	0.43	0.96
19	221	526	0.70	1.66
21	307	833	0.97	2.62
23	441	1274	1.39	4.01
25	617	1891	1.94	5.95
27	833	2724	2.62	8.58
29	1147	3871	3.61	12.19
31	1559	5430	4.91	17.10
33	1918	7348	6.04	23.13
35	2287	9635	7.20	30.33
37	2743	12378	8.64	38.97
39	3019	15397	9.50	48.47
41	3222	18619	10.14	58.62
43	3045	21664	9.59	68.21
45	2651	24315	8.35	76.55
47	2237	26552	7.04	83.59
49	1721	28273	5.42	89.01
51	1239	29512	3.90	92.91
53	822	30334	2.59	95.50
55	547	30881	1.72	97.22
57	343	31224	1.08	98.30
59	204	31428	0.64	98.95
61	125	31553	0.39	99.34
63	63	31616	0.20	99.54
65	53	31669	0.17	99.70
67	31	31700	0.10	99.80
69	15	31715	0.05	99.85
71	11	31726	0.03	99.88
73	8	31734	0.03	99.91
75	7	31741	0.02	99.93
77	8	31749	0.03	99.96
79	2	31751	0.01	99.96
81	1	31752	0.00	99.97
83	1	31753	0.00	99.97
85	2	31755	0.01	99.97
87	1	31756	0.00	99.98
89	0	31756	0.00	99.98
91	1	31757	0.00	99.98
93	1	31758	0.00	99.98
95	1	31759	0.00	99.99
97	0	31759	0.00	99.99
99	4	31763	0.01	100.00

/proj1/EDARinDenver-OCT2019/Analysis/analyze_Fleet_Wind_1.sas 06MAY20 17:28

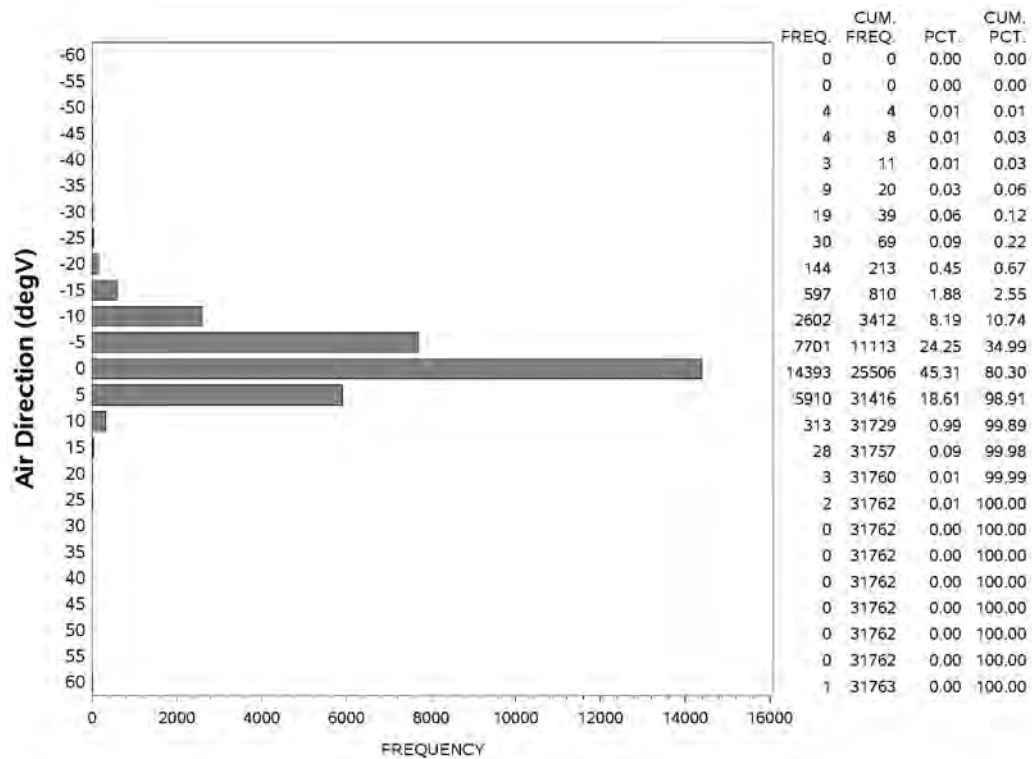## Figure 6-4. Vehicle Reference Frame: Fleet Air Direction Distribution

Air Direction (degV)	FREQ	CUM. FREQ	PCT	CUM. PCT
-60	0	0	0.00	0.00
-55	0	0	0.00	0.00
-50	4	4	0.01	0.01
-45	4	8	0.01	0.03
-40	3	11	0.01	0.03
-35	9	20	0.03	0.06
-30	19	39	0.06	0.12
-25	30	69	0.09	0.22
-20	144	213	0.45	0.67
-15	597	810	1.88	2.55
-10	2602	3412	8.19	10.74
-5	7701	11113	24.25	34.99
0	14393	25506	45.31	80.30
5	5910	31416	18.61	98.91
10	313	31729	0.99	99.89
15	28	31757	0.09	99.98
20	3	31760	0.01	99.99
25	2	31762	0.01	100.00
30	0	31762	0.00	100.00
35	0	31762	0.00	100.00
40	0	31762	0.00	100.00
45	0	31762	0.00	100.00
50	0	31762	0.00	100.00
55	0	31762	0.00	100.00
60	1	31763	0.00	100.00

Figure 6-5. Vehicle Reference Frame: Fleet Distribution of Air Movement

/proj1/EDARinDenver-OCT2019/Analysis/analyze_Fleet_Wind_1.sas 06MAY20 17:28
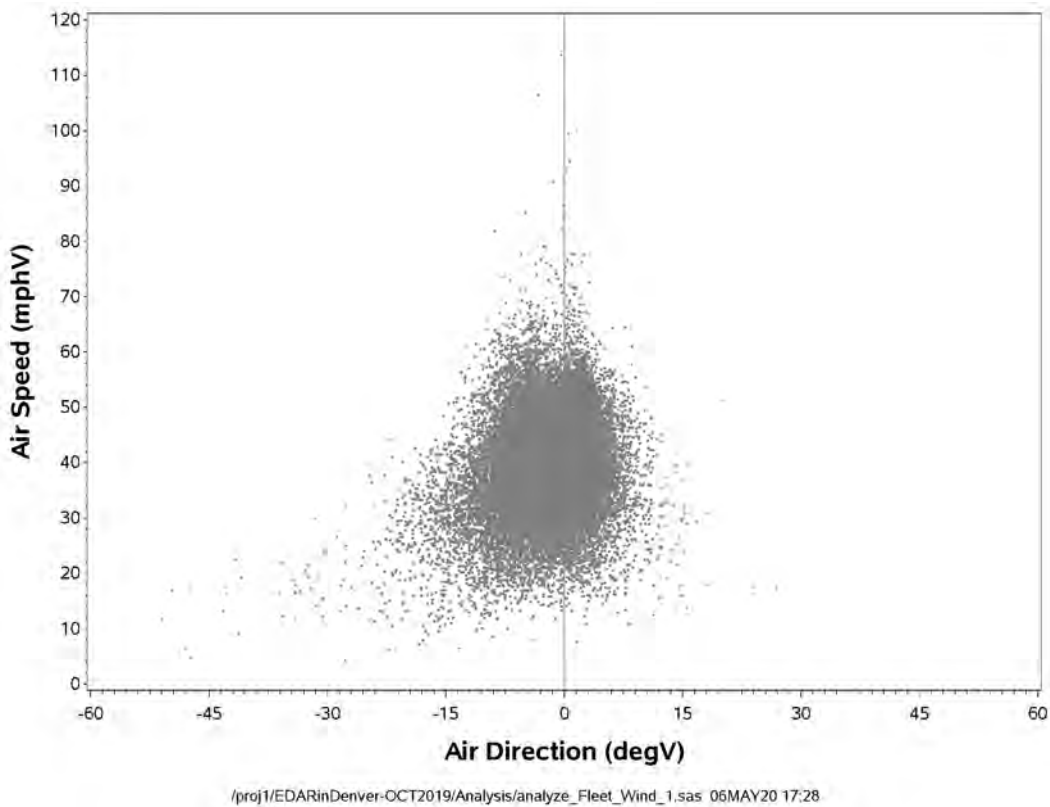
6.2   Vehicle Footprint Length and Width

As described above and demonstrated in Figure 5-4, when a vehicle is on top of the pavement tape, the laser beam is not returned to the overhead EDAR instrument. This causes missing detailed data values, which when imaged as in Figure 6-6, produce a "vehicle footprint." In this figure, the vehicle footprint is the evenly colored blue area to the left of the red/yellow/green vortex area which contains the emissions mass. The size of the footprint is related to the size and shape of the vehicle. Since the vehicle footprint is made up of pixels with missing values, we can calculate the dimensions of the footprint by examining the pattern of the missing pixels.

Figure 6-6. Image of an EDAR Detailed Data Array
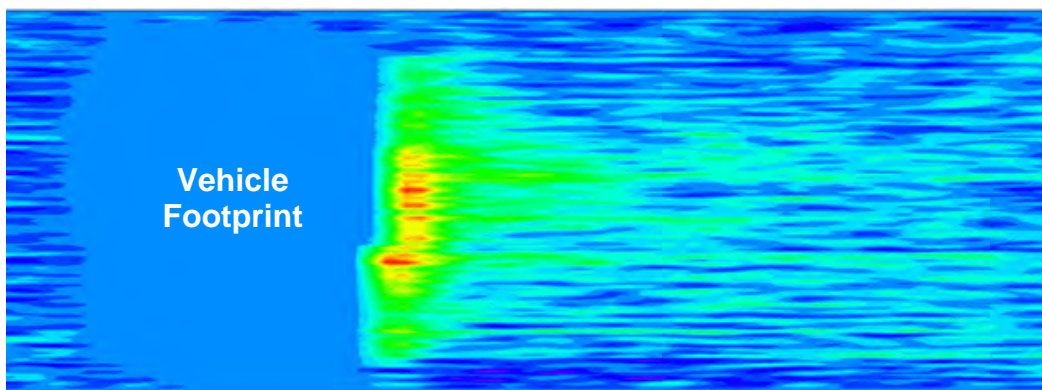
The length of the footprint, which is in the direction of vehicle motion, is a function of the vehicle speed, which is measured by the EDAR system, and the vehicle length. In this study, the laser beam always scanned at a constant 20 scans/s rate. For a given vehicle length, vehicles moving at low speeds produce more scans with missing-value pixels than vehicles moving at high speeds. For example, a 17.6-foot-long vehicle moving at 30 mph would have about 8 missing-value footprint scans, while the same vehicle moving at 60 mph would have about 4 missing-value footprint scans.

The width of the footprint is affected by the vehicle width, the vehicle height, and the length of the laser scan on the pavement tape. Because of the triangular scan pattern of the laser beam, as shown in Figure 2-3, tall vehicles, as well as wide vehicles, produce a wide footprint. For example, the top of a 53-foot, 102-inch wide, 13.5-foot-tall, 18-wheeler box trailer would be so close to the overhead EDAR instrument that the footprint would be the entire 256 pixels wide. On the other hand, if the EDAR instrument were 15 feet above the pavement with a 12-foot pavement tape, a 60-inch-high, 66-inch-wide car would have a footprint only about 82 inches wide or about 145 pixels.

The number of scans and number of pixels with missing values in each transit, pavement tape length, laser scan rate, and vehicle speed were used to calculate the length and width of each transit's vehicle footprint.

Locating vehicle front and rear – Before we could calculate the length and width of each transit's vehicle footprint, we needed to determine which EDAR scans were associated with the front and rear of the vehicle. Because a CO_2 signal is always present in the vortex of a vehicle with a fossil-combusting engine, we used the EDAR CO_2 detailed data to locate the vehicle footprint. While we could locate the footprints of a small number of transits by examining the CO_2 detailed data by eye, because the Westminster dataset contains more than 30,000 transits, we developed an automated method for determining the scans associated with the front and rear of each footprint.

We used the raw CO_2 detailed data of the 1180 test vehicle transits as a dataset to develop an automated algorithm for determining the scan number of the first scan after the vehicle's rear bumper, which we call BumperCounter=1. For each of those transits, we made a plot of the sum of the CO_2 measurements in each scan vs. scan number overlaid with a plot of the number of missing (blank) CO_2 values in each scan vs. scan number. Then, we examined each transit's plot by eye and recorded the scan number that we judged was the first scan after the rear of the vehicle.

We wrote a SAS program[22] that used hand-observed after-vehicle scan numbers of the 1180 test vehicle transits to develop a draft automatic method for determining those values. The first scan after the end of the footprint was defined as the scan after the last scan where the number blank CO_2 pixels was greater than three pixels. Three pixels were used as the detection threshold since occasionally three pixels could have blank CO_2 values as a consequence of HEAT's raw data post-processing that was not indicative of the footprint. The program determined the last scan

---

[22] P:\EDARinDenver-OCT2019\Analysis_MLout\211108/OCT19_bumper.sas

before the beginning of the footprint by reversing the order of sorting of the scan numbers and then applying the same detection method.

The program was then applied to the Westminster dataset to validate the front and rear footprint assignments by visual checks against a random set of the fleet vehicle transits.

Footprint length – Figure 6-7 shows an example of scans assigned to a vehicle transit. The black trace and right axis show the counts of the number of blank pixels in each scan. On the basis of the automated assignment, a vertical black, dashed reference line is placed at the last scan that intersects the vehicle at After-Vehicle Scan =0. The next scan is the first-after-vehicle scan, which is assigned After-Vehicle Scan=1. In a similar manner, with reverse scan sorting, the last-before-vehicle scan is located at After-Vehicle Scan = -7 and is marked by a small green triangle symbol. The result is that all scans between After-Vehicle Scan = -7 and 1 have at least three blank pixels, which indicates the presence of the vehicle. Because the vehicle footprint has seven scans and the measured vehicle speed was 45.5 mph, we calculate a vehicle length of 23 feet (=45.5 * 5280 * (7/20) / 3600). Since we are using just whole numbers of scans, this calculated length is approximate. The red trace and left axis of Figure 6-7 show the CO_2 scansums for the transit. Notice that the CO_2 scansum is low before After-Vehicle Scan =1. After the vehicle clears the laser beam, the CO_2 scansum rises rapidly and then decays back toward zero as the exhaust CO_2 disperses.

Figure 6-7. CO_2 ScanSums and Blank Pixel Counts for a Car (45.5 mph, Series_Transit=505_000299)

/proj1/EDARinDenver-OCT2019/Analysis_MLout/211108/Anal_MLout/OCT19_bumper.sas 01DEC21 11:32
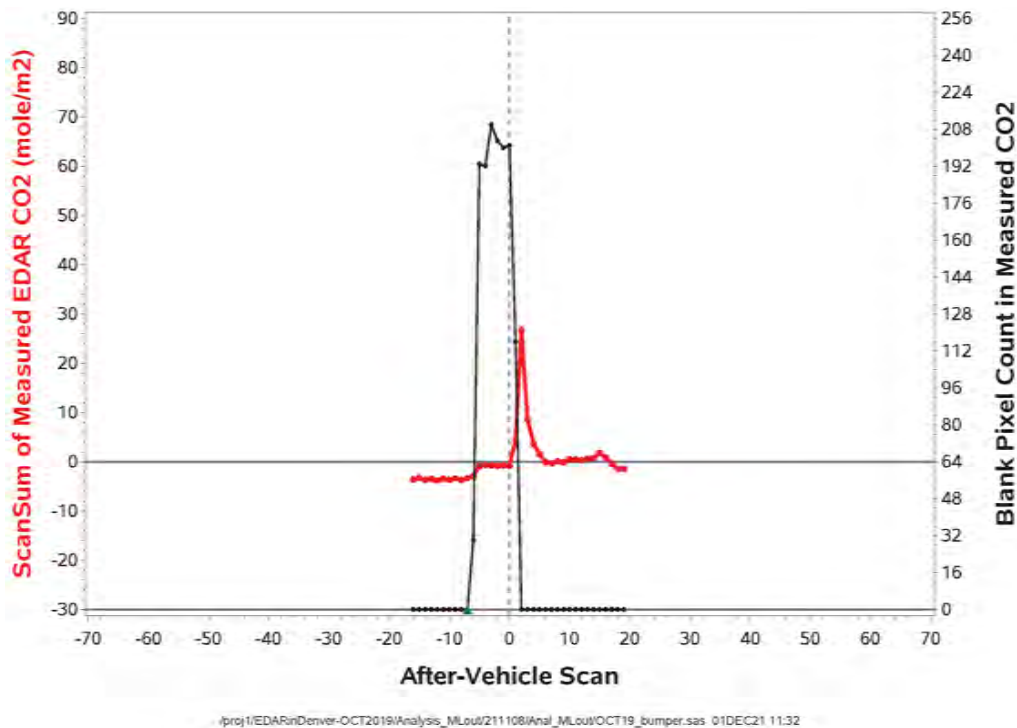
Figure 6-8. CO₂ ScanSums and Blank Pixel Counts for a Vehicle with Trailer (19.8 mph, Series_Transit=505_000262)

/proj1/EDARinDenver-OCT2019/Analysis_MLout/211108/Anal_MLout/OCT19_bumper_trailers.sas 19NOV21 12:37
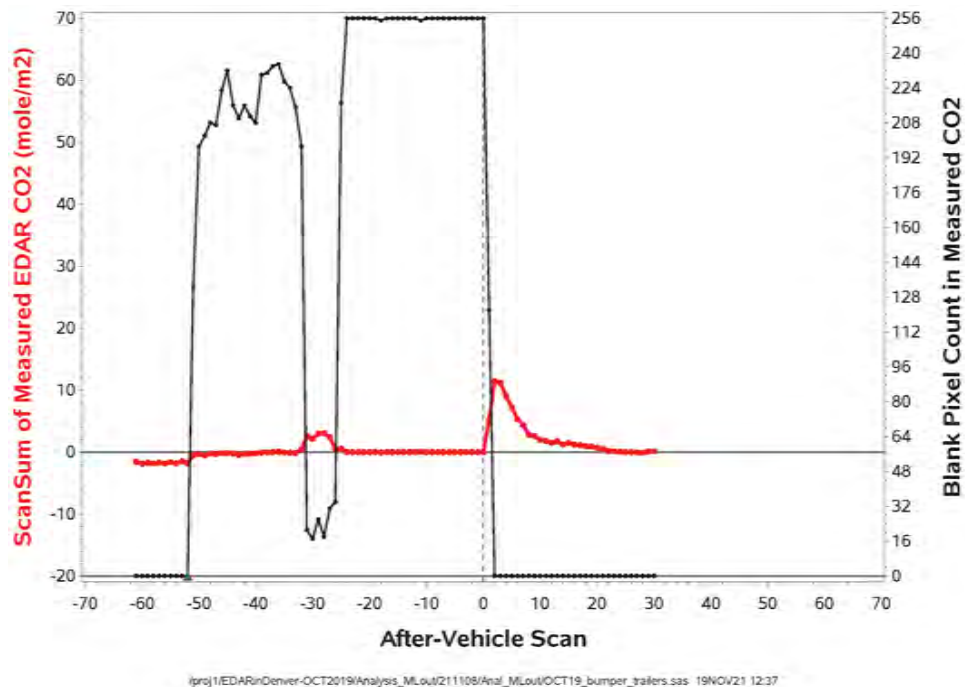
Figure 6-8 shows a result for a vehicle pulling a trailer with a footprint between After-Vehicle Scan = -52 and 1 (i.e., 52 scans) traveling at 19.8 mph for a calculated vehicle/trailer length of 75 feet. The red CO_2 scansum trace clearly shows CO_2 at the hitch, zero CO_2 on the sides of the trailer because the trailer blanks out virtually all of the 256 pixels, and a large CO_2 signal behind the trailer.

Footprint width – To estimate the width of the vehicle footprint, the length in feet of each scan with blank pixels is calculated as the length of the retro-reflective pavement tape (12 feet) by the number of blank pixels in each scan to the number of pixels the number of pixels in each scan (256). Then, we assign the second longest scan length in feet to the vehicle footprint width. Using the second longest scan length reduces the influence of protrusions from the vehicle body such as side-view mirrors.

Vehicles with trailers – Once we developed an automated method to locate the front and rear of a vehicle in a transit, we wrote code[23] to attempt to identify vehicles that were pulling trailers. The code looked for abrupt, large changes in the number of blank pixels in the scans between the front bumper and the rear bumper as an estimate of the presence of a hitch. About 159 transits of the Westminster dataset were identified by this method as having trailers. Because we decided to put understanding the emissions of vehicles with trailers as part of future work, we did not further investigate these transits.

---

[23] P:\EDARinDenver-OCT2019\Analysis_MLout\211108/OCT19_bumper.sas

Footprint size trends – For many of the transits produced by vehicles registered in Colorado, the registration database contained various types of vehicle descriptions, for example, fuel type (gasoline, diesel, electric, …), vehicle type (car, motorcycle, incomplete, …), body type (bus, ambulance, convertible, pickup truck, …), and GVWR. We examined vehicle size trends as a function of these descriptors. For example, Figure 6-9 shows the footprint length and width as a function of GVWR. The plots show that the footprint length and width tend to increase with GVWR.

Figure 6-9. Footprint Size as a Function of GVWR for the Westminster Set

6-10
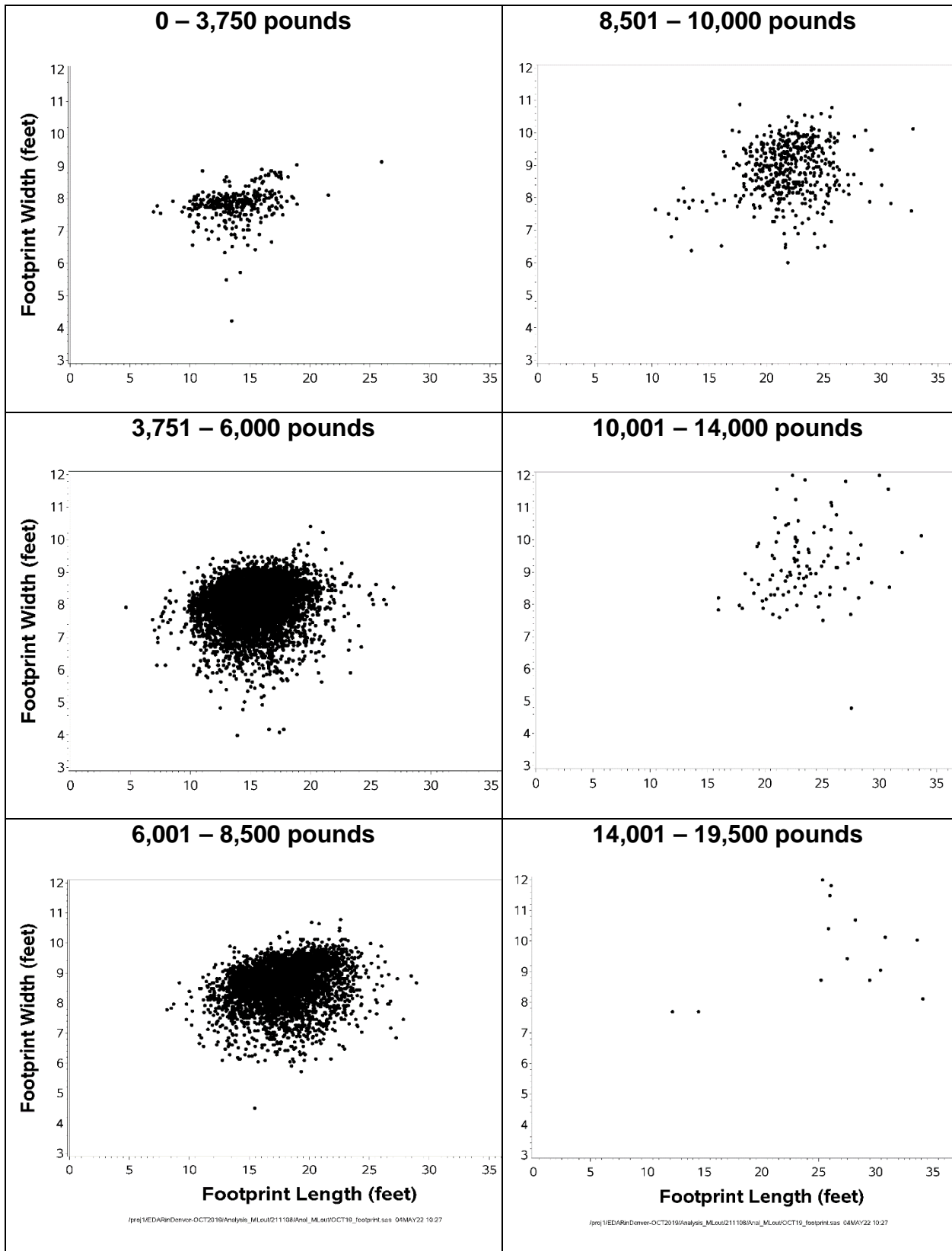
6.3   100% Illumination Speed for this Study

The 100% illumination speed (100%IS) is a characteristic constant for a given RSD instrument geometrical set-up that is used to correct the RSD signal for the speed of the vehicle, as used in Equation 5-14. This subsection describes how the 100%IS is calculated for the EDAR set-up used in this study. The 100%IS for other RSD set-ups might be calculated similarly.

The purpose of Step 6 is to calculate the RSD 100% Illumination Speed (100%IS), which is the road speed at which the vehicle/vortex would have to move to produce an RSD signal that would equal the RSD signal produced if the RSD light beam illuminated the scan path once and only once. The 100%IS is independent of other variables including vehicle, road speed, pollutant, release rate, release location, and wind.

As shown in Figure 5-4, in the reference frame of the vehicle/vortex, the laser beam optically samples the vortex with a zigzag pattern from above the roadway. Of course, the instrument can make measurements only where pixels are illuminated, that is, where blue dots are. The pollutant mass in the white areas between the scans and around the blue dots is not illuminated and therefore does not contribute to the RSD signal. The pitch of the zigzag in the vehicle/vortex reference frame is a function of the road speed. At higher speeds, the pitch is larger. After pre-processing, the arrangement of the processed measurements is on a rectangular grid, but the shape and size of the measurement region remains the same. Because the diameter of the laser beam is independent of road speed, but the distance in the vortex between successive scans depends on road speed, the fraction of the vortex that is illuminated by the light beam depends on road speed.

In addition, the overlap of pixels is a function of vortex speed. At road speeds below the 100%IS, all pixels have some degree of overlap with other pixels.

To calculate the 100%IS, the speed at which the total area illuminated by the RSD would be equal to the total area of the scan path is determined. The scan path is the path that the RSD instrument is scanning. The fraction of vortex illuminated is a function of the road speed and characteristics of the RSD instrument. When the RSD instrument scans the roadway from above:

Fraction of Vortex Illuminated   = $\dfrac{\text{Area of Illumination for 1 second}}{\text{Area of Scan Path for 1 second}}$ **Equation 6-1**

The Area of Illumination for 1 second is the sum of the areas illuminated by each pixel for all pixels illuminated in 1 second. The areas of all pixels are to be summed even if pixels overlap. This is appropriate since while overlapping pixels cause over-sampling of the pollutants in the vortex, overlapping pixels do contribute to the RSD signal.

An example serves to illustrate Equation 6-1. Suppose the vortex, which moves at the same speed as the vehicle, is moving at 25 m/s. The scan length is 3.66 m (=12 feet), which is the length of the retro-reflective tape on the pavement. Thus, the Area of the Scan Path for 1 second is 91.5 m^2 (=25m * 3.66m). Since the RSD laser beam has a radius of 1.0 cm, scans the retro-reflective tape 20 times per second, and each scan has 256 pixels, the Area of Illumination for 1 second is 1.61 m^2 (=π*(0.01m)^2 * 20 * 256). Thus, the Fraction of Vortex Illuminated is 1.75% (=1.61 / 91.5). This means that the mass of pollutant in the vortex moving at 25 m/s past the

instrument is actually 57 times larger (=1/0.0175) than the mass illuminated by the RSD laser beam.

This example shows that the fraction of the vortex illuminated is given by:

Fraction of Vortex Illuminated **Equation 6-2**

$$= \frac{\text{Number of Pixels/Scan } * \text{ Effective Pixel Area (m}^2\text{/pixel) } * \text{ Scan Rate (scan/s)}}{\text{Road Speed (m/s) } * \text{ Scan Length (m)}}$$

Note that Equation 6-2 is specific to this RSD instrument, which scans the full width of the vortex from above the pavement and which is accordingly believed to obtain a representative optical sample of the vortex. For other types of RSD instruments that are believed to obtain a representative optical sample, Equation 6-2 would be replaced with a different appropriate relationship. RSD instruments that make measurements using a horizontal beam at a fixed height above the pavement may or may not be able to get a representative optical sample of the vortex.

To derive an expression for the 100%IS, Equation 6-2 is simply solved for Road Speed for a value of Fraction of Vortex Illuminated =1, which produces Equation 5-13.

For the RSD set-up used in this study, the 100%IS would be calculated as:

$$\frac{256 \text{ pixels/scan } * \pi *(0.01 \text{ m})^2\text{/pixel } * 20 \text{ scan/s}}{3.66 \text{ m}}$$

which equals 0.44 m/s (=0.97 mph).

6.4 Vortex Entrainment Time (VET) Functionality

Vortex Entrainment Time (VET) is key to this method for measuring pollutant emission rate using RSD because it establishes a connection between the RSD-measured pollutant Mass in Vortex and pollutant Release Rate (g/hr) as described by Equation 5-17.

The Vortex Entrainment Time (VET) can be defined by a re-arrangement of Equation 5-17:

$$\text{VET (hr) } = \frac{\text{Mass in Vortex (g)}}{\text{Release Rate (g/hr)}} \qquad \textbf{Equation 6-3}$$

The VET is influenced by 1) the volume of the vortex, and 2) the efficiency of entrainment of emissions released from the vehicle into the vortex. Consider Equation 6-3 for the case of a large vehicle and a small vehicle that have the same pollutant release rates. The larger vehicle will have a larger vortex, which, at equilibrium, will contain a larger pollutant mass and produce a larger RSD signal than the smaller vehicle will. Accordingly, the larger vehicle will have a larger VET. Now, consider another comparison of two vehicles of the same size and shape having the same pollutant release rate, but one vehicle has the release at the vehicle rear and the other vehicle has the release under the hood. The vehicle with the under-the-hood release will likely have a smaller VET since a smaller portion of its release is likely to become entrained in the

vortex compared to the vehicle with the rear release – especially if the vehicles are in a strong cross wind.

Characteristic VET values depend on the size and shape of the vehicle, the location of the release from the vehicle, and the speed and direction of air moving across the vehicle (i.e., the vehicle's air velocity). VET values do not depend on the pollutant release rate. Thus, methods to compute the VET value can use the physical outline of the vehicle in the measurement data, the spatial locations of large-amplitude plume components in the processed measurements, and the wind velocity as measured by the RSD system during the transit event.

The dependencies of VET on vehicle properties, vehicle operation, pollutant release location, and ambient conditions were studied using the test vehicle data from the September 2016 and October 2019 studies. Test vehicles with metered pollutant releases were driven past the RSD. For each transit, the release rate was metered and the mass in the vortex was calculated from the RSD data. Then, Equation 6-3 was used to calculate the VET for each transit.

The analysis that is described below effectively separates the dependence of VET into three multiplicative factors for: 1) vehicle air speed, 2) the location on the vehicle of emissions released, and 3) the drag area of the vehicle.

Air Speed Effects

The first step in examining VET functionalities looks at the effects of air speed. Because all fossil-fueled vehicles have exhaust plumes containing high concentrations of CO_2, because most light-duty vehicles release exhaust at a location at their rear, and because RSD instruments get strong signals from the CO_2 in exhaust plumes, we will analyze the trends of VETs calculated from CO_2 signals to determine how vehicle air speed influences VET. Indeed, as will become apparent later, we will use the CO_2 in light-duty vehicle exhaust plumes as a reference for evaluating the effect of emissions location on VET.

In this October 2019 study, exhaust gas was metered from EV-1 and EV-2, which were the electric vehicles that had been fitted with fake tailpipes and bottle gas. Therefore, the CO_2 from EV-1 and EV-2 can be used to calculate VETs. The only difference in the bodies of EV-1 and EV-2 was that EV-1 had the fake tailpipe on the left rear corner and EV-2 had the tailpipe on the right rear corner. While exhaust gas was released from all five test vehicles, the exhaust gas from the F150, GMC, and Subaru was natural engine exhaust, and its composition and flow rate was neither metered nor measured. Therefore, the exhaust data from those three vehicles cannot be used to calculate VETs.

The calculated VET values from EV-1 and EV-2 exhaust CO_2 releases are plotted with red and blue symbols against the AirSpeed Para in Figures 6-10 and 6-11. Clearly, VETs are higher for lower air speeds. Regression analysis of this CO_2 VET data, as well as the analysis of EvapHC VET data on all five test vehicles, indicated that VETs followed a trend that was approximately proportional to the inverse of the square root of the AirSpeed Para. The solid lines in Figures 6-10 and 6-11 are fits using that functionality. The figures show substantial scatter in the VET values. Because the flow of air around the vehicle is complex, turbulent in the vortex, and varies across replicates, the VETs vary to produce the observed scatter. However, on average over a

period of time, VET values for a given operating condition converge to a finite, repeatable value. The figures show that a typical value for emissions from the rear of a light-duty vehicle with a 30-mph airspeed is around 4 seconds.

We examined the ratio of the measured VET to the fit VET to determine if the residual scatter in the measured VETs was dependent on AirSpeed Perp, that is, the speed of the air blowing perpendicular to the direction of vehicle motion. Figures 6-12 and 6-13 show the ratios plotted against AirSpeed Perp. The plots show that for EV-1 the ratios increase with increasing AirSpeed Perp, and for EV-2 they decrease with increasing AirSpeed Perp.

Those trends can be understood by considering the fake tailpipe location and the direction of cross air movement. Positive values of AirSpeed Perp represent air blowing toward the left side of the vehicle; negative values of AirSpeed Perp represent air blowing toward the right side of the vehicle. EV-1 had its fake tailpipe on the left rear corner of the vehicle. Therefore, positive values of AirSpeed Perp tend to move exhaust gas toward the centerline of the vortex and thereby tend to increase the mass of CO_2 in the vortex, which in turn produces a higher VET value. Negative AirSpeed Para values tend to move EV-1's exhaust gas farther to the left and therefore away from the vortex, which tends to decrease the VET value. Because EV-2's fake tailpipe is on the right rear, the trend of the ratio measured VET to predicted VET is opposite of that for EV-1. While the scatter in Figures 6-12 and 6-13 is substantial, it appears that cross air movement of 3 mph typically causes changes of around ± 30% with respect to the VET value with no cross-air movement.

The results in Figures 6-12 and 6-13 show that as AirSpeedPerf gets large the VET value is affected. Even more extreme values of AirSpeed Perp could reduce the VET value to zero, which essentially means that the release is blown so strongly to the side that it has no chance of becoming entrained in the vortex. We expect that the effect is worse for emissions release locations farther forward on the vehicle, such as for under-hood evaporative emissions releases. For strong side winds, the EDAR instrument would have little chance of obtaining a usable emissions signal. An EDAR flag could be developed to avoid outputting results when cross winds are likely to blow plumes away.

Low AirSpeed also can be a risk to good RSD measurements. All RSDs are based on measurement of the pollutants entrained in a vortex that follows a vehicle. At low vehicle air speeds, it may be possible that no vortex forms at all or that the vortex is so poorly defined that RSDs cannot get reliable measurements. Low AirSpeeds can occur when a vehicle is moving slowly in calm air, but they can also occur when a vehicle is driving at normal speeds but in a strong tailwind.

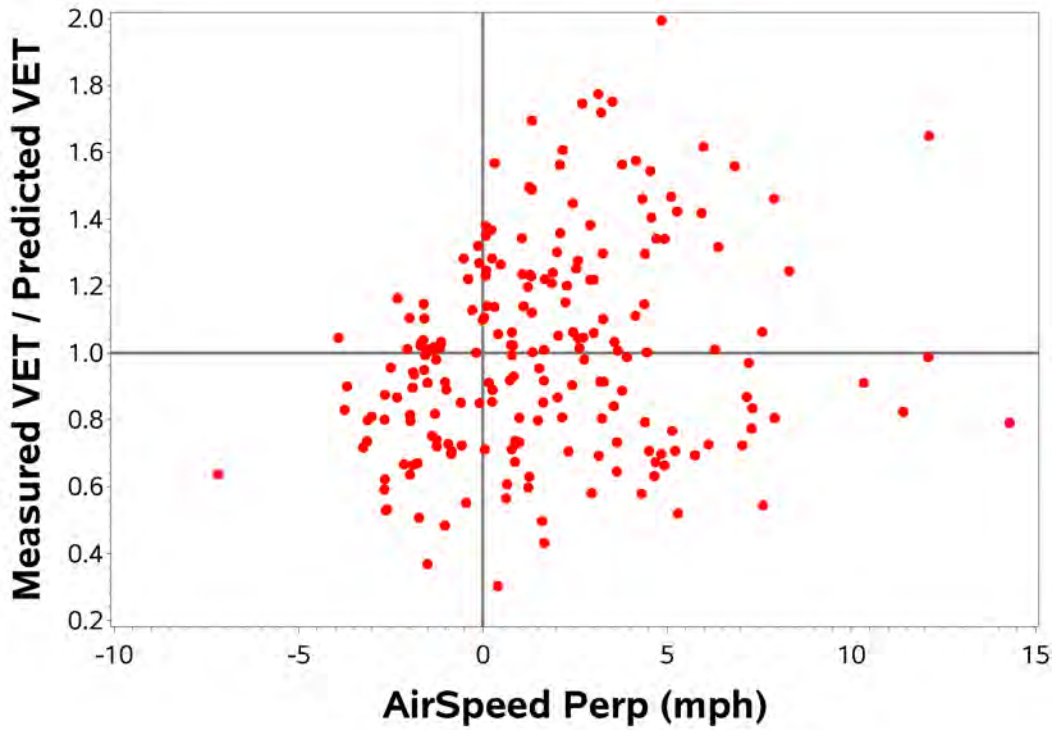**Figure 6-10. Exhaust CO₂ VET vs. AirSpeed Para for EV-1**
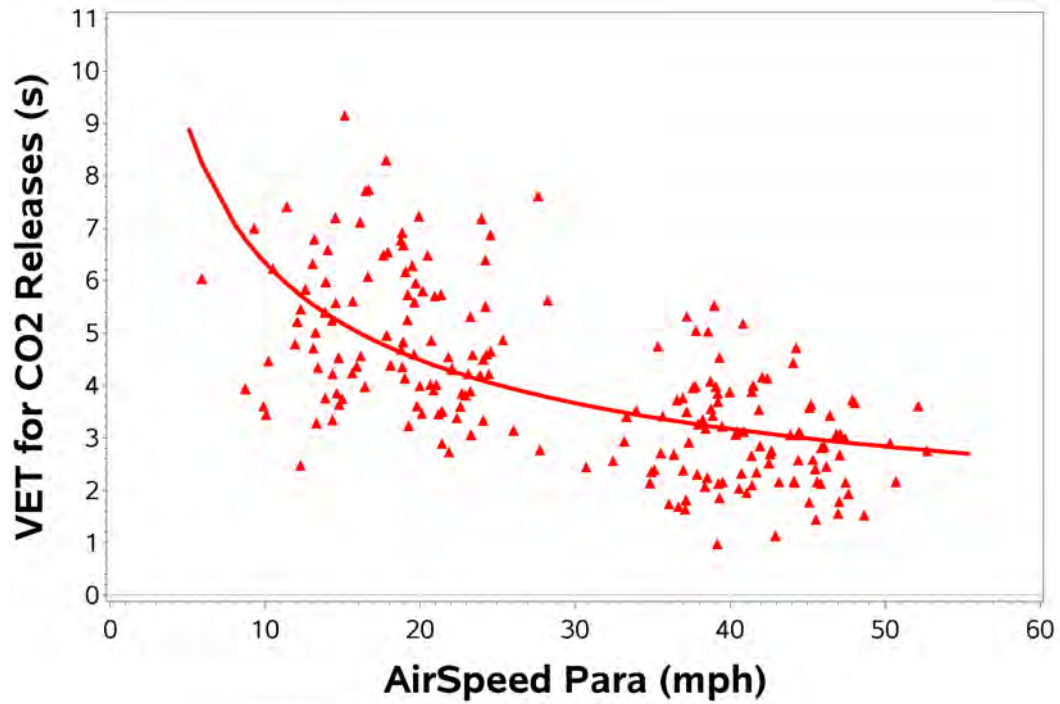
/proj1/EDARinDenver-OCT2019/Analysis_MLout/211220/Anal_MLout/OCT19_TOT_2_THD.sas 28JUL22 13:17

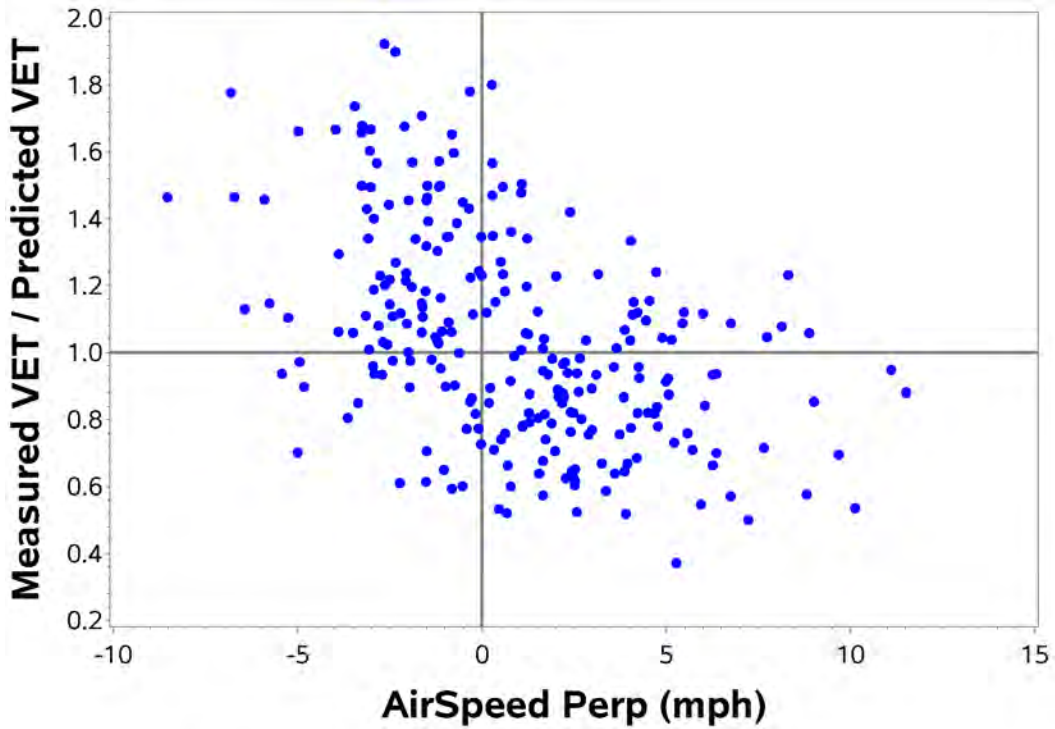**Figure 6-11. Exhaust CO₂ VET vs. AirSpeed Para for EV-2**
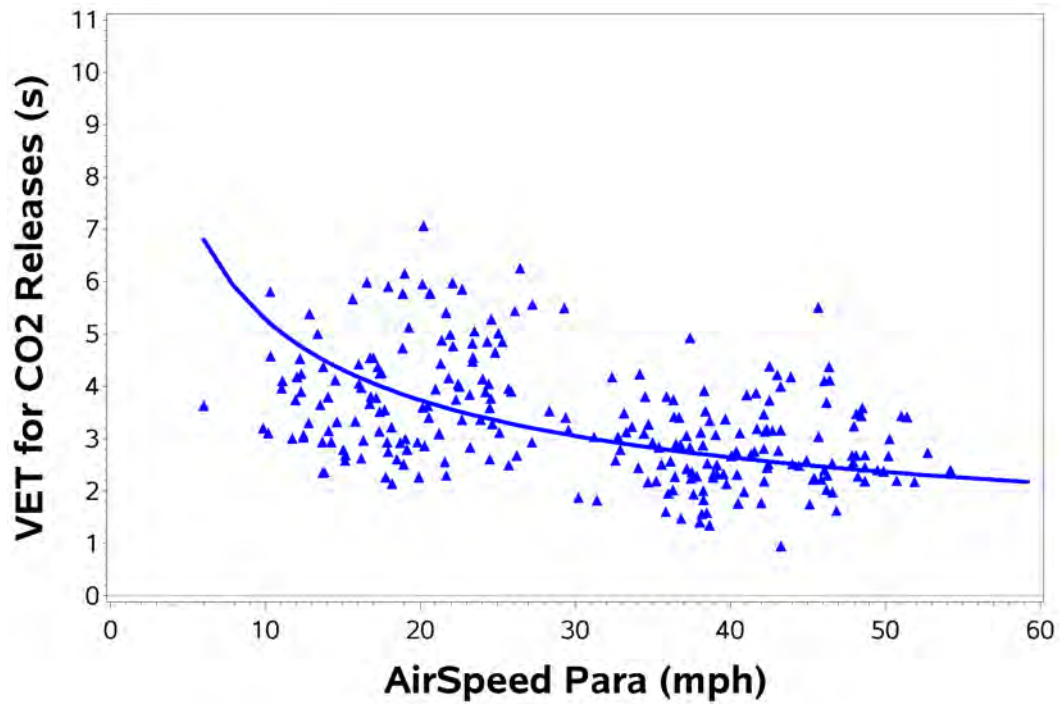
/proj1/EDARinDenver-OCT2019/Analysis_MLout/211220/Anal_MLout/OCT19_TOT_2_THD.sas 28JUL22 13:17

Figure 6-12. Residual VET Trend vs. AirSpeed Perp for EV-1

/proj1/EDARinDenver-OCT2019/Analysis_MLout/211220/Anal_MLout/OCT19_TOT_2_THD.sas 28JUL22 13:17

Figure 6-13. Residual VET Trend vs. AirSpeed Perp for EV-2

/proj1/EDARinDenver-OCT2019/Analysis_MLout/211220/Anal_MLout/OCT19_TOT_2_THD.sas 28JUL22 13:17

Release Location Effect

To determine the effect of release location, we need to have RSD transits with metered releases from different release locations at different air speeds. In this October 2019 study, artificial exhaust and artificial EvapHC emissions were metered in releases from the five test vehicles. The dependence of VET on emissions release location and vehicle AirSpeed Para was determined from these releases.

Artificial evaporative emissions (propane) were metered from all five test vehicles at three different locations and at 6400, 3200, 1600, 800, 400, 200, 100, and 50 mg/mile emission rates. Some of the resulting tests can be used to calculate VETs for releases from the locations as long as natural ExhHC emissions and natural EvapHC emissions are small relative to the artificial evaporative releases.

For EV-1, the artificial exhaust contained no HC, and since EV-1 was an all-electric vehicle, it had no gasoline on board. Its evaporative HC should be quite small since it would be derived only from outgassing of HC from vehicle construction materials. However, we also used only the test data from the 6400, 3200, and 1600 mg/mile artificial evaporative emission rates from EV-1 to maximize the signal-to-noise ratio of the RSD HC signals. Finally, we could use no EV-2 evaporative test data to calculate VETs because EV-2's artificial exhaust HC was quite high (402 ppm propane). Thus, none of EV-2's artificial evaporative HC emission rates were substantially higher than its exhaust HC emission rate.

Similarly, we used only the test data from the 6400, 3200, and 1600 mg/mile artificial evaporative emission rates for the F150, GMC, and Subaru test vehicles to ensure that the artificial evaporative release rates were substantially larger than the natural ExhHC and EvapHC emissions from those vehicles.

The calculated VET values from the 6400, 3200, and 1600 mg/mile artificial evaporative releases from EV-1, F150, GMC, and Subaru test vehicles are plotted in Figures 6-14, 6-15, 6-16, and 6-17. For EV-1 and Subaru, the three release locations were at the fuel fill door (Door=purple) at the rear of the quarter panel, on top of the under-vehicle fuel tank (Tank=orange), and on top of the engine under the hood (Hood=green). For the F150 and GMC, the fuel fill door (Side = blue) was just aft of the driver's door on the left side of the vehicle.

Test regressions of the trends of VETs for artificial EvapHC (EV-1, F150, GMC, and Subaru) as a function of release location and AirSpeed Para indicated, just as for CO_2-based VETs, that VET was inversely proportional to approximately the square root of the AirSpeed Para. In addition, the regressions indicated that the proportionality constants were connected to the release location. Based on those findings, we used regression to determine the proportionality constants for all of the selected test vehicle transits. For the EvapHC releases, we used regression weights proportional to the 6400, 3200, and 1600 mg/mile emission rate values to account for the less variable VETs associated with the higher emission rates. The resulting proportionality constants are shown in the fourth column of Table 6-1. The first three columns of Table 6-1 show the test vehicle identifier, drag area, and emission release location for the data under consideration. The solid curves in Figures 6-14, 6-15, 6-16, and 6-17 show the regression fits of the measured VETs.

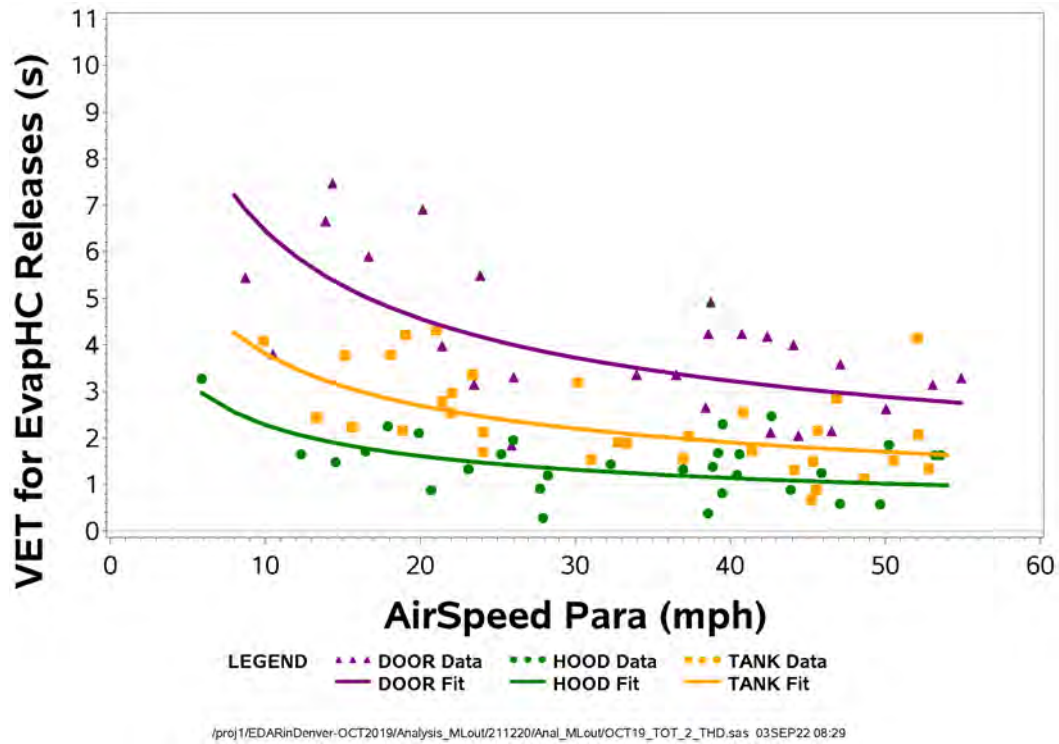**Figure 6-14. VET vs. EvapHC Release Location and Air Speed for EV-1**

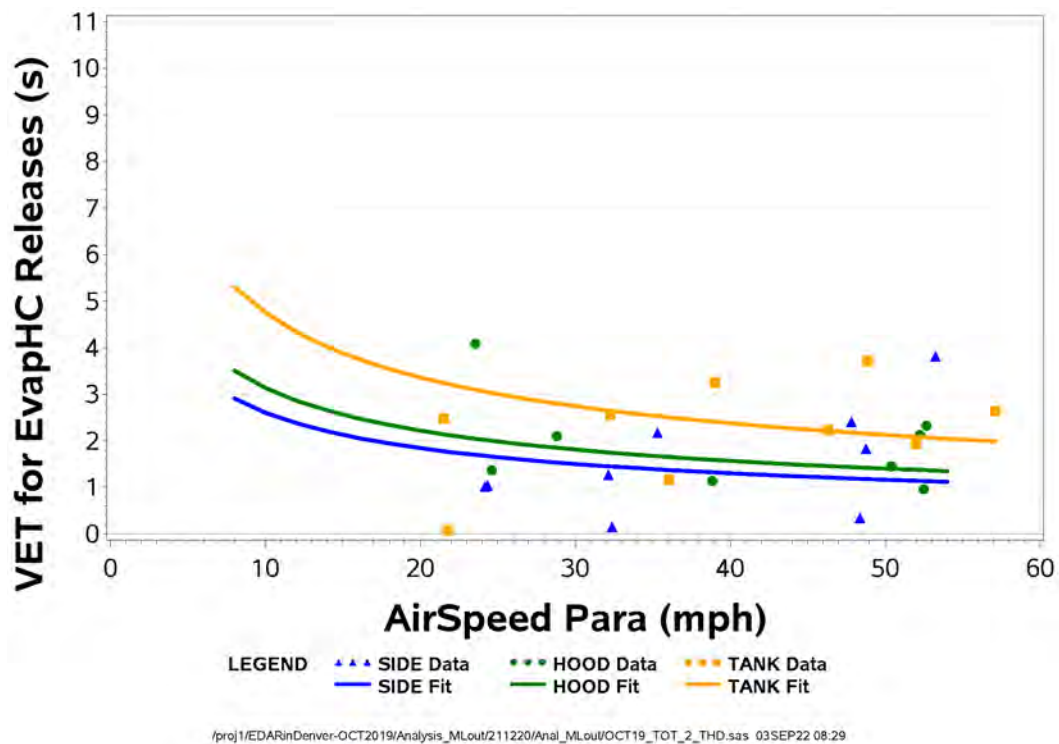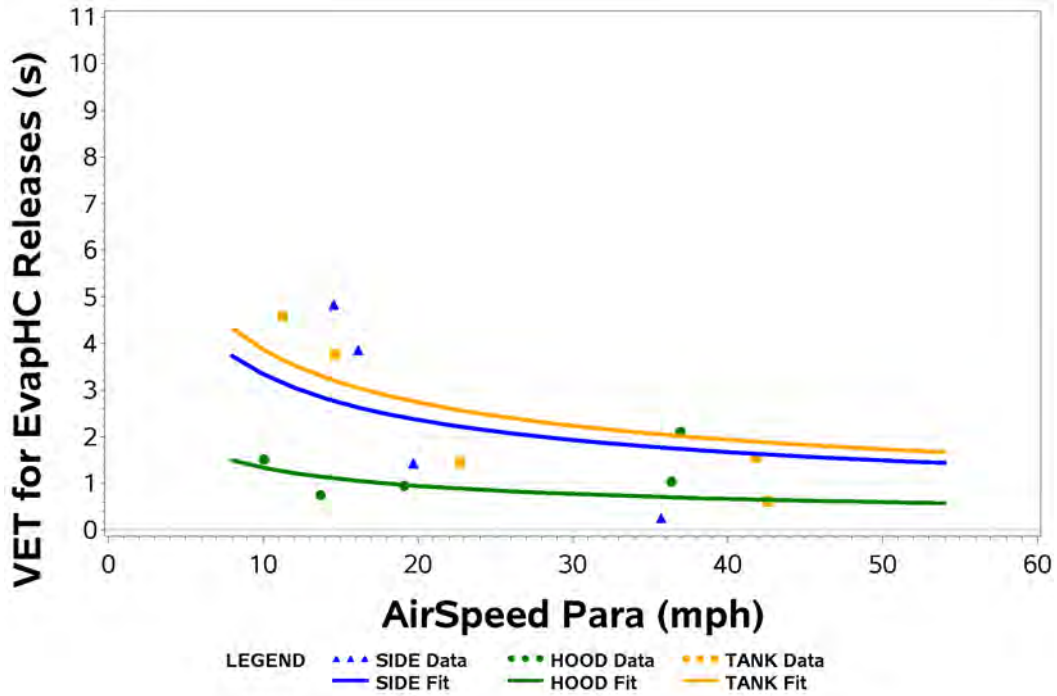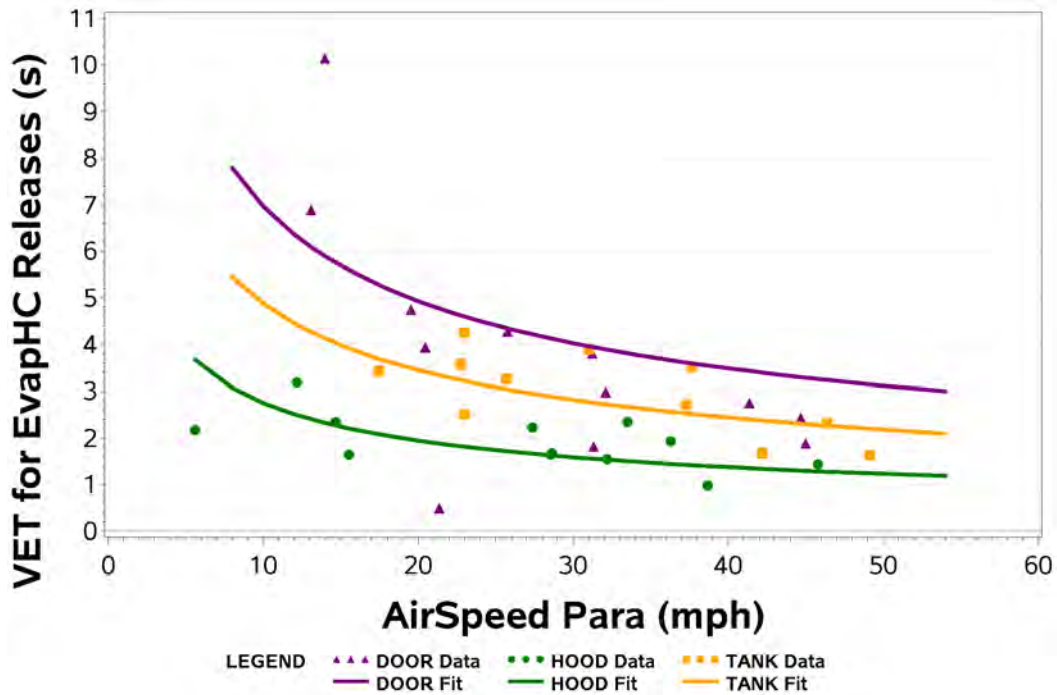**Figure 6-15. VET vs. EvapHC Release Location and Air Speed for F150**

Figure 6-16. VET vs. EvapHC Release Location and Air Speed for GMC

Figure 6-17. VET vs. EvapHC Release Location and Air Speed for Subaru

Table 6-1. Release Location Factors for Test Vehicles

Test Vehicle	Drag Area (ft2)	Release Location	Proportionality Constant VET vs. sqrt (AirSpeed Para)	Release Location Factor
EV-1	8.0	Tailpipe CO2	20.2	≡1.00
EV-1	8.0	Door	20.4	1.02
EV-1	8.0	Tank	12.1	0.60
EV-1	8.0	Hood	7.2	0.36
EV-2	8.0	Tailpipe CO2	16.9	
EV-2	8.0	Door	n/a	n/a
EV-2	8.0	Tank	n/a	n/a
EV-2	8.0	Hood	n/a	n/a
F150		Tailpipe CO2	n/a	n/a
F150		Side	8.2	
F150		Tank	15.0	
F150		Hood	9.9	
GMC		Tailpipe CO2	n/a	n/a
GMC		Side	10.6	
GMC		Tank	12.2	
GMC		Hood	4.2	
Subaru	10.2	Tailpipe CO2	n/a	n/a
Subaru	10.2	Door	22.0	
Subaru	10.2	Tank	15.4	
Subaru	10.2	Hood	8.7	

To get a better view of the trends in the proportionality constants, they are shown in Table 6-2 in a vehicle-versus-release-location grid.

Table 6-2. VET Proportionality Constant vs. Vehicle and Release Location

	EV-1	EV-2	F150	GMC	Subaru
Tail	20.2	16.9			
Door	20.4				22.0
Tank	12.1		15.0	12.2	15.4
Side			8.2	10.6	
Hood	7.2		9.9	4.2	8.7

Table 6-2 shows a trend of decreasing VET proportionality constant as location moves from vehicle rear to front (Tail Door Tank Side Hood). This makes physical sense since plumes of releases tend to spread horizontally and vertically as they move away from their release point. Thus, a smaller portion of pollutant releases from the front of a vehicle is likely to become entrained in the vortex that follows the vehicle rear in comparison with releases from the vehicle rear.

We would like to estimate the relative VET proportionalities among the five release locations even though only 14 of the 25 cells in Table 6-2 have measured values of the VET proportionality constant. We smoothed the relative VET proportionalities by assuming that the

VET proportionality constants differ by location factors across the five locations and also differ by vehicle factors across the five vehicles. We built a categorical model[24] that used these assumptions to arrive at the fitted VET proportionality constants given in Table 6-3.

Table 6-3. Fit of VET Proportionality Constant vs. Vehicle and Release Location

	EV-1	EV-2	F150	GMC	Subaru
Tail	20.2	16.9	22.6	17.3	23.9
Door	19.5	16.3	21.8	16.6	23.0
Tank	13.2	11.0	14.7	11.3	15.6
Side	9.5	8.0	10.7	8.1	11.3.
Hood	6.9	5.8	7.7	5.9	8.2

The model had an r-square of 0.88, an F-value of 144, and the effect of release location was significant at greater than the 99% confidence level. Even though the model did not find that vehicle ID was a statistically significant factor, we left it in the model since we know that vehicles with different drag areas will have different VET proportionality constants. Comparison of the measured VET constants in Table 6-2 with the corresponding fit values in Table 6-3 shows good agreement. The agreement for the F150 and GMC test vehicles, which had fewer transits on which to base their VET constants, is not quite as good as for the other test vehicles.

We then used any column from Table 6-3 to calculate the VET proportionality constant relative to the tailpipe (Tail) location as shown in Table 6-4. The Relative VET factors for release location are appealing because they directly relate to the relative front-to-rear location of the release point: Hood releases are effectively at the firewall (one-third to the rear: 0.34 factor); Sides releases (one-half to the rear, 0.47 factor); Tank releases (two-thirds to the rear, 0.67 factor); quarter-panel fuel-fill-Door releases (almost all the way to the rear, 0.96 factor), and Tailpipe releases (at the rear, 1.00 factor).

Table 6-4. Relative VET Proportionality vs. Release Location

Release Location	Relative VET
Tail	$\equiv$1.00
Door	0.96
Tank	0.65
Side	0.47
Hood	0.34

It is important to note that none of the factors are zero and the factors range from 0.3 to 1. This indicates that there is always a significant chance that a portion of emissions released from a vehicle can get into the vortex that follows the vehicle and that the emissions will always potentially be present for detection by an RSD instrument.

---

[24] P:\EDARinDenver-OCT2019\Analysis_MLout\220817\Anal_MLout\RefVehs/ RelVET.sas

Drag Area Effect

In the September 2016 study, artificial EvapHC was metered at a constant Emission Rate (10,913 mg/mile) from four late-model, light-duty test vehicles while driving the vehicles at four different road speeds. That emission rate was chosen to be large so that any natural EvapHC or ExhHC emissions from the test vehicles would be trivially small in comparison.

Table 6-5 shows the September 2016 study results of the 50 transits made on each of the four test vehicles with a metered, constant EvapHC Emission Rate. The results show that vehicles with larger drag areas had higher VETs than those with lower drag areas. The results also show that for these four light-duty vehicles, drag area had a mild effect on VET. Specifically, the ratio of largest to smallest drag area was 2:1, but the ratios of VETs was only 1.3:1. Thus, for this dataset VET appears to be proportional to approximately the one-third root of the drag area.

Table 6-5. Relative VET by Vehicle Drag Area

Test Vehicle ID	Drag Area (ft2)	Relative VET
1	7.2	0.85
3	10.7	1.10
4	6.7	0.95
5	13.4	1.06

Overall, the analysis indicates that light-duty vehicle VETs follow the relationship given by Equation 5-8 with VET proportional to the relative location of the release point from front to rear, proportional to the one-third root of the drag area, and inversely proportional to the square root of AirSpeed Para. We have not yet quantified the dependence of VET on AirSpeed Perp.

6.5   Vortex Shape (Weights) Functionality

Because in most instances evaporative emissions from well-maintained, latest-technology vehicles are quite low, attempting to quantify or even just detect evaporative emissions using remote sensing devices is challenging. While RSD instruments can make thousands of detailed measurements around each vehicle driving past the instrument, each individual measurement has low signal and high noise. We need to find ways to enhance RSD signals.

When we think about it, we realize that we do not need to know exactly where the emissions are, that is, we do not need to analyze the emissions location in great detail – even though RSDs provide such information. We anticipate that a portion of emissions from vehicles get entrained in the vortex and otherwise disperse behind the vehicle in patterns that may be predictable. If we could predict the pattern, then we could use the pattern as a template for quantifying the emissions in the pattern or cloud of emissions and thus enhance the signal-to-noise ratio.

In this subsection, we analyze the patterns of emissions of vehicles moving through the air to understand the pattern or shape of the emissions clouds around moving vehicles. We minimize the effects of noise for this analysis by using either large artificial gas releases or large natural

vehicle emissions (exhaust CO_2). And we do this with the knowledge that, whether the release rates are tiny or large, the patterns are the same – even though the magnitude of emissions in the pattern is different. Thus, once we understand the shape well enough to predict it, we can use the pattern to quantify the emission magnitude – to convert the thousands of detailed measurements collected for a single vehicle transit into a single emissions value.

Early Trends from September 2016 Data

Although the scientific literature contains results of many computational fluid dynamics (CFD) studies that detail how gases flow around moving bodies, for this methodology a more general description of the dependence of RSD signals from pollutants in the vortex on vehicle operation and pollutant release characteristics is preferred.

The weight functionality characterizes the shape of the vortex as viewed by the RSD when pollutants are released from a vehicle under a range of conditions that are expected from in-use vehicles.

The scansum, which is the sum of all pixels in each RSD scan for each pollutant, is calculated. Figure 6-18 shows scansum time traces for fifteen transits in the September 2016 study when artificial evaporative HC (butane) was released at 10,913 mg/mile from a test vehicle when it was driving under the RSD at 37.5 mile/hour. Each dot in the figure is one scansum. The fifteen transits are made up of four replicate transits with releases from the fuel fill door (Door=purple), under the hood (Hood=green), on top of the fuel tank (Tank=orange), and inside the left-rear wheel well (Well=red).

The traces in Figure 6-18 have been aligned in time at the vehicle rear (Scan=0). The traces in the figure are generally made up of a peak at about Scan 2. After the peak, the traces decay in a variety of paths toward a scansum of zero. This diversity of scansum trace shapes is attributed to turbulence and instrumental noise. Because of this diversity and to get a clearer picture of the overall tendency of the scansum trace shape, the 207 traces for 10,913 mg/mile HC releases were averaged across all four test vehicles, all four test speeds, all four artificial evaporative HC release locations, and all replicates to produce a grand mean trace, which is shown by the black dots on a linear scale in Figure 6-19 and a log scale in Figure 6-20. These figures show that after the initial peak the RSD signal tends to decay exponentially.

Figure 6-18. ScanSum Traces for Vehicle with 10,913 mg/mile HC at 37.5 mph
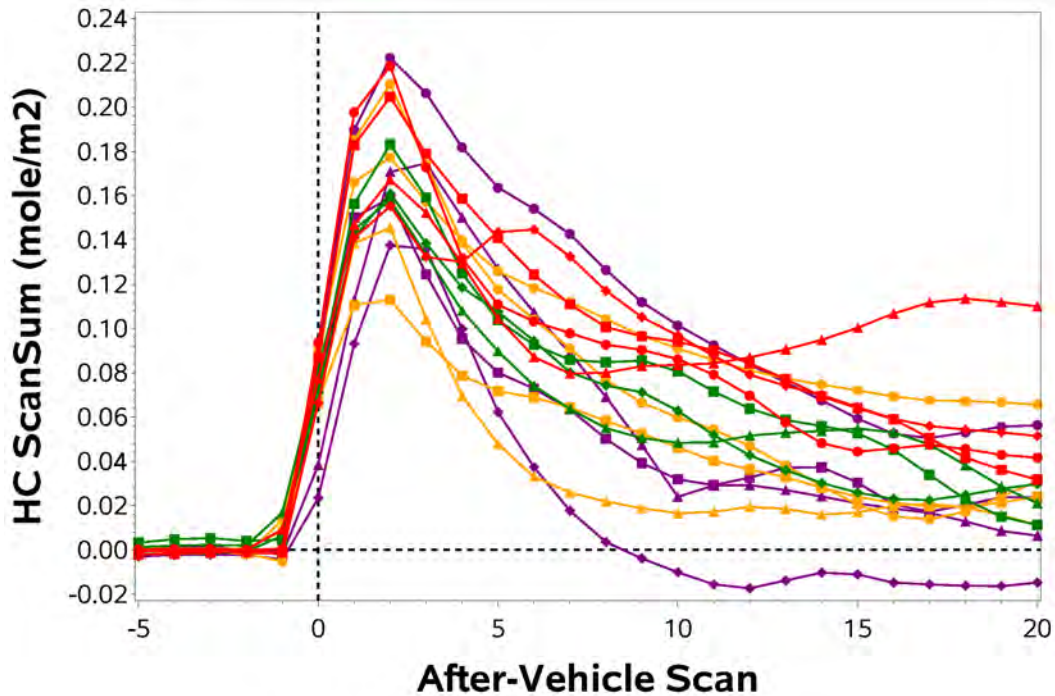
To examine the influences on the grand scansum shape, the 207 scansum time traces were averaged in categories of vehicle identity, road speed, and HC release location. Figures 6-21, 6-22, and 6-23 show the log of the average scansum time traces for the four different levels of each of those categories. Each curve is the average of approximately 50 traces. Just as seen in the grand average log plot in Figure 6-20, the curves in Figures 6-21, 6-22, and 6-23 are characterized by a peak at Scan=2 followed by an exponential decay. The plots indicate that all levels of those categories have close to, but perhaps not exactly, the same scansum time trace shape.

Note that while the <u>shapes</u> of the traces are quite similar, the <u>magnitudes</u> of the traces, as seen by vertical shifts of curves in the log plots of Figures 6-21, 6-22, and 6-23 do vary with the different levels of vehicle, road speed, and pollutant release location even though the HC emission rate was a constant 10,913 mg/mile.

Overall, the analysis of the first measurement dataset with 207 RSD transits on four test vehicles indicated that the shape of scansum time traces depends on time after the vehicle rear and seems to be independent of road speed and vehicle shape. Each scansum time trace shape is characterized by a peak at Scan 2 followed by an exponential decay.

Figure 6-19. Grand Average HC ScanSum Trace for HC Releases
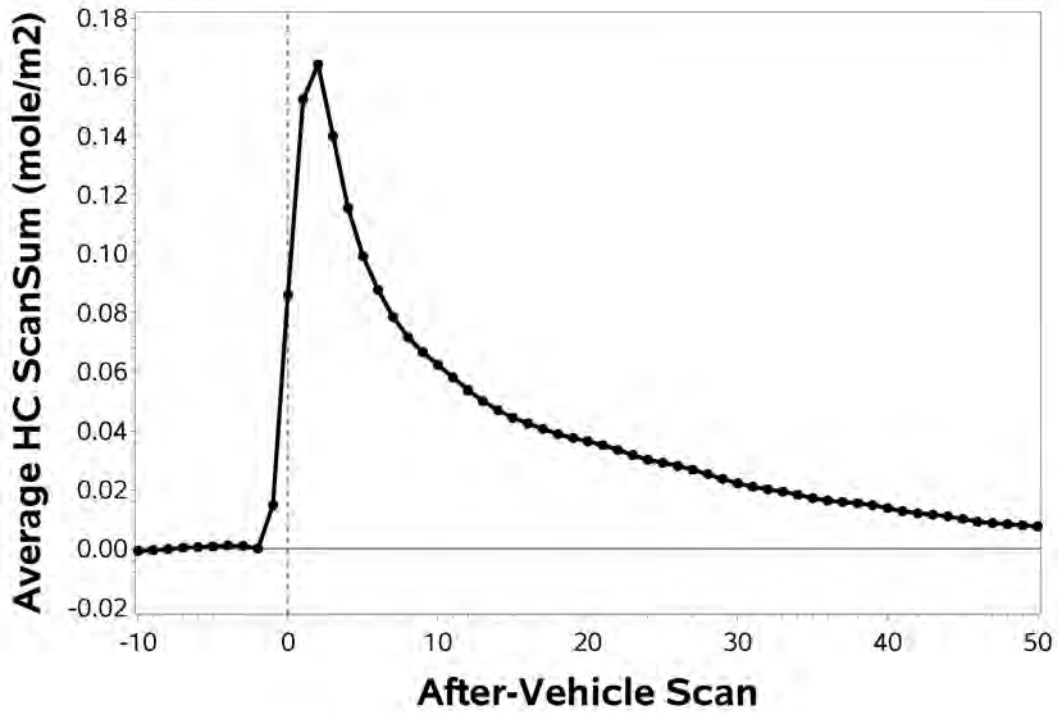
/proj1/EDARatTTI-SEP2016/RunLoss/Analysis/TTI_analysis_HCgrp3_5.sas 13JUL22 09:41

Figure 6-20. Log of Grand Average HC ScanSum Trace for HC Releases
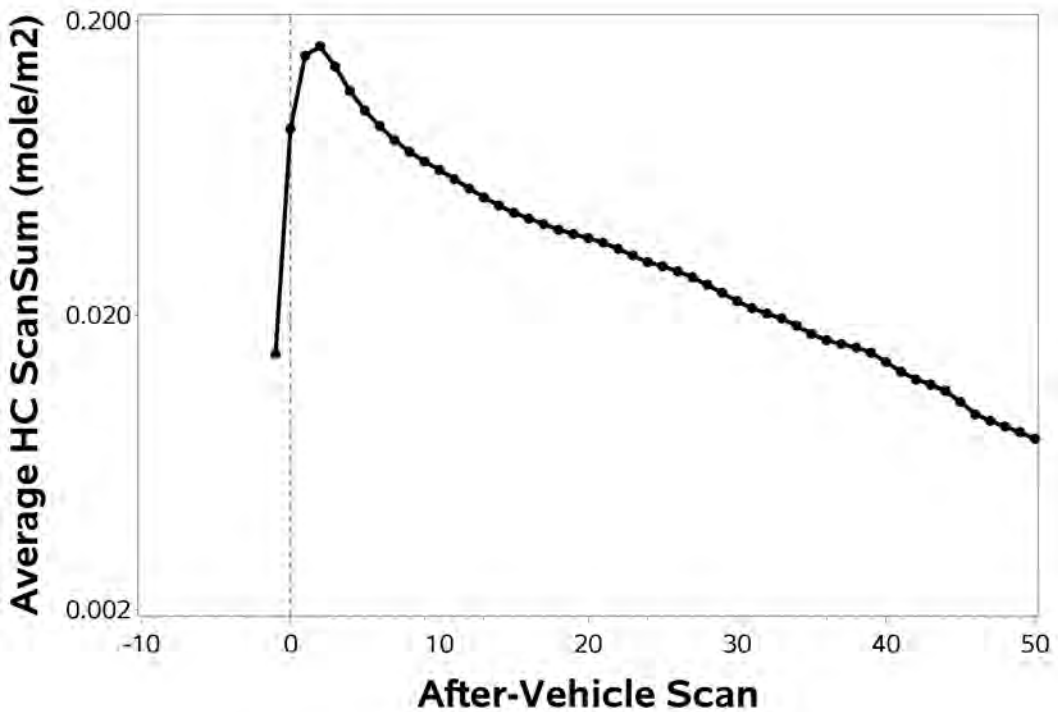
/proj1/EDARatTTI-SEP2016/RunLoss/Analysis/TTI_analysis_HCgrp3_5.sas 13JUL22 09:41

Figure 6-21. Log of HC ScanSum Traces Averaged by Vehicle ID
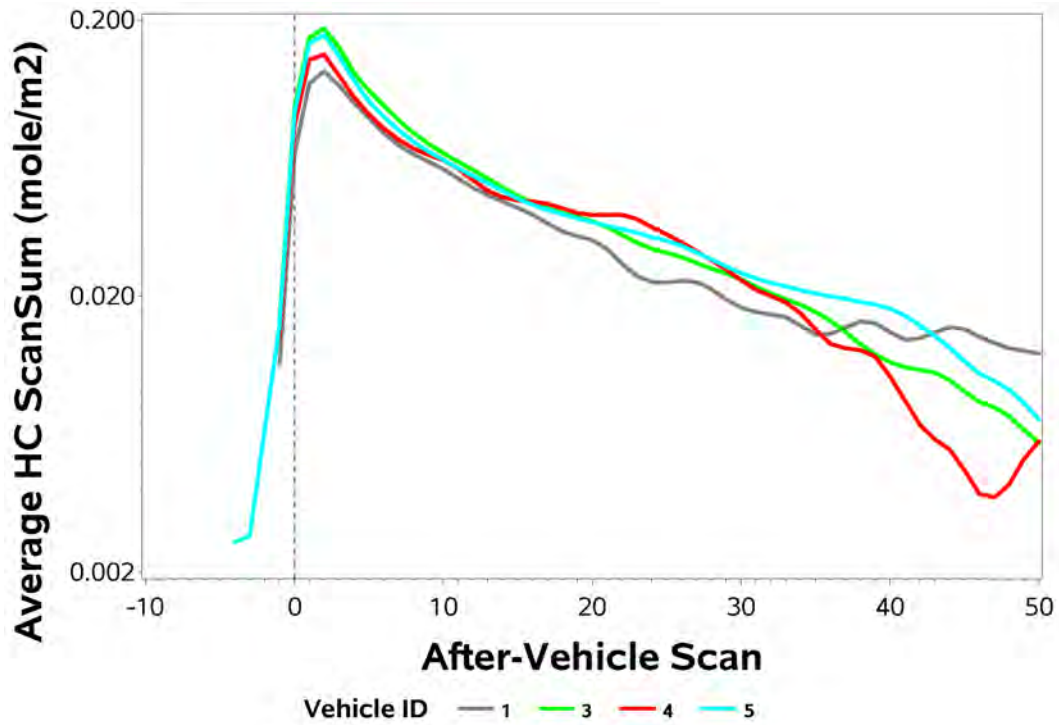
Figure 6-22. Log of HC ScanSum Traces Averaged by Road Speed
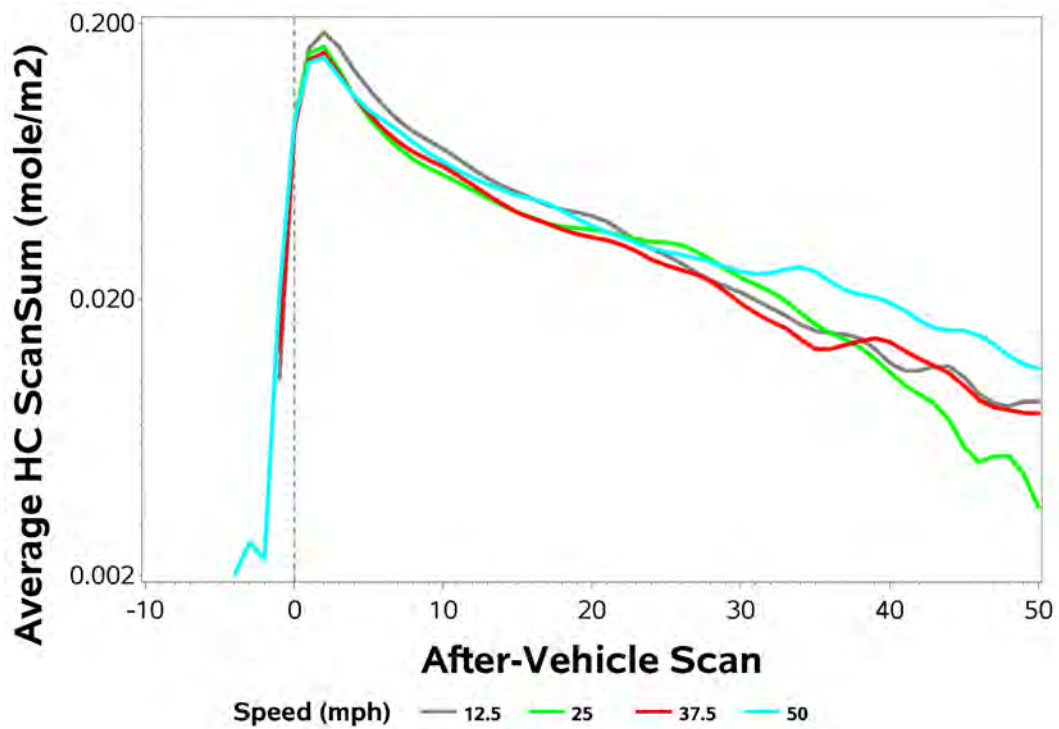
Figure 6-23. Log of HC ScanSum Traces Averaged by Release Location
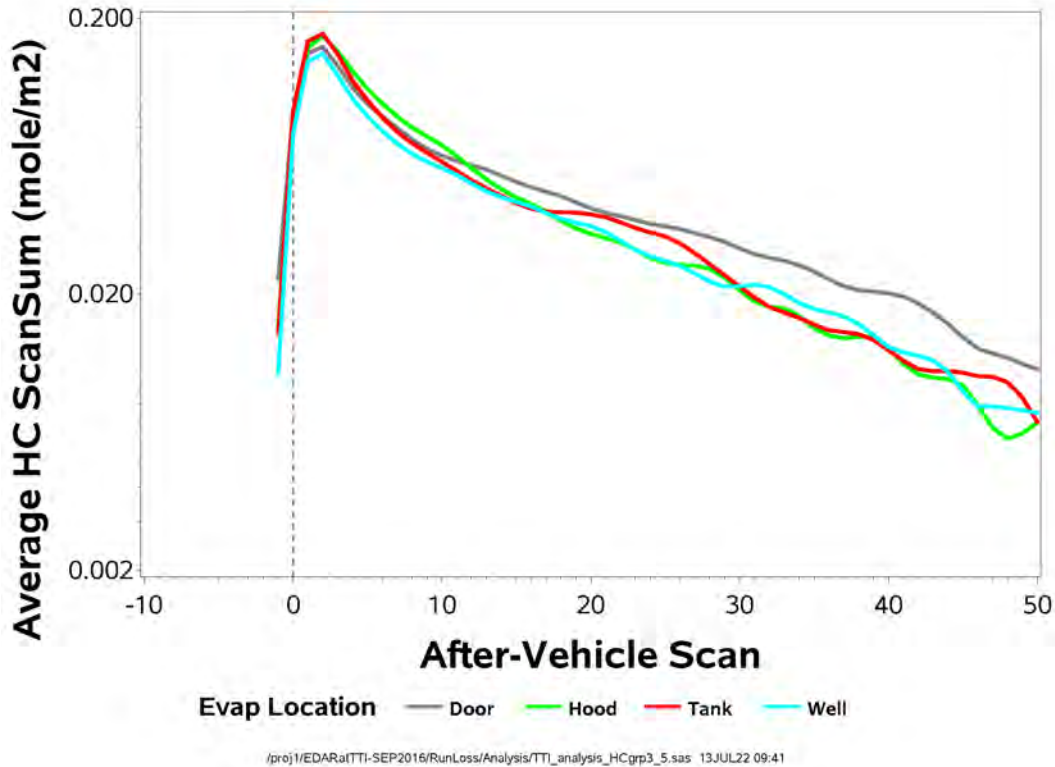
Refined Trends from Westminster October 2019 Data

Analysis of the September 2016 staged data taken on test vehicles indicated that the shape of scansum traces for both exhaust and evaporative emissions in the vortex had the same shape and could be described as a peak followed by an exponential decay. We wanted to confirm that finding using the Westminster data. Further, we wanted to determine the dependence of the shape of scansum traces on vehicle and vehicle operation variables.

The fleet vehicles that produced the 30,000 transits in the Westminster dataset have a variety of shapes and sizes and most use gasoline or diesel fuel and have exhaust plumes containing CO_2. Therefore, we used the CO_2 data collected by the EDAR instrument to examine influences on the shape of the scansum traces.

The CO_2 scansum traces were used to quantify the scansum trace shape. However, to provide accurate scansum shapes, the CO_2 pixel zero baseline must be accurate. The MatLab processing of the raw EDAR data used a histogram of the log of the pixel counts to initially zero-adjust the measured CO_2 detailed data. These initial MatLab baseline offset adjustments will be described in Section 7.1. We then used a SAS program[25] to verify and further adjust the zero of the CO_2 scansums.

---

[25] P:\EDARinDenver-OCT2019\Analysis_MLout\211122\Anal_MLout/OCT19_shapeCO2.sas

We provided the second and final zero-baseline adjustment by considering the CO_2 scansums between the last-before-vehicle scan and the first-after-vehicle scan. Since exhaust CO_2 is not usually present in front of the tailpipe exit, all of these CO_2 scansums should be zero. The SAS program found the median of the scansums in this zone and adjusted all CO_2 pixels for the transit to make the median be exactly zero.

Figure 6-24 shows an example of the procedure. The red scansum trace shows that the sum provided by the initial MatLab zeroing is slightly negative during the vehicle footprint. The green scansum trace is after the median scansum value (at the small orange triangle) is set to zero.

Figure 6-24. Example Showing CO₂ ScanSum Zero Adjustment

/proj1/EDARinDenver-OCT2019/Analysis_MLout/211122/Anal_MLout/OCT19_shapeCO2.sas 21DEC21 10:51
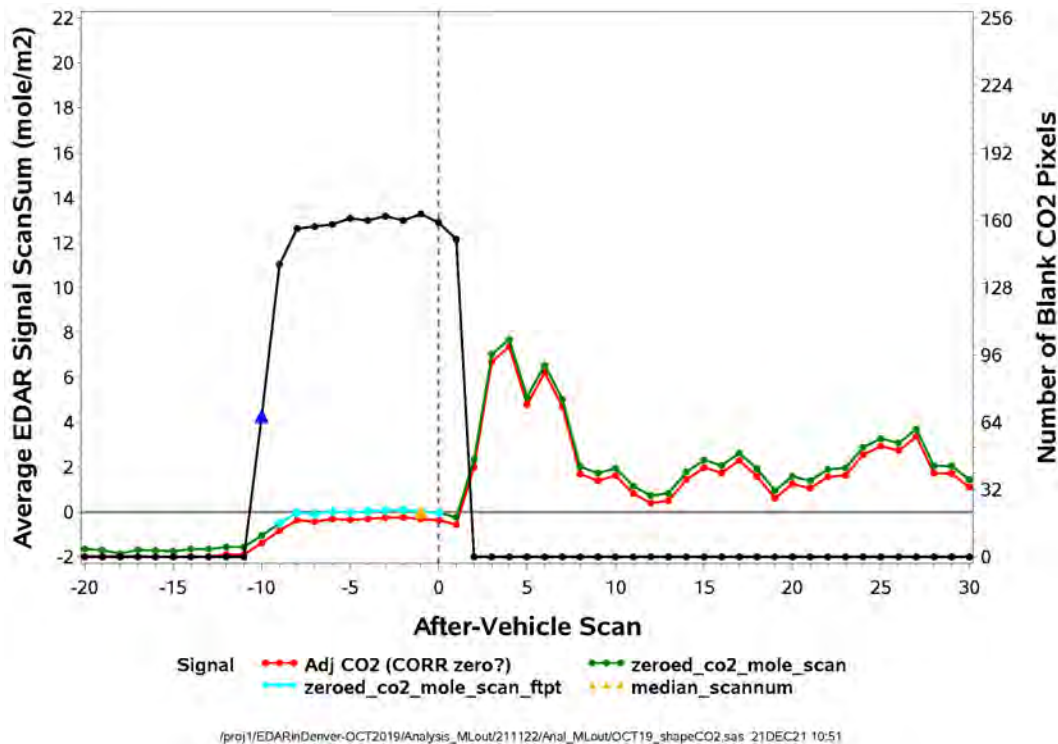
We expected that vehicle air speed has a more intimate influence on vortex shape than vehicle road speed since the movement of air around the vehicle body produces the vortex. Further, based on our examination of average plume contours for different air speed directions, we expected that the component of the air speed parallel to the major axis of the vehicle is the most important component to the formation of the vortex. Figure 6-25 shows a histogram of the air speed parallel component for fleet vehicle transits in the Westminster dataset.

We also expected that the scansum trace shape could also be influenced by the vehicle length. Figure 6-26 shows a histogram of vehicle length for the fleet vehicles in the Westminster dataset as estimated as described in Section 6.2. Most vehicles in this dataset have a length between 9 and 26 feet.

Figure 6-25. Distribution of the Parallel Component of the Vehicle Air Speed

/proj1/EDARinDenver-OCT2019/Analysis_MLout/211122/Anal_MLout/OCT19_interpshapeCO2_2.sas 09MAY22 15:09

Figure 6-26. Distribution of Vehicle Length for Westminster Fleet Vehicles

/proj1/EDARinDenver-OCT2019/Analysis_MLout/211122/Anal_MLout/OCT19_interpshapeCO2_2.sas 09MAY22 15:09

Figure 6-27 shows a scatter plot of all transits as a function of Vehicle Length and AirSpeed Para. Black symbols represent fleet vehicles, and red symbols represent test vehicles. Figure 6-28 zooms in to the region of abundant data.

Because turbulence is always present behind a moving vehicle, scansum shapes are variable – even for replicate transits. Accordingly, we examined averages of shapes of CO_2 scansum traces. We averaged CO_2 scansums of transits in categories of Vehicle Length and AirSpeed Para.

Figure 6-29 shows the averages of CO_2 scansum traces for the Westminster fleet transits in categories of Vehicle Length. Figure 6-31 shows the averages taken for essentially the same transits but in categories of AirSpeed Para. The curves in the two plots have the same general shape – a peak followed by a decay. Figure 6-30 and Figure 6-32 show log versions of the same data. These plots show that beyond After-Vehicle Scan 8 the decays are close to exponential since the lines are straight. Also, the slopes of the straight portions for different levels of Vehicle Length and AirSpeed Para are all about the same – except for low values of AirSpeed Para where the data is less abundant.

At this point in the analysis, we are concerned mainly about the shape of these average CO_2 time traces – not their magnitudes since many things affect the relative magnitudes of the traces including engine displacement, engine RPM during the transit, and frontal area of the vehicle. We present the analysis of the shape of the time traces.

Figure 6-27. Full Distribution of Vehicle Length and Parallel Air Speed
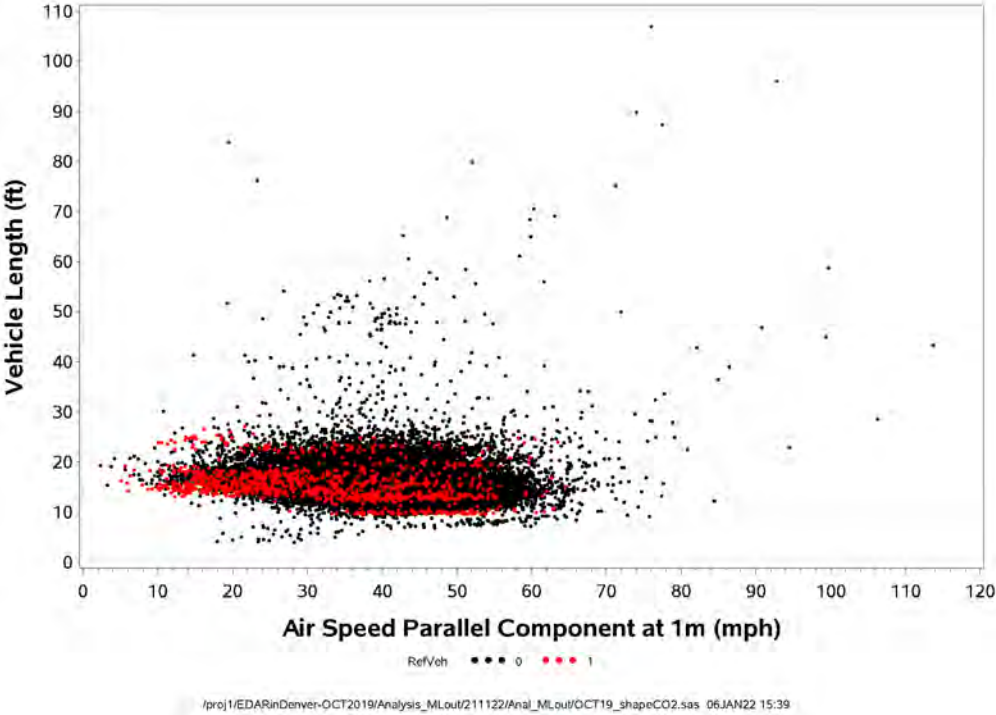
Figure 6-28. Zoomed Distribution of Vehicle Length and Parallel Air Speed
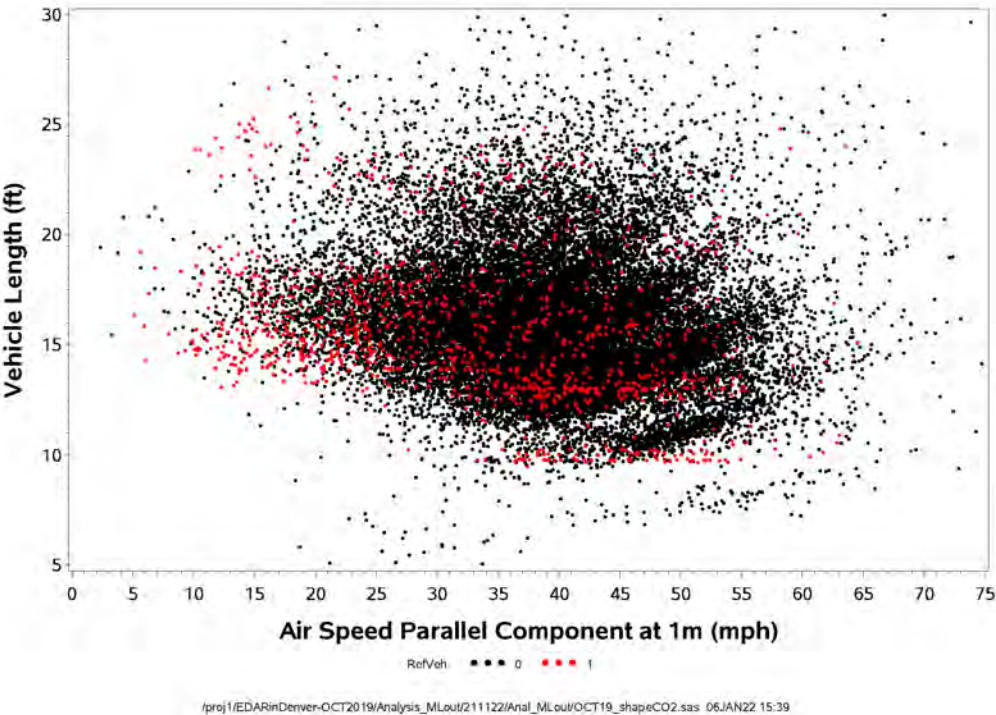
Figure 6-29. CO_2 Mass Trace Averaged by Vehicle Length
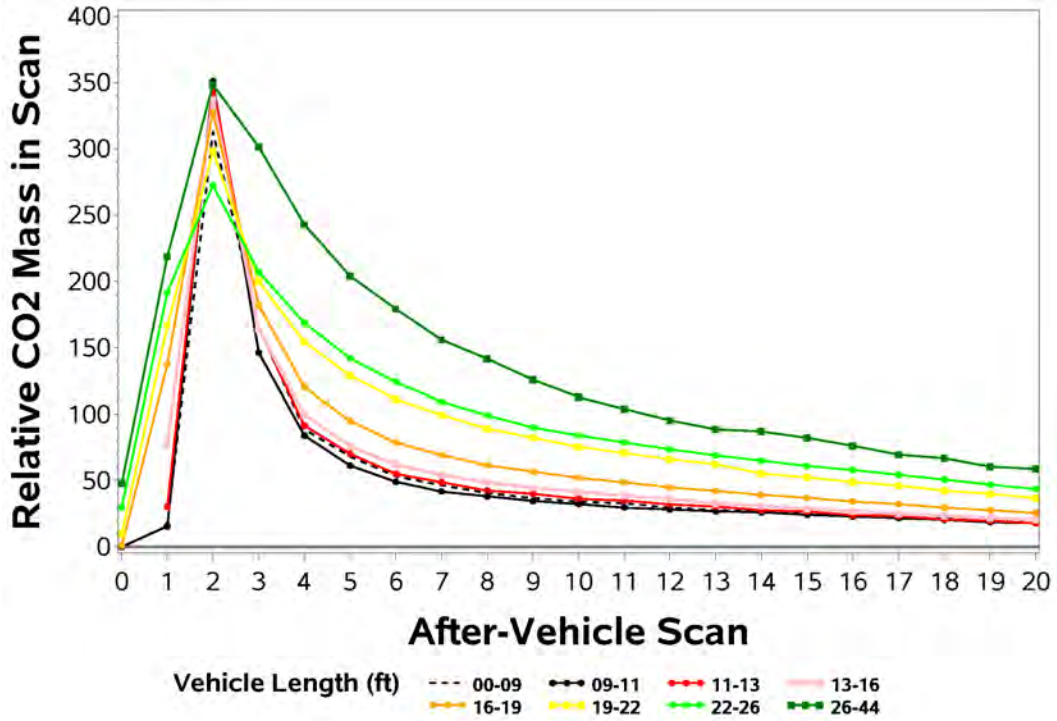
Figure 6-30. Log CO_2 Mass Trace Averaged by Vehicle Length
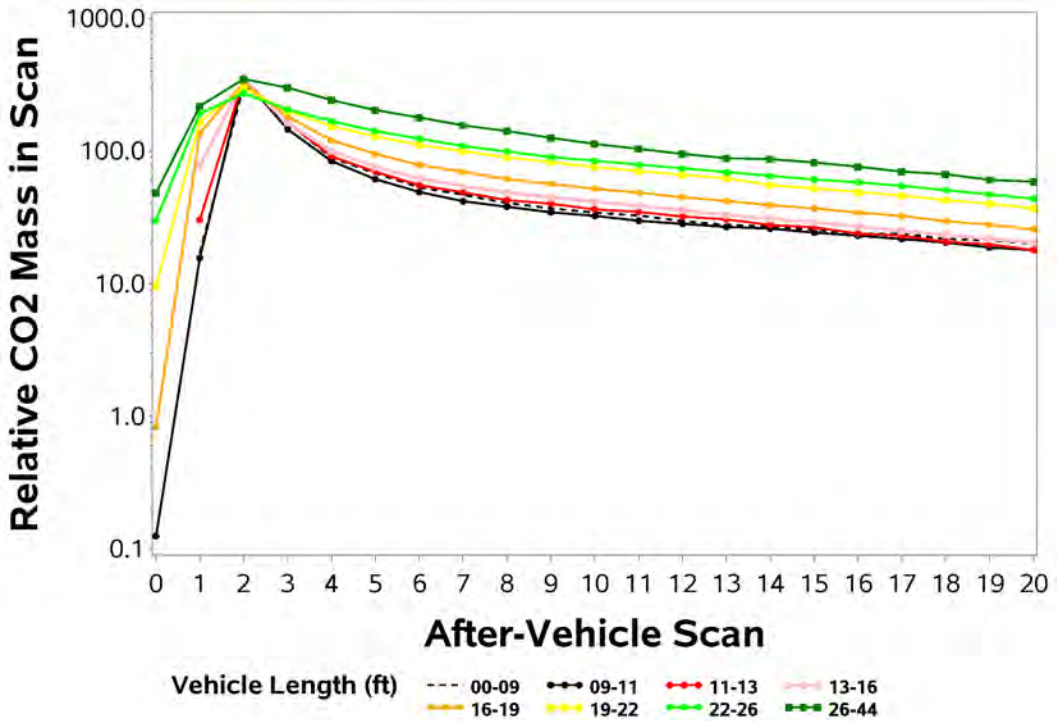
Figure 6-31. CO_2 Mass Trace Averaged by AirSpeed Para
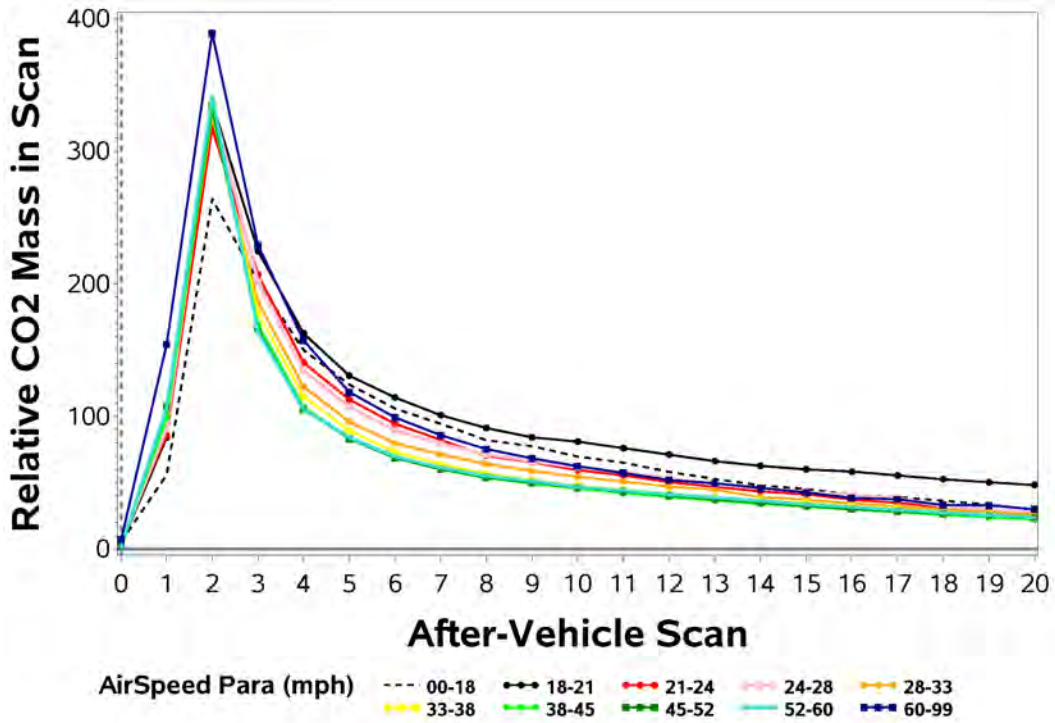
Figure 6-32. Log CO_2 Mass Trace Averaged by AirSpeed Para
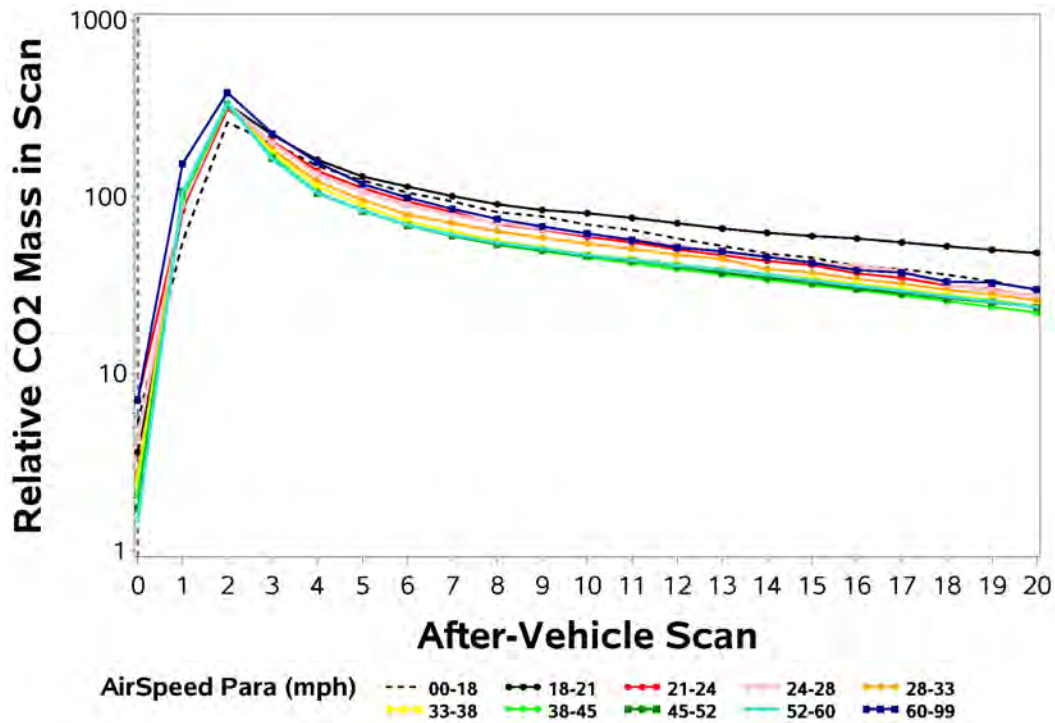
Since the plots in Figure 6-30 and Figure 6-32 indicated that the average slopes beyond After-Vehicle Scan 8 were close to the same value for Vehicle Length categories and AirSpeed Para categories, we quantified the average exponential decay rate for the entire Westminster dataset for After-Vehicle Scan 10 to 20 (0.5 to 1.0 s) using a regression model[26]. Figure 6-33 shows the fit of the Westminster CO_2 scansum traces to an exponential decay with a decay constant of -1.38 +- 0.03 (2 standard errors) s^{-1}.

Figure 6-33. Fit of 30,559 CO₂ ScanSum Traces to an Exponential Decay
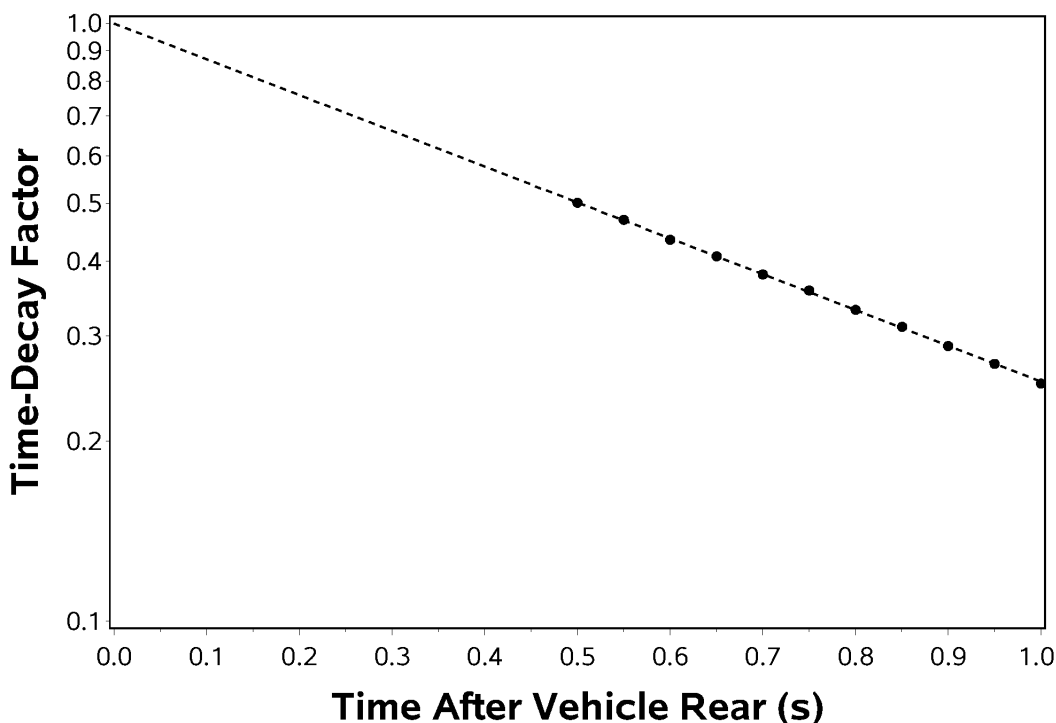
/proj1/EDARinDenver-OCT2019/Analysis_MLout/211122/Anal_MLout/OCT19_interpshapeCO2_5.sas 03SEP22 10:23

We also determined the decay constants for AirSpeed Para and Vehicle Length strata of the dataset. The analysis indicated that the decay constant was the same across all levels of those two variables, which confirms the exponential trends seen in Figure 6-30 and Figure 6-32. Table 6-6 shows mean decay constants and the 95% confidence intervals for the strata and the entire dataset. The table shows that the decay constant has no significant trend across the two stratification variables, since the dataset mean value of -1.38 s^{-1} is within the 95% confidence interval of almost all strata.

These results indicate that the stripping of pollutants from the low-pressure zone, which is quite close to the vehicle rear, into the wake behind the vortex is a first-order process, which can be expressed by the first-order differential rate law:

---

[26] P:\EDARinDenver-OCT2019\Analysis_MLout\211122\Anal_MLout\ OCT19_interpshapeCO2_5.sas

$$\frac{dM}{dt} \quad = \quad k * M \qquad\qquad \textbf{Equation 6-1}$$

where M = Mass of pollutant
        t = time

The rate law says that the rate that the pollutant mass moves out of the low-pressure zone (dM/dt) and into the wake behind the vortex is directly proportional to the mass of the pollutant in the low-pressure zone. If the ambient air has a zero pollutant mass, the integrated form of Equation 6-1 gives the time dependence of the mass in the tail of the vortex:

$$M(t) \quad = \quad M_0 * \exp(k * t) \qquad\qquad \textbf{Equation 6-2}$$

where M_0 is the mass in the low-pressure zone just behind the vehicle.

The RSD instrument takes measurements at constant time intervals since it uses 20 scans per second. Because the pollutants leave the vortex following the time dependence of Equation 6-2, the RSD-measured decay of pollutants in the vortex appears to be independent of the stratification variables. Thus, in terms of time, the vortex length is constant, but in terms of distance, the vortex length is proportional to AirSpeed Para.

Table 6-6. Exponential Vortex Time-Decay Constants for Various Dataset Strata

Stratification Variable	Bin	$N_{transits}$	k Decay Constant (s^{-1})		
			LCLM95	Mean	UCLM95
AirSpeed Para (mph)	00-18	503	-1.38	-1.68	-1.98
	18-21	422	-0.52	-1.04	-1.57
	21-24	793	-1.30	-1.55	-1.80
	24-28	1610	-1.37	-1.51	-1.64
	28-33	3235	-1.27	-1.37	-1.47
	33-38	6119	-1.27	-1.34	-1.41
	38-45	8989	-1.38	-1.43	-1.49
	45-52	6598	-1.24	-1.30	-1.37
	52-60	1980	-1.23	-1.34	-1.45
	60-99	310	-1.11	-1.49	-1.86
Vehicle Length (ft)	00-09	166	-0.60	-1.09	-1.58
	09-11	985	-0.99	-1.15	-1.30
	11-13	4456	-1.33	-1.41	-1.49
	13-16	11525	-1.36	-1.41	-1.46
	16-19	9053	-1.34	-1.40	-1.45
	19-22	3166	-1.22	-1.33	-1.45
	22-26	917	-1.14	-1.28	-1.42
	26-44	206	-0.96	-1.29	-1.62
	44-73	77	-0.87	-1.46	-2.06
	73-99	8	-0.66	-2.54	-4.42
None	All	30559	1.35	**-1.38**	1.41

In the next modeling step, we divided all CO_2 scansum traces by the exponential decay shown in Figure 6-33 to determine the residual of the traces for further analysis. We assigned the residuals to Vehicle Length bins and calculated the average residual trace and its 95% confidence limits for each vehicle length bin.

As an example, Figure 6-34 shows the result for the 19-22 ft vehicle length bin. The blue and red symbols show the lower and upper 95% confidence limits for the mean. The analysis revealed that for all After-Vehicle Scans > 8, a constant value of the Length Factor for each Length Bin plot would stay between the red and blue limits. For example, in Figure 6-34, a value of about 1.5 was within the upper and lower confidence limits for After-Vehicle Scans >8. Therefore, the mean value at After-Vehicle Scan 8 or 9 was held constant for all later After-Vehicle Scans as shown in the figure. For all Vehicle Length bins, these "padded" values remained inside the 95% confidence limits for all Vehicle Length bins.

Figure 6-34. Average Residual CO₂ Scansum Trace for 19-22 ft Length Bin
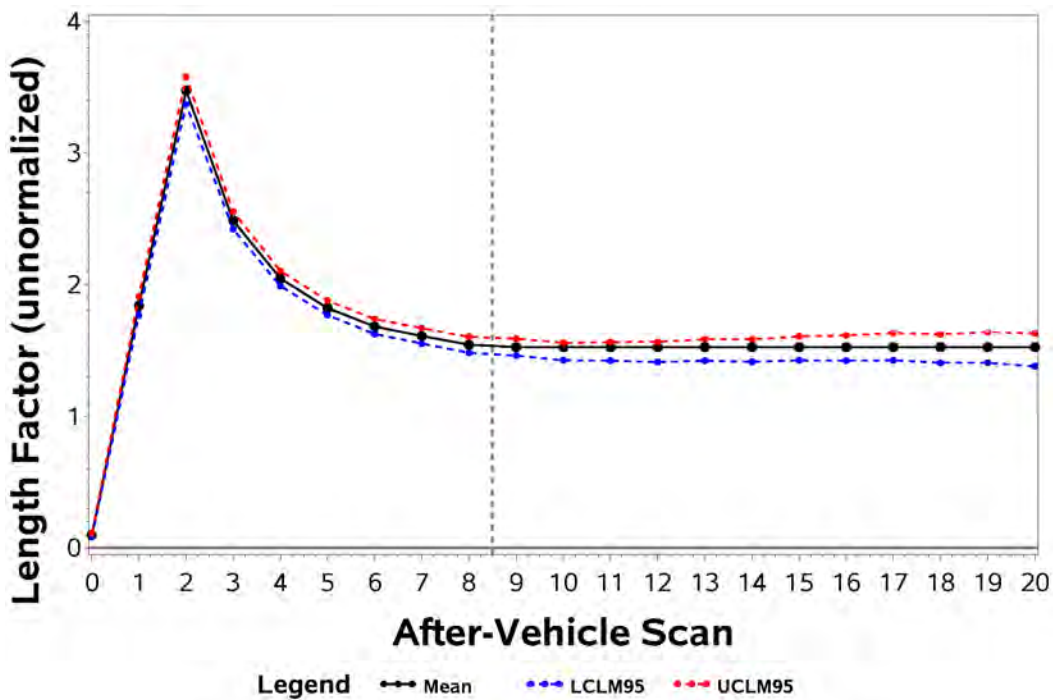
/proj1/EDARinDenver-OCT2019/Analysis_MLout/211122/Anal_MLout/OCT19_interpshapeCO2_5.sas 03SEP22 10:23

The results of this procedure are shown in Figure 6-35 for the eight Vehicle Length bins up to 44 feet. The top two bins (44-73 ft and 73-99 ft) had too few transits to provide reliable results. Since the analysis focuses on the shape of the traces, each average unnormalized trace in Figure 6-35 was then normalized by dividing the trace by the asymptotic value that was used for After-Vehicle Scans > 8. This produced the normalized traces by Vehicle Length bin shown in Figure 6-36. Figure 6-36 shows a constant asymptotic value of 1 for all After-Vehicle Scans > 8, and all of the Vehicle Length effects are concentrated in the first several scans (Scans 0 to 6, 0.0 to 0.3 s) just behind the vehicle. Since the average AirSpeed Para value for each Vehicle Length bin and for the entire dataset was near 40mph, the curves in Figures 6-35 and 6-36 are the effects of Vehicle Length for airspeed Para values near 40 mph.

Figure 6-35. Average Residual CO₂ Scansum Traces for Vehicle Length Bins

Figure 6-36. Normalized Average Residual CO₂ Scansum Traces by Length for 40mph AirSpeed Para
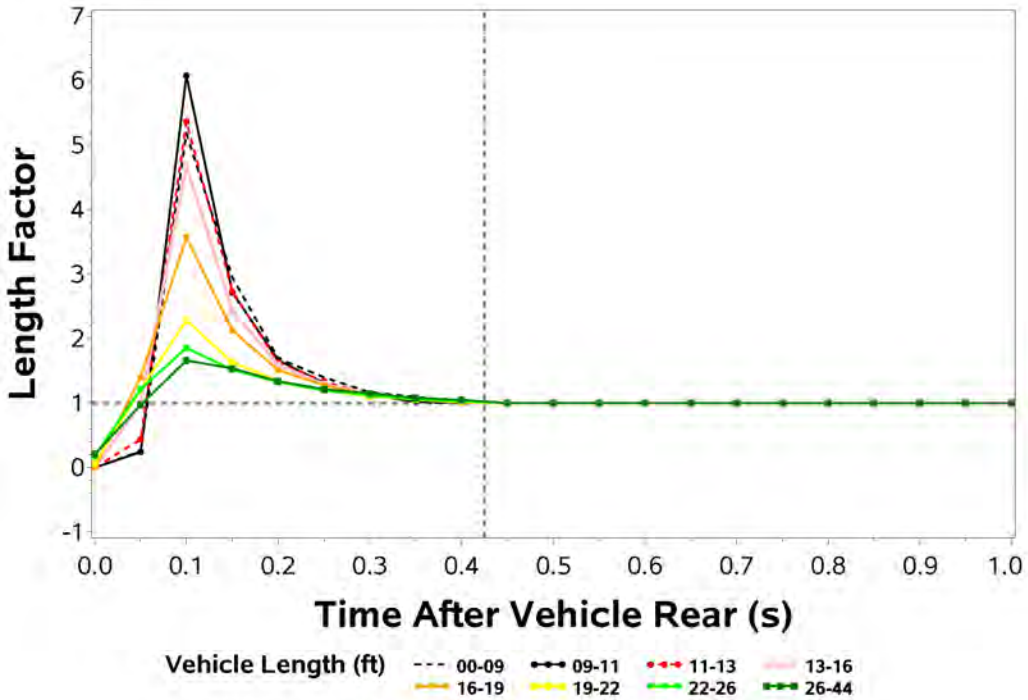
Next, we determine the effects of AirSpeed Para on CO_2 trace shape by removing the effect of Vehicle Length, as well as the time decay. First, all transits were divided by the exponential time decay of Figure 6-33. Second, all transits were divided additionally by the Vehicle Length bin traces of Figure 6-36. Next, the residual traces were grouped by AirSpeed Para bins, and the average residual trace and the 95% confidence interval for each AirSpeed Para bin was calculated. For example, Figure 6-37 shows the result for the 18-21 mph AirSpeed Para bin. The results indicated that for After-Vehicle Scans > 4 the unnormalized AirSpeed Factor could be padded at a constant value for the remainder of the scans without straying outside of the 95% confidence intervals.

The unnormalized AirSpeed Para residual traces for the various bins are superimposed in Figure 6-38. It is apparent the trace shape effects of AirSpeed Para are confined to the first four scans behind the vehicle, which is the first 0.2 seconds of the vortex. Just as for the Vehicle Length factors, we divide each AirSpeed Para residual trace by its asymptotic value to produce Figure 6-39.

Figure 6-37. Average Residual CO$_2$ Scansum Trace for 18-21 mph AirSpeed Para Bin

/proj1/EDARinDenver-OCT2019/Analysis_MLout/211122/Anal_MLout/OCT19_interpshapeCO2_5.sas 03SEP22 10:23
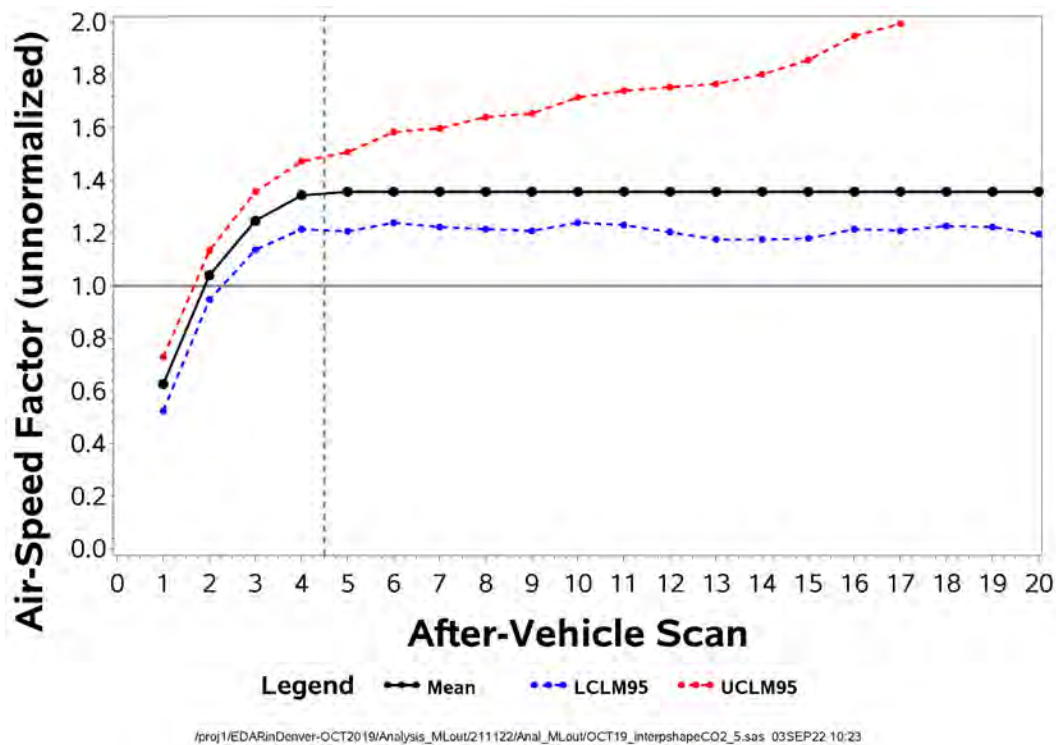
Figure 6-39 shows that if the AirSpeed Para is 40mph, the Air-Speed Factor is 1 for all times after the vehicle rear. If the AirSpeed Para is different from 40mph, Figure 6-39 gives the factor to make the correction to the expected scansum time trace. AirSpeed Paras below 40 mph have values less than 1 near the vehicle rear, and therefore we expect less pollutant mass near the vehicle rear.

By calculating the Air-Speed Factors for Vehicle Length subsets of the dataset, we found that the Air-Speed Factors as shown in Figure 6-39 were relatively independent of Vehicle Length.

Figure 6-38. Average Residual CO$_2$ Scansum Traces for AirSpeed Para Bins
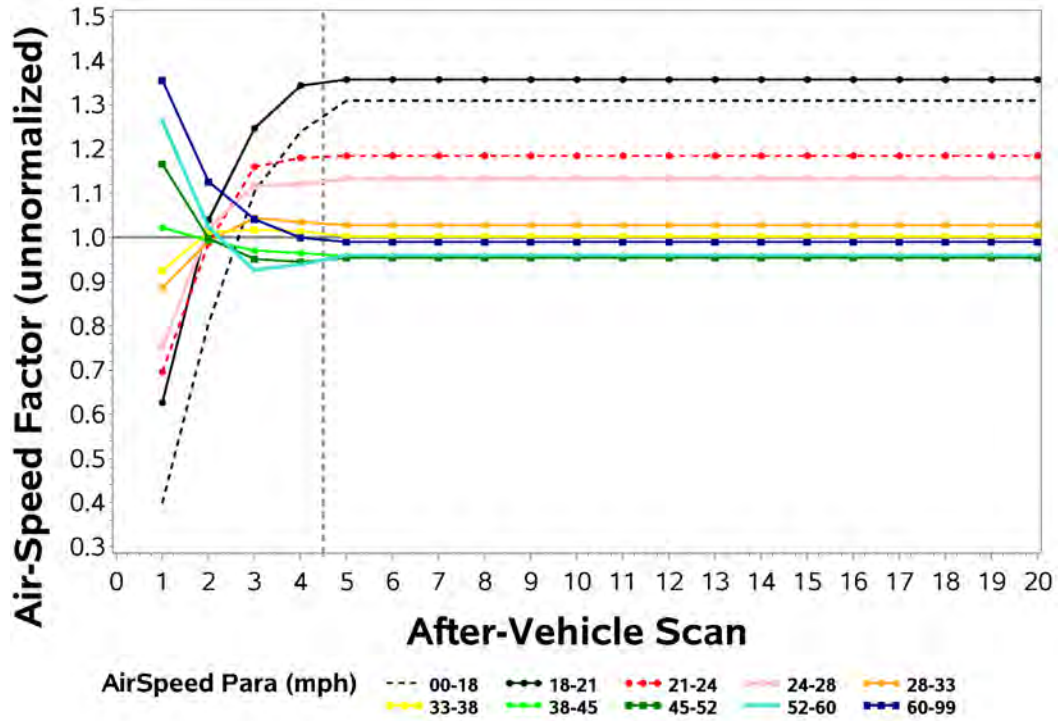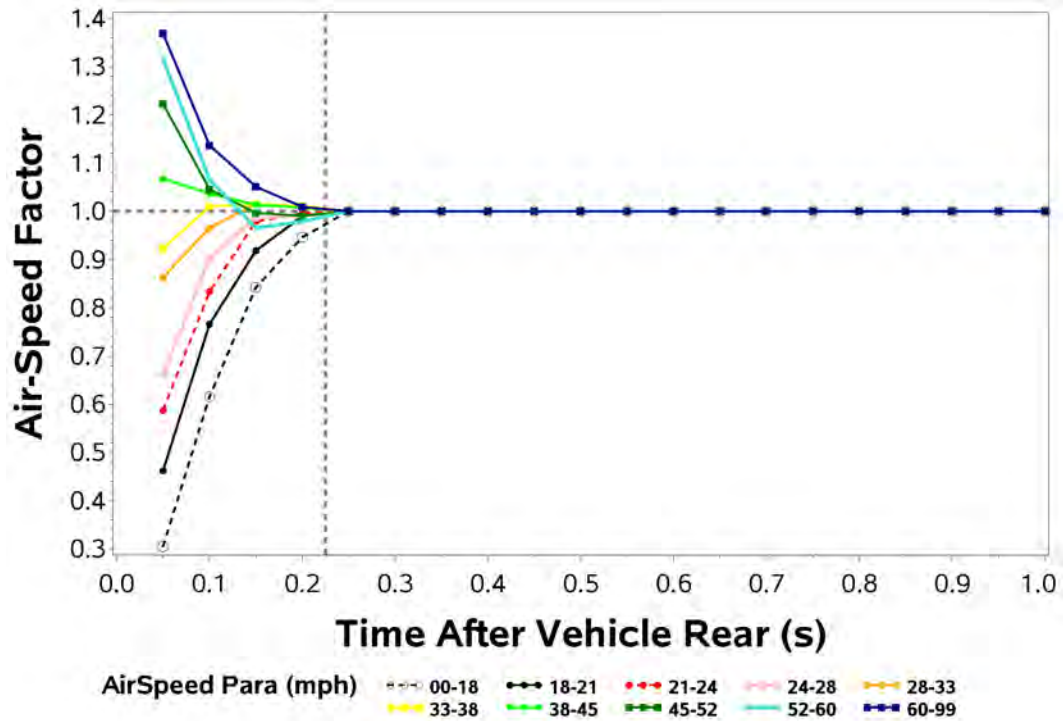

Figure 6-39. Normalized Average Residual CO$_2$ Scansum Traces by AirSpeed

The 207 test vehicle transits of the September 2016 dataset were sufficient to show that the shape of the vortex time traces is characterized by a peak at Scan 2, which is 0.1 seconds after the vehicle rear, followed by an exponential decay. Those 207 transits also indicated that time traces near the vehicle rear had additional dependencies, but the number of transits was insufficient to determine the functionality of the dependencies.

The 30,559 transits of the October 2019 Westminster study confirmed that the exponential decay rate in the tail of the vortex (beyond After-Vehicle Scan 8, which is beyond 0.4 s after the vehicle rear) is independent of vehicle, road speed, vehicle air speed parallel component, release location, vehicle length, and pollutant.

The shape of the vortex peak, which extends from the vehicle rear to After-Vehicle Scan 8, which is 0.4 seconds after the vehicle rear, is additionally influenced by vehicle length and air speed parallel component. The analysis of the exhaust CO_2 in the 30,559 transits quantified the vortex scansum time trace.

Overall, the shape of the scansum time trace is expressed as the product of the Time-Decay Factor of Figure 6-33, the Vehicle-Length Factor of Figure 6-36, and the AirSpeed-Para Factor of Figure 6-39. Parameterizations of these three factors are given by Equations 5-10a, 5-10b, and 5-10c in Section 5.4.

The parameterizations express the expected scansum time trace shape of any vehicle emission in the vortex as a function of Vehicle Length and the component of the air speed in the direction of vehicle motion (AirSpeed Para), which is a function of vehicle velocity and wind velocity.

The average scansum trace shape is important to know because in the current method it is used to smooth and reduce the noise in the EDAR signals obtained from each transit.

6.6   Future Improvement: EvapHC Release Location Detection

The data analysis in Section 6.4 showed that when the EvapHC source location is known, the Vortex Entrainment Time estimate improves, directly enhancing release rate and emission rate calculations. Therefore, we did a scoping analysis to investigate the possibility of detecting emissions zones around the vehicle to determine the approximate location of the EvapHC sources. Further refinement of zone boundaries, ranking plumes based on physical likelihood, and outlier removal may help in EvapHC predictions of greater reliability.

Vehicles can emit EvapHC from various locations. The location of the source affects the emission dispersion and changes the measured EDAR signature. Initially, we looked at the average scansum traces of test vehicle transits grouped by evaporative release location. Figures 6-40, 6-41, and 6-42 show EDAR scansums v. after-vehicle scan number for aggregated Door, Hood, and Tank EvapHC releases from test vehicle transits at 22.5 mph. The black lines track blank CO_2 pixels to show where the vehicle is. Blank CO_2 pixels occur when the vehicle passes over the pavement retro-reflective tape. The blue lines track RSD HC signal strength. Since each scan takes 50 ms, these scansum traces track emissions over time. We see that the signal trace varies depending on the release location. While the Door, Hood, and Tank release rates were equal, the Door signal shows the largest vortex peak. In contrast, portions of the Hood release are blocked from RSD detection during the vehicle transit. These emissions, being farther forward

on the vehicle, are partially masked because of the coincident vehicle footprint, thereby reducing a portion of the signal that the RSD instrument would otherwise obtain. Tank releases are a middle ground between Door and Hood releases; tank emissions have a medium-strength peak that is partially masked by the vehicle footprint.

Knowledge of post-vehicle peak signal intensity alone cannot distinguish among Door, Hood, and Tank releases. For instance, a medium-emission rate Door release and a high-emission rate Tank release may have similar maxima. Additionally, integrating the area tends to underrepresent the emission rate of Tank releases due to the emissions masking by the vehicle footprint. As HC levels increase within the vehicle footprint, the vortex peak decreases. From observing the gradual buildup of emissions during the vehicle footprint in Figure 6-41 (After-Vehicle Scans -11 to 0), we theorized that with additional spatial analysis of the EDAR array, we could estimate the release location of a given transit.

We created aggregate heatmaps to detect release location trends. Averaging enhances location information by mitigating outliers and reducing apparent noise to more clearly image trends than can be seen in the heatmap of a single transit. Figure 6-43 shows RSD field test results from releases of artificial EvapHC and artificial ExhHC from the EV-2 all-electric test vehicle. Each panel, which was made by averaging approximately fifty transits, includes a vehicle footprint, depicted by the white pixels, moving towards the left. For each panel, substantial perpendicular air speed was blowing from the bottom of the figure towards the top. The ExhHC emission rate was metered at 1660 mg/mile and was released from the tailpipe, whose location is denoted with a black circle. EvapHC was released at 1600 mg/mile from the Hood, Tank, or Door with positions denoted by the black triangle in the second, third, and fourth panels. No EvapHC was released in the first panel.

The ExhHC releases are seen as regions of high intensity in the panels, directly behind (to the right of) the black circle, which weaken with increasing distance from the point of highest intensity. The clouds of ExhHC appear with similar spread and false color in all four panels.

By examining the differences among the panels, we begin to see the regions that evaporative emissions tend to populate. The second panel with its under-Hood EvapHC release shows a high-mass HC plume on the right side of the vehicle (near the top of the panel) as well as light EvapHC Mass in Vortex area behind the vehicle (right of the footprint). In the third panel, the Tank EvapHC release, originating from below the vehicle, shows an even dispersion of HC behind the vehicle. In the fourth panel, the fuel Door EvapHC release shows a high concentration (red pixels) of HC mass at the release location with a bright yellow plume being pulled into the vortex.

The different patterns of EvapHC releases from different release locations suggests that a pattern recognition algorithm could be used to estimate the approximate location of EvapHC sources. Estimated EvapHC emissions location coupled with the measured AirSpeed Perp would be used to improve the selection of an appropriate relative VET factor for the effect of release location (see Table 6-4) for the transit.

Figure 6-40. EDAR Scansums v. Scan Number for DOOR Evaporative Releases

Figure 6-41. EDAR Scansums v. Scan Number for HOOD Evaporative Releases

Figure 6-42. EDAR Scansums v. Scan Number for TANK Evaporative Releases
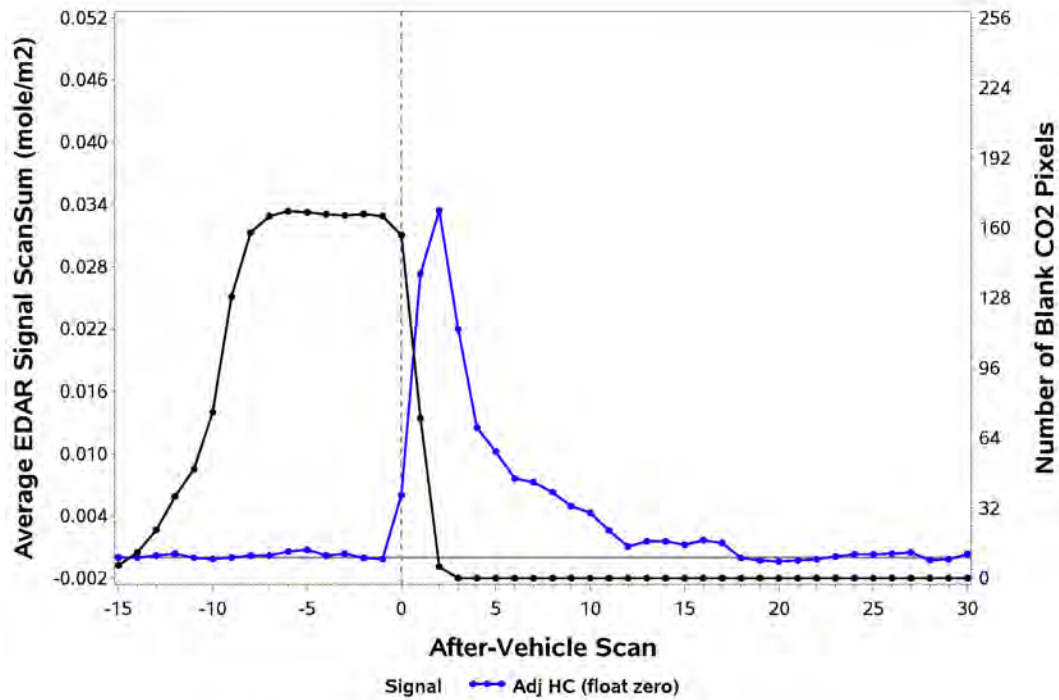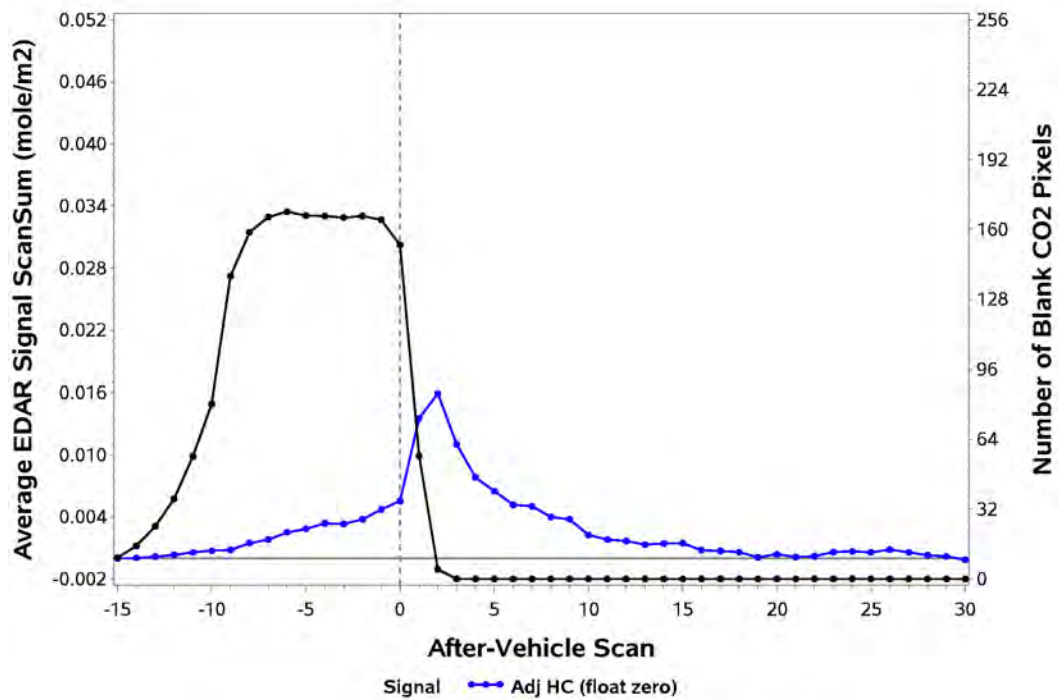
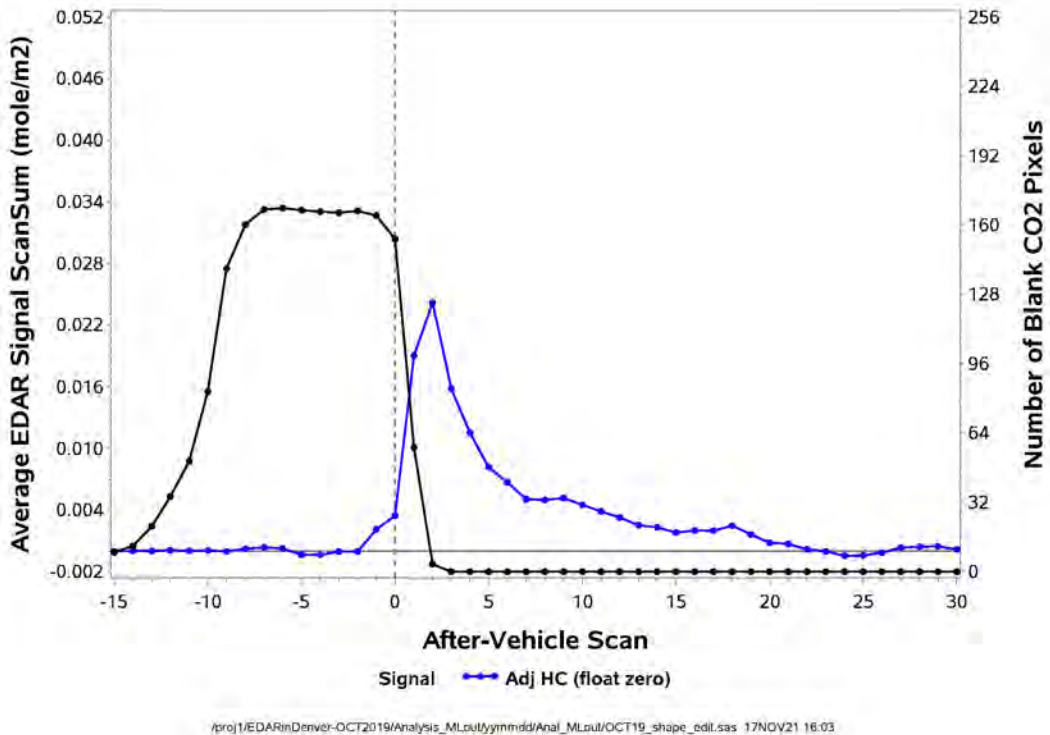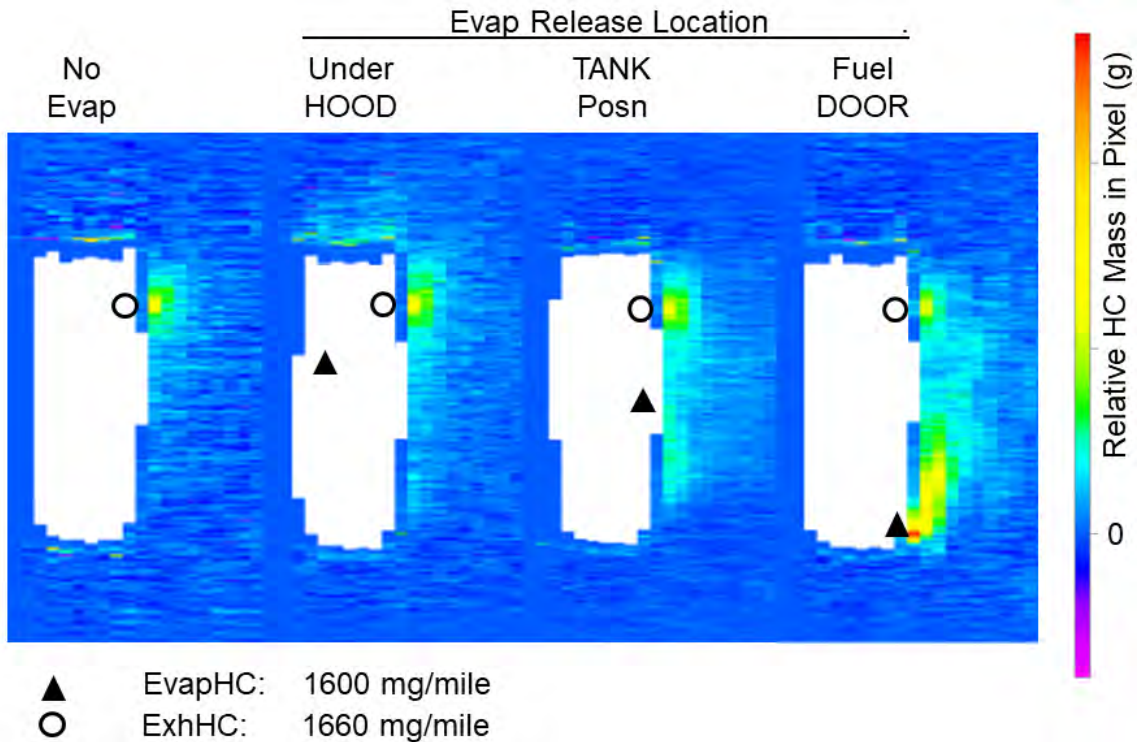/proj1/EDARinDenver-OCT2019/Analysis_MLout/yymmdd/Anal_MLout/OCT19_shape_edit.sas 17NOV21 16:03

Figure 6-43. EV-2 HC Releases from Different Locations in a Transverse Air Flow

The dispersion patterns of EvapHC for different release locations were enhanced in the panels of Figure 6-43 by averaging the arrays of approximately 50 high-EvapHC individual transits per panel. For standard RSD field operation, EvapHC release location would need to be estimated from just a single transit when the EvapHC release rate may or may not be high. Under these circumstances, noise in the RSD signal becomes an issue because noise in individual pixels obscures the EvapHC signal.

To reduce the effects of noise, we began the development of zones around and behind the vehicle to locate the origin of various emissions. Zones help classify emissions surrounding a vehicle. By comparing the average signals of different zones, we protect against outliers and can lower the detection limit. Figure 6-44 shows a conceptualization of zones that could be used to help determine emission release location. If, for instance, the zone-average EvapHC signals were greater than the average noise level in Zones 4 and 6, and if the airspeed data indicated substantial air flow from vehicle left to vehicle right, one possible explanation would be an under-hood EvapHC release. The morphology of these emissions would match that of the second panel of Figure 6-43, where an under-hood evaporative release dispersed to one side of the vehicle and also to the vortex. However, if similarly sized EvapHC signals were found in Zones 5 and 6, but not in Zone 4, then the finding could indicate an EvapHC release location closer to the rear of the vehicle as for the Tank location in the third panel of Figure 6-43. Thus, it is possible that classifying EvapHC release location by assessing the relative strength of RSD signals found in distinct zones can help explain the emissions and its associated factors.

During our preliminary analysis[27], we identified rectangular zones around and behind the vehicle. From the test vehicle data, we correctly identified the evaporative release location at a rate greater than 50%. A single transit with a high-release rate at the Hood of a test vehicle is shown in Figure 6-45. In this figure, the vehicle footprint is moving down towards the bottom of the page, with a back bumper position at about 30 on the y-axis. Here, we see a significant plume emanating from the side of the vehicle. Test vehicle data, however, represent ideal conditions with known releases of large amounts of EvapHC. Due to the typically low emission rates of fleet vehicles, we did not apply our model to the fleet. Novel test transits, in addition to a more sophisticated or machine-learning model, could enable fleet-level EvapHC emissions detection.

Test transits tailored to enhance release location detection could be part of a future evaporative emission study. We would like to improve release location detection because of the enhancement it brings to Vortex Entrainment Time, which directly affects release rate and emission rate calculations. During the 2019 Westminster study, the test transits focused around two all-electric sedans. We now know that Vortex Entrainment Time is mildly correlated with both vehicle shape and emission release location. Due to the high variability of a single transit, multiple Door, Tank, and Hood test releases on larger SUVs, light duty trucks, and medium/heavy duty trucks would strengthen the release location prediction model. Furthermore, the latest noise reduction and separation techniques have enhanced the overall signal-to-noise ratio. Such improvements promote focusing on medium-to-low HC release rates, which have greater applicability to fleet-level evaporative emissions.

---

[27] P:/EDARinDenver-OCT2019/Analysis_MLout/211118/Anal_MLout/
OCT19_hoodEvapProfile_standard.sas

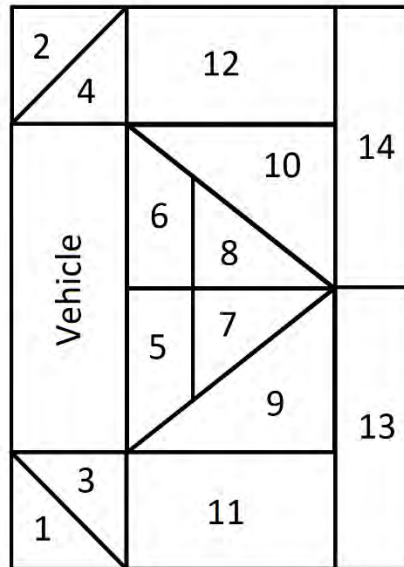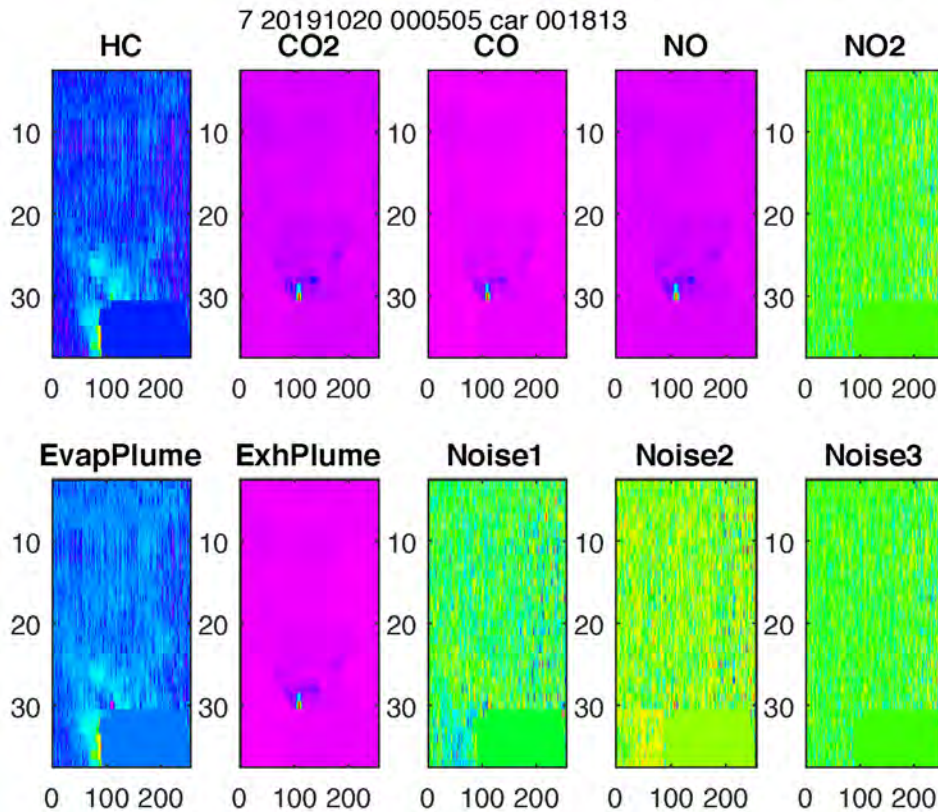**Figure 6-44. Example Zones for Detecting Releases from Vehicle Locations**

Figure 6-45. EvapHC Hood Release for a Single Transit in a Transverse Air Flow

7.0 Demonstration of Signal Analysis of RSD Detailed Data

7.1 Adjustment and Improvement of RSD Detailed Data

Figure 7-1 displays raw EDAR detailed data for an example vehicle transit from the Westminster dataset. The direction of vehicle motion for each panel is vertically toward the bottom. The colors shown represent relative amounts of each pollutant for the five data channels: HC, CO_2, CO, NO, and NO_2. No corrections have been applied to this example dataset.

Figure 7-1. Detailed Data Patterns for Example Westminster Transit

7 20191023 000512 car 001188
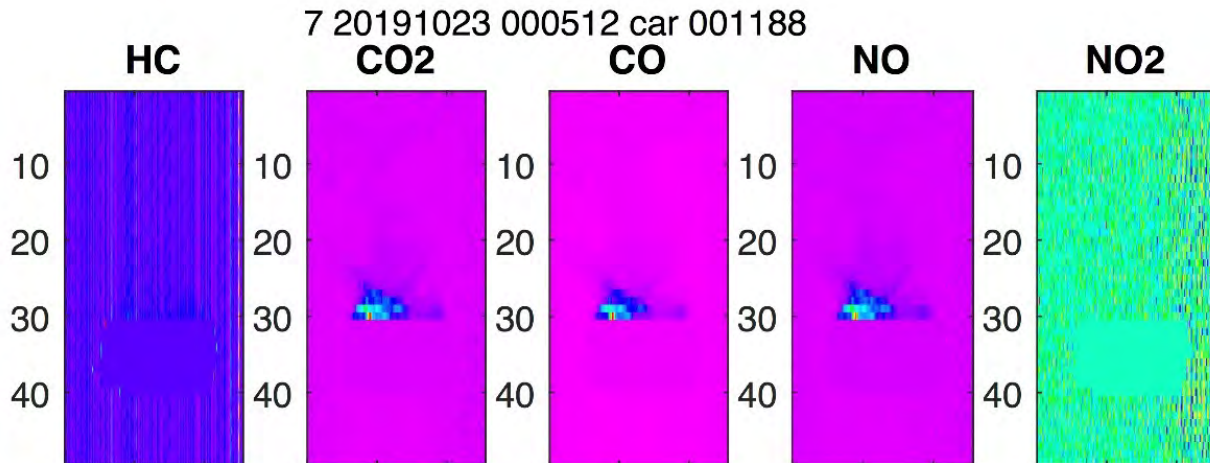
The Pre-Processing Device performs the following four signal improvements to the incoming EDAR measurements presented to it, in the order shown:

1. Adjust constant-level offsets
2. Remove outliers
3. Filter non-physical components

   a. De-stripe in the direction of vehicle travel using multi-tonal cancellation (HC only)

   b. Adaptive notch filter in the direction of the across-road scans

4. Interpolate measured transit data to a rectangular grid

Each channel of incoming EDAR measurements is treated independently and identically in terms of its processing, with two exceptions:

- When filtering non-physical components, the HC channel is processed differently from the other measurement channels. The HC channel data is processed using multi-tonal cancellation followed by adaptive notch filtering, whereas the other channels (CO_2, CO, NO, NO_2) are processed using adaptive notch filtering only.
- When applying adaptive notch filtering to all data channels, the NO_2 channel is used to adaptively estimate the frequency of the notch disturbance to be removed.

Table 7-1 shows which processing step is performed on each of the data channels.

Table 7-1. Application of Improvement Steps to Transit Data

Improvement Step \ Data Channel	HC	CO$_2$	CO	NO	NO$_2$
1. Offset Adjustment	X	X	X	X	X
2. Outlier Removal	X	X	X	X	X
3. De-striping via Multi-Tonal Cancellation	X				
4. Adaptive Notch Filtering	X	X	X	X	XO
5. ZigZag Interpolation to Rectangular Grid	X	X	X	X	X

X - Applied to each data channel independently
O - Used in procedure across all applied channels

Each of the five signal adjustments is now considered.

Adjusting Constant-Level Offsets

Processing Rationale – As provided, the EDAR detailed data measurements have been calibrated by HEAT such that the values nominally represent mass measurements (mole/m^2). Since mass is always non-negative, these calibrations would appear to be straightforward to do. On examination of the data, however, it became clear that measurement noise causes some of the values in the EDAR data to be negative, which is non-physical. This means that the zero reference of each channel is not obvious. Moreover, the zero reference may not be set exactly by the EDAR instrument. An inaccurate setting of the zero reference would create a bias of the mass measurements[28] in any data channel, thus leading to a bias in any calculations using these mass measurements. Fortunately, the statistical behavior of this noise is a feature that can be used to set a zero reference for each measurement channel in each transit independently.

The procedure for finding the zero reference is based on the following concept. If the noise in each channel is additive and Gaussian with a bell-shaped histogram, then the peak of this noise will define the zero reference. The peak can be found precisely by the following steps:

1. Compute the histogram of each measurement channel in each transit.

2. Take the logarithm of the number of counts in each histogram bin. The logarithm turns the histogram count values around the zero reference into a parabola facing downward.[29]

3. Fit a parabola to the log-histogram points for values below a data-dependent threshold. Currently, this threshold is set as 20% of the maximum histogram pixel count for each bin count. This threshold removes bin values that contain both outliers and likely plume pixels.

---

[28] Note that zero-offset inaccuracies have little effect on EDAR's routinely reported exhaust concentration values.

[29] The expected parabolic shape is a consequence of the functional form for the bell-shaped curve.

4. Find the peak of this parabola. This is the zero reference for the measurement channel for the given transit.

This method does not make use of the locations of the signal-free measurements in the transit.

The values used for this offset estimation process include all pixels in each channel except the following:

1. Pixels that have been determined to be clipped values. As delivered, the Westminster data has been adjusted by HEAT with certain pixels clipped to an arbitrary negative value. It is presumed that these pixels have been deemed to be "too negative to be valid." The negative value that replaces these pixels is non-physical and alters the histogram counts in an erroneous manner. These pixels are easily identified, as they are set to the same minimum value. These pixels are detected and removed from the histogram formation.

2. Pixels that have been artificially adjusted to near-zero. As delivered, the Westminster data has a number of pixel values that are unnaturally close to zero, yet these pixels are not vehicle pixels. The non-zero value of these pixels registers as a peak in the histogram, and this peak is ignored in the processing.

3. Pixels counts that fall below a percentage threshold. The noise histogram need only have pixel counts that extend across the two sides of the parabola after the log has been applied. Thus, we limit the range of these pixel counts to those bins whose counts are at least 20% of the maximum count of any one bin. The 20% rule used in this detection appears to provide good performance for the image sizes and pixel counts contained in the Westminster dataset.

This method assumes that there are many samples (pixels) in each measurement channel that have little to no signal in them. When a plume is present, it typically has a limited spatial extent, such that the number of low-level values in the plume is small relative to the number of measurements in the entire transit. Therefore, this assumption is often reasonable. The method might have difficulty in situations where a) the measured transit is short, with not many scan lines after the vehicle, b) the plume has a large spatial extent in terms of the number of nonzero values relative to the number of sample measurements in the transit, and/or c) the background of the transit channel is not flat, e.g. there is an unnatural shape or curvature to the overall channel image. In the first two of these cases, the method is data-starved for the particular channel. In the last case, the image data does not fit the histogram model.

Figure 7-2 shows an annotated plot for all pixels in the CO_2 raw detailed data in Figure 7-1. The CO_2 pixel optical masses were binned with a bin width of 0.00145 mole/m^2. Figure 7-2 shows the log of the pixel count in each bin vs. the midpoint value of each bin. Bins from -0.03 to about 0.01 contain counts of CO_2 optical mass values that are dominated by noise and create the concave-downward parabolic shape. A quadratic fit to these points provides an estimate of the zero reference and the standard deviation of the noise. These values correspond to most of the pink area of the second panel of Figure 7-1. Values larger than about 0.01 mole/m^2 are smaller in number than for noise, but they begin to deviate from the parabola because they are influenced by signal. The figure shows that there are only three pixels that have CO_2 optical masses greater than 0.40 mole/m^2. These three important pixels are for the CO_2 mass just behind the tailpipe exit and are the red pixels in the second panel of Figure 7-1.

Figure 7-2. Histogram of CO_2 Pixel Counts for Series=512 Transit=1188
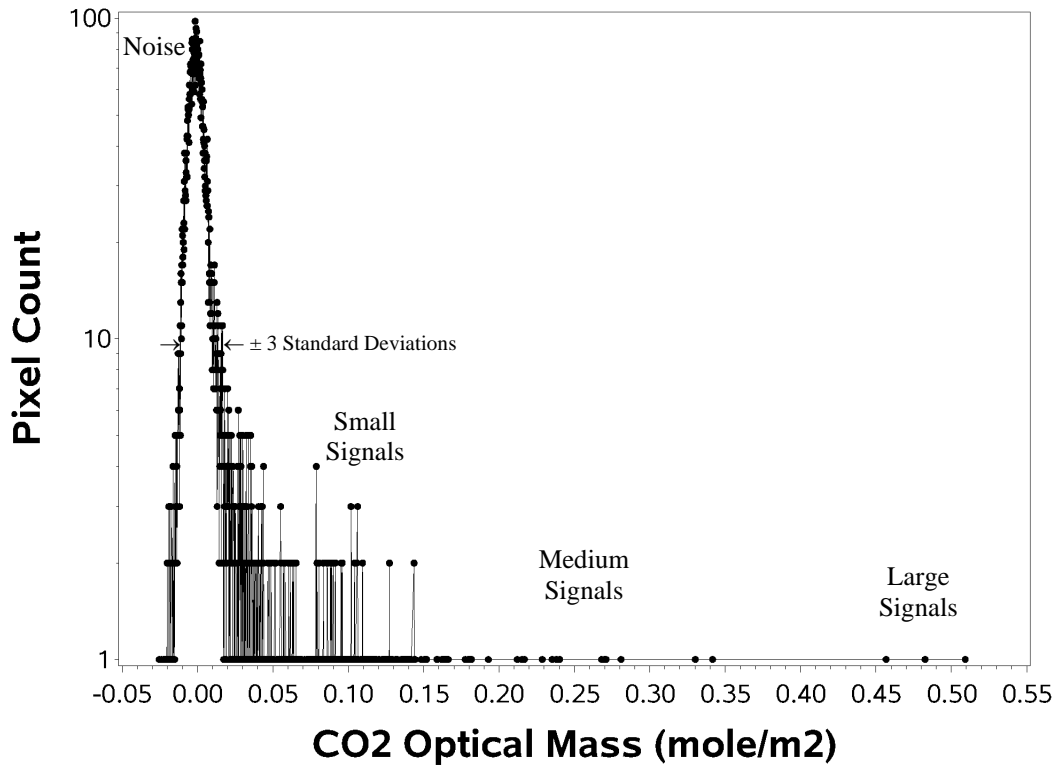
/proj1/EDARinDenver-OCT2019/Analysis_MLout/220817/Anal_MLout/OCT19_CO2_bin_plot.sas 27FEB23 12:46

Processing Examples – We now provide examples of the offset estimation method as applied to example transit data from the test vehicle datasets. In each figure, the five raw images from the measured transit are shown in the first row, and the log-histograms and quadratic data fit plots are shown in the second row. The log-histograms shown are only for the portion of the data that is dominated by noise, for example, in Figure 7-2 for CO_2 optical masses less than 0.01 mole/m^2.

Figure C-1 (in Appendix C) provides an example of a test vehicle with a low amount of HC evaporative emissions, a simulated CO_2 exhaust emission, no other tailpipe emissions, and moving at a low speed. In this case, the log-histograms form inverted parabolas in each data channel, and the data is easily fitted to a parabolic shape.

Figure C-2 provides an example of a test vehicle with a high amount of HC evaporative emissions, a simulated CO_2 exhaust emission, no other tailpipe emissions, and moving at a low speed. Again, the log-histograms form inverted parabolas in each data channel, and the data is easily fitted to a parabolic shape.

Figure C-3 provides an example of a test vehicle with a low amount of HC evaporative emissions, simulated HC/CO_2/CO/NO exhaust emissions, and moving at a low speed. Again, the log-histograms form inverted parabolas in each data channel, and the data is easily fitted to a parabolic shape.

Figure C-4 provides a second example of a test vehicle with a low amount of HC evaporative emissions, simulated HC/CO_2/CO/NO exhaust emissions, and moving at a low speed. In this

case, the HC and CO log-histograms show non-parabolic shapes, and the amplitudes of the CO channel in particular deviate significantly from the model. This behavior was observed rarely, but it tended to occur with transits that exhibited some amount of CO emissions.

Figure C-5 provides an example of a test vehicle with a high amount of HC evaporative emissions, simulated $HC/CO_2/CO/NO$ exhaust emissions, and moving at a low speed. In this case, the CO log-histogram exhibits a highly non-parabolic shape. It was more likely to find an erroneous CO offset model in high HC emission environments for this test vehicle, suggesting that there is an interaction between HC and CO measurements when HC emission values are high and CO emissions are non-zero.

Other examples of the failure of the offset adjustment procedure to adequately characterize the CO offset value can be found. Figure C-6 shows an example from the fleet where the shape of the log-histogram CO values is concave upward. This situation implies that the noise variance is negative – an impossibility – and means the additive noise model is not appropriate for this channel of this dataset.

Processing Summary – As conceived and developed, offset adjustment provides a simple and accurate method for determining the constant offsets in each channel of an EDAR measured transit when the data in each channel obeys an additive noise model. The method assumes a constant background level for each measured channel, an assumption that is physically justified. In most scenarios, it works well. It also provides an estimate of the background noise level in the form of a noise signal power for each channel on a per-transit basis, determined from the curvature of the inverse-parabolic model of the log-histogram data points.

The primary drawback of the offset adjustment procedure is the parsimony of the additive noise model for certain measurement scenarios. For example, when the CO channel measurements are significantly positive, indicating the presence of a CO signal, the offset adjustment procedure can fail. Such situations can likely be detected and flagged, although such detection methods are currently not implemented. A qualitative review of these particular scenarios indicates that they tend to occur in situations where the underlying shape of the CO channel background is not very flat and has some form of curvature to it in terms of Scan Position. It is unclear why the CO channel would exhibit this artifact. It may be useful to study this phenomenon further and either correct for it or provide feedback to the RSD manufacturer to help address it in future data collection campaigns. For the Westminster data, if fleet measurements are considered plentiful enough such that some fraction of them could be rejected, a simple detector based on the following reasoning could be built:

a. Find all transits with significant CO components.

b. Determine the similarity of the CO channel to the CO_2 channel in a normalized way (i.e. based on relative shape similarity and not dependent on mass or plume size). If the two channels are dissimilar, reject the transit.

For future work, some possible enhancements to the procedure can be developed. A partial list follows.

1. Use a goodness-of-fit measure between the log-histogram values and the inverse-parabolic model to identify transit channels and/or transits that do not fit the additive noise model. The goodness-of-fit could take into account various quantities, such as the error in the inverse-parabolic fit or the number of pixels being used in the overall model.

2. Test the value of the variance estimated in each channel – for example, a negative estimated variance value – to determine data channels for each transit that do not fit the additive noise model. Flag these channels and/or transits for further analysis and/or alternative processing.

3. Explore the dependence between the CO channel and other data channels in terms of degree-of-fit to the additive noise model. An example question thread that could be explored: Does the goodness-of-fit of the CO channel to the additive noise model correlate with the goodness-of-fit of other data channels? If so, how often does this occur? Can this correlation be used as a flag to identify problematic transits for omission or further processing?

Removing Outliers

Processing Rationale – The EDAR instrument relies on a reflective strip on the roadway to reflect laser light back to the detector. Thus, the measurements are only valid when this reflective strip is not covered by an object, such as a vehicle's body. As provided by HEAT, the EDAR measurements that have been determined by the EDAR instrument to be occluded are set to zero values. These determinations are not error-free, however. Problems can occur near the corners of the vehicle where large outlier values or "spikes" can sometimes be observed. If these outlier values were left in the measurement, they would greatly distort the results of later processing stages, particularly the separation processing.

For this reason, the following procedure is used to find these outlier values and set them to zero:

1. From the histogram generated from the constant-level adjustment procedure, determine the width of the noise histogram, also known as the standard deviation of the noise.

2. Test all non-zero measurement values that are next to the vehicle footprint. If these measurement values are larger than a threshold – currently set as twice the noise standard deviation – these are possibly "spike" values.

3. Make sure that these large values are not next to other large values and are also behind the vehicle footprint, because those are likely legitimate measurements. Those measurements are kept. The remaining detected values are outliers and are removed.

Processing Examples – We now provide examples of the outlier removal method as applied to example transit data from the test vehicle datasets. In each figure, the five raw images from the measured transit are shown in the first row, and corresponding images of the transit data with the outlier pixels removed are shown in the second row. Due to auto-scaling of the colormaps, the images in the second row have a different color palette due to the different amplitude ranges of each of the data channels. Thus, a "tell-tale sign" of an outlier pixel being removed is an overall

color shift of a second-row image to a lighter shade of blue or yellow, as one or more large-scale pixels have been removed.

Figure C-7 (in Appendix C) provides an example of the EV-2 test vehicle with a low amount of HC evaporative emissions, simulated $HC/CO_2/CO/NO$ exhaust emissions, and moving at a low speed. As can be seen, the main difference between the first- and second-row images is the HC data channel image. All other images have a similar background shade. Moreover, the detected outliers are found to be typically at the sides, corners, and the front of the vehicle. The HC emissions are clearly more evident in the processed images.

Figure C-8 provides an example of the EV-2 test vehicle with a high amount of HC evaporative emissions, simulated $HC/CO_2/CO/NO$ exhaust emissions, and moving at a low speed. Again, the main difference between the first- and second-row images is the HC data channel image. All other images have a similar background shade. As in the previous case, the detected outliers are found to be typically at the sides, corners, and the front of the vehicle. The HC emissions are again clearly more evident in the processed images.

Processing Summary – The purpose of outlier detection for the EDAR measurement instrument is to identify and remove erroneous pixels that occur near the boundary of the vehicle footprint. To provide some context, the EDAR instrument data was originally delivered with this vehicle footprint obscured by a larger rectangle that also removed pixels that were near the back of the vehicle bumper. This was viewed as a loss of data, so the EDAR instrument data was re-delivered with the rear bumper pixels left intact. Outliers were then discovered in the original data measurements that were clearly "wrong," as they were large, isolated pixels next to the vehicle. The outlier detection method identifies these pixels in a per-transit technique that is data-dependent within each channel. The use of a per-channel variance calculation for setting the detection threshold allows this test to be statistically robust.

The only potential drawback of this technique is its connection to the offset estimation step described previously. The offset estimation method can fail, and if it does, then the variance calculation it produces and used in the outlier detection method to set the detection threshold can be incorrect. This is expected to be a rare occurrence. Thus, this technique is likely to be useful as-is for future data processing campaigns.

De-Striping via Multi-Tonal Cancellation

A preliminary analysis of the Westminster dataset indicated that every transit measurement contains non-physical additive noise components. These components show up as periodic sine wave artifacts in each channel of each transit and are structured. It is unclear why these artifacts are present, but they can be identified, characterized, and largely mitigated through numerical processing.

Two types of non-physical artifacts were identified. These two artifacts are dealt with independently in the data processing. The first of the processing methods to be applied to the Westminster data is termed multi-tonal cancellation. The second of the processing methods is

termed adaptive notch filtering. This subsection discusses multi-tonal cancellation; the next subsection discusses adaptive notch filtering.

Processing Rationale – The first type of artifact is something that mainly affects the HC channel measurement in each EDAR dataset in the Westminster dataset. The artifact shows up as a series of lines and periodic waves that extend in time from the front to the rear of the transit data in the direction of vehicle motion. These lines and periodic waves are random in amplitude and phase for each position across the vehicle width. The resulting image looks like it has both "stripes" and sine waves in it. The stripes are oriented vertically and look like streaks of light and dark pixels. The sine waves are undulating vertically and appear to produce light and dark regions on the order of every four to five scan lines. To preview such an image, the upper-left corner of Figure C-9 (in Appendix C) shows an example HC image from a particular EDAR dataset in the Westminster dataset. Other examples of these types of images are shown in the upper-left corner of Figure C-10 through Figure C-20.

Because this type of data artifact appears in other EDAR measurement sets from other instruments in other measurement campaigns, several different methods for its removal have been developed.

a. **Adaptive Linear Prediction**: Apply a common single-channel adaptive least-squares linear predictor (4 samples of prediction, 11 taps for filtering) from back-to-front of each transit. This operation is termed adaptive line enhancement in the adaptive filtering literature.

b. **Multi-Transit Prediction**: Use noise-only data fields from several transits before and several transits after to predict the current transit's noise field. This operation is similar to how a video encoder performs when compressing a video signal.

c. **Multi-Tonal Cancellation**: Employ multi-tonal cancellation of each data column with fixed noise frequencies. This operation is a form of adaptive noise cancellation common in digital signal processing when a) the noise disturbances are known to be sinusoidal in nature and b) the frequencies of these tonal disturbances are known.

Figure 7-3 shows examples of both linear prediction (middle) and multi-transit prediction (right) as applied to a particular HC dataset example shown on the left. This figure does not show an example of multi-tonal cancellation. This figure is meant to illustrate the types of improvements that can be obtained using the first two methods listed above. In the final analysis for this report, it was determined that the third method not shown in Figure 7-3 – multi-tonal cancellation – was most suitable for the Westminster dataset. Thus, it is the only one discussed in depth in this report.

Figure 7-3. Example of Linear and Multi-Transit Prediction for HC Channel

Original HC Data	Linear Prediction	Multi-Transit Prediction
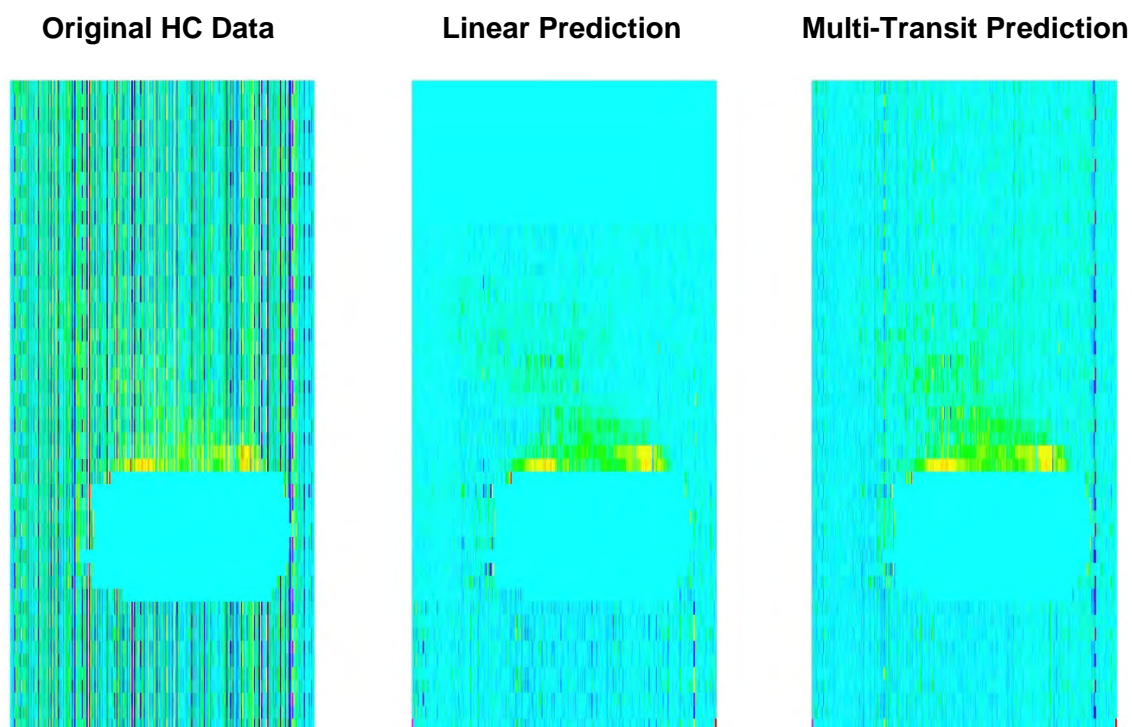
An analysis of the entire Westminster dataset showed that the frequencies of these disturbances in the HC channel were essentially the same for every transit, although the amplitudes and phases of these disturbances change on a per-position basis uniquely across each transit. Figure 7-4 shows the power spectra of the five data channels for all 33,636 transits in the direction of vehicle motion, where we only considered the data away from the vehicle along the edges of each transit – usually the first few and last few pixels of each side of each transit. The purpose of this analysis is to attempt to ignore any emission signal that may be present in the transit data without having to build a detector for this condition. Thus, the resulting scan line power spectrum is simply the frequency content of the noise field of the vertical lines of all signal-free Westminster data in the aggregate. The HC data has a scan line power spectrum with peaks at the following digital frequencies, where $f = 1$ corresponds to half the sampling rate: $f = 0$, $f = 0.21875$ ($= 7/32$), $f = 0.5$, and $f = 1$. We assume that these periodic disturbances are additive. So, to remove them, we process the HC channel according to the method described in Section 5.2. We call this processing multi-tonal cancellation.

Figure 7-4. Noise Power Spectra for RSD Channels in the Vehicle Direction
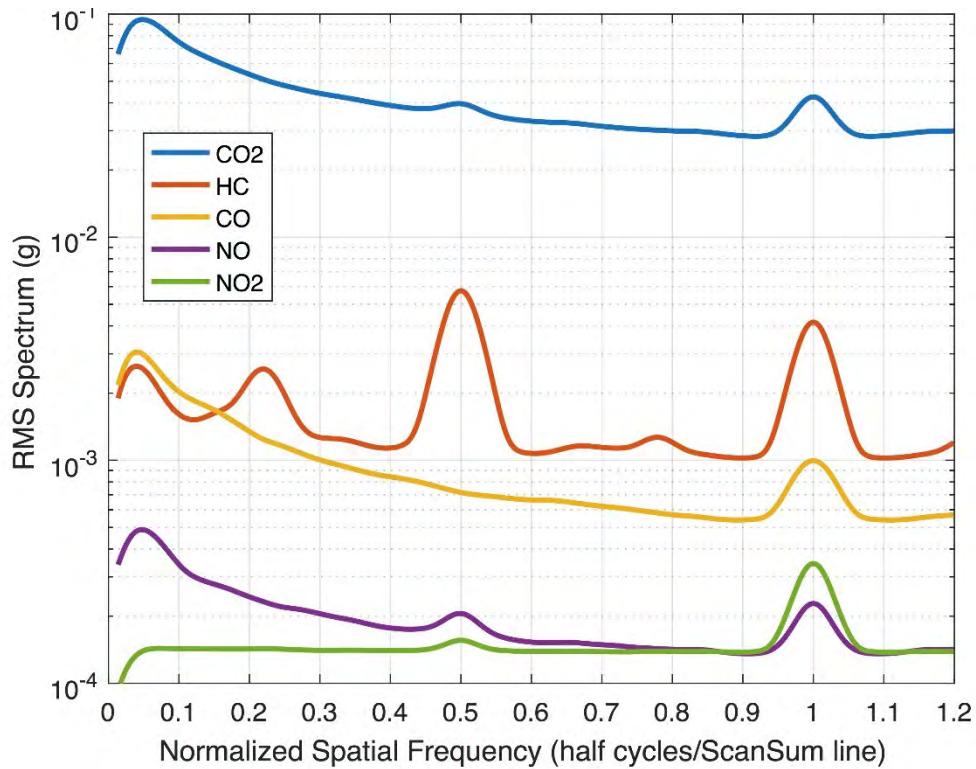

Figure 7-5 shows the power spectra before and after processing using the multi-tonal cancellation method and the best competing method to this chosen one at the time of writing – multi-transit prediction – for all of the transits in the Westminster dataset, where we again only considered the data away from the vehicle along the edges of each transit. In this example, we applied a fourth tonal cancellation frequency at $f = 0.779$ ($= 399/512$) to address the small tonal component at this frequency but found that there was no improvement at that frequency; hence, this fourth tonal cancellation was removed for final processing. As can be seen, multi-tonal cancellation does a better job of reducing the tonal peaks of the HC noise field in the direction of vehicle motion than does multi-transit prediction, except at $f = 0$, which corresponds to the offset baseline. The improvement at $f = 0.5$ is about 12.5 dB, and the improvement at $f = 1.0$ is about 10.5 dB.

Figure 7-5. De-Striping Evaluation using HC Noise Power Spectra
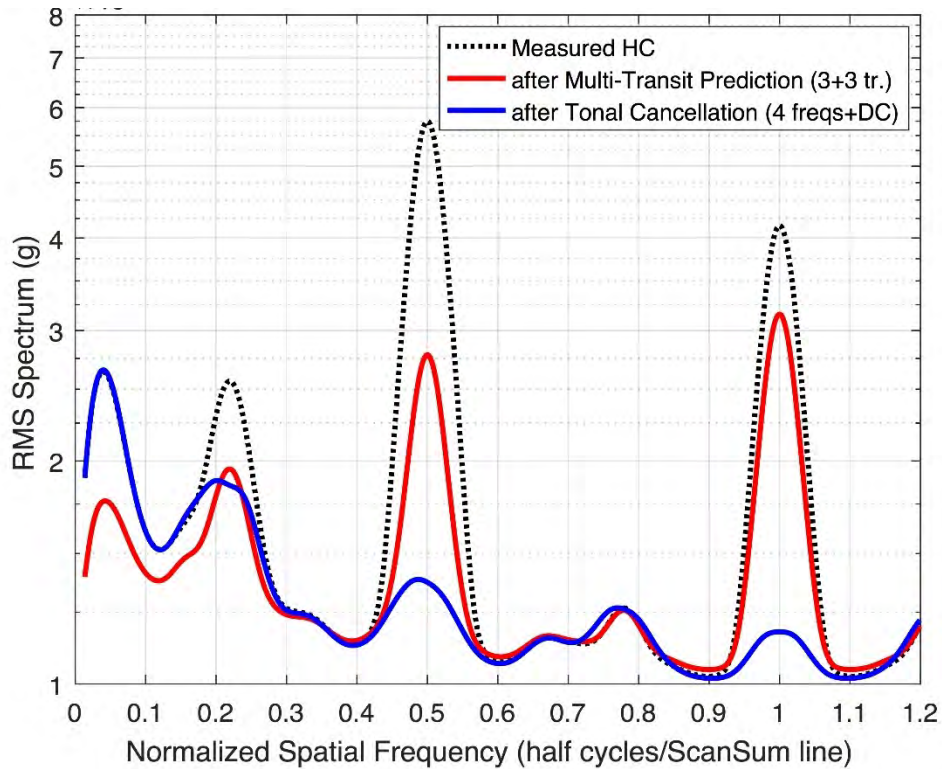
Processing Examples – To illustrate the effects of multi-tonal cancellation, we consider only the HC data channel from selected transits of the Westminster dataset corresponding to the following known measurement conditions:

Test Vehicles	EV-1
	EV-2
EvapHC Release Locations	DOOR
	TANK
	HOOD
EvapHC Emission Rates	200 mg/mile (low)
	6400 mg/mile (high)
Nominal Road Speed	22.5 mph

Considering one example from each possible combination of the above conditions results in twelve transits from the Westminster dataset.

For each selected transit, we present one figure per page. An example of the first figure page is shown in Figure C-9 in Appendix C. The upper-left corner of this figure shows the original measured HC data for the selected transit after outliers have been removed. The right side of this figure shows plots of the scanlines corresponding to pixel positions 100 (top right of the figure) and 200 (bottom right of the figure), respectively, which are easily located vertical lines corresponding to pixel values shown in the images on the left of the figure. Two lines on each of the two right-side plots are provided: the original scan line in red, and the processed scan line in

blue in which multi-tonal cancellation has been applied. The two lines on each plot show an example of the type of interference that multi-tonal cancellation reduces in its operation.

On each page, the lower-left image shows the processed HC data after multi-tonal cancellation. Comparison of the upper-left and lower-left images illustrates the visual improvement that multi-tonal cancellation provides in reducing interference for the HC data channel.

Figure C-9 through Figure C-20 provide the twelve pairs of the figure pages for the different EV-1 and EV-2 vehicle transits discussed previously. Although these twelve figure sets will not be discussed individually in this report, several comments are now provided that summarize the types of improvements that the processing method achieves.

Improvement #1: When plumes are present, multi-tonal cancellation enables them to be more easily seen visually in the data. This improvement is evident for strong plume signals for the portions of the plumes that are ten or more scanlines after the vehicle (e.g. Figures C-9, C-11, C-15, C-17). This improvement is also evident for weak plume signals near the vehicle (e.g. Figures C-13, C-19, C-20).

Improvement #2: Multi-tonal cancellation removes oscillations and offsets that are clearly erroneous, while preserving waveforms that do not exhibit such effects. Good examples of this performance can be seen in the plots in Figure C-19 and Figure C-9, in which the plots at Line 100 each show a fairly clean original signal and the plots at Line 200 show an extremely noisy signal that is improved significantly through multi-tonal cancellation.

Improvement #3: Multi-tonal cancellation addresses constant-level offsets that vary with pixel position, effectively performing image de-striping. These improvements are found in all Figures C-9 through C-20. They are exhibited in the signal plots as well. See Figures C-10, C-12, C-14, and C-19 for plots that show negative scan line values that are clearly incorrect.

Processing Summary – Multi-tonal cancellation is a processing method that addresses two specific problems in the EDAR measurements. One of these problems – striping – is common to all multispectral "pushbroom" sensors. The other problem – tonal components in the direction of motion – is clearly present in the Westminster HC data, but the source of these artifacts is unclear. Both artifacts appear to be additive, such that estimation and subtraction is a viable methodology to address them.

While the multi-tonal cancellation method works well, there are some open issues regarding its performance that could be addressed in future work:

1. Improve the performance of the method for low frequency striping effects. From Figure 7-5, it appears that the performance of multi-transit prediction is better at lower frequencies than multi-tonal cancellation. It is possible to combine the two techniques to obtain better performance than using either one alone. Such a combination would be useful to consider.

2. Develop quantitative emission-based strategies for evaluating the performance of these methods. The quantitative evaluation provided in Figure 7-4 and Figure 7-5 is well-founded but only includes the noise field in the Westminster data. Determining the

quality of the noise suppression should consider the level of signal present in the data as well.

Adaptive Notch Filtering

Processing Rationale – The second type of artifact is a tonal disturbance in the form of a low-level sine wave that appears in the one-dimensional signal that makes up the zigzag measurement of an entire channel of a transit. Figure 7-6 shows the spatial structure of this scan. To make the one-dimensional signal, we put the scan lines for each channel in an end-to-end fashion, removing the common value at the ends of each scan line.

Figure 7-6. Spatial Structure of EDAR Pixels for ZigZag Collection Pattern
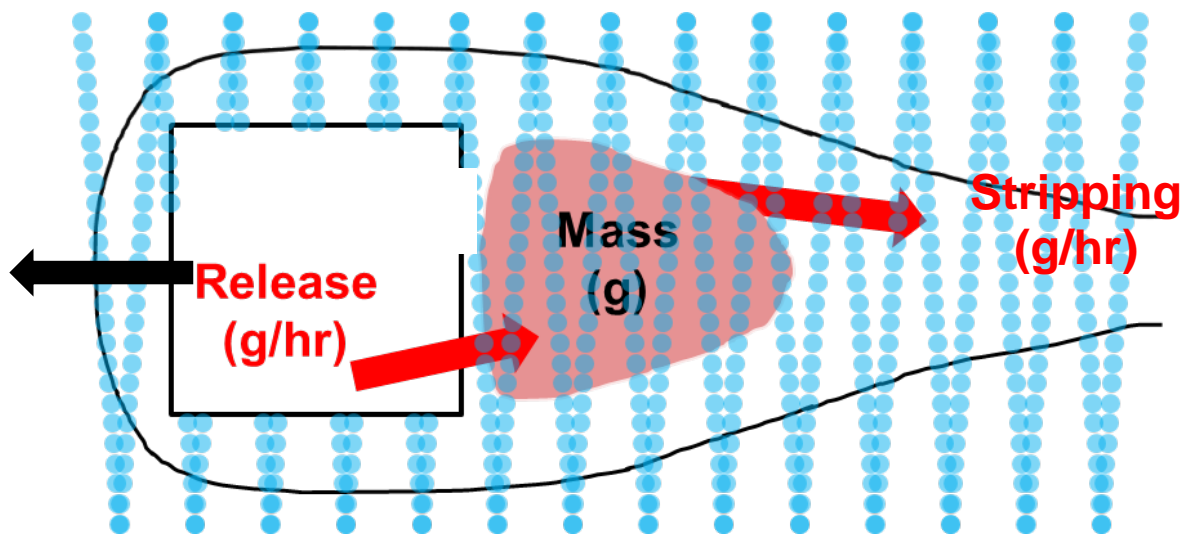
Figure 7-7 shows an example NO_2 dataset as an image (lower left) and its corresponding one-dimensional signal as a time plot (upper plot). The flat regions in the upper plot are the portions of the EDAR scan that are the vehicle footprint. The red boxes in the NO_2 image and one-dimensional time plot represent two scan lines – a "zig" and a "zag" – of the EDAR measurement process across the roadway. These 512 samples are plotted in the smaller plot on the lower right, also outlined in red. The zoomed NO_2 signal shows an obvious tonal artifact of varying amplitude across this scanning process. This tonal artifact shows up as a moire-type noise pattern in the NO_2 image in the lower left and is similar to the type of interference an old cathode ray tube (CRT) television set would show when it had oscillatory interferences in its display electronics.

**Figure 7-7. Example of EDAR NO₂ Signal Collected for One Transit**
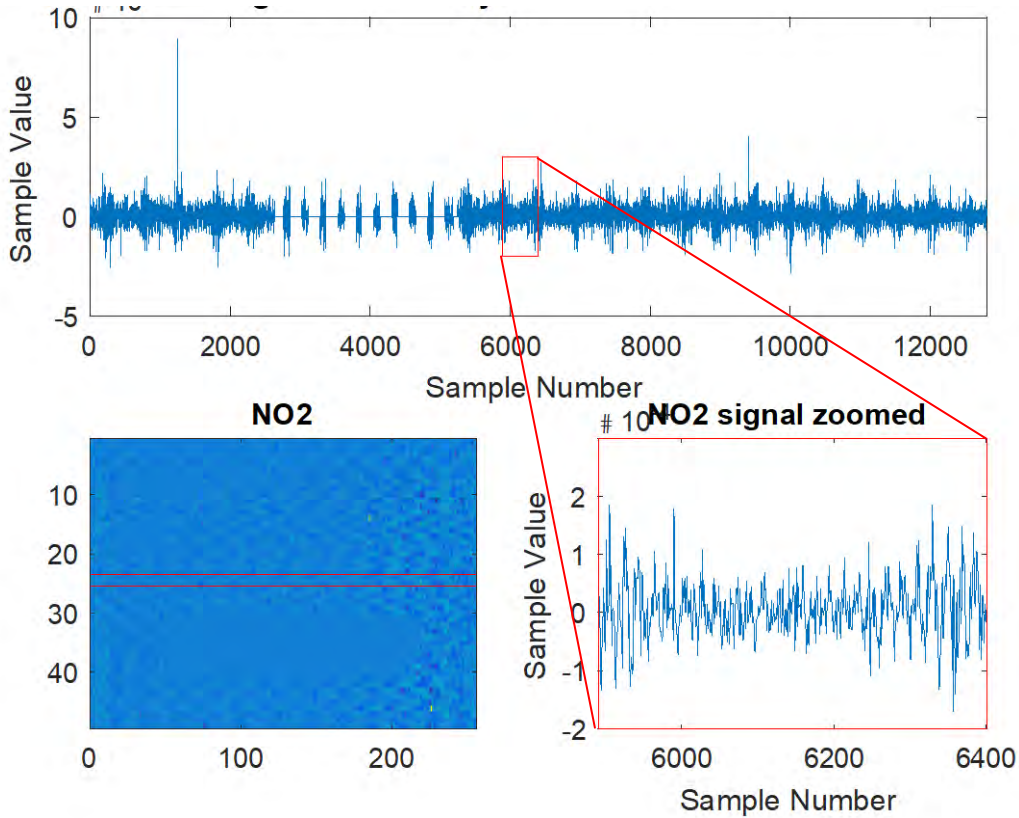
This sine wave can be seen in the NO₂ channel of each transit, as this channel is usually signal-free except for this sine wave. The frequency of this sine wave is different for each transit, and it appears to slowly change over the entire set of 33,636 measurements. This issue was determined through an analysis of a slope error in the test vehicle data that occurred when the notch filter frequency falls to a low value. More recently, it has been determined that the frequency of this interfering sine wave is a function of temperature. Figure 7-8 shows an analysis that illustrates this fact. The upper half of this figure shows the field value "EDAR_Ambient_Temperature" contained in the metadata of the Westminster measurement dataset for the first transit of each hour of the Westminster data collection campaign – from 12:00am, Sunday, October 20, 2019Z to 2:00pm, Thursday, October 25, 2019 – whenever such data is available. The lower half of this figure shows the notch filter frequency determined via frequency analysis on each of these transits in blue, along with a best linear fit of the "EDAR_Ambient_Temperature" value to this notch filter frequency determined by optimal least-squares methods to be:

$$f = 1.0342 - 0.01592 * EDAR\_Ambient\_Temperature.$$

Thus, the frequency of the noise disturbance in the one-dimensional scan signals of the EDAR instrument is approximately negatively linear with temperature. This correspondence likely means that some physical aspect of the EDAR instrument is sensitive to temperature. Identifying the cause of this disturbance could lead to mitigation strategies in future data collection campaigns.

Figure 7-8. Change in Tonal Disturbance Frequency for Test Vehicle Transits
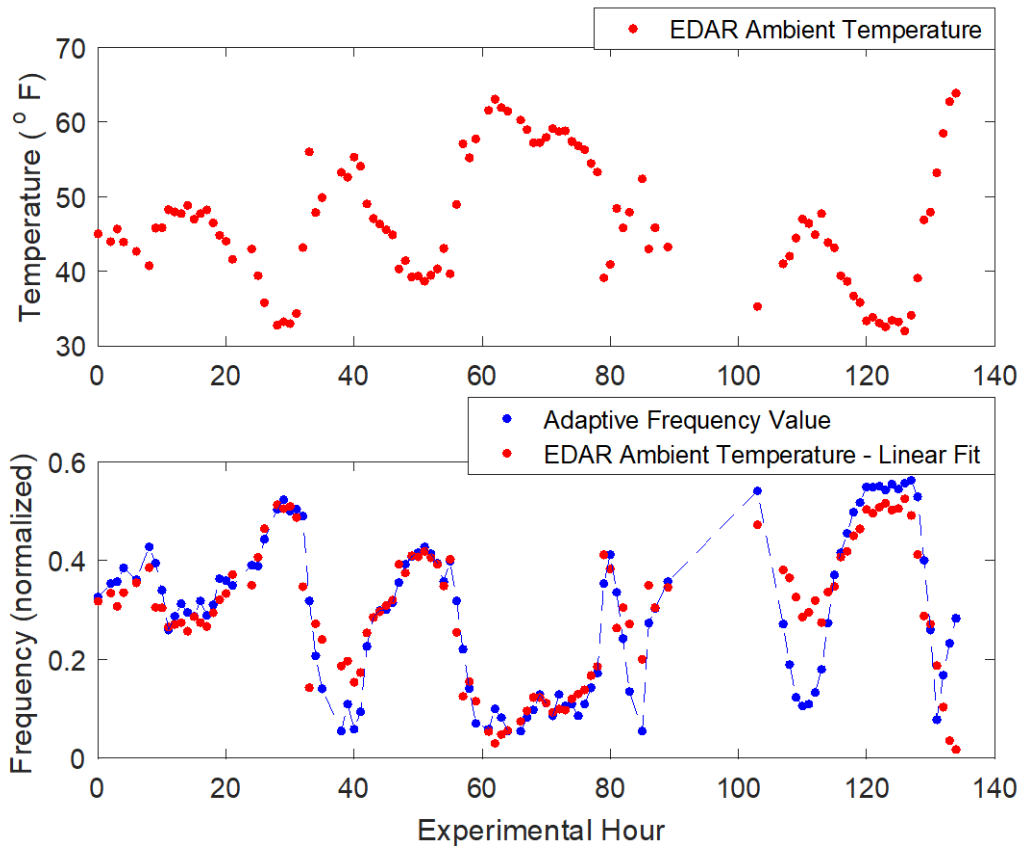
To reduce this sine wave component, we apply the processing described in Section 5.2. Because the processing uses a notch filter with an adaptive frequency, we call this processing *adaptive notch filtering*. This form of adaptive notch filtering has one effective adaptive parameter: the notch frequency. The notch frequency for each transit is estimated from the NO_2 channel using standard power spectrum methods. For each transit, the same filter is applied independently to all data channels.

For the HC channel, both the multi-tonal cancellation and adaptive notch filtering help to improve data integrity. The striping effects in the HC channel are generally much larger than the effects due to the presence of the tone in the zigzag form of the HC measurement data. Because of this, the multi-tonal cancellation is applied first to the HC channel, followed by adaptive notch filtering. For the other four EDAR channels – CO_2, CO, NO, and NO_2 – only adaptive notch filtering is applied.

Processing Examples – We illustrate the effects of adaptive notch filtering through selected transits of the Westminster dataset corresponding to the following known measurement conditions:

Test Vehicles	EV-1
	EV-2
EvapHC Release Locations	DOOR
	TANK
	HOOD
EvapHC Emission Rates	200 mg/mile (low)
	6400 mg/mile (high)
Nominal Road Speed	22.5 mph

Considering one example from each possible combination of the above conditions results in twelve transits from the Westminster dataset.

Figure C-21 (in Appendix C) through Figure C-32 show images from these twelve transits in the same data ordering as Figure C-9 through Figure C-20. The top row of each figure slide shows the five channels of transit data, where the HC channel has been processed using multi-tonal cancellation. The bottom row of each figure slide shows the five channels of transit data after adaptive notch filtering. These data can be explored and compared individually from top row to bottom row to see the qualitative effects of the processing. In some cases, the improvements are subtle, whereas in others, the improvements are more obvious.

Highlighted improvements include the following:

Figure C-22 uses the dataset used to generate the images in plots in Figure 7-7. In this figure, images from all five EDAR channels are shown, both before (top) and after (bottom) adaptive notch filtering. The improvement in the NO_2 channel is obvious, although this result is not very interesting given the design of the processing method. Examining the HC, CO, and NO channels, however, there is clearly an improved visual structure in the associated plume images after processing, as the noise field in these images is of lower amplitude. This qualitative improvement likely results in a quantitative improvement in mass assessment as this data is processed using subsequent methods.

Figure C-26 shows an improvement in plume structure from before to after adaptive notch filtering processing as well. The periodic components that appear in the original data within the CO_2 and NO channels is reduced after processing.

Figure C-29 illustrates an improvement in the plume structure of the HC channel through adaptive notch filtering. The bottom HC image looks clearer and has a better defined plume structure as compared to the top HC image. Note that these effects are most easily seen in situations where the data channel contains a strong signal of interest.

Note that if the tonal disturbance is not strong, then the improvement provided by adaptive notch filtering is not as apparent. Examples where this is likely the case include Figure C-25 and Figure C-30. Even when the processing provides minimal qualitative effects, there are

improvements that can be gleaned. For example, Figure C-31 shows an HC channel that has a better-defined plume structure after processing (bottom) as compared to before (top). It is clear, however, that there are other artifacts in the data, particularly in the NO and NO$_2$ channels for this transit, that are not being addressed by adaptive notch filtering processing. Fortunately, these other noise artifacts are spatially-correlated across multiple data channels, which implies that they can be addressed using spatially-oriented methods such as blind source separation.

Processing Summary – Adaptive notch filtering is a modification of a fixed notch filtering method originally developed for the September 2016 EDAR dataset collected at TTI. The primary modification to this method was to make the frequency of the tonal reduction adaptive, as the Westminster dataset exhibited a changing tonal frequency value.

Adaptive notch filtering is based on the fundamental way the EDAR instrument functions. The EDAR instrument collects a one-dimensional signal over time. This one-dimensional signal is then mapped to a two-dimensional array through the position of the scanning laser on the roadway and the travel time of the vehicle as it passes under the instrument. Any noise or errors that are generated as part of the scanning process are ideally addressed in the form that these disturbances were introduced. This is why adaptive notch filtering is inherently a one-dimensional filtering technique.

It is clear that the tonal disturbance in the EDAR data that adaptive notch filtering addresses is related to something physical and/or numerical about the way the EDAR instrument collects its data. Periodic signals in sampled physical waveforms can be due to many things: physical resonances, detuned oscillators within electronics, aliasing due to under-sampling, and even interference patterns due to the combinations of high-frequency signals. One cannot figure out what causes this disturbance without additional knowledge of the EDAR instrument itself. In addition, the only way to completely remove this interference would be to modify the data collection and/or processing of the EDAR data before it is delivered by the data collection contractor. Adaptive notch filtering represents a reasonable way to address the tonal artifacts in the EDAR data as delivered absent these modifications.

Interpolating Measured Pixel Positions to a Rectangular Grid

Processing Rationale – Each channel of each transit is measured according to the zigzag pattern shown in Figure 7-6. So far, we have treated each zigzag measured pattern as if it is a two-dimensional image, showing pixel values on a rectangular grid according to an approximate spatial mapping of the EDAR data scan onto the roadway over time. It is clear, however, that this type of representation is not entirely accurate. In reality, each dataset is a zigzag sampling of the two-dimensional image of the mass in each data channel that passes under the EDAR instrument. This zigzag pattern does not characterize mass in all regions similarly.

To illustrate how the zigzag sampling of the EDAR instrument affects the representation of the two-dimensional data, Figure 7-9 shows a simple cartoon of what a completely smooth exponentially decaying plume after a vehicle might look like using the standard color palate employed throughout this report. The left-most panel shows what the EDAR instrument would collect in such an idealized situation, where we show the measured values as a two-dimensional

image. It is clear that there is "something wrong" in this image. There are discontinuities on the left and right sides of this image despite the fact that this idealized plume has no discontinuities in it. The center panel shows what is occurring with the measurement device. As the instrument scans left-right-left-right-…, the plume signal is decreasing in the vertical direction only. If one knows the position of the scanning element, then the representation in the center panel can be interpolated in the vertical direction to reconstruct the underlying plume accurately. This interpolation restores the equal spacing that is expected in a two-dimensional Cartesian coordinate sampling of an image. The right-most panel shows this interpolated image. It was generated using the measurements in the center panel only. The smoothness of the original data is recovered, and there are no discontinuities in it. More importantly, the right panel represents a spatially-accurate distribution of the measured quantity – in this case, mass – that the left-most panel can only approximate.

Figure 7-9. Cartoon Demonstrating Interpolation to Rectangular Grid
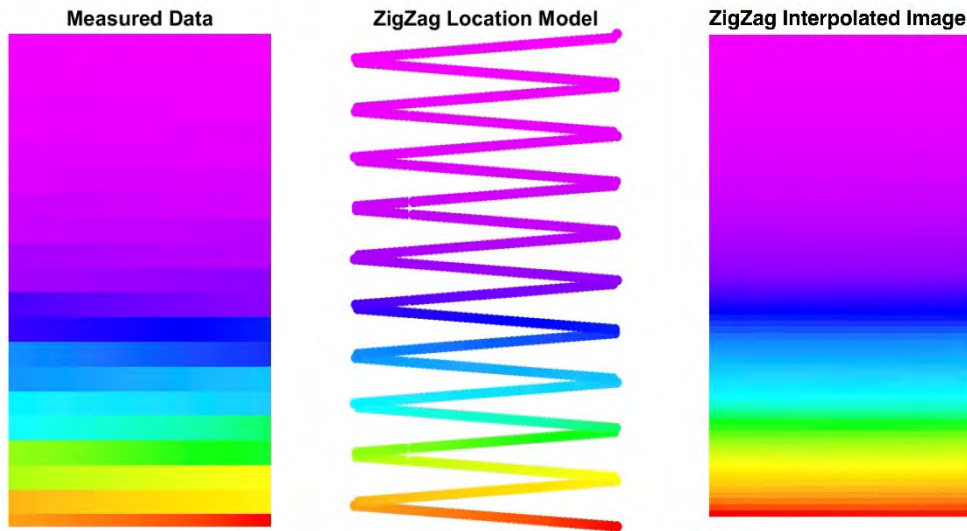
Fortunately, the representation provided with the EDAR data allows us to recover the zigzag nature of the sampling and perform this interpolation easily. This interpolation is done after the adaptive notch filtering described in the previous subsection, and thus takes advantage of all noise reduction methods applied previously, including the de-striping of the HC transit data and the filtering of disturbances via adaptive notch filtering.

As an initial check of the methodology, Figure 7-10 shows an example interpolation performed on the CO_2 channel of an example transit. In this figure, the left-most "image" is the raw data. This data exhibits the same discontinuities seen in the left panel of Figure 7-9. The center image is an interpolated-and-upsampled version of the data in the left panel, where we have used the proper zigzag placement of the data values to do the linear interpolation. It is important to recognize that this enhanced image is not simply a two-dimensional extension of the data on the left. The physical location of the zigzag pattern as illustrated in the center image of Figure 7-9 has been used to interpolate the values in the zigzag pattern in the left image of Figure 7-10 to

make them two-dimensional with equal spacing between each row value in the center image of Figure 7-10. A highly detailed plume structure with physically plausible plumes is reconstructed.

However, this upsampled version of the data has too many scan lines and would require modification of all subsequent processing steps within the Westminster data analysis. Thus, we instead use a subsampled version of this upsampled dataset, as shown on the right-most image of Figure 7-10. Comparing the left-most image with the right-most image, one can surmise that the interpolation method used here reconstructs a more physically plausible plume structure and thus a more accurate representation of the mass measurements being collected by the EDAR instrument.

Figure 7-10. Example of Interpolation of CO_2 Data to a Rectangular Grid

Raw CO_2 Data   **Interpolated + Upsampled**   **Then Downsampled**
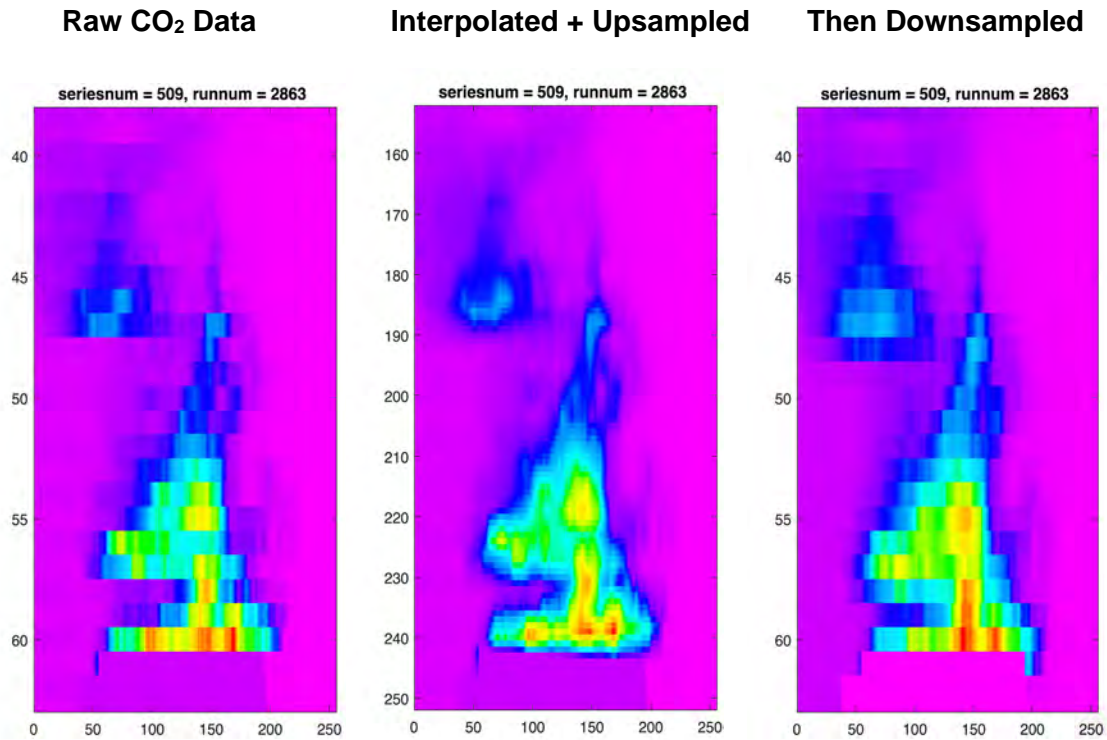
Processing Examples – We illustrate the effects of zigzag interpolation through selected transits of the Westminster dataset corresponding to the following known measurement conditions:

Test Vehicles	EV-1
	EV-2
EvapHC Release Locations	DOOR
	TANK
	HOOD
EvapHC Emission Rates	200 mg/mile (low)
	6400 mg/mile (high)
Nominal Road Speed	22.5 mph

Considering one example from each possible combination of the above conditions results in twelve transits from the Westminster dataset.

Figure C-33 (in Appendix C) through Figure C-44 show images from these twelve transits in the same data ordering as Figure C-21 through Figure C-32. In these datasets, the HC and CO_2 data channels show specific plume structures, so these two channels are used to illustrate the behavior of the zigzag interpolation process in each case. This choice allows us to use more of the printed or viewed page for zoomed-in image content. The four figures show the HC and CO_2 data channels for the selected transit. The two images on the left show the HC channel before and after zigzag interpolation after both have been processed with multi-tonal cancellation and adaptive notch filtering. The two figures on the right show the corresponding CO_2 data channel before and after zigzag interpolation after both have been processed with adaptive notch filtering. The elongated view of each image allows one to more easily assess the effects of zigzag interpolation as well.

These data can be explored and compared individually to see the qualitative effects of the processing. In some cases, the improvements are subtle, whereas in others, the improvements are more obvious.

As an example, Figure C-33 shows plume structures for both the HC and CO_2 data channels that are less "blocky" after interpolation as compared to before interpolation. The tell-tale sign for the zigzag artifact is plume discontinuities that occur every two scan lines. There are fewer of these discontinuities in the interpolated images.

As another example, Figure C-39 has an HC channel with a plume that is more physically plausible after interpolation as compared to before interpolation. Generally, plumes should have smoothly changing amplitudes in the direction of vehicle motion, and the HC interpolated image exhibits this character in this example.

Figure C-40 shows obvious "blocky" artifacts in both the HC and CO data channels before interpolation that are largely eliminated through the zigzag interpolation process. Finally, Figure C-40 illustrates the measurement issue with the EDAR instrument in the CO_2 channel. The discontinuities in the CO_2 plume on the right side of the image after the vehicle are largely gone in the interpolated image.

Processing Summary – As a point of background, almost all traditional optical cameras in use today – phone cameras, laptop cameras, and the like – use a two-dimensional lens-based collection process with an image sensor that measures pixels on a rectangular grid. A traditional document copier or scanner uses a one-dimensional detector of parallel sensors and moves the image across this parallel detector array uniformly, again creating pixels on a rectangular grid but with potentially non-uniform spacing. The EDAR instrument has effectively only one sensor that must move in a two-dimensional pattern to sense an image. It differs both from a traditional camera and a copier or scanner. Moreover, because this instrument must move its sensing point around, there are physical limits to where and when the device can sense information.

Using a zigzag scanning motion creates a sampling process that is non-uniform in the direction of vehicle motion depending on the lateral position of the information across the roadway. Pixels sensed in the center of the EDAR field of view are uniformly sampled. Pixels sensed near either edge of the EDAR field of view are non-uniformly sampled and inherently have less spatial detail in them.

The interpolation process described in this report takes care of the baseline issue with the zigzag measurement process of the EDAR instrument: The pixels of the original EDAR measurement are not true assessments of the mass in any Cartesian coordinate position except along the center line of the camera field of view. After interpolation, each pixel of the interpolated image represents a scaled version of the actual spatial information contained in the pixel quadrant.

An important issue is now raised. Because the EDAR instrument is performing spatial sampling of a two-dimensional image field, the theory behind its sampling operation can be understood using traditional 2D signal processing concepts. For example, for a plume to be properly sampled, its spatial shape must satisfy a sampling criterion as understood via Nyquist sampling theory. The zigzag form of the scanning process complicates this analysis somewhat, but it is possible to do. But most importantly, it is not clear that the EDAR instrument is performing an adequate sampling of the spatial plume field. Said more simply, we do not really know how "spatially rough" the plumes are behind travelling vehicles. Maybe there are peaks and valleys in these plumes that are being missed by the EDAR instrument, or maybe the plumes themselves are smooth. As far as we are aware, no one has measured the smoothness of a plume behind a travelling vehicle. If these physical details about the underlying signals were known, then the EDAR data collection process could be designed to specify a scanning rate to ensure that the entire mass of the plume could be captured and assessed. In any event, for the purposes of better quantifying pollutant release rate (g/hr) and emission rate (g/mile), it would be worthwhile to explore new collection strategies – and even new sensor designs – that would capture more scan lines in the direction of vehicle motion with a much smaller spacing or timing between them.

For the original EDAR design goal of measuring pollutant concentrations, the zigzag scanning method is, by no means, a limitation or problem. The reason is that EDAR's determination of concentrations is based on measurement of the ratio of a pollutant signal to the CO_2 signal at each pixel. The locations or spacings of the pixels are of little consequence to accurate determinations of concentration as long as many pixels are in the vortex.

7.2   Blind Source Separation by Independent Component Analysis

Processing Rationale – A vehicle powered by an internal combustion engine (ICE) emits compounds as it travels along the road. These emitted compounds create different spatial patterns depending on the location of their emission from the vehicle. Some of these spatial patterns correspond to multiple material types. For example, for an internal combustion engine vehicle, multiple emitted materials are typically expended from the exhaust, including CO_2, CO, HC, and NOx. The spatial patterns of these emitted compounds are largely the same if they are present. In other cases, the spatial pattern corresponds to one material type. For example, a vehicle leaking hydrocarbon vapor from the fuel fill door will not have any other compounds, such as CO_2 or NO, emitted from the same fuel fill door location. There are typically a small number of locations around the vehicle from which compounds are emitted, where the chemical makeup of these emissions is different at each emitted location. This situation is what allows blind source separation processing to yield useful results.

Blind source separation is used in this project to identify unique spatial patterns that can correspond to different plumes of emitted materials around the vehicle. Blind source separation tries to make output images that are spatially different from each other using the five channels of RSD data (HC, CO_2, CO, NO, and NO_2) obtained for each transit. This processing is performed on the improved data from each transit separately after the pre-processing steps are performed. The mathematical procedure is described in Section 5.3.

Note that the spatial patterns produced after separation are images that look like plume images of a particular compound, but their amplitudes are no longer in units of mass. In other words, the separation procedure produces normalized plume patterns as outputs. They do not have the correct amplitude to correspond to any particular mass of any particular chemical compound. That is why a second step of processing – estimation – is performed, to be described later.

Since there are five RSD channels going into the BSS procedure, five possible plume patterns are produced from the procedure. If a smaller number of channels from the RSD are selected for processing, then the number of possible plume patterns produced from the BSS procedure is also reduced. Because of how ICE-powered vehicles work, only two types of situations are expected. Either 1) only an exhaust plume is present, or 2) both an exhaust plume and an evaporative plume are present. The exhaust plume will contain some amount of CO_2. The evaporative plume, if it is present, will be most similar to the HC data channel. Thus, we use the procedure described in Section 5.3 to select two of the BSS spatial patterns to identify an exhaust plume and an evaporative plume for each transit. What remains after these patterns are considered noise plumes and are discarded. No processing is performed on these noise patterns other than to identify them as noise.

Processing Examples – In order to show various processing scenarios of interest, we have selected the dataset types shown in Table 7-2 from the test vehicle set to illustrate BSS results in this section.

Table 7-2. Criteria for Selection of Processing Examples

Test Vehicles	EV-1:
	        Metered CO_2 artificial exhaust emissions
	EV-2:
	        Metered HC, CO_2, CO, and NO artificial exhaust emissions
	Subaru:
	        Sedan shape with natural exhaust emissions
	F-150:
	        "Capped" pickup truck shape with natural exhaust emissions

EvapHC Release Locations	DOOR TANK HOOD

EvapHC Emission Rates	6400 mg/mile (high)
	  800 mg/mile (medium)
	  200 mg/mile (low)

Nominal Road Speed	22.5 mph (slow) 45.0 mph (fast)

Using these choices along with some controlled zero-emission EV transits, and selecting fewer fast-speed transits, results in 52 different separation examples. These are shown in Appendix D. All of these examples have the following form. Ten images are shown. The top five images are the transit data channels input to the standard BSS procedure, labeled by compound type and given by HC, CO_2, CO, NO, and NO_2. The bottom five images are the separated plume outputs, labeled as evaporative plume (EvapPlume), exhaust plume (ExhPlume), and the three remaining output channels, termed Noise1, Noise2, and Noise3, respectively.

Regarding all of the results, some general comments can be made:

1. The exhaust plume, when present, typically looks most like the CO_2 input channel. Note that BSS uses all data channels to estimate each plume. So, in fact, this plume is typically cleaner than the CO_2 channel alone when other data channels also have clear exhaust plume structures, such as in the EV-2 transits.

2. The evaporative plume, when present, typically looks mostly like the HC channel with any HC exhaust emissions removed. For the EV-1 transits, there is no HC exhaust emissions, so successful processing should result in the HC channel and the EvapPlume looking highly similar. For the EV-2 transits, there is HC exhaust emissions present, so successful processing should result in EvapPlume appearing to be the portion of the HC channel that is different from ExhPlume.

3. Any apparent plume signal in Noise1, Noise2, or Noise3 is indicative of some aspect of the process – either inherent within the measurements or due to the processing – that does not fit the standard evaporative emissions / exhaust emissions model. However, if these "noise plumes" correspond to an apparent signal within the CO, NO, or NO_2 channels that looks different from the CO_2 channel, then BSS has successfully isolated these "erroneous plumes" into channels that effectively isolate them from the EvapPlume and

ExhPlume outputs. Such a processing result is considered successful given the nature of the input signals to the BSS process.

4. One tell-tale error that can occur with standard BSS processing is a type of "over-subtraction" of the evaporative plume portion of the HC transit signal, causing a negative value that is typically hole-shaped due to the concentrated nature of the exhaust plume at the vehicle tailpipe. This "blue-hole" phenomenon is understandable from the constraints imposed by standard BSS processing, which assumes no spatial overlap of plumes. These observed artifacts were the inspiration behind the development of the BSScov separation procedure developed under this project and discussed in the next subsection.

With these general comments in place, we now discuss the individual transit results.

Figure D-1 shows a separation example for EV-1 where no emissions of any kind are present. In this case, BSS produces a near-zero EvapPlume and a near-zero ExhPlume, as it should. No spurious signals are created.

Figure D-2 shows a separation example for EV-1 where only CO_2 tailpipe emissions are present. In this case, BSS produces a zero EvapPlume and an ExhPlume that is nearly-identical to the CO_2 input signal – a correct result.

Figure D-3 shows a separation example for EV-1 where a high-level evaporative release occurs from the simulated fuel-fill door away from the simulated tailpipe location where CO_2 is released. In this case, BSS correctly estimates an EvapPlume similar to the HC input signal and estimates an ExhPlume similar to the CO_2 input signal – a correct result. There is little spatial overlap of these two plumes.

Figure D-4 shows a separation example for EV-1 where a medium-level evaporative release occurs from the simulated fuel-fill door away from the simulated tailpipe location where CO_2 is released. As in Figure D-3, BSS correctly estimates an EvapPlume similar to the HC input signal and estimates an ExhPlume similar to the CO_2 input signal – a correct result. The evaporative plume is weaker due to the lower-level release rate. There is little spatial overlap of these two plumes.

Figure D-5 shows a separation example for EV-1 where a low-level evaporative release occurs from the simulated fuel-fill door away from the simulated tailpipe location where CO_2 is released. As in Figure D-3 and Figure D-4, BSS correctly estimates an EvapPlume similar to the HC input signal and estimates an ExhPlume similar to the CO_2 input signal – a correct result. The evaporative plume is weaker still due to the low-level release rate. There is little spatial overlap of these two plumes.

Figure D-6 shows a separation example for EV-1 for a high-speed transit, in which a medium-level evaporative release occurs from the simulated fuel-fill door away from the simulated tailpipe location where CO_2 is released. As in Figure D-4 and Figure D-5, BSS correctly estimates an EvapPlume similar to the HC input signal and estimates an ExhPlume similar to the CO_2 input signal – a correct result.

Figure D-7 shows a separation example for EV-1 where a high-level evaporative release occurs from the simulated gas tank underneath the center of the vehicle rear and close to the simulated tailpipe location where CO_2 is released. There is a large spatial overlap between the evaporative plume and the exhaust plume. In this case, BSS estimates EvapPlume as the portion of the HC input signal that overlaps with, yet is spatially different from, the CO_2 input signal that largely makes up ExhPlume. While this result looks reasonable, it is in fact incorrect for this particular transit, as no HC was released from the tailpipe for EV-1. This result is largely due to the constraint imposed by standard BSS procedures that use statistical independence as the separation measure. EvapPlume and ExhPlume are two plumes that are spatially distinct, but they do not fit the measurement scenario in this case due to plume overlap. The BSScov procedure discussed in the next subsection was designed for this type of scenario.

Figure D-8 shows a separation example for EV-1 where a medium-level evaporative release occurs from the simulated gas tank underneath the vehicle rear and close to the simulated tailpipe location where CO_2 is released. As in Figure D-7, there is a large spatial overlap between the evaporative plume and the exhaust plume. Like this previous example, BSS estimates EvapPlume as the portion of the HC input signal that overlaps with, yet is spatially different from, the CO_2 input signal that largely makes up ExhPlume. Again, the result is reasonable for an independence-based separation system but does not fit this measurement scenario. EvapPlume is also noisier due to the weaker evaporative emissions release.

Figure D-9 shows a separation example for EV-1 where a low-level evaporative release occurs from the simulated gas tank underneath the vehicle rear and close to the simulated tailpipe location where CO_2 is released. Due to the low-level release, there is less apparent spatial overlap of the two plumes. BSS estimates EvapPlume as the portion of the HC input signal that overlaps with, yet is spatially different from, the CO_2 input signal that largely makes up ExhPlume. The result appears to be more reasonable here because of the low-level nature of the evaporative release.

Figure D-10 shows a separation example for EV-1 for a high-speed transit, in which a medium-level evaporative release occurs from the simulated tank near the simulated tailpipe location where CO_2 is released. Because of the weak nature of the evaporative signal, and its dispersed spatial signature, there is little spatial relationship between it and the tailpipe plume seen in the CO_2 channel. Thus, standard BSS does a good job of maintaining the evaporative signal in EvapPlume.

Figure D-11 through Figure D-15 all show separation examples for EV-1 where the evaporative release occurs from underneath the hood. For this vehicle shape, the precise release location under the hood, and wind velocity, the resulting evaporative plume largely appears on the side of the vehicle and away from the simulated tailpipe location where CO_2 is released. Since there is little spatial overlap between the evaporative and exhaust plumes, EvapPlume and ExhPlume in all four separation examples are distinct and largely are correct in their isolation of the HC channel in EvapPlume and the isolation of the CO_2 channel in ExhPlume. The main differences in all four of these examples is the relative levels of signal in the HC channel input to the standard BSS procedure.

Figure D-15 shows a separation example for EV-2 where no emissions of any kind are present. Like Figure D-1, BSS produces a near-zero EvapPlume and a near-zero ExhPlume – as it should. No spurious signals are created.

Figure D-16 shows a separation example for EV-2 where tailpipe emissions with four different pollutants – HC, CO_2, CO, and NO – are present, and there are no evaporative emissions. In this case, BSS produces a nearly-zero EvapPlume and an ExhPlume that is similar to all four of the different plumes for each of the four different pollutants. The BSS procedure correctly merges the four different compound signals into one plume pattern.

Figure D-17 shows a separation example for EV-2 where tailpipe emissions with four different pollutants – HC, CO_2, CO, and NO – are present, and where a high-level HC evaporative release occurs from the simulated fuel-fill door which is located near the rear bumper but on the other side of the vehicle's tailpipe location. This is our first example of a composite release of both evaporative HC and exhaust HC in a transit signal. Here, EvapPlume has a "blue hole" in the tailpipe location, indicating that standard BSS has over-subtracted the emissions component in the evaporative plume and created a negative-valued signal in the tailpipe location. This result is to be expected due to the independence criterion used by standard BSS techniques and is one of the motivating scenarios for which BSScov was designed. Standard BSS does a good job of estimating the evaporative plume in EvapPlume from the multiple input signals.

Figure D-18 shows a separation example for EV-2 where tailpipe emissions with four different pollutants – HC, CO_2, CO, and NO – are present, and where a medium-level HC evaporative release occurs from the simulated fuel-fill door which is located near the rear bumper but on the other side of the vehicle's tailpipe location. In this case, standard BSS processing produces a reasonable result, isolating the evaporative plume in EvapPlume from the exhaust plume in ExhPlume, and correctly combining the multiple tailpipe signals into one ExhPlume. No spurious artifacts are created in any Noise outputs.

Figure D-19 shows a separation example for EV-2 where tailpipe emissions with four different pollutants – HC, CO_2, CO, and NO – are present, and where a low-level HC evaporative release occurs from the simulated fuel-fill door which is located near the rear bumper on the other side of the vehicle's tailpipe location. In this case, standard BSS processing produces a fairly reasonable result for EvapPlume and ExhPlume, but it also generates spurious artifacts in at least one of the Noise outputs near the tailpipe location. The performance of standard BSS in this case is somewhere in-between the results of the previous two examples.

Having provided these three examples, we can consider the performances of the remaining EV-2 transit examples in Figure D-20 through Figure D-27 as being similar in characteristics to one of these three above. Examining the figures, we find that:

BSS performance similar to Figure D-18 (reasonable): Figures D-20, 21, 23, 26, 28

BSS performance similar to Figure D-19 (in the middle): Figures D-22, 24, 27

BSS performance similar to Figure D-17 (blue hole): Figure D-25

These behaviors are likely due to the specific plume structures and emission levels of these various transit examples matching those of the three initial EV-2 examples provided above.

Figure D-29 through Figure D-40 show separation examples for the Subaru test vehicle, which has natural CO_2 tailpipe emissions and perhaps a small amount of HC tailpipe emissions as well, although the latter is likely much below the release amounts from the simulated evaporative emissions in every measured case. In addition, it is possible for the Subaru to emit other compounds, like CO, depending on its engine state. Examining these twelve figures, we can classify them into three different performance categories:

> Reasonable BSS performance, CO present: Figures D-32, D-34, D-36. In these cases, the vehicle appears to emit similar exhaust plumes containing both CO_2 and CO. ExhPlume largely follows the spatial pattern of these CO_2 and CO emissions. The HC channel contains emissions that are largely different from the tailpipe emissions, and these are correctly isolated in EvapPlume.

> Reasonable BSS performance, no CO emissions present: Figures D-30, D-36, D-39. In these cases, the vehicle appears to emit only a CO_2 exhaust plume. ExhPlume largely follows the spatial pattern of the CO_2 emissions. The HC channel contains emissions that are largely different from the tailpipe emissions, and these are correctly isolated in EvapPlume.

> Artifacts in the CO channel: Figures D-29, D-31, D-33, D-35, D-37, D-40. In these cases, the vehicle appears to emit at least two different kinds of plumes in the CO_2 and CO channels. This type of behavior is non-physical, as internal combustion engines would generate similar CO_2 and CO plumes if they are being produced from the same engine – even if the engine generating the CO is from another nearby vehicle or combustion source. Thus, it is initially unclear how to evaluate the performance of standard BSS in these cases. However, it can be seen that, if the CO channel is thought to be in error, then the so-labelled erroneous components within the CO channel are isolated in the Noise1 channel – a correct result. In addition, the separation performance for EvapPlume and ExhPlume under this interpretation appears to be reasonable.

Figure D-41 through Figure D-52 show separation examples for the F-150 pickup truck test vehicle, which has natural CO_2 tailpipe emissions and perhaps a small amount of HC tailpipe emissions as well, although the latter is likely much below the release amounts from the simulated evaporative emissions in every measured case. Examining these twelve figures, we can classify them into two different performance categories:

> Reasonable BSS performance, no CO emissions present: Figures D-48, D-49, D-52. In these cases, the vehicle appears to emit only a CO_2 exhaust plume. ExhPlume largely follows the spatial pattern of the CO_2 emissions. The HC channel contains emissions that are largely different from the tailpipe emissions, and these are correctly isolated in EvapPlume.

> Artifacts in the CO channel: Figures D-41, D-42, D-43, D-44, D-45, D-46, D-47, D-50, D-51. In this case, a large number of the measured transits for the F-150 test vehicle

contain artifacts in the CO data channel. These artifacts are non-physical and make evaluating the separation performance of standard BSS challenging for this vehicle type. A particular standout in this group is Figure D-46, which appears to contain three different plume structures in the CO_2, CO, and NO channels despite this scenario being an impossibility from a physical perspective.

Processing Summary – The goal of BSS processing in this project is to isolate specific candidate plume patterns from spatially-oriented RSD measurements of moving vehicles without regard to, and without knowledge of, the exact emission characteristics of any one vehicle being analyzed. If one knows the exact nature of the emissions from a vehicle, then one can design a specific processing method to extract the requisite plume patterns from the vehicle. The problem of course is the lack of knowledge of this exact nature for any one vehicle. Applying a precise processing method to a vehicle with an unknown state would likely result in erroneous results. This is the reason for using BSS methods in this project. They generally work well without having precise knowledge of the emissions characteristics of any one vehicle being analyzed. The examples provided show that standard BSS often does a reasonable job of estimating the exhaust plume of vehicles and, when present, isolating the evaporative plume of emitted HC components from the exhaust plume. This is the first step in performing an estimation of the evaporative and exhaust components of a specific pollutant, such as HC.

Standard BSS also appears to deal with non-idealities in the measured RSD data that do not fit the emissions model. In particular, non-physical CO components generate "noise plumes" that are then rejected for further processing.

The primary drawback to standard BSS processing occurs when exhaust and evaporative plumes have a significant spatial overlap. In such cases, standard BSS processing can sometimes create erroneous results by "over-subtracting" the measured signals from each other, leading to negative plume regions. This issue was recognized early on in this project, and the BSScov algorithm, described in the next section, is one possible methodology that can be used to address the issue when it occurs.

7.3   Enhanced Blind Source Separation using Correlation Constraints

Processing Rationale – Blind source separation based on independent component analysis uses the property that the signals being separated – in this case, spatial plume signatures – are statistically independent of each other. This property is a good one to use for RSD measurements in this project when the evaporative and exhaust plumes are very different – for example, when the locations of the plume signatures do not overlap very much. This property is less accurate if there is a lot of overlap between the exhaust plume and the evaporative plume. For this reason, a new BSS method was developed under this effort to handle this situation. Called **BSScov**, the separation algorithm allows one to specify a parameter, called a *correlation parameter* and denoted as ρ (the Greek symbol "rho"), to specify the amount of overlap between the two plumes. This parameter should ideally be adjusted based on the amount of overlap of the two plume types, and it is likely best chosen using the emission location of the evaporative plume. The BSScov procedure is described in mathematical detail in Section 5.3.

While BSScov provides a potential solution to the issue of overlapping plumes and the proper assignment of plume structure to EvapPlume and ExhPlume for real-world RSD measurements, it should be noted that a precise procedure for specifying the value of the correlation parameter ρ has not yet been developed. However, evaluations of the candidate procedure on the Westminster and other similar RSD measurements of vehicle transits indicate that:

- The correlation parameter need only be specified for the relationship between EvapPlume and ExhPlume. Hence, there is only one parameter to be set for each processed transit.

- A typical range of the correlation parameter is $0 \leq \rho \leq 0.3$. A zero value yields the standard BSS procedure. Values greater than 0.3 lead to non-physical results.

- Since BSScov includes standard BSS processing as a special case, we can obtain our existing results by selecting $\rho = 0$. There is no need to "switch" between algorithms. Non-switching processing strategies are more robust.

- Performance varies smoothly for small changes in the correlation parameter value. In other words, if the value of the parameter has a small error, then performance will degrade by a small amount. Thus, adjusting the correlation parameter does not involve significant risk.

- When the correlation parameter ρ is chosen properly, non-physical artifacts, such as large negative values in the extracted plume signatures, tend to be suppressed. Thus, the algorithm has the potential to achieve the desired goal of artifact-free plumes for estimating both exhaust and evaporative emissions.

Processing Examples – In this section, we illustrate the behavior of the BSScov algorithm through selected examples. Each of these examples illustrates the separation behavior of the BSScov algorithm on a specific vehicle transit dataset for a range of correlation parameter values. The purpose of these examples is to show that a proper value of the correlation parameter can likely be set once a specific criterion for its design has been chosen. The examples also illustrate the limitations of the standard BSS approach.

Figure 7-11 shows the input data channels (top five images) and the results of standard BSS processing (bottom five images) for an EV-1 vehicle transit with a large evaporative release at the TANK location. Recall that the TANK release location typically results in an evaporative plume that significantly overlaps with the exhaust plume, especially for high-level releases. Standard BSS processing leads to negative values in EvapPlume at the locations where ExhPlume is large. These can be seen by the two "blue holes" in EvapPlume next to the back bumper of the vehicle.

Figure 7-12 shows the same input data illustrated in Figure 7-11 (top five images) processed by the BSScov algorithm with the choice $\rho = 0.1$. The "blue holes" in EvapPlume are mitigated without significant changes in ExhPlume.

Figure 7-13 shows just the HC and CO_2 data channels (left two images) as well as the corresponding EvapPlume and ExhPlume results for standard BSS processing (second-from-the-left two images) along with the BSScov algorithm's plume outputs for the values of $\rho = 0.05$, $\rho = 0.1$, and $\rho = 0.15$ (right six images). One can see that, as the correlation parameter is increased, the plume patterns in EvapPlume and ExhPlume slowly change, and a value of this parameter can be selected to mitigate the "negative holes" issue identified in the previous standard BSS example. The proper choice of this correlation parameter is currently an open issue. This figure illustrates, however, that the algorithm's outputs have the desired range of outputs to mitigate the undesired artifacts of standard BSS processing.

Figures E-1 through E-12 show the examples shown in Figures 7-11, 7-12 and 7-13 plus three more examples comparing standard BSS processing with the results of the BSScov algorithm, in which differing release locations (DOOR, HOOD) and differing amounts of evaporative releases are considered. In each case, the BSScov algorithm provides a range of outputs that enable a reasonable selection of the correlation parameter to obtain physically plausible patterns of EvapPlume and ExhPlume.

Processing Summary – The BSScov algorithm was designed with the specific goal of mitigating a known artifact in standard BSS processing when applied to data that does not precisely fit a statistically-independent source model. It is impossible for two positive-valued signals that have any degree of overlap to be statistically independent, because they must be non-negative wherever they overlap, by definition.

The primary issue in using the BSScov algorithm is setting the value of the correlation parameter. Some exploration has been performed in this direction. It is likely a problem involving calibration of the processing approach to the specific RSD measurement instrument collecting the data, where test vehicles with known release amounts can serve as training data. It is also likely that knowledge of the evaporative emission location, if such information could be identified on a per-transit basis, could be used to choose a reasonable value of the correlation parameter. Such procedures are the subject of potential future work.

Figure 7-11. BSS ICA Separation (ρ=0) of Example: EV-1, High EvapHC from TANK
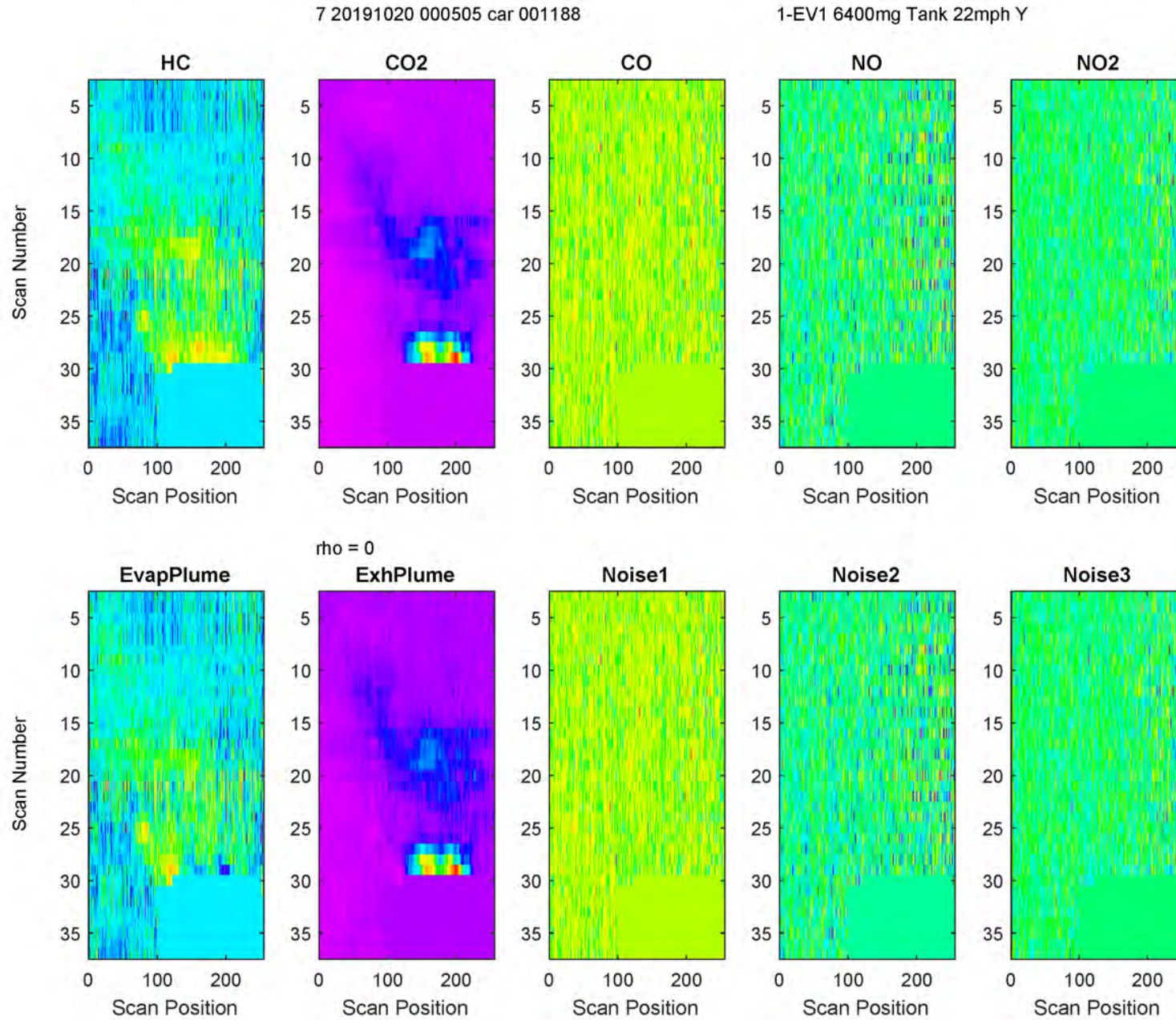
Figure 7-12. BSScov Separation (ρ=0.1) of Example: EV-1, High EvapHC from TANK

7 20191020 000505 car 001188   1-EV1 6400mg Tank 22mph Y
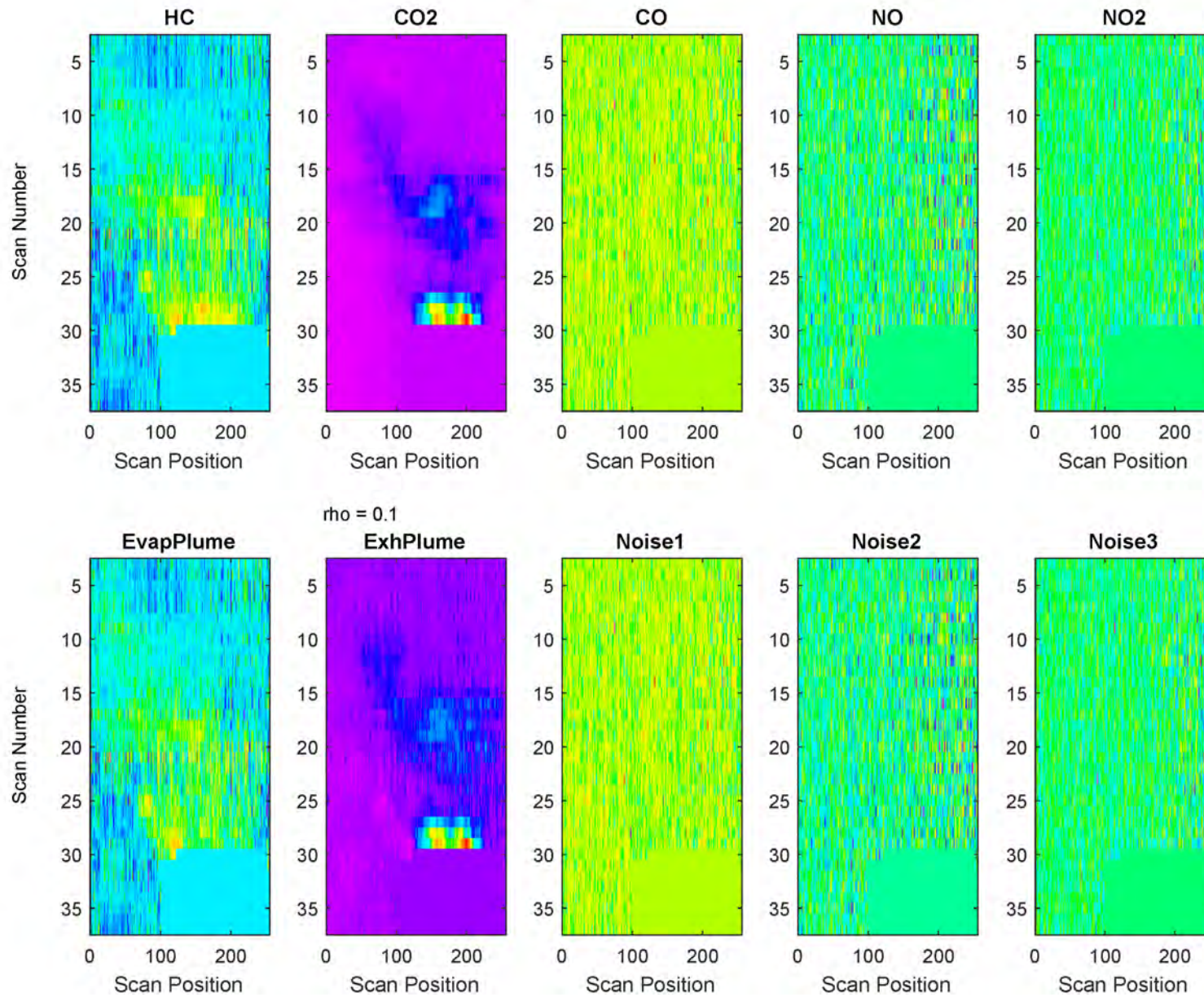
Figure 7-13. Evaluation of Plume Outputs while Varying ρ for Example: EV-1, High EvapHC from TANK

7 20191020 000505 car 001188   1-EV1 6400mg Tank 22mph Y
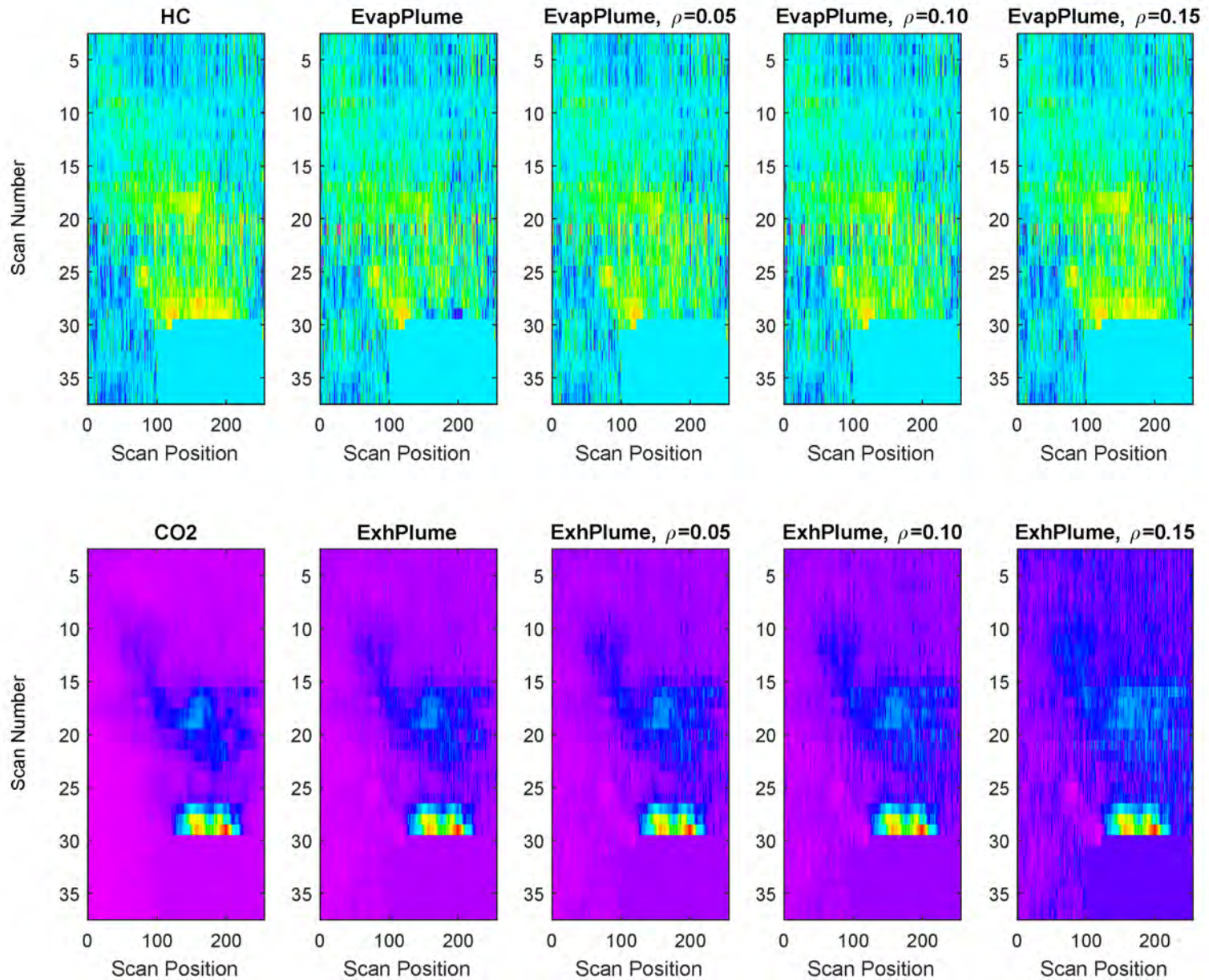
7.4   Estimation of EvapHC and ExhHC from Candidate Plumes

Processing Rationale – The Blind Source Separation portion of the Separation/Estimation Device creates an ExhPlume pattern and an EvapPlume pattern from the improved RSD signals presented to it. These plumes are effectively unitless. They are spatial patterns, but they do not specify the amounts of any one compound in any measurement from the RSD. To find these amounts, an estimation procedure must be performed. The estimation portion of the Separation/Estimation Device is a mathematical procedure that combines the ExhPlume and the EvapPlume from the BSS portion with the improved RSD signals to figure out the scaling of each plume needed to match the portion of that plume in the corresponding RSD signal. The output of the estimation procedure is a mass image corresponding to the type of emission plume for each compound that we choose to estimate. In this project, we applied estimation to the improved HC signal only, although it could be applied to other RSD signals as well.

Using this procedure, we have the following advantages:

1. The plumes produced by the BSS procedure are further "cleaned up" with respect to the improved RSD signals, so they can be more accurate than any one improved RSD signal.

2. Using an exhaust plume and an evaporative plume allows us to "divvy up" the HC signal into an ExhHC component and an EvapHC component. The two components are not obtainable by direct examination of the HC signal alone.

The problem of estimating the height of a signal given a candidate template for this signal is well-known and involves an estimation procedure called regression. In this project, we used the structure of the data to better estimate the exhaust HC plume and the evaporative HC plume. In particular, we used weighting factors determined from the analysis of the entire Westminster dataset as described in other portions of this document, and as detailed in Section 5.4. This procedure is called weighted least squares.

Weighted least-squares is a standard approach in regression analysis. How the weighting is applied to the Westminster data is now explained. This process involves three steps:

1. Generation of one-dimensional weighting functions

2. Extension of these one-dimensional weighting functions to two-dimensional weighting functions within the transit data

3. Multiplication of the two-dimensional weighting functions with measured data.

These procedures are used to combine the estimated plume patterns, EvapPlume and ExhPlume, with the measured HC transit data to determine the proper height of the component of each of these plumes that make up the HC transit data. The end results are scalar values that scale the "unitless" plumes into estimated components of the measured data, with units of mass that match the units of the measured data. There is a single scalar value for each particular plume type, EvapPlume and ExhPlume, for each transit.

Note that the resulting images of both the ExhHC plume and the EvapHC plume for each transit look just like the unitless ExhPlume and EvapPlume produced by the BSS procedure. Thus, we do not show the images of this process here. This estimation procedure is required to leverage the outcomes produced by the BSS procedure, however.

There are additional choices of least-squares methods that could be made. For example, we could use a constraint to specify the total amount of hydrocarbon produced in the two estimated HC plumes. This procedure is known as constrained least squares. We could also use an estimate of the baseline noise level in the improved HC signal to adjust the estimates to account for the noise amount. This procedure is known as total least squares. Both constrained least squares and total least squares could use weighting factors to improve their accuracy, resulting in weighted constrained least squares and weighted total least squares procedures, respectively. There are many possible choices for this estimation procedure. We chose weighted least squares due to its simplicity and the lack of additional knowledge required for the transit data.

Processing Examples – In this section, we illustrate, via several examples, how the one-dimensional weight functions are extended to two dimensions so that they can be applied to measured RSD data.

Figure 7-14 shows two identical one-dimensional plots along the first column of the figure. These one-dimensional plots are the weighting functions determined by the data analysis procedure described in Section 5.4. They have been rotated by 90 degrees so that they are oriented along the scan number of the transit data. They have also been shifted to the back bumper position so that they match the position of the vortex as it appears after the vehicle in the transit data. The peak of this function is typically at the same position as the first full line of pixel values after the back bumper of the vehicle.

The second column of Figure 7-14 shows the two-dimensional weighting image generated from the one-dimensional weighting function. This image is simply the weighting function applied to every scan position in the image, where we have turned this function into pixel values and displayed the weighting function as a two-dimensional image. The weighting function is only non-zero over pixels that are not vehicle pixels. Hence, there are portions of the weighting function that are "zeroed-out" by the position of the vehicle in the transit data.

The third column of Figure 7-14 shows the HC and CO_2 data after pre-processing.

The fourth column of Figure 7-14 shows the HC and CO_2 data after it has been weighted by the two-dimensional weighting function in the second column. In this weighted image, the weighting suppresses pixels that are far from the back bumper, because these pixels are likely to contain only noise and very little plume mass of any type. Thus, using weighting functions helps to improve the robustness of the estimation by suppressing noise pixels that add little to the accuracy of the assessment.

The fifth column of Figure 7-14 shows the EvapPlume and ExhPlume generated by standard BSS that is then combined with the weighted data in the fourth column to determine the proper height of the estimated evaporative and exhaust components. These plumes can be combined with either the weighted HC or the weighted CO_2 image data. If both EvapPlume and ExhPlume

are combined with weighted HC, one obtains the height of the evaporative HC plume and the exhaust HC plume, respectively. Similarly, ExhPlume can be combined with the weighted CO_2 to determine a more-accurate exhaust CO_2 plume. Since CO_2 is not an evaporative emission, it makes no sense physically to combine EvapPlume with weighted CO_2 in this application.

Figures 7-15, 7-16, and 7-17 show three additional examples of the weight function used in estimation of emission components, the corresponding weight images, the measured HC and CO_2 after pre-processing, the weighted versions of this data, and the corresponding EvapPlume and ExhPlume patterns generated from standard BSS for this data in the same ten-image format as Figure 7-14. In each case, the weighting images applied to the pre-processed data suppress noise pixels and provide for an improved estimation accuracy. In some cases, the weighting function suppresses signal energy that is not located right after the vehicle. Such an example can be found in Figure 7-17 for a high-level hood release for the EV-1 test vehicle.

Figure 7-14. Use of Weights for Estimation for Example: EV-1, High EvapHC from DOOR, Low Speed
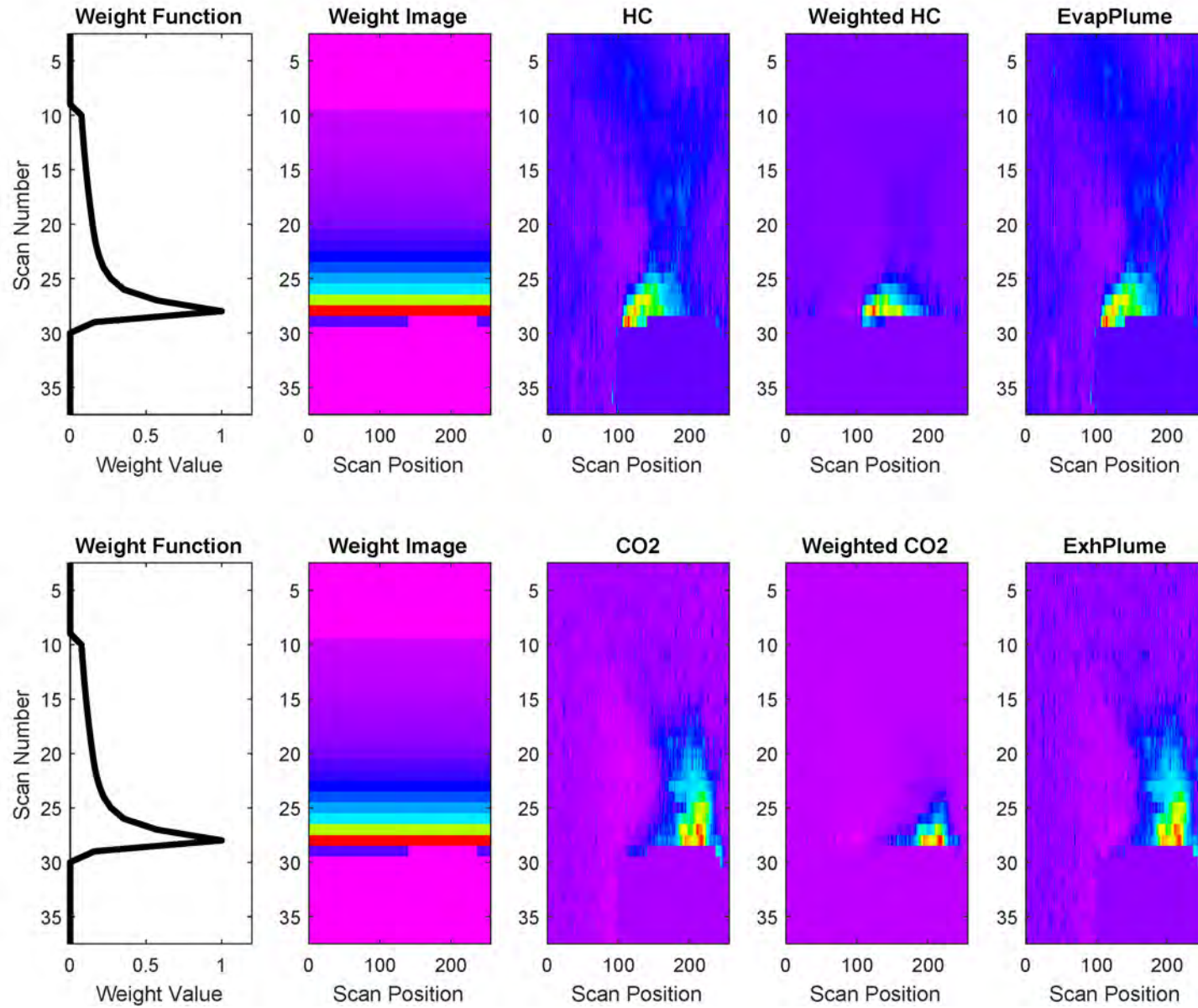
Figure 7-15. Use of Weights for Estimation for Example: EV-1, Low EvapHC from TANK, Low Speed
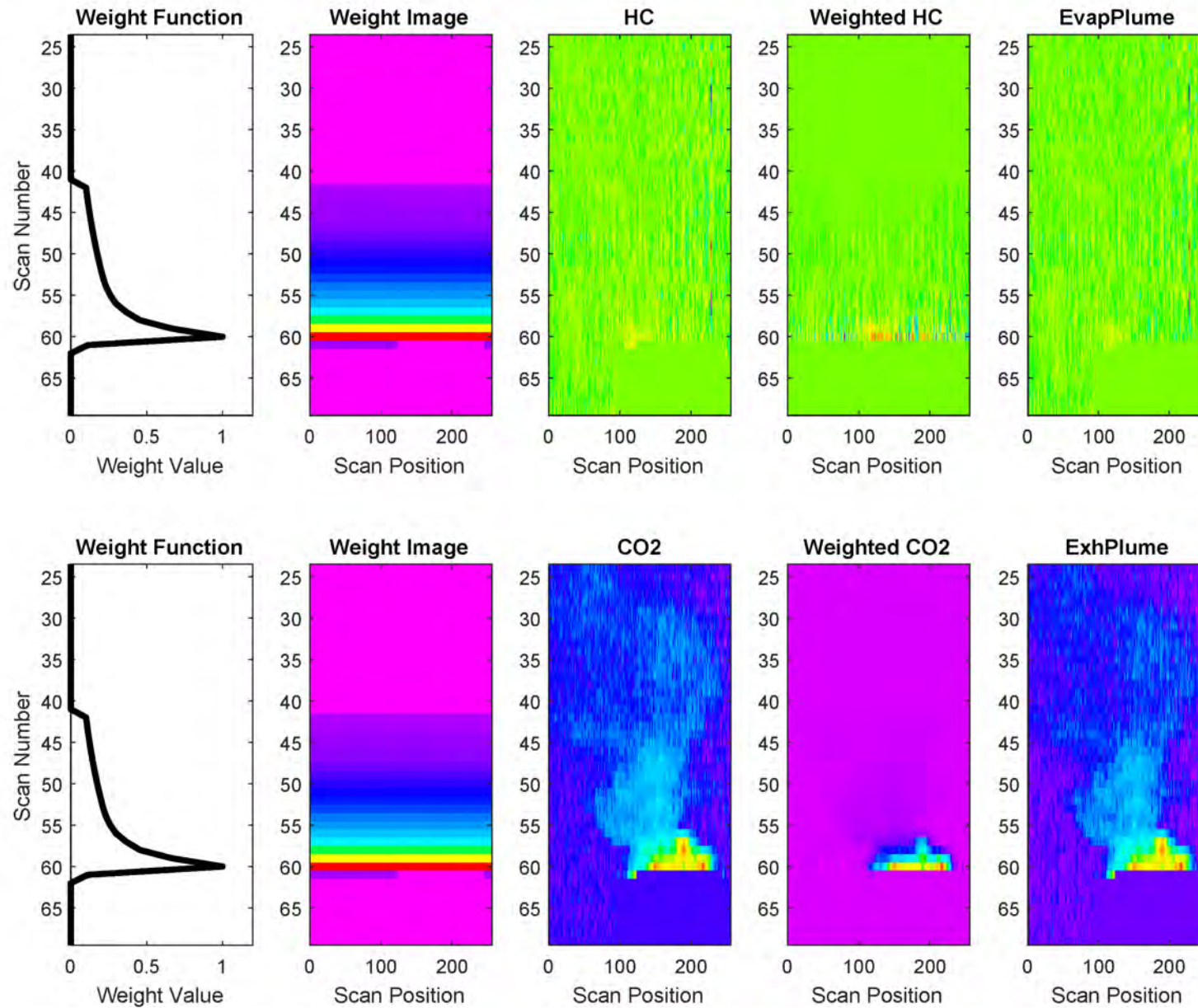
Figure 7-16. Use of Weights for Estimation for Example: EV-1, Medium EvapHC from TANK, High Speed

7 20191020 000505 car 001347

1-EV1 800mg Tank 45mph Y
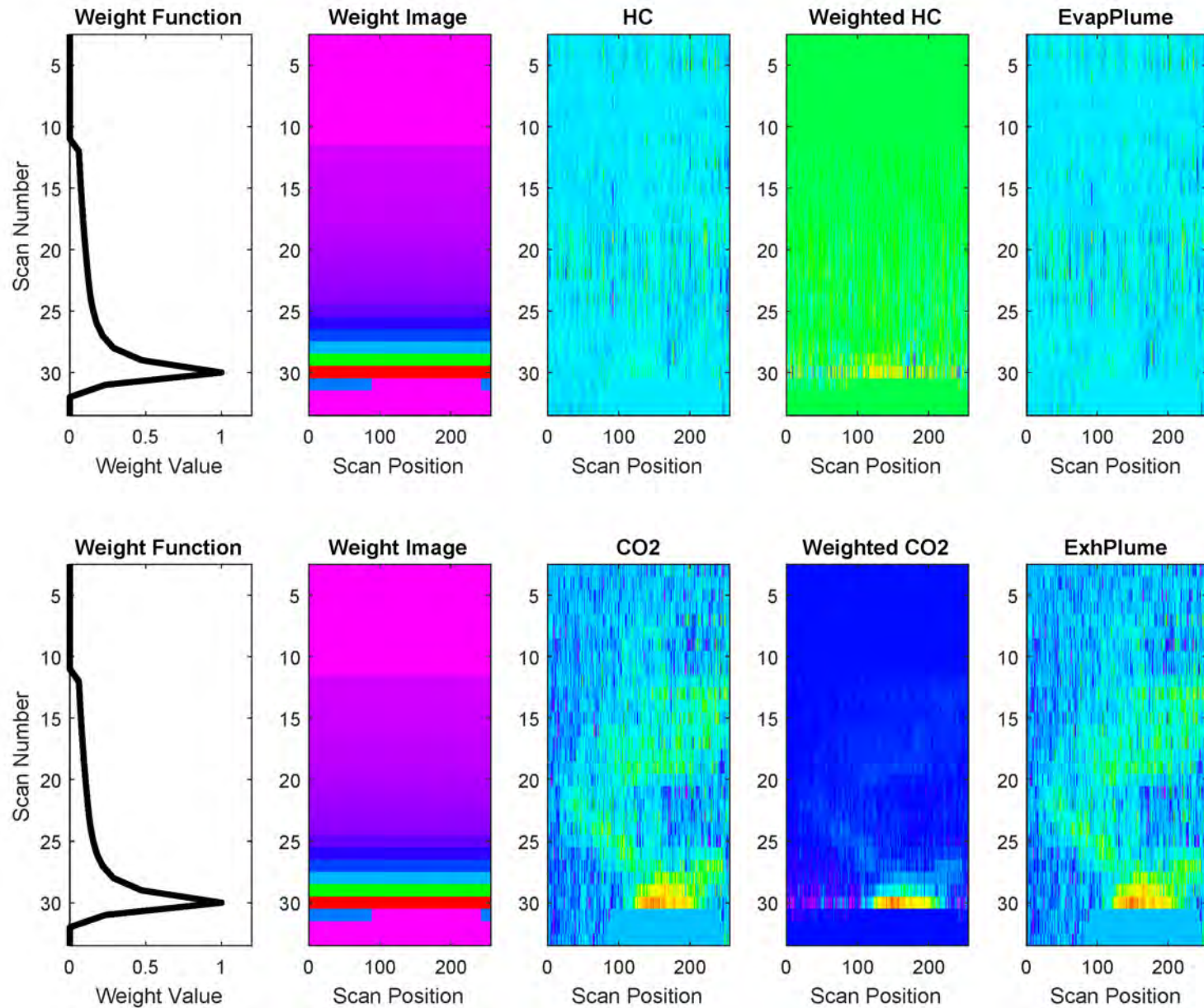
Figure 7-17. Use of Weights for Estimation for Example: EV-1, High EvapHC from HOOD, Low Speed

7 20191020 000505 car 001812   1-EV1 6400mg Hood 22mph Y
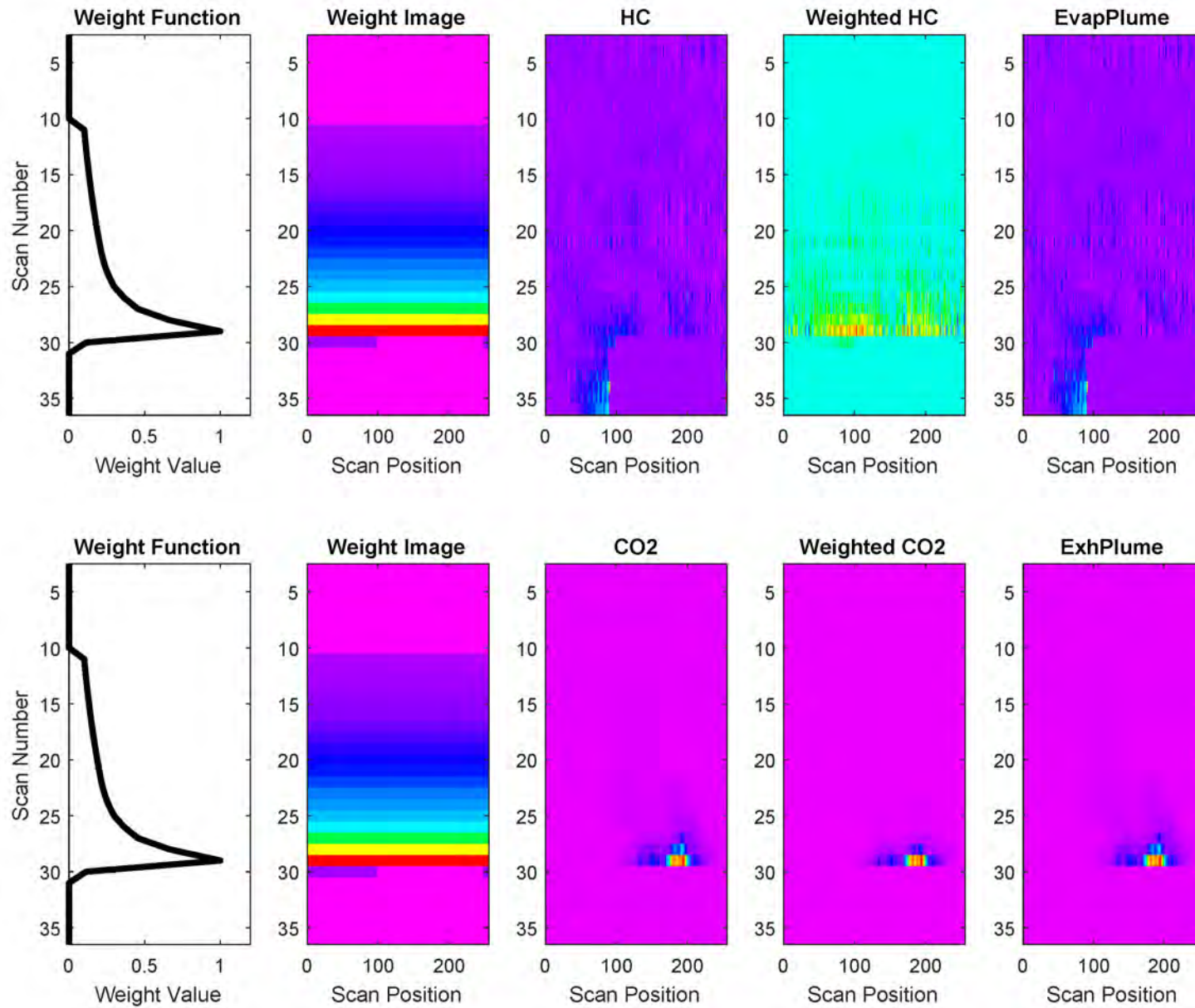
Processing Summary – The goal of weighted least-squares is to improve upon standard least-squares regression by using weightings that emphasize useful signals and suppress noise. Generally, large weight values are used whenever desirable signal components are much larger than undesirable noise components. Conversely, small weight values are used if the measured signals values are dominated by noise. The ideal weighting function is a computed function of the signal-to-noise-ratio of the measured data, from signal processing theory. In this application, we do not have a clear idea of where the plume pixel values will be present or absent precisely. However, we can accurately assume that any plume of interest will be strongest nearest the back of the vehicle, and its strength will decrease with distance from the back bumper. The one-dimensional weighting functions used in the estimation procedure have this precise structure.

The one-dimensional weight functions ignore the precise position of the plume as it appears along the vehicle bumper within the vortex. It is likely that using this lateral position information could further improve the estimation accuracy of the procedure. Applying a two-dimensional weight function to the estimation procedure is mathematically straightforward, as a simple two-dimensional weighting function is already being employed within the software. Two issues remain: 1) an understanding of the proper weighting template as a function of plume and transit parameters and b) a mathematical model that encodes this understanding in numerical form.

As a preview of the former issue, Figure 7-18 shows average CO_2 plumes generated from EV-1 test vehicle data (top row) and EV-2 test vehicle data (bottom row) as a function of the airspeed component parallel to the direction of vehicle motion. In this case, each transit has been aligned to a reference position so that the appropriate pixel average across non-zero transit pixels can be accurately performed. Each of these figures can be compared to the second column of Figures 7-14 through Figure 7-17. The images in Figure 7-18 contain plume structure from side-to-side in the vehicle transit that is not apparent in the weight images of the previous figures. These two-dimensional plume patterns can potentially be a source of more-accurate weight functions for estimating plume components.

Figure 7-19 shows average CO_2 plumes generated from EV-1 for two different nominal road speeds – 22.5 mph (top row) and 45 mph (bottom row). Similar data for EV-2 is provided in Figure 7-20. In these images, the different images from left to right illustrate average plumes as a function of the airspeed component perpendicular to the direction of vehicle motion. The structures of these two-dimensional plumes have not been analyzed, but they could represent a starting point for improved weighting functions as they are easily generated.

Figure 7-18. 2-Dimensional CO₂ Plume Averages for Different Parallel AirSpeed Ranges: EV-1 and EV-2

Top Row: EV-1   Bottom Row: EV-2
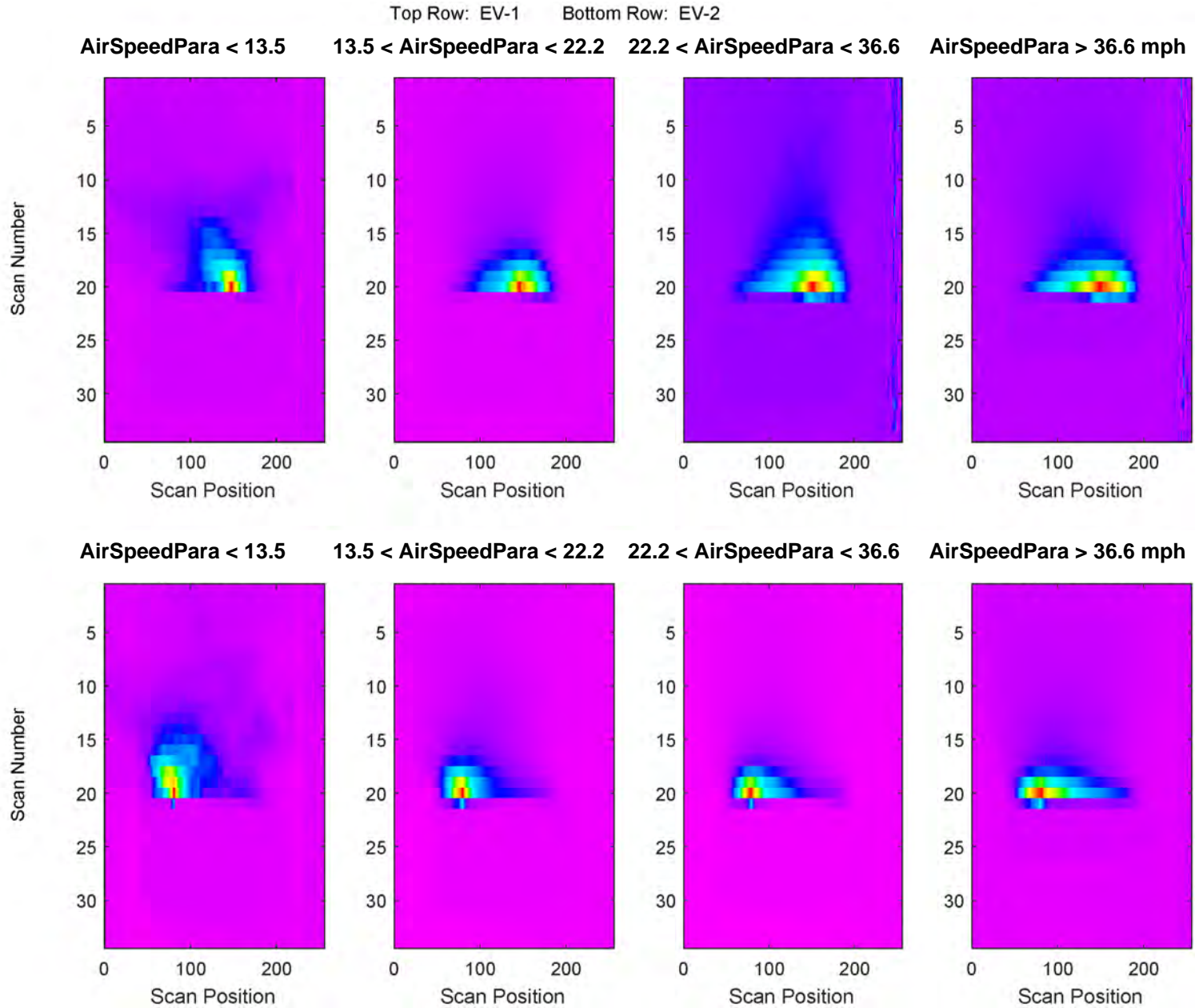
Figure 7-19. 2-Dimensional CO₂ Plume Averages for Different Perpendicular AirSpeed Ranges: EV-1 at Low and High Speeds
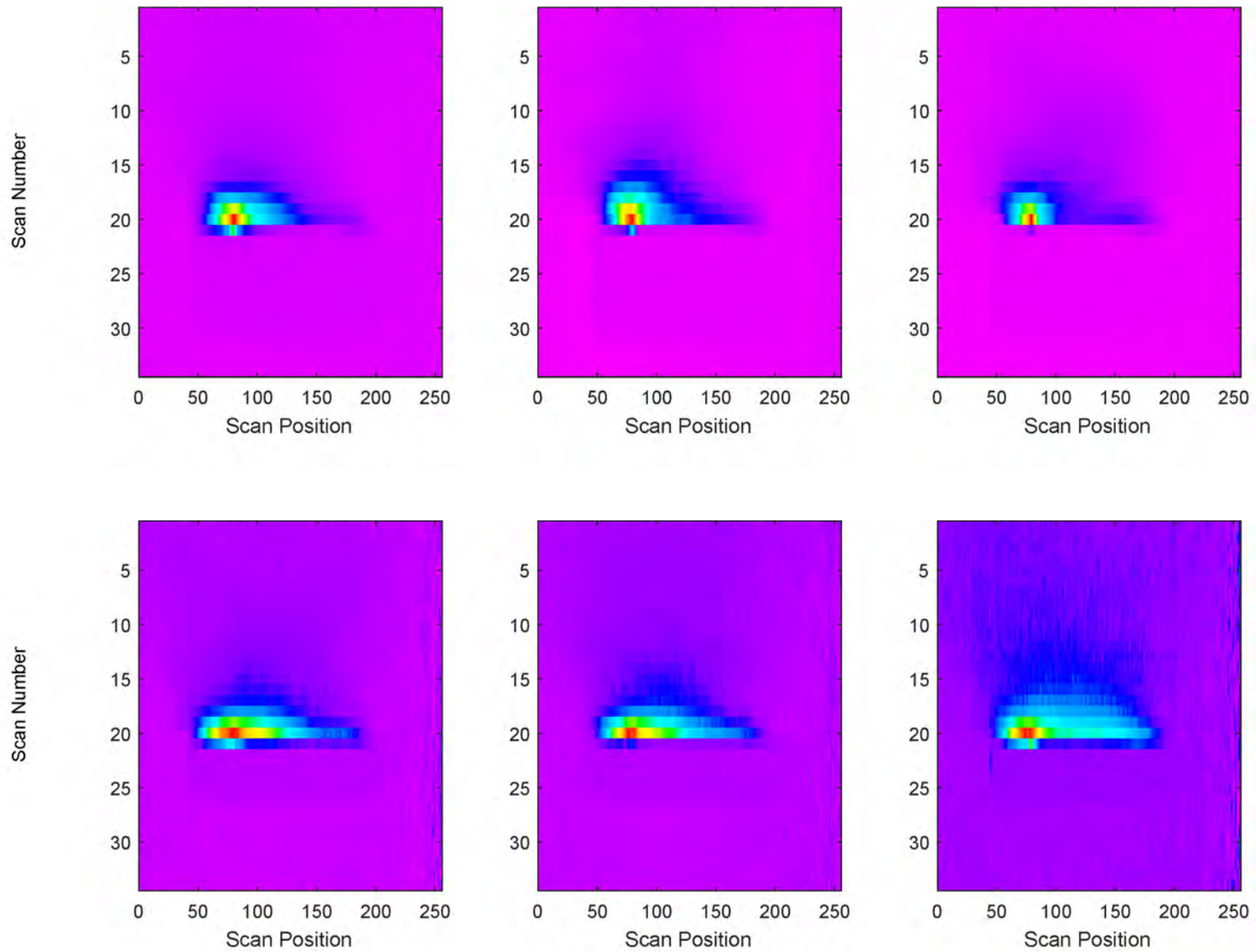
Top Row: EV-1, 22.5 mph   Bottom Row: EV-1, 45 mph
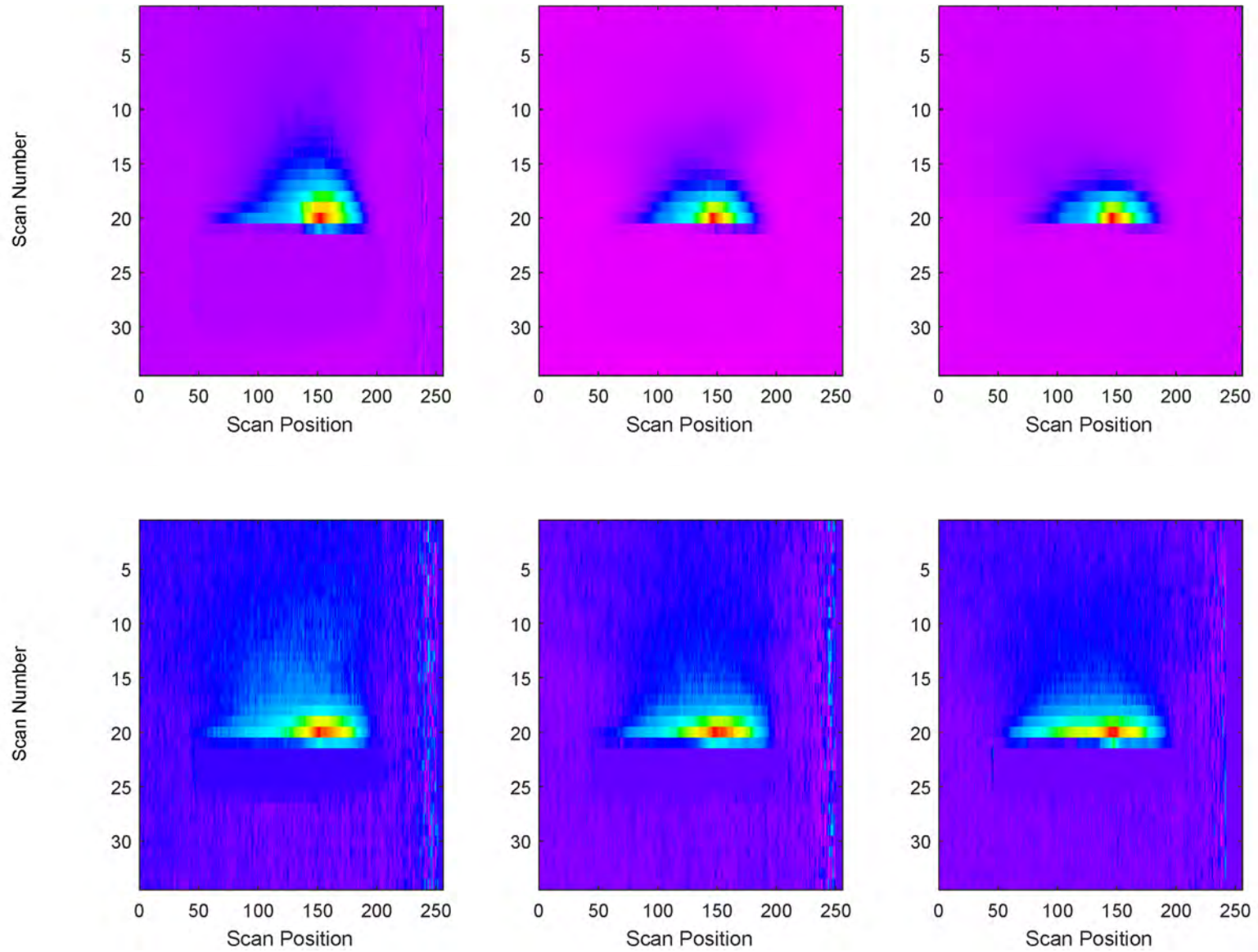
Figure 7-20. 2-Dimensional CO$_2$ Plume Averages for Different Perpendicular AirSpeed Ranges: EV-2 at Low and High Speeds

Top Row: EV-2, 22.5 mph   Bottom Row: EV-2, 45 mph

7.5   Development of Flags to Qualify Processed Detailed Data

The RSD detailed data from some vehicle transits are sometimes contaminated with severe noise or have low CO_2 signal strength. Such events are common in all types of RSD instruments. In such cases in the Westminster dataset, the noise reduction techniques described above are insufficient to produce a transit's adjusted data that will result in proper blind source separation and/or accurate reported emission rates. Just as for traditional RSD outputs, flags that can identify problematic transits need to be developed for the new methodology to avoid including such transits in a dataset that will be used to identify high-emitting vehicles or to characterize the emissions of a fleet sample.

An example will serve to demonstrate how flags can be used to qualify transit data for inclusion in a dataset. A set of 127 transits from the Westminster dataset were selected to preliminarily evaluate performance of noise reduction and blind source separation. The transits were not randomly selected but were selected in groups of light-duty diesels, old gasoline vehicles operating on warm days, test vehicles, and transits that showed detailed data with various levels of noise including some with severe noise.

Figure 7-21 shows the set of ten heatmaps for one example transit: Series=515 Transit=1131. In each heatmap the vehicle is at the bottom of the panel where the color is uniform. The vehicle is moving downward. The top five panels show the heatmap for each RSD channel after noise reduction processing, that is, the heatmaps of the adjusted detailed data. Pollutants CO_2, CO, NO, and NO_2 can only be exhaust pollutants and therefore, if there is any detectable pollutant present, they should have similar heatmaps. While no NO_2 is visible, CO_2, CO, and NO have detectable signals. The spatial patterns of the heatmaps for CO_2 and NO look similar, but CO looks different. In particular, the high-intensity (red) portion of CO is not at the same location as those for CO_2 and NO. Therefore, the CO heatmap is a concern.

The bottom five panels show the output of the blind source separation. A good separation would show a heatmap for ExhPlume that is similar to the heatmap for CO_2 and heatmaps for Noise1, Noise2, and Noise3 that are just a field of random speckles. If substantial EvapHC is detected, it would appear in EvapPlume, as shown in the bottom left panel. The problem is that while Noise2 and Noise3 are predominantly random speckles, Noise1 shows a strong signal that looks like the heatmap for CO. Evidently, BSS "thought" that the heatmaps for CO_2 and CO were substantially different and therefore assigned most of the CO signal to the Noise1 heatmap.

One flag that we have begun to develop is designed to determine if the adjusted CO heatmap is well correlated with the adjusted CO_2 heatmap. More specifically, the question is: What is the probability that the adjusted CO heatmap is the same as the adjusted CO_2 heatmap? Based on the visual examination of the heatmaps in Figure 7-21, we would say that it was a low probability, but we want to quantify the probability so that we can remove the worst offending transits from the analysis dataset.

We visually examined the ten heatmaps of the 127 transits in the selected sample. While it is practical to visually examine the heatmaps of the 127-transit sample set, it is not practical to do so for the entire 30,000-transit Westminster dataset. Therefore, we need to develop flags that can be used to identify suspect transits automatically.

Figure 7-21. Heatmaps for an Example Westminster Transit
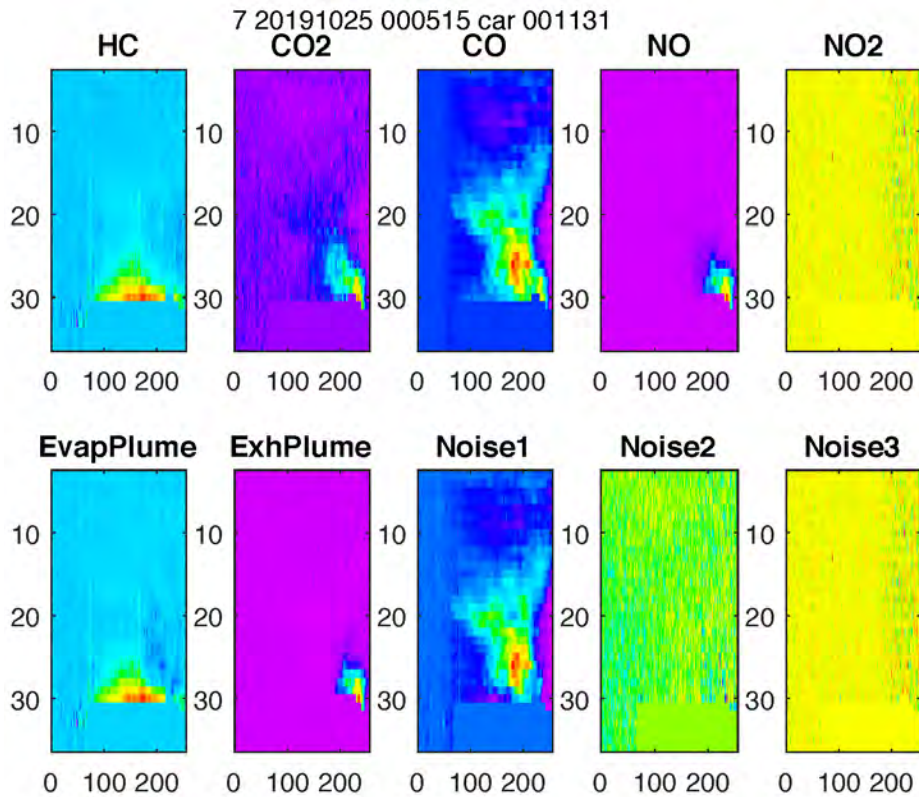
For each of the 127 transits in the selected set, we visually examined the CO_2 and CO heatmaps and answered the questions: 1) Does the CO heatmap show a detectable signal? and 2) If there is a detectable CO signal, is the CO heatmap correlated with the CO_2 heatmap? Then, we used SAS to calculate two statistics: 1) the probability that the pixel values used by the CO heatmap were NOT normally distributed, and 2) the correlation coefficient, R, between the CO pixel values and the CO_2 pixel values.

The results of the exercise are shown in Figure 7-22. The x-axis gives the probability that the pixel values used by the CO heatmap were NOT normally distributed. High x-values indicate that a signal was present in the CO heatmap; low x-values indicate that the CO values were likely just noise. The y-axis gives the correlation between CO pixel values and CO_2 pixel values. High y-values near 1 indicate the pixel values are highly, positively correlated. Y-values near 0 indicate poor correlation.

The symbols in the figure indicate the results of the visual examination of the heatmaps. Blue triangles indicate that a signal was observed in the CO heatmap and that it appeared to be correlated with the CO_2 heatmap. Black dots indicate that no or a very weak signal was seen in the CO heatmap and therefore it was not possible to visually determine if a correlation with CO_2 was present or not. Red dots indicate that a signal was seen in the CO heatmap and that it was not correlated with the CO_2 heatmap. The figure shows overlap between the "good" (blue and black) transits from the "bad" (red) transits. The red dot at (0.25, 0.66) is the symbol for the transit examined in Figure 7-21.

Figure 7-22. Statistics for Adjusted CO and CO₂ for the 127-Transit Sample Set
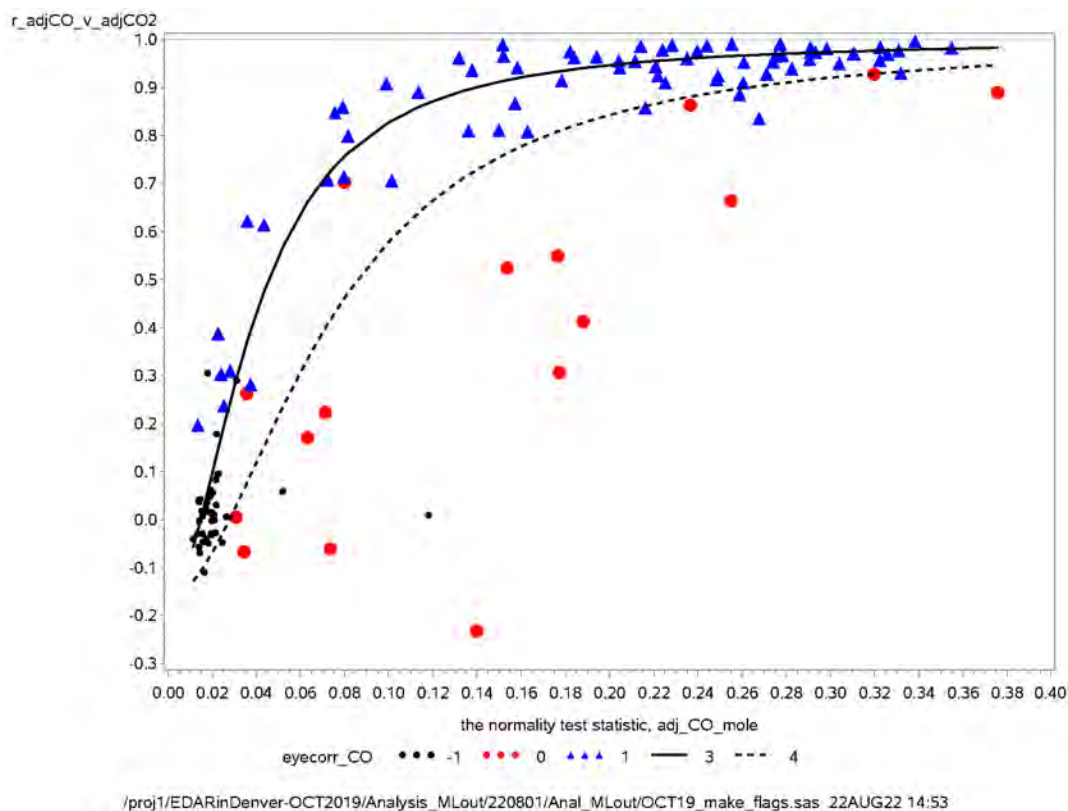
We built a model[30] to approximate the trend through the black dots and blue triangles, which were visually judged to be "good" transits with respect to CO and CO_2 correlation. The modeling dataset did not include any red dots and did not include the two black dots that are among the red dots. All of those transits were judged as "bad." The resulting model is the black solid curve in the figure. The model also provided an estimate of the standard deviation of the distribution of measured y-values above and below the black curve. We drew the dashed black line at -1.645 standard deviations, which provides an estimate of the location of the one-tailed 5% probability curve. That means that a CO heatmap that has its symbol below the dashed line has less than a 5% probability of being correlated with the CO_2 heatmap.

The standard deviation can also be used to calculate the correlation probability for each transit. For example, the probability that the CO heatmap of the transit examined in Figure 7-21 is correlated with its CO_2 heatmap is only 0.015%. These individual probabilities can be used to choose the probability levels used to cull out suspect transits.

Development of flags is underway but not yet completed. Therefore, the fleet emissions characteristics that are reported below have not had their underlying transit detailed datasets screened by flags. Accordingly, the findings below must be regarded as preliminary.

---

[30] /proj1/EDARinDenver-OCT2019/Analysis_MLout/220801/Anal_MLout/OCT19_make_flags.sas

8.0   Exhaust Concentrations Reported by EDAR

The primary goal of this study was to study on-road running loss emissions. However, EDAR routinely reports exhaust emissions for each vehicle transit. In the subsections below, we use the test vehicle data and the fleet data to characterize the exhaust emissions performance of the EDAR instrument.

In Section 2.9, Table 2-5 showed that the EDAR QC flag assigned values of "valid," "interfering plume," "low CO_2," or "no plate" to each transit. Interfering plumes and small CO_2 plumes are likely to cause reported EDAR concentration values that have larger error than otherwise. Therefore, for the analysis results reported below, transits with EDAR QC flag values of "interfering plume" or "low CO_2" were not used.

8.1   EDAR Exhaust Concentrations on Test Vehicles

As part of the study, the exhaust emissions of the test vehicles were reported by the EDAR instrument. For most of the test runs, the EV-1, EV-2, F-150, GMC, and Subaru test vehicles drove past the RSD while releasing real or simulated exhaust emissions <u>and</u> simulated running loss emissions. But for some planned test runs, they drove past releasing only exhaust emissions. In addition, the Infiniti, which never released simulated running loss emissions, drove past the RSD for every convoy transit. We identified 425 individual test vehicle transits when no artificial running losses were released (ref_MeasuredReleaseRate = 0 g/hr), when the test conditions were satisfied (ref_QualityFlag = G or Q), and when the EDAR RSD reported that the result was valid (EDAR_QC = valid). The reported exhaust emissions of those runs with date and time are provided in Appendix A.

Histograms for the reported HC, CO, NO, and CO_2 emissions are shown using uniform concentration axes in Figures 8-1 to 8-4 for EV-1, EV-2, the Subaru, and the Infiniti. These four vehicles had the largest number of measurements. Table 8-1 gives statistics describing the eligible exhaust emissions values for all six test vehicles.

As described earlier, the EV-1 and EV-2 test vehicles released a puff of a stoichiometric blend of dry, simulated exhaust gas mixtures just before each RSD transit. Because these simulated exhaust gas blends came from a cylinder, the blend concentrations were the same for every transit. On the other hand, the exhaust from the F-150, GMC, Subaru, and Infiniti was just their usual, natural exhaust; they did not release artificial exhaust gas mixtures. Consequently, their exhaust contained water of combustion. Also, emissions concentrations could possibly change concentrations from run to run depending on engine and catalyst operation. The exhaust gas concentrations were known for the EV-1 and EV-2 from the labels on the cylinders, but the exhaust concentrations of the other four test vehicles were not measured except by the EDAR instrument.

Figure 8-1. EDAR Exhaust Concentration Measurements on EV-1
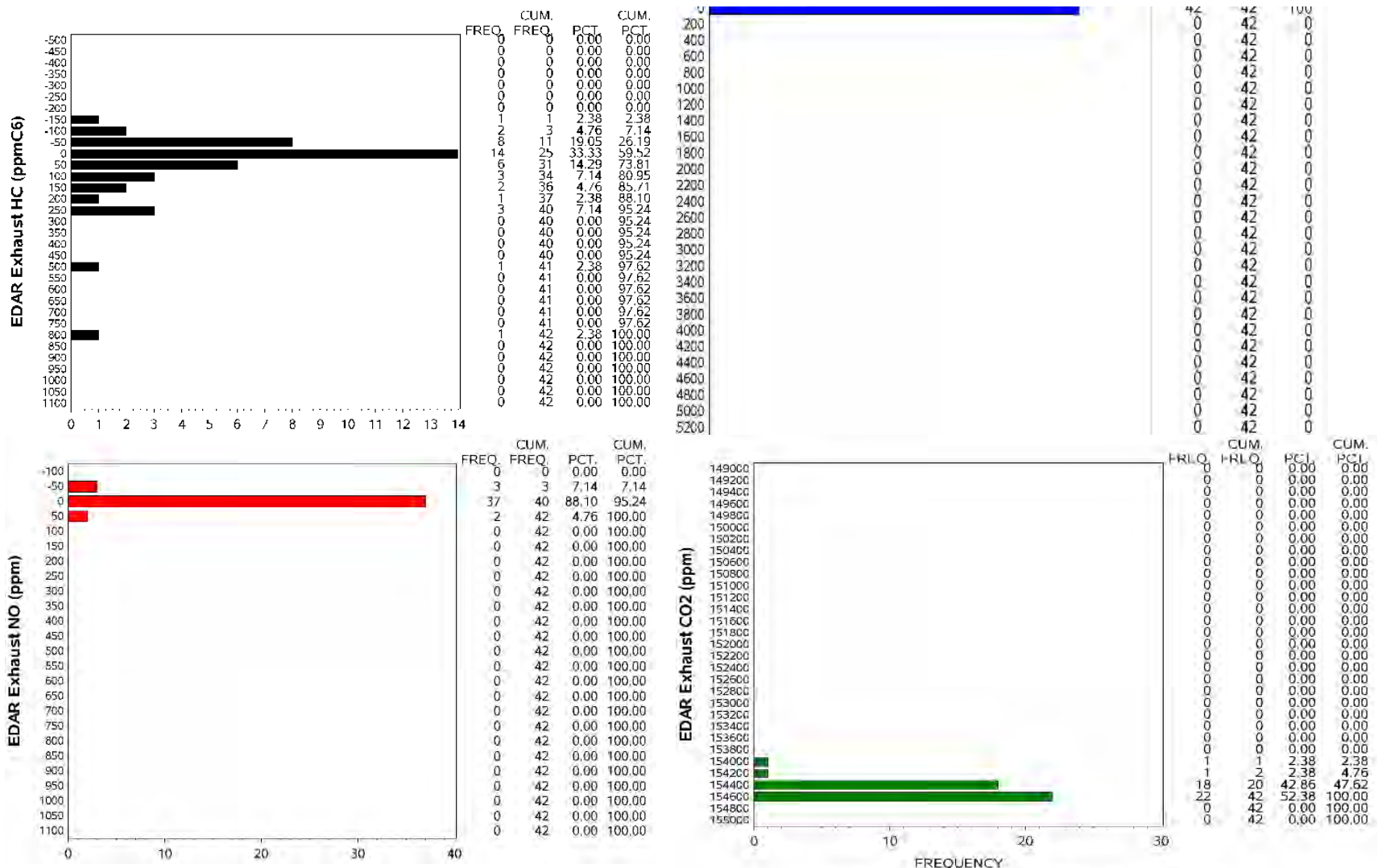
Figure 8-2. EDAR Exhaust Concentration Measurements on EV-2

Figure 8-3. EDAR Exhaust Concentration Measurements on Subaru
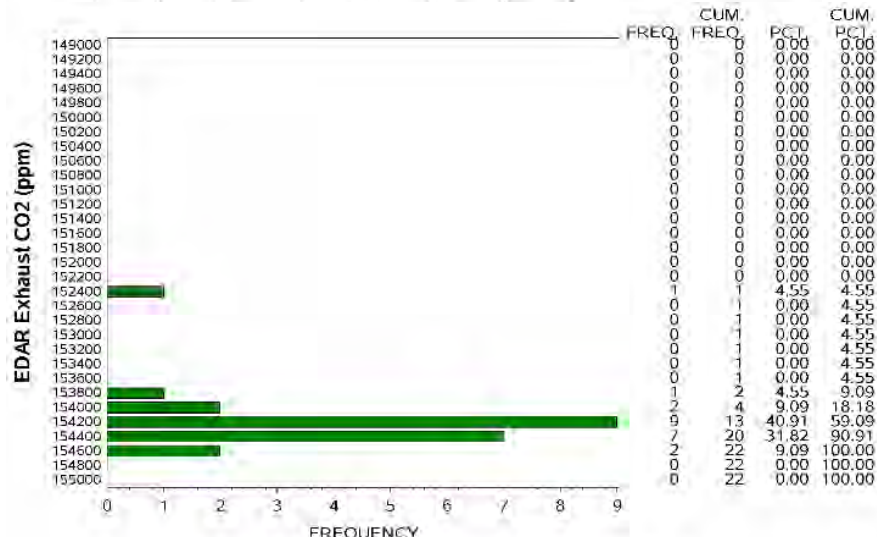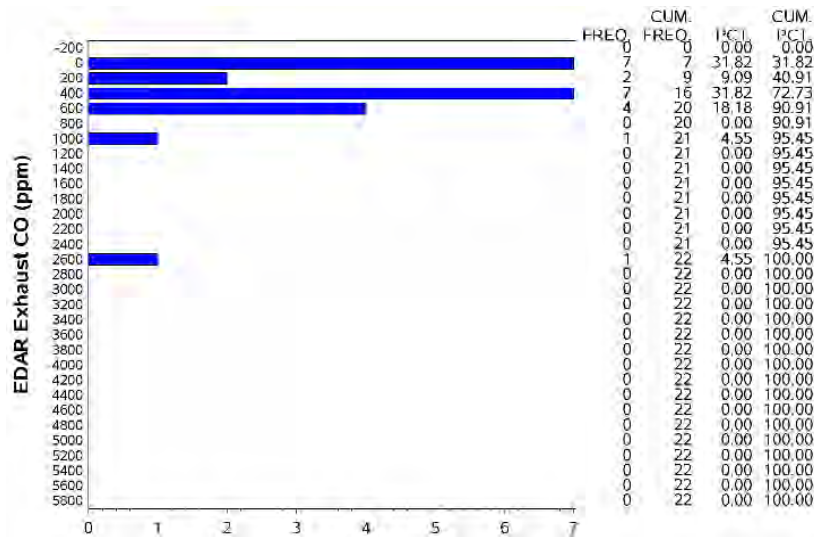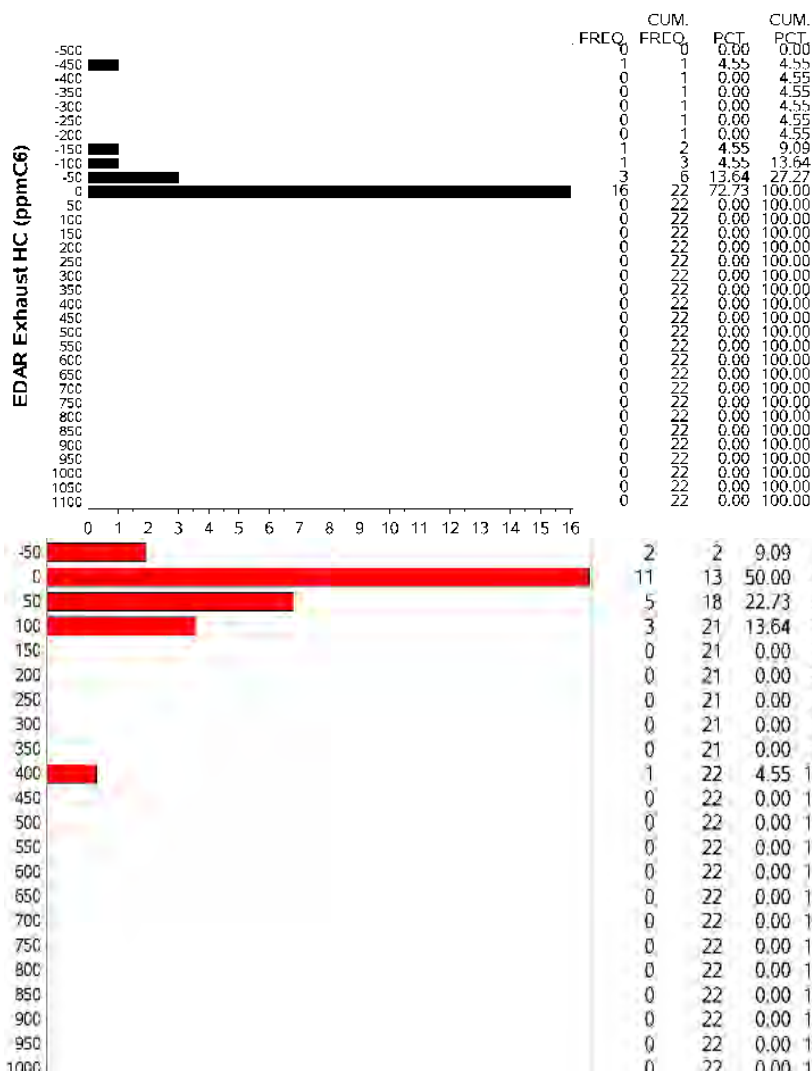
Figure 8-4. EDAR Exhaust Concentration Measurements on Infiniti

Table 8-1. Reported Exhaust Concentrations for the Test Vehicles

a)

Reference Vehicle ID	Label HC (ppmC3)	N	EDAR Reported Exhaust HC (ppmC6)								
			Percentiles					Mean	Std Dev	Min.	Max.
			16th	25th	50th	75th	84th				
1-EV1	0	42	-53	-29	2	78	164	55	163	-135	791
2-EV2	402	49	80	123	169	233	271	178	115	-75	554
3-F150	n/a	18	-69	-19	0	2	6	-20	44	-160	17
3-GMC	n/a	4	-1	-1	0	1	1	0	1	-1	1
3-Subaru	n/a	22	-73	-27	-9	4	6	-43	102	-455	15
4-Infiniti	n/a	290	-13	-7	-2	0	1	3	86	-300	1047

b)

Reference Vehicle ID	Label CO (ppm)	N	EDAR Reported Exhaust CO (ppm)								
			Percentiles					Mean	Std Dev	Min.	Max.
			16th	25th	50th	75th	84th				
1-EV1	0	42	-8	-5	1	7	25	5	22	-48	80
2-EV2	5043	49	5030	5076	5294	5460	5551	5210	385	4053	5699
3-F150	n/a	18	6	11	44	109	137	80	107	-6	421
3-GMC	n/a	4	58	94	130	345	558	219	229	58	558
3-Subaru	n/a	22	22	79	336	551	608	425	555	-7	2651
4-Infiniti	n/a	290	109	143	251	433	595	778	4071	-91	47348

c)

Reference Vehicle ID	Label NO (ppm)	N	EDAR Reported Exhaust NO (ppm)								
			Percentiles					Mean	Std Dev	Min.	Max.
			16th	25th	50th	75th	84th				
1-EV1	0	42	-10	-2	1	7	12	0	18	-57	49
2-EV2	996	49	861	881	922	977	1023	917	101	531	1060
3-F150	n/a	18	7	12	22	42	54	29	23	-12	83
3-GMC	n/a	4	-2	0	3	7	9	4	5	-2	9
3-Subaru	n/a	22	-2	3	17	52	80	42	91	-43	416
4-Infiniti	n/a	290	1	3	6	14	18	10	19	-26	226

d)

Reference Vehicle ID	Label CO_2 (ppm)	N	EDAR Reported Exhaust CO_2 (ppm)								
			Percentiles					Mean	Std Dev	Min.	Max.
			16th	25th	50th	75th	84th				
1-EV1	150500	42	154395	154427	154509	154534	154543	154471	101	154009	154555
2-EV2	147600	49	149998	150051	150215	150319	150425	150234	296	149530	151155
3-F150	n/a	18	154328	154405	154468	154509	154527	154436	98	154166	154532
3-GMC	n/a	4	154136	154295	154454	154472	154489	154383	166	154136	154489
3-Subaru	n/a	22	154067	154112	154245	154431	154486	154177	445	152368	154532
4-Infiniti	n/a	290	154008	154159	154334	154414	154447	153921	3001	119640	154545

The distributions of the reported exhaust emissions concentrations for EV-1 are shown in Figure 8-1. The distributions for CO (blue), NO (red), and CO_2 (green) are relatively tight, but the distribution for HC (black) has two elevated values that appear to be outliers. Appendix A indicates that these values, which are shaded with yellow backgrounds, are 498 and 791 ppmC6. The CO, NO, and CO_2 values associated with these two transits do not appear to be outliers.

Table 8-1 shows statistics for the 42 EV-1 transits in the first data row of sub-tables a), b), c), and d). Comparison of the 50 percentile (median) values (light blue) with the mean values (light green) provides an indication of the influence of outlier values. For HC, the mean of 55 ppmC6 is somewhat higher than the median 2 ppmC6 value. This difference is presumably caused by the two high HC values increasing the mean. On the other hand, median and mean values are comparable for EV-1's CO, NO, and CO_2: 1 vs. 5ppm, 1 vs. 0 ppm, and 154,509 vs. 154,471 ppm.

Table 8-1 also shows the comparisons of the statistics with the labeled concentrations for the cylinders used for EV-1 and EV-2 for the artificial dry exhaust gas mixtures. EV-1 was releasing a "clean" artificial exhaust gas mixture that had only 15.05 vol% CO_2 with balance nitrogen. Table 8-1 shows percentiles and standard deviations to judge variability. Like means, standard deviations can be more susceptible to outliers than percentiles – at least for percentiles that are not near the extremes of distributions. For a normal distribution, the -1 standard deviation point and the +1 standard deviation points are at approximately the 16 and 84 percentile values.

Table 8-2 helps to focus on the EDAR performance for measuring the "clean" artificial exhaust gas mixture released from EV-1. The table uses only the medians to describe trends since medians are less susceptible to extreme measured values. The EDAR medians in the third column are very close to the cylinder values in the second column. The 95% confidence limits of the medians are shown in the fourth and fifth columns. The confidence limits are quite close to the medians for CO, NO, and CO_2 and are larger for HC. The CO_2 deviations, expressed as percents with respect to (wrt) the CO_2 median, are given in the sixth and seventh columns. The last column shows that EDAR was reporting CO_2 about 2.7% higher than the label concentration on the gas cylinder.

Table 8-2. Dry, Artificial Exhaust Zero Performance by EV-1 Test Vehicle[31]

Pollutant	Concentration (ppm vol)		Confidence Limits on Median (ppm vol)		Deviation (Δ% wrt Median)		Accuracy (% wrt Cylinder)
	Cylinder Value	EDAR Median	Lower 95%CL	Upper 95%CL	Lower 95%CL	Upper 95%CL	Median Cylinder
HC	0	2	-9	40	n/a	n/a	n/a
CO	0	1	-2	3	n/a	n/a	n/a
NO	0	1	-1	3	n/a	n/a	n/a
CO_2	150500	154509	154469	154523	-0.03%	+0.01%	102.7%

---

[31] P:\EDARinDenver-OCT2019\Analysis/refveh_out.xlsx

Test vehicle EV-2 released an artificial, dry exhaust gas mixture that can be called "dirty" since it had cylinder label concentrations of 402 ppmC3 HC, 5043 ppm CO, 996 ppm NO, and 147,600 ppm CO_2, as shown in the second column of Table 8-1. Thus, while exhaust mixture releases from EV-1 can be used to evaluate EDAR performance at zero, the exhaust mixture releases from EV-2 can be used to evaluate EDAR performance at high values – essentially a span evaluation.

Note that EDAR reports HC in units of ppmC6, that is, ppm on a hexane basis. Since the exhaust gas cylinders used propane as the HC gas, the cylinder HC concentrations are in units of ppmC3, that is, ppm on a propane basis. The conversion factor between ppmC6 and ppmC3 is roughly a factor of 2. For example, 402 ppmC3 ≈ 201 ppmC6. That means that when evaluating EDAR HC performance for measuring the dirty mixture, we should compare EDAR HC reported values against the 201 ppmC6 value.

Figure 8-2 shows histograms for the 49 valid test runs of EV-2 when artificial exhaust was released but artificial running losses were not released. The following extreme values, although not necessarily outliers, are observed in the histograms and are shaded in yellow in Appendix A: -75 ppmC6 HC, 554 ppmC6 HC, 4070 ppm CO, 531 ppm NO, and 624 ppm NO. The appendix shows that the 4070 ppm CO and 531 ppm NO occurred on the same transit. Similarly, the 554 ppmC6 HC and 624 ppm NO occurred on a different transit. These associated extreme reported values suggest that some sort of noise threw off the calculations of the reported values for these transits.

The presence of extreme reported values has an influence on evaluating the EDAR "span" performance using mean and standard deviation, which are shown in Table 8-1. The median values for EV-2 are condensed in Table 8-3. Table 8-3 shows that for the exhaust span mixture, the relative deviations (columns six and seven), expressed as a percent with respect to the median, were low for CO, NO, and CO_2, but were high for HC. The last column shows the accuracy, as measured by the median, relative to the cylinder concentrations. HC was 16% low, CO was 5% high, NO was 7% low, and CO_2 was 2 % high.

Table 8-3. Dry, Artificial Exhaust Span Performance by EV-2 Test Vehicle[32]

Pollutant	Concentration (ppm vol)		Confidence Limits on Median (ppm vol)		Deviation (Δ% wrt Median)		Accuracy (% wrt Cylinder)
	Cylinder Value	EDAR Median	Lower 95%CL	Upper 95%CL	Lower 95%CL	Upper 95%CL	**Median** Cylinder
HC	201	169	148	185	-12.6%	+ 9.2%	84.3%
CO	5043	5294	5210	5399	-1.6%	+ 2.0%	105.0%
NO	996	922	898	941	-2.6%	+ 2.1%	92.6%
CO₂	147600	150215	150119	150271	-0.06%	+0.04%	101.8%

The four non-electric test vehicles (F-150, GMC, Subaru, and Infiniti) did not release artificial exhaust gas mixtures. Instead, they released their natural tailpipe exhaust at their usual flow

---

[32] P:\EDARinDenver-OCT2019\Analysis/refveh_out.xlsx

rates. Also, their exhaust compositions were natural, which means they included water of combustion and a wide variety of hydrocarbon compounds. Depending on the methods used by EDAR, these differences could affect the measurements. These potential influences were the reason that gasoline vehicles were used as part of the test vehicle convoy.

For NO, Table 8-1c shows that for the four non-electric test vehicles, EDAR reported NO mean and median values that were somewhat (2 to 42 ppm) higher than those reported for EV-1. Such NO levels can be expected from properly operating current technology vehicles. The 16th and 25th percentile NO values for the non-electric test vehicles were comparable to those for EV-1. However, for the 75th and 84th percentiles, the NO values tended to be higher than for EV-1. This trend could be the result of real changes in NO concentrations of the non-EVs as their real engines and catalyst systems operated.

For HC, Table 8-1a shows that the four non-EVs had reported median HC values near 0 ppmC6 and near the 2 ppmC6 median value reported for EV-1. In addition, the non-EV's reported HC values for the upper and lower percentiles seemed to be substantially tighter (i.e., closer to the median) than for the EV-1. The tailpipe emissions of gasoline vehicles is a mixture of many HC compounds, contains water of combustion, and is emitted at flow rates generally larger than those used on the EVs. Since the EDAR instrument is intended to measure the emissions of real vehicles, and not artificial exhaust emissions, it is possible that EDAR performance on real exhaust may be superior to performance on simulated exhaust.

For CO, the EV-1 statistics in Table 8-1b show that EDAR reports CO values with low bias and good repeatability when challenged with an artificial zero gas. For the non-EVs, Table 8-1c shows that the non-EVs apparently have CO concentrations somewhat above zero. Additionally, the variability in the reported median (or mean) values is monotonically increasing with the median (or mean) values. There are two indistinguishable contributions to this trend in variability: 1) actual vehicles with higher emissions will tend to have higher emissions variability, and 2) measured values will tend to have higher variability due to noise in the measuring process.

Appendix A shows that the Infiniti occasionally had high reported CO values. Of the 290 eligible transits, the highest four values, which are shaded in yellow, were 5098, 34380, 38009, and 47348 ppm CO. We have no reason to not believe these values and suggest that they may have occurred because of enrichment while accelerating in traffic.

8.2 EDAR Exhaust Concentrations on Fleet Vehicles

We can also evaluate EDAR's exhaust emissions measurement performance by examining the reported emissions of fleet vehicles as they drove under the instrument. Of the 33,636 transits recorded during the testing, 21,398 transits were determined to be from 13,480 private gasoline vehicles with recognizable Colorado plates, decodable VINs, and with EDAR_QC = "valid". Model years ranged from 1947 through 2020. For calculating emissions statistics, the 1947 through 1989 model year vehicles were combined into a ≤1989 model year group.

The gray dot symbols in Figures 8-5, 8-6, and 8-7 show EDAR's measured values for HC, CO, and NO for the 21,398 transits as a function of model year. The plots have constrained upper and lower y-axis ranges so that some detail in model-year trends can be seen. Consequently, several

emissions values are "off scale." All three plots show some negative emissions measurements. Negative measurements can occur because of random noise in the instrument's underlying optical measurements. Substantially more negative HC values are reported than CO and NO values. That trend is in agreement with the test vehicle results, which were described in the previous subsection.

The lines in the plots denote the model-year trends of the following percentiles: 5 (dark blue), 10 (medium blue), 20 (light blue), 50 (black), 80 (orange), 90 (red), and 95 (dark red). All three figures show a generally downward trend with movement toward newer model years. Figure 8-5 shows the HC downward trend from 1990 to 2004. For model years newer than 2004, no further HC decrease can be seen. For CO and NO in Figures 8-6 and 8-7, the percentile lines show the downward trend throughout the entire model year range.

Table 8-4 gives statistics by model year for the HC, CO, and NO emissions measurements reported by the EDAR instrument. For each pollutant, the table gives the mean and its 95% confidence limits (tan background) and the median and its 95% confidence limits (green background). Both mean and median are useful measures of the central tendency of each distribution. Because the emissions distribution within each model year is positively skewed, there is a strong tendency for the mean emissions value to be larger than the median emissions value. For example, for the 96 mean-median pairs in Table 8-4, the mean is larger than the median 93 times. However, as discussed in the previous subsection, the mean and its confidence limits are quite susceptible to outliers, while the median and its confidence limits are less susceptible to outliers. There is also a strong tendency for the 95% confidence interval for the median to be narrower (and usually much narrower) than the 95% confidence interval for the mean. For example, for the 96 mean-median pairs of intervals in Table 8-4, the interval for the mean is larger than the interval for the median 90 times.

Figure 8-5. Model Year Distribution of Fleet HC Concentration Measurements
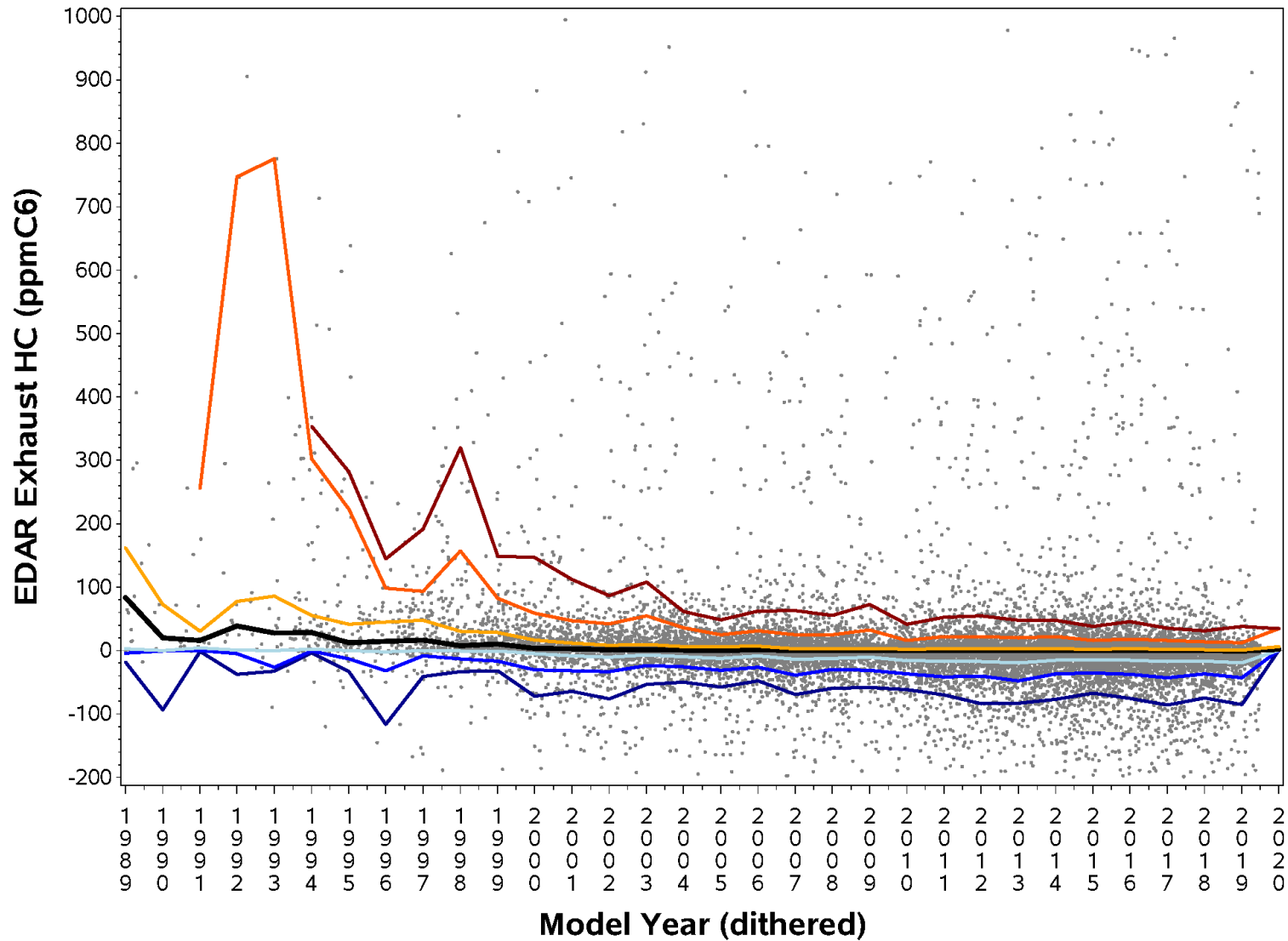
/proj1/EDARinDenver-OCT2019/Analysis/analyze_Fleet_Exh_1.sas 04MAY20 16:46

Figure 8-6. Model Year Distribution of Fleet CO Concentration Measurements
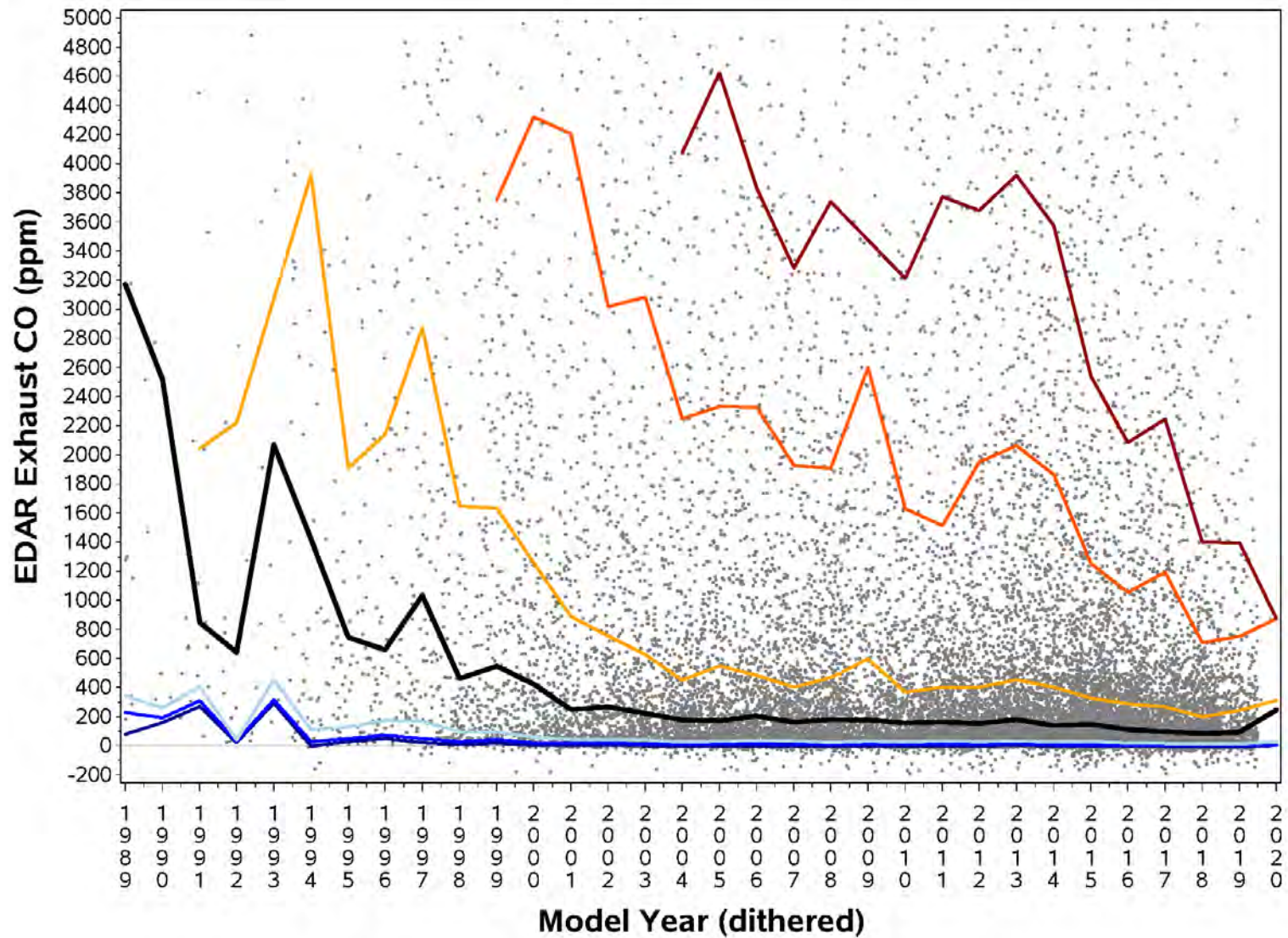
/proj1/EDARinDenver-OCT2019/Analysis/analyze_Fleet_Exh_1.sas 04MAY20 16:46

Percentile: — 5 — 10 — 20 — 50 — 80 — 90 — 95

Figure 8-7. Model Year Distribution of Fleet NO Concentration Measurements
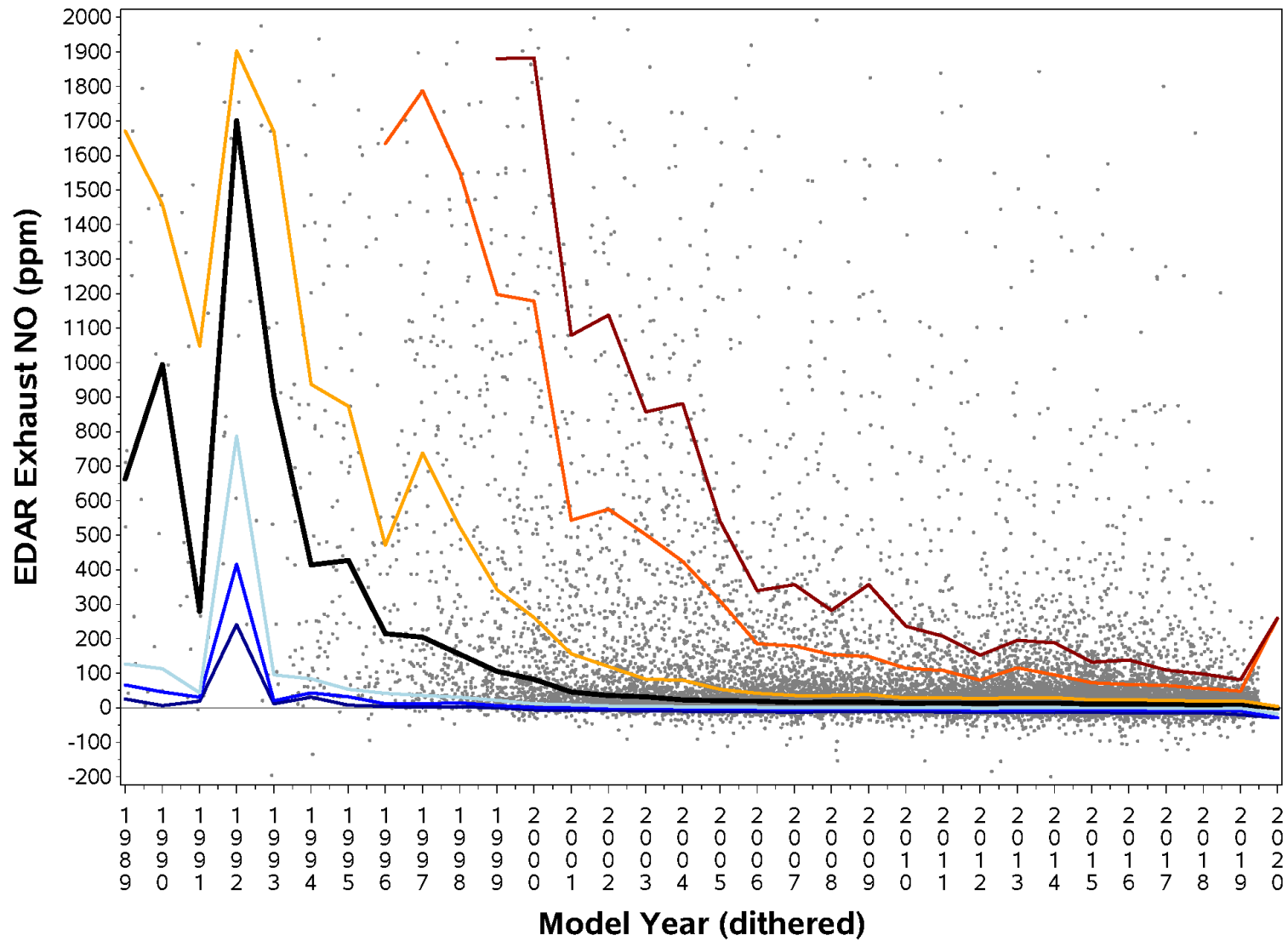
/proj1/EDARinDenver-OCT2019/Analysis/analyze_Fleet_Exh_1.sas 04MAY20 16:46

Percentile: 5   10   20   50   80   90   95

Table 8-4. Fleet Vehicle Model-Year-Mean and Median Concentration Measurements and Confidence Intervals

Model Year	Count	HC (ppmC6)						CO (ppm)						NO (ppm)					
		Lower 95%CL	Mean	Upper 95%CL	Lower 95%CL	Median	Upper 95%CL	Lower 95%CL	Mean	Upper 95%CL	Lower 95%CL	Median	Upper 95%CL	Lower 95%CL	Mean	Upper 95%CL	Lower 95%CL	Median	Upper 95%CL
≤1989	32	52	158	264	15	83	161	3922	10812	17702	1151	3170	8871	688	1031	1374	368	662	1671
1990	15	-30	366	762	0	20	167	1368	8660	15952	320	2516	12157	502	1206	1911	177	993	1485
1991	21	-56	214	484	4	16	70	888	1921	2953	481	847	2095	314	619	924	162	279	1143
1992	18	8	138	268	14	39	91	388	2220	4052	86	643	2746	1126	1568	2011	797	1702	2339
1993	24	-24	280	584	5	28	110	2758	6908	11057	896	2067	6823	660	1135	1609	242	906	1687
1994	81	58	90	122	19	28	42	2769	4505	6241	449	1418	3177	569	773	977	188	413	786
1995	77	30	59	87	7	12	30	1603	3262	4920	571	744	1272	566	751	936	244	427	711
1996	85	-17	58	134	8	14	30	1724	2980	4236	484	660	1511	354	536	718	105	214	388
1997	151	20	32	43	12	16	23	1779	2550	3321	624	1031	1746	480	616	752	128	205	367
1998	195	28	50	73	3	8	12	1790	2874	3958	312	461	782	408	505	603	118	155	240
1999	250	25	46	67	6	10	16	1344	2373	3401	382	545	813	313	387	462	77	105	168
2000	360	7	25	43	2	3	5	1399	1918	2437	321	421	630	299	369	439	67	83	114
2001	390	8	24	41	1	2	3	1242	1840	2438	184	248	338	166	210	254	40	45	59
2002	483	-2	9	20	0	1	2	907	1160	1414	217	267	338	170	215	259	27	35	44
2003	563	10	20	29	0	1	2	891	1159	1427	180	223	273	140	177	214	25	32	40
2004	723	-15	49	114	0	0	1	766	1148	1530	144	177	209	137	170	203	18	23	28
2005	764	-4	3	10	0	0	0	758	1084	1410	144	169	209	93	115	137	17	20	23
2006	816	1	7	13	1	1	1	753	937	1120	164	203	234	69	92	114	16	19	21
2007	980	-4	6	16	0	0	0	637	784	930	146	161	183	64	81	97	13	15	18
2008	1013	-2	6	15	0	0	0	721	861	1002	156	180	216	58	74	91	15	16	18
2009	628	-3	10	23	0	0	0	842	1089	1336	143	176	214	62	84	105	13	16	20
2010	862	-5	2	8	-1	0	0	553	718	883	134	156	178	40	51	62	11	13	15
2011	1104	-3	3	9	0	0	0	614	731	848	143	162	180	45	61	76	12	14	15
2012	1168	-41	42	125	0	0	0	666	811	955	139	153	167	32	39	47	11	12	14
2013	1380	-8	-2	4	0	0	0	697	795	893	157	179	203	47	60	74	12	13	15
2014	1551	-19	26	72	0	0	0	692	810	928	121	138	156	40	49	58	13	14	15
2015	2235	-5	0	4	-1	0	0	553	674	795	134	147	160	31	37	43	9	10	11
2016	1749	-3	6	14	0	0	0	426	514	602	96	109	120	28	34	40	10	11	13
2017	1585	-4	4	12	-1	-1	0	424	514	605	84	94	106	27	34	41	9	10	11
2018	1418	-11	-8	-4	-1	-1	0	315	404	493	72	83	92	23	31	40	8	9	10
2019	672	-4	7	19	-2	-1	-1	274	369	464	81	92	107	15	18	22	8	9	11
2020	5	-10	8	27	0	1	34	-137	295	728	2	247	872	-105	45	196	-29	-1	261

Figure 8-8. Model Year Distribution of Fleet Mean [HC] Measurements
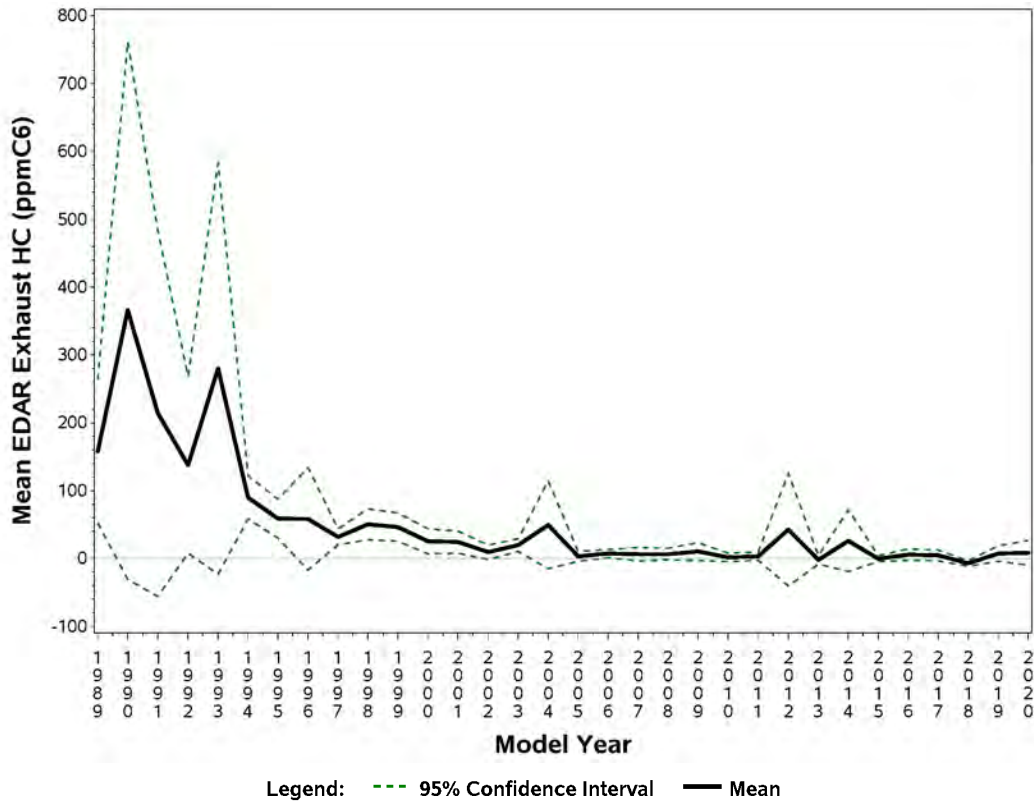
Figure 8-9. Model Year Distribution of Fleet Median [HC] Measurements
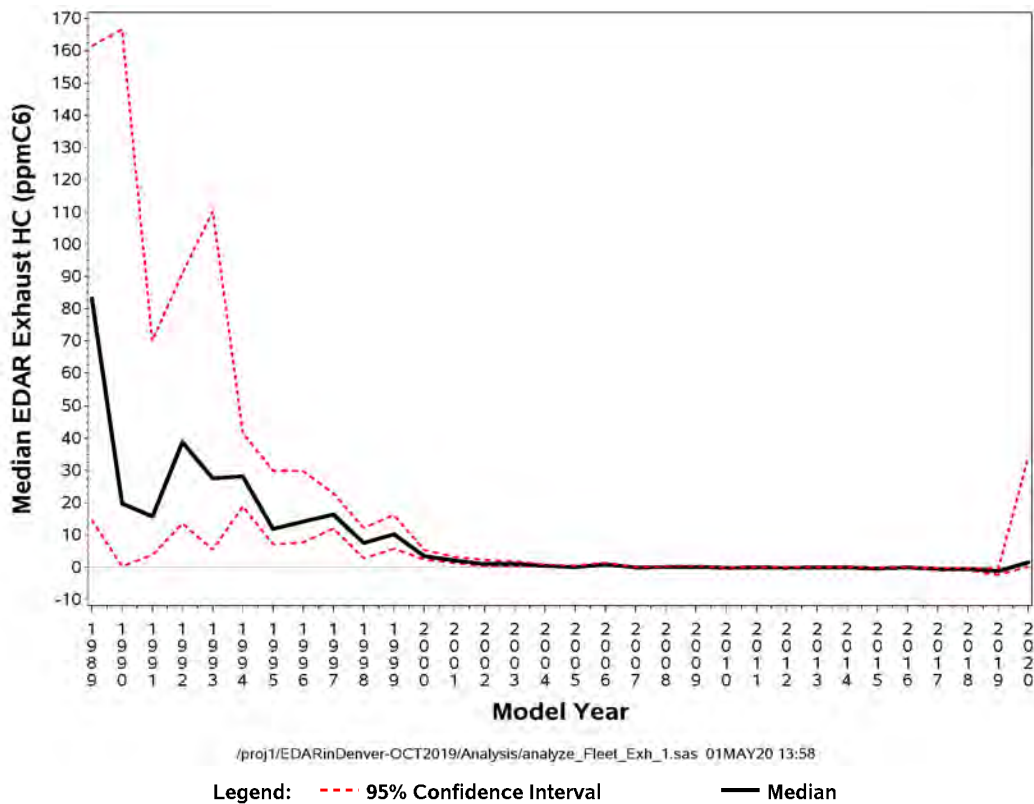
Figure 8-10. Model Year Distribution of Fleet Mean [CO] Measurements

Legend: - - - 95% Confidence Interval   —— Mean
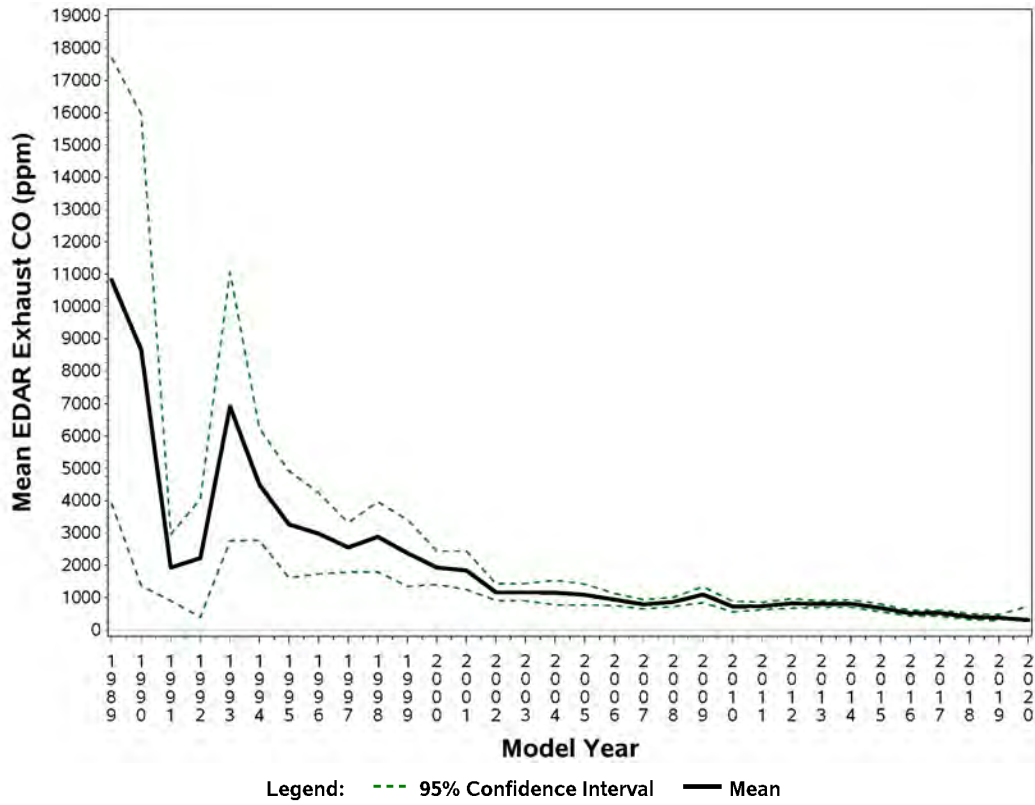
Figure 8-11. Model Year Distribution of Fleet Median [CO] Measurements

/proj1/EDARinDenver-OCT2019/Analysis/analyze_Fleet_Exh_1.sas 01MAY20 13:58

Legend: - - - 95% Confidence Interval   —— Median
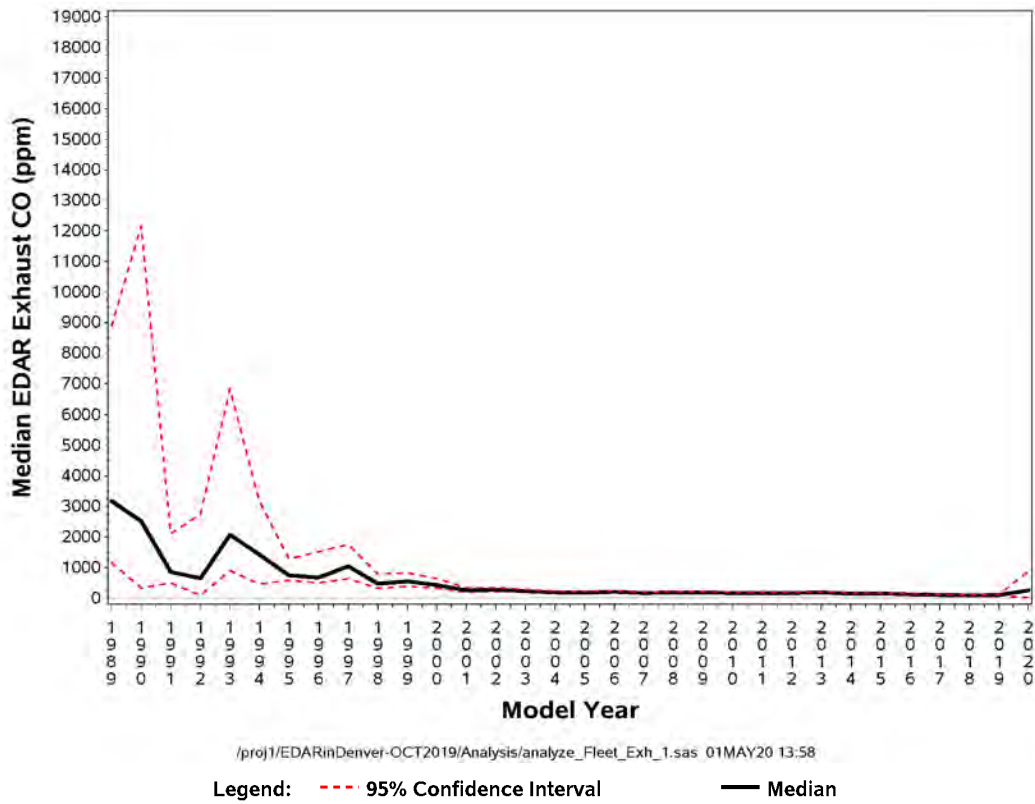
Figure 8-12. Model Year Distribution of Fleet Mean [NO] Measurements
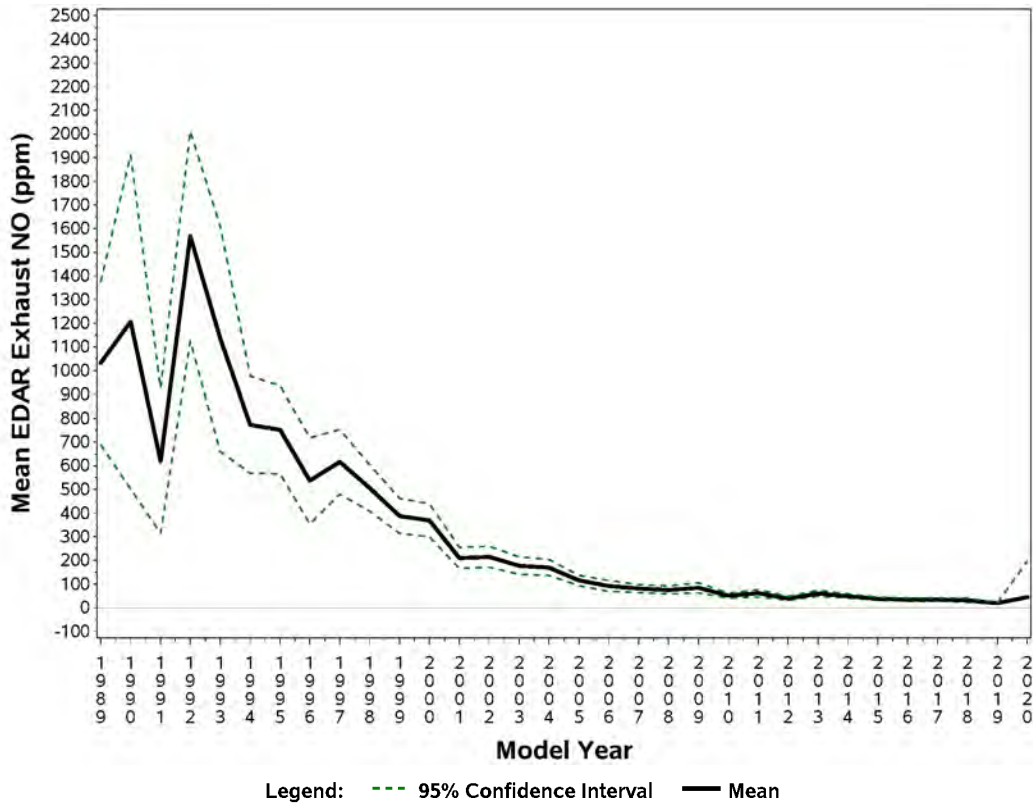
Figure 8-13. Model Year Distribution of Fleet Median [NO] Measurements
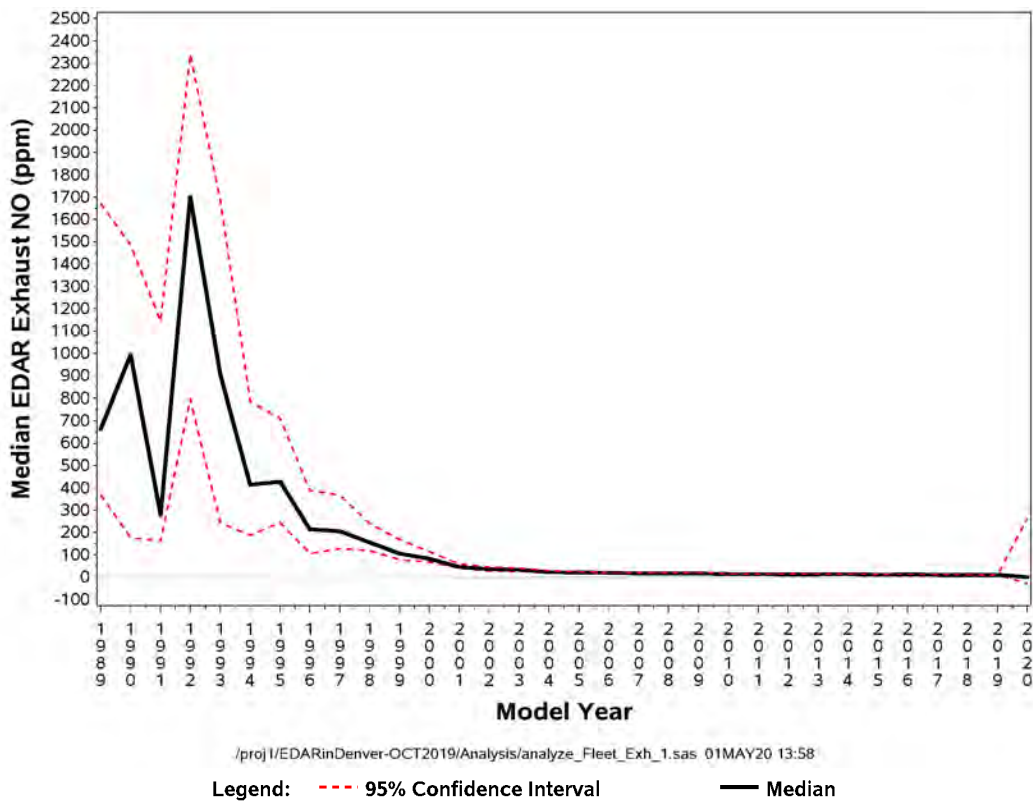
In addition to Table 8-4, Figures 8-8 through 8-13 show the model-year trends of the mean and median HC, CO, and NO values. The dashed green lines in the mean plots give the lower and upper 95% confidence limits on the mean, and the dashed red lines in the median plots give the lower and upper 95% confidence limits on the median.

The Table 8-4 median values for HC from 2002 through 2020 are noteworthy. The medians are all within 1 ppm of zero for those model years. The volatility in the corresponding HC means makes it difficult to discern a downward trend from 2002 to 2020. For CO and NO, Table 8-4 and the figures show distinct downward trends in means and medians throughout the 2000+ model-year period.

9.0   Performance of the Emissions Rate Measurement Methodology

In this section, the methodology's performance is evaluated by comparing the method's calculated Release Rates (g/hr) for the test vehicles with their metered rates. The comparisons can be made only in those cases where the pollutant releases from vehicles are known because the pollutants were metered. Table 9-1 shows the corresponding cases.

Table 9-1. Combinations of Test Vehicles and Pollutant Types[33]

Test Vehicle	Adjusted CO	Adjusted NO	Zeroed CO_2	Adjusted THC	EvapHC	ExhHC
EV-1	Sec 9.1	Sec 9.1	Sec 9.1	Sec 9.2	Sec 9.2	Sec 9.2
EV-2	Sec 9.1	Sec 9.1	Sec 9.1	Sec 9.2	Sec 9.2	Sec 9.2
F150	*	*	*	*	Sec 9.3	*
GMC	*	*	*	*	Sec 9.3	*
Subaru	*	*	*	*	Sec 9.3	*
Infiniti	*	*	*	*	*	*

* Emissions were not metered for these tests.

For EV-1 and EV-2, all exhaust emissions and evaporative emissions were produced by releases from gas cylinders or tanks. These two all-electric test vehicles had no evaporative emissions of their own except for the presumably trivial emissions from vehicle construction materials. The measurement performance of exhaust CO, NO, and CO_2 can be evaluated using data only from EV-1 and EV-2. That analysis is presented in Section 9.1. The measurement performance for EV-1 and EV-2 of Total HC (i.e., before BSS separation), and EvapHC and ExhHC (i.e., after BSS separation) is presented in Section 9.2.

The F150, GMC, and Subaru test vehicles can be used to evaluate measurement performance of EvapHC in those cases where the metered EvapHC release rates are believed to be substantially larger than the vehicles' natural EvapHC and ExhHC release rates. That analysis is presented in Section 9.3. The measurements of exhaust CO, NO, and CO_2 from these test vehicles cannot be used since those pollutants were not metered on those vehicles. Finally, no emissions measurements for the Infiniti test vehicle can be used since neither exhaust nor evaporative emissions were metered for that vehicle.

For the evaluations below, the measured EDAR detailed data collected in Westminster in October 2019 was noise-reduced using the methods described in Section 7.1 to produce so-called adjusted arrays (adjTHC, adjCO, adjNO, adjNO2, adjCO2) for each EDAR channel and each transit. All five adjusted arrays were then used by BSS (standard FastICA) as described in Section 7.2 to produce relative arrays assigned to EvapPlume and ExhPlume plus the three Noise arrays. EvapHC and ExhHC arrays were determined by weighted regression of the adjTHC array against the EvapPlume and ExhPlume arrays. The weights were the ScanSum weights described in Section 6.5. Then, the baseline of adjCO2 was additionally adjusted in SAS, as described in

---

[33] P:\EDARinDenver-OCT2019\Analysis_MLout\220113\Anal_MLout/
OCT19_VSPbins_2_EV_RefVeh.xlsx

Section 6.5, to produce ZeroedCO2. The Vortex Entrainment Time (VET) values for the tailpipe location described in Section 6.4 were used to convert the RSD-measured vortex masses to release rates. Using tailpipe VETs is appropriate for exhaust emissions when the tailpipe exit is near the vehicle rear. In the calculations below, rear-vehicle VETs were used for all tests – even those where releases were from farther forward on the vehicle. This approach allows the deviations between RSD-measured release rates and metered release rates to be evaluated in Section 9.2 in terms of the known release locations of EvapHC on the test vehicles.

9.1   Exhaust CO, NO, and CO_2 Release Rates from Reference EVs

The only vehicles in the Westminster study for which the emission rates of the exhaust emissions were measured were the two all-electric test vehicles EV-1 and EV-2. As described earlier, the exhaust emissions were entirely artificial by conducting metered releases of dry gas from gas cylinders. The artificial dry exhaust from EV-1 simulated clean emissions, which contained 15.05 % CO_2 in nitrogen. EV-2 artificial exhaust emissions simulated a dirty vehicle with 402 ppm propane, 5043 ppm CO, 996 ppm NO, and 14.76 % CO_2 in nitrogen. For both vehicles, the simulated exhaust gas was released at 30 scfm. Since the artificial exhaust gas releases were replicated independently of the various release rates used for artificial evaporative emissions, many replicate measurements of the exhaust emissions are available for analysis.

To obtain exhaust emission rates using the methodology, the detailed RSD data for the NO, CO, and CO_2 data undergo the processing steps shown in Figure 5-1. Specifically, no BSS separation or estimation is needed to convert the raw RSD detailed data to Release Rates (g/hr) and Emission Rates (g/mile).

Table 9-2 shows the Metered release rates in Column 3 and the corresponding Mean RSD-measured release rates in Column 4 with standard error, lower 95% confidence limit on the mean, upper 95% confidence limit on the mean, and the t-value in subsequent columns. The last column gives the percent recovery, which is the ratio of Mean divided by Metered. The recoveries range from 66% to 87%.

Table 9-2. Comparison of Metered and RSD-Measured Exhaust CO, NO, and CO_2 Release Rates for EV-1 and EV-2

Vehicle ID	Nobs	Exh NO (g/hr)						Recovery
		Metered	Mean	Std Err	LCLM	UCLM	t	
EV1	159	0.00	0.37	0.25	-0.13	0.86	1.5	
EV2	260	63.1	41.9	1.08	39.8	44.1	39.0	66%

Vehicle ID	Nobs	Exh CO (g/hr)						Recovery
		Metered	Mean	Std Err	LCLM	UCLM	t	
EV1	159	0.00	1.74	2.20	-2.60	6.08	0.79	
EV2	260	298	227	6.04	215	239	37.6	76%

Vehicle ID	Nobs	Exh CO2 (g/hr)						Recovery
		Metered	Mean	Std Err	LCLM	UCLM	t	
EV1	159	13991	12239	361	11526	12953	33.9	87%
EV2	260	13721	10715	253	10218	11213	42.4	78%

9.2   Total HC, Evaporative HC, Exhaust HC Release Rates from Reference EVs

The performance of the methodology for unambiguously determining the methodology's performance for measuring HC Release Rates (g/hr) can be done using only data from the EV-1 and EV-2 test vehicles. Only for those two vehicles were all EvapHC and ExhHC release rates metered. During testing, the other test vehicles (F150, GMC, Subaru) emitted their natural EvapHC and ExhHC emissions; however, as shall be shown in the next subsection, those emissions appear to be quite low.

For EV-1, the artificial dry exhaust gas was released at 30 scfm, but the gas contained no HC. Therefore, the EV-1 Metered ExhHC release rate was 0 g/hr. For EV-2, the artificial dry exhaust gas was released at 30 scfm, and the gas contained 402 ppm propane, which produces a release rate of 37.4 g/hr HC. For both EV-1 and EV-2, propane was released from either the fuel fill door (DOOR), under the hood (HOOD), or at the center of the rear axle (TANK) and at either 0, 1.1, 2.3, 4.5, 9, 18, 36, 72, 144, or 288 g/hr. Additionally, the test vehicles were driven at either 22.5 or 45 mph past the RSD instrument.

The processing described by Figure 5-1 was used to convert the raw RSD HC channel data into THC (Total HydroCarbon) release rates. Specifically, BSS separation and estimation is not needed and was not used to calculate the THC release rates. On the other hand, since the raw RSD HC channel must be split to arrive at the separate release rates for EvapHC and ExhHC, the processing described by Figure 5-2 was used to provide the separation (by ICA) and estimation.

Because of the different processing paths used for THC vs. EvapHC and ExhHC, comparison of Measured vs. Metered THC provides evaluation of different processing steps than the comparison of Measured vs. Metered EvapHC and Measured vs. Metered ExhHC. Calculated values of THC are affected by the processing steps in Figure 5-1, namely, pre-processing, vortex shape calculation, and emission calculation. Calculated values of EvapHC and ExhHC are additionally affected by the additional processing step in Figure 5-2, namely, separation/estimation.

Because test vehicles EV-1 and EV-2 were driven in every transit of the convoy past the RSD instrument, many replicate RSD measurements are available for analysis. The analysis begins by examining the trends of averages of replicate transits. Tables 9-3 and 9-4[34] show the average results for THC, EvapHC, and ExhHC for EV-1 and EV-2. Later, we will examine plots of the data from the table, and in the next section, we will examine data tables and plots for similar calculations for the gasoline test vehicles.

Because the tables and plots for all five test vehicles have the same format, we will describe and discuss the results for EV-1 in some detail.

---

[34] P:\EDARinDenver-OCT2019\Analysis_MLout\220817\Anal_MLout\RefVehs/ OCT19_perf_RefVeh.xlsx, which was derived from P:\EDARinDenver-OCT2019\Analysis_MLout\220817\Anal_MLout\RefVehs / OCT19_perf_RefVeh.sas and *.lst

Table 9-3. Metered HC and Measured HC Average Responses for Test Vehicle EV-1

Vehicle ID Evap Release Location	N obs	Metered fake EvapHC (g/hr)	Evap HC (g/hr) Measured			Metered fake ExhHC (g/hr)	ExhHC (g/hr) Measured			Metered fake THC (g/hr)	THC (g/hr) Measured		
			Mean	Std Err	t		Mean	Std Err	t		Mean	Std Err	t
EV-1	61	0	**-1.2**	1.9	-0.6	0.0	1.6	0.6	2.8	0.0	1.1	2.0	0.5
EV1 Door	5	1.1	**7.6**	2.0	3.8	0.0	7.9	3.2	2.4	1.1	15.6	4.0	3.9
	10	2.3	**7.8**	6.5	1.2	0.0	13.0	5.5	2.4	2.3	21.2	6.7	3.2
	10	4.5	**14.0**	8.9	1.6	0.0	5.8	2.3	2.5	4.5	20.1	7.7	2.6
	10	9	**26.9**	6.9	3.9	0.0	6.8	1.4	5.0	9.0	34.0	7.3	4.7
	10	18	**14.5**	2.6	5.7	0.0	16.1	4.0	4.0	18.0	31.0	4.8	6.4
	9	36	**36.0**	9.2	3.9	0.0	14.1	4.4	3.2	36.0	50.8	8.8	5.8
	9	72	**56.4**	9.6	5.9	0.0	22.5	7.0	3.2	72.0	79.9	14.3	5.6
	10	144	**136.5**	13.2	10.4	0.0	28.4	14.1	2.0	144.0	165.7	11.7	14.1
	5	288	**250.6**	35.9	7.0	0.0	79.5	35.8	2.2	288.0	334.7	48.2	6.9
EV1 Hood	5	1.1	**3.6**	1.8	2.0	0.0	1.0	0.4	2.4	1.1	4.5	1.6	2.8
	10	2.3	**4.9**	4.6	1.1	0.0	2.9	1.5	1.9	2.3	8.9	5.2	1.7
	10	4.5	**13.1**	5.8	2.3	0.0	4.2	1.4	3.1	4.5	17.4	5.1	3.4
	10	9	**9.7**	5.5	1.8	0.0	3.6	2.1	1.7	9.0	14.1	6.3	2.2
	10	18	**8.0**	4.1	2.0	0.0	6.9	1.8	3.9	18.0	15.5	4.9	3.2
	9	36	**14.1**	6.1	2.3	0.0	5.5	2.3	2.4	36.0	20.1	6.7	3.0
	10	72	**29.8**	4.0	7.5	0.0	10.0	3.3	3.1	72.0	39.9	4.7	8.4
	10	144	**75.1**	10.6	7.1	0.0	11.9	3.3	3.7	144.0	89.0	10.5	8.5
	5	288	**104.1**	18.0	5.8	0.0	38.0	18.5	2.1	288.0	143.8	28.7	5.0
EV1 Tank	5	1.1	**5.5**	3.3	1.7	0.0	4.7	1.1	4.4	1.1	10.5	3.7	2.9
	11	2.3	**6.5**	2.8	2.4	0.0	5.2	1.0	5.3	2.3	11.9	3.4	3.5
	10	4.5	**-0.5**	7.0	-0.1	0.0	10.9	2.1	5.2	4.5	16.9	3.1	5.5
	10	9	**13.4**	5.2	2.6	0.0	10.0	1.7	5.7	9.0	23.4	5.2	4.5
	10	18	**5.7**	8.6	0.7	0.0	10.4	2.9	3.6	18.0	17.5	9.7	1.8
	12	36	**23.6**	8.9	2.7	0.0	19.2	3.5	5.4	36.0	43.0	8.5	5.0
	10	72	**37.1**	11.4	3.2	0.0	23.8	5.2	4.6	72.0	69.2	8.9	7.8
	12	144	**65.8**	11.8	5.6	0.0	58.8	16.9	3.5	144.0	125.3	8.2	15.4
	5	288	**118.7**	8.8	13.5	0.0	62.2	17.0	3.7	288.0	181.6	11.7	15.6

Table 9-4. Metered HC and Measured HC Average Responses for Test Vehicle EV-2

Vehicle ID Evap Release Location	N obs	Metered fake EvapHC (g/hr)	Evap HC (g/hr) Measured			Metered fake ExhHC (g/hr)	ExHC (g/hr) Measured			Metered fake THC (g/hr)	THC (g/hr) Measured		
			Mean	Std Err	t		Mean	Std Err	t		Mean	Std Err	t
EV-2	62	0	**-0.9**	2.0	-0.5	37.4	19.9	1.8	10.9	37.4	20.6	2.6	7.8
EV-2 Door	5	1.1	**-0.6**	4.5	-0.1	37.4	33.1	2.8	11.9	38.5	32.5	5.7	5.7
	10	2.3	**6.5**	5.8	1.1	37.4	30.9	4.7	6.5	39.7	42.6	5.8	7.3
	10	4.5	**8.7**	4.3	2.0	37.4	27.5	5.7	4.9	41.9	42.9	6.0	7.1
	10	9	**6.9**	4.2	1.6	37.4	30.0	4.8	6.3	46.4	38.3	6.3	6.1
	10	18	**10.0**	3.3	3.1	37.4	35.0	2.7	13.0	55.4	45.6	4.0	11.5
	10	36	**43.4**	8.9	4.9	37.4	29.7	4.9	6.1	73.4	73.7	11.2	6.6
	10	72	**56.1**	10.0	5.6	37.4	36.6	5.4	6.7	109.4	97.4	8.8	11.1
	10	144	**155.2**	19.2	8.1	37.4	47.6	10.8	4.4	181.4	203.4	22.2	9.2
	5	288	**131.2**	25.8	5.1	37.4	65.3	34.9	1.9	325.4	245.3	36.2	6.8
EV-2 Hood	5	1.1	**3.1**	3.4	0.9	37.4	26.1	5.6	4.7	38.5	30.4	7.2	4.2
	10	2.3	**1.6**	3.1	0.5	37.4	30.2	3.9	7.8	39.7	32.2	3.1	10.4
	10	4.5	**1.9**	8.6	0.2	37.4	35.1	5.6	6.2	41.9	44.0	8.8	5.0
	10	9	**9.2**	5.7	1.6	37.4	29.3	4.7	6.3	46.4	45.4	7.3	6.2
	10	18	**11.4**	6.4	1.8	37.4	34.1	3.4	10.1	55.4	50.4	6.1	8.3
	10	36	**13.4**	2.3	5.8	37.4	34.7	4.7	7.3	73.4	48.5	5.5	8.8
	10	72	**17.3**	4.2	4.1	37.4	45.8	6.9	6.6	109.4	69.5	5.0	13.9
	10	144	**59.9**	4.4	13.5	37.4	55.8	13.2	4.2	181.4	118.9	12.0	9.9
	5	288	**53.4**	14.6	3.7	37.4	72.3	19.0	3.8	325.4	151.6	14.7	10.3
EV-2 Tank	5	1.1	**8.3**	2.8	3.0	37.4	30.7	5.2	5.9	38.5	39.5	6.1	6.5
	12	2.3	**8.0**	3.0	2.6	37.4	35.0	3.1	11.4	39.7	44.9	4.6	9.7
	10	4.5	**4.3**	5.9	0.7	37.4	37.5	4.2	8.9	41.9	42.6	3.6	11.8
	12	9	**5.9**	3.6	1.6	37.4	39.3	5.4	7.3	46.4	46.0	5.5	8.3
	10	18	**7.1**	3.2	2.3	37.4	38.3	2.7	14.4	55.4	46.0	4.8	9.5
	12	36	**31.9**	4.6	6.9	37.4	32.5	4.1	7.9	73.4	69.1	6.1	11.2
	10	72	**21.0**	6.5	3.3	37.4	44.7	10.0	4.5	109.4	86.2	6.6	13.0
	11	144	**72.2**	12.2	5.9	37.4	73.5	7.7	9.5	181.4	146.7	11.6	12.7
	5	288	**76.2**	22.2	3.4	37.4	131.6	37.9	3.5	325.4	225.9	22.8	9.9

Table 9-3 shows the average results for EvapHC, ExhHC, and THC for EV-1. The table has fourteen columns in three groups of columns for EvapHC, ExhHC, and THC. Columns 3, 7, and 11 show the Metered release rates. Column 3 shows the various EvapHC release rates. Column 7 shows the constant ExhHC release rate of 0.0 g/hr. Column 11 is just the sum of Columns 3 and 7. The means, standard errors, and t-values for each average measured release rate are shown in Columns 4, 5, 6; 8, 9, 10; and 12, 13, 14. The standard error can be viewed as the standard deviation of the mean value. The t-value is just the mean divided by the standard error. Column 2 gives the number of replicates that are used to calculate the statistics in each row.

The table has four horizontal sections (groups of rows). The top section (first row) shows the results when no EvapHC was released. The remaining sections show results for EvapHC releases from Door, Hood, and Tank locations. Throughout the table, it is useful to compare a measured value with the metered value just to the left of it. This provides information on the accuracy of the methodology for that particular test condition represented by the row.

The first row shows that for EvapHC the measured mean plus or minus the standard error of -1.2 ± 1.9 is in agreement with the metered value of 0 g/hr. This is an important result because it means that the separation/estimation processing produces good EvapHC values when no EvapHC is present. In the same row, the measured mean ExhHC value of 1.6 ± 0.6 g/hr is higher than the metered ExhHC value of 0.0 g/hr, but it is not substantially higher.

As we move down the EvapHC columns, the measured values (Column 4) tend to increase but not necessarily at the same rate of increase as the metered values (Column 3). The reasons for the different rates of increase arise from the EvapHC release locations and will be considered later.

The same exercise can be done for the ExhHC columns. However, for ExhHC, the measured values (Column 8) should stay constant as the metered values (Column 7) do. The table shows that this is only somewhat true. At each of the three release locations (Door, Hood, Tank), there is a tendency for "leakage" or "crosstalk" of some of the EvapHC into the ExhHC channel. This tendency is a measure of the performance of the separation/estimation processing.

The features of Table 9-4 for EV-2 are similar to those of Table 9-3 for EV-1. One important feature to be pointed out is the result in Table 9-4 in the first row for transits when no EvapHC was released. For these transits, the release rate of ExhHC was quite high at 37.4 g/hr (402 ppm exhaust HC). In spite of this large ExhHC release rate, the separation/estimation processing produced an average EvapHC value of -0.9 ± 2.0 g/hr, which is not significantly different from the metered EvapHC value of 0.0 g/hr.

The plots in Figures 9-1 and 9-2 use the data from Tables 9-3 and 9-4 to show the trends for EV-1 and EV-2 more clearly.

In Figure 9-1b, which is for the fuel-fill-Door releases, the blue line shows that the measured EvapHC increases close to linearly with the metered EvapHC values on the x-axis. The slope of the blue line is also close to the ideal value of 1. The red, dashed line shows the much milder increase of ExhHC as the metered EvapHC on the x-axis increases. If the separation/estimation process were perfect, the red, dashed line would stay horizontal and be at the metered ExhHC value of 0 g/hr, which is shown by the red solid horizontal reference line.

Figure 9-1. HC Performance (Average) for Test Vehicle EV-1

a) EV-1: THC Overview
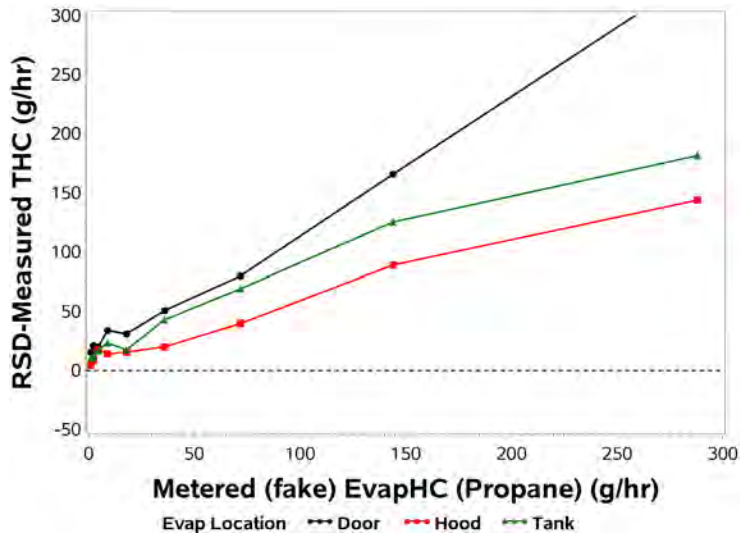
b) EV-1: Evap release at DOOR
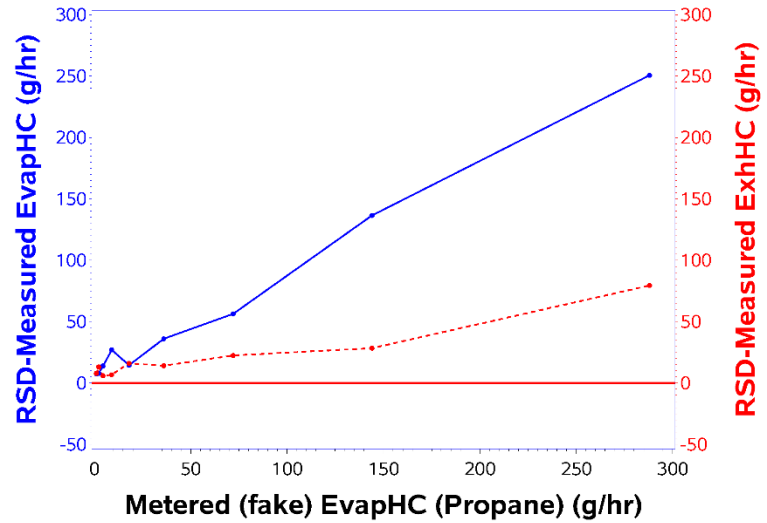
c) EV-1: Evap release at HOOD
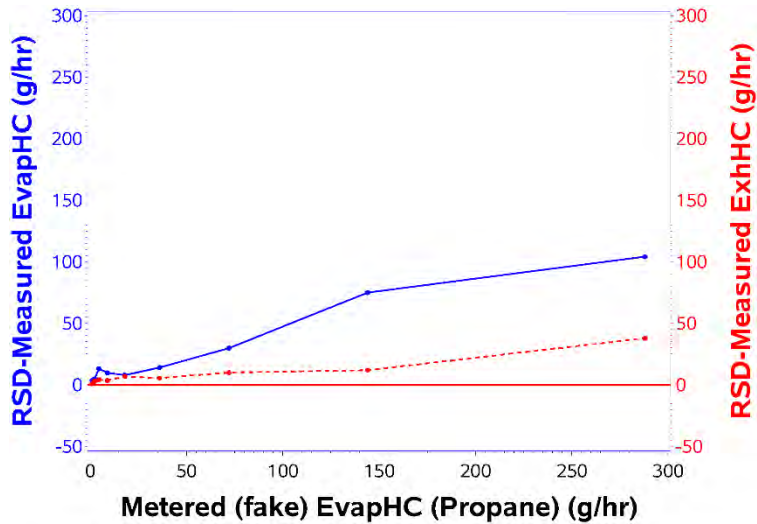
d) EV-1: Evap release at TANK
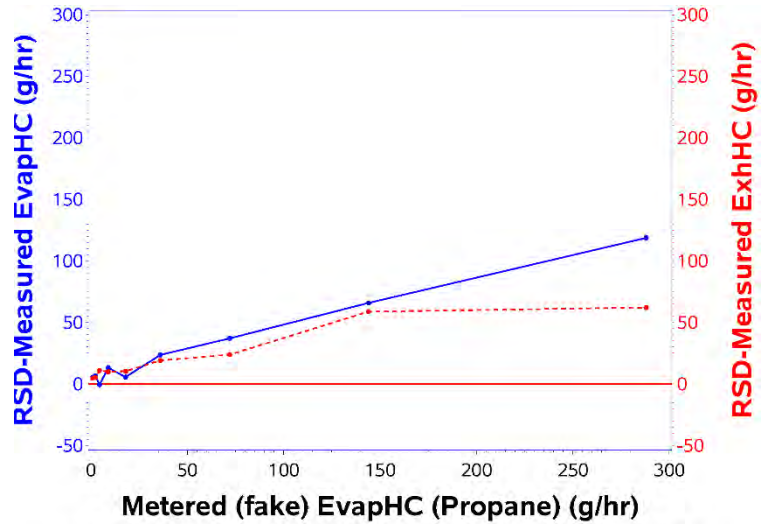
Figure 9-2. HC Performance (Average) for Test Vehicle EV-2

a) EV-2: THC Overview
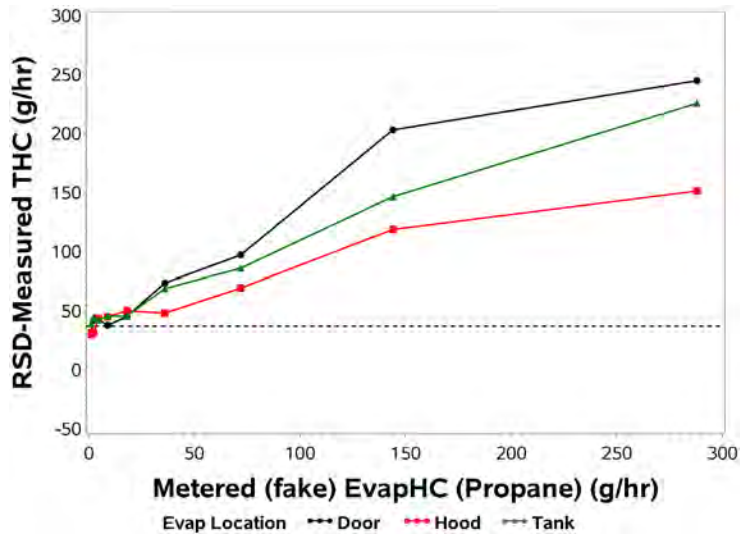
b) EV-2: Evap release at DOOR
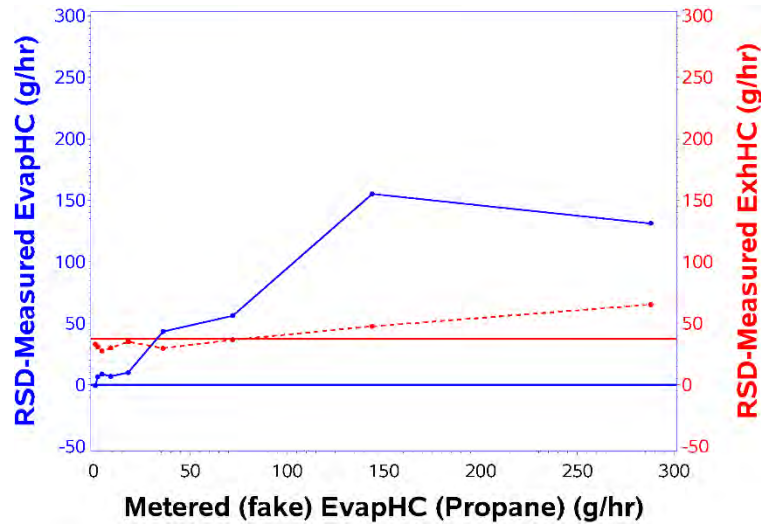
c)

d)

e) EV-2: Evap release at HOOD
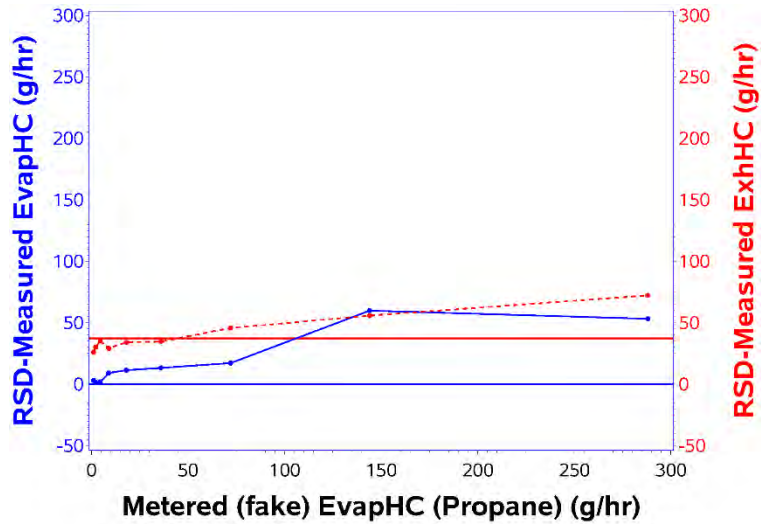
f) EV-2: Evap release at TANK
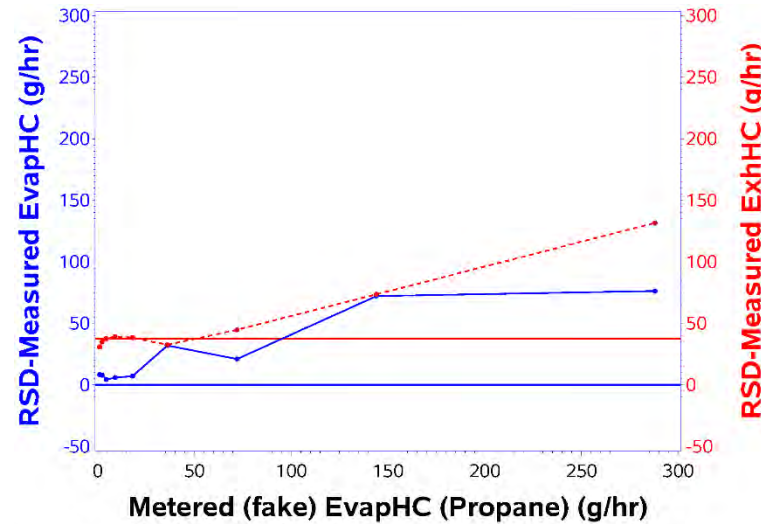
/proj1/EDARinDenver-OCT2019/Analysis_MLout/220817/Anal_MLout/RefVehs/OCT19_perf_RefVeh.sas 28AUG22 09:44

/proj1/EDARinDenver-OCT2019/Analysis_MLout/220817/Anal_MLout/RefVehs/OCT19_perf_RefVeh.sas 28AUG22 09:44

The plots in Figures 9-1c and 9-1d show the same plots for releases from Hood and Tank locations for the same vehicle EV-1. The notable difference of these plots, compared with Figure 9-1b for Door, is that the slope of the blue lines is much lower for Figure 9-1c and 9-1d. This is a consequence of the lower entrainment efficiency (VET) for releases farther forward on the vehicle (Hood, Tank) in comparison with those at the vehicle rear (Door) in the case of EV-1.

Figure 9-1a shows an overview of the effect of increasing the metered EvapHC release rate (x-axis) on the THC release rate (y-axis) as a function of release location. The trend of the slopes is: Door > Tank > Hood. Again, this is a consequence of the lower entrainment efficiency for EvapHC release locations farther forward on the vehicle. The portion of THC that is contributed by ExhHC is not greatly affected by its tailpipe release location since the VET factor for tailpipe releases (if they are near the rear of the vehicle) of 0.96 is close to 1 (see Table 6-4).

The corresponding ExhHC and EvapHC plots for EV-2 are shown in Figure 9-2. The ExhHC dashed curves (red) in Figure 9-2b, c, and d are compared to the red solid horizontal reference line at 37.4 g/hr since that was the metered ExhHC release rate. Just as for the ExhHC curves for EV-1 in Figure 9-1, these ExhHC curves show some crosstalk of EvapHC signal into the deduced ExhHC signal. The blue curves for EV-2 EvapHC in Figure 9-2 are quite similar to the corresponding curves for EV-1 EvapHC in Figure 9-1. And just as for EV-1, the EV-2 EvapHC curves show the effects of release location.

Figures 9-3 and 9-4 show additional details for the performance of the methodology as applied to the EV-1 and EV-2 test vehicles.

Figures 9-3a and 9-4a show a comparison of the average RSD-measured EvapHC release rates, to which the release-location factors of Table 6-4 have been applied, against the metered EvapHC release rates. For these plots, all curves should be on the 1:1 parity trend. Except for the highest metered release rate at 288 g/hr, the location-corrected, RSD-measured trends of EvapHC release rate are reasonably close to parity.

Plots in panels b, c, and d for Figures 9-3 and 9-4 show the individual transit measurements of EvapHC vs. the metered values. These values are not corrected for release location and are the values used to get the averages in Figures 9-1 and 9-2 for the corresponding panels. The data points at each test condition show the considerable amount of scatter, which we attribute to plume variability from turbulence behind the moving vehicle. The plots also show that the variability increases with increasing levels of metered EvapHC.

Figure 9-3. HC Performance (Details) for Test Vehicle EV-1

a) EV-1: Location-corrected EvapHC Overview
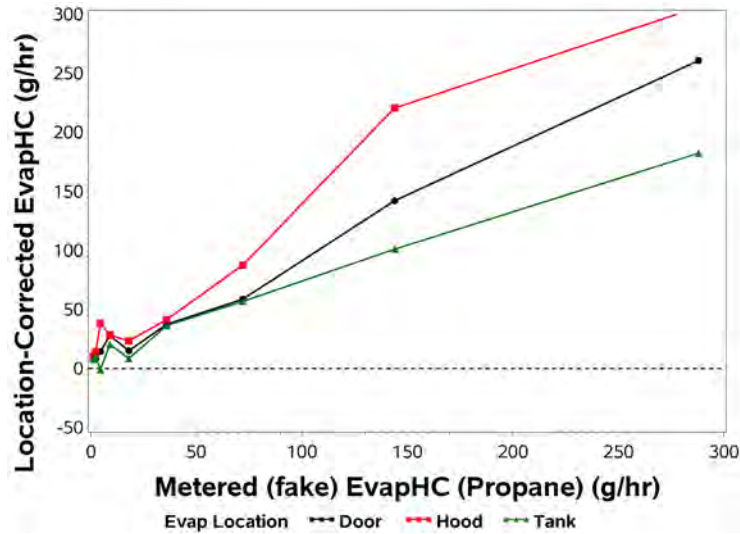
b) EV-1: Evap at DOOR (scatter)
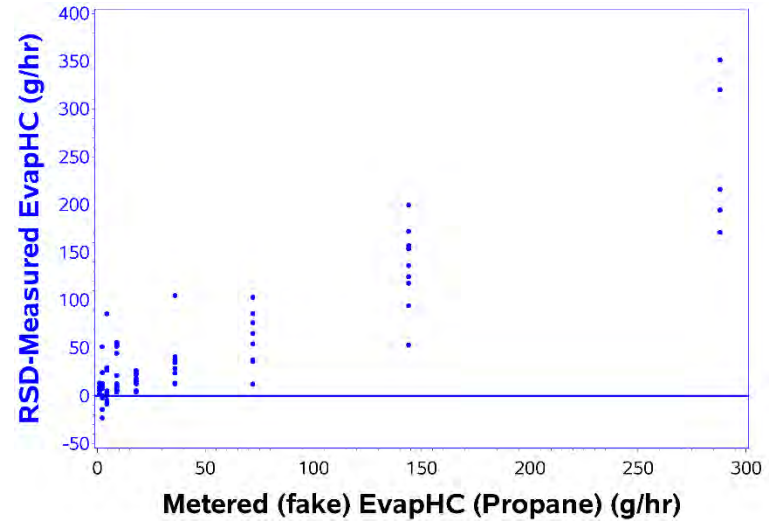
c)

d)

e) EV-1: Evap at HOOD (scatter)
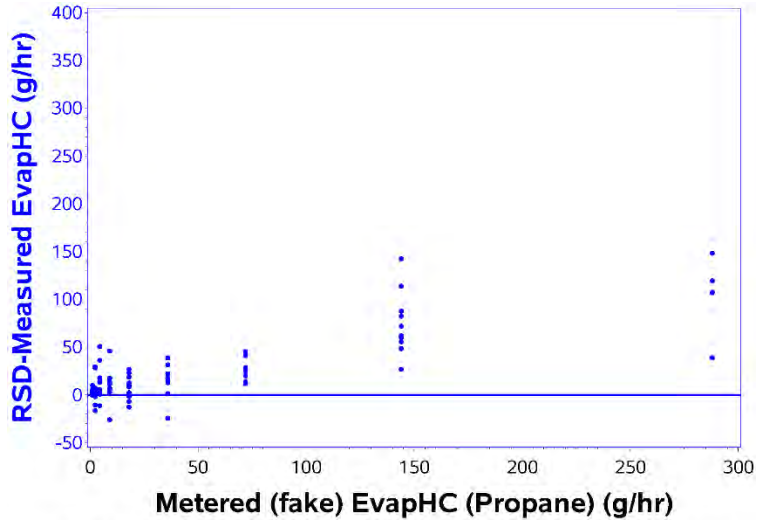
f)   EV-1: Evap at TANK (scatter)
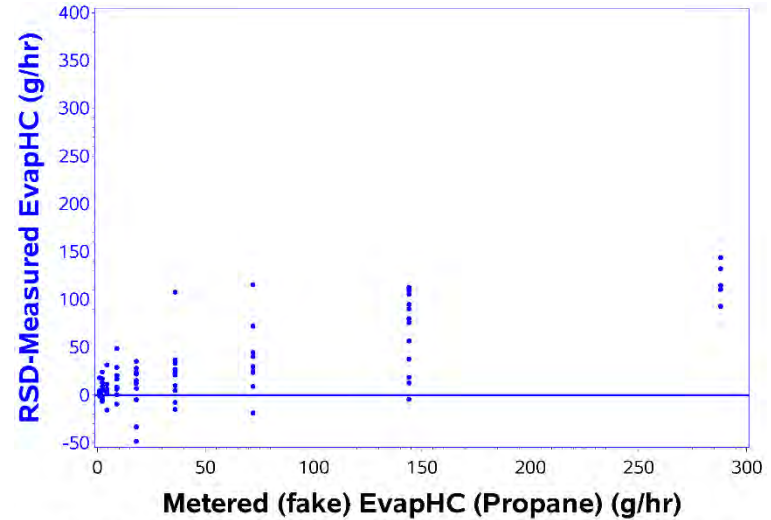
/proj1/EDARinDenver-OCT2019/Analysis_MLout/220817/Anal_MLout/RefVehs/OCT19_perf_RefVeh_scatter.sas 29AUG22 15:17

/proj1/EDARinDenver-OCT2019/Analysis_MLout/220817/Anal_MLout/RefVehs/OCT19_perf_RefVeh_scatter.sas 29AUG22 15:17

Figure 9-4. HC Performance (Details) for Test Vehicle EV-2

g) EV-2: Location-corrected EvapHC Overview
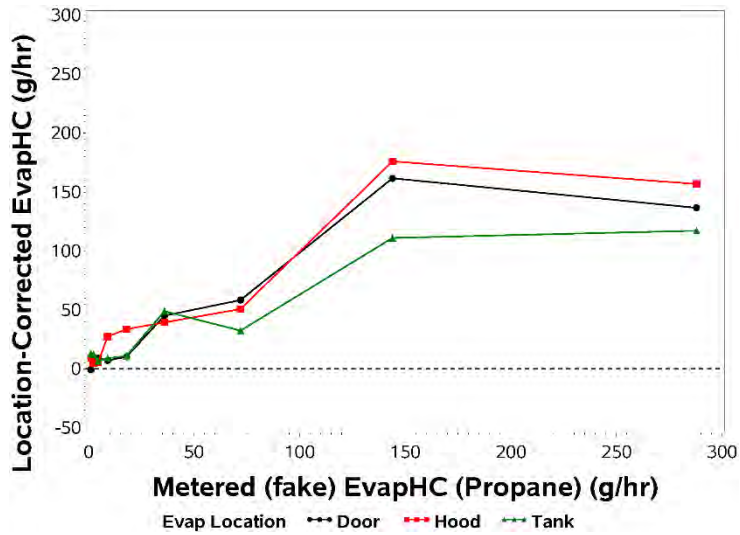
h) EV-2: Evap at DOOR (scatter)
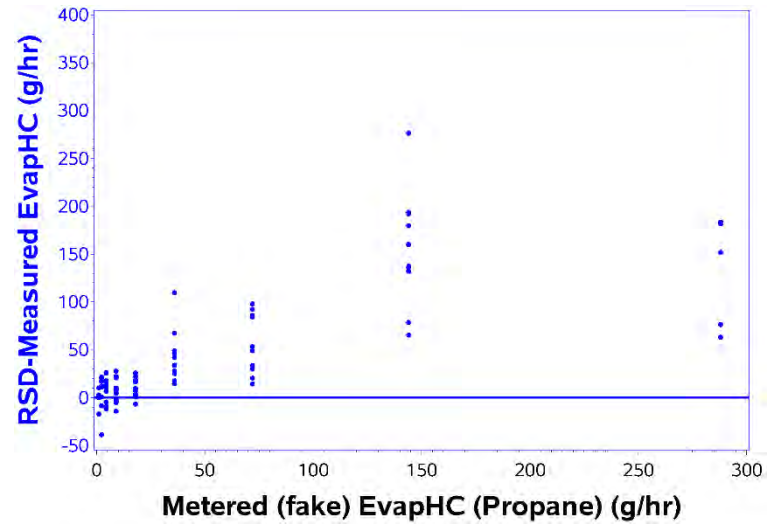
i) EV-2: Evap at HOOD (scatter)
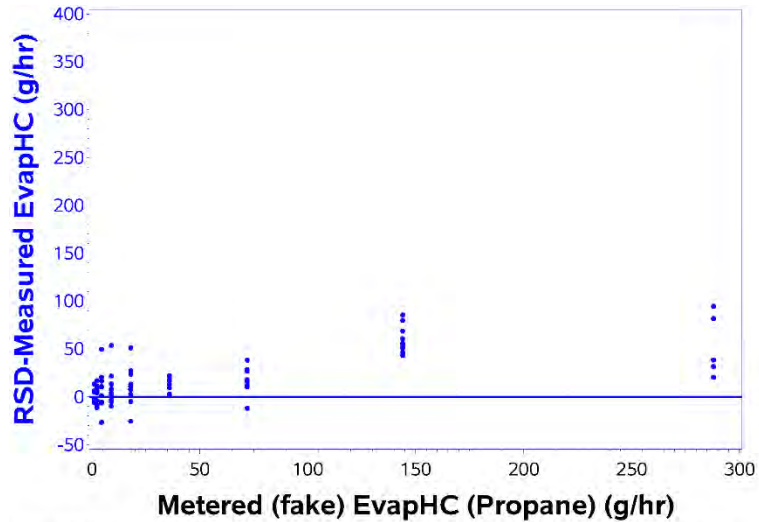
/proj1/EDARinDenver-OCT2019/Analysis_MLout/220817/Anal_MLout/RefVehs/OCT19_perf_RefVeh_scatter.sas 29AUG22 15:17

j) EV-2: Evap at TANK (scatter)
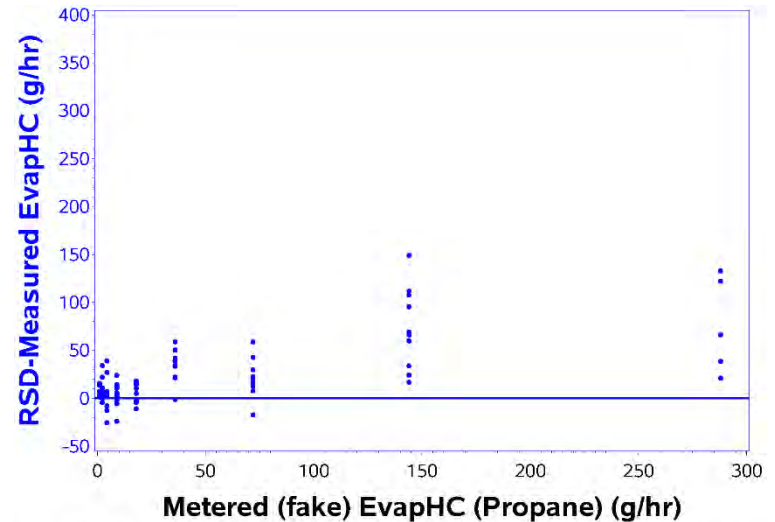
/proj1/EDARinDenver-OCT2019/Analysis_MLout/220817/Anal_MLout/RefVehs/OCT19_perf_RefVeh_scatter.sas 29AUG22 15:17

9.3　Evaporative HC Release Rates from Reference Gasoline Vehicles

The performance of the methodology to determine EvapHC release was examined in the previous subsection by examining the responses for EV-1 and EV-2, which are all-electric vehicles. The advantage of the test conditions for those vehicles was that the composition and release rates were well known. However, there were a few differences that could have an influence on the performance results. First, the composition of the artificial exhaust gas was relatively simple. HC was simulated using only propane, and NOx was simulated using only NO. Second, the simulated exhaust did not contain any gaseous water of combustion, which makes up a huge fraction of real exhaust. Third, because the simulated exhaust came from gas cylinders, the exhaust flow rate used was 30 scfm, which is quite low compared to exhaust flow rates from engines under moderate to high loads. Fourth, the EV test vehicles were Chevrolet Bolts, which have bodies substantially smaller than many light-duty vehicles that are typically on the road.

Thus, it is also important to examine the performance of the methodology for test situations that come closer to real-world operating environments of conventional gasoline-fueled vehicles – even if some of the advantages of testing all-electric vehicles need to be relaxed. The three gasoline vehicles tested were the F150, GMC, and Subaru. Their exhausts were natural, and their flow and composition were not metered or measured, but since the vehicles were all 2016 model year or newer, we expected that their exhaust and evaporative emissions would be well controlled. Since the exhaust was a real product of combustion, its composition was complex with a mixture of HC compounds, NOx compounds, and water of combustion. The exhaust flows were likely typical of a variety of light-duty vehicles passing by the RSD instrument during data collection. Finally, these vehicles had larger bodies than the EVs. The F150 was a pick-up with a full-size cap over the bed; the GMC was a pick-up with an open bed; the Subaru Outback was a small SUV with no distinct rear deck over a trunk.

Tables 9-5, 9-6, and 9-7 show the average measured release rates for EvapHC, ExhHC, and THC for the three gasoline test vehicles using the same format as Tables 9-3 and 9-4 for the two EVs. The values in Tables 9-5, 9-6, and 9-7 can be examined just as those for EV-1 and EV-2 in Tables 9-3 and 9-4. Note that for the F150 and GMC pick-ups, the fuel fill door and therefore the artificial EvapHC release point were located just aft of the driver's door. In the tables and figures, this location is called Side.

The first row of all three tables shows that when no EvapHC was released, the methodology produced average EvapHC release rates that were not significantly different from zero. We conclude that the natural EvapHC of the three vehicles was basically 0 g/hr. Also, from the first row, the mean ExhHC release rates were near 13.4, 9.6, and 6.2 g/hr, which are low values but statistically significantly above zero (since their t-values are greater than 1.96). These values can be viewed as the typical ExhHC release rates for these vehicles.

Table 9-5. Metered HC and Measured HC Average Responses for Test Vehicle F150

Vehicle ID Evap Release Location	N obs	Metered fake EvapHC (g/hr)	Evap HC (g/hr) Measured			Metered fake ExhHC (g/hr)	ExhHC (g/hr) Measured			Metered fake THC (g/hr)	THC (g/hr) Measured		
			Mean	Std Err	t		Mean	Std Err	t		Mean	Std Err	t
F150	19	0.0	-6.1	7.0	-0.9	Natural	13.4	4.6	2.9	n/a	12.2	7.9	1.6
F150 Side	1	1.1	-41.6	.	.	Natural	-0.1	.	.	n/a	-33.1	.	.
	4	2.3	-2.1	2.9	-0.7	Natural	18.6	10.6	1.8	n/a	20.3	8.8	2.3
	2	4.5	0.0	9.5	0.0	Natural	2.2	3.3	0.7	n/a	26.6	24.4	1.1
	4	9	5.3	6.1	0.9	Natural	18.5	7.6	2.4	n/a	37.0	12.4	3.0
	2	18	8.8	34.7	0.3	Natural	5.7	2.1	2.7	n/a	32.5	19.8	1.6
	4	36	4.3	6.9	0.6	Natural	5.6	8.3	0.7	n/a	19.5	16.0	1.2
	2	72	60.0	56.5	1.1	Natural	11.8	13.3	0.9	n/a	95.8	47.9	2.0
	4	144	94.8	13.2	7.2	Natural	13.0	7.2	1.8	n/a	150.8	38.0	4.0
	1	288	171.8	.	.	Natural	36.4	.	.	n/a	242.0	.	.
F150 Hood	1	1.1	-24.6	.	.	Natural	0.1	.	.	n/a	-18.8	.	.
	4	2.3	19.4	20.9	0.9	Natural	12.9	4.4	2.9	n/a	36.1	23.7	1.5
	2	4.5	17.6	4.5	3.9	Natural	7.0	3.0	2.3	n/a	26.6	0.1	355.3
	4	9	-7.0	17.5	-0.4	Natural	18.4	9.0	2.0	n/a	13.7	22.5	0.6
	2	18	9.3	16.7	0.6	Natural	24.8	7.5	3.3	n/a	52.7	15.6	3.4
	4	36	-7.1	22.6	-0.3	Natural	19.8	10.4	1.9	n/a	13.5	19.5	0.7
	2	72	11.4	0.7	17.1	Natural	30.8	7.5	4.1	n/a	60.5	6.8	8.9
	4	144	65.1	24.8	2.6	Natural	55.1	16.0	3.4	n/a	131.3	28.9	4.5
	1	288	215.9	.	.	Natural	163.9	.	.	n/a	385.6	.	.
F150 Tank	1	1.1	23.2	.	.	Natural	5.8	.	.	n/a	31.3	.	.
	4	2.3	-27.5	14.4	-1.9	Natural	22.2	13.4	1.7	n/a	17.9	13.2	1.4
	2	4.5	-23.3	48.5	-0.5	Natural	15.5	12.6	1.2	n/a	-5.3	32.7	-0.2
	4	9	4.0	18.9	0.2	Natural	12.5	7.4	1.7	n/a	26.4	10.2	2.6
	2	18	-13.6	34.2	-0.4	Natural	16.9	2.8	6.0	n/a	14.4	28.1	0.5
	4	36	39.7	13.4	3.0	Natural	18.8	11.2	1.7	n/a	61.7	20.3	3.0
	2	72	-9.7	45.7	-0.2	Natural	48.0	19.8	2.4	n/a	39.7	26.6	1.5
	4	144	98.7	38.4	2.6	Natural	54.8	25.0	2.2	n/a	178.1	4.9	36.6
	1	288	391.9	.	.	Natural	23.2	.	.	n/a	417.1	.	.

Table 9-6. Metered HC and Measured HC Average Responses for Test Vehicle GMC

Vehicle ID Evap Release Location	N obs	Metered fake EvapHC (g/hr)	Evap HC (g/hr) Measured			Metered fake ExhHC (g/hr)	ExhHC (g/hr) Measured			Metered fake THC (g/hr)	THC (g/hr) Measured		
			Mean	Std Err	t		Mean	Std Err	t		Mean	Std Err	t
GMC	12	0.0	**-4.2**	5.9	-0.7	Natural	9.6	2.7	3.5	n/a	10.7	5.8	1.8
GMC Side	1	1.1	**-54.0**	.	.	Natural	-2.2	.	.	n/a	-54.8	.	.
	2	2.3	**5.0**	19.5	0.3	Natural	23.5	8.7	2.7	n/a	29.1	27.7	1.0
	2	4.5	**-15.3**	3.1	-5.0	Natural	18.3	2.9	6.2	n/a	15.9	12.5	1.3
	2	9	**-37.8**	37.5	-1.0	Natural	46.7	36.1	1.3	n/a	10.3	0.2	55.8
	2	18	**-1.3**	5.4	-0.2	Natural	11.3	5.4	2.1	n/a	45.0	17.5	2.6
	2	36	**6.0**	12.3	0.5	Natural	5.1	2.4	2.1	n/a	11.2	10.0	1.1
	2	72	**58.6**	58.1	1.0	Natural	12.4	3.4	3.7	n/a	78.8	53.7	1.5
	2	144	**66.5**	18.5	3.6	Natural	50.0	46.3	1.1	n/a	117.8	26.7	4.4
	1	288	**-15.4**	.	.	Natural	45.7	.	.	n/a	38.5	.	.
GMC Hood	1	1.1	**2.4**	.	.	Natural	3.8	.	.	n/a	8.2	.	.
	2	2.3	**26.3**	18.7	1.4	Natural	3.4	3.9	0.9	n/a	35.1	27.6	1.3
	2	4.5	**-16.5**	22.6	-0.7	Natural	24.3	19.7	1.2	n/a	9.3	3.1	3.0
	2	9	**-21.4**	29.8	-0.7	Natural	6.0	0.4	14.3	n/a	9.4	4.7	2.0
	2	18	**8.6**	10.0	0.9	Natural	10.5	2.6	4.1	n/a	18.4	8.2	2.3
	2	36	**61.0**	53.8	1.1	Natural	5.5	2.2	2.5	n/a	66.4	56.0	1.2
	2	72	**-7.6**	3.3	-2.3	Natural	6.8	10.8	0.6	n/a	0.2	15.2	0.0
	2	144	**-44.9**	57.1	-0.8	Natural	25.1	0.4	64.9	n/a	111.6	74.0	1.5
	1	288	**13.0**	.	.	Natural	91.7	.	.	n/a	146.6	.	.
GMC Tank	1	1.1	**21.0**	.	.	Natural	7.7	.	.	n/a	28.5	.	.
	2	2.3	**-2.7**	0.6	-4.6	Natural	2.6	4.3	0.6	n/a	2.7	4.9	0.6
	2	4.5	**-33.5**	34.2	-1.0	Natural	17.8	2.7	6.5	n/a	13.6	2.4	5.6
	2	9	**-24.8**	9.0	-2.7	Natural	15.3	8.2	1.9	n/a	-0.5	6.9	-0.1
	2	18	**4.4**	9.8	0.5	Natural	44.1	18.2	2.4	n/a	50.4	10.3	4.9
	2	36	**0.7**	12.6	0.1	Natural	25.4	3.7	6.9	n/a	26.3	16.2	1.6
	2	72	**18.5**	20.9	0.9	Natural	24.1	4.7	5.2	n/a	42.7	25.6	1.7
	1	144	**-8.8**	.	.	Natural	69.6	.	.	n/a	128.0	.	.
	1	288	**71.3**	.	.	Natural	96.6	.	.	n/a	263.0	.	.

Table 9-7. Metered HC and Measured HC Average Responses for Test Vehicle Subaru

Vehicle ID Evap Release Location	N obs	Metered fake EvapHC (g/hr)	Evap HC (g/hr) Measured			Metered fake ExhHC (g/hr)	ExhHC (g/hr) Measured			Metered fake THC (g/hr)	THC (g/hr) Measured		
			Mean	Std Err	t		Mean	Std Err	t		Mean	Std Err	t
Subaru	23	0.0	**-1.0**	4.5	-0.2	Natural	6.2	2.6	2.4	n/a	5.2	2.7	2.0
Subaru Door	2	1.1	**-3.9**	0.8	-5.0	Natural	4.6	4.5	1.0	n/a	0.7	3.7	0.2
	4	2.3	**-2.6**	8.4	-0.3	Natural	2.3	1.3	1.8	n/a	16.3	6.3	2.6
	4	4.5	**11.8**	2.4	5.0	Natural	8.6	4.4	2.0	n/a	21.7	5.7	3.8
	4	9	**8.3**	8.6	1.0	Natural	4.9	2.2	2.3	n/a	14.5	8.9	1.6
	4	18	**21.9**	4.7	4.7	Natural	16.1	1.0	16.6	n/a	39.1	5.0	7.8
	4	36	**30.0**	8.1	3.7	Natural	19.9	5.7	3.5	n/a	57.3	1.7	33.5
	4	72	**49.9**	10.3	4.8	Natural	14.9	7.4	2.0	n/a	71.0	3.0	23.6
	4	144	**159.4**	33.4	4.8	Natural	22.6	10.7	2.1	n/a	183.3	38.1	4.8
	2	288	**198.3**	21.1	9.4	Natural	98.8	17.9	5.5	n/a	296.6	3.0	99.0
Subaru Hood	2	1.1	**1.7**	9.7	0.2	Natural	5.4	2.3	2.3	n/a	13.3	1.3	10.2
	3	2.3	**-5.0**	7.1	-0.7	Natural	4.9	3.7	1.3	n/a	2.7	7.3	0.4
	4	4.5	**-5.6**	6.0	-0.9	Natural	15.2	4.8	3.1	n/a	15.0	2.4	6.3
	4	9	**10.9**	4.7	2.3	Natural	8.4	2.4	3.6	n/a	20.7	7.3	2.8
	4	18	**8.5**	5.6	1.5	Natural	10.3	4.8	2.1	n/a	15.8	6.2	2.5
	4	36	**4.9**	8.6	0.6	Natural	12.8	2.2	5.8	n/a	33.7	8.3	4.0
	4	72	**23.2**	6.3	3.7	Natural	24.4	7.0	3.5	n/a	47.8	11.1	4.3
	4	144	**59.9**	8.9	6.7	Natural	34.5	8.0	4.3	n/a	99.4	8.6	11.5
	2	288	**127.2**	3.1	41.4	Natural	51.7	3.5	14.7	n/a	179.5	7.0	25.5
Subaru Tank	2	1.1	**6.5**	1.5	4.2	Natural	6.3	4.0	1.6	n/a	13.1	5.2	2.5
	4	2.3	**-10.1**	5.6	-1.8	Natural	6.0	1.8	3.4	n/a	2.5	4.6	0.5
	4	4.5	**-11.2**	7.0	-1.6	Natural	13.4	9.7	1.4	n/a	13.1	5.4	2.4
	4	9	**5.1**	2.7	1.9	Natural	6.6	2.6	2.5	n/a	23.2	5.7	4.1
	4	18	**28.4**	25.9	1.1	Natural	15.9	4.8	3.3	n/a	58.5	43.0	1.4
	4	36	**9.9**	17.9	0.6	Natural	13.0	5.6	2.3	n/a	35.8	9.3	3.9
	4	72	**68.2**	25.7	2.7	Natural	34.3	7.6	4.5	n/a	105.0	26.5	4.0
	4	144	**108.5**	16.6	6.5	Natural	41.9	27.6	1.5	n/a	154.5	12.9	12.0
	2	288	**171.8**	29.3	5.9	Natural	63.2	8.3	7.6	n/a	237.5	40.2	5.9

The mean and metered values in Table 9-5, 9-6, and 9-7 are plotted in Figures 9-5, 9-6, and 9-7. The solid purple lines provide a comparison of the RSD-measured EvapHC (g/hr) on the y-axis with the metered EvapHC (g/hr) on the x-axis. Since for these test vehicles the ExhHC was neither measured nor metered, we used, as a best estimate, the RSD-measured ExhHC (g/hr) values from the first row of Tables 9-5, 9-6, and 9-7 to draw the solid red horizontal reference lines that designate the ExhHC release rates in panels b, c, and d. The RSD-measured trends for ExhHC, as the metered EvapHC increases, are shown by the dashed red lines. Generally, these dashed red lines rise monotonically above the solid red reference lines indicating the presence of crosstalk between the EvapHC and ExhHC signals.

The trends seen in Figures 9-5 and 9-7 for the F150 and the Subaru agree with the trends seen for EV-1 and EV-2:

a) The response of measured EvapHC tends to increase linearly with the metered EvapHC.
b) The calculated values of ExhHC tend to increase as metered EvapHC increases, which suggests that the separation/estimation processing is not operating optimally.
c) For the F150, the responses to EvapHC releases from the Side and Hood locations are smaller than to releases from the Tank location.
d) For the Subaru, the responses to EvapHC releases from the Tank and Hood locations are smaller than to releases from the Door location.

For the GMC pick-up, the mean EvapHC responses shown in Figure 9-6 do not show reliable linear trends. We attribute this to the relatively small number of transits driven by the GMC.

Figures 9-8, 9-9, and 9-10 show details of the trends for these vehicles. The trends for the F150 and the Subaru show good evidence of increasing measured EvapHC trends as the metered EvapHC is increased.

Figure 9-5. HC Performance (Average) for Test Vehicle F150

a) F150: THC Overview
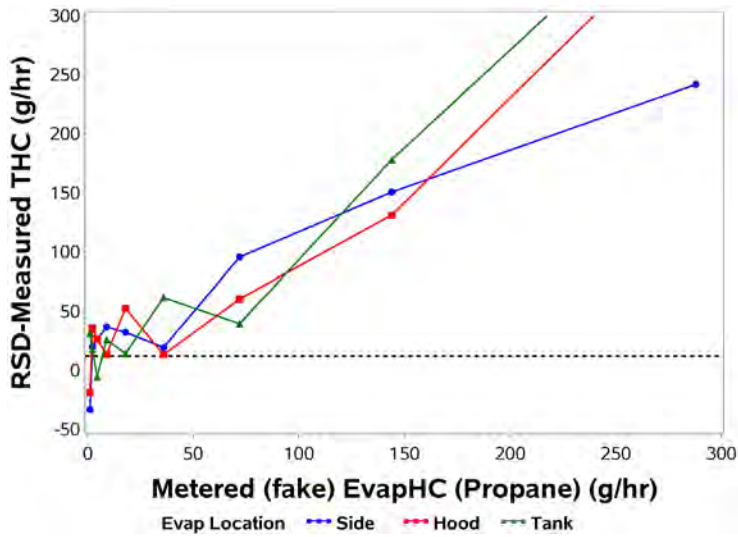
b) F150: Evap release at SIDE
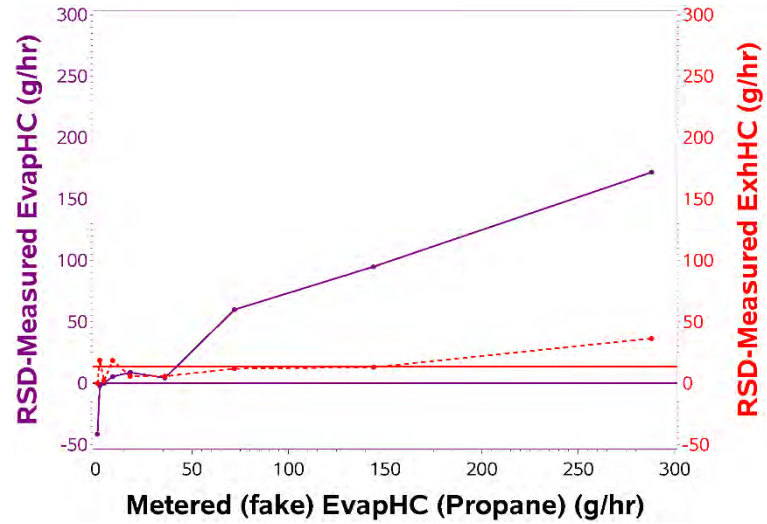
c) F150: Evap release at HOOD
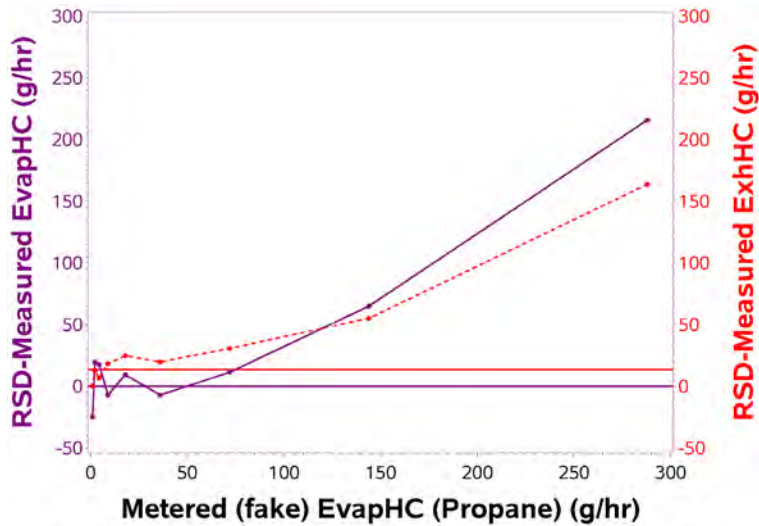
d) F150: Evap release at TANK

/proj1/EDARinDenver-OCT2019/Analysis_MLout/220817/Anal_MLout/RefVehs/OCT19_perf_RefVeh.sas 28AUG22 09:44
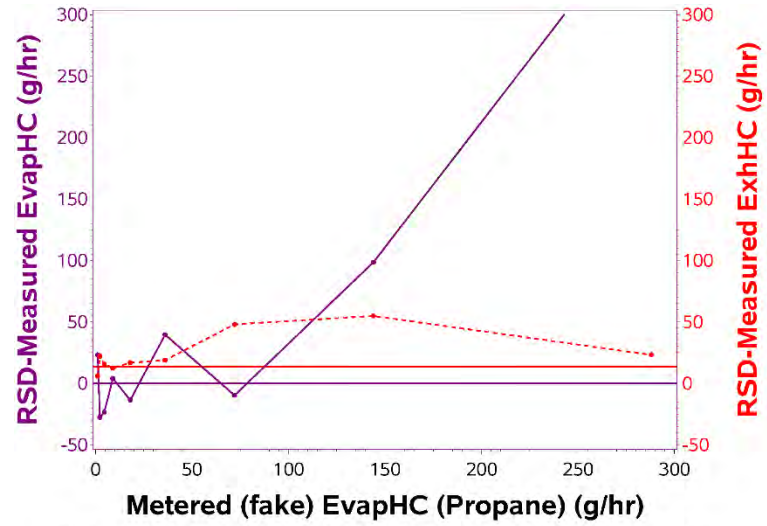
/proj1/EDARinDenver-OCT2019/Analysis_MLout/220817/Anal_MLout/RefVehs/OCT19_perf_RefVeh.sas 28AUG22 09:44

Figure 9-6. HC Performance (Average) for Test Vehicle GMC

a) GMC: THC Overview
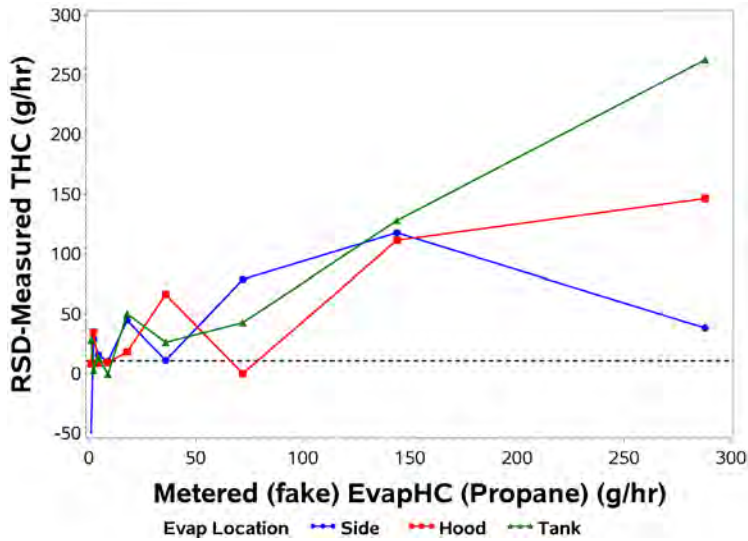
b) GMC: Evap release at SIDE
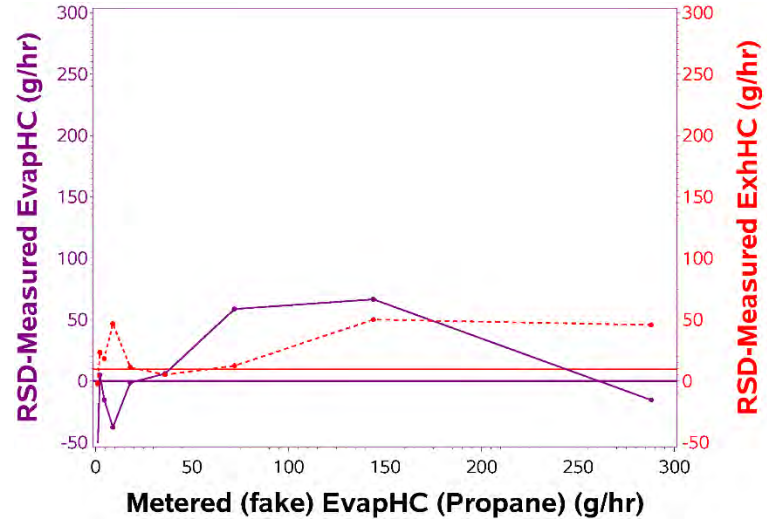
c) GMC: Evap release at HOOD
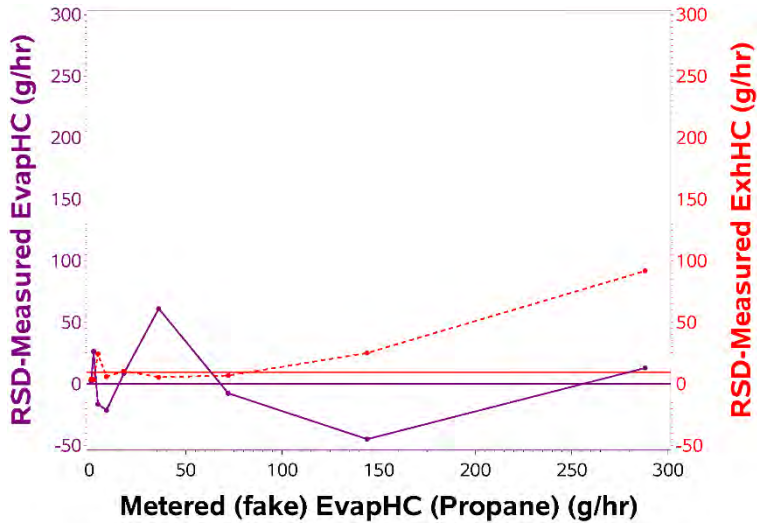
d) GMC: Evap release at TANK
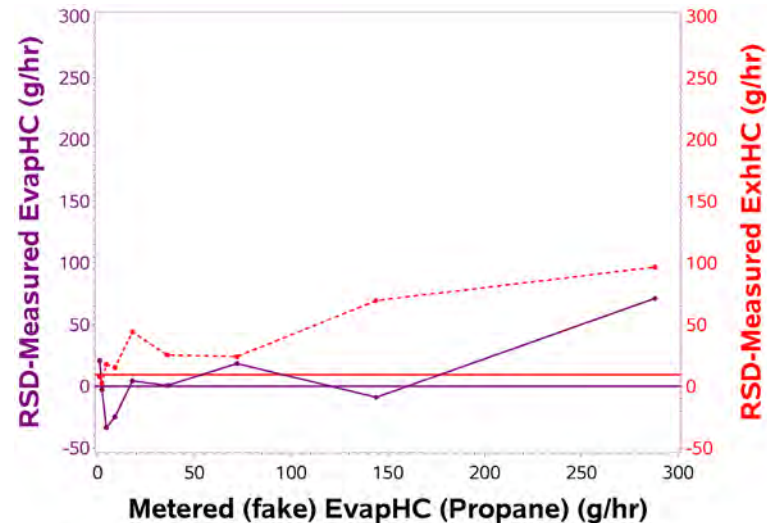
/proj1/EDARinDenver-OCT2019/Analysis_MLout/220817/Anal_MLout/RefVehs/OCT19_perf_RefVeh.sas 28AUG22 09:44

Figure 9-7. HC Performance (Average) for Test Vehicle Subaru

a) Subaru: THC Overview
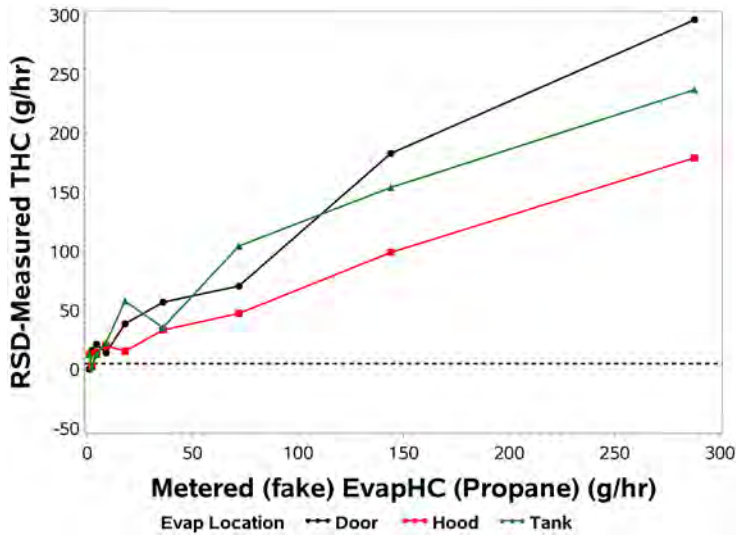
b) Subaru: Evap release at DOOR
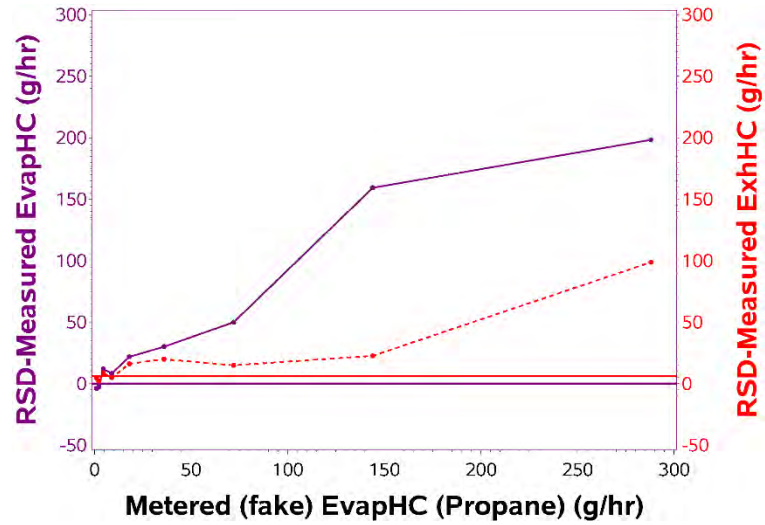
c) Subaru: Evap release at HOOD
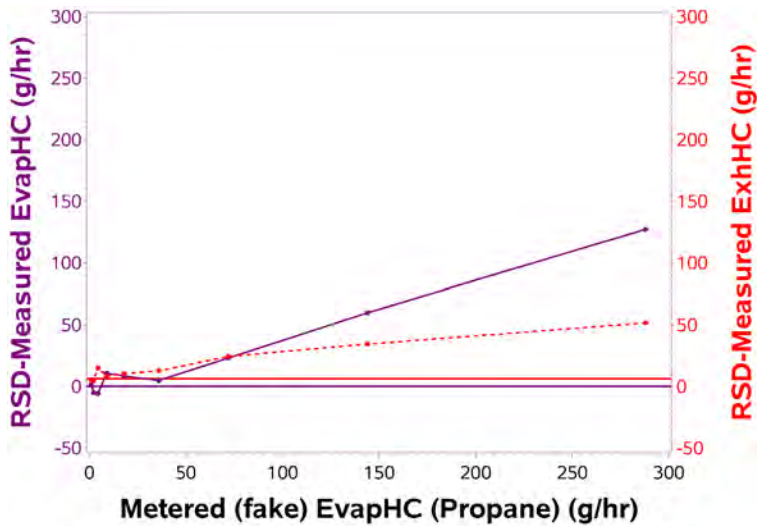
d) Subaru: Evap release at TANK
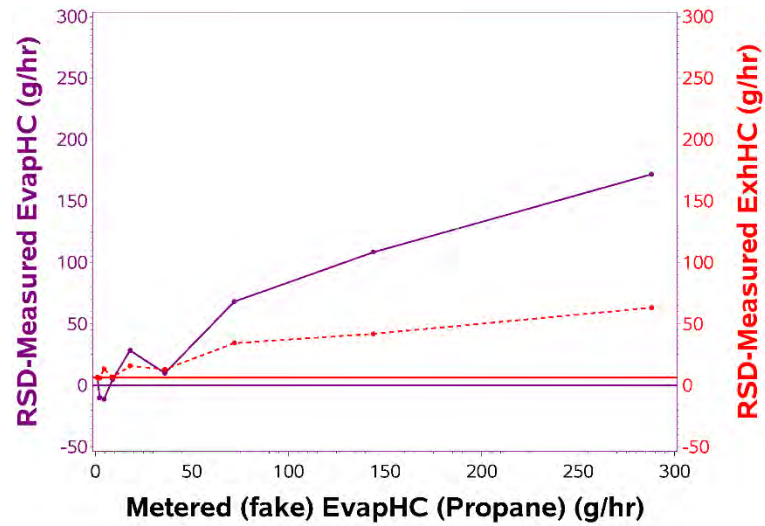
/proj1/EDARinDenver-OCT2019/Analysis_MLout/220817/Anal_MLout/RefVehs/OCT19_perf_RefVeh.sas 28AUG22 09:44

Figure 9-8. HC Performance (Details) for Test Vehicle F150

a) F150: Location-corrected EvapHC Overview
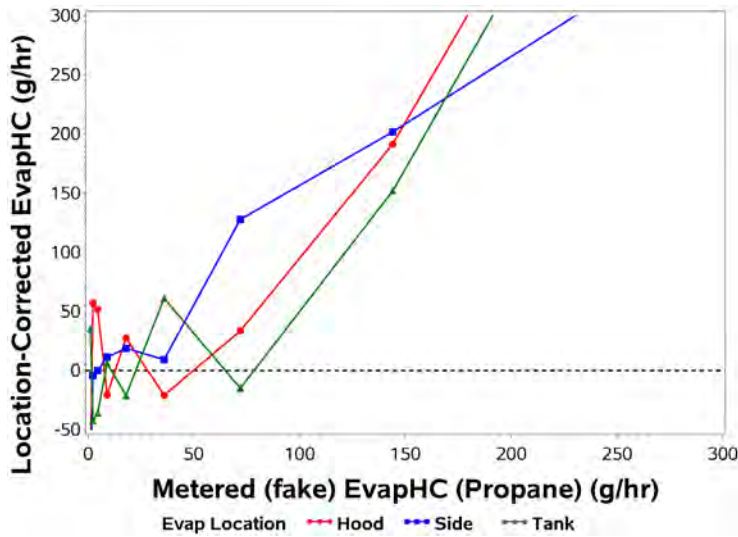
b) F150: Evap at SIDE (scatter)
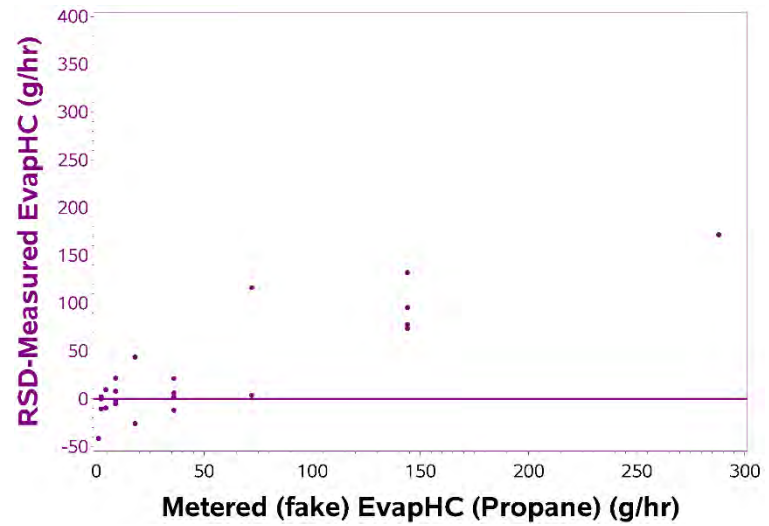
c) F150: Evap at HOOD (scatter)

/proj1/EDARinDenver-OCT2019/Analysis_MLout/220817/Anal_MLout/RefVehs/OCT19_perf_RefVeh_scatter.sas 29AUG22 15:17
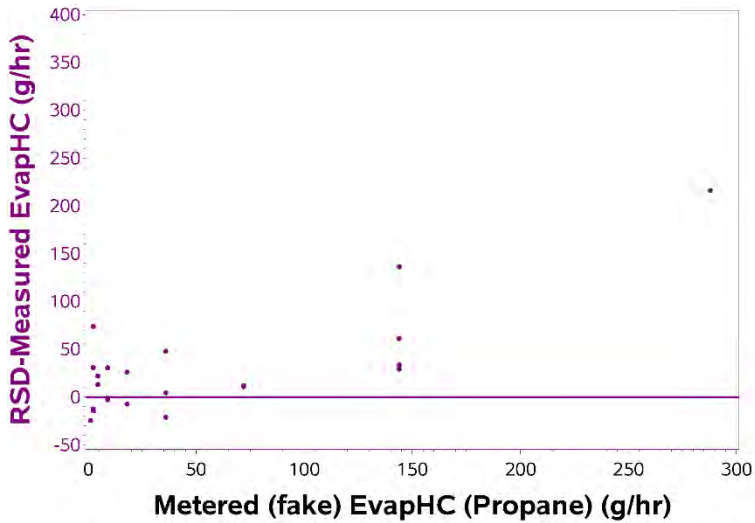
d) F150: Evap at TANK (scatter)
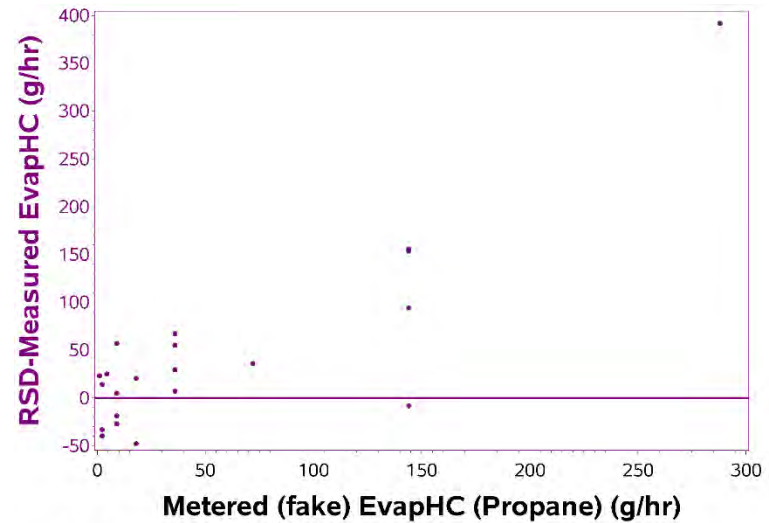
/proj1/EDARinDenver-OCT2019/Analysis_MLout/220817/Anal_MLout/RefVehs/OCT19_perf_RefVeh_scatter.sas 29AUG22 15:17

Figure 9-9. HC Performance (Details) for Test Vehicle GMC

a) GMC: Location-corrected EvapHC Overview
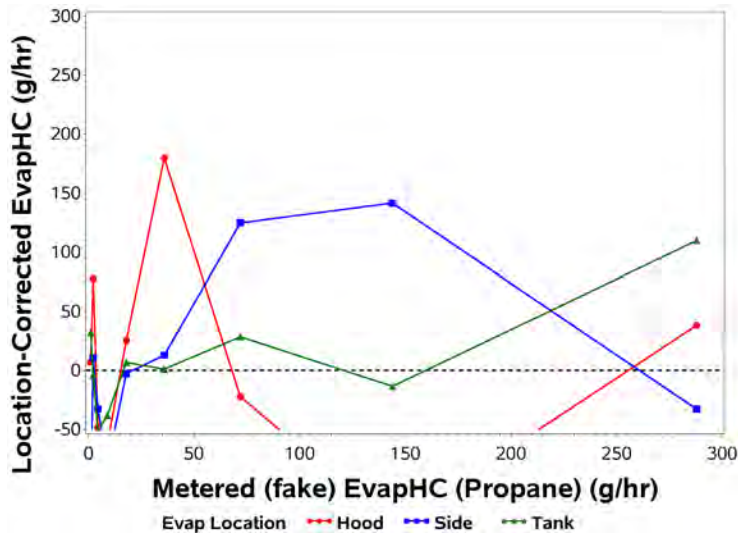
b) GMC: Evap at SIDE (scatter)
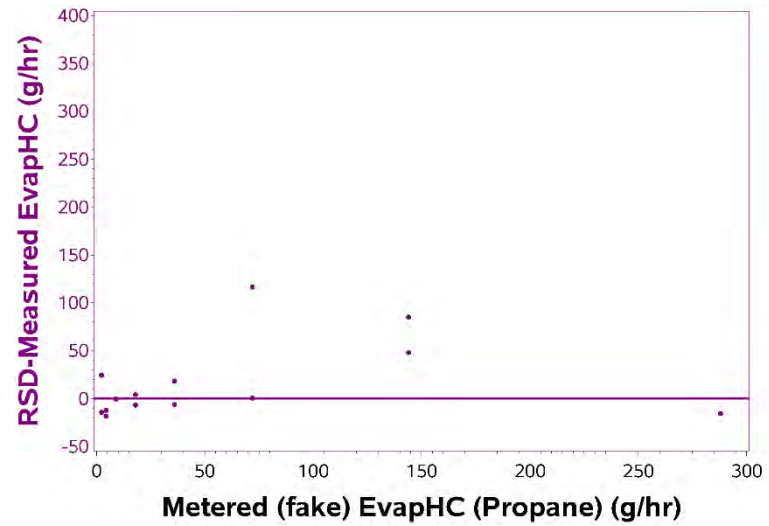
c) GMC: Evap at HOOD (scatter)

/proj1/EDARinDenver-OCT2019/Analysis_MLout/220817/Anal_MLout/RefVehs/OCT19_perf_RefVeh_scatter.sas 29AUG22 15:17
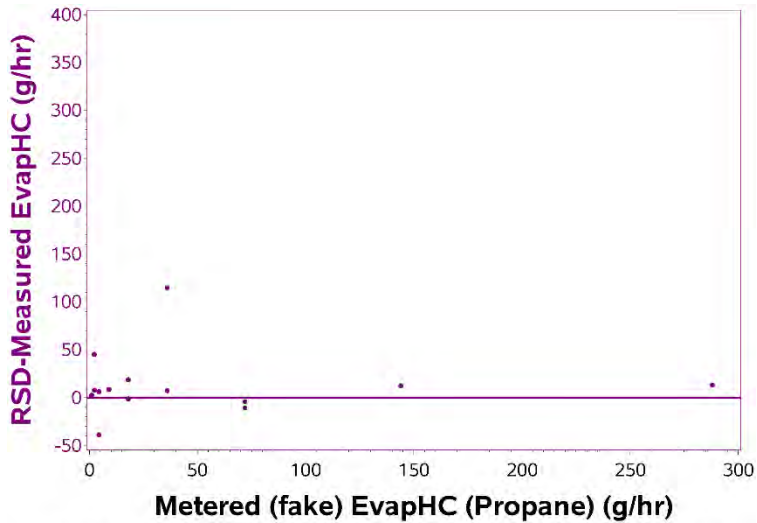
d) GMC: Evap at TANK (scatter)
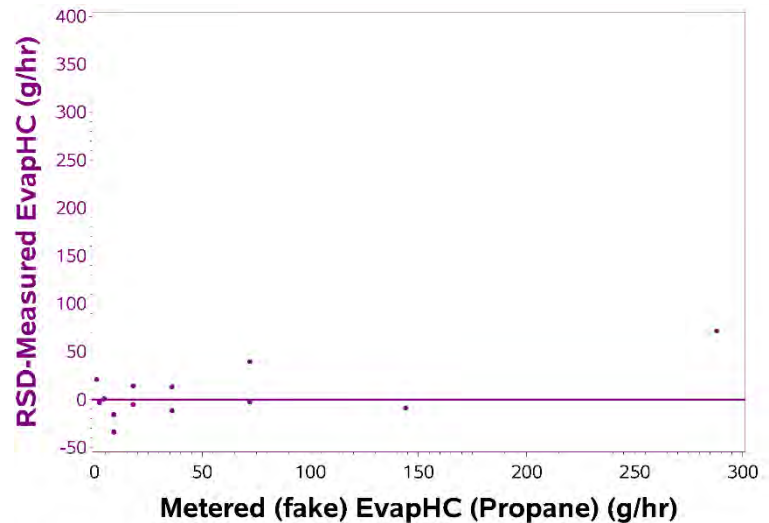
/proj1/EDARinDenver-OCT2019/Analysis_MLout/220817/Anal_MLout/RefVehs/OCT19_perf_RefVeh_scatter.sas 29AUG22 15:17

Figure 9-10. HC Performance (Details) for Test Vehicle Subaru

a) Subaru: Location-corrected EvapHC Overview
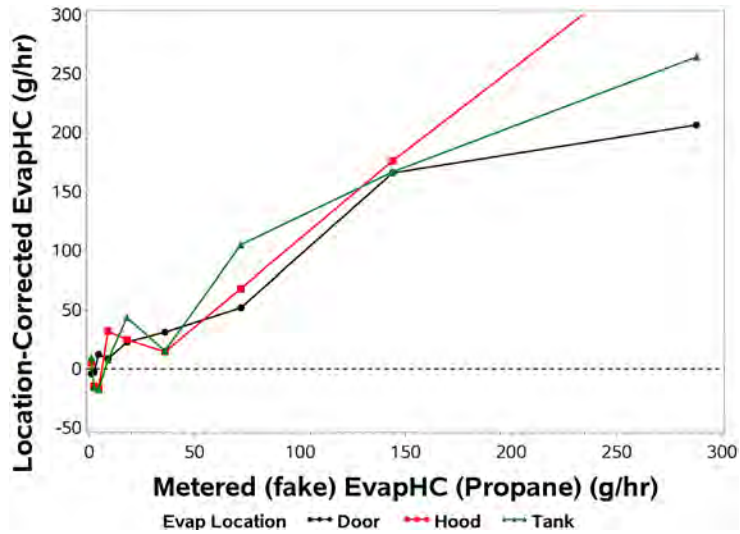
b) Subaru: Evap at DOOR (scatter)
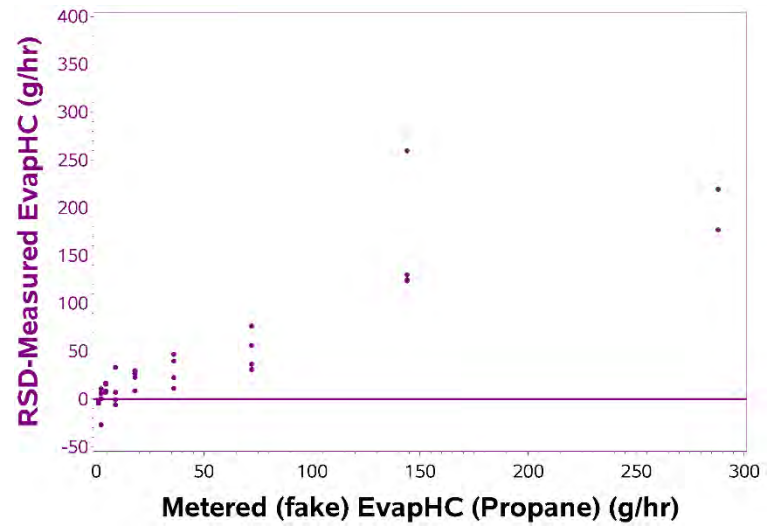
c) Subaru: Evap at HOOD (scatter)

/proj1/EDARinDenver-OCT2019/Analysis_MLout/220817/Anal_MLout/RefVehs/OCT19_perf_RefVeh_scatter.sas 29AUG22 15:17
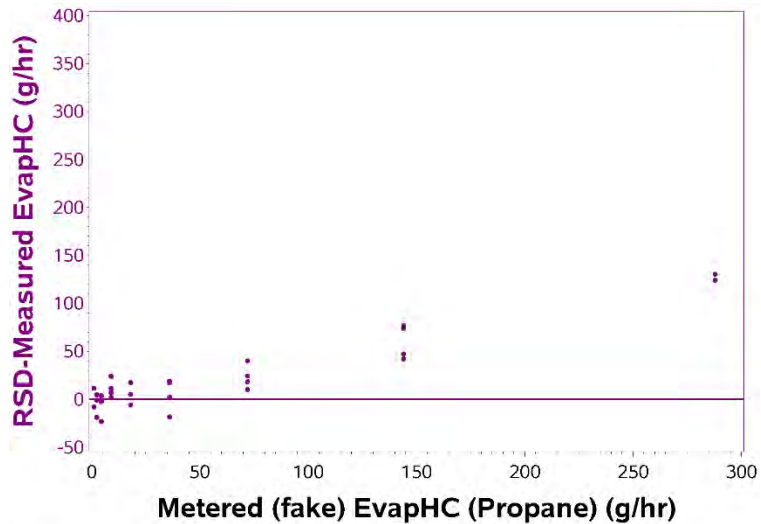
d) Subaru: Evap at TANK (scatter)
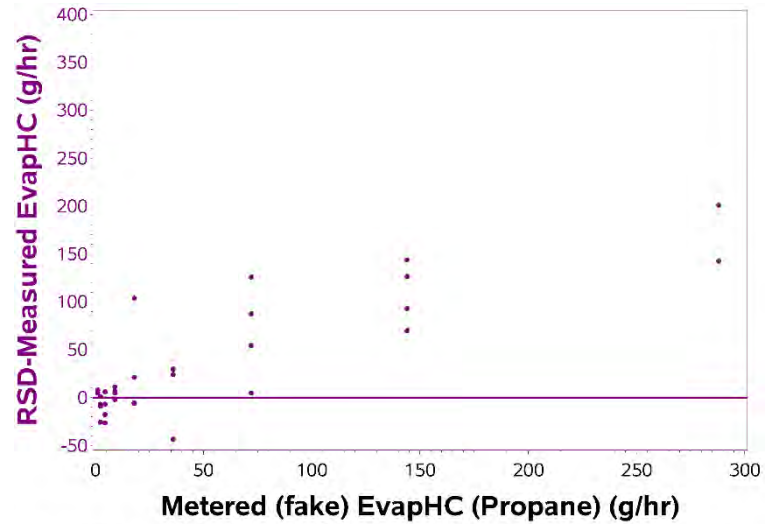
/proj1/EDARinDenver-OCT2019/Analysis_MLout/220817/Anal_MLout/RefVehs/OCT19_perf_RefVeh_scatter.sas 29AUG22 15:17

9.4   Recommendations for Development of the RSD Emission Rate Method

This study shows that, with different processing of detailed RSD data, direct estimations of vehicle release rate (g/hr) and emission rate (g/mile) are possible. The traditional RSD method for exhaust concentration (ppm) and fuel-specific mass emission rates (g/gFuel) cannot obtain emission release and emission rates, and exhaust HC values are subject to potentially large errors introduced by evaporative emissions. However, the traditional RSD method has a great advantage in that it is straight-forward and minimizes certain types of interferences and vehicle-specific dependencies. The traditional method has these attractive properties because its calculations are based on the ratio of each pollutant's RSD signal to the simultaneous CO_2 RSD signal. In contrast, the new RSD emission rate method is based, not on a ratio of pollutant signals, but on the single, absolute RSD signal of each pollutant. Consequently, the new method will benefit from additional development. This subsection briefly describes sixteen suggested areas to improve the method in general and to extend it to medium- and heavy-duty on-road vehicles. These are ordered with the most important areas for improvement at the top of each list.

To improve the method in general:

1. Poor Correlations among Exhaust Pollutant Detailed Data
2. RSD Signal Dependence on Laser Pathlength
3. Vortex Entrainment Time (VET)
4. Release Location Detection of Light-Duty EvapHC
5. Vortex Shape (Weights)
6. RSD Signal Accuracy
7. RSD Signal Attenuation
8. Evaporative Plume Signal-to-Noise Improvement
9. Drag Area
10. Enhanced Blind Source Separation
16. Interfering Plumes

To extend the method to medium-duty and heavy-duty vehicles

3. Vortex Entrainment Time (VET) – specific to MDVs and HDVs
5. Vortex Shape (Weights) – specific to MDVs and HDVs
11. Release Location Detection of Medium- and Heavy-Duty Exhaust
12. Diesel Engine Load
13. Particulate Material Pollutant Correction Factor
14. Trailer Configuration Detection
15. Emissions of Vehicles with Trailers

1. Poor Correlations among Exhaust Pollutant Detailed Data – The investigation of flags (see Section 7.5) seems to indicate that correlations of CO and NO with CO_2 are relatively good for the test vehicles and for diesel vehicles but are frequently poor for the vehicles that dominate the fleet – gasoline vehicles. Since CO, NO, and CO_2 can originate only from exhaust sources, their RSD detailed data should always be highly correlated. So, poor correlation among them is a major concern. The BSS separations help identify poor correlations by displaying the remnant

signals seen in the BSS output heatmaps of Noise 1, 2, and 3. Our analyses do not indicate that the problem arises from our signal improvement processing.

Since the vortex contains releases from the last 5 to 10 seconds of engine operation, our hypothesis is that recent changes in engine operation cause shifts between CO and CO_2 mass that is reflected in the spatial distributions of pollutants in the vortex. For gasoline vehicles, changes in engine operation in response to load causes a time-varying shift of carbon between CO and CO_2. Thus, unless the engine has been operating under chemically steady-state conditions over the last 5 to 10 seconds, none of the pollutant signals precisely represent the exhaust plume. Nevertheless, it may be possible to determine the combustion-independent exhaust plume signal by accounting for the stoichiometry differences seen in all pollutant channels for a given transit.

2. RSD Signal Dependence on Laser Pathlength – The EDAR instrument is positioned above the lane, and the laser scans back and forth. This geometry causes the optical pathlength to be longer for pixels near the edge of the lane and shorter for pixels near the center of the lane. This geometry is not a problem for the traditional RSD concentration method. While the 400ppm ambient CO_2 produces about 20% of the total CO_2 signal, HEAT has a proprietary method to correct for the ambient CO_2.

For the RSD emission rate method, the varying pathlength needs to be corrected for every pollutant channel. We believe that the proposed O_2 channel, discussed below, could be used to make this correction in addition to correcting for signal attenuation.

Another possibility is to use both the CO_2 and O_2 channels to monitor and correct for the changing pathlength. The O_2 and CO_2 optical masses at each pixel are simply a proportional blend of the O_2 and CO_2 concentrations in ambient air and the O_2 and CO_2 concentrations at the tailpipe exit. By taking advantage of that fact, it should be possible to use O_2 and CO_2 pixel measurements to verify that the signals of all RSD channels have been consistently corrected to changing laser pathlengths in each scan.

3. Vortex Entrainment Time (VET) – The VET of a transit is just the ratio of the Mass in Vortex (g) to the Release Rate (g/hr). Thus, if the RSD measures a pollutant's Mass in Vortex, the VET can be conveniently used to estimate the pollutant release rate. For the light-duty vehicles in this study, the VET was found to depend on vehicle air velocity, vehicle drag area, and emission release location, and VET was independent of pollutant and release rate. In future data collection efforts, we would like to 1) confirm the dependencies of light-duty VETs and 2) collect data that can be used to extend VET knowledge to medium- and heavy-duty vehicles.

To determine generalized values and dependencies of VETs, repeated RSD measurements of representative test vehicles must be made while releases of a pollutant are being measured as the vehicles are driven under carefully controlled conditions. These requirements suggest test vehicles in a staging area out of traffic.

For confirming light-duty VETs, we suggest releasing 30,000 ppm NO in nitrogen from gasoline-fueled test vehicles with a wide range of drag areas while they drive at two speeds under a variety of wind conditions. We suggest using the high NO concentration so that the natural NO emissions of the test vehicles will only trivially affect the RSD signal – thus avoiding

procuring electric test vehicles. Using NO as the metered pollutant will produce strong RSD signals. To determine EvapHC release location dependencies, the NO can be released from Door, Tank, Hood, Side, and Well locations. To simulate exhaust emissions location dependencies, the NO can be injected into the exhaust system between the catalyst and upstream of the muffler. Light-duty test vehicles will have to operate at constant speed and release at constant conditions for at least 15s (= ~3 VETs) before arriving at the RSD.

For discovering medium- and heavy-duty VETs, we suggest using the natural CO_2 emissions of test vehicles with a wide range of sizes while they drive at two speeds and a variety of wind conditions. The test vehicles would also be chosen so that the fuel rate could be monitored with an OBD data stream. During each test transit the engine would have to be operated so that the fuel rate remains constant for 30s (= ~3 VETs) before passing the RSD so that the CO_2 Mass in Vortex (box trucks have a large vortex to fill) is substantially in dynamic equilibrium with the CO_2 release rate. Test vehicles should also be chosen to cover the range of exhaust release locations (e.g., under-chassis tailpipe, over-cab stacks, rear bumper) seen in the fleet.

4. Release Location Detection of Light-Duty EvapHC – This Westminster study found that light-duty VETs were dependent on emission release location. Therefore, to promote more accurate EvapHC emission rate values, a method to get a general idea of EvapHC emission release location is desirable. We suggest staged testing of test vehicles out of traffic to generate transits with detailed data that can be used to develop a method.

One of the main challenges of EvapHC release location detection is the need for an improved signal-to-noise ratio of the HC signal. Specifically, even with large EvapHC release rates (g/hr) from test vehicles, finding the EvapHC plume is difficult. To judge the performance of candidate signal processing release location detection methods using the HC channel data alone, we need an EvapHC plume tracer gas that produces a strong signal. Therefore, we suggest releasing a mixture of butane and 30,000 ppm NO. The butane simulates the EvapHC since it is a major component of EvapHC emissions. Butane will be metered over a wide range. The release rate of the NO will be kept high so that the true location of the EvapHC plume can be easily seen in the RSD NO detailed data stream. Then, signal processing techniques for estimating EvapHC release location can be developed on the butane detailed data and tested against the NO detailed data, which defines the true location of the EvapHC plume.

The effort will focus on determining release location for moderate and high EvapHC release rates since knowing the release location of low EvapHC releases is less important and is expected to be quite difficult to achieve. Because we will not attempt low butane release rates, the test vehicles can be gasoline-fueled vehicles, whose natural ExhHC and EvapHC release rates will be lower than the butane release rates. Three different vehicle shapes (sedan, sport-utility vehicle, and pick-up with open bed) will be a minimum to generate widely different EvapHC plume dispersion patterns from a few locations (Door, Tank, Hood, Side). As usual, tests will be conducted at two speeds, under a variety of wind conditions, and with RSD approaches at constant release and operating conditions for at least 15s (= ~3 VETs).

5. Vortex Shape (Weights) – The RSD emission rate method uses the expected shape of the vortex that follows the vehicle to weight the measured optical masses at each pixel. The shape is the <u>relative</u> magnitude of optical absorption of emissions at different scans and/or pixel positions

in the vortex. The weights are used to effectively improve the signal-to-noise ratio of the RSD signal of each pollutant channel and thereby improve the detection limit of the calculated emission rates (g/mile). In this report's analysis, we developed one-dimensional (1D) weights with one weight for each RSD scan behind the vehicle. We developed these weights primarily for light-duty vehicles. These light-duty 1D weights were found to be a function of time after the vehicle rear, the parallel component of the airspeed, and vehicle length. Light-duty 1D weights were found to be independent of pollutant. We expect that two-dimensional (2D) weights, which are effectively weights on individual pixels, will be additionally dependent on the perpendicular component of the airspeed.

In future work, we would like to confirm the 1D weights on light-duty vehicles, extend the 1D weights to medium- and heavy-duty vehicles, and collect EDAR detailed data for and develop 2D weights for light-, medium-, and heavy-duty vehicles. These extensions to weights can be made by analyzing the CO_2 in vortexes of thousands of fleet vehicles in traffic. The light-duty 1D weights did not seem to be a function of vehicle drag area or pollutant release location. However, because exhaust release locations vary considerably among individual medium- and heavy-duty vehicles, it would be prudent to plan to examine future field data for these possible influences.

Metered releases are not needed to determine vortex shape (weights) since only relative, not absolute, magnitude is determined. And any pollutant can be used to determine weights. This Westminster study used the CO_2 in the vortexes of the 30,000 fleet vehicles to determine the 1D weights and their dependencies. We also found that we needed at least this many transits to determine the dependencies. When a small subset of the 30,000 transits was analyzed for dependencies, the trends became confused. We expect that this was a consequence of the turbulence that is always present around vehicles moving through air.

6. RSD Signal Accuracy – In its detailed data files, the EDAR instrument reports the optical mass measurements at each pixel of each pollutant channel in moles/m^2. Unlike the traditional RSD concentration method, which uses ratios, the RSD emission rate method uses absolute RSD optical mass values and therefore requires accurate reported detailed data values. This Westminster study assumed that the reported optical mass values were accurate. To be certain that EDAR's reported optical masses are accurate, we need to have a field method to verify or measure the accuracy of the reported optical mass values for each EDAR pollutant channel. HEAT may already have a method such as a gas cell within the EDAR instrument. Using a gas cell to check calibration at the RSD site could provide data to correct for any variations in reflection efficiencies of different areas of the retro-reflective pavement tape.

7. RSD Signal Attenuation – Also because the RSD emission rate method uses the absolute RSD optical mass values, the RSD signals on which the method's reported values of emission release rate are based, are subject to attenuation caused by wear of and dirt on the retro-reflective tape and by particulate material in the air between the EDAR instrument and the pavement. The traditional RSD concentration method, which is used by EDAR, is not affected by such attenuation sources. We need to develop a way to monitor and to correct for these attenuations so that the calculated emission rates (g/mile) are not biased low.

The attenuation of the EDAR optical path could be monitored continuously by getting an RSD signal from gases that occur naturally in the atmosphere. Ambient CO_2 could be used since its

global concentration is about 400 ppm. However, the ambient CO_2 concentration around a busy roadway is likely higher since the vehicles on the road emit large exhaust volumes of CO_2 with concentrations around 15% (=150,000 ppm). This method might work in out-of-traffic staging areas, on roadways with light traffic, or roadways that have non-polluted air blowing across them, but it will not work on busy roadways since ambient CO_2 levels are greater than 400ppm there.

A procedure for correcting for signal attenuation might be tested by artificially attenuating the RSD signals by placing and removing an attenuation grid on top of the retro-reflective tape.

8. Evaporative Plume Signal-to-Noise Improvement – The noise that is present in the BSS output channel called Evap Plume causes uncertainty in the calculated EvapHC emission rate (g/mile). In turn, this causes the detection limit of the EvapHC emission rate to be higher than it would otherwise be. Therefore, reduction of the noise in Evap Plume is desirable. Generally, most of the noise in Evap Plume is from the noise in the adjusted HC channel, which is one of the inputs to the BSS. Even though the noise in raw detailed HC data is reduced by the signal analysis techniques described in this report, because the typical EvapHC emission rates (g/mile) of fleet vehicles are small, the S/N ratio of EvapHC is small. Therefore, to improve the detection limit of EvapHC emission rates, either the noise in Evap Plume or in adjusted HC needs to be reduced and/or the EvapHC signal in the RSD HC channel needs to be increased.

One method that might be used to increase the EvapHC signal in the RSD HC channel is to select an EDAR infrared (IR) wavelength that focuses on the IR spectrum of butane, which is the dominant gas in EvapHC emissions. Reducing noise and artifacts in the Evap Plume signal, that is, the BSS output, might also yield improved S/N ratios.

Another candidate for improving the evaporative plume S/N ratio is to use ethanol vapor as a tracer for the EvapHC plume. Our modeling of gasoline blends with 10 wt% ethanol, which is now universally used in the United States, indicates that its headspace is about 20 mole% ethanol and the whole evaporated blend contains about 18 mole% ethanol. Thus, whether an evaporative emission is produced by an evaporative emission control system vapor leak or by an evaporated gasoline liquid leak, the emission is about 20 mole% ethanol. On the other hand, only about 3 mole% of the NMHC of ExhHC is ethanol. The infrared spectrum contains about eight sharp spectral lines that are candidates for evaluation as targets for measurements of ethanol by the DiAL method. If relatively free of interferences from other compounds, one of the ethanol lines might be able to increase the evaporative S/N compared to using the EDAR HC channel's signal as done in this study.

9. Drag Area – The analysis of the September 2016 (TTI) data and the October 2019 (Westminster) data indicates that the drag area of a vehicle mildly affects the VET. Therefore, knowledge of the drag area of the vehicle in each transit would help improve the calculated emissions rate. For some, but not all, vehicles, drag areas can be obtained from a look-up table using the VIN obtained from the license plate. In a further development, it might be possible to apply machine learning to the vehicle footprint (when the laser beam is occluded by the vehicle) and perhaps an image of the side profile of the vehicle to estimate the drag area of the vehicle. Such a method would be able to the estimate drag area of <u>any</u> vehicle without using a look-up table.

10. Enhanced Blind Source Separation – The Independent Component Analysis (ICA) method using FastICA was the BSS method used in this first analysis of the Westminster dataset to split the RSD HC signal into an EvapHC signal and an ExhHC signal. This method produces very good separations when the EvapHC and ExhHC plumes do not overlap. However, we found that in circumstances where the EvapHC and ExhHC plumes substantially overlap, the standard ICA separations produce only mediocre "first-order" separations, which are usable but are not optimal. In these situations in the portion of the vortex just behind the tailpipe, too much HC mass is assigned to ExhHC and not enough mass to EvapHC. In some cases, the mass assigned to EvapHC at the tailpipe exit location is a slightly negative – seen in heatmaps as the "blue hole" – a physical impossibility.

To address the problem, we developed a new BSS technique called BSScov (see Section 7.3) in which one of the constraints in the matrix algebra is relaxed to produce better separation results when plumes overlap, which is the usual case for vehicles in light-duty fleets. However, we have not yet developed a method to determine when the adjustable parameter, rho, is at an optimum. Without the BSScov method, the standard ICA method produces usable results, but developing a method to optimize BSScov's rho will produce superior results.

11. Release Location Detection of Medium- and Heavy-Duty Exhaust – Just as for EvapHC, the release location of exhaust emissions can affect the VET of exhaust plumes. For light-duty exhaust emissions, the release location will always be from the vehicle rear, and therefore determination of release location for light-duty exhaust is not needed. On the other hand, on medium- and heavy-duty vehicles, exhaust exit locations vary. For example, medium-duty trucks may release exhaust from just behind and below the cab or below the rear of the cargo box. We expect that these different locations will have different release location fingerprints.

A method for detecting different exhaust release locations of medium- and heavy-duty vehicles can be developed from the same data that is collected for the VET effort described above. That is, we suggest using the natural CO_2 emissions of test vehicles with a wide range of sizes while they drive at two speeds and a variety of wind conditions. The test vehicles would also be chosen with an OBD data stream so that the fuel rate can be monitored. During each test transit the engine would have to be operated so that the fuel rate remains constant for 30s (= ~3 VETs) before passing the RSD so that the CO_2 Mass in Vortex (box trucks have a large vortex to fill) is substantially in dynamic equilibrium with the CO_2 release rate. Test vehicles should also be chosen to cover the range of exhaust release locations seen in the fleet.

Stewart Hager of HEAT indicates that for large trucks releasing exhaust emissions near the front of the truck 1) vehicle speeds of at least 17 mph are needed to produce a significant vortex behind the box or trailer, and 2) exhaust emissions "hug" the sides of the box (Bernoulli) on their way to the vortex. The second of these observations might be verified by collecting EDAR data using a set of two EDAR instruments placed above the left and right edge of the lane but looking across the full width of the lane. Such a set-up might allow seeing emissions move past the side of the box or trailer and establish the point at which transverse air movement causes a reduction of emissions entrainment in the vortex behind the vehicle.

12. Diesel Engine Load – The load on an in-use diesel engine is important to know to judge if the engine emissions are elevated with respect to the emission certification standards of the

engine. An emission-compliant engine operating under high load might have the same high emissions as a non-emissions-compliant engine operating under light load. While road grade contributes to engine load, for cargo-hauling diesel vehicles the weight of the cargo is an important factor. While we do not have a method to remotely determine vehicle weight, we believe that the RSD emission rate method applied to CO_2 can provide an estimate of diesel engine load.

Diesel engines tend to have similar CO_2 emission rates (g/mile) when operating under similar loads – pretty much regardless of engine displacement, design, RPM, and rated horsepower. This is a consequence of the heat content of the fuel. If we assume that all diesel engines have about the same efficiency, the gross load on the engine (including internal frictional losses) is proportional to the fuel rate (g/hr). Since the carbon in the fuel becomes primarily exhaust CO_2, the CO_2 release rate (g/hr) is directly proportional to the fuel rate. Because the RSD emission rate method can determine CO_2 release rate, it can determine gross engine load. Thus, the RSD method can not only measure pollutant release rates (g/hr) and emission rates (g/mile), it should be able to estimate the gross engine load. Knowledge of the engine load would allow the distinction between an emission-compliant engine operating under high load and a non-emissions-compliant engine operating under light load.

By looking up the license plate in the vehicle registration database, decoding the heavy-duty VIN, and determining the engine's displacement, the estimated minimum and maximum non-boost fuel rates could be determined and compared to the RSD-measured fuel rate to estimate relative engine load at the instant of the RSD transit. The minimum fuel rate can be determined by assuming that an idling diesel will have an air:fuel ratio near 100:1. The maximum fuel rate can be determined by assuming that a diesel engine operating near 100% non-boosted load will have an equivalence ratio[35] near 0.6. Thus, dividing the RSD-estimated absolute fuel rate by the displacement-estimated maximum fuel rate will provide an estimate of the relative load on the engine. We would expect that turbo-boosted operation would simply produce relative loads greater than 100%.

The ability of the RSD emission rate method to determine diesel engine load and relative load using this technique could be evaluated during staged testing. The diesel test vehicles that were equipped with a monitor of OBD fuel rate would be used to generate load and fuel rate data for comparison with values determined by the RSD emission rate method. The diesel test vehicles would be operated under a variety of engine loads and RPMs.

13. Particulate Material (PM) Pollutant Correction Factor – The exhaust PM emission rates of diesel vehicles could be measured by the RSD emission rate method if the RSD optical signals produced by the PM can be used to estimate the PM Mass in Vortex. The conversion from RSD optical signal to PM mass depends on 1) the method used by the RSD and on 2) the Mie light scattering of diesel particles. EDAR reports PM in units of particles/m^2.

---

[35] Equivalence ratio is the ratio of the actual air:fuel ratio to the stoichiometric air:fuel ratio. For diesel fuel combustion, the stoichiometric air:fuel ratio is about 14.4:1. Therefore, diesel engines are usually designed to operate at actual air:fuel ratios no less than about 25:1 to avoid excessive generation of smoke.

The sensitivity of EDAR to diesel PM could be determined on a diesel test vehicle in an out-of-traffic staging area. The PM release rate (g/hr) and ideally size distribution would be determined using a PEMS installed on the vehicle while the vehicle drove past the RSD under a variety of engine loads to produce a variety of PM release rates.

An accompanying Mie light scattering modeling effort of reported diesel particle size distributions would be able to determine the sensitivity of EDAR's measurement and the calculated PM emission rate (g/mile) to the literature-reported variations in size distribution, refractive index, and particle morphology.

14. Trailer Configuration Detection – In this Westminster study, the analysis eliminated transits that appeared to be from vehicles pulling trailers since quantifying the emissions from those vehicles was not the focus of the study. We developed SAS code to identify such vehicles. However, if the efforts to quantify emissions from combination tractor-trailers is successful, we would want to distinguish them from medium-duty pick-ups pulling work trailers. We think that applying machine learning techniques to the RSD detailed data would be more productive for solving this problem than using further in-depth SAS efforts.

15. Emissions of Vehicles with Trailers – With the determination of VETs, vortex shapes, and an exhaust release location method, we expect that the exhaust emissions rate (g/mile) of medium-duty box trucks and heavy-duty combination tractor-trailers could be determined using RSD. However, quantification for medium-duty pick-ups pulling a wide variety of work trailers may be more difficult. The Westminster data shows that vortexes for these transits are formed behind the vehicle and behind the trailer. Accordingly, at this point, we do not propose work to quantify the emissions of these types of vehicle assemblages.

16. Interfering Plumes – The EDAR QC flag assigned "interfering plume" to 7.2% (=2302/31763) of the transits in the dataset of fleet vehicles at the relatively light-traffic Westminster site. Interfering plumes can occur when a transit has emissions from another vehicle detected by EDAR in front of the subject vehicle. Such emissions cause incorrect reported emission concentrations when the standard calculations are used. So, standard protocol is to throw out measurements where an interfering plume is detected. However, we think that it may be possible to use signal processing to process the transit's raw data so that the interfering plume can be separated from the subject vehicle's data and thereby obtain good emissions measurements on the subject vehicle. This would reduce the number of transits that are thrown out and would allow use of the EDAR instrument in heavier-traffic situations.

10.0 Application of the RSD Emission Rate Method to the Fleet Sample

In this section, we evaluate the RSD emission rate method by comparing the exhaust release rates measured in Westminster in October 2019 with MOVES model predictions of exhaust release rates for the same time period. To be able to make that comparison, we need to describe the bases of the release rate values for the MOVES predictions and the RSD measurements.

Portable emissions measurement systems (PEMS) are sometimes used in field studies to measure the rapid up and down changes on emissions concentrations, release rates, and flows on a second-by-second basis. The exhaust gas is sampled using a probe that is inserted in the tailpipe. The gas sample is conducted via a small-diameter, heated sample line, without dilution, to the PEMS instrument package installed on board the vehicle. The PEMS analyzers typically have fast response times to attempt to preserve the rapidly varying time traces.

MOVES predictions for newer model year light-duty vehicles are based primarily on dynamometer tests that use a constant-volume sampling (CVS) procedure. The exhaust gases are conducted through a heated pipe to the CVS system for dilution and concentration measurement. During this procedure, the rapid ups and downs of concentrations and flows are smoothed slightly. Thus, the dynamometer CVS measurements do not reflect the rapid second-by-second changes that a PEMS instrument would have, but still CVS measurements preserve the rapid changes relatively well.

Rather than conducting a sample of gas from the tailpipe exit, as PEMS and CVS systems do, RSDs measure pollutants in-situ in the vortex without taking a sample of the gas. Because RSDs measure optically, the RSD measurement process for one vehicle transit takes only about 0.5s. While the measurement is fast, the RSD results reflect the mass of pollutants in the vortex – not the pollutant flows from or concentrations in the tailpipe. The reason for this is that the mass of pollutants in the vortex at any given instant is the result of entrainment of emissions released from the vehicle and stripping of pollutants from the vortex by air moving across the surface of the vortex as described by Figure 5-4. In this study, we have found that for light-duty vehicles the vortex entrainment time (VET) is around 4 seconds. The mass of pollutants in the vortex is influenced by the emissions released from the vehicle over at least the last 2 VETs or about 8 seconds. Thus, even though RSDs measure almost instantaneously, the masses in the vortex that they measure are influenced by the changes in vehicle and engine operation over a comparatively long time.

So, MOVES predictions are based on relatively rapid changes in exhaust, and RSD measurements of the vortex mass reflect the relatively slowly changing effects of the entrainment process. Thus, evaluating the RSD emission rate method by comparing MOVES predictions with the Westminster RSD results must be done with the differences of time scales in mind.

10.1 Simulation of Vortex Entrainment using PEMS Data

An RSD measures the mass in a vehicle's vortex at one instant, but, of course, vortex entrainment of pollutant releases is occurring constantly as the vehicle drives on the road. Thus, the RSD is simply getting one measurement of a long time series of vortex masses. This study

has given us an understanding of the entrainment process. Now, we can simulate that process to determine the validity of comparing RSD measurements with MOVES predictions. We use historical PEMS data to evaluate the validity.

We retrieved PEMS data collected from two vehicles that were procured for the Kansas City PM Characterization Study. Table 10-1 shows information taken from Table 4-14 of the report.[36] The test notes for the Forester say that it was malfunctioning with abnormally high exhaust temperature. The vehicle had NOx emissions of 5.764 g/mile – a quite elevated value. The Trail Blazer had relatively low NOx emissions.

Table 10-1. Kansas City PEMS Data on Two Vehicles

CTR_TST_ID	D_KS2_904_1	D_KS2_795_1
Test Date	3/28/2005	3/9/2005
Vehicle Description	2001 Subaru Forester	2002 Chevrolet Trail Blazer
Displacement	2.5 L	4.2 L
Test Distance	23.4 miles	56.9 miles
Composite CO2	362.2 g/mile	479.5 g/mile
Composite CO	3.774 g/mile	2.272 g/mile
Composite NOx	5.764 g/mile	0.255 g/mile
Composite THC	0.136 g/mile	0.047 g/mile
PEMS Data File Location	P:\KansasCity\SEMTECH \Round2\Driveaways/ pp_MO_690SBG_DRIVEAWAY _Test0_M0-M3.csv	P:\KansasCity\SEMTECH \Round2\Driveaways/ pp_MO_TBL970_DRIVEAWAY _Test0_M0-M5.csv

Figure 10-1[37] demonstrates the simulation procedure using a 250-second portion of the PEMS data for the Forester from Second 3050 to Second 3300 of the PEMS file.

---

[36] S. Kishan, A.D. Burnette, S.W. Fincher, M.A. Sabisch, B. Crews, R. Snow, M. Zmud, R. Santos, S. Bricka, E. Fujita, D. Campbell, P. Arnott, "Kansas City PM Characterization Study, Final Report," prepared for U.S. Environmental Protection Agency, prepared by Eastern Research Group, BKI, NuStats, and Desert Research Institute, EPA-061027, October 27, 2006.

[37] C:\Users\TDeFries\Documents\EPA WA5-13 (MAR22-FEB23)\8_Reports/ pp_MO_690SBG_DRIVEAWAY_Test0_M0-M3_THDplay.xlsx

Figure 10-1. Vortex/RSD Simulation using PEMS Data for the Forester
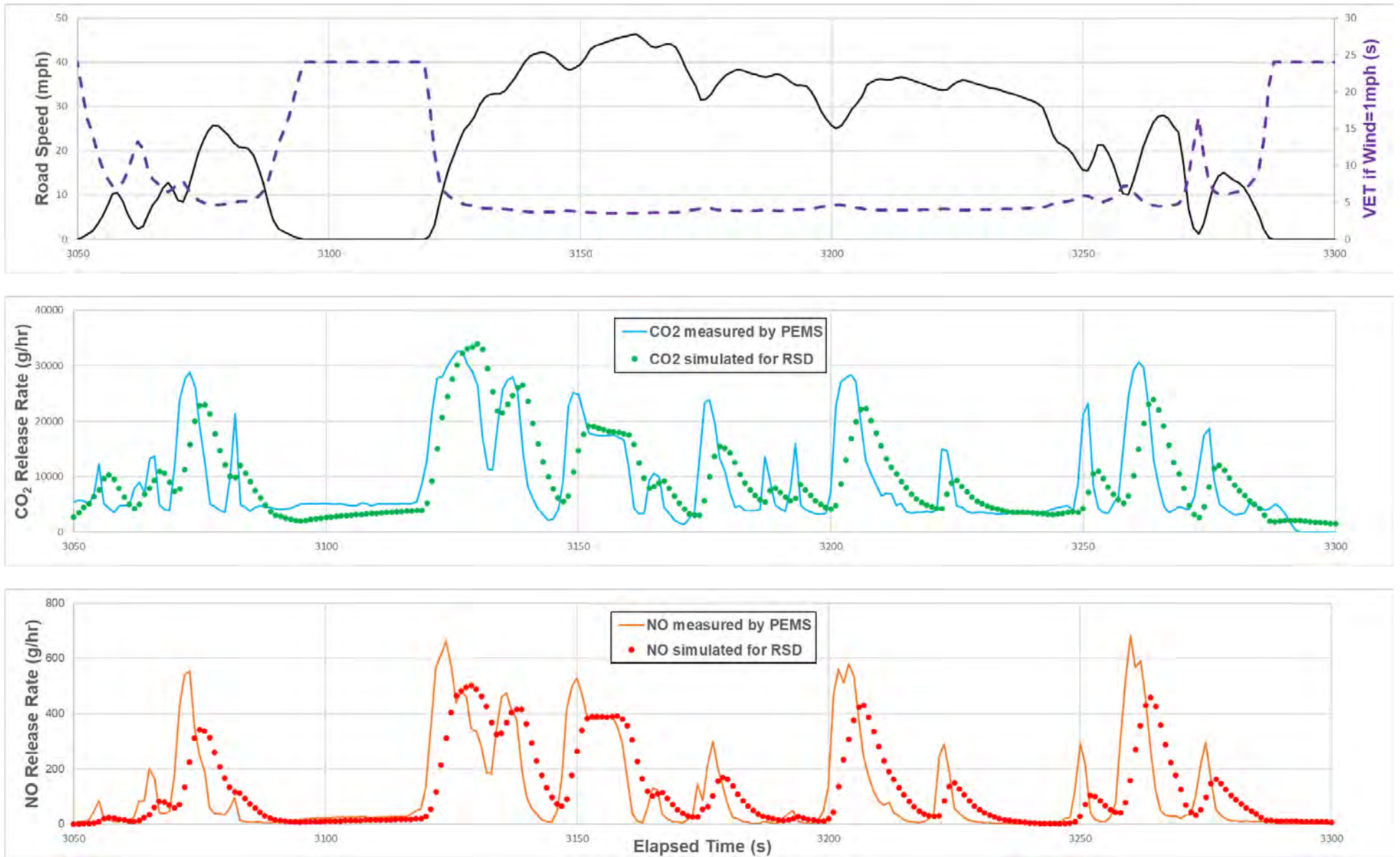
The top panel of Figure 10-1 shows the road speed (black, solid line). To calculate the VET (purple, dashed line), we used the proportionality constant for the Subaru test vehicle at the tailpipe location, which is given in Table 6-3 as 23.9. To calculate airspeed, we assumed that there is always a 1mph light breeze. This prevents the VET from going to infinity when the vehicle is stopped. Therefore, the VET line in the top panel of Figure 10-1 is given by:

$$VET(s) = 23.9 / \text{sqrt}(RoadSpeed\_mph + 1mph)$$

We used the second-by-second VET to simulate the vortex entrainment of released emissions to determine the release rate values that would be measured by an RSD instrument that incorporated the RSD emission rate method. Note that the VET is independent of exhaust pollutant.

The middle panel of Figure 10-1 shows the PEMS-measured CO_2 release rate (g/hr) (light-blue line), and the bottom panel shows the PEMS-measured NO release rate (g/hr) (orange line).

The entrainment is easily simulated in a spreadsheet using this procedure:

Initialization:

1) In Second 1, the release rate is given by the PEMS Release Rate,
2) In Second 1, the Mass in Vortex is an arbitrary value (which will converge after a few iterations)
3) In Second 1, the Stripping Rate is the Mass in Vortex divided by the VET

Iteration:

4) For Second 2, the Mass in Vortex is calculated as Second 1's Mass in Vortex plus Second 1's PEMS Release Rate, minus Second 1's Stripping Rate,
5) For subsequent seconds, iterate Step 4.

The simulated RSD release rate time series is just the Mass in Vortex time series divided by the VET time series, as described by Equation 5-17. This is equivalent to the stripping rate in the spreadsheet.

This procedure was used to calculate the simulated release rate as would be measured by an RSD instrument using the RSD emission rate method. The green dots in the middle panel give the simulated CO_2 release rate values, and the red dots in the bottom panel give the simulated NO release rate values. Any one of these red dots is the expected release rate value that an RSD instrument would obtain at a given second.

There are several things to notice about the plots in Figure 10-1:

1) The top panel shows that at speeds higher than about 15 mph, the changes in VET are relatively small.

2) A comparison of the blue CO_2 PEMS and orange NO PEMS data with the black Road Speed data shows that relatively minor changes in speed produce large, sharp spikes in the PEMS

tailpipe CO_2 and NO release rates. This is a consequence of high engine load and the corresponding high fuel rate needed to produce power at the wheels.

3) When the engine is idling with the vehicle at rest or when the vehicle decelerating, the PEMS CO_2 release rate is about 4000 g/hr, which is generally the lowest CO_2 release rate in the vehicle's dataset.

4) The simulated release rates (green CO_2 dots and red NO dots) follow the PEMS release rate values, but the simulated values are smoother and have rounded peaks that are delayed compared to the PEMS peaks. In general, the simulated release rates do not go as high or as low as the PEMS release rates.

5) As a consequence of the time-dependent entrainment of emissions in the vortex, second-by-second PEMS and RSD measurements almost never agree, as demonstrated by the second and third plots in Figure 10-1. Thus, matching a PEMS emissions measurement with an RSD measurement on the same second cannot be a reliable method for checking RSD accuracy – unless the emissions release rates are verified as constant over at least 2 VETs before the RSD transit.

Given the substantial observed differences between the PEMS-measured release rate time series and the simulated RSD emission rate method release rate time series, we begin wondering if the RSD emission rate method's release rates capture the emission trends that the PEMS data does. To help address that concern, we show the 250-second Forester snippet's PEMS NO vs. CO_2 release rate in Figure 10-2 and the simulated RSD NO vs. CO_2 release rate in Figure 10-3.

The log-log plot of the Forester PEMS NO vs. CO_2 release rates in Figure 10-2 shows a locus of 1-second points that forms a "dog leg." The vertical branch of the dog leg is produced by conditions when the engine is idling since the CO_2 release rate values are around 4000 g/hr. For these conditions, the NO release rate varied from 0 to about 60 g/hr. The angular branch of the dog leg is formed by conditions with CO_2 release rates greater than about 5000 g/hr, which occurs when the engine is under at least some load greater than at idle. The key feature of the angular branch is that most of the points are within a relatively tight clump with a slope somewhat greater than 1. The angular branch indicates that, when the engine is operating under some load even just slightly greater than at idle, the NO release rate usually increases with the CO_2 release rate.

Figure 10-3 plots NO vs. CO_2 release rates for the same Forester data snippet, but for release rates in the vortex as simulated for the RSD emission rate method using the PEMS data. Clearly, the plot has a shape quite similar to Figure 10-2. The points in the vertical branch are more scattered than for the PEMS data in Figure 10-2, but the angular branches are quite similar.

Figure 10-2. NO v CO₂ Release Rates as Measured by PEMS for Forester Snippet
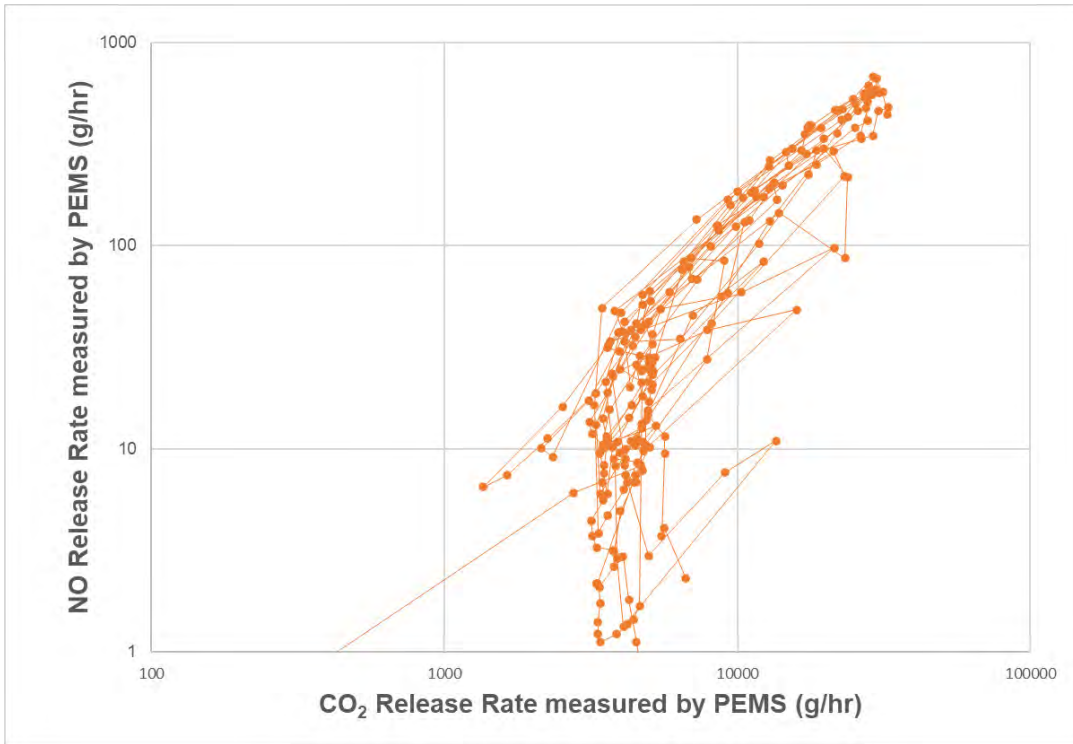
Figure 10-3. NO v CO₂ Release Rates as Simulated for RSD for Forester Snippet
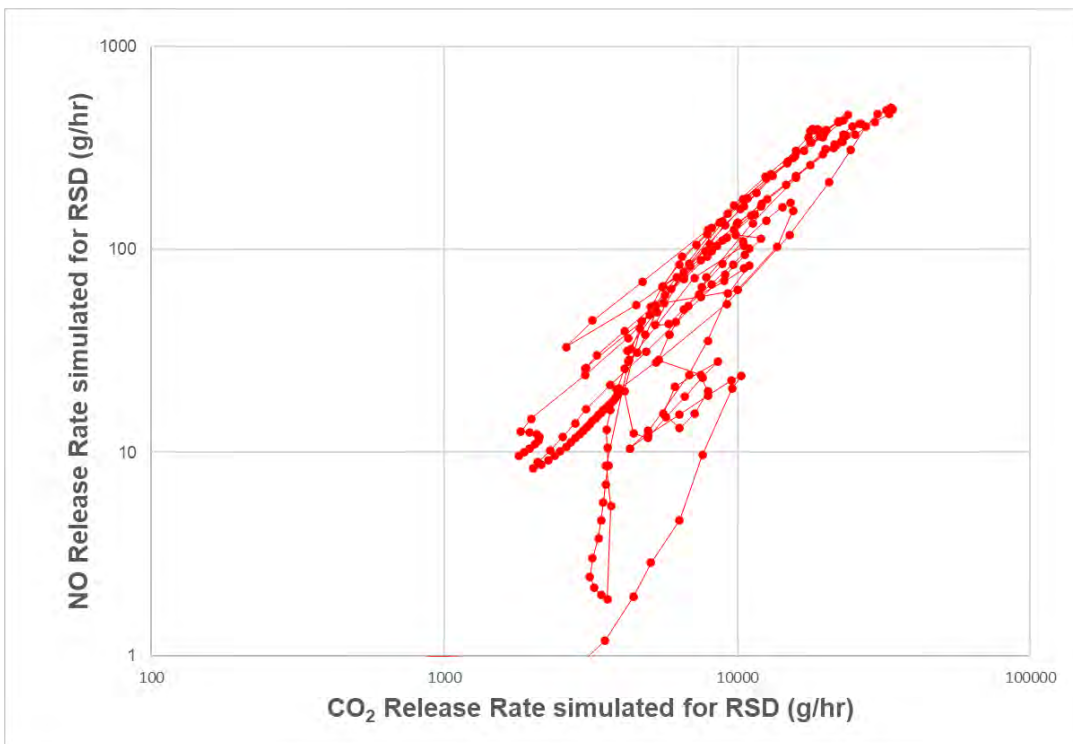
Figure 10-4. NO v CO$_2$ Release Rates as Measured by PEMS for Forester
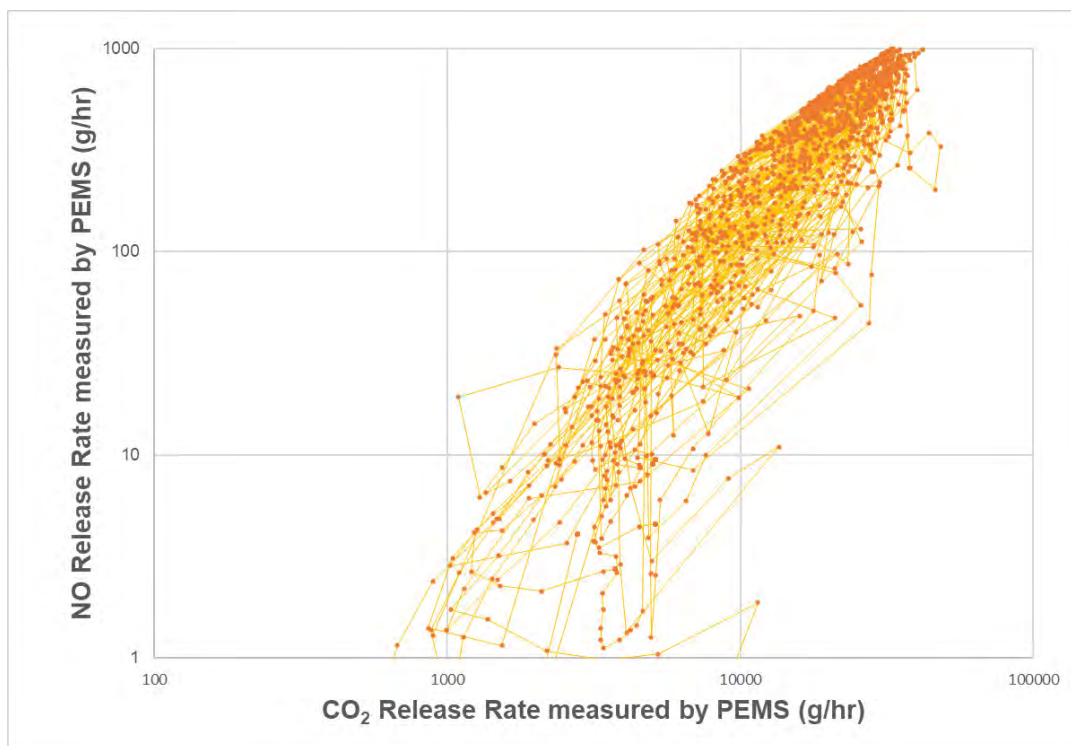
Figure 10-5. NO v CO$_2$ Release Rates as Simulated for RSD for Forester
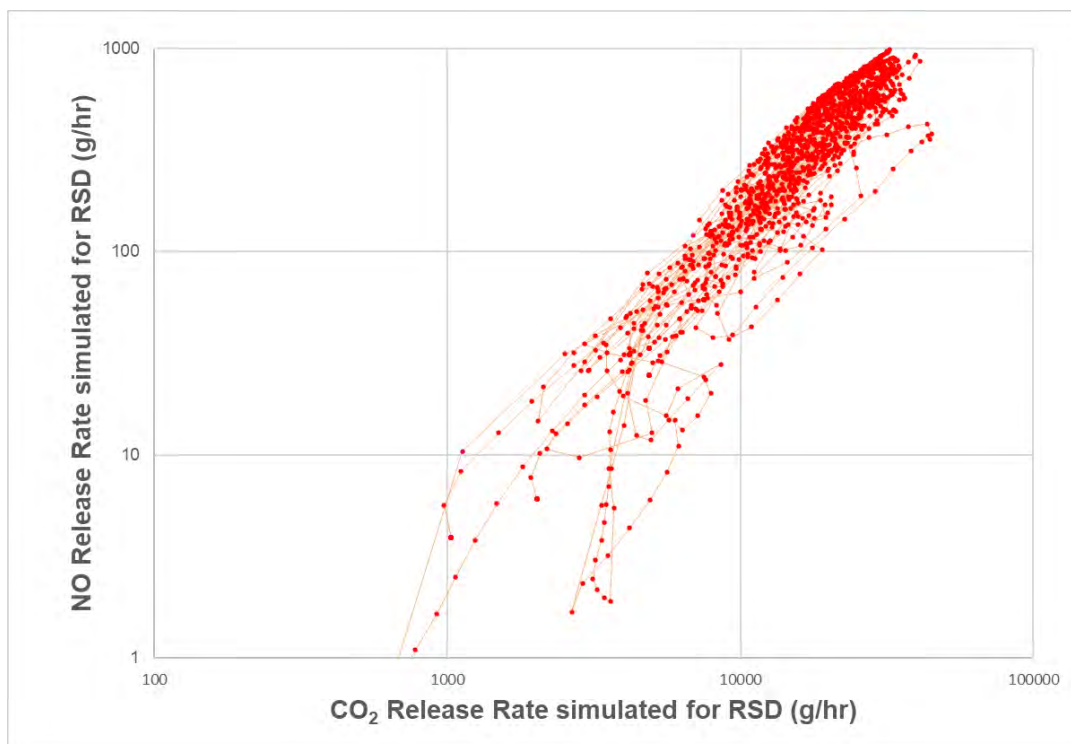
Figures 10-4 and 10-5 show the same plots for the entire 1843-second Forester dataset when the vehicle was moving faster than 15 mph. The figures show the same trends for this large dataset as for the snippet plots. Figure 10-5 shows that the simulated RSD release rates have the same trend as the PEMS data in Figure 10-4 when the CO_2 release rate is larger than about 10,000 g/hr, which is about twice the idle CO_2 release rate. One of the benefits of the accumulation of emissions releases in the vortex is a decrease in the scatter of the simulated RSD release rates relative to the measured PEMS release rates. Specifically, the scatter of points in the region above 10,000 g/hr CO_2 is less in Figure 10-5 than in Figure 10-4.

Figures 10-6 and 10-7 show the corresponding figures for the lower-NO-emitting Trail Blazer. The symbols are shown only for the 6,836 observations when the vehicle speed was greater than 15 mph. The simulated RSD values in Figure 10-7 show lower scatter than for the PEMS measurements in Figure 10-6. Comparison of Figure 10-5 for the Forester with Figure 10-7 for the Trail Blazer shows that the clump of simulated RSD release rates for the Forester (red points) are much higher on the plot field than for the Trail Blazer (green points). Consequently, the RSD emission rate method can clearly distinguish these high- and low-emitting vehicles.

Figure 10-6. NO v CO_2 Release Rates as Measured by PEMS for Trail Blazer
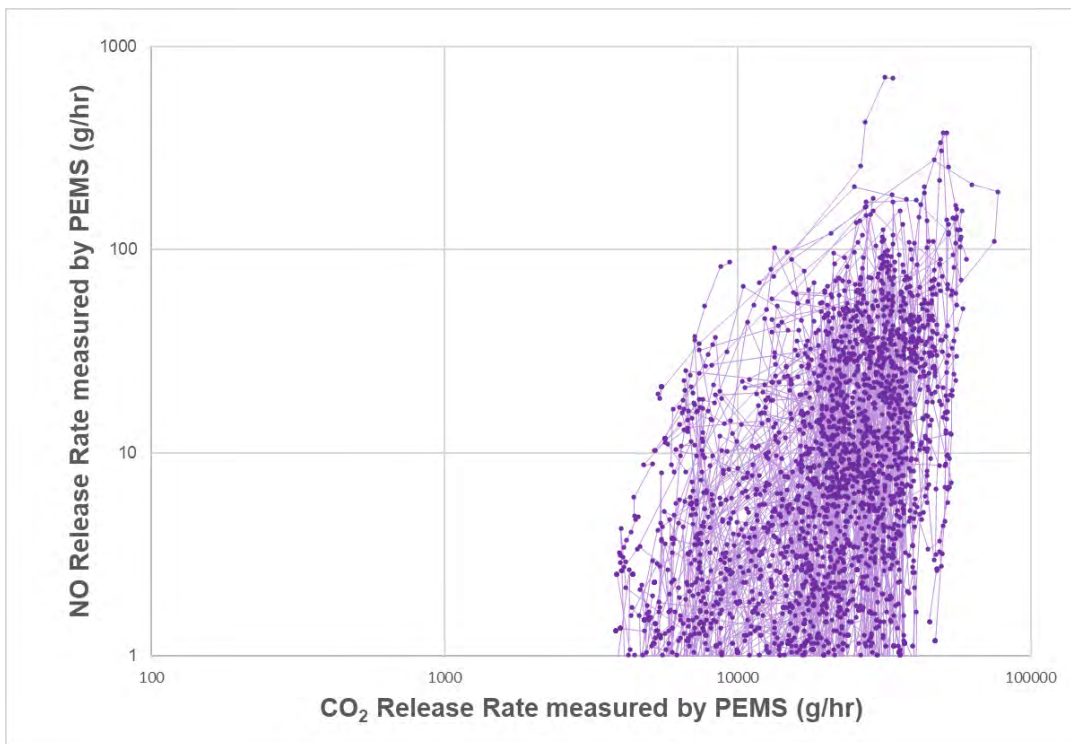
Figure 10-7. NO v CO_2 Release Rates as Simulated for RSD for Trail Blazer
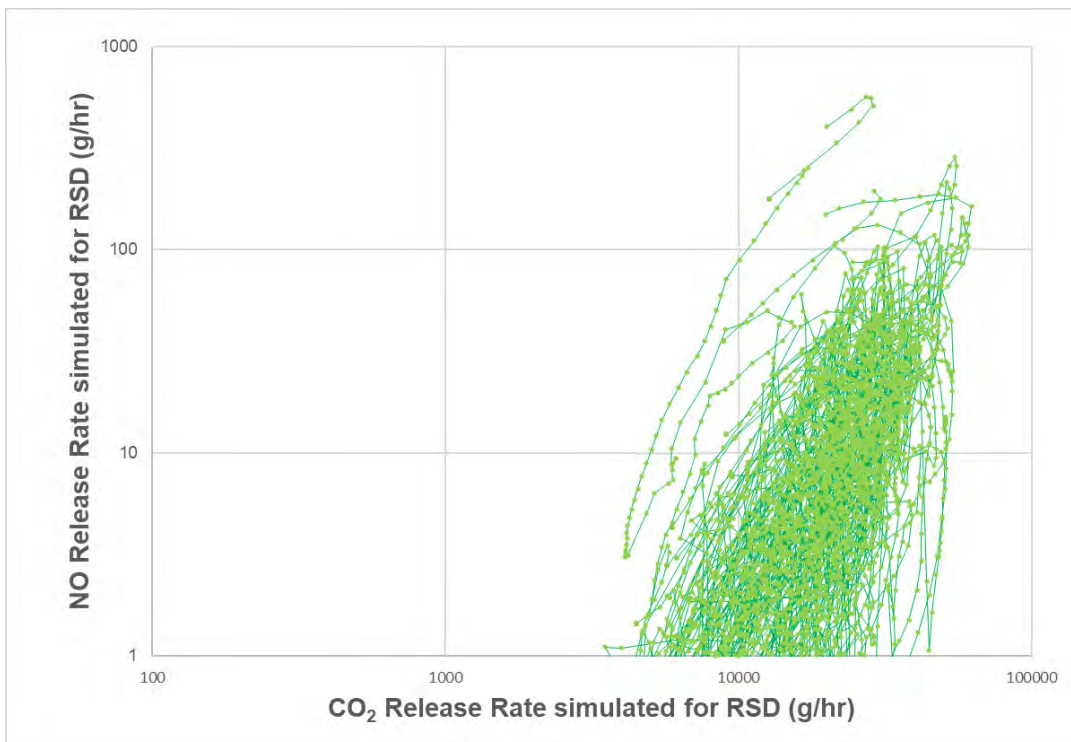
10.2 Comparison of RSD Emission Rates and MOVES Release Rates

The previous sections of this report describe the RSD emission rate method that uses RSD detailed data to calculate mass release rate (g/hr) and, by dividing by vehicle speed, the mass emissions rate (g/mile). Section 9 compared the method's RSD-determined release rates (g/hr) of the test vehicles that we imbedded in the Westminster traffic with their metered emissions releases. In this section, we compare the method's calculated release rates of the fleet vehicles with MOVES (MOtor Vehicle Emission Simulator) modeled estimates of the release rates of the vehicle fleet. Although the method has estimated release rates for all combinations of fleet vehicle fuel type and regulatory class, the comparisons focus only on gasoline LDVs and LDTs since they are by far the most common vehicle types in the Westminster fleet sample.

For the comparison, we selected MOVES3, EPA's well developed mobile source modeling system, whose emission release rate information is derived from laboratory dynamometer measurements and inspection/maintenance program dynamometer with some validation using PEMS measurements. The purpose of the comparison is <u>not</u> to judge the accuracy of MOVES. Instead, we anticipate that if both the RSD emission rate method and MOVES are reasonably accurate, then emission release rates from both methods should compare well. We do not necessarily expect to find a close match in emission rates between these two sources of data. From the Westminster data, we have observed RSD signal strength to be correlated with factors such as position within the road lane and wind speed – factors that are not present within MOVES. Although we have taken steps towards accounting for such factors that increase or decrease the measured RSD signal strength, an additional understanding of the problem is needed so that further improvements to the RSD emission rate method can be made.

Release rate information with high specificity can be acquired from within MOVES, that is, from MOVES internal tables, not from making MOVES runs. The latest MOVES3 database version (movesdb20220802) was used to extract MOVES emission factors for the exhaust pollutants of interest – exhaust CO_2, NOx, CO, and Total HC[38]. The NOx, CO, and Total HC exhaust emission rates are expected to change over the lives of the modeled vehicles; these rates are found in the *emissionratebyage* table.

The *emissionratebyage* table uses the variable *sourceBinID*. This variable is 19 digits long and can be parsed to decode specific fuel types, engine technologies, regulatory classes, and model years. This Westminster field study occurred in 2019, so we kept only the model year and age group combinations relevant for our data. For instance, for the 0-to-3-year-old age group contained only model years 2020 through 2017. Exhaust emission rates for NOx, CO, and Total HC were separated into distinct fuel type, regulatory class, vehicle specific power (VSP), and age groups. These extracted rates show the expected behavior of different vehicle classes as their emissions systems degrade over time.

Comparison of the RSD emission rate method and MOVES for LDTs and LDVs and for exhaust CO_2, NOx, CO, and HC are explored by the log scale plots in Figures 10-8 to 10-15. We use log

---

[38] Here, Total HC refers to the MOVES context. Total HC means the sum of all hydrocarbon species coming from the exhaust. Thus, Total HC includes exhaust methane and exhaust non-methane hydrocarbon (NMHC). Total HC does not include EvapHC.

plots so that we can see trends over a wide range of release rate values. On each plot, the exhaust release rates (g/hr) are displayed on the vertical axis. The vehicle specific power (VSP) is displayed in bins on the horizontal axis. While the bin labels are evenly spaced on the x-axis, please note that the ranges within each bin are expanded on the left and right ends of the x-axis and compressed in the middle of the x-axis. As shown in the legends, each age group is given its own color, but the MOVES results are shown with colored lines, and the RSD emission rate method results are shown with colored dots.

Exhaust CO_2 – Unlike for exhaust NOx, CO, and Total HC, MOVES does not store CO_2 emission factors in the *emissionratebyage* or *emissionrate* tables (i.e. CO_2 g/hr rates are not directly available from MOVES table). However, total energy consumption, which is found in the *emissionrate* table of the MOVES database, can be used to produce MOVES estimates of CO_2 release rates. The CO_2 release rates are calculated from total energy consumption, fuel carbon content, the fraction of carbon oxidized to form CO_2, and the ratio of the molecular weight of CO_2 to the atomic mass of carbon. The resulting emission factors represent CO_2 release rates in g/hr.

Figures 10-8 and 10-9 show the comparisons of the RSD emission rate method CO_2 release rates (dots) and the MOVES CO_2 release rates (lines) for LDTs and LDVs, respectively. The two figures have similar trends. Overall, the RSD emission rate method's CO_2 release rates are roughly in same range as the MOVES rates. Also, the vertical scatter of the dots and lines among the age groups are similar and indicate that the influence of vehicle age is about the same for the two methods across the range of age groups. MOVES indicates that CO_2 rates are about 50% higher for 20-years-and-older vehicles than for 0-to-3-year-old vehicles. While the trend of MOVES CO_2 rates shows an increase as age increases, the RSD trend is too scattered to notice a trend with age group. The differing VSP trends of the RSD emission rate method and MOVES is a concern. While both have linear, upward trends with respect to the VSP bins, the RSD emission rate method has substantially higher rates in the low VSP bins (e.g. an RSD/MOVES ratio of 3/2 in the 3-to-6 kW/Mg bin) and substantially lower rates in the high VSP bins (e.g., an RSD/MOVES ratio of 2/3 in the 24-to-30 kW/Mg bin) than MOVES does.

Exhaust NOx – For gasoline engines, 95% or more of NOx is NO. Therefore, we expect minimal differences between exhaust NO and NOx emission rates. Consequently, Figures 10-10 and 10-11 compare NOx g/hr rates from MOVES against NO g/hr rates from the Westminster dataset.

Just as for the CO_2 comparisons, the figures show similar trends for MOVES and the RSD emission rate method. The general range of MOVES NOx and RSD NO rates are the same. The NOx/NO comparison additionally shows that the age-group order is the same for MOVES NOx and RSD NO. The vertical scatter by age group is similar with NOx/NO release rates about 50 times lower for 0-to-3-year-old vehicles compared to 20-years-and-older vehicles. The VSP trends for MOVES and RSD are both generally upward and linear. However, just as for CO_2, the VSP slopes are lower for the RSD emission rate method than for MOVES.

Figure 10-8. LDT Exhaust CO$_2$ Release Rates v. VSP Bin and Age Group
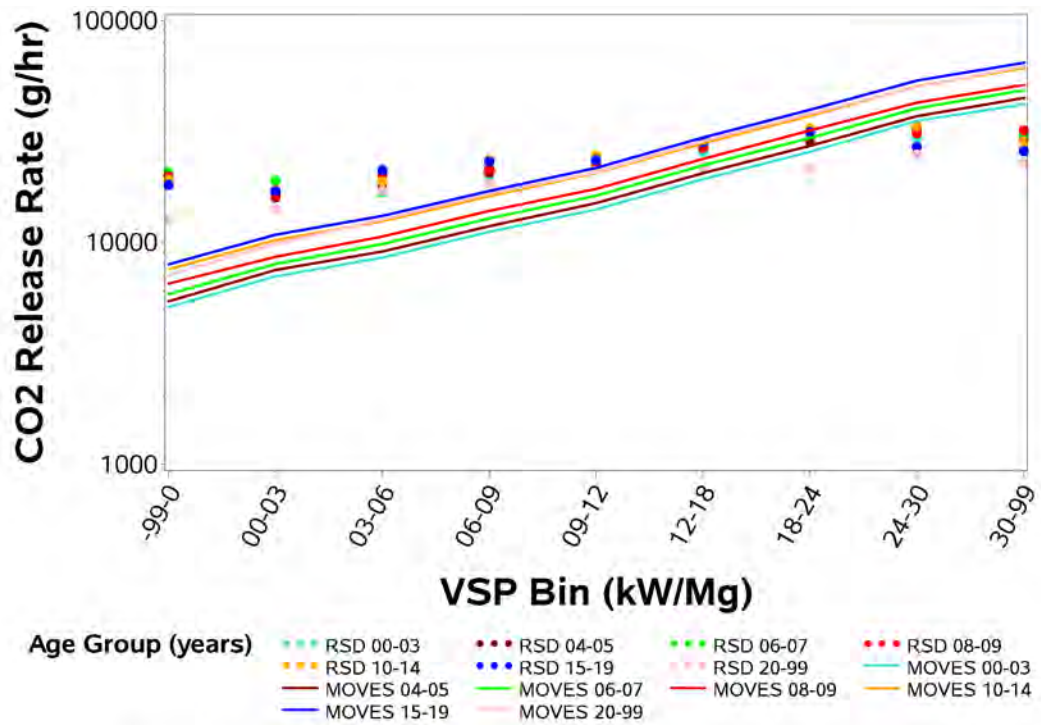
Figure 10-9. LDV Exhaust CO$_2$ Release Rates v. VSP Bin and Age Group
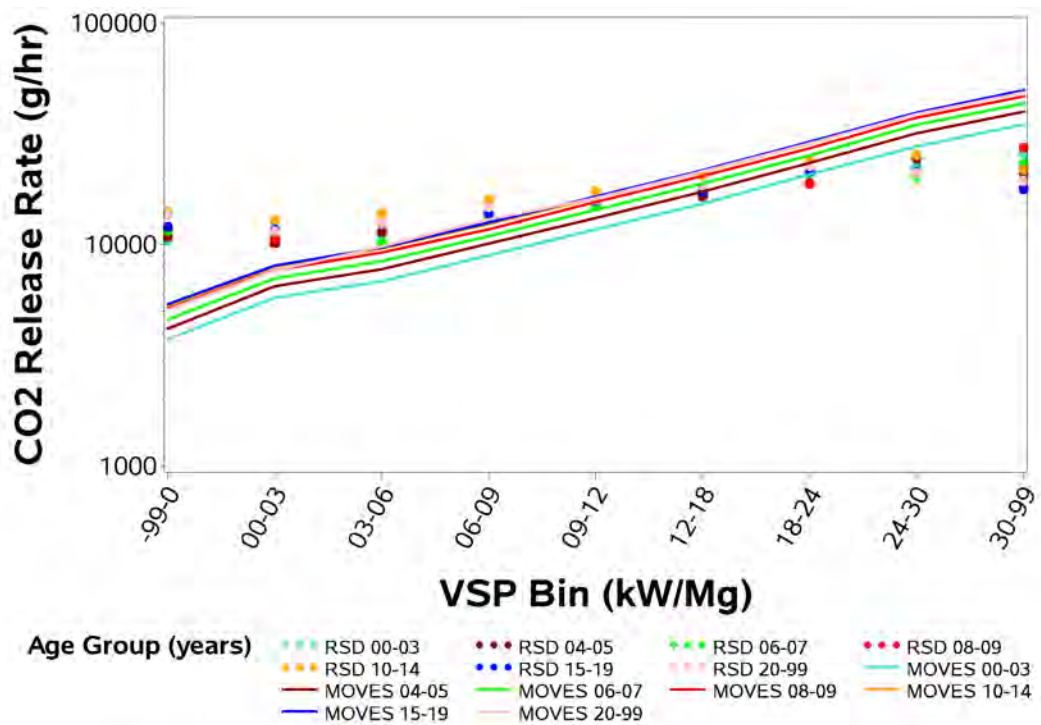
Figure 10-10. LDT Exhaust NOx/NO Release Rates v. VSP Bin and Age Group
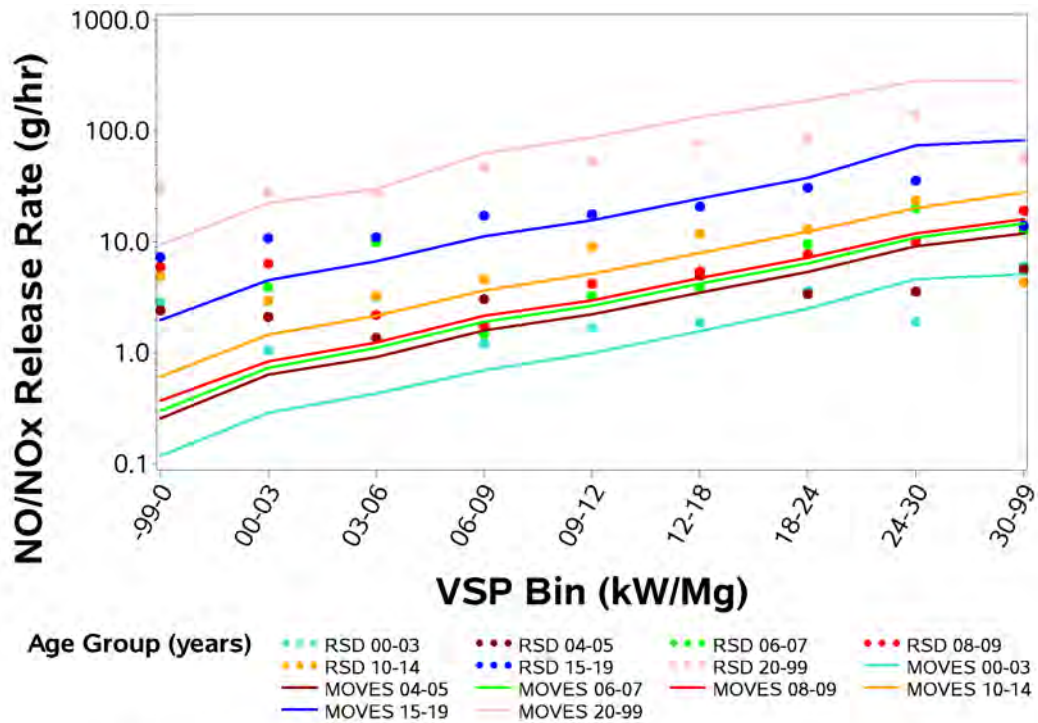
Figure 10-11. LDV Exhaust NOx/NO Release Rates v. VSP Bin and Age Group
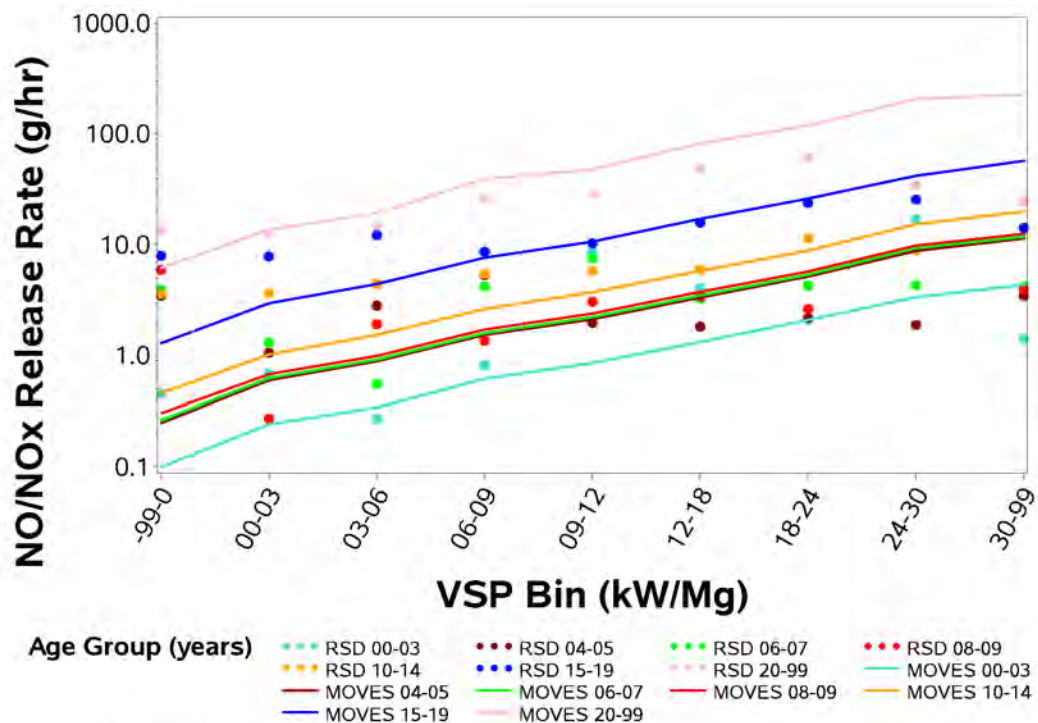
Figure 10-12. LDT Exhaust CO Release Rates v. VSP Bin and Age Group
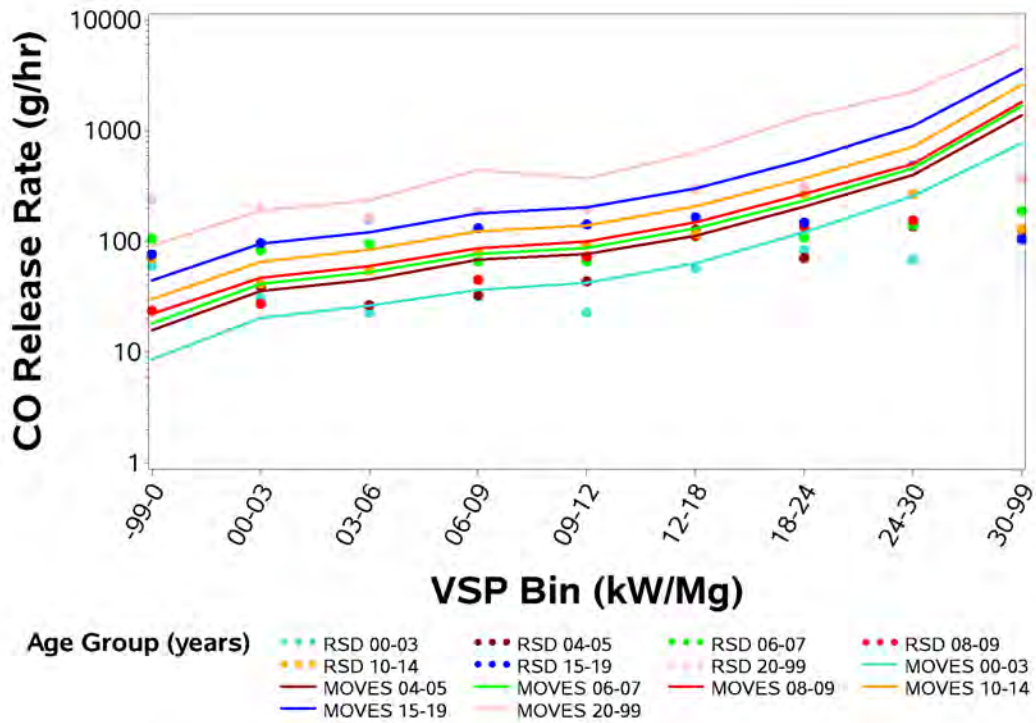
/proj1/EDARinDenver-OCT2019/Analysis_MLout/220113/Anal_MLout/OCT19_VSPbins_3.sas 23DEC22 15:42

Figure 10-13. LDV Exhaust CO Release Rates v. VSP Bin and Age Group
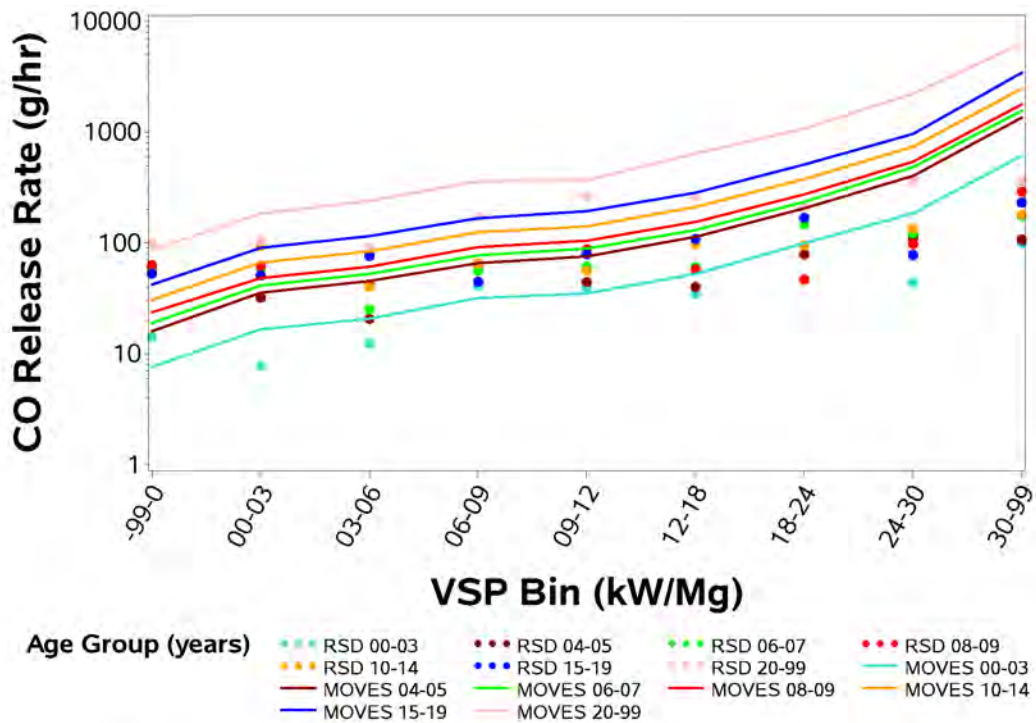
/proj1/EDARinDenver-OCT2019/Analysis_MLout/220113/Anal_MLout/OCT19_VSPbins_3.sas 23DEC22 15:42

Figure 10-14. LDT Exhaust Total HC Release Rates v. VSP Bin and Age Group
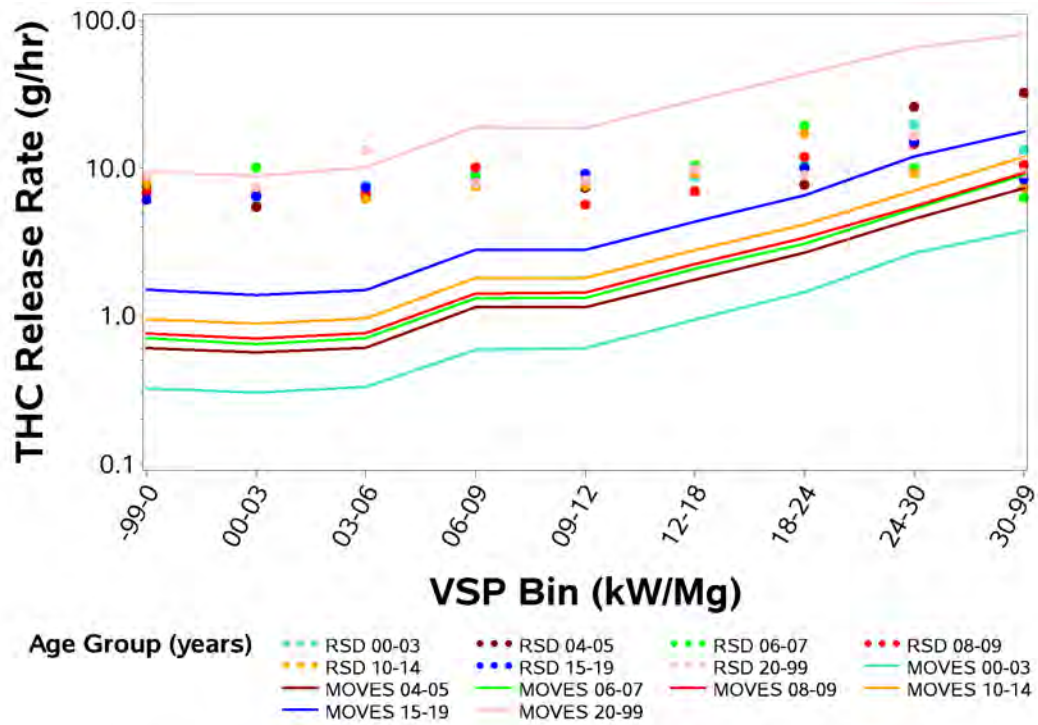
Figure 10-15. LDV Exhaust Total HC Release Rates v. VSP Bin and Age Group
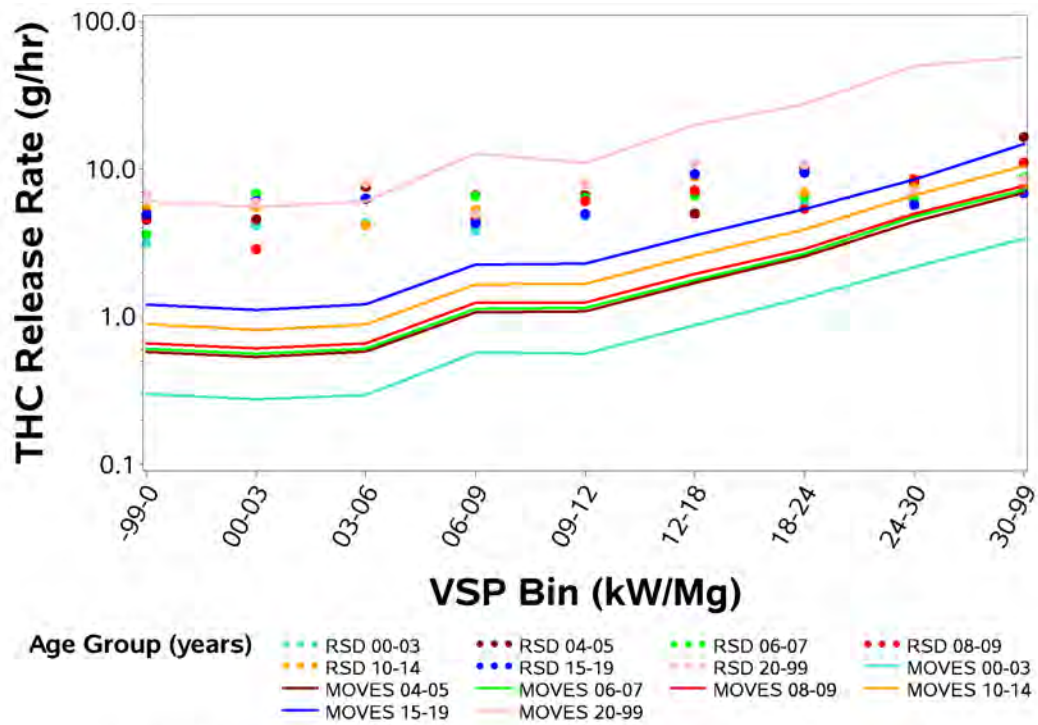
Exhaust CO – Figures 10-12 and 10-13 show the comparisons for CO for LDTs and LDVs. Again, the general range of CO rates and the size of the age-group scatter are similar for MOVES and the RSD emission rate method. Also, there is evidence that the order of age-groups is the same for MOVES and for the RSD emission rate method, for example, the 0-to-3-year-olds (light blue) are at the bottom and the 20-year-and-olders (pink) are at the top. The size of the vertical scatter associated with vehicle age is similar for MOVES and RSD with CO rates about 10 times lower for 0-to-3-year-old vehicles compared to 20-year-and-older vehicles.

Again, the biggest concern with the comparison of CO rates between MOVES and the RSD emission rate method is the relative twist between VSP dependencies. The evidence of the twist is seen at high VSPs by the substantially lower RSD release rates for the RSD emission rate method compared to MOVES. In terms of VSP trends, the MOVES lines show increasing slopes at high VSP bins, while the RSD emission rate method dots show a more muted increase with VSP.

Exhaust Total HC – For the comparisons of exhaust Total HC shown in Figures 10-14 and 10-15, the RSD g/hr values are substantially above the MOVES values. In general, the MOVES versus RSD emission rate method comparisons that we made for other pollutants are poor for exhaust Total HC. A large part of this difference may be due to noise in the RSD HC channel. Noise in the RSD HC channel tends to increase the quantified Total HC release rate. We have used signal processing techniques to reduce the noise in all RSD pollutant channels, but additional work is needed for the HC channel.

Overall, the release rate trends by the RSD emission rate method and by MOVES correlate and indicate that the RSD emission rate method shows promise. Still, there are some caveats. In Figures 10-8 to 10-13 for CO_2, NOx/NO, and CO, and for each combination of vehicle type and age, there is a twist in the VSP trends. That is, low-VSP RSD values tend to be higher than low-VSP MOVES values, and high-VSP RSD values tend to be lower than high-VSP MOVES values. At middle-VSP values (9-18 kW/Mg), there is usually good agreement between RSD values and MOVES values.

Why the twist? – We have an explanation for the worrisome "twist" in the VSP dependencies of the RSD-based release rates vs. the MOVES-based release rates. Since all of the graphical comparisons of all four pollutants in Figures 10-8 through 10-13 exhibit the twist, the twist is likely independent of pollutant. A VSP is determined for each second of vehicle operation – whether that operation is on the dynamometer for MOVES or on the road for RSD. Additionally, the actual measurements of the emissions by the laboratory instruments or by the RSD instrument are also both relatively fast. The CVS quickly aspirates a sample of the tailpipe, and therefore the measurement is an almost instantaneous measure of tailpipe concentrations and flows. But on the road, the entrainment of tailpipe releases (and any other source of releases) into the vortex is slow because the mass of pollutants in the vortex at any given instant comes from the releases over about at least 2 VETs, which for a typical light-duty vehicle in a 30-mph air flow is about 8 seconds.

For example, for a vehicle moving with a constant 4-second VET and releasing a pollutant at a constant rate (g/hr), Figure 10-16 shows the fraction of the pollutant mass in the vortex contributed during each previous second's release. The first previous second's release

contributes only 25% of the vortex pollutant mass. Similarly, the five previous seconds together contribute 76% of the pollutant mass, and the remaining 24% of the vortex mass is contributed by all seconds prior to the fifth previous second. Clearly, if the release rate of a pollutant changes during previous seconds, the portion of the mass in the vortex for each previous second will vary from that shown in the figure. Also, if the VET is substantially larger, for example for the 53-foot box trailer of an 18-wheeler, the vortex will contain contributions from many more previous seconds. The point is that the mass measured by an RSD during a vehicle transit is not a measure of the instantaneous (or even almost instantaneous) emissions release rate, emission rate, or tailpipe concentrations. It is a measure of the weighted emissions over the most recent many seconds.

Figure 10-16. Portions of Pollutant Mass in a 4-Second-VET Vortex
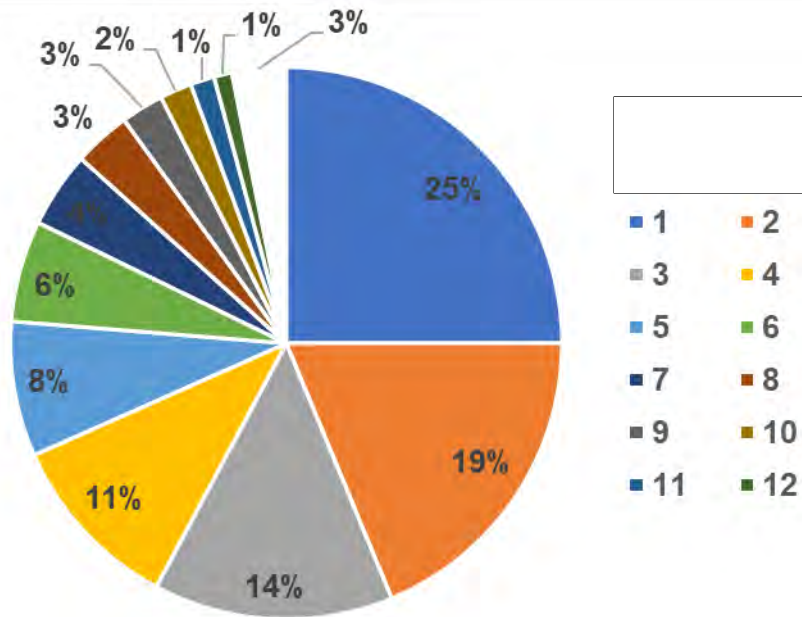
So, the mass of pollutants in the on-road vortex has "memory" of the engine operation, including fuel rate, over a much longer time than for the dynamometer or PEMS testing.

In Figures 10-8 through 10-15 , the MOVES release rate "lines" have VSP coordinates that are the almost instantaneous VSP of the MOVES release rate measurement. But for the RSD release rate "dots," the VSP coordinate is simply the VSP at the time of the RSD measurement, while the RSD release rate value is a measurement of pollutant mass in the vortex accumulated over the previous many seconds. Since for high VSP values, the VSPs of these previous many seconds are most likely less than the VSP coordinate value, the RSD-measured release rate is likely to be lower than for the corresponding MOVES release rate value. The opposite is true of low VSP values. Because of this difference of VSP basis between the MOVES and RSD release rate values, Figures 10-8 through 10-15 artificially introduce the apparent twist when comparing the two data sources. This twist might cause the analyst to incorrectly conclude that the MOVES and the RSD emission rate method do not agree.

If vortex entrainment explains all of the apparent MOVESvRSD twist, it is likely that the middle-level VSP values (perhaps the 9-12 kW/Mg bin) do not have much VSP bias between the MOVES and RSD release rate values. Accordingly, if we compare the MOVES and RSD release rate values for just the 9-12 kW/Mg bins in Figures 10-8 through 10-15, we conclude that the values and the range of by-age values of MOVES and RSD release rate agree well for CO_2, NO, and CO. However, for Total Hydrocarbon, the RSD values are substantially higher than the MOVES values.

Now, we consider an alternative method for comparing MOVES and RSD release rates while using fuel rate to account for VSP. The blue dots in the log-log plot in Figure 10-17 show the RSD NO vs. RSD CO_2 release rates calculated for 15-to-19-year-old LDVs in the Westminster dataset. Because both the RSD NO and the RSD CO_2 are obtained from RSD, they both are measures of those pollutants in the vortex at the same instant of the RSD transit and therefore they both are influenced in exactly the same way by vortex entrainment. Also, because the measures are optical – not via extraction of a gas sample (as CVS or PEMS do) – the RSD NO and RSD CO_2 are perfectly time-aligned with each other, and with all other pollutants in the vortex.

Unless the CO release rate is high, the CO_2 release rate is directly proportional to the engine fuel rate. Therefore, the highest fuel rates, and therefore, the highest engine loads are usually on the right side of the figure. An examination of the blue dots at around 40,000 g/hr CO_2 release rate shows that some vehicles were releasing around 1 gNO/hr while others were releasing around 600 gNO/hr. Keep in mind that those NO release rates are for vehicles operating at high fuel rates. The top edge of the blue-dot field in the figure shows the NO-release trend of the highest releasing vehicles in this data subset.

We can use the MOVES trends of release rates as a reference for the RSD release rates.[39] The basis of the MOVES values for NOx and CO_2 release rates is the same, that is, both are based on dynamometer testing. While the basis of the MOVES values is different than the basis of RSD values, the trends for MOVES vs. RSD can be compared. The black line in Figure 10-17 shows the trend of the MOVES NOx vs. MOVES CO_2 release rates for the MOVES *opModeID*s averaged over the four LDV model years in the 15-19-year-old age group in Calendar Year 2019. The *opModeID*s for the highest CO_2 release rates, VSPs, and fuel rates are on the upper right end of the black line. Note that the upper edge of the blue-dot field of RSD transit release rates is roughly parallel to the MOVES line.

The values of the RSD NO and RSD CO_2 release rates, which determine the location of each blue dot in Figure 10-17, are calculated as described earlier using each transit's EDAR signal divided by the estimated VET. The value of the VET is independent of pollutant, and therefore, the same value of the VET is used to calculate both the RSD NO and the RSD CO_2 release rate – that is, both coordinates of each blue dot.

---

[39] Note that we are not trying to evaluate MOVES quality. The idea is that if RSD trends somehow agree with MOVES trends, then we gain comfort with the RSD results.

Figure 10-17. Comparison of NO v CO₂ Release Rates by RSD for Westminster 15-to-19-Year-Old LDVs
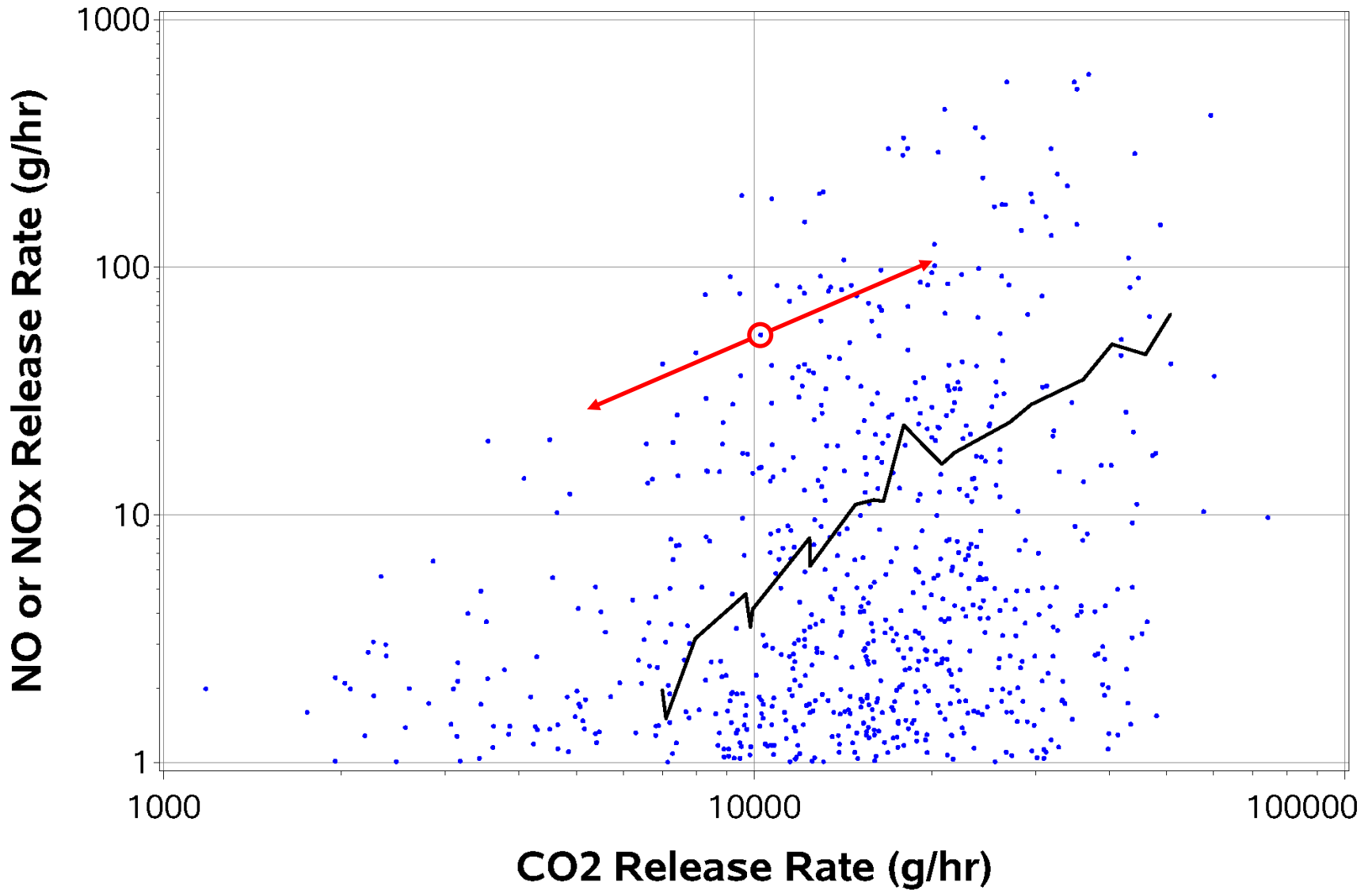
Source: • • • Westminster: 2000-2004 LDVs in 2019 ——— MOVES: Average 2000-2004 LDV in 2019

/proj1/EDARinDenver-OCT2019/Analysis_MLout/220113/Anal_MLout/OCT19_VSPbins_4_CP.sas 03MAR23 10:51

Because of turbulence, the estimated VET for a given transit has some uncertainty. Figures 6-10, 6-11, and 6-14 to 6-17 indicate that the approximate size of the uncertainty in VET might be at most -50% and +100% of the estimated value. For example, the true value of an estimated VET of 4s might be somewhere between 2s and 8s.

Since the uncertainty affects both blue-dot coordinates by the same amount, the true location of a blue dot would be on a 1:1 line passing through the blue-dot location in Figure 10-17. To demonstrate the effect of VET uncertainty, Figure 10-17 is annotated with a red circle around a selected blue dot. The blue-dot location for the release rates using the true VET would be somewhere on the red line with the arrowheads. Thus, even taking the uncertainty of the VET into account, the location of the selected blue dot will remain in the same general location in the blue-dot field, that is, near the top-left angled edge of the blue-dot field. Importantly, regardless of wherever the true blue-dot location might be along the red line, the location will be approximately the same distance from the black MOVES reference line – because the MOVES reference line and the red 1:1 line have approximately the same slope.

Forty-two plots comparing CO_2, NO, CO, and THC, for LDVs and LDTs, and for all seven age groups are shown in Appendix F. Overall, the results for NO vs. CO_2, and CO vs. CO_2 suggest that the RSD emission rate method provides results that are consistent with the trends modeled by MOVES by vehicle class, vehicle age, and fuel rate. The THC results for the RSD results are not consistent with MOVES modeled THC values. We suspect that the RSD values are elevated either by noise or by a calculation error. We do not suspect the MOVES values.

Because the MOVES and RSD results in Figure 10-17 are consistent with each other, we wondered whether the vertical distance of a transit's blue point from the MOVES black line could be used to determine if the vehicle was a high or low emitter. To evaluate that possibility, we overlaid the simulated second-by-second RSD NO vs. RSD CO_2 results from the Kansas City 2001 Forester high-emitter (5.8 gNO/mile) from Figure 10-5 and the 2002 Trail Blazer low-emitter (0.3 gNO/mile) from Figure 10-7 onto the plot shown in Figure 10-17 to create Figure 10-18. The overlay is appropriate since both the Forester and the Trail Blazer would be 15-19-year-olds in 2019.

Figure 10-18 shows that most of the red pluses for the 2001 Forester fall at the top edge of the blue-dot field of Westminster 15-19-year-old LDVs. The lime-green pluses for the Trail Blazer fall much lower in the figure and are near the MOVES black line. The idea is that if either the Forester or the Trail Blazer would pass under the EDAR instrument at any second of their PEMS time series, then the simulated RSD NO vs. RSD CO_2 release rates would almost always fall in a location in Figure 10-18 that would correctly characterize them as either a high or low NO emitter.

Figure 10-18. Comparison of NO v CO₂ Release Rates for Datasets of 15-to-19-Year-Old LDVs
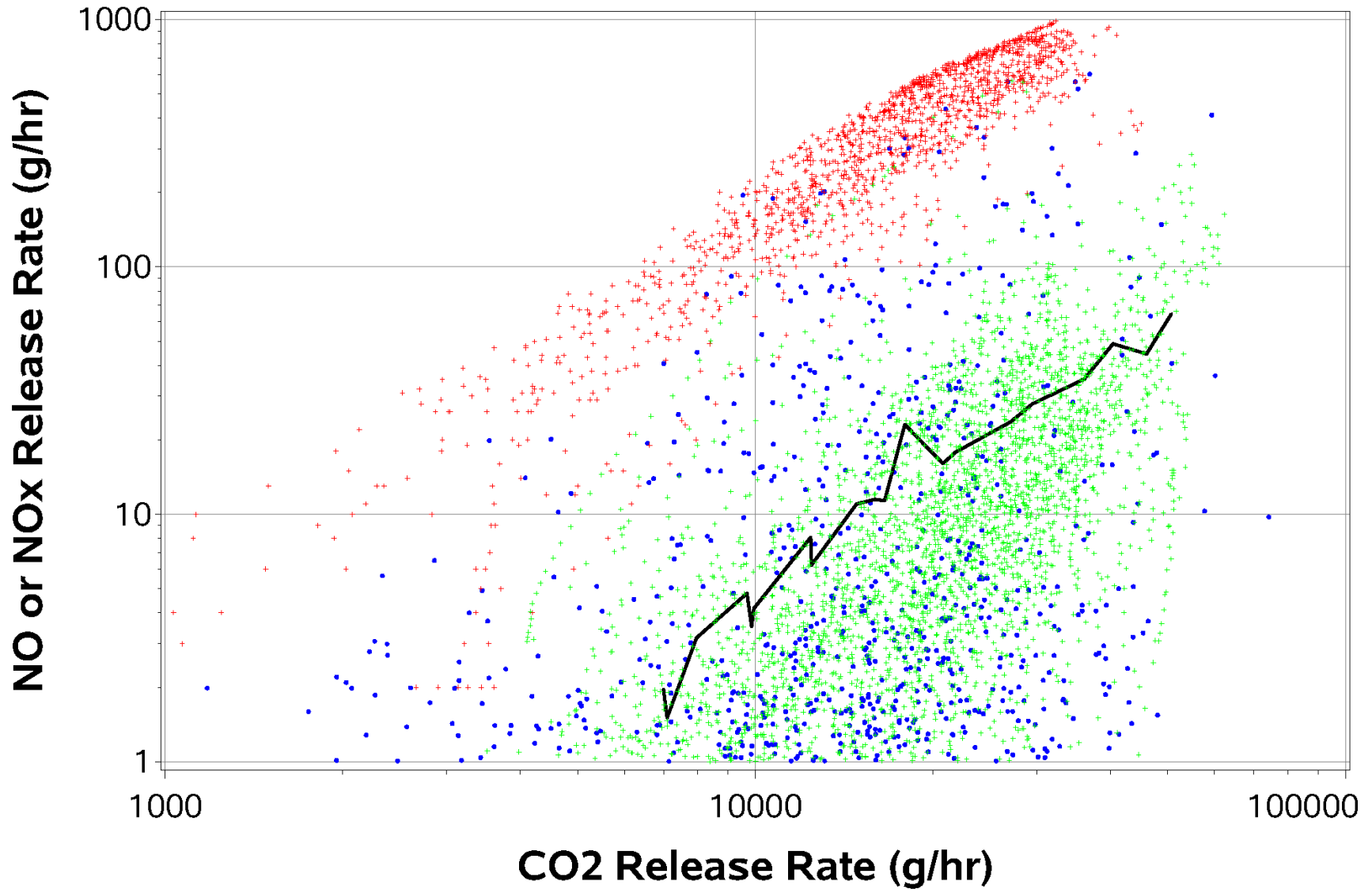
Source:
- • • • Westminster: 2000-2004 LDVs in 2019
- + + + Kansas City: 2001 Forester (5.8 gNO/mile)
- —— MOVES: Average 2000-2004 LDV in 2019
- + + + Kansas City: 2002 Trail Blazer (0.3 gNO/mile)

/proj1/EDARinDenver-OCT2019/Analysis_MLout/220113/Anal_MLout/OCT19_VSPbins_4_CP.sas 03MAR23 10:51

Careful examination of Figure 10-18 shows that, for a small fraction of the seconds, some red pluses fall below where the bulk of the Forester symbols are located. This suggests that occasionally, the history of engine operation just before the RSD transit could cause the RSD-observed NO release rate to be somewhat lower than what the general NO release rate for the vehicle might more typically be. Similarly, but in the other direction, a few lime-green pluses appear at higher NO release rates than the bulk of symbols for the Trail Blazer. If the vehicle got an RSD during one of those seconds, it would appear to be a somewhat higher NO emitter than it is most of the time. Further analysis of the PEMS time series might help eliminate some of these classification errors through selected siting of the RSD instrument.

10.3 Comparison of the Traditional RSD Concentration Method with the RSD Emission Rate Method

This subsection uses the detailed data obtained during an example Westminster transit to compare the traditional RSD method used to calculate exhaust emissions concentrations with the new RSD method to calculate mass emissions rate (g/mile).

As an overview, traditional calculations can be described by the schematic in Figure 10-19. The calculations start with the RSD detailed data for CO_2, CO, NO, and HC on the left. The method then assumes that all pollutants are exhaust pollutants emitted at the tailpipe, which leads to the expectation that all exhaust pollutants are well mixed and diffuse and disperse together from the tailpipe exit.[40] Consequently, the optical masses of all pollutants should be directly proportional to each other, which means that plots of the detailed data for pairs of pollutants will produce lines passing through the origin.

To demonstrate and compare the RSD methods, we will use the transit (Series=515, Transit=2469, 10/25/19:13:27:23.6) of a 2001 pickup truck that happened to drive by. Figure 10-20 shows the pairwise detailed data plots against CO_2 and regression fits for this transit. The blue and orange trends in the top two plots for NO vs. CO_2 and CO vs. CO_2 are close to linear, have positive slopes, and pass near the origin. The green points in the lower left plot show the trend for the RSD HC channel, which reports measurements of Total HC, that is, for ExhHC plus EvapHC. The apparent[41] noise in this plot makes it difficult to determine if the trend is linear or not, but the linear regression indicates that the trend passes near the origin, and if the trend is linear, it has a negative slope.

---

[40] Gases with different molecular weights actually would diffuse at different rates. For example, CO2 (MW=44) would diffuse more slowly than CO (MW=28). However, given the time scale of each transit's RSD detailed data collection (about 0.5s) and the accuracy of RSD detailed data measurements, the assumption of equal diffusion rates for all gases is reasonable.

[41] We say "apparent" because we will see that a large part of the apparent noise is actually from EvapHC.

Figure 10-19. Diagram of Traditional RSD Method for Calculating Exhaust Concentration from Detailed Data

Assume all Pollutants are Exhaust

If gasoline, Assume Stoichiometric Combustion

RSD
Detailed Data

CO2
CO
NO
HC

Regression
Slopes

n/a
CO v CO2
NO v CO2
HC v CO2

Exhaust
Concentration

% CO2
% CO
ppm NO
ppm HC
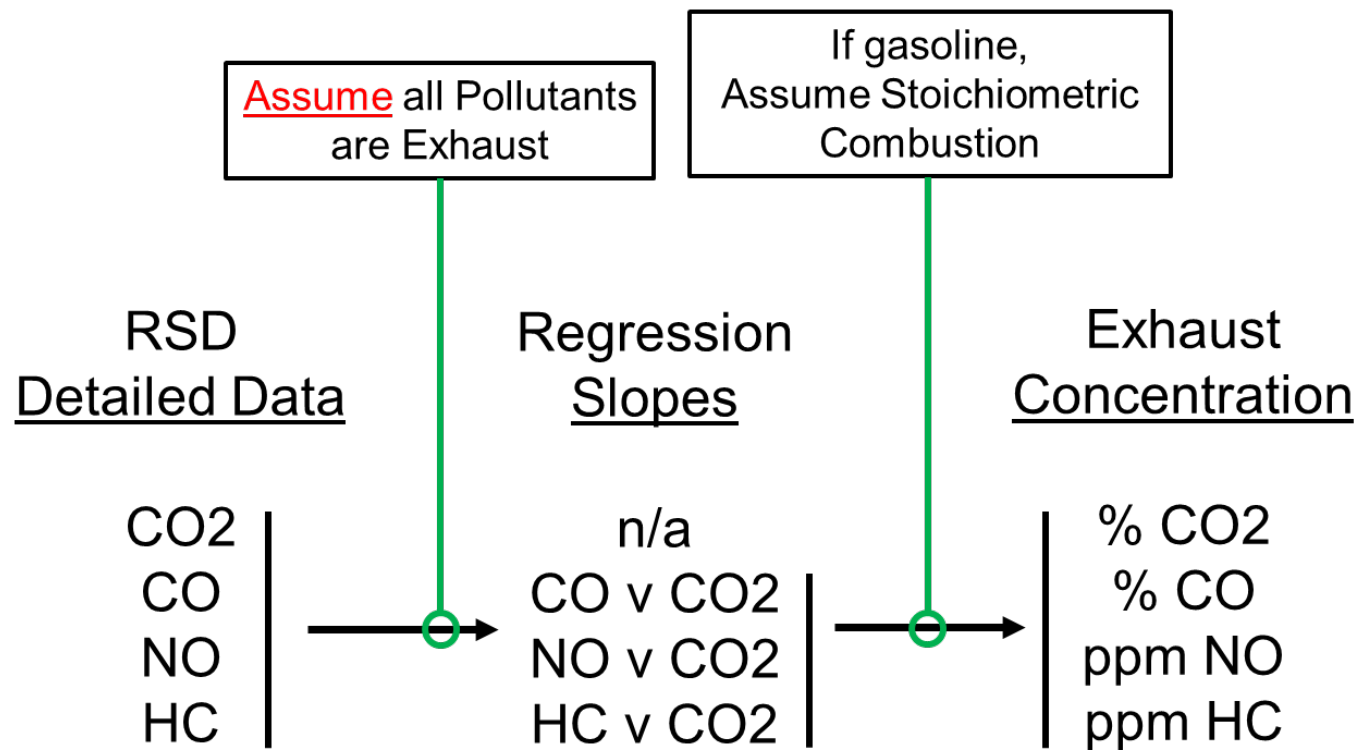
Figure 10-20. Pairwise Optical Mass Plots for the Example Transit (Series=515, Transit=2469)
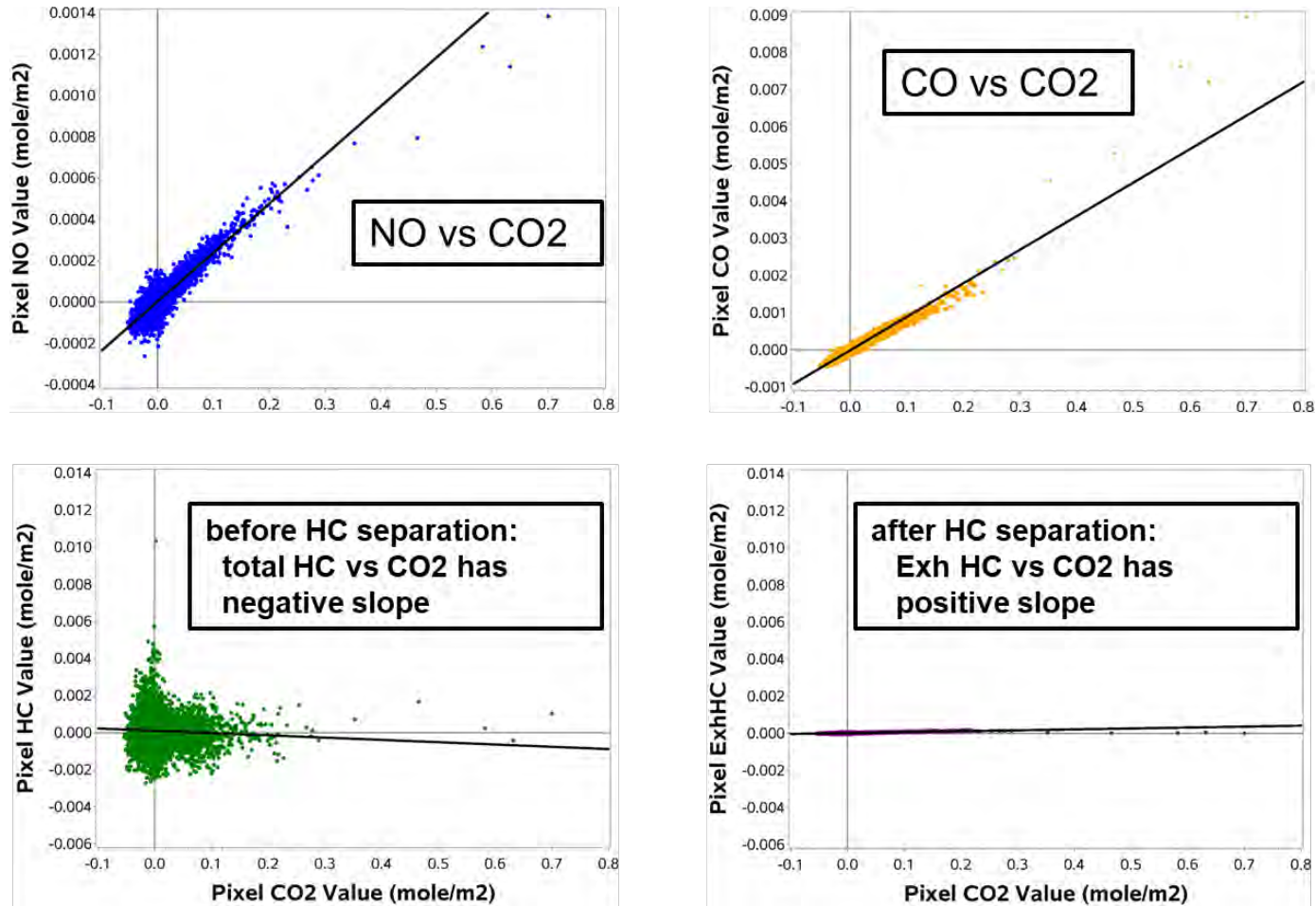
The traditional RSD method then uses the regression slopes of CO, NO, and HC against the CO_2 to estimate exhaust emissions concentrations – if the vehicle is assumed to be a stoichiometrically operating engine, for example, a gasoline engine. To perform the concentration calculations for this example, we will use the algebraic equation that ESP has used in the past[42] for its Accuscan 4600 RSD instrument:

$$ppmCO \quad = \quad Slope\ COvCO2 \ * \ ppmCO2$$
$$ppmNO \quad = \quad Slope\ NOvCO2 \ * \ ppmCO2 \qquad \textbf{Equation 10-1}$$
$$ppmHC \quad = \quad Slope\ HCvCO2 \ * \ ppmCO2$$

where $ppmCO2 =$

$$\frac{150538}{(1 + \ 0.7168 * Slope\ COvCO2 \ + \ 0.3584 * Slope\ NOvCO2 \ + \ 0.3011 * Slope\ HCvCO2)}$$

Following the traditional RSD method, the slopes of the regression lines shown in the first three subplots (blue, orange, green) of Figure 10-20 were used with Equation 10-1 to calculate the estimated exhaust concentrations shown in the right column of Figure 10-21. The negative estimated concentration for ExhHC is a concern. An incorrect interpretation of this value would be that the vehicle has a near-zero exhaust HC emissions concentration. The negative value is the result of the negative regression slope of the green points in Figure 10-20.

The left column of Figure 10-21 shows the plume heatmaps of the four RSD channels as observed by the RSD from above the pavement. Those heatmaps clearly show that CO_2, CO, and NO have plumes of the same shape, but the HC heatmap shows that the HC plume is substantially different from the others. We conclude that most of the HC mass cannot be exhaust HC, otherwise the HC heatmap would have the same shape as the heatmaps for CO_2, CO, and NO. Thus, although there may be some evidence of ExhHC in the HC heatmap, we claim that most of the HC must be EvapHC. Since the heatmaps indicate that EvapHC, as well as some ExhHC, is present, the traditional RSD assumption that all pollutants are from the tailpipe is violated. We cannot be certain that the calculated value of -184 ppm ExhHC is correct.

[42] T.H. DeFries, J.H. Lindner, C.F. Palacios, S. Kishan, "Investigation of RSD for High Evaporative Emissions Vehicle Detection: Denver Summer 2008 Pre-Testing Study," Version 1, EPA-090306, prepared for U.S. Environmental Protection Agency, March 6, 2009.

Figure 10-21. Traditional RSD Method Exhaust Concentration Results for the Example Transit

	Detailed Data	Est. Exhaust Conc.
Veh	CO_2	14.95 %
Veh	CO	0.13 %
Veh	NO	353 ppm
Veh	HC	-184 ppm

62.8 °F
24.96 in
26.3 % RH
4.5 mph S

Appears to be Clean HC
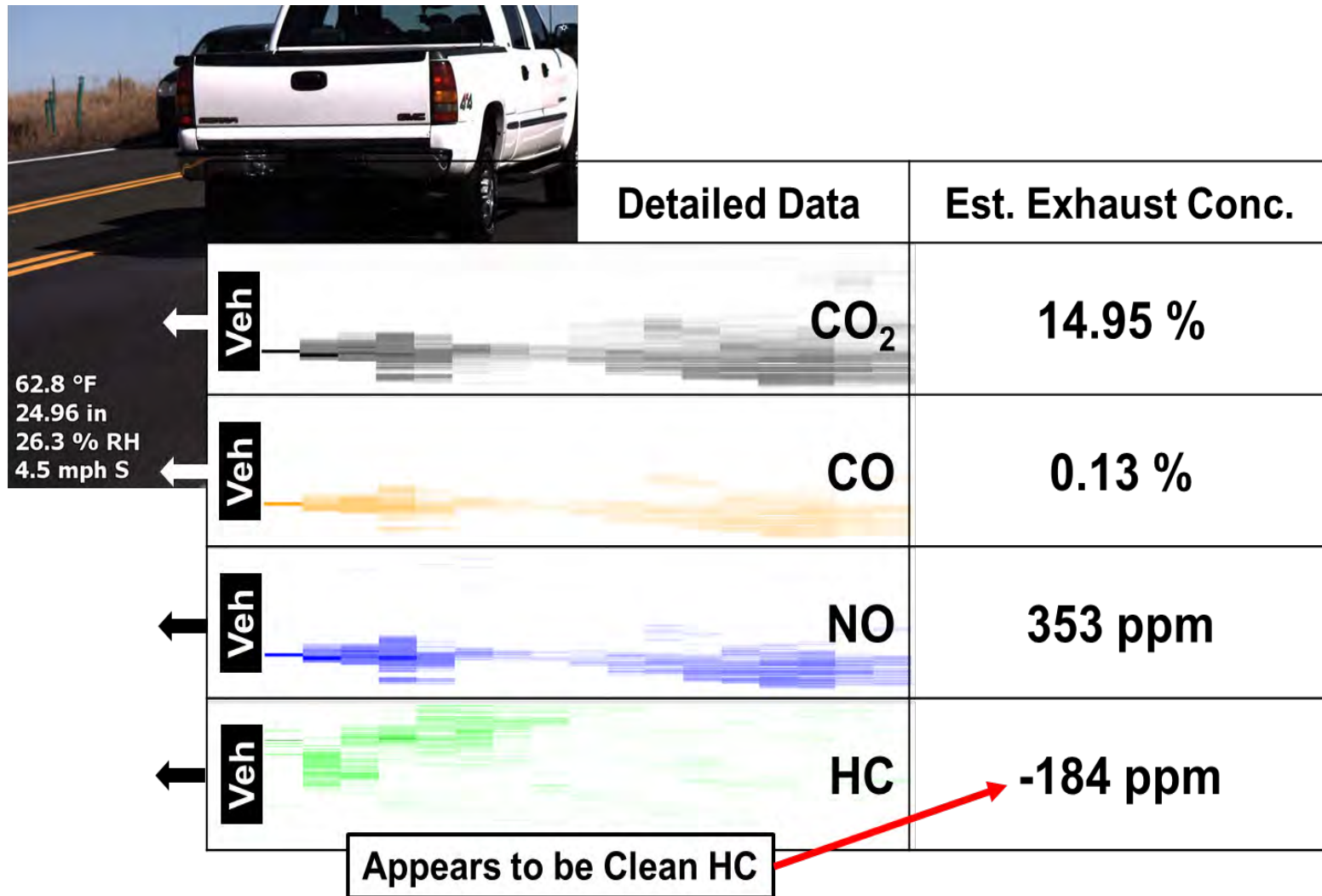
The next step in the analysis of the example transit is to use the Blind Source Separation method to split the RSD HC detailed data into an ExhHC portion and an EvapHC portion. This BSS converted the green Total HC heatmap at the bottom left of Figure 10-21 into the purple ExhHC heatmap and the red EvapHC heatmaps at the bottom left of Figure 10-22. The re-calculated exhaust concentrations are estimated using the same Equation 10-1 but now the regression slopes are obtained from the blue NO vs. CO_2, the orange CO vs. CO_2, and the purple ExhHC vs. CO_2 shown in Figure 10-20. The resulting exhaust concentrations are listed in the right column of Figure 10-22. The re-calculated CO_2, CO, and NO concentrations are virtually the same values as originally calculated and shown in Figure 10-21 and the second column of Figure 10-22. However, the new value of ExhHC is +74 ppm, which is a much more reasonable value than the original -184 ppm value. Overall, we believe that the concentration results shown in Figure 10-22 are reasonably accurate concentration results for the exhaust emissions for the example transit.

Of course, since concentration has no meaning for EvapHC, the value is listed as "n/a" in Figure 10-22. Still, we want to have some measure of the EvapHC emissions – especially since the green HC heatmap in Figure 10-21 indicates that the EvapHC emissions are substantially larger than the ExhHC emissions. We will use the RSD emission rate method to estimate the magnitude of the EvapHC emissions rate (g/mile).

The schematic shown in Figure 10-23 shows an overview of the calculation using the RSD emission rate method. Just as for the schematic for the traditional RSD concentration method shown in Figure 10-19, the flow begins on the left with the detailed RSD data. The first step is the application of the BSS separation method to effectively split the Total HC detailed data into ExhHC detailed data and EvapHC detailed data. Then, following Equation 5-19, the RSD Signal (g) from each of the RSD channels is simply divided by the RSD instrument's 100% Illumination Speed (mile/hr) and the Vortex Entrainment Time (hr) to produce each pollutant's Emission Rate (g/mile).

The last column of Figure 10-24 shows the resulting mass emission rates (g/mile) for the five pollutants. The estimated EvapHC emission rate of 8.6 g/mile is over 100 times the EvapHC running loss emission standard of 0.05 g/mile and more than 10 times the estimated ExhHC emission rate of 0.8 g/mile. This is an example where the traditional RSD method had failed to identify this vehicle as an elevated HC emitter. The fundamental cause of the erroneous conclusion was that the emission circumstances did not satisfy the assumptions made by the traditional RSD method.

It's important to recognize that the new RSD emission rate method and the improved results use the same detailed, internal data that all RSD instruments are collecting.

Figure 10-22. Re-Calculation of Exhaust Concentrations after separating ExhHC from EvapHC Plumes for the Example Transit

Detailed Data	Traditional	ReCalc Result	
CO_2	14.95 %	14.94 %	*Same*
CO	0.13 %	0.13 %	
NO	353 ppm	353 ppm	
ExhHC	-184 ppm	74 ppm	*Larger*
EvapHC	n/a	n/a	

11

Figure 10-23. Diagram of RSD Method for Calculating Mass Emission Rates (g/mile) from Detailed Data
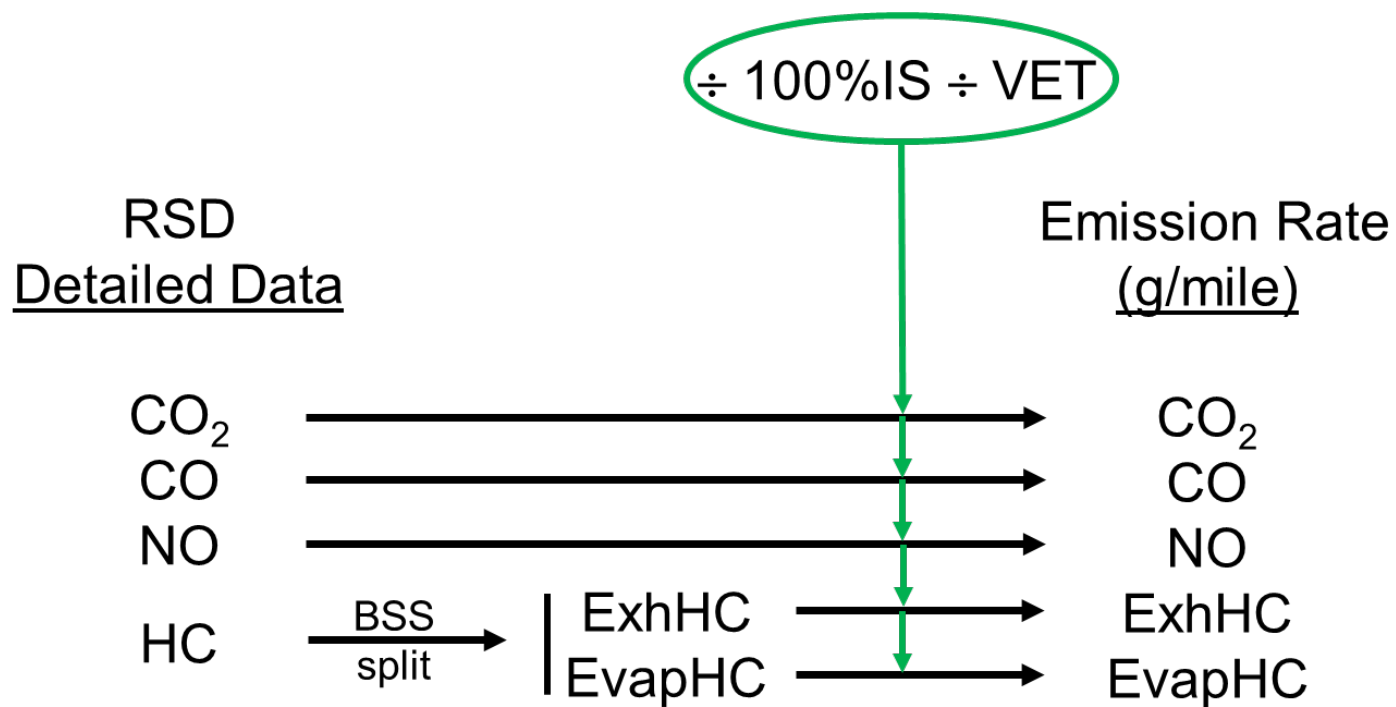
Figure 10-24. Calculation of Mass Emission Rates (g/mile) for the Example Transit

Massive EvapHC

Detailed Data	Traditional	ReCalc Result	Emission Rate
CO_2	14.95 %	14.94 %	546. g/mile
CO	0.13 %	0.13 %	12.3 g/mile
NO	353 ppm	353 ppm	3.1 g/mile
ExhHC	-184 ppm	74 ppm	0.8 g/mile
EvapHC	n/a	n/a	8.6 g/mile

10.4 Characterization of NO Mass in the Westminster Fleet Sample

Figures 10-10 and 10-11 in Section 10-2 showed that MOVES NOx release rates (g/hr) and the RSD emission rate method NO release rates (g/hr) were comparable over a wide range of VSP bins and vehicle age bins. Accordingly, this subsection uses the Westminster sample's NO measurements to demonstrate the type of fleet analysis that can be performed using mass emission rate (g/mile) measures that the RSD emission rate method can provide.

We used the RSD emission rate method to calculate the NO emission rates (g/mile) for the transits of fleet vehicles that drove past the RSD instrument. The left side of Figure 10-25 shows that the distribution of the number of vehicles has a peak at around 0.03 g/mile. In this plot, equal areas represent equal numbers of vehicles. Therefore, the plot shows that the youngest vehicles (blue) have low NO emission rates and the oldest vehicles (orange + red) have higher average emission rates. The areas also indicate that a large part of the fleet is made up of vehicles less than 16 years old (blue + green + yellow). The vertical reference line at 1 gNO/mile shows that only a small fraction of the fleet vehicles has NO emission rates above 1 gNO/mile.

The right side of Figure 10-25 shows the distribution of NO mass for the same analysis set of transits. Equal areas on this plot represent equal NO mass. The plot was produced by summing[43] the calculated NO emission rate (g/mile) for every transit in the analysis set. The right plot shows that even though large numbers of vehicles are present at low NO emission rates on the left plot, they do not contribute much NO mass to the fleet emissions. For example, the fraction of the fleet NO mass below 1 gNO/mile of the right plot is much smaller than the fraction of vehicles with NO emission rates below 1 gNO/mile on the left plot.

These two plots help us focus on the portion of the fleet that produces the largest part of the fleet emissions problem. In Figure 10-26 the shaded areas on the left and right plots show that vehicles 11 years and older (yellow + orange + red) make up only about 8% of the fleet but contribute 64% of the fleet NO mass. On the other hand, vehicles less than 11 years old (blue + green) contribute a small portion of the fleet NO mass.

These observations are really nothing new to the mobile sources emissions research community. What is new is the ability of RSD measurements to provide data that can quantify the mass distributions.

It is important to recognize that, just like for any RSD measurement, using measured emissions values from 1-second snapshots of many vehicles to infer the mass of emissions of the entire fleet is an extrapolation. The extrapolation is affected by using a single RSD instrument location and by how the visual presence of the RSD equipment may affect how drivers operate their vehicles as they drive past the RSD. For example, some drivers may take their foot off the accelerator, which will produce a small exhaust plume and thereby greatly affect the emission rates (g/mile) of all pollutants during the transit.

---

[43] We assumed that all vehicles in the analysis set have equal annual mileage accumulation.

Figure 10-25. Distributions of Number of Vehicles and NO Mass by NO Emission Rate and Age
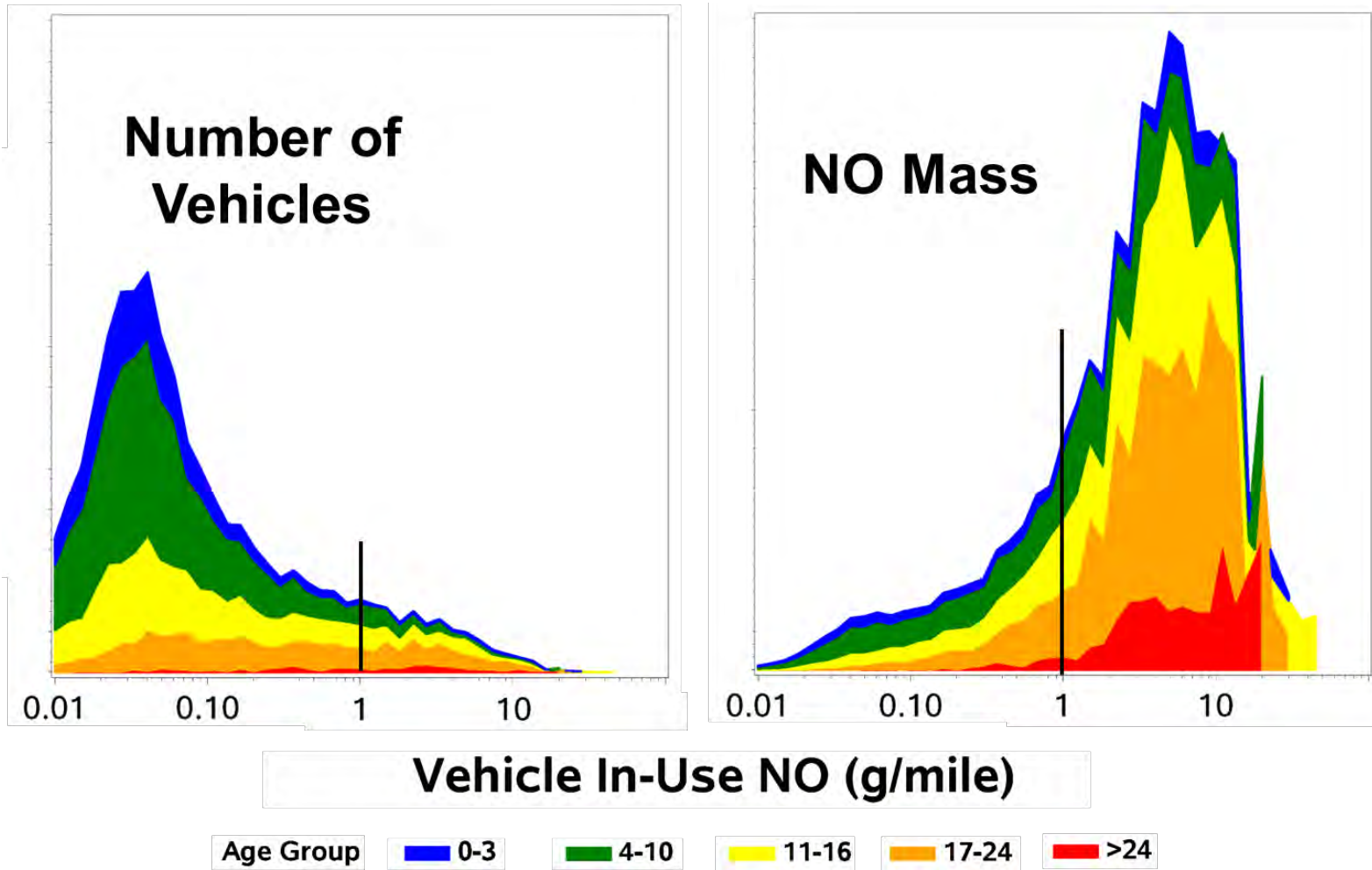
Figure 10-26. Fleet Fraction that Produces Most NO Mass
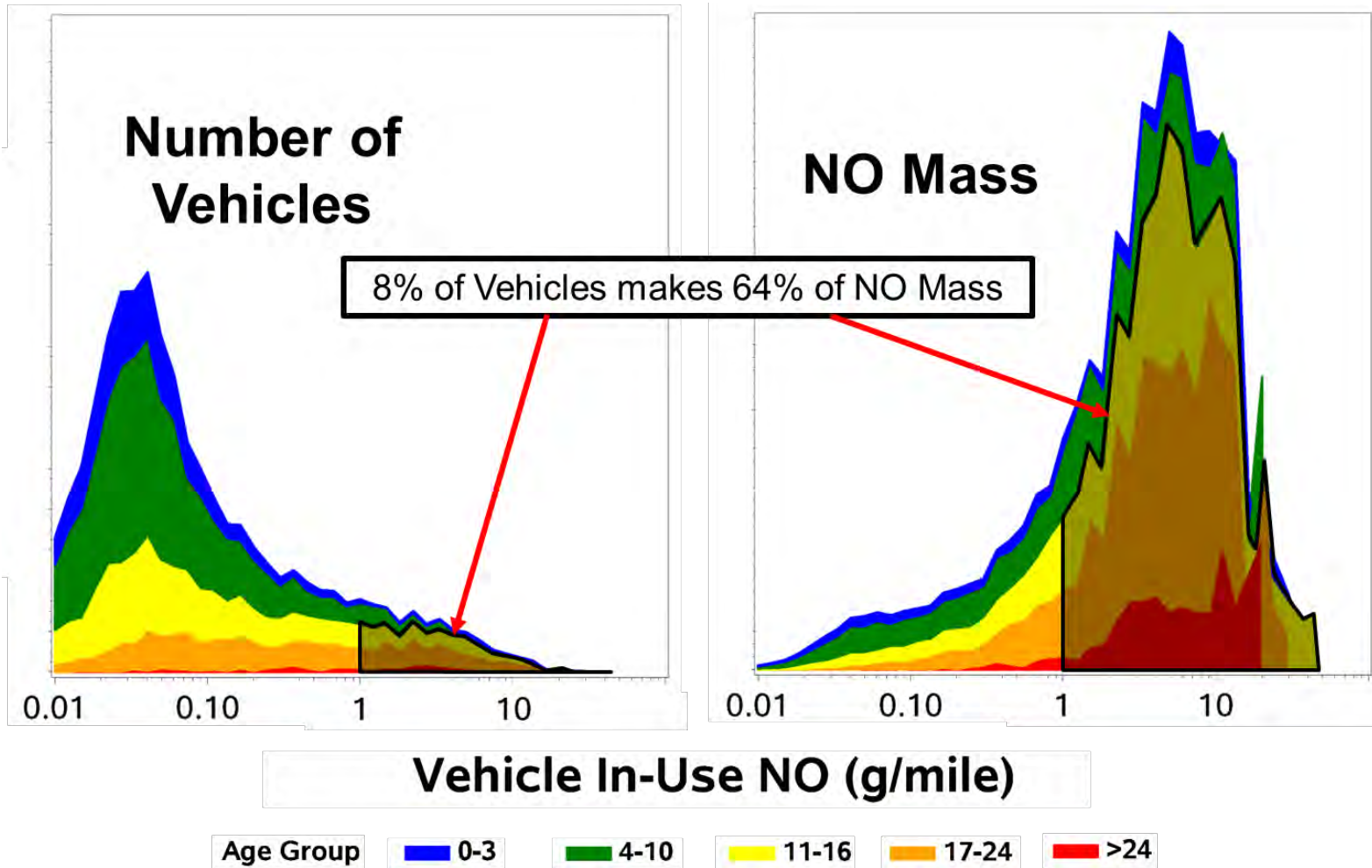
**Appendix A:
Test Vehicle EDAR Exhaust Emissions Measurements[1]**

---

[1] P:\EDARinDenver-OCT2019\Analysis/refveh_out.xlsx

Convoy Position - Reference Vehicle ID	Nominal Vehicle Speed (mph)	Exhaust HC (ppmC6)	Exhaust CO (ppm)	Exhaust NO (ppm)	Exhaust CO_2 (ppm)	Transit Date	Transit Time
1-EV1	22.5	32	-3	-2	154535	10/20/2019	11:54:55 AM
1-EV1	22.5	-35	-7	0	154542	10/20/2019	12:38:32 PM
1-EV1	22.5	46	-27	-19	154496	10/20/2019	1:18:45 PM
1-EV1	22.5	-29	-1	2	154543	10/20/2019	3:51:05 PM
1-EV1	22.5	-71	-9	10	154527	10/20/2019	4:09:15 PM
1-EV1	22.5	-42	4	1	154541	10/21/2019	9:37:09 AM
1-EV1	22.5	-135	-4	-1	154512	10/21/2019	10:21:06 AM
1-EV1	22.5	-3	3	8	154552	10/21/2019	11:25:10 AM
1-EV1	22.5	-9	2	0	154554	10/21/2019	12:37:08 PM
1-EV1	22.5	-33	9	9	154534	10/21/2019	1:03:07 PM
1-EV1	22.5	40	-6	0	154522	10/22/2019	10:49:03 AM
1-EV1	22.5	4	1	2	154555	10/22/2019	11:43:22 AM
1-EV1	22.5	-87	3	12	154520	10/22/2019	12:30:50 PM
1-EV1	22.5	16	3	1	154543	10/22/2019	3:29:19 PM
1-EV1	22.5	30	3	-2	154526	10/22/2019	4:05:13 PM
1-EV1	22.5	234	38	16	154372	10/23/2019	9:00:15 AM
1-EV1	22.5	78	25	-32	154468	10/23/2019	9:46:50 AM
1-EV1	22.5	0	67	-21	154398	10/23/2019	10:30:44 AM
1-EV1	22.5	185	-4	4	154414	10/23/2019	11:56:44 AM
1-EV1	22.5	0	3	7	154427	10/23/2019	12:30:47 PM
1-EV1	22.5	==498==	-12	-15	154231	10/23/2019	1:48:51 PM
1-EV1	22.5	-111	15	-1	154469	10/23/2019	2:34:46 PM
1-EV1	22.5	-14	-2	-5	154546	10/24/2019	2:16:35 PM
1-EV1	22.5	-60	2	-1	154533	10/24/2019	2:36:48 PM
1-EV1	22.5	19	1	-1	154546	10/24/2019	3:09:12 PM
1-EV1	45	-73	-14	16	154516	10/20/2019	12:13:42 PM
1-EV1	45	54	2	-2	154515	10/20/2019	12:55:51 PM
1-EV1	45	24	-8	-9	154523	10/20/2019	1:36:09 PM
1-EV1	45	-14	-5	24	154516	10/20/2019	3:09:38 PM
1-EV1	45	226	0	-57	154378	10/20/2019	3:28:05 PM
1-EV1	45	47	2	45	154494	10/21/2019	11:04:02 AM
1-EV1	45	0	44	4	154378	10/21/2019	11:44:02 AM
1-EV1	45	-11	-5	7	154506	10/21/2019	12:16:02 PM
1-EV1	45	0	-12	2	154481	10/22/2019	11:07:49 AM
1-EV1	45	88	7	0	154494	10/22/2019	12:03:51 PM
1-EV1	45	109	25	16	154465	10/22/2019	12:49:50 PM
1-EV1	45	164	-1	-10	154450	10/22/2019	2:33:49 PM
1-EV1	45	158	-48	-10	154411	10/22/2019	2:53:50 PM
1-EV1	45	==791==	0	49	154009	10/23/2019	3:44:37 PM
1-EV1	45	-53	27	-36	154479	10/24/2019	1:31:43 PM
1-EV1	45	0	80	3	154395	10/24/2019	1:55:44 PM
1-EV1	45	232	8	1	154384	10/24/2019	3:28:04 PM
2-EV2	22.5	178	4340	772	150967	10/20/2019	11:54:58 AM
2-EV2	22.5	112	5399	922	150173	10/20/2019	12:38:36 PM

Convoy Position - Reference Vehicle ID	Nominal Vehicle Speed (mph)	Exhaust HC (ppmC6)	Exhaust CO (ppm)	Exhaust NO (ppm)	Exhaust CO$_2$ (ppm)	Transit Date	Transit Time
2-EV2	22.5	149	5294	965	150214	10/20/2019	1:18:49 PM
2-EV2	22.5	147	5237	948	150262	10/20/2019	3:51:12 PM
2-EV2	22.5	193	5246	932	150229	10/20/2019	4:09:20 PM
2-EV2	22.5	159	5041	881	150425	10/21/2019	9:37:13 AM
2-EV2	22.5	171	4818	833	150596	10/21/2019	10:21:11 AM
2-EV2	22.5	170	5085	886	150379	10/21/2019	11:25:14 AM
2-EV2	22.5	148	5411	919	150147	10/21/2019	12:37:14 PM
2-EV2	22.5	169	5304	898	150215	10/21/2019	1:03:13 PM
2-EV2	22.5	150	5357	895	150194	10/22/2019	10:49:08 AM
2-EV2	22.5	271	5558	941	149938	10/22/2019	11:43:26 AM
2-EV2	22.5	218	5529	925	150010	10/22/2019	12:30:54 PM
2-EV2	22.5	241	5674	940	149886	10/22/2019	3:29:26 PM
2-EV2	22.5	160	5565	1057	149998	10/22/2019	4:05:20 PM
2-EV2	22.5	141	5440	1025	150119	10/23/2019	9:00:19 AM
2-EV2	22.5	185	5585	1032	149983	10/23/2019	9:46:55 AM
2-EV2	22.5	-3	5505	1023	150051	10/23/2019	10:30:47 AM
2-EV2	22.5	226	5517	1020	150016	10/23/2019	11:56:51 AM
2-EV2	22.5	80	5349	977	150232	10/23/2019	12:30:53 PM
2-EV2	22.5	143	5492	1052	150068	10/23/2019	1:48:55 PM
2-EV2	22.5	409	5551	1017	149880	10/23/2019	2:34:51 PM
2-EV2	22.5	98	5607	1060	150017	10/23/2019	3:21:18 PM
2-EV2	22.5	205	5339	940	150154	10/24/2019	2:16:42 PM
2-EV2	22.5	112	5232	932	150292	10/24/2019	2:36:54 PM
2-EV2	22.5	144	5051	885	150424	10/24/2019	3:09:17 PM
2-EV2	45	163	4558	812	150794	10/20/2019	12:13:45 PM
2-EV2	45	55	4583	816	150832	10/20/2019	12:55:54 PM
2-EV2	45	76	5166	970	150346	10/20/2019	1:36:12 PM
2-EV2	45	424	5069	861	150242	10/20/2019	3:09:42 PM
2-EV2	45	302	5110	898	150271	10/20/2019	3:28:11 PM
2-EV2	45	247	5210	907	150225	10/21/2019	9:56:06 AM
2-EV2	45	233	5132	873	150309	10/21/2019	11:04:05 AM
2-EV2	45	0	4070	531	151155	10/21/2019	11:44:05 AM
2-EV2	45	183	5069	861	150335	10/21/2019	12:16:07 PM
2-EV2	45	0	4519	805	149530	10/21/2019	2:00:03 PM
2-EV2	45	123	5235	875	150288	10/22/2019	11:07:52 AM
2-EV2	45	163	5699	961	149907	10/22/2019	12:03:55 PM
2-EV2	45	237	5460	909	150051	10/22/2019	12:49:54 PM
2-EV2	45	331	5647	907	149852	10/22/2019	2:33:54 PM
2-EV2	45	0	5359	869	150146	10/22/2019	2:53:55 PM
2-EV2	45	285	5371	1029	150076	10/23/2019	9:21:55 AM
2-EV2	45	175	5428	1006	150107	10/23/2019	10:05:54 AM
2-EV2	45	233	5443	1012	150070	10/23/2019	10:49:53 AM
2-EV2	45	554	4053	624	150777	10/23/2019	12:33:54 PM
2-EV2	45	-75	5236	1029	150319	10/23/2019	1:25:53 PM

Convoy Position - Reference Vehicle ID	Nominal Vehicle Speed (mph)	Exhaust HC (ppmC6)	Exhaust CO (ppm)	Exhaust NO (ppm)	Exhaust CO_2 (ppm)	Transit Date	Transit Time
2-EV2	45	94	5076	900	150425	10/24/2019	1:31:48 PM
2-EV2	45	175	5249	925	150247	10/24/2019	1:55:49 PM
2-EV2	45	381	5030	896	150289	10/24/2019	3:28:08 PM
3-F150	22.5	1	246	36	154278	10/23/2019	9:00:24 AM
3-F150	22.5	-13	-6	17	154527	10/23/2019	9:47:00 AM
3-F150	22.5	-160	45	4	154412	10/23/2019	10:10:59 AM
3-F150	22.5	2	134	38	154411	10/23/2019	10:30:52 AM
3-F150	22.5	2	18	20	154461	10/23/2019	11:56:56 AM
3-F150	22.5	0	6	18	154530	10/23/2019	1:49:00 PM
3-F150	22.5	-10	421	83	154166	10/23/2019	2:34:55 PM
3-F150	22.5	-19	10	59	154499	10/23/2019	2:59:01 PM
3-F150	22.5	5	5	20	154532	10/23/2019	3:21:22 PM
3-F150	45	17	137	42	154405	10/23/2019	9:22:00 AM
3-F150	45	6	19	54	154511	10/23/2019	9:26:02 AM
3-F150	45	-46	109	35	154415	10/23/2019	10:49:57 AM
3-F150	45	-83	86	50	154404	10/23/2019	12:33:58 PM
3-F150	45	1	28	-12	154328	10/23/2019	1:25:58 PM
3-F150	45	-69	44	23	154494	10/23/2019	2:07:57 PM
3-F150	45	0	11	7	154509	10/23/2019	2:11:55 PM
3-F150	45	6	43	9	154491	10/23/2019	2:53:56 PM
3-F150	45	0	73	12	154474	10/23/2019	3:44:44 PM
3-GMC	22.5	-1	58	2	154489	10/22/2019	10:49:13 AM
3-GMC	22.5	0	558	5	154136	10/22/2019	4:05:26 PM
3-GMC	45	1	131	9	154454	10/22/2019	11:07:56 AM
3-GMC	45	-1	129	-2	154453	10/22/2019	11:11:59 AM
3-Subaru	22.5	4	2651	416	152368	10/20/2019	11:55:01 AM
3-Subaru	22.5	-112	96	13	154431	10/20/2019	12:38:39 PM
3-Subaru	22.5	-9	250	23	154335	10/20/2019	1:18:52 PM
3-Subaru	22.5	6	16	9	154486	10/20/2019	3:51:18 PM
3-Subaru	22.5	1	22	7	154532	10/20/2019	4:09:24 PM
3-Subaru	22.5	-14	639	100	153949	10/21/2019	9:37:15 AM
3-Subaru	22.5	-45	315	57	154244	10/21/2019	10:21:14 AM
3-Subaru	22.5	6	-7	-2	154478	10/21/2019	11:01:13 AM
3-Subaru	22.5	-9	458	80	154167	10/21/2019	11:25:18 AM
3-Subaru	22.5	-23	39	3	154518	10/21/2019	12:37:20 PM
3-Subaru	22.5	-27	266	35	154317	10/21/2019	1:03:19 PM
3-Subaru	45	-24	551	81	154100	10/20/2019	12:13:48 PM
3-Subaru	45	15	439	22	154143	10/20/2019	12:17:26 PM
3-Subaru	45	-174	352	52	154259	10/20/2019	12:55:56 PM
3-Subaru	45	-73	401	52	154221	10/20/2019	1:36:14 PM
3-Subaru	45	4	376	3	154127	10/20/2019	3:09:46 PM
3-Subaru	45	-22	-2	-27	154499	10/20/2019	3:28:15 PM
3-Subaru	45	1	556	43	154112	10/21/2019	9:56:09 AM
3-Subaru	45	1	79	9	154425	10/21/2019	10:00:08 AM

Convoy Position - Reference Vehicle ID	Nominal Vehicle Speed (mph)	Exhaust HC (ppmC6)	Exhaust CO (ppm)	Exhaust NO (ppm)	Exhaust CO_2 (ppm)	Transit Date	Transit Time
3-Subaru	45	7	608	-43	154067	10/21/2019	11:04:07 AM
3-Subaru	45	-8	918	-1	153867	10/21/2019	12:16:12 PM
3-Subaru	45	-455	321	-10	154246	10/21/2019	2:00:07 PM
4-Infiniti	22.5	0	48	6	154481	10/20/2019	11:40:01 AM
4-Infiniti	22.5	-1	414	36	154197	10/20/2019	11:47:20 AM
4-Infiniti	22.5	9	176	15	154372	10/20/2019	11:50:58 AM
4-Infiniti	22.5	-2	54	14	154446	10/20/2019	11:55:04 AM
4-Infiniti	22.5	0	114	1	154344	10/20/2019	12:22:09 PM
4-Infiniti	22.5	-1	17	10	154536	10/20/2019	12:25:51 PM
4-Infiniti	22.5	-7	15	5	154512	10/20/2019	12:29:30 PM
4-Infiniti	22.5	8	282	5	154334	10/20/2019	12:33:12 PM
4-Infiniti	22.5	4	136	3	154414	10/20/2019	12:38:42 PM
4-Infiniti	22.5	4	275	4	154349	10/20/2019	1:00:42 PM
4-Infiniti	22.5	1	399	4	154251	10/20/2019	1:04:23 PM
4-Infiniti	22.5	0	595	5	154101	10/20/2019	1:08:08 PM
4-Infiniti	22.5	0	230	5	154375	10/20/2019	1:11:44 PM
4-Infiniti	22.5	0	261	1	154334	10/20/2019	1:15:20 PM
4-Infiniti	22.5	-62	32	0	154519	10/20/2019	1:18:54 PM
4-Infiniti	22.5	6	2025	8	153051	10/20/2019	2:08:38 PM
4-Infiniti	22.5	-4	190	2	154414	10/20/2019	2:27:17 PM
4-Infiniti	22.5	9	656	5	154062	10/20/2019	2:36:01 PM
4-Infiniti	22.5	0	222	4	154385	10/20/2019	2:45:50 PM
4-Infiniti	22.5	2	254	14	154354	10/20/2019	2:54:24 PM
4-Infiniti	22.5	0	-10	-26	154527	10/20/2019	3:01:40 PM
4-Infiniti	22.5	0	88	1	154490	10/20/2019	3:21:32 PM
4-Infiniti	22.5	4	1140	6	153710	10/20/2019	3:25:35 PM
4-Infiniti	22.5	1	64	4	154498	10/20/2019	3:44:03 PM
4-Infiniti	22.5	-80	439	3	154220	10/20/2019	3:47:38 PM
4-Infiniti	22.5	0	236	1	154384	10/20/2019	3:51:21 PM
4-Infiniti	22.5	-8	135	4	154450	10/20/2019	4:02:13 PM
4-Infiniti	22.5	0	464	2	154207	10/20/2019	4:05:50 PM
4-Infiniti	22.5	4	248	4	154350	10/20/2019	4:09:29 PM
4-Infiniti	22.5	1	144	7	154399	10/21/2019	9:21:17 AM
4-Infiniti	22.5	-9	156	6	154416	10/21/2019	9:25:18 AM
4-Infiniti	22.5	-1	205	8	154389	10/21/2019	9:29:18 AM
4-Infiniti	22.5	-7	320	15	154308	10/21/2019	9:33:15 AM
4-Infiniti	22.5	-1	105	5	154457	10/21/2019	9:37:18 AM
4-Infiniti	22.5	-7	219	6	154304	10/21/2019	10:05:13 AM
4-Infiniti	22.5	-4	168	8	154421	10/21/2019	10:13:13 AM
4-Infiniti	22.5	-1	346	14	154288	10/21/2019	10:17:16 AM
4-Infiniti	22.5	0	393	4	154267	10/21/2019	10:21:17 AM
4-Infiniti	22.5	-2	470	3	154205	10/21/2019	11:01:16 AM
4-Infiniti	22.5	-1	494	31	154134	10/21/2019	11:09:20 AM
4-Infiniti	22.5	-3	565	8	154135	10/21/2019	11:13:20 AM

Convoy Position - Reference Vehicle ID	Nominal Vehicle Speed (mph)	Exhaust HC (ppmC6)	Exhaust CO (ppm)	Exhaust NO (ppm)	Exhaust CO_2 (ppm)	Transit Date	Transit Time
4-Infiniti	22.5	0	160	7	154429	10/21/2019	11:17:17 AM
4-Infiniti	22.5	-8	103	-1	154467	10/21/2019	11:21:21 AM
4-Infiniti	22.5	-8	405	6	154247	10/21/2019	11:25:20 AM
4-Infiniti	22.5	0	231	5	154376	10/21/2019	12:09:17 PM
4-Infiniti	22.5	-8	894	7	153891	10/21/2019	12:13:22 PM
4-Infiniti	22.5	0	594	4	154109	10/21/2019	12:29:23 PM
4-Infiniti	22.5	-3	7	5	154542	10/21/2019	12:33:08 PM
4-Infiniti	22.5	0	522	4	154169	10/21/2019	12:37:23 PM
4-Infiniti	22.5	0	207	28	154379	10/21/2019	12:51:21 PM
4-Infiniti	22.5	0	123	-1	154465	10/21/2019	12:55:23 PM
4-Infiniti	22.5	-4	215	4	154387	10/21/2019	1:03:22 PM
4-Infiniti	22.5	-15	589	10	154088	10/21/2019	1:11:24 PM
4-Infiniti	22.5	-1	178	3	154424	10/21/2019	1:19:20 PM
4-Infiniti	22.5	0	104	7	154458	10/21/2019	1:47:19 PM
4-Infiniti	22.5	-4	1001	27	153694	10/21/2019	1:57:27 PM
4-Infiniti	22.5	0	734	3	154013	10/21/2019	2:05:18 PM
4-Infiniti	22.5	0	76	-2	154462	10/22/2019	10:33:15 AM
4-Infiniti	22.5	0	152	0	154008	10/22/2019	10:37:12 AM
4-Infiniti	22.5	0	99	3	154467	10/22/2019	10:41:12 AM
4-Infiniti	22.5	-2	140	6	154429	10/22/2019	10:45:16 AM
4-Infiniti	22.5	-8	98	3	154457	10/22/2019	10:49:16 AM
4-Infiniti	22.5	-2	126	1	154393	10/22/2019	11:23:05 AM
4-Infiniti	22.5	-7	307	8	154314	10/22/2019	11:27:04 AM
4-Infiniti	22.5	-4	331	-4	154282	10/22/2019	11:31:21 AM
4-Infiniti	22.5	0	179	1	154423	10/22/2019	11:39:17 AM
4-Infiniti	22.5	-16	172	18	154415	10/22/2019	11:43:34 AM
4-Infiniti	22.5	-1	128	3	154463	10/22/2019	12:09:13 PM
4-Infiniti	22.5	-1	72	0	154495	10/22/2019	12:14:57 PM
4-Infiniti	22.5	-11	141	6	154442	10/22/2019	12:19:00 PM
4-Infiniti	22.5	-2	269	-2	154355	10/22/2019	12:22:58 PM
4-Infiniti	22.5	-9	38	6	154523	10/22/2019	12:26:59 PM
4-Infiniti	22.5	-1	759	19	153967	10/22/2019	12:31:02 PM
4-Infiniti	22.5	-5	326	3	154288	10/22/2019	1:51:02 PM
4-Infiniti	22.5	-12	124	3	154458	10/22/2019	1:59:03 PM
4-Infiniti	22.5	-3	461	4	154215	10/22/2019	2:07:08 PM
4-Infiniti	22.5	-5	161	12	154412	10/22/2019	2:15:03 PM
4-Infiniti	22.5	-40	636	36	154066	10/22/2019	2:23:02 PM
4-Infiniti	22.5	0	212	0	154388	10/22/2019	2:31:07 PM
4-Infiniti	22.5	2	1252	1	153611	10/22/2019	2:47:16 PM
4-Infiniti	22.5	-2	158	5	154304	10/22/2019	3:26:12 PM
4-Infiniti	22.5	0	107	7	154439	10/22/2019	3:29:37 PM
4-Infiniti	22.5	1	289	-1	154316	10/22/2019	3:57:31 PM
4-Infiniti	22.5	0	10	1	154545	10/22/2019	4:01:33 PM
4-Infiniti	22.5	0	384	6	154268	10/22/2019	4:05:30 PM

Convoy Position - Reference Vehicle ID	Nominal Vehicle Speed (mph)	Exhaust HC (ppmC6)	Exhaust CO (ppm)	Exhaust NO (ppm)	Exhaust CO_2 (ppm)	Transit Date	Transit Time
4-Infiniti	22.5	0	29	7	154526	10/22/2019	4:09:31 PM
4-Infiniti	22.5	-3	167	115	154385	10/23/2019	8:44:21 AM
4-Infiniti	22.5	0	109	4	154450	10/23/2019	8:48:22 AM
4-Infiniti	22.5	-3	187	7	154415	10/23/2019	8:52:25 AM
4-Infiniti	22.5	-2	203	4	154391	10/23/2019	8:56:22 AM
4-Infiniti	22.5	0	189	6	154414	10/23/2019	9:00:28 AM
4-Infiniti	22.5	-4	228	3	154372	10/23/2019	9:31:05 AM
4-Infiniti	22.5	-6	352	9	154239	10/23/2019	9:35:01 AM
4-Infiniti	22.5	-3	628	1	154075	10/23/2019	9:38:58 AM
4-Infiniti	22.5	-21	367	11	154251	10/23/2019	9:42:57 AM
4-Infiniti	22.5	-3	102	13	154475	10/23/2019	9:47:03 AM
4-Infiniti	22.5	-1	605	3	154110	10/23/2019	10:11:01 AM
4-Infiniti	22.5	-6	161	8	154418	10/23/2019	10:15:11 AM
4-Infiniti	22.5	-2	281	12	154344	10/23/2019	10:18:58 AM
4-Infiniti	22.5	0	478	21	154197	10/23/2019	10:22:59 AM
4-Infiniti	22.5	-2	130	3	154457	10/23/2019	10:26:56 AM
4-Infiniti	22.5	0	235	6	154360	10/23/2019	10:30:54 AM
4-Infiniti	22.5	-7	330	24	154267	10/23/2019	11:26:57 AM
4-Infiniti	22.5	-1	275	6	154347	10/23/2019	11:31:08 AM
4-Infiniti	22.5	-8	116	13	154438	10/23/2019	11:47:06 AM
4-Infiniti	22.5	-20	117	6	154446	10/23/2019	11:50:58 AM
4-Infiniti	22.5	9	318	15	154303	10/23/2019	11:56:59 AM
4-Infiniti	22.5	0	264	-13	154342	10/23/2019	12:21:47 PM
4-Infiniti	22.5	-2	288	17	154326	10/23/2019	12:27:02 PM
4-Infiniti	22.5	-102	236	6	154322	10/23/2019	12:31:02 PM
4-Infiniti	22.5	-13	103	13	154460	10/23/2019	12:43:03 PM
4-Infiniti	22.5	-2	61	1	154426	10/23/2019	12:50:58 PM
4-Infiniti	22.5	0	326	4	154292	10/23/2019	12:59:01 PM
4-Infiniti	22.5	-16	256	-9	154298	10/23/2019	1:07:00 PM
4-Infiniti	22.5	-15	263	1	154264	10/23/2019	1:14:58 PM
4-Infiniti	22.5	-2	643	-4	154002	10/23/2019	1:23:05 PM
4-Infiniti	22.5	-10	126	-4	154443	10/23/2019	1:32:24 PM
4-Infiniti	22.5	0	230	1	154355	10/23/2019	1:36:59 PM
4-Infiniti	22.5	-32	363	0	154276	10/23/2019	1:41:02 PM
4-Infiniti	22.5	-5	115	37	154010	10/23/2019	1:45:05 PM
4-Infiniti	22.5	-3	369	2	154265	10/23/2019	1:49:03 PM
4-Infiniti	22.5	-1	147	-10	154408	10/23/2019	2:16:58 PM
4-Infiniti	22.5	-15	184	6	154398	10/23/2019	2:21:01 PM
4-Infiniti	22.5	-1	161	8	154400	10/23/2019	2:25:00 PM
4-Infiniti	22.5	0	283	-11	154326	10/23/2019	2:29:05 PM
4-Infiniti	22.5	-2	276	4	154352	10/23/2019	2:34:58 PM
4-Infiniti	22.5	8	289	7	154311	10/23/2019	2:59:04 PM
4-Infiniti	22.5	-10	411	-2	154180	10/23/2019	3:03:09 PM
4-Infiniti	22.5	-9	359	11	154262	10/23/2019	3:07:21 PM

Convoy Position - Reference Vehicle ID	Nominal Vehicle Speed (mph)	Exhaust HC (ppmC6)	Exhaust CO (ppm)	Exhaust NO (ppm)	Exhaust CO_2 (ppm)	Transit Date	Transit Time
4-Infiniti	22.5	-7	746	13	153794	10/23/2019	3:13:24 PM
4-Infiniti	22.5	0	15	9	154468	10/23/2019	3:17:25 PM
4-Infiniti	22.5	-11	134	5	154448	10/23/2019	3:21:24 PM
4-Infiniti	22.5	-2	-16	-1	154536	10/24/2019	12:28:51 PM
4-Infiniti	22.5	-7	268	11	154334	10/24/2019	12:36:51 PM
4-Infiniti	22.5	-2	370	2	154227	10/24/2019	12:44:46 PM
4-Infiniti	22.5	-1	177	36	154395	10/24/2019	1:12:53 PM
4-Infiniti	22.5	0	315	5	154312	10/24/2019	1:20:50 PM
4-Infiniti	22.5	-6	334	16	154277	10/24/2019	1:28:46 PM
4-Infiniti	22.5	3	488	5	154179	10/24/2019	1:48:51 PM
4-Infiniti	22.5	0	342	16	154294	10/24/2019	1:52:48 PM
4-Infiniti	22.5	-5	230	15	154370	10/24/2019	2:12:47 PM
4-Infiniti	22.5	0	61	1	154512	10/24/2019	2:16:46 PM
4-Infiniti	22.5	-1	105	7	154458	10/24/2019	2:28:56 PM
4-Infiniti	22.5	0	168	8	154429	10/24/2019	2:32:53 PM
4-Infiniti	22.5	-3	-91	-13	154469	10/24/2019	2:36:58 PM
4-Infiniti	22.5	-1	184	15	154401	10/24/2019	2:52:59 PM
4-Infiniti	22.5	-4	124	8	154456	10/24/2019	2:56:50 PM
4-Infiniti	22.5	-1	119	25	154451	10/24/2019	3:00:48 PM
4-Infiniti	22.5	-7	238	19	154365	10/24/2019	3:05:18 PM
4-Infiniti	22.5	-4	174	14	154417	10/24/2019	3:09:21 PM
4-Infiniti	45	-6	109	4	154474	10/20/2019	11:59:14 AM
4-Infiniti	45	5	323	6	154311	10/20/2019	12:02:48 PM
4-Infiniti	45	6	37	-20	154414	10/20/2019	12:06:29 PM
4-Infiniti	45	8	699	33	154025	10/20/2019	12:10:08 PM
4-Infiniti	45	4	231	3	154378	10/20/2019	12:13:51 PM
4-Infiniti	45	-26	68	-6	154463	10/20/2019	12:17:29 PM
4-Infiniti	45	1	566	14	154074	10/20/2019	12:41:21 PM
4-Infiniti	45	-2	368	9	154221	10/20/2019	12:44:58 PM
4-Infiniti	45	5	173	9	154364	10/20/2019	12:48:39 PM
4-Infiniti	45	4	5098	7	150728	10/20/2019	12:52:19 PM
4-Infiniti	45	-11	79	5	154407	10/20/2019	12:55:59 PM
4-Infiniti	45	1	949	3	153837	10/20/2019	1:32:39 PM
4-Infiniti	45	29	351	-13	154087	10/20/2019	1:39:56 PM
4-Infiniti	45	-3	886	3	153877	10/20/2019	2:02:03 PM
4-Infiniti	45	35	319	15	154286	10/20/2019	2:11:12 PM
4-Infiniti	45	0	8	7	154533	10/20/2019	2:31:26 PM
4-Infiniti	45	0	364	5	154283	10/20/2019	2:38:43 PM
4-Infiniti	45	-20	217	-1	154386	10/20/2019	2:49:42 PM
4-Infiniti	45	-9	77	-6	154472	10/20/2019	2:57:02 PM
4-Infiniti	45	-7	134	33	154384	10/20/2019	3:09:50 PM
4-Infiniti	45	-23	112	10	154445	10/20/2019	3:13:30 PM
4-Infiniti	45	6	100	5	154475	10/20/2019	3:17:10 PM
4-Infiniti	45	1	211	4	154384	10/20/2019	3:28:19 PM

Convoy Position - Reference Vehicle ID	Nominal Vehicle Speed (mph)	Exhaust HC (ppmC6)	Exhaust CO (ppm)	Exhaust NO (ppm)	Exhaust CO$_2$ (ppm)	Transit Date	Transit Time
4-Infiniti	45	0	482	4	154171	10/20/2019	3:31:51 PM
4-Infiniti	45	0	979	11	153755	10/20/2019	3:57:32 PM
4-Infiniti	45	-1	726	20	153959	10/20/2019	4:12:11 PM
4-Infiniti	45	-15	795	8	153927	10/20/2019	4:15:51 PM
4-Infiniti	45	-14	31	9	154518	10/21/2019	9:40:18 AM
4-Infiniti	45	-15	237	18	154371	10/21/2019	9:45:52 AM
4-Infiniti	45	-41	138	18	154424	10/21/2019	9:48:16 AM
4-Infiniti	45	-10	267	3	154336	10/21/2019	9:52:13 AM
4-Infiniti	45	-5	213	4	154356	10/21/2019	9:56:12 AM
4-Infiniti	45	-12	153	10	154412	10/21/2019	10:00:10 AM
4-Infiniti	45	423	433	43	153957	10/21/2019	10:24:12 AM
4-Infiniti	45	0	515	6	154159	10/21/2019	10:48:15 AM
4-Infiniti	45	-5	324	28	154294	10/21/2019	10:52:11 AM
4-Infiniti	45	1	2134	5	152968	10/21/2019	11:04:10 AM
4-Infiniti	45	-3	872	5	153893	10/21/2019	11:28:13 AM
4-Infiniti	45	98	276	26	154256	10/21/2019	11:32:13 AM
4-Infiniti	45	1	396	3	154161	10/21/2019	11:36:11 AM
4-Infiniti	45	-45	75	25	154466	10/21/2019	11:40:12 AM
4-Infiniti	45	-189	91	43	154430	10/21/2019	11:44:11 AM
4-Infiniti	45	-3	207	4	154392	10/21/2019	12:00:13 PM
4-Infiniti	45	2	1006	1	153808	10/21/2019	12:04:12 PM
4-Infiniti	45	0	549	8	154132	10/21/2019	12:16:15 PM
4-Infiniti	45	-19	92	4	154473	10/21/2019	12:20:16 PM
4-Infiniti	45	-2	449	16	154219	10/21/2019	12:24:14 PM
4-Infiniti	45	-1	240	6	154374	10/21/2019	12:40:16 PM
4-Infiniti	45	-17	1286	-1	153579	10/21/2019	12:46:12 PM
4-Infiniti	45	-3	109	6	154405	10/21/2019	1:06:15 PM
4-Infiniti	45	-5	780	1	153973	10/21/2019	1:14:16 PM
4-Infiniti	45	12	55	26	151221	10/21/2019	1:24:12 PM
4-Infiniti	45	-300	911	-8	153848	10/21/2019	1:32:14 PM
4-Infiniti	45	37	175	4	154366	10/21/2019	1:42:14 PM
4-Infiniti	45	77	38009	2	126574	10/21/2019	1:52:12 PM
4-Infiniti	45	175	47348	6	119640	10/21/2019	2:00:12 PM
4-Infiniti	45	0	120	9	154406	10/22/2019	10:52:04 AM
4-Infiniti	45	-1	210	11	154391	10/22/2019	10:56:05 AM
4-Infiniti	45	-3	279	19	154339	10/22/2019	11:00:05 AM
4-Infiniti	45	3	583	10	154073	10/22/2019	11:07:59 AM
4-Infiniti	45	0	228	11	154366	10/22/2019	11:18:01 AM
4-Infiniti	45	-14	212	1	154367	10/22/2019	11:48:03 AM
4-Infiniti	45	-16	279	-2	154311	10/22/2019	11:56:02 AM
4-Infiniti	45	0	463	3	154186	10/22/2019	12:04:01 PM
4-Infiniti	45	465	389	52	153955	10/22/2019	12:34:01 PM
4-Infiniti	45	-8	28	4	154477	10/22/2019	12:38:04 PM
4-Infiniti	45	-33	284	-2	154339	10/22/2019	1:47:11 PM

Convoy Position - Reference Vehicle ID	Nominal Vehicle Speed (mph)	Exhaust HC (ppmC6)	Exhaust CO (ppm)	Exhaust NO (ppm)	Exhaust CO_2 (ppm)	Transit Date	Transit Time
4-Infiniti	45	-7	835	7	153909	10/22/2019	1:54:28 PM
4-Infiniti	45	-5	935	2	153824	10/22/2019	2:10:05 PM
4-Infiniti	45	-30	351	23	154203	10/22/2019	2:18:03 PM
4-Infiniti	45	-12	575	8	154120	10/22/2019	2:26:05 PM
4-Infiniti	45	5	436	29	154051	10/22/2019	2:34:03 PM
4-Infiniti	45	-6	890	16	153895	10/22/2019	2:38:03 PM
4-Infiniti	45	0	227	8	154350	10/22/2019	2:42:02 PM
4-Infiniti	45	0	184	13	154394	10/22/2019	2:58:03 PM
4-Infiniti	45	-10	636	20	154006	10/22/2019	3:02:03 PM
4-Infiniti	45	-9	279	7	154334	10/22/2019	3:53:07 PM
4-Infiniti	45	79	34380	7	129227	10/22/2019	4:17:10 PM
4-Infiniti	45	0	383	1	154227	10/23/2019	9:04:05 AM
4-Infiniti	45	-4	207	0	154360	10/23/2019	9:08:00 AM
4-Infiniti	45	-4	342	29	154239	10/23/2019	9:12:02 AM
4-Infiniti	45	1	683	14	154036	10/23/2019	9:18:02 AM
4-Infiniti	45	0	306	11	154281	10/23/2019	9:22:03 AM
4-Infiniti	45	2	186	17	154388	10/23/2019	9:26:07 AM
4-Infiniti	45	-37	143	-5	154348	10/23/2019	9:50:03 AM
4-Infiniti	45	288	151	5	154267	10/23/2019	9:54:04 AM
4-Infiniti	45	485	383	8	153972	10/23/2019	9:58:03 AM
4-Infiniti	45	-1	121	-7	154447	10/23/2019	10:02:04 AM
4-Infiniti	45	0	158	2	154426	10/23/2019	10:34:03 AM
4-Infiniti	45	-5	364	21	154265	10/23/2019	10:38:03 AM
4-Infiniti	45	-2	241	12	154363	10/23/2019	10:42:02 AM
4-Infiniti	45	-6	184	16	154402	10/23/2019	10:50:01 AM
4-Infiniti	45	-18	291	16	154313	10/23/2019	10:53:59 AM
4-Infiniti	45	-3	581	7	153996	10/23/2019	11:18:05 AM
4-Infiniti	45	1	835	29	153729	10/23/2019	11:22:03 AM
4-Infiniti	45	0	278	8	154350	10/23/2019	11:38:03 AM
4-Infiniti	45	-8	294	12	154323	10/23/2019	11:42:01 AM
4-Infiniti	45	0	2488	8	152682	10/23/2019	12:00:02 PM
4-Infiniti	45	-25	752	8	153998	10/23/2019	12:04:05 PM
4-Infiniti	45	50	398	114	154141	10/23/2019	12:34:00 PM
4-Infiniti	45	17	134	-6	154403	10/23/2019	12:38:04 PM
4-Infiniti	45	-5	174	28	154249	10/23/2019	12:46:03 PM
4-Infiniti	45	-3	1412	13	153403	10/23/2019	12:54:03 PM
4-Infiniti	45	-13	160	20	154077	10/23/2019	1:02:02 PM
4-Infiniti	45	-10	236	1	154319	10/23/2019	1:10:02 PM
4-Infiniti	45	-15	545	-11	153359	10/23/2019	1:18:04 PM
4-Infiniti	45	-1	335	2	154303	10/23/2019	1:52:02 PM
4-Infiniti	45	-83	268	-1	154260	10/23/2019	1:56:02 PM
4-Infiniti	45	1047	366	32	153602	10/23/2019	2:00:00 PM
4-Infiniti	45	-50	272	-5	154256	10/23/2019	2:04:00 PM
4-Infiniti	45	-2	55	-3	154496	10/23/2019	2:08:00 PM

Convoy Position - Reference Vehicle ID	Nominal Vehicle Speed (mph)	Exhaust HC (ppmC6)	Exhaust CO (ppm)	Exhaust NO (ppm)	Exhaust CO_2 (ppm)	Transit Date	Transit Time
4-Infiniti	45	0	194	6	154368	10/23/2019	2:11:59 PM
4-Infiniti	45	-71	120	1	154448	10/23/2019	2:37:59 PM
4-Infiniti	45	-28	56	12	154419	10/23/2019	2:42:02 PM
4-Infiniti	45	5	215	-15	154383	10/23/2019	2:45:58 PM
4-Infiniti	45	-164	178	23	154360	10/23/2019	2:50:00 PM
4-Infiniti	45	-7	208	16	154378	10/23/2019	2:53:59 PM
4-Infiniti	45	1	29	16	154323	10/23/2019	3:24:26 PM
4-Infiniti	45	2	706	7	154023	10/23/2019	3:28:48 PM
4-Infiniti	45	1	940	20	153387	10/23/2019	3:32:34 PM
4-Infiniti	45	5	563	1	154058	10/23/2019	3:36:27 PM
4-Infiniti	45	-21	186	5	154366	10/23/2019	3:44:47 PM
4-Infiniti	45	-10	282	16	154276	10/24/2019	12:21:21 PM
4-Infiniti	45	-7	343	49	154000	10/24/2019	12:39:51 PM
4-Infiniti	45	13	1419	19	153494	10/24/2019	1:07:57 PM
4-Infiniti	45	-1	1308	32	153467	10/24/2019	1:15:54 PM
4-Infiniti	45	-5	410	12	154240	10/24/2019	1:23:55 PM
4-Infiniti	45	0	315	10	154290	10/24/2019	1:31:52 PM
4-Infiniti	45	-157	91	19	154399	10/24/2019	1:35:51 PM
4-Infiniti	45	-83	17	16	154484	10/24/2019	1:39:56 PM
4-Infiniti	45	2	1782	23	153236	10/24/2019	1:43:54 PM
4-Infiniti	45	2	1924	23	153108	10/24/2019	1:55:53 PM
4-Infiniti	45	-21	574	-9	154085	10/24/2019	1:59:53 PM
4-Infiniti	45	-39	187	-4	154404	10/24/2019	2:03:53 PM
4-Infiniti	45	-22	173	12	154414	10/24/2019	2:19:55 PM
4-Infiniti	45	-16	1000	28	153785	10/24/2019	3:16:55 PM
4-Infiniti	45	0	571	-5	154122	10/24/2019	3:20:16 PM
4-Infiniti	45	-2	191	14	154254	10/24/2019	3:24:11 PM
4-Infiniti	45	-52	949	83	153772	10/24/2019	3:28:12 PM
4-Infiniti	45	1	297	226	154236	10/24/2019	3:32:13 PM

**Appendix B:
Westminster Dataset and Analysis Program Locations**

Tables B-1 and B-2 provide the locations of the datasets and analysis programs that were used to archive and analyze the Westminster data.

Table B-1. Vehicle Description Data for the Westminster Sample[2]

	Directory	Dataset	SAS program	Inputs	Outputs
V	P/Colorado_OBD_IM240/ RegistrationData/2019_RegData/	col_reg_2019_julyupdate.sas7bdat			
U	P/CDPHE/Regis2019		copy2022_COreg_find _mk_mod_yr.sas	V @ Line 41	T @ Line 157
T	P/CDPHE/Regis2019	co_reg_2019_wts.sas7bdat			
A	P/EDARinDenver-OCT2019/Analysis/	Westminster_OCT2019Results_200124Reprocess-200219_modified.CSV			
B	P/EDARinDenver-OCT2019/Analysis/	VIN_output.CSV			

---

[2] P/EDARinDenver-OCT2019/Analysis_MLout/SAS Program Flow.xlsx

Table B-2. Analysis Programs for the Westminster Sample

	P:/EDARinDenver-OCT2019/	Dataset	SAS program	Inputs	Outputs
C	Analysis_MLout/		OCT19_metadata.SAS	A @ Line 50 B @ Line 304	D @ Line 510
D	Analysis_MLout/	spreadsheet_vin_211115.sas7bdat			
Y	Analysis_MLout/211108/Data_MLout	Results_Westminster_Series5##-211108.zip			
H	Analysis_MLout/211108/Anal_MLout		OCT19_read_matlab.sas	Y @ Line 74	I @ Line 725
I	Analysis_MLout/211108/Anal_MLout	OCT19_scansubset-211108.sas7bdat			
E	Analysis_MLout/211108/Anal_MLout		OCT19_bumper.sas	D @ Line 52 I @ Line 167	F @ Line 1583 G @ Line 1585
F	Analysis_MLout/211108/Anal_MLout	scansum_autofronttrailer_211108.sas7bdat			
G	Analysis_MLout/211108/Anal_MLout	BumperLocations-211108_v2.CSV			
AA	Analysis_MLout/211122/Data_MLout	Results_Westminster_Series5##-211122.zip			
Z	Analysis_MLout/211122/Anal_MLout		OCT19_read_matlab.sas	AA @ Line 82	J @ Line 734
J	Analysis_MLout/211122/Anal_MLout	OCT19_scan_211122_standard.sas7bdat			
K	Analysis_MLout/211122/Anal_MLout		OCT19_interpshapeCO2_5.sas	D @ Line 175 F @ Line 303 J @ Line 132	L @ Line 1705 M @ Line 1729
L	Analysis_MLout/211122/Anal_MLout	BumperLocations_211122_draft_v3.CSV			
M	Analysis_MLout/211122/Anal_MLout	CO2shapes_by_udst.sas7bdat			
Q	Analysis_MLout/220817/Data_MLout	OCT19_Unit_Date_Series_Transit_"rundate"*.CSV			
N	Analysis_MLout/220817/Anal_MLout		OCT19_read_matlab.sas	Q @ Line 117 F @ Line 512 M @ Line 576 D @ Line 625	O @ Line 661 P @ Line 727: std (741: bootstrap 755: lsmean)
O	Analysis_MLout/220817/Anal_MLout	OCT19_pixel_readout_"rundate".sas7bdat			
P	Analysis_MLout/220817/Anal_MLout	OCT19_scan_readout_"rundate".sas7bdat			
W	Analysis_MLout/220801/Anal_MLout		**temp:** OCT19_make_flags.sas	O @ Line 57	X @ Line 812 AB @ Line 807
X	Analysis_MLout/220801/Anal_MLout	**temp:** udstplusflags.sas7bdat			
AB	Analysis_MLout/220801/Anal_MLout	**temp:** pixelplusflags.sas7bdat			
R	Analysis_MLout/220817/Anal_MLout		OCT19_scan_postprocess.sas	P @ Line 96 D @ Line 141 T @ Line 296 F @ Line 341 M @ Line 365 X @ Line TBD	S @ Line 539
	Analysis_MLout/220817/Anal_MLout	OCT19_scanmetaflag.sas7bdat			

**Appendix C:
Plots for Signal Adjustment Demonstration**

Figure C-1. Offset Adjustment Example for no CO and NO Emissions: EV-1, Low EvapHC from DOOR, Low Speed

7 20191020 000506 car 000108
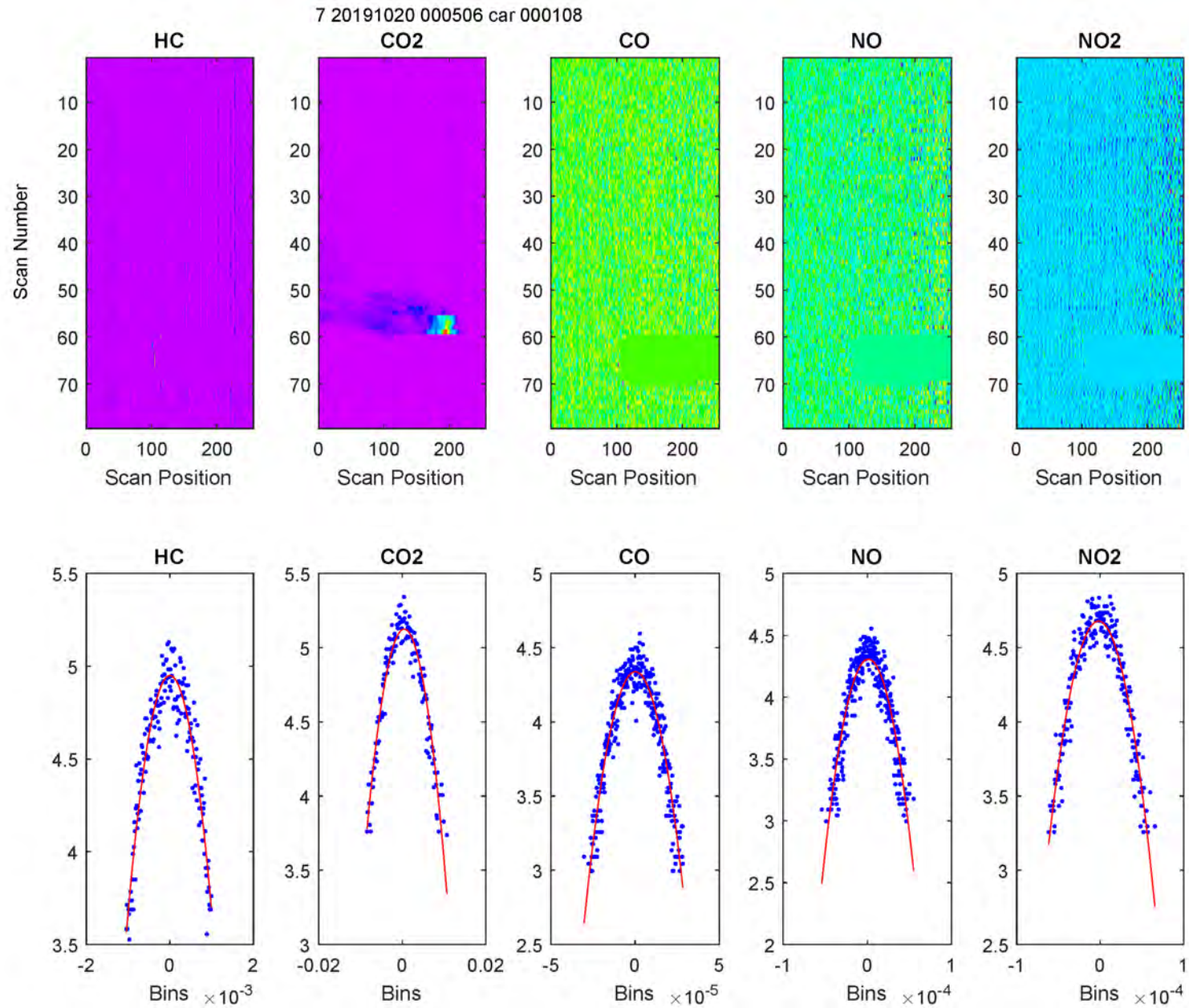
Figure C-2. Offset Adjustment Example for no CO and NO Emissions: EV-1, High EvapHC from DOOR, Low Speed

7 20191022 000509 car 001735
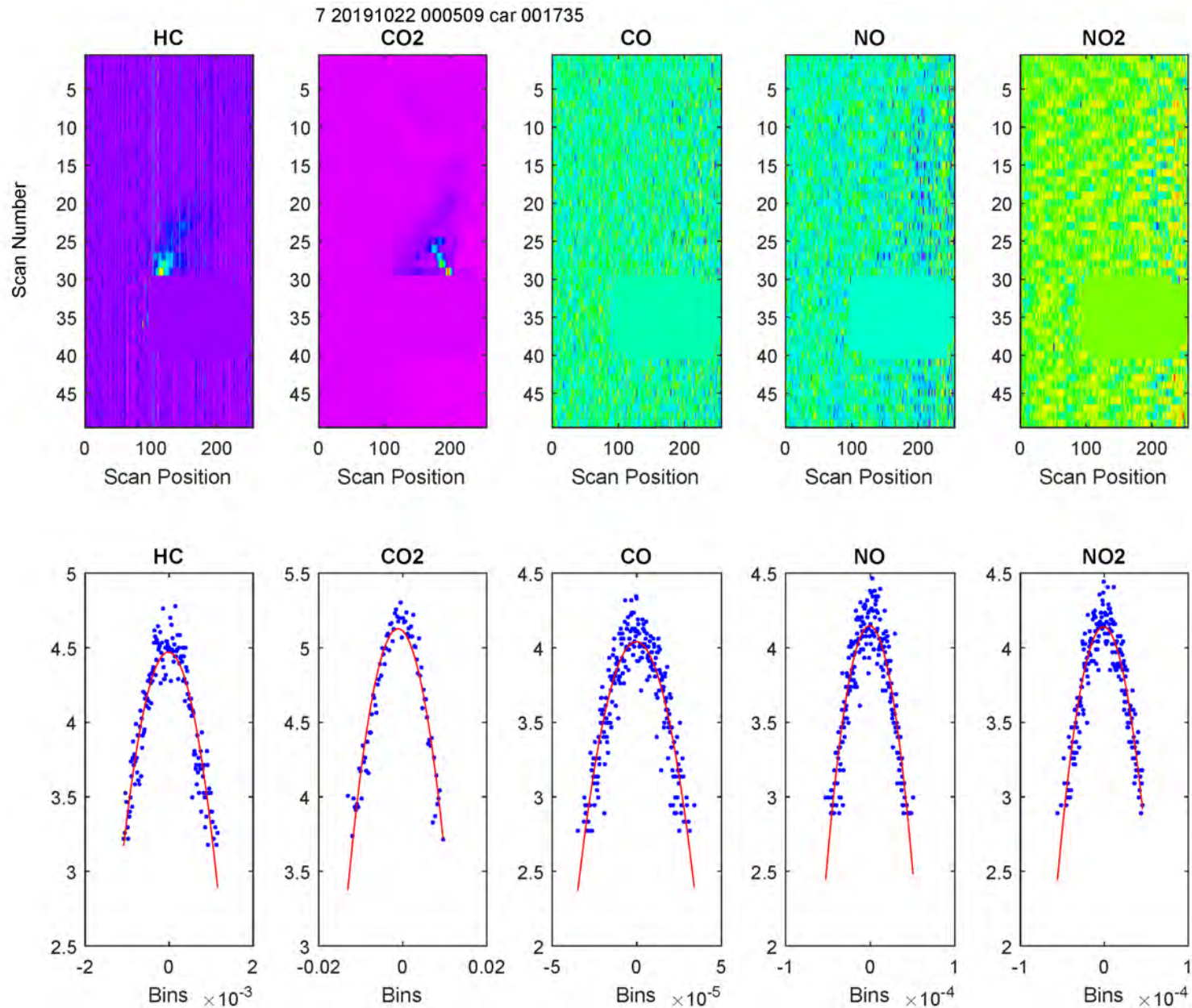
Figure C-3. Offset Adjustment Example with CO and NO Emissions: EV-2, Low EvapHC from DOOR, Low Speed
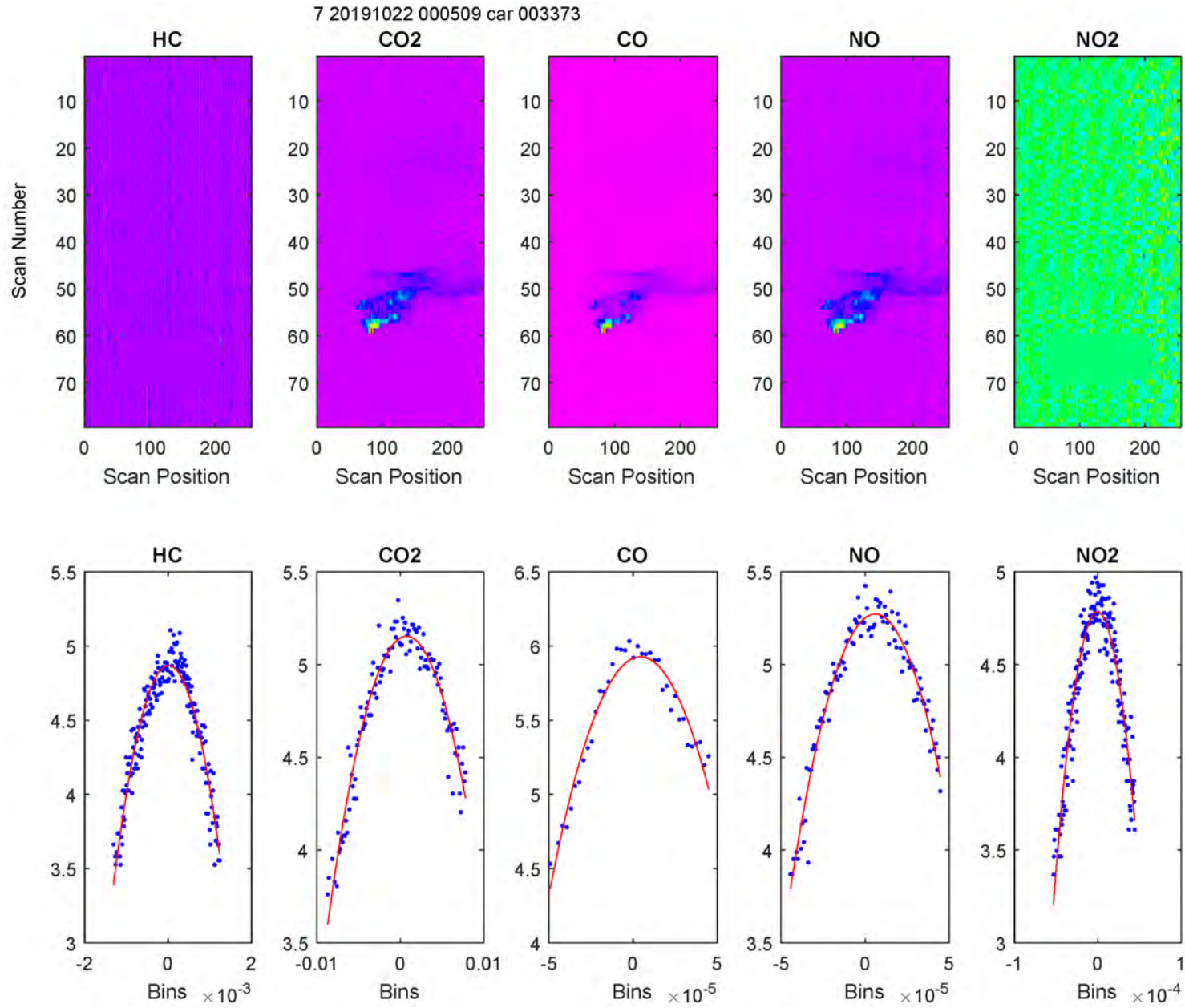
Figure C-4. Offset Adjustment Example with CO and NO Emissions: EV-2, Low EvapHC from DOOR, Low Speed
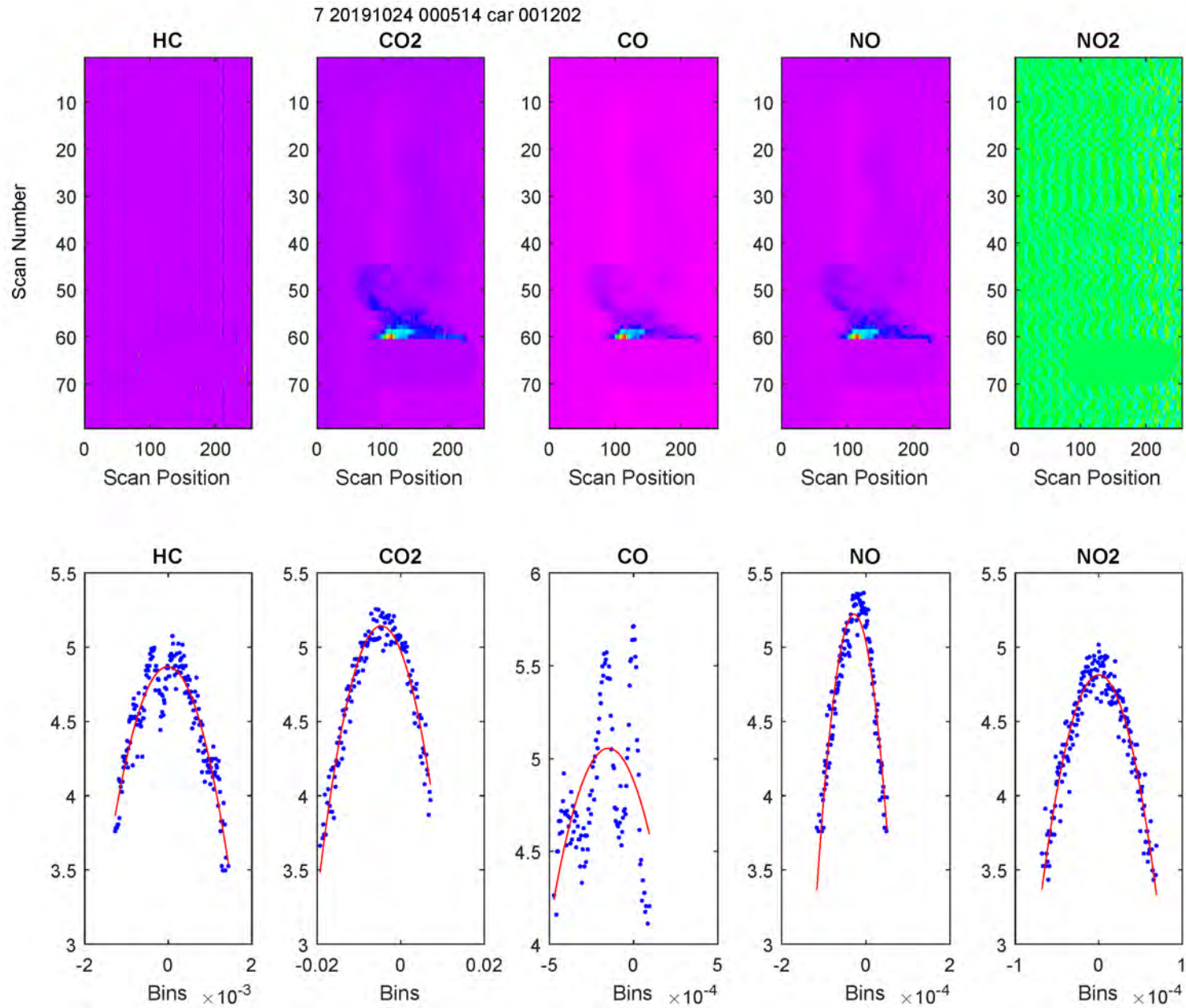
Figure C-5. Offset Adjustment Example with CO and NO Emissions: EV-2, High EvapHC from DOOR, Low Speed
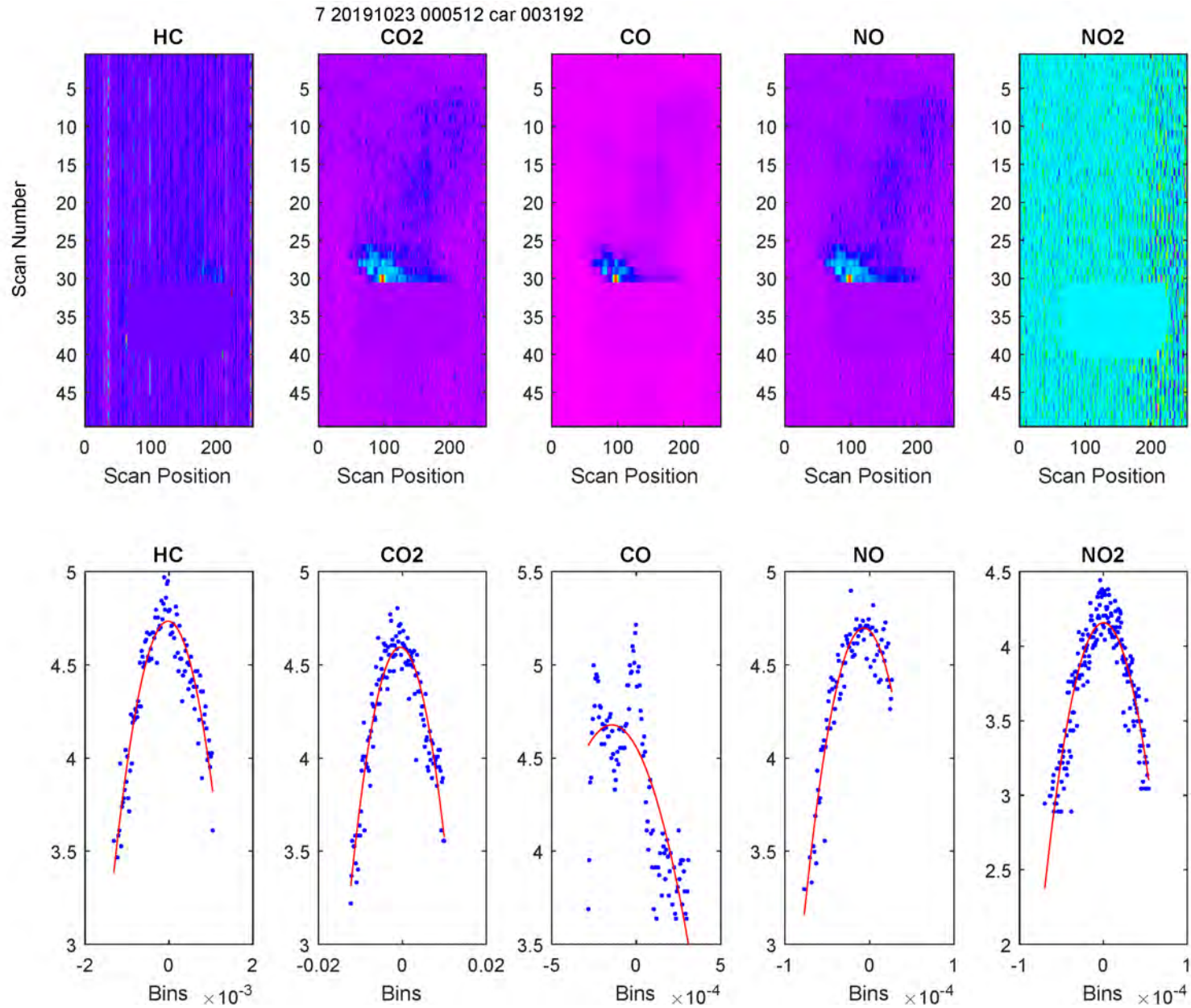
Figure C-6. Offset Adjustment Example indicating CO Channel Failure: 2013 Ford F-150 (Fleet Vehicle)
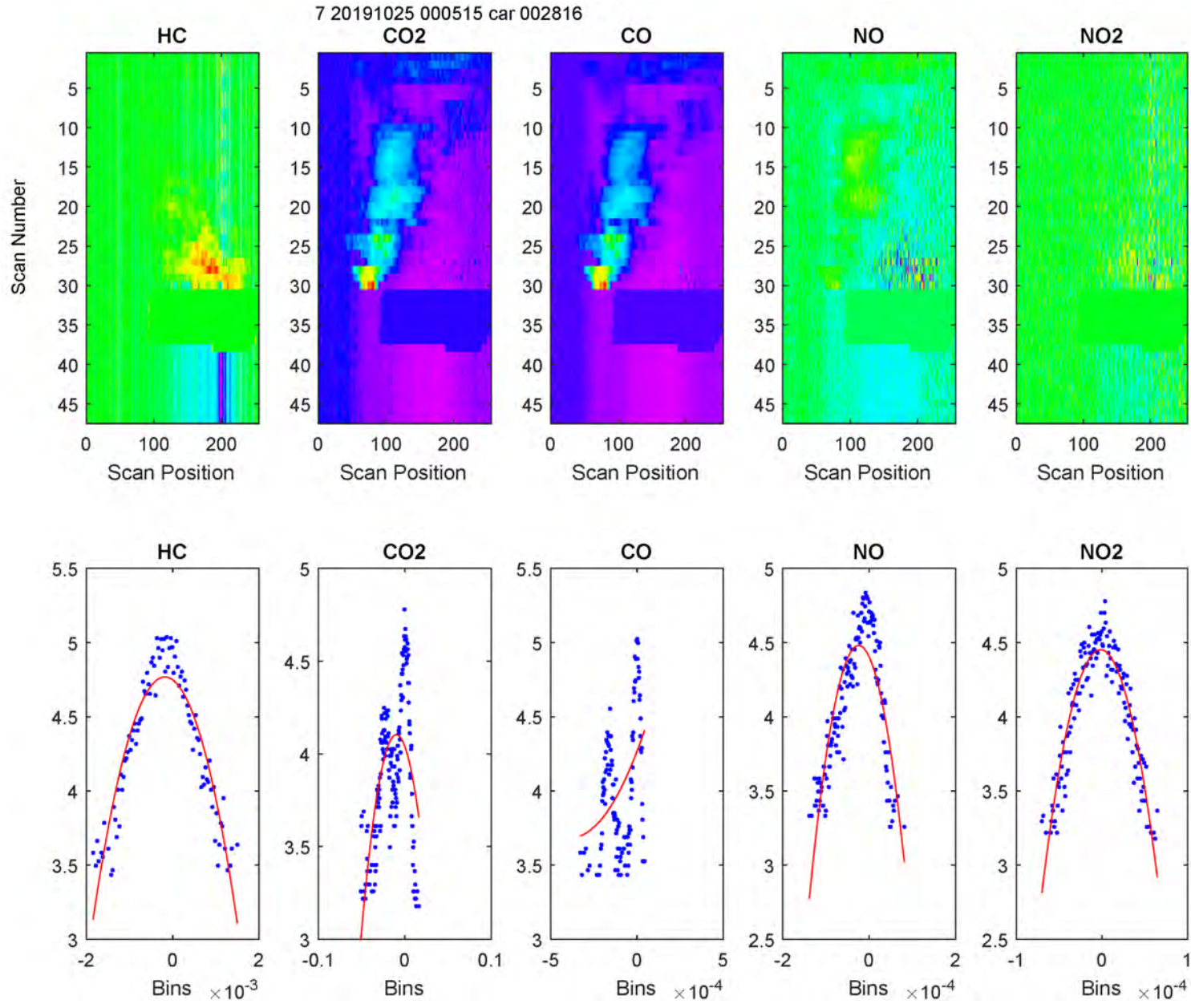
Figure C-7. Outlier Removal Example: EV-2, Low EvapHC from HOOD, Low Speed

7 20191023 000512 car 001834
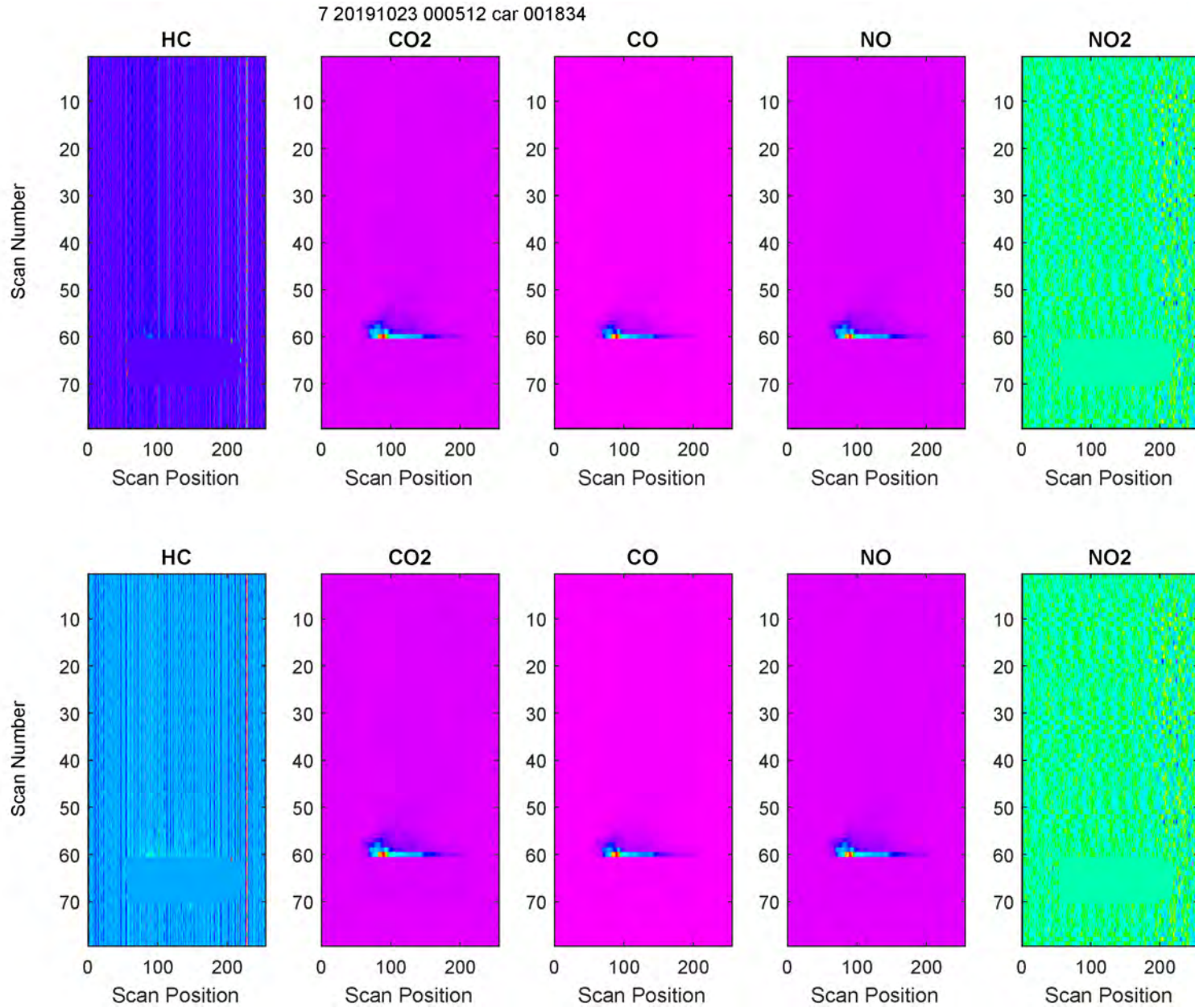
Figure C-8. Outlier Removal Example: EV-2, High EvapHC from DOOR, Low Speed

7 20191021 000507 car 001351
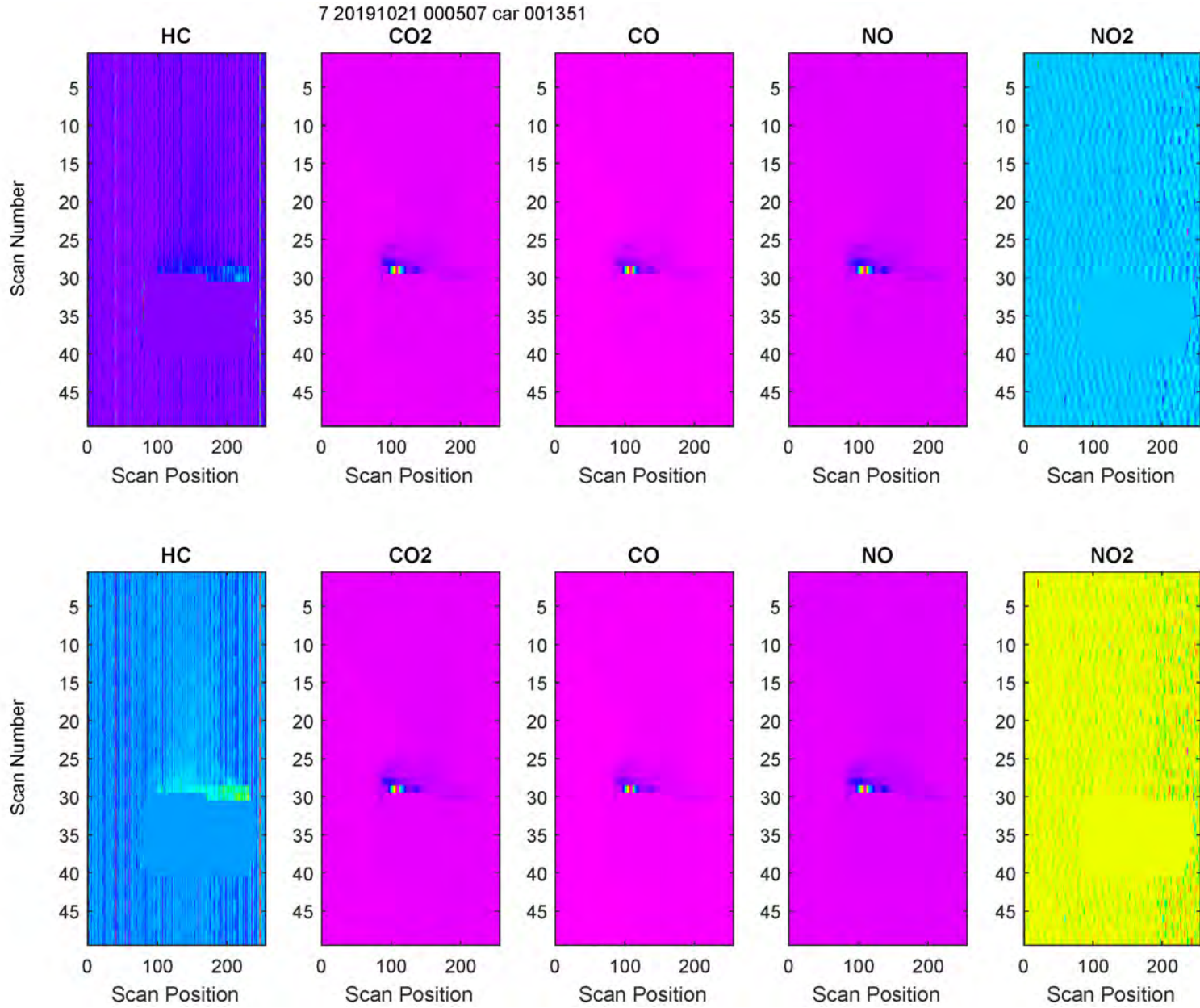
Figure C-9. HC Multi-Tonal Cancellation Example: EV-2, High EvapHC from DOOR

7 20191023 000512 car 001168
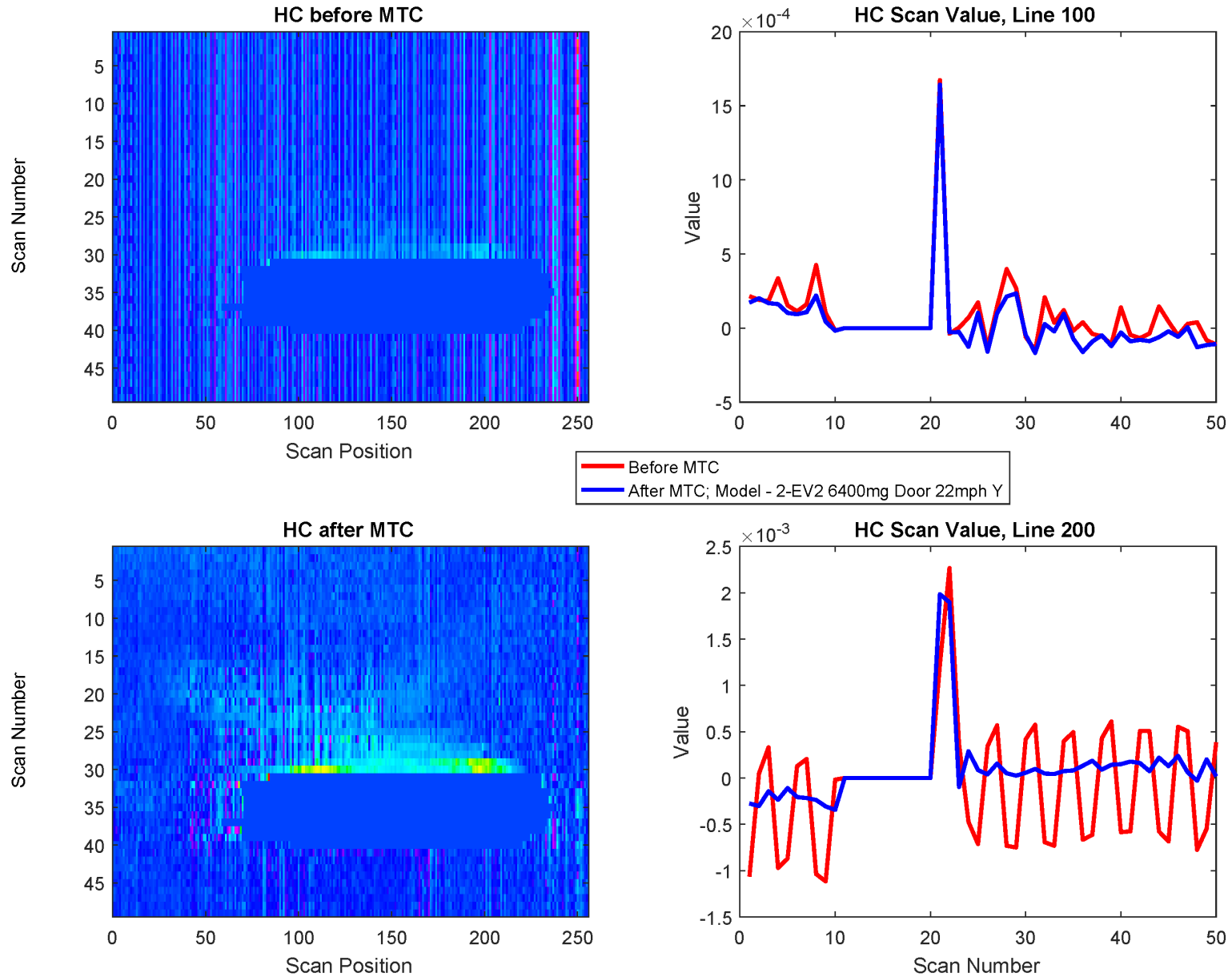
Figure C-10. HC Multi-Tonal Cancellation Example: EV-2, High EvapHC from TANK

7 20191024 000514 car 001635
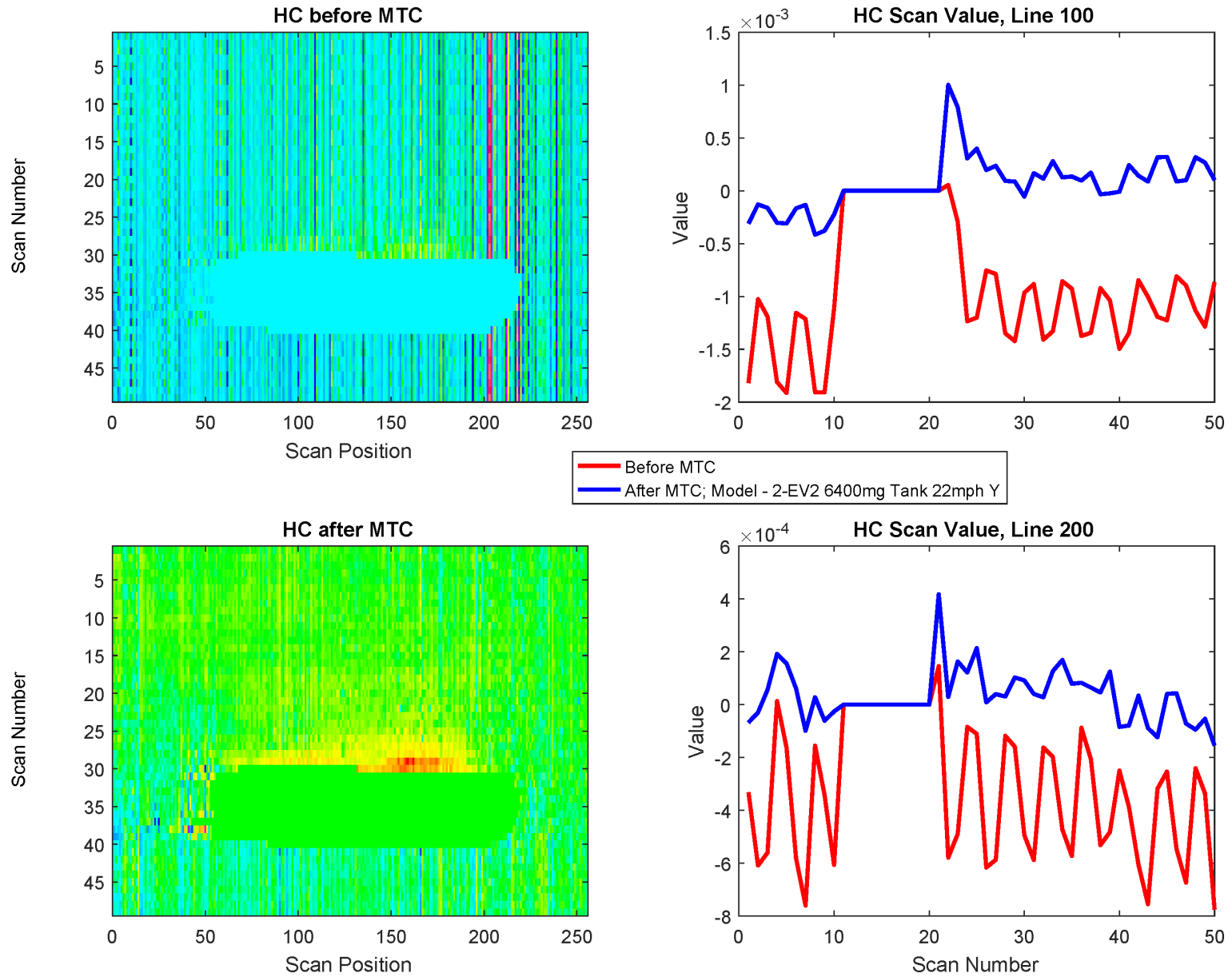
Figure C-11. HC Multi-Tonal Cancellation Example: EV-2, High EvapHC from HOOD

7 20191020 000505 car 001813
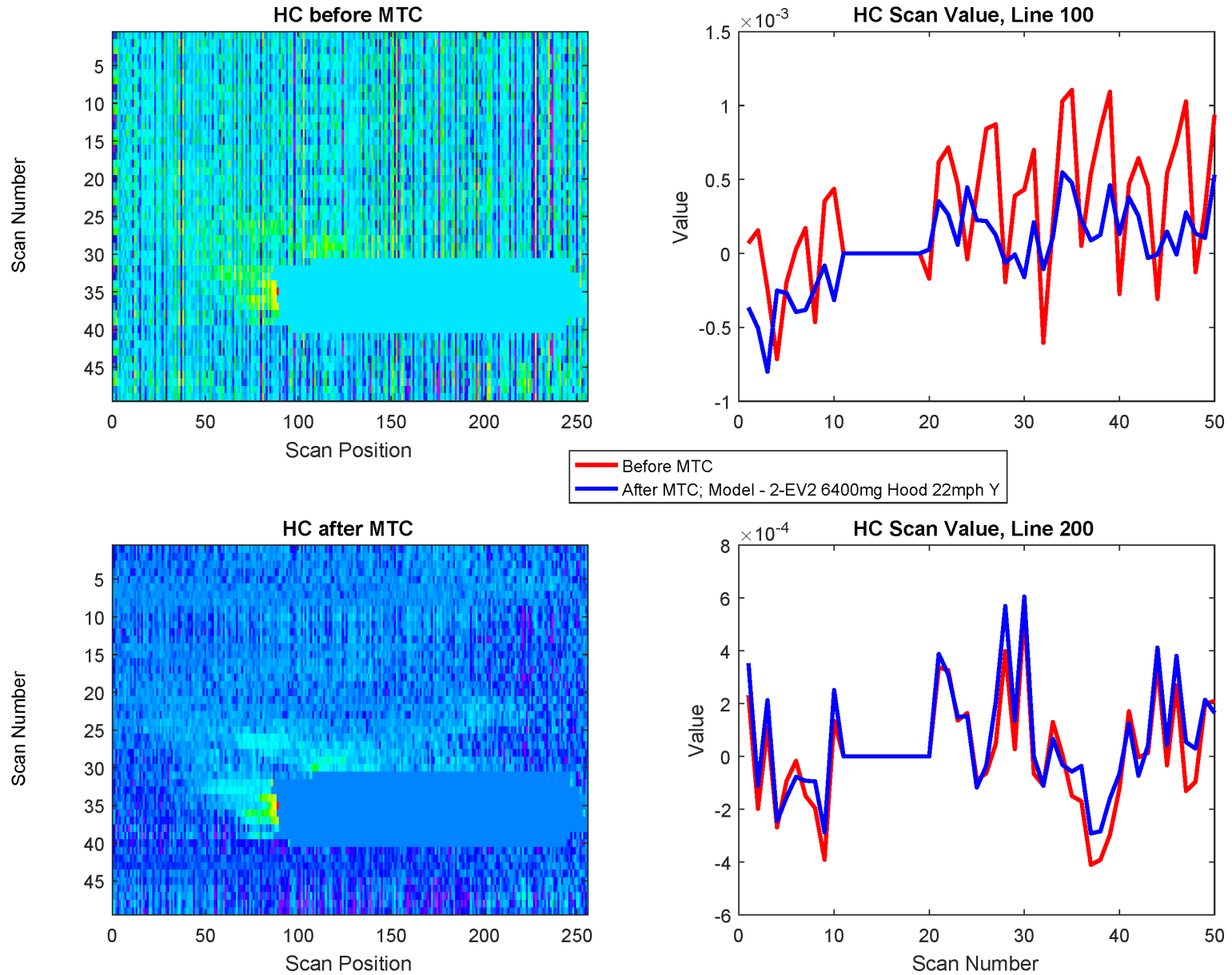
Figure C-12. HC Multi-Tonal Cancellation Example: EV-2, Low EvapHC from DOOR

7 20191024 000514 car 001202
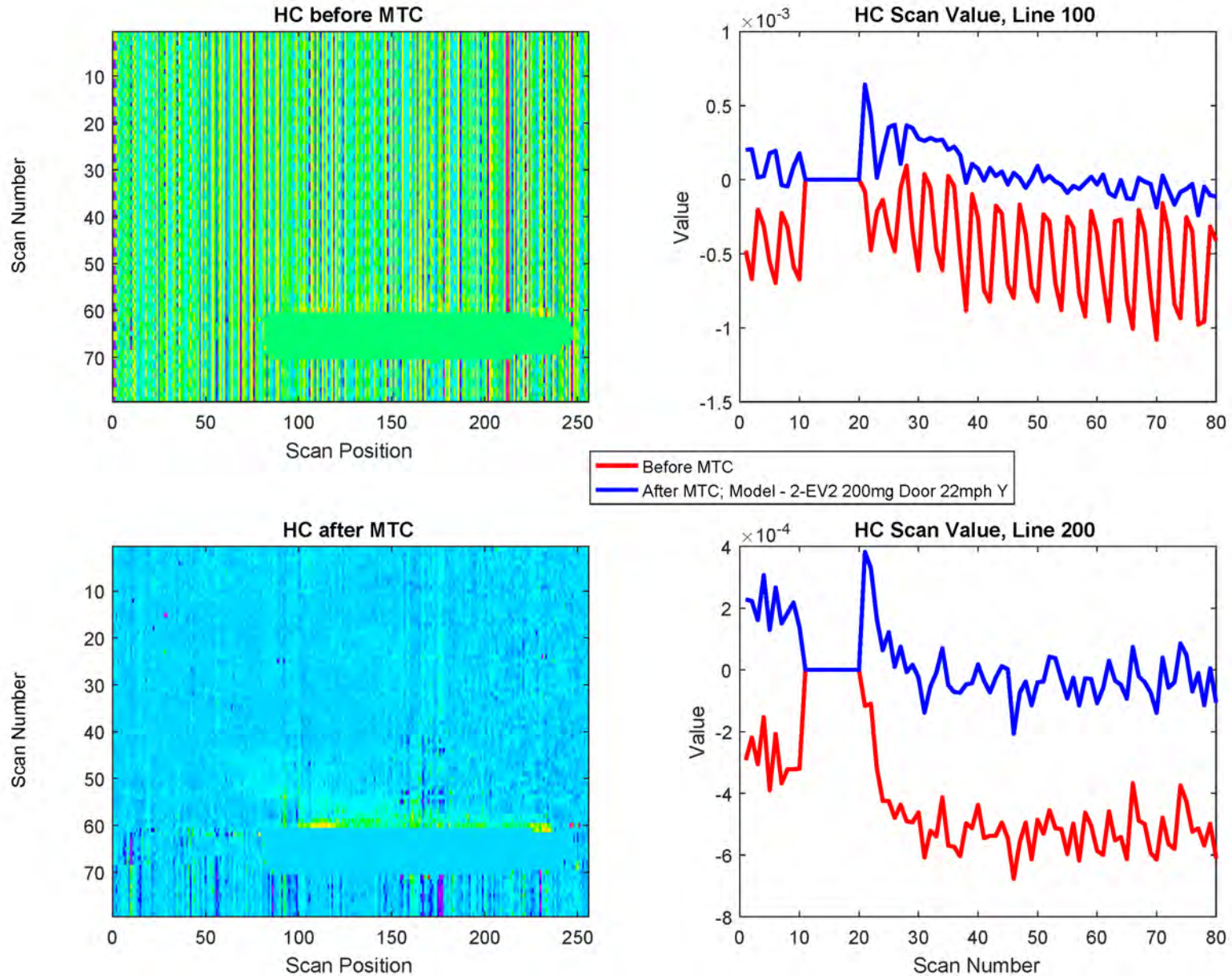
Figure C-13. HC Multi-Tonal Cancellation Example: EV-2, Low EvapHC from TANK

7 20191023 000512 car 002206
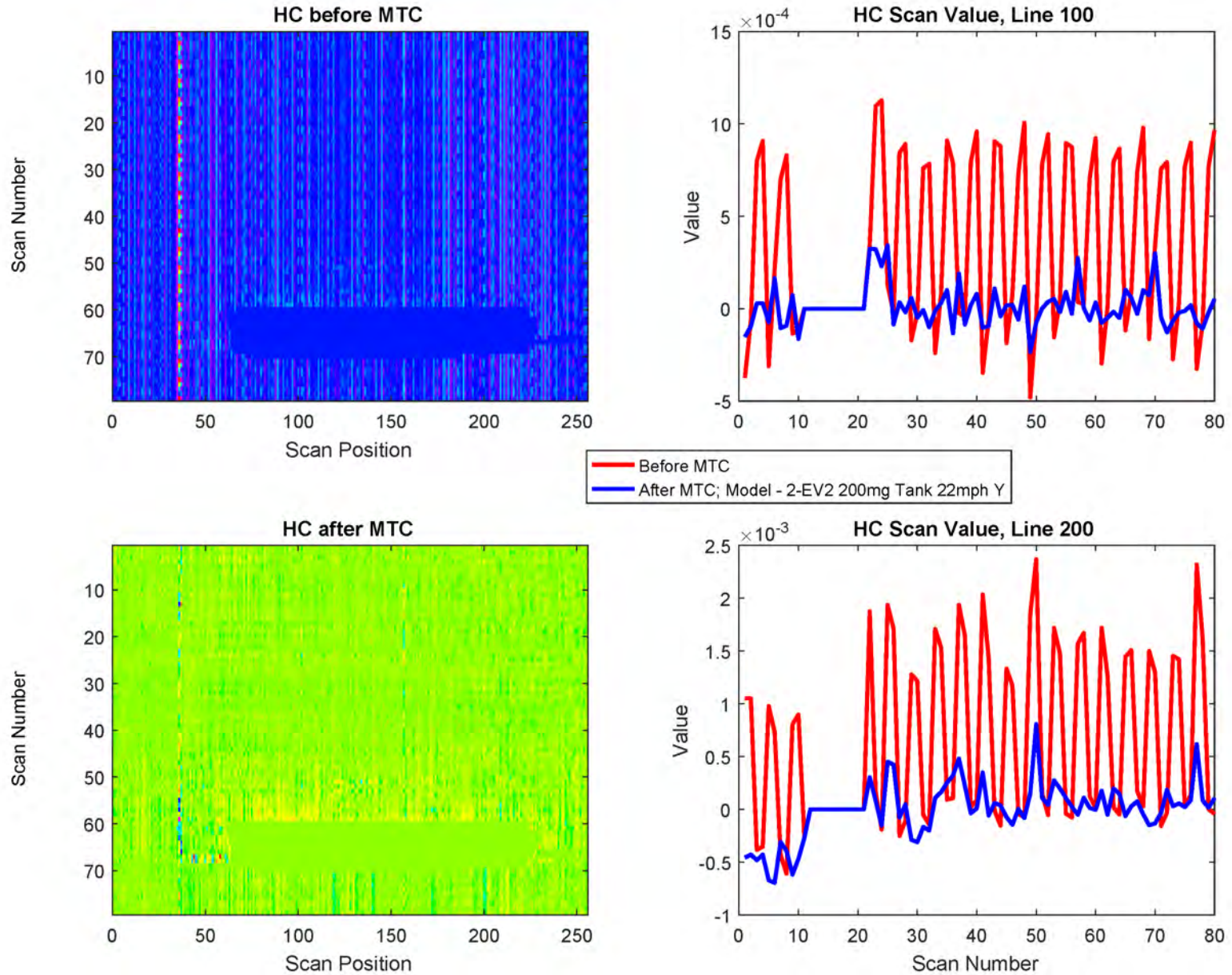
Figure C-14. HC Multi-Tonal Cancellation Example: EV-2, Low EvapHC from HOOD

7 20191024 000514 car 001053
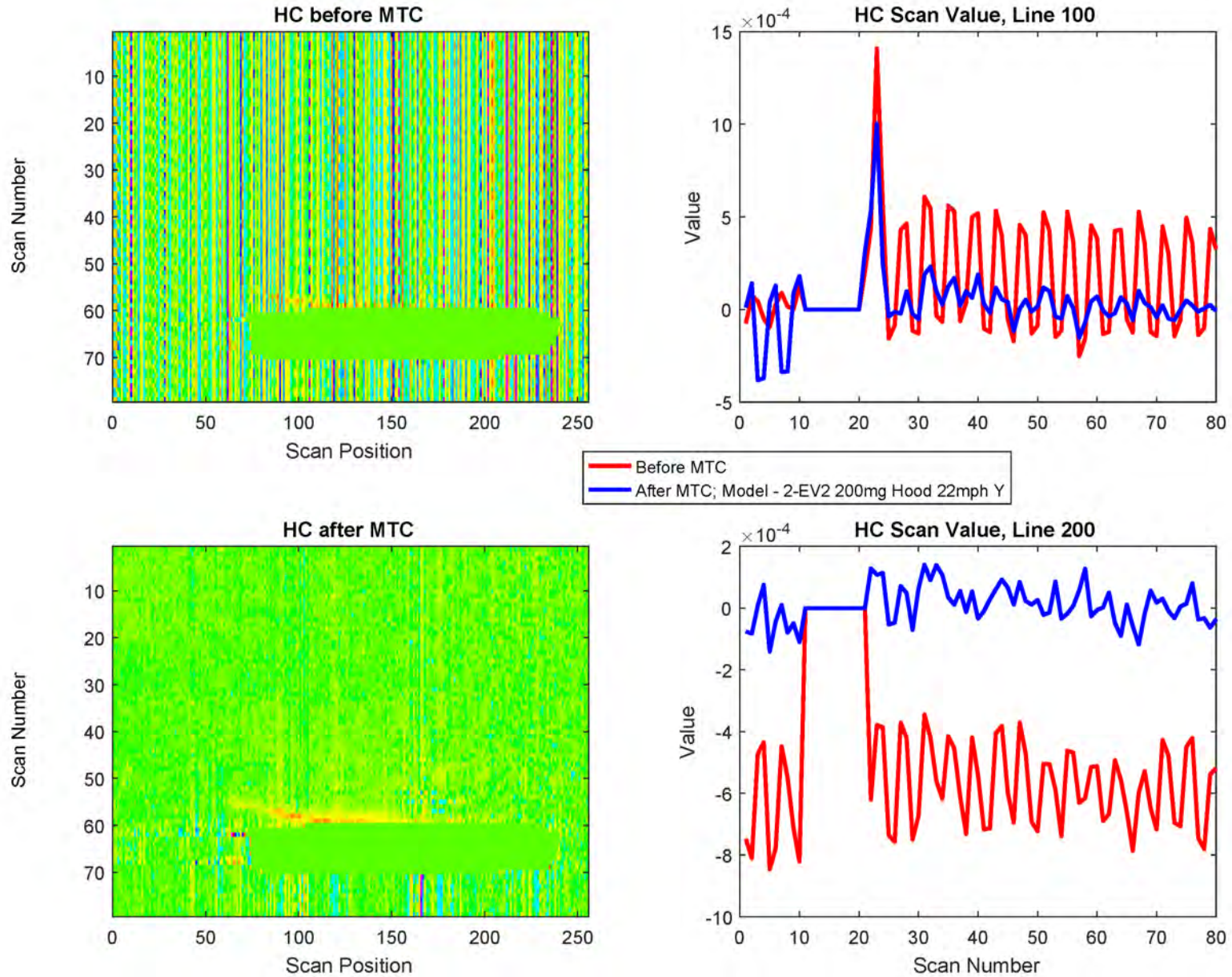
Figure C-15. HC Multi-Tonal Cancellation Example: EV-1, High EvapHC from DOOR

7 20191023 000512 car 001167
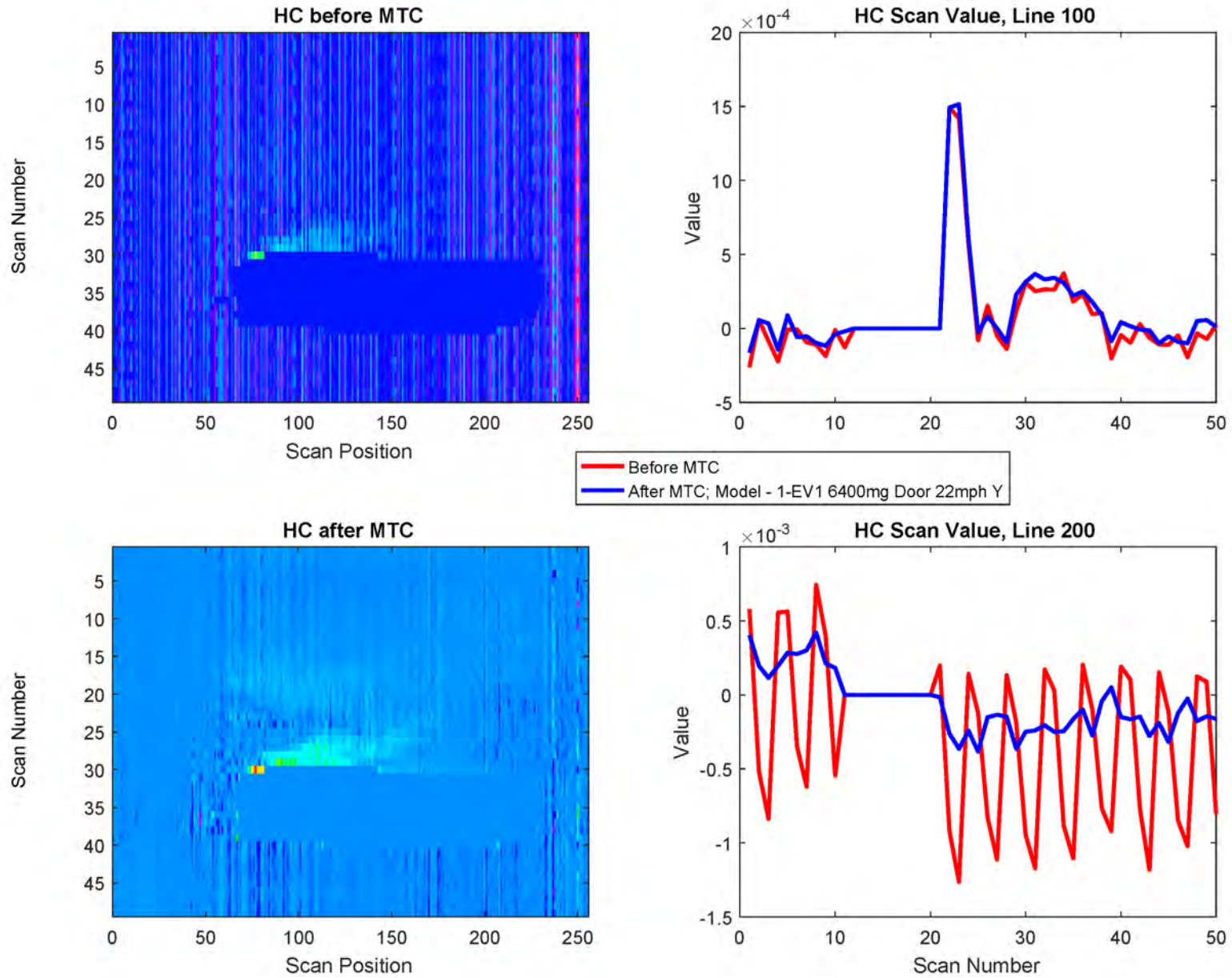
Figure C-16. HC Multi-Tonal Cancellation Example: EV-1, High EvapHC from TANK

7 20191022 000509 car 001451
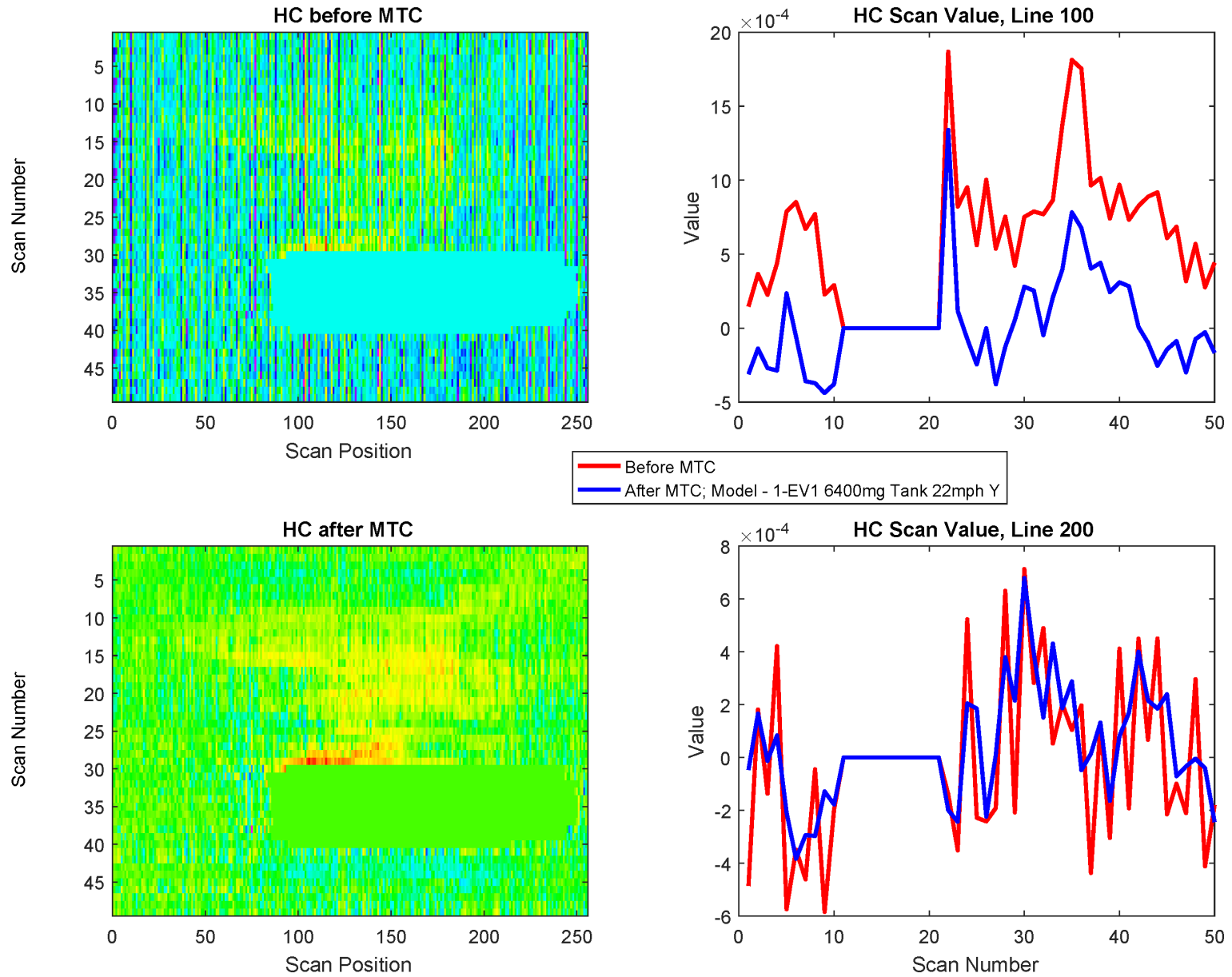
Figure C-17. HC Multi-Tonal Cancellation Example: EV-1, High EvapHC from HOOD

7 20191022 000509 car 002092
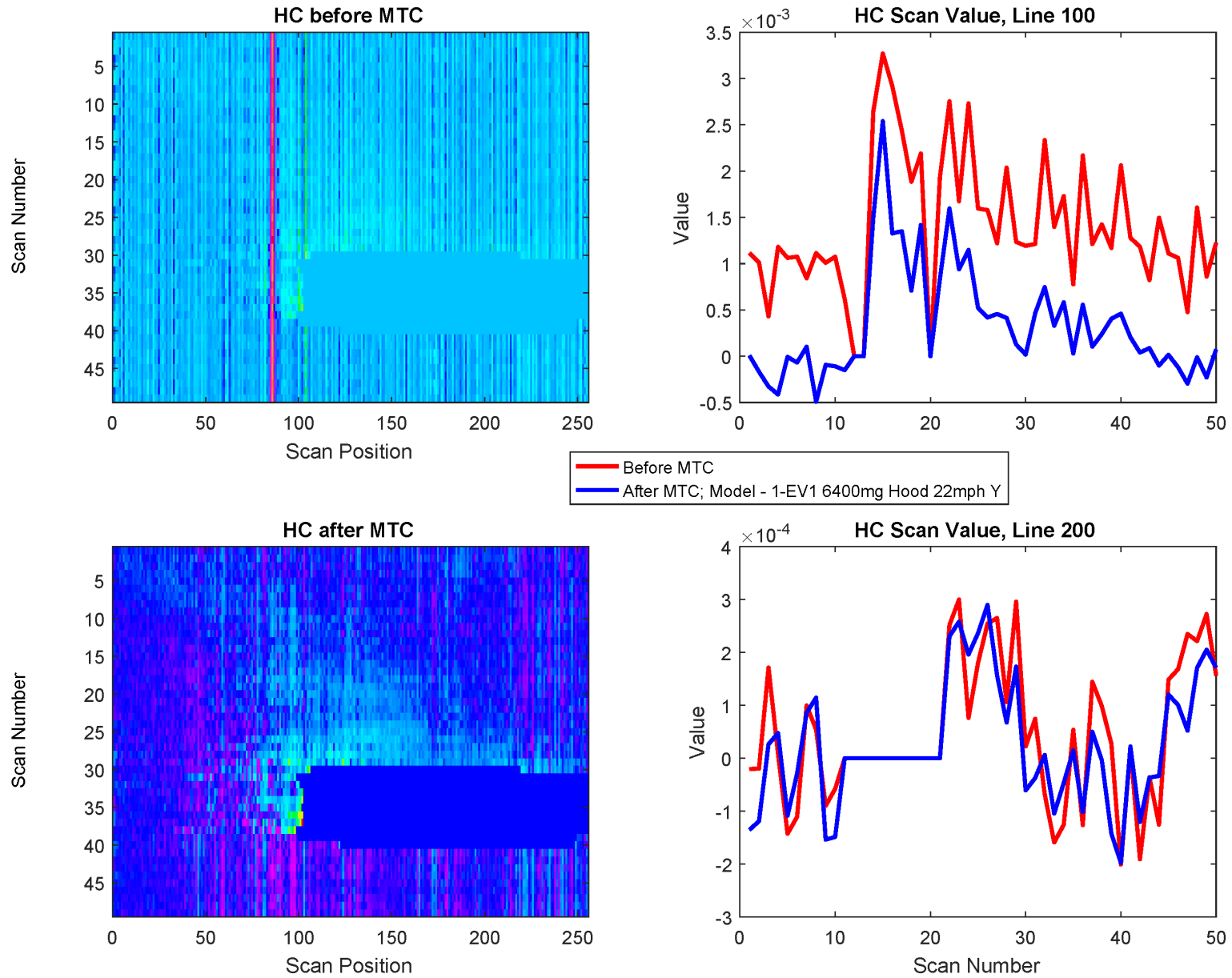
Figure C-18. HC Multi-Tonal Cancellation Example: EV-1, Low EvapHC from DOOR

7 20191020 000506 car 000108
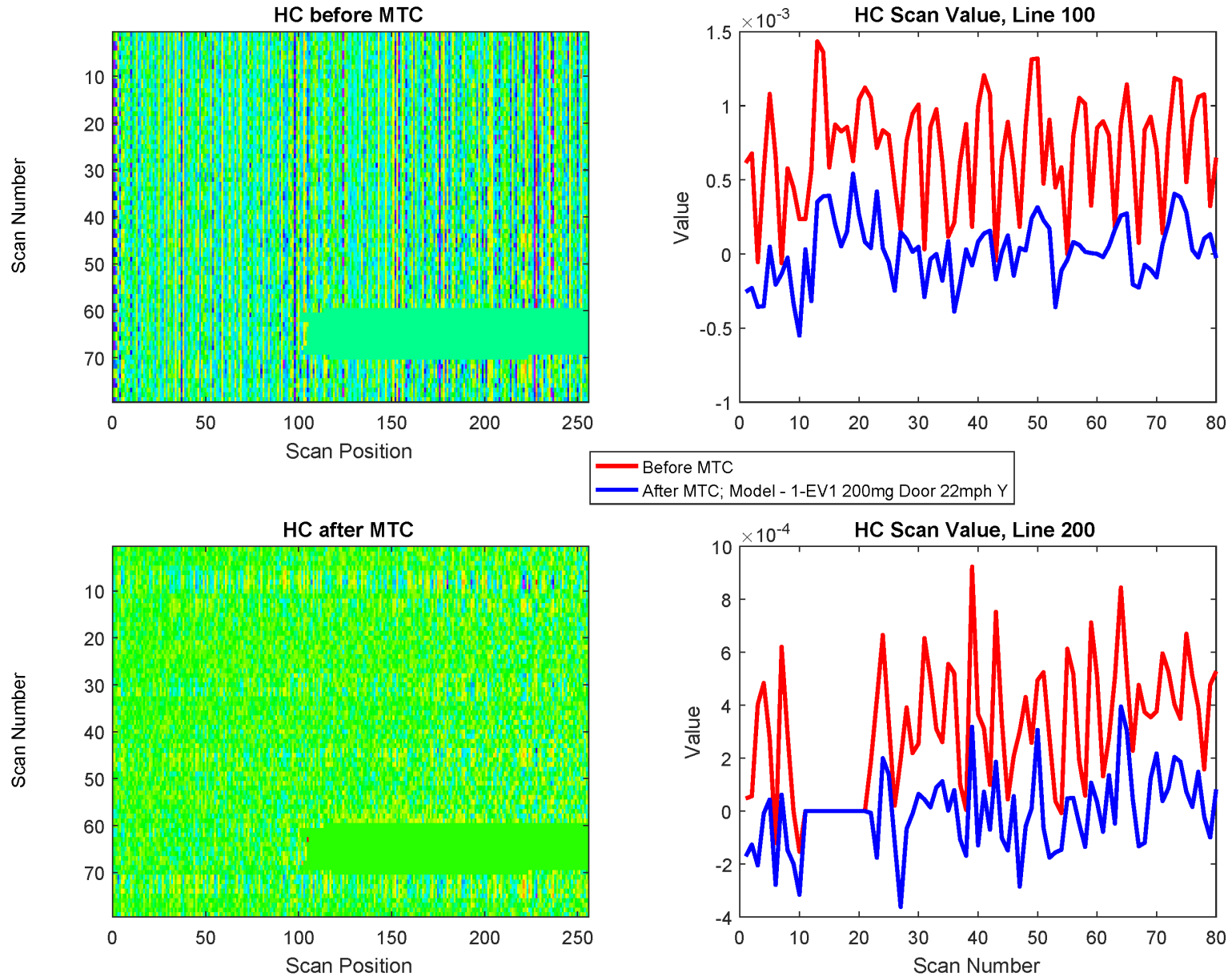
Figure C-19. HC Multi-Tonal Cancellation Example: EV-1, Low EvapHC from TANK

7 20191021 000507 car 002354
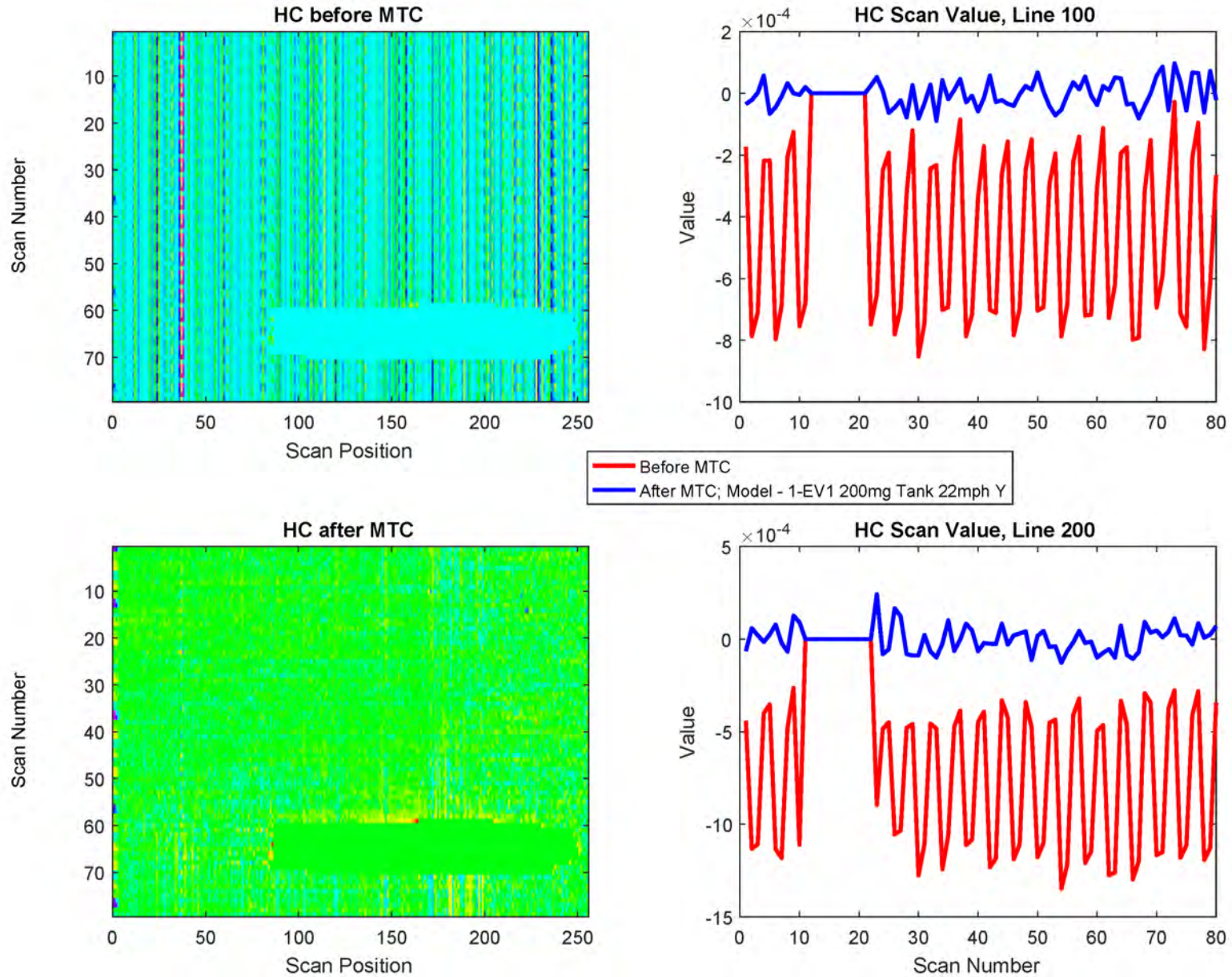
Figure C-20. HC Multi-Tonal Cancellation Example: EV-1, Low EvapHC from HOOD

7 20191020 000505 car 002864
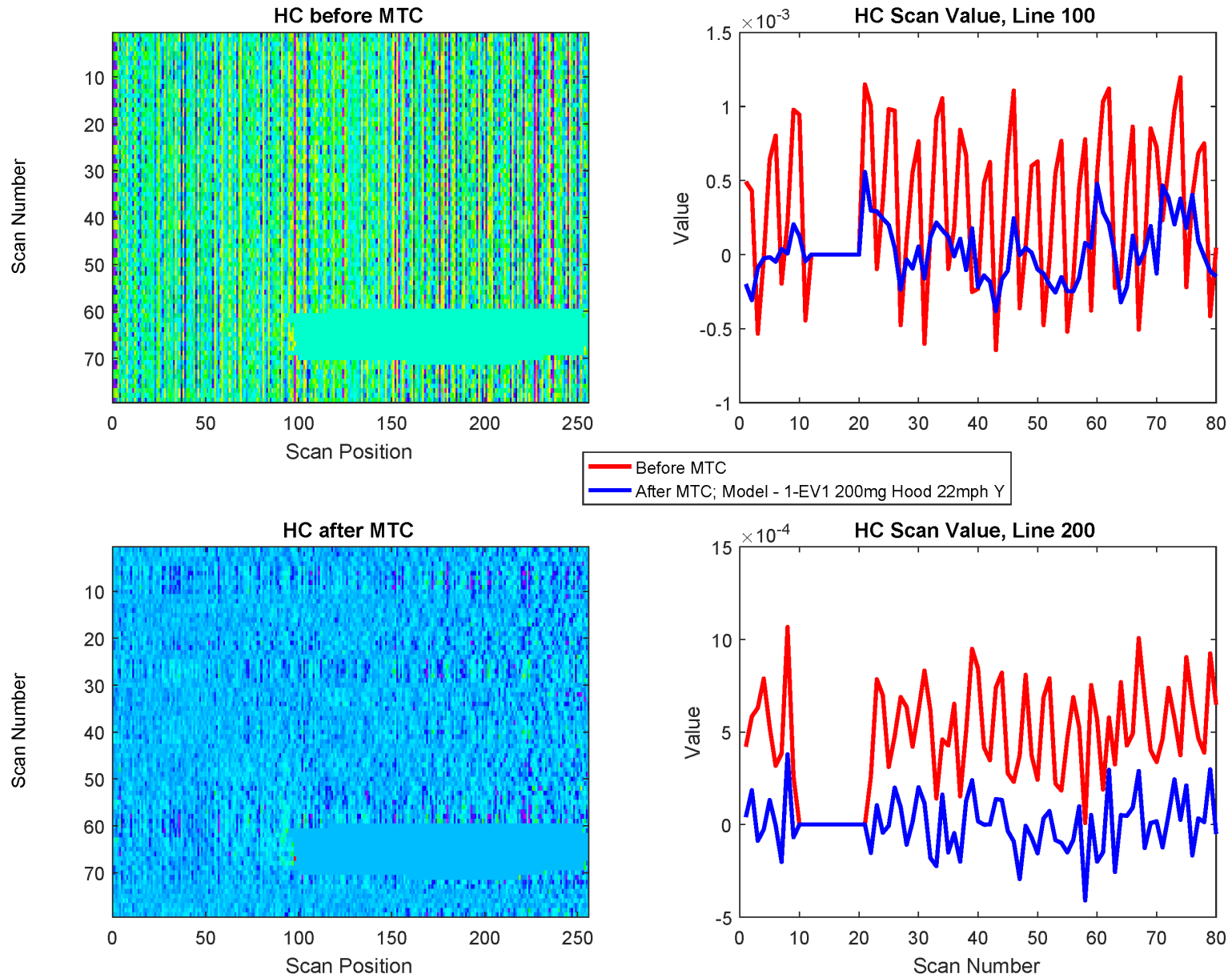
Figure C-21. Before (top) and After (bottom) Adaptive Notch Filtering. Example: EV-2, High EvapHC from DOOR
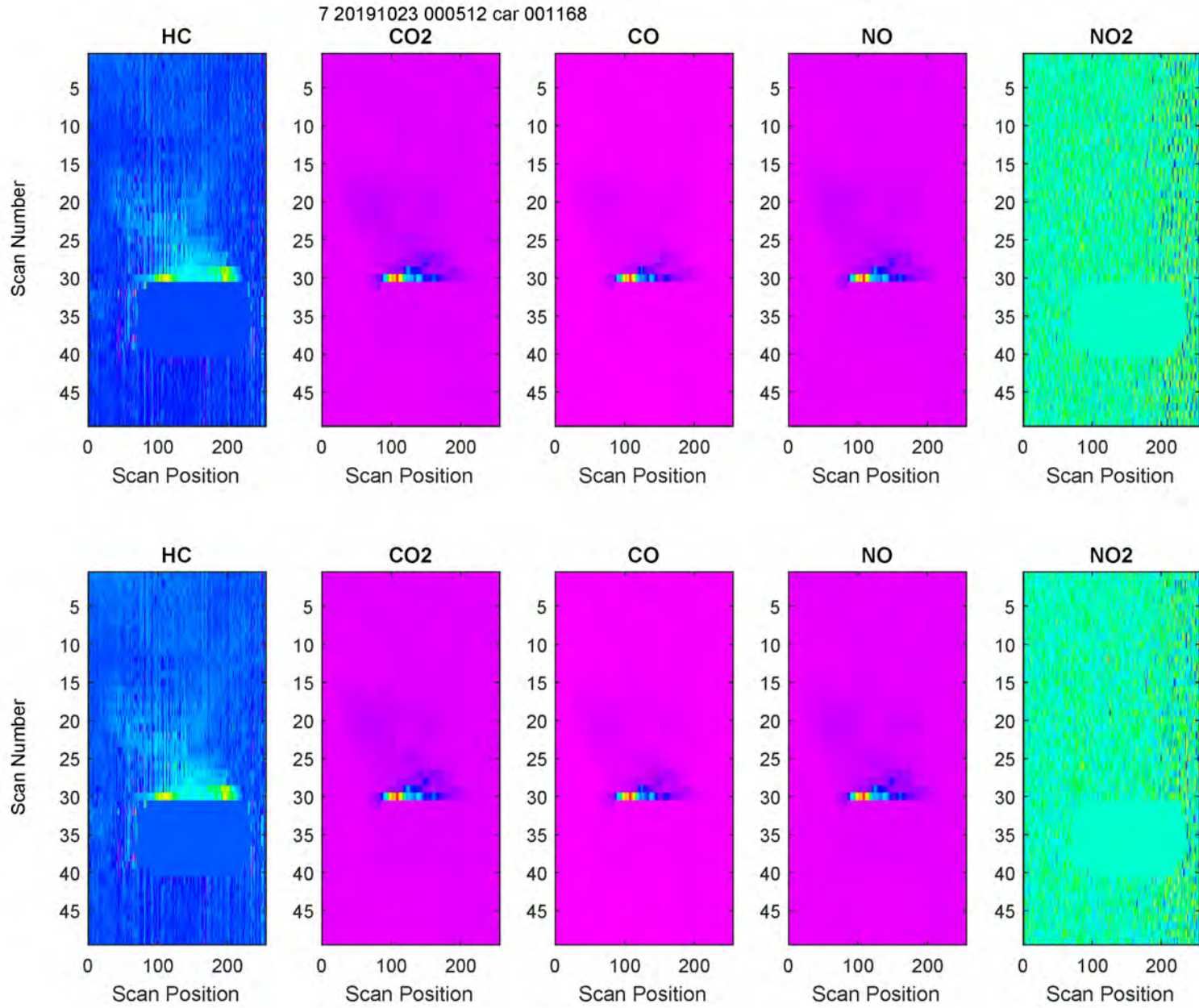
Figure C-22. Before (top) and After (bottom) Adaptive Notch Filtering. Example: EV-2, High EvapHC from TANK
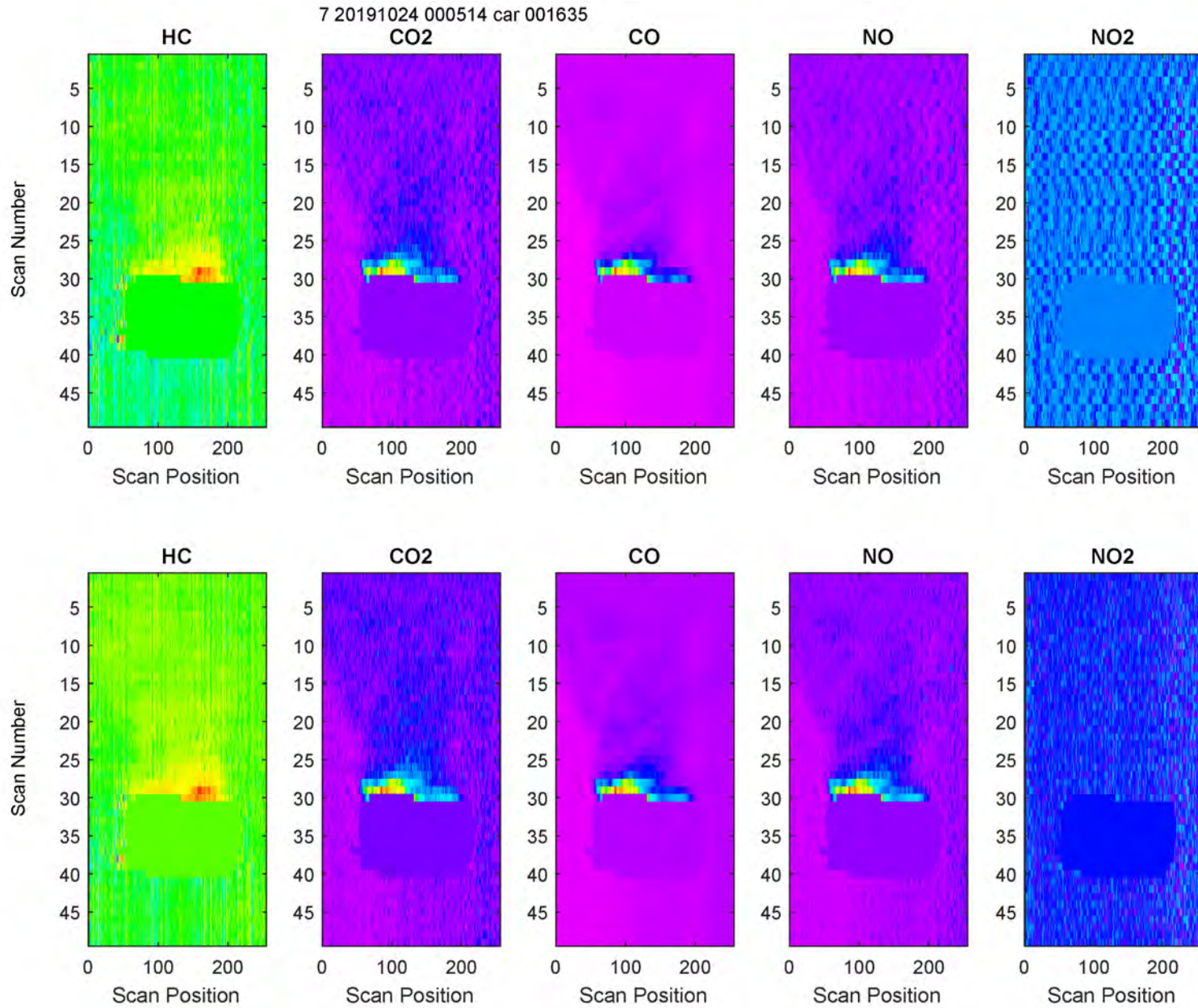
Figure C-23. Before (top) and After (bottom) Adaptive Notch Filtering. Example: EV-2, High EvapHC from HOOD

7 20191020 000505 car 001813
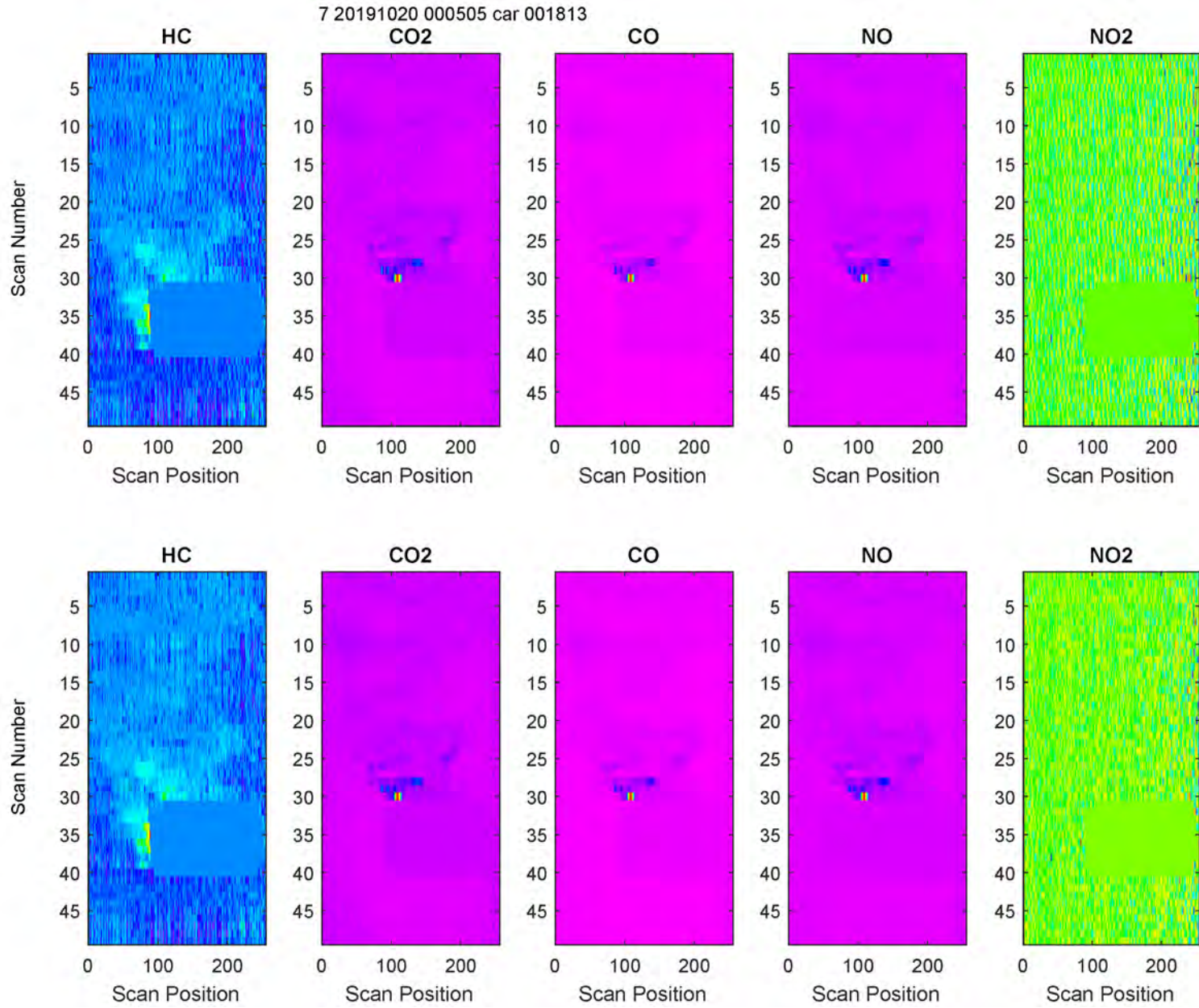
Figure C-24. Before (top) and After (bottom) Adaptive Notch Filtering. Example: EV-2, Low EvapHC from DOOR
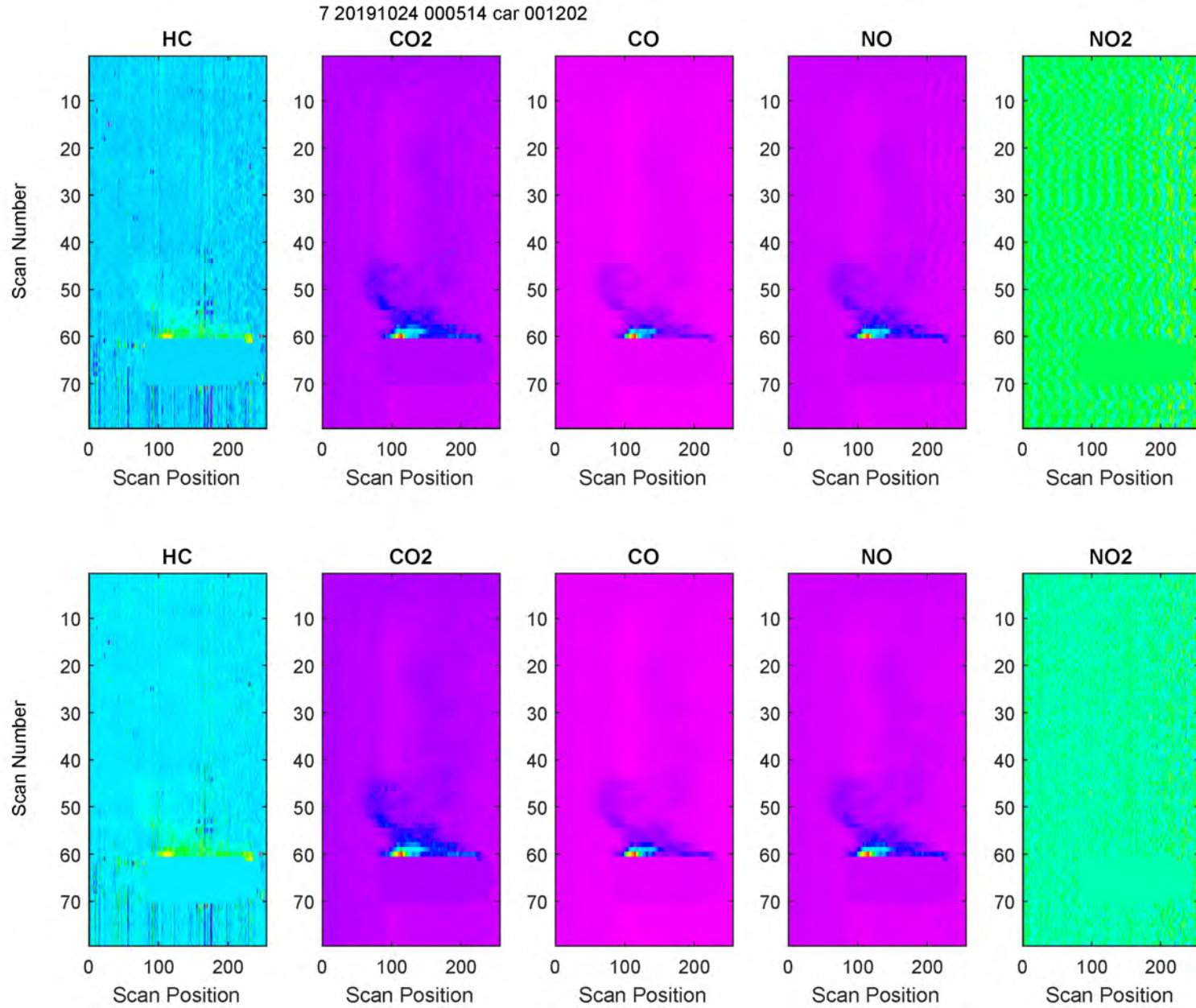
Figure C-25. Before (top) and After (bottom) Adaptive Notch Filtering. Example: EV-2, Low EvapHC from TANK

7 20191023 000512 car 002206
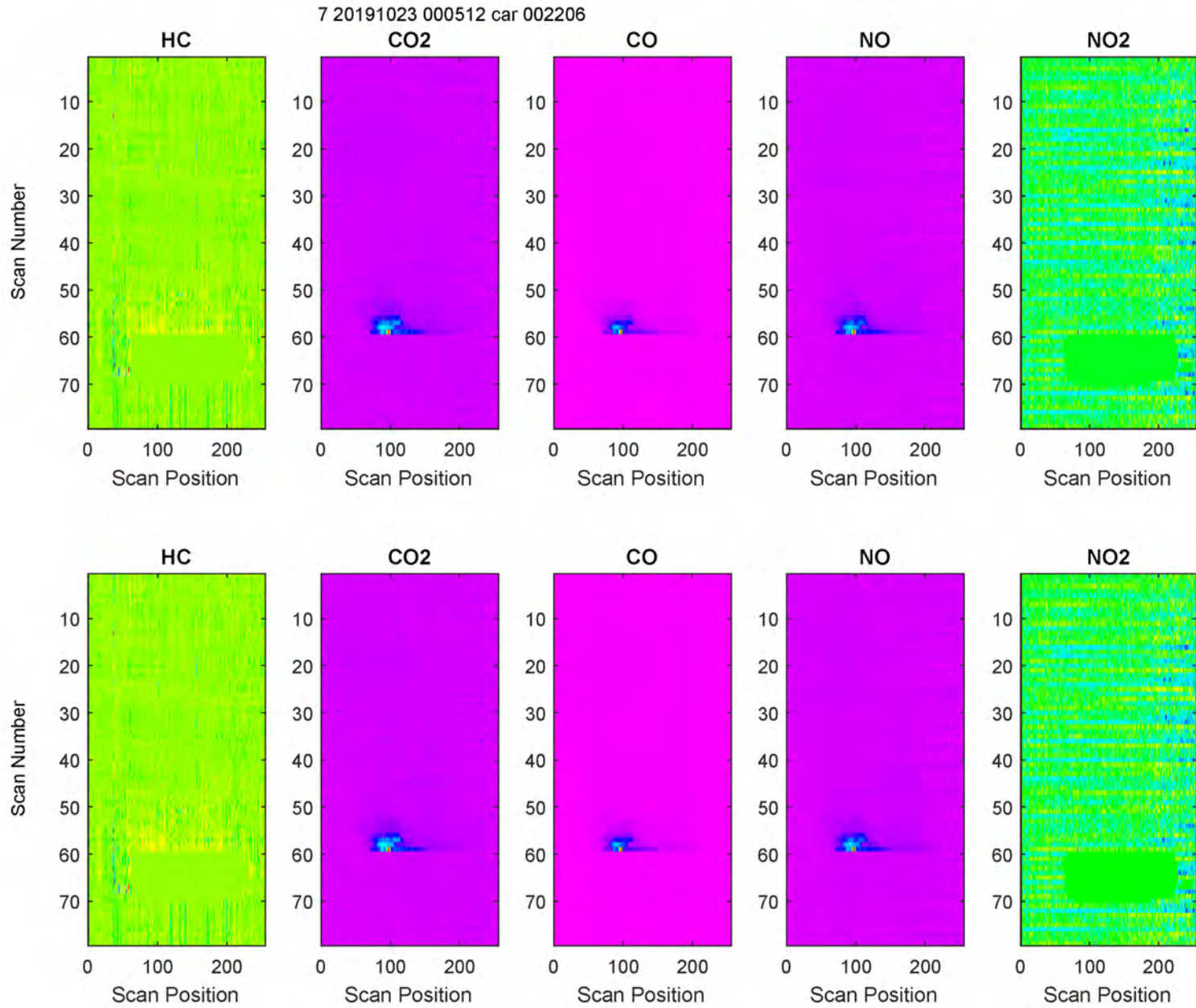
Figure C-26. Before (top) and After (bottom) Adaptive Notch Filtering. Example: EV-2, Low EvapHC from HOOD

7 20191024 000514 car 001053
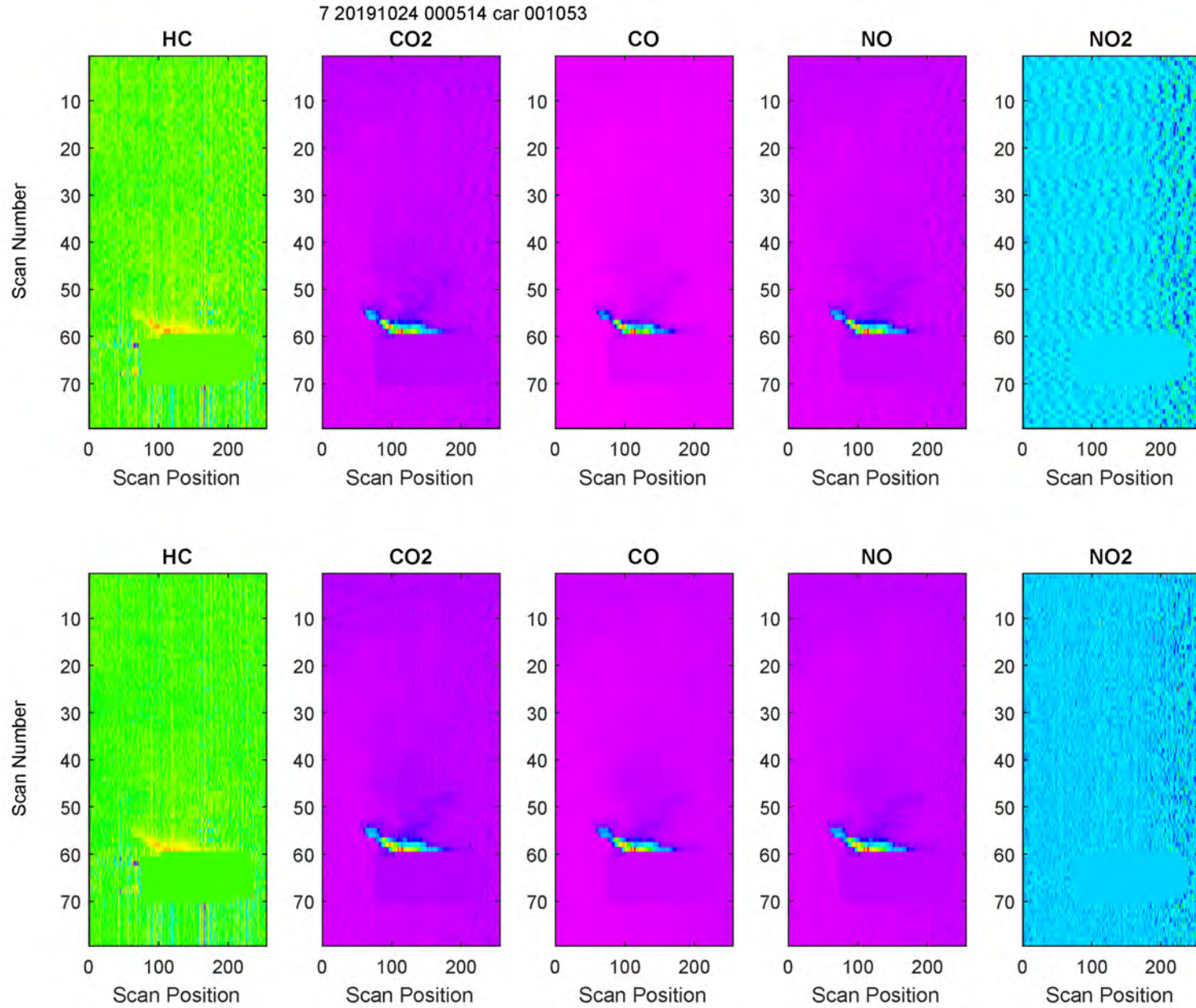
Figure C-27. Before (top) and After (bottom) Adaptive Notch Filtering. Example: EV-1, High EvapHC from DOOR

7 20191023 000512 car 001167
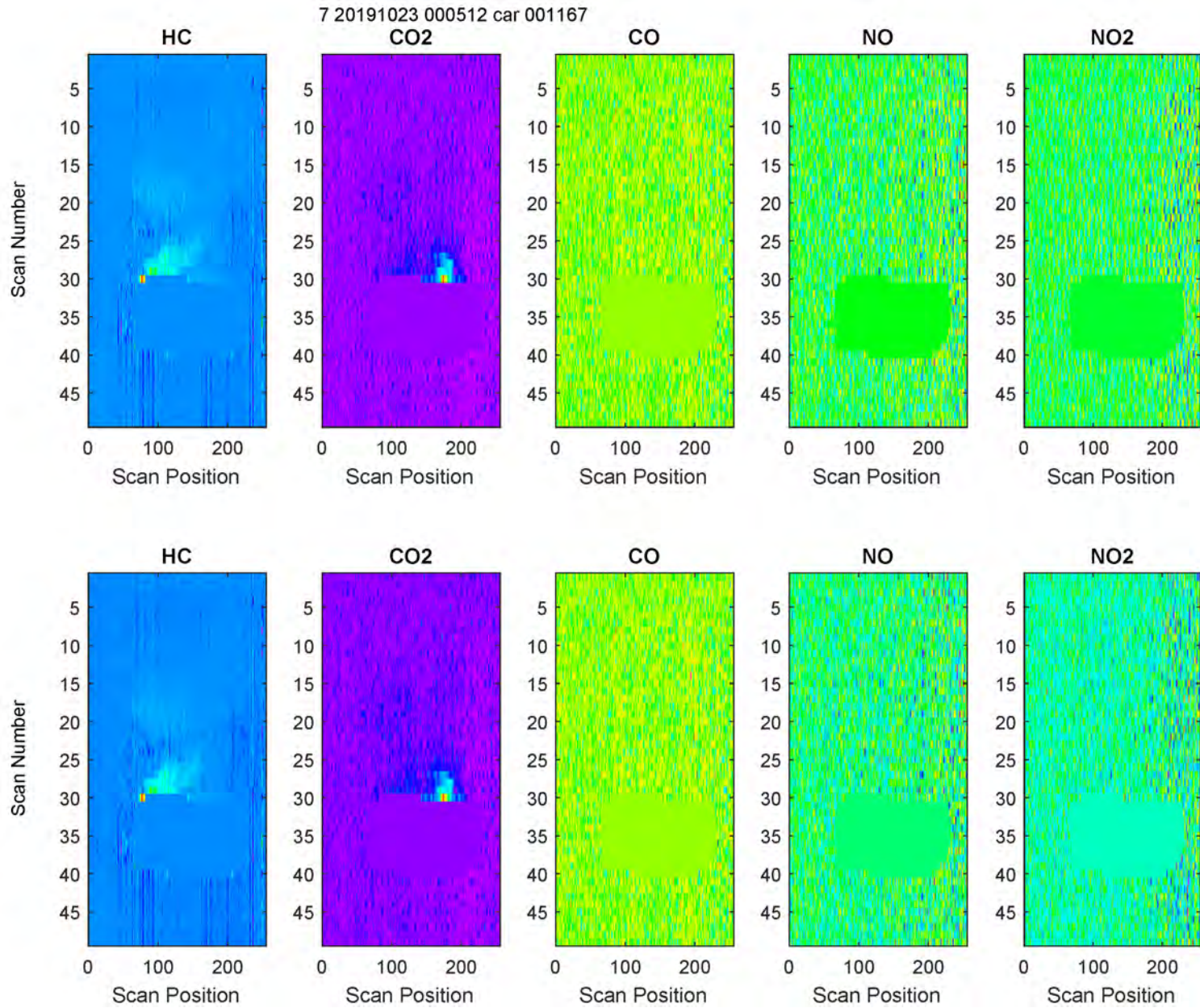
Figure C-28. Before (top) and After (bottom) Adaptive Notch Filtering. Example: EV-1, High EvapHC from TANK

7 20191022 000509 car 001451
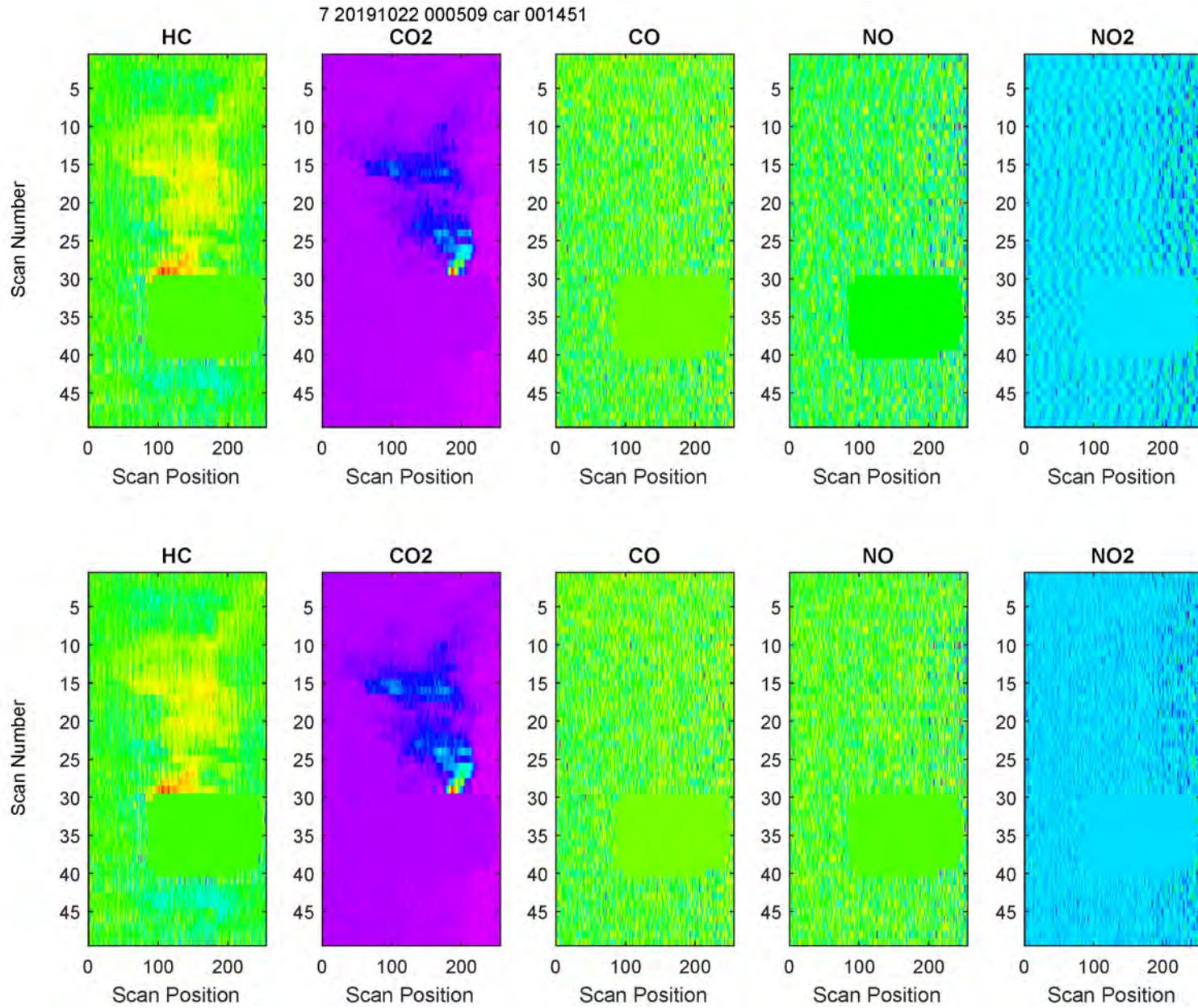
Figure C-29. Before (top) and After (bottom) Adaptive Notch Filtering. Example: EV-1, High EvapHC from HOOD
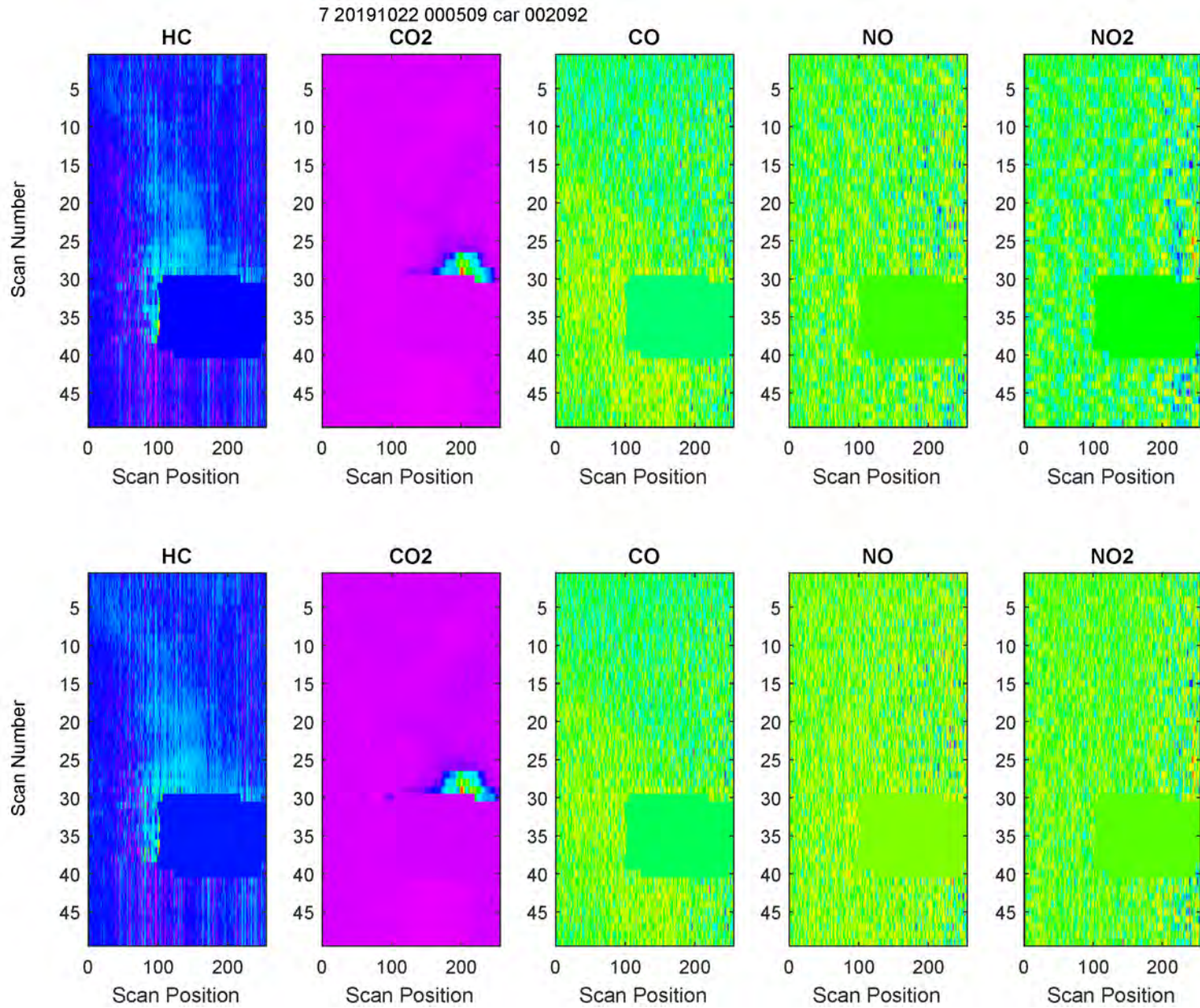
Figure C-30. Before (top) and After (bottom) Adaptive Notch Filtering. Example: EV-1, Low EvapHC from DOOR

7 20191020 000506 car 000108
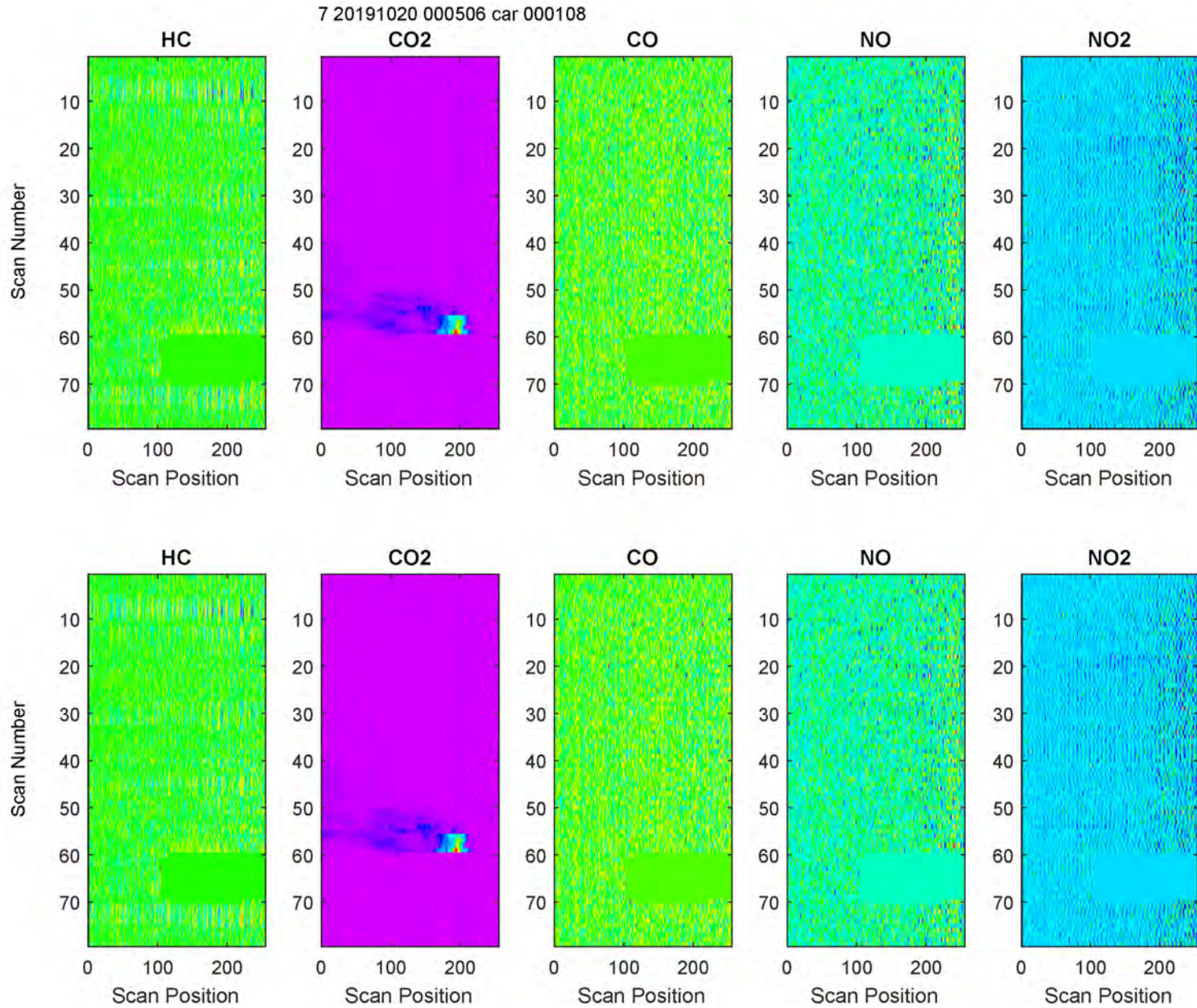
Figure C-31. Before (top) and After (bottom) Adaptive Notch Filtering. Example: EV-1, Low EvapHC from TANK

7 20191021 000507 car 002354
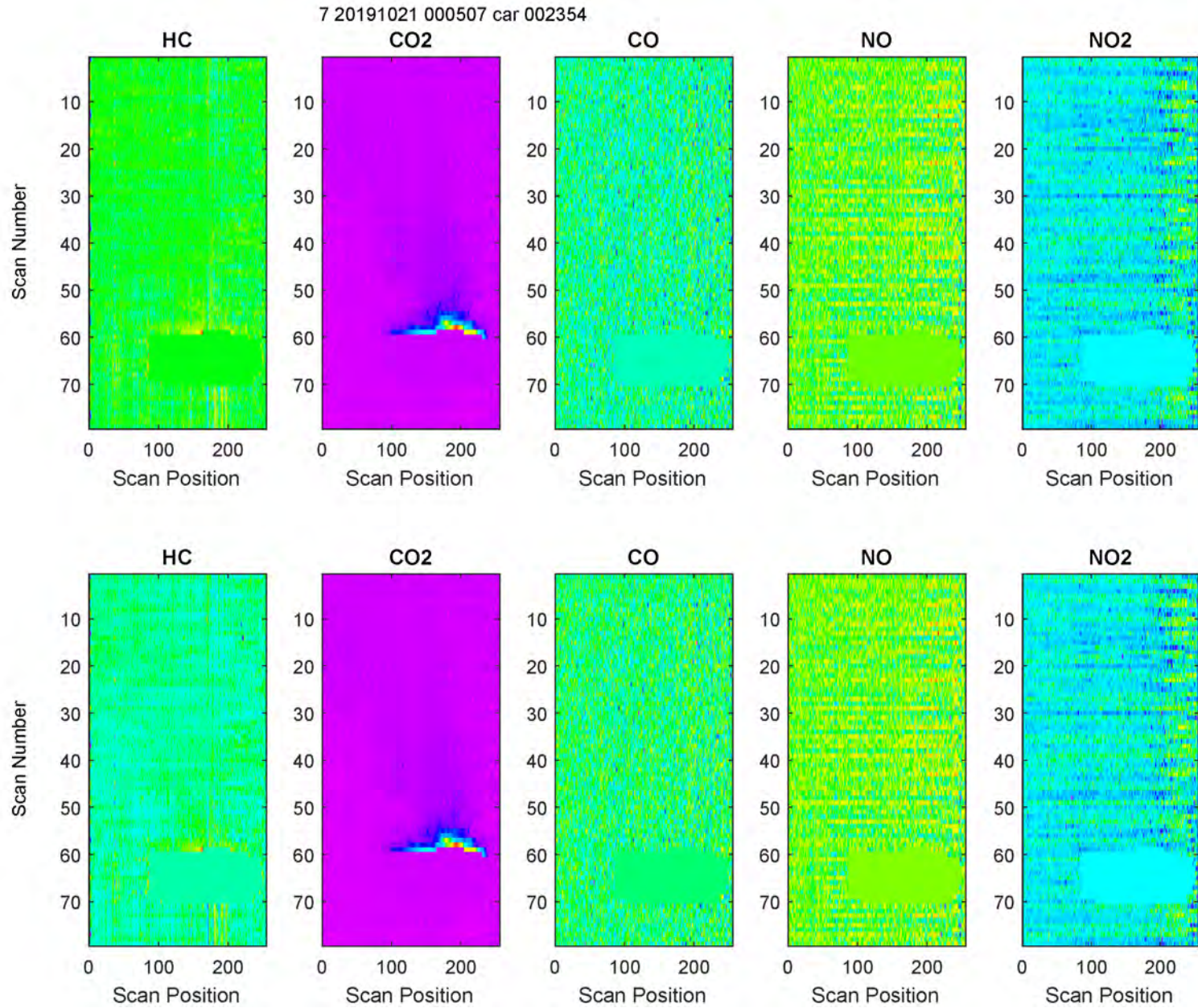
Figure C-32. Before (top) and After (bottom) Adaptive Notch Filtering. Example: EV-1, Low EvapHC from HOOD

7 20191020 000505 car 002864
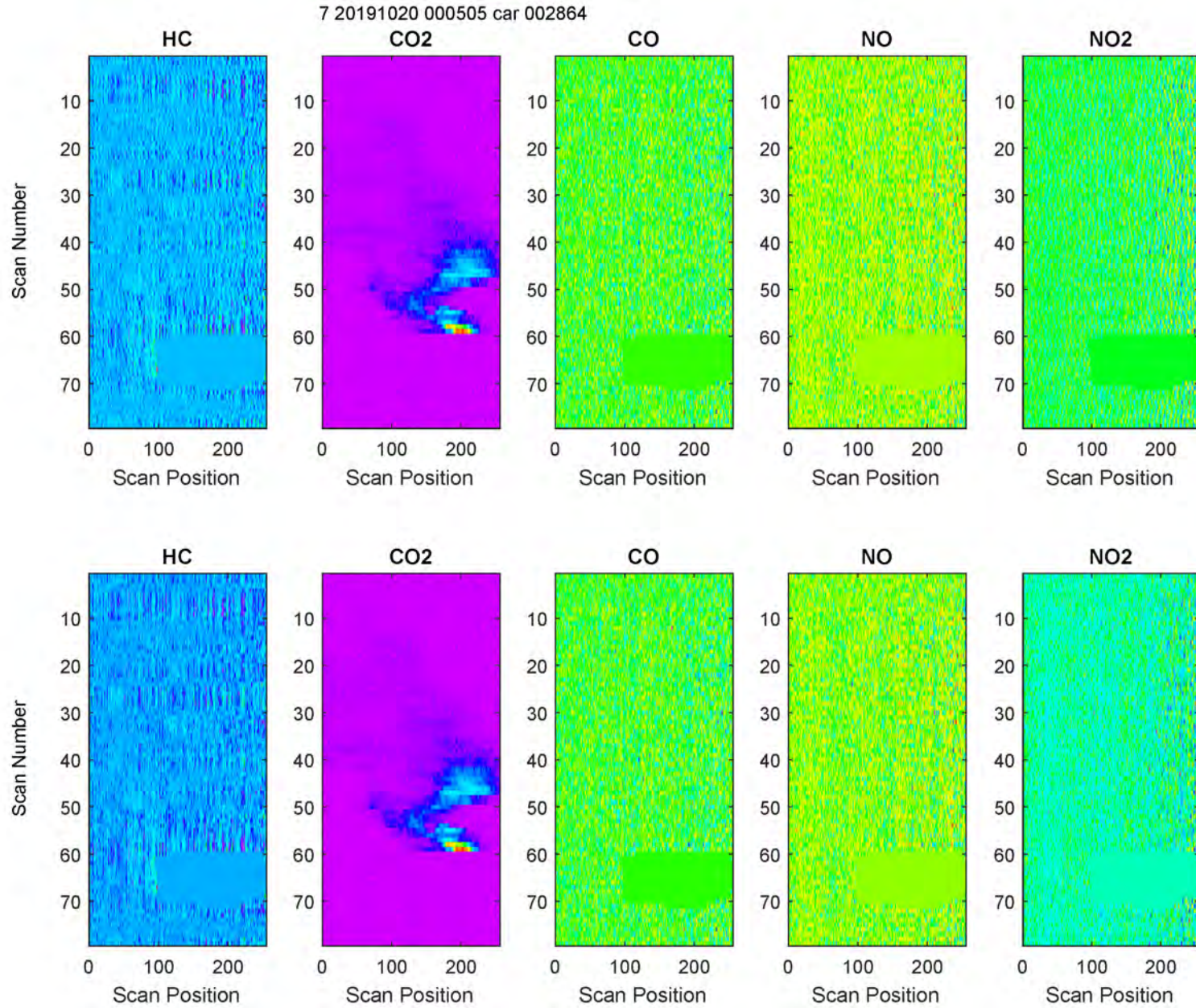
Figure C-33. ZigZag Interpolation Example: EV-2, High EvapHC from DOOR

7 20191023 000512 car 001168
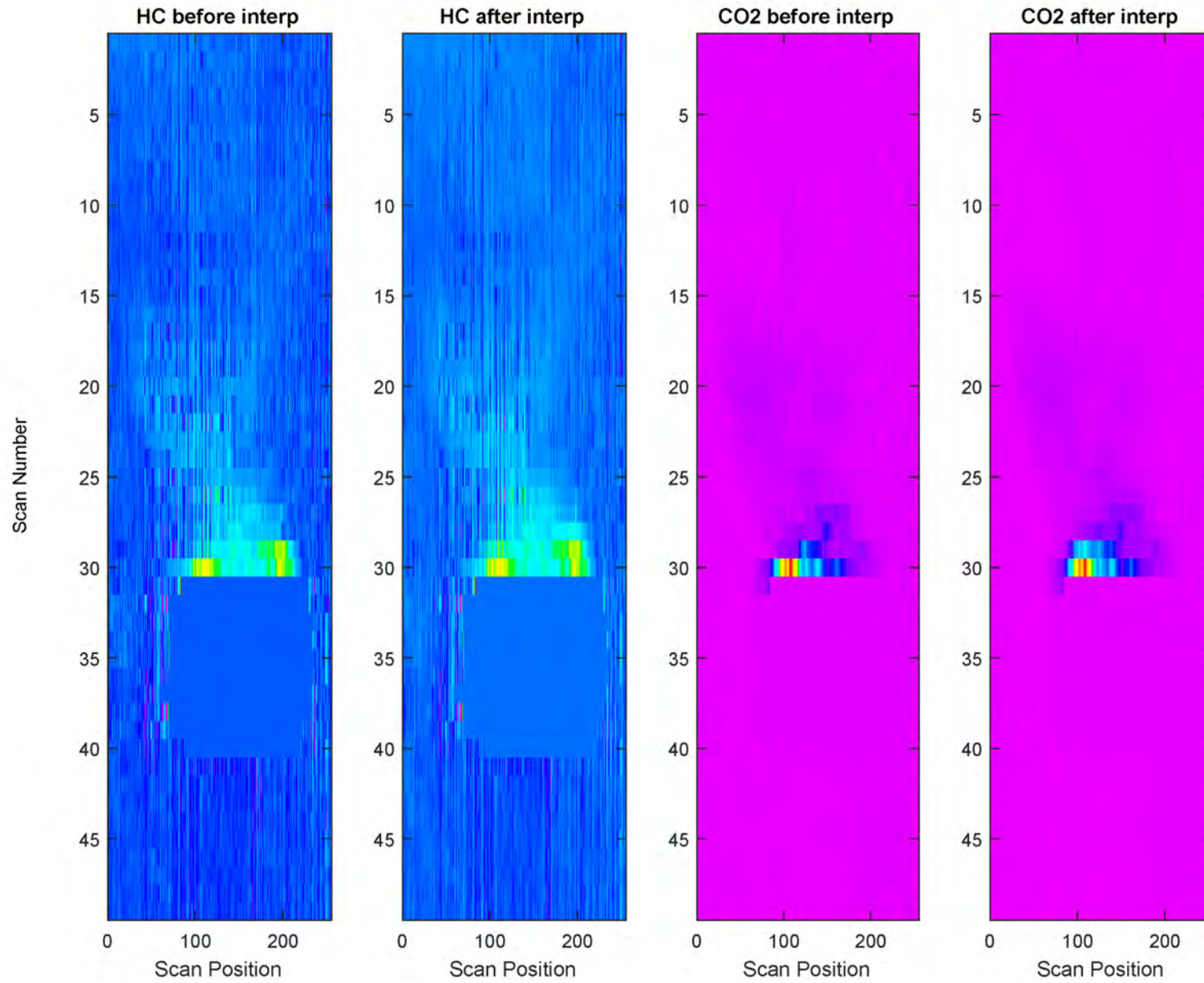
Figure C-34. ZigZag Interpolation Example: EV-2, High EvapHC from TANK

7 20191024 000514 car 001635
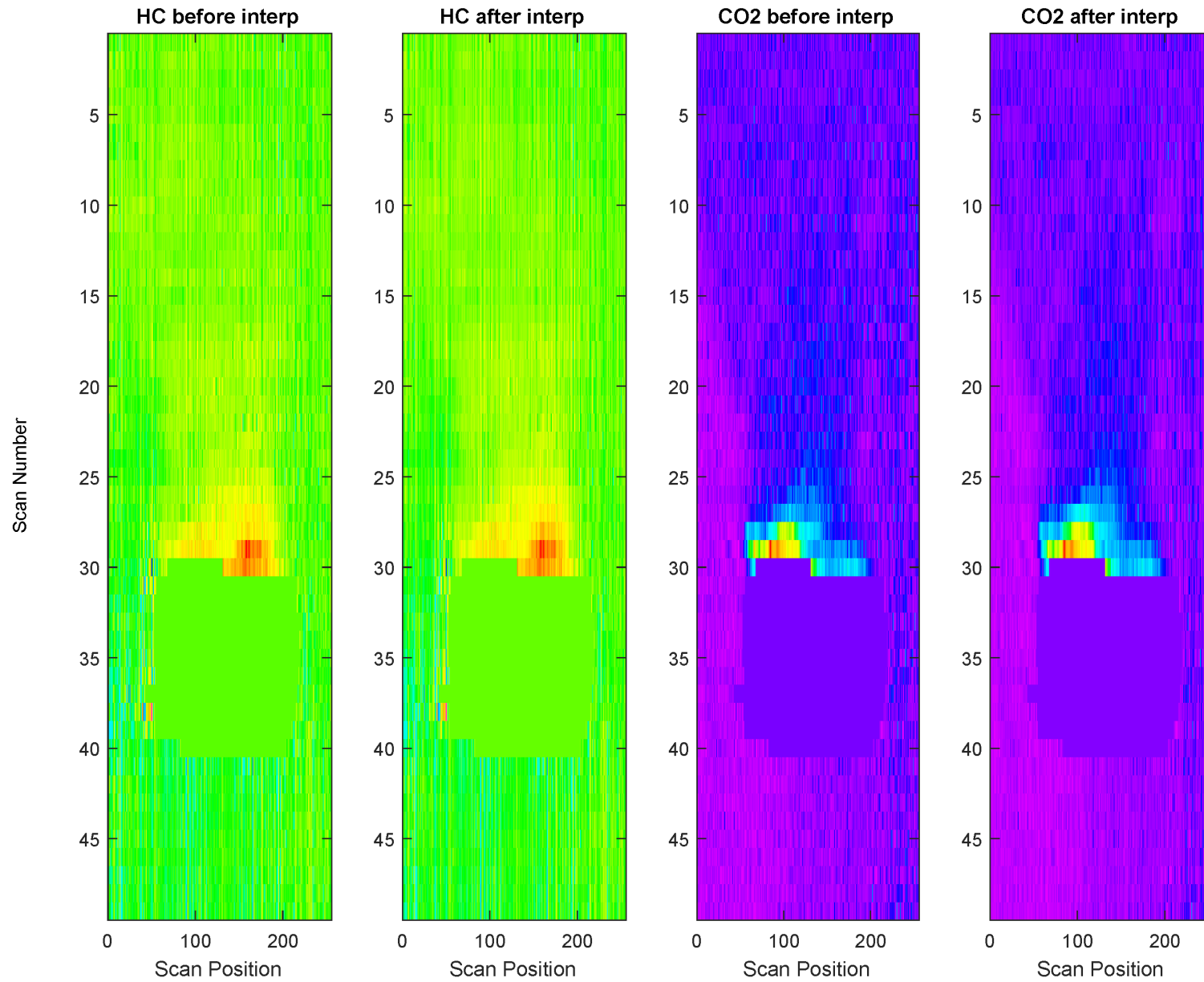
Figure C-35. ZigZag Interpolation Example: EV-2, High EvapHC from HOOD

7 20191020 000505 car 001813
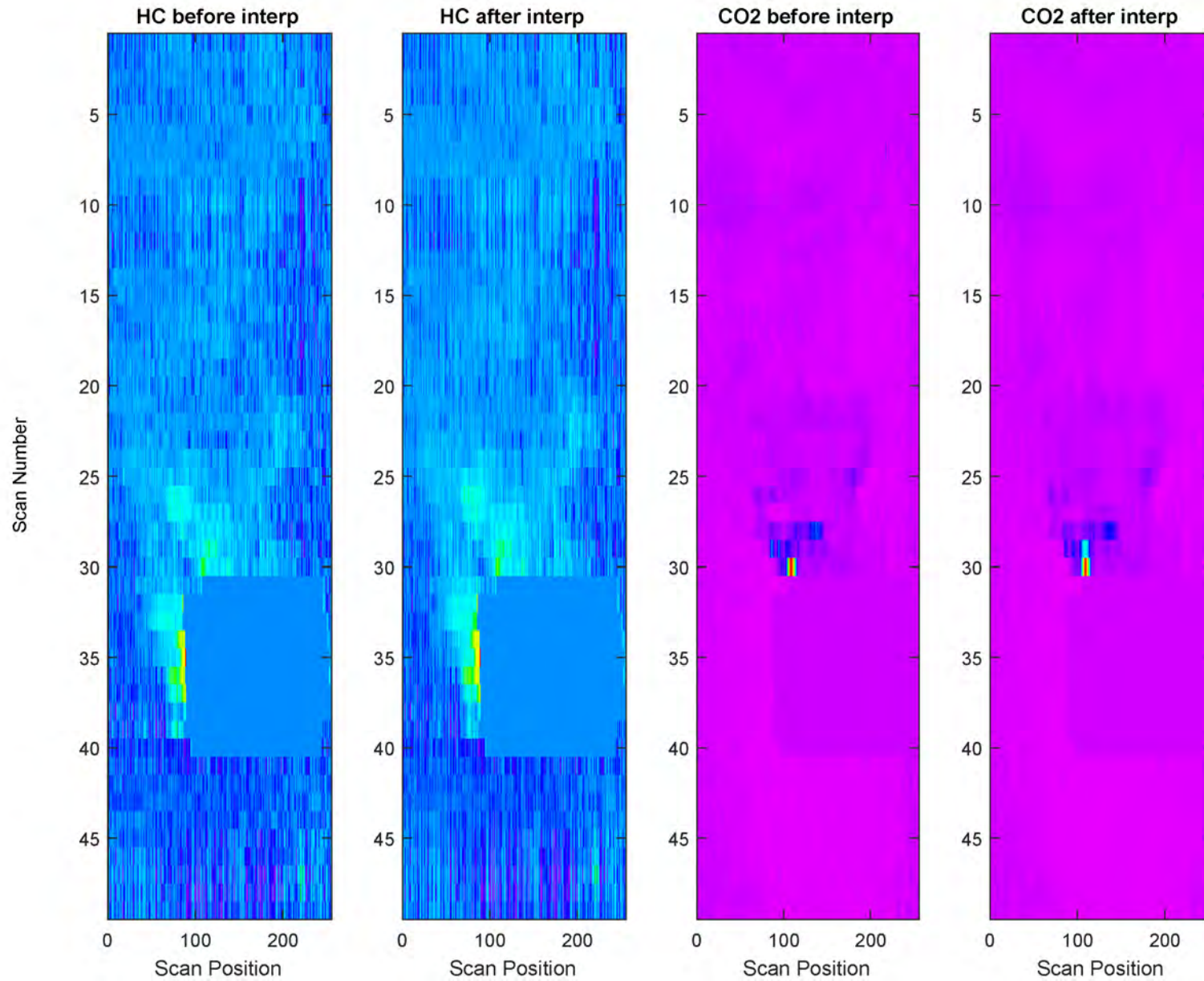
Figure C-36. ZigZag Interpolation Example: EV-2, Low EvapHC from DOOR

7 20191024 000514 car 001202
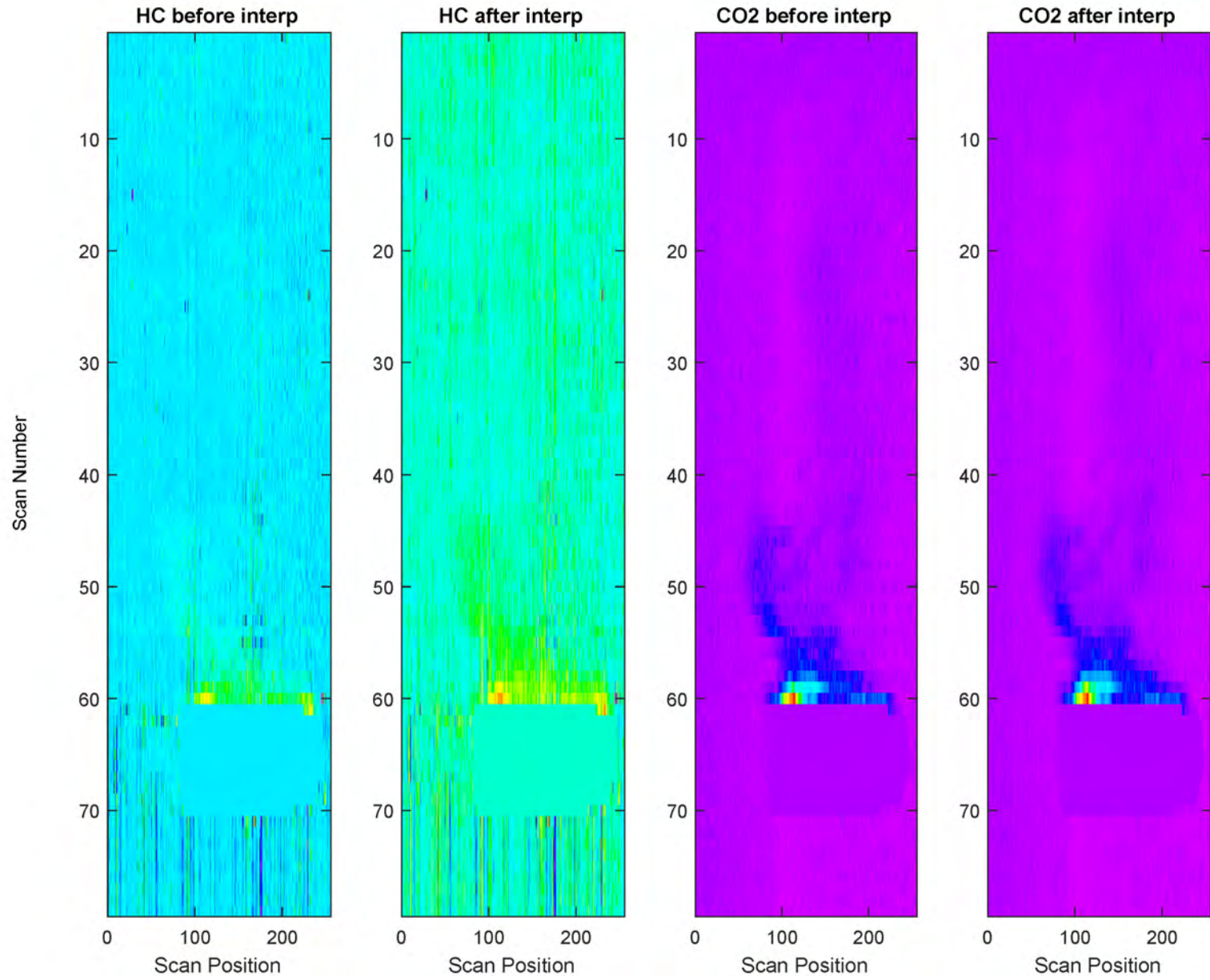
Figure C-37. ZigZag Interpolation Example: EV-2, Low EvapHC from TANK

7 20191023 000512 car 002206
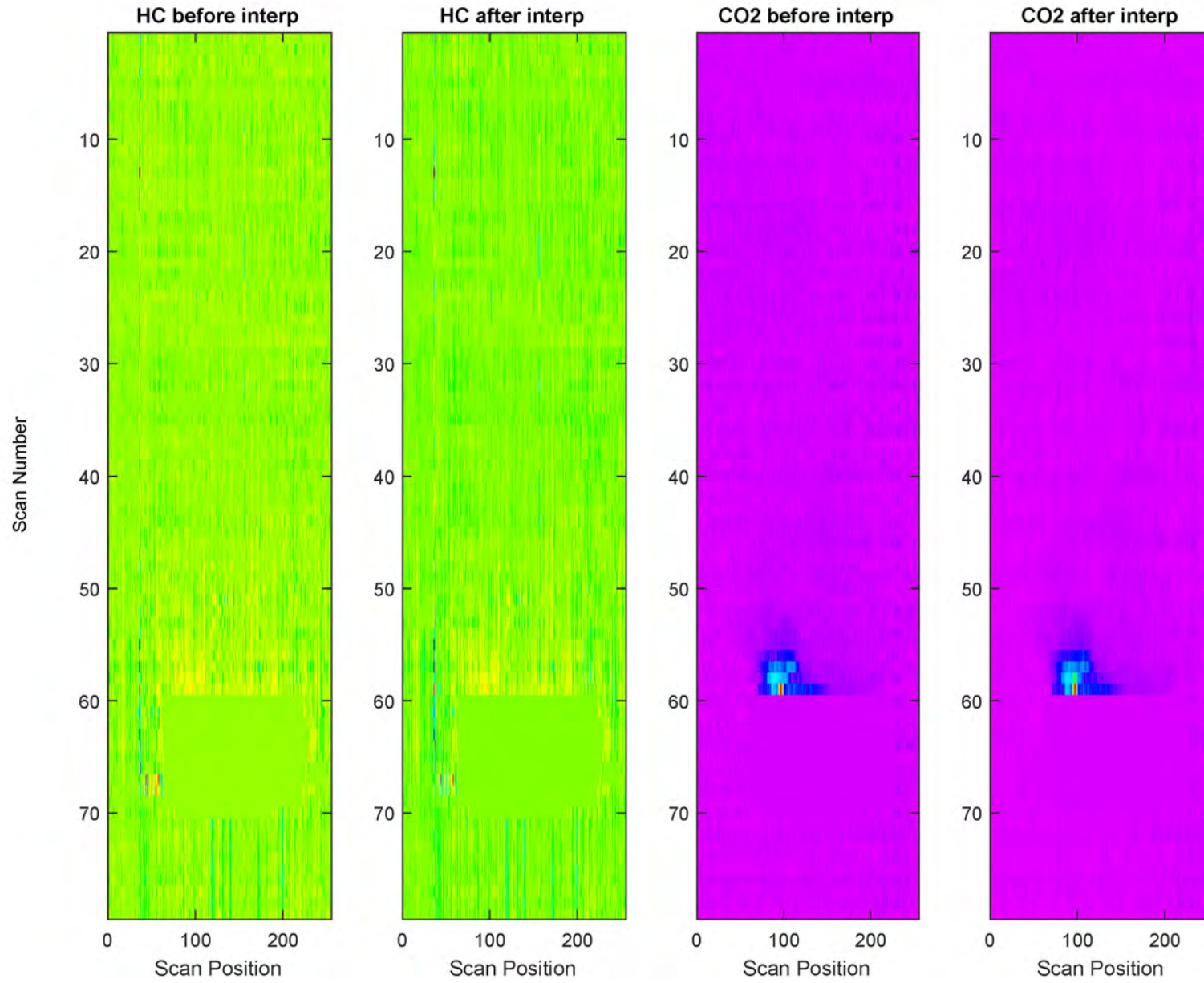
Figure C-38. ZigZag Interpolation Example: EV-2, Low EvapHC from HOOD

7 20191024 000514 car 001053
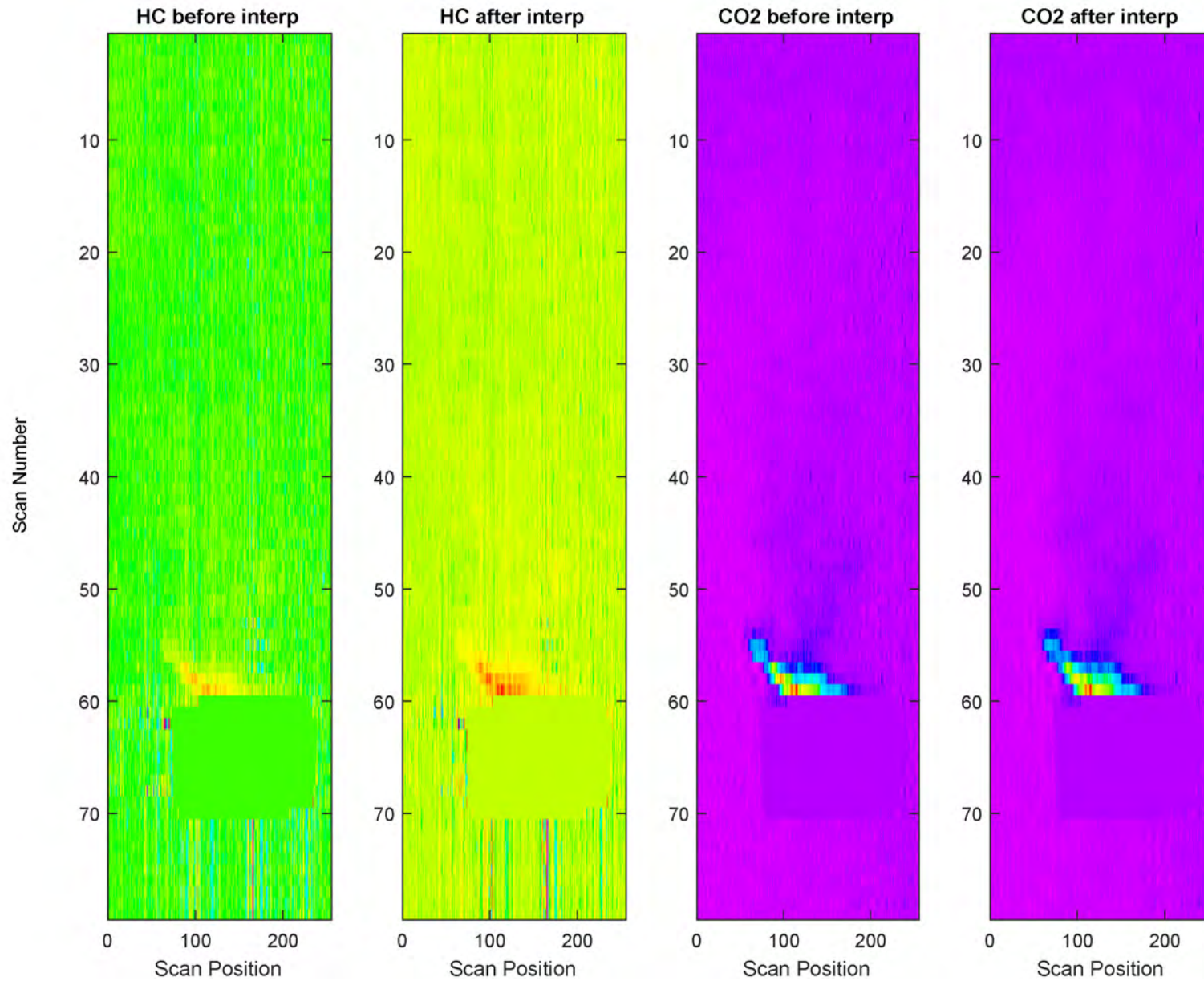
Figure C-39. ZigZag Interpolation Example: EV-1, High EvapHC from DOOR

7 20191023 000512 car 001167
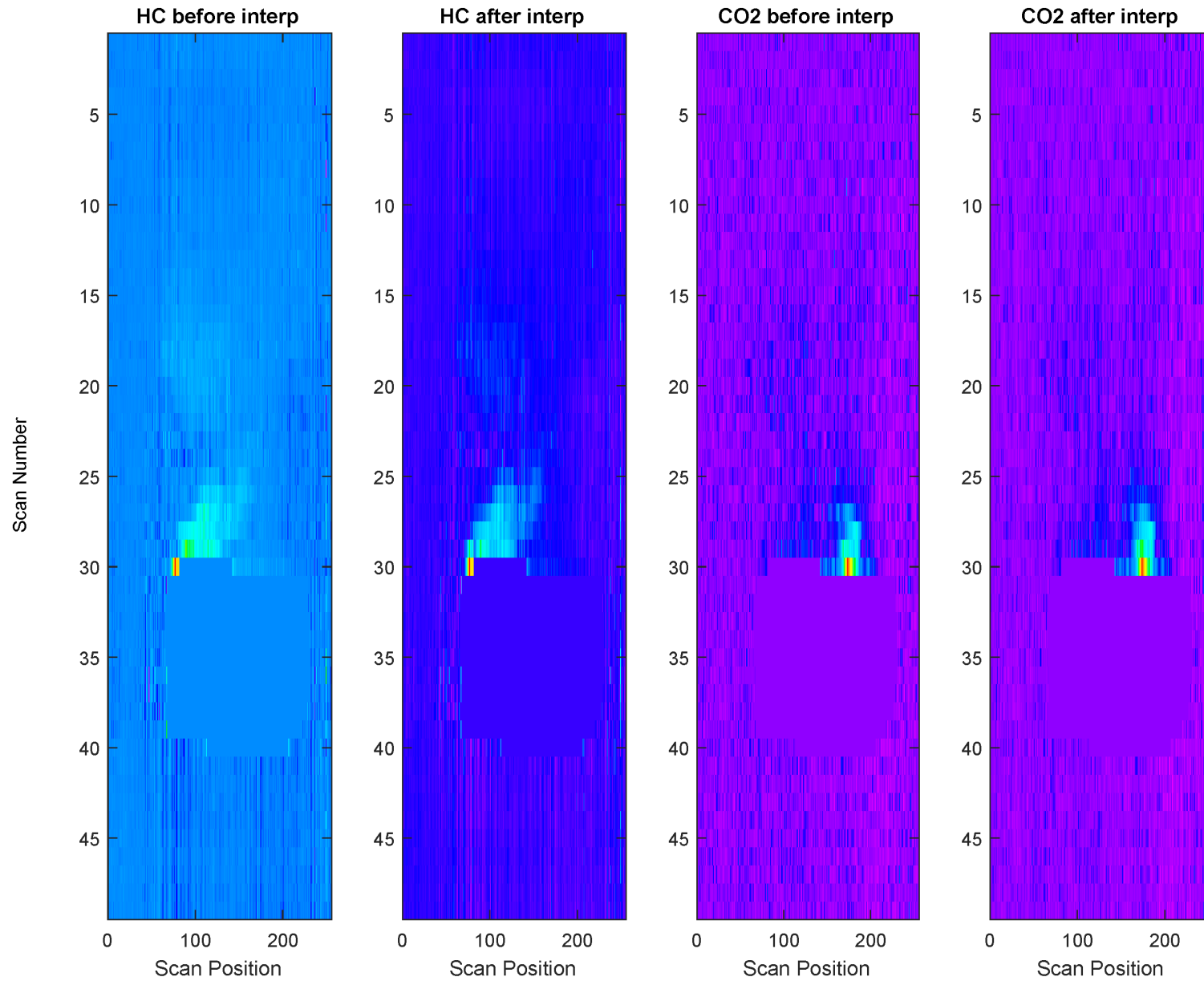
Figure C-40. ZigZag Interpolation Example: EV-1, High EvapHC from TANK

7 20191022 000509 car 001451
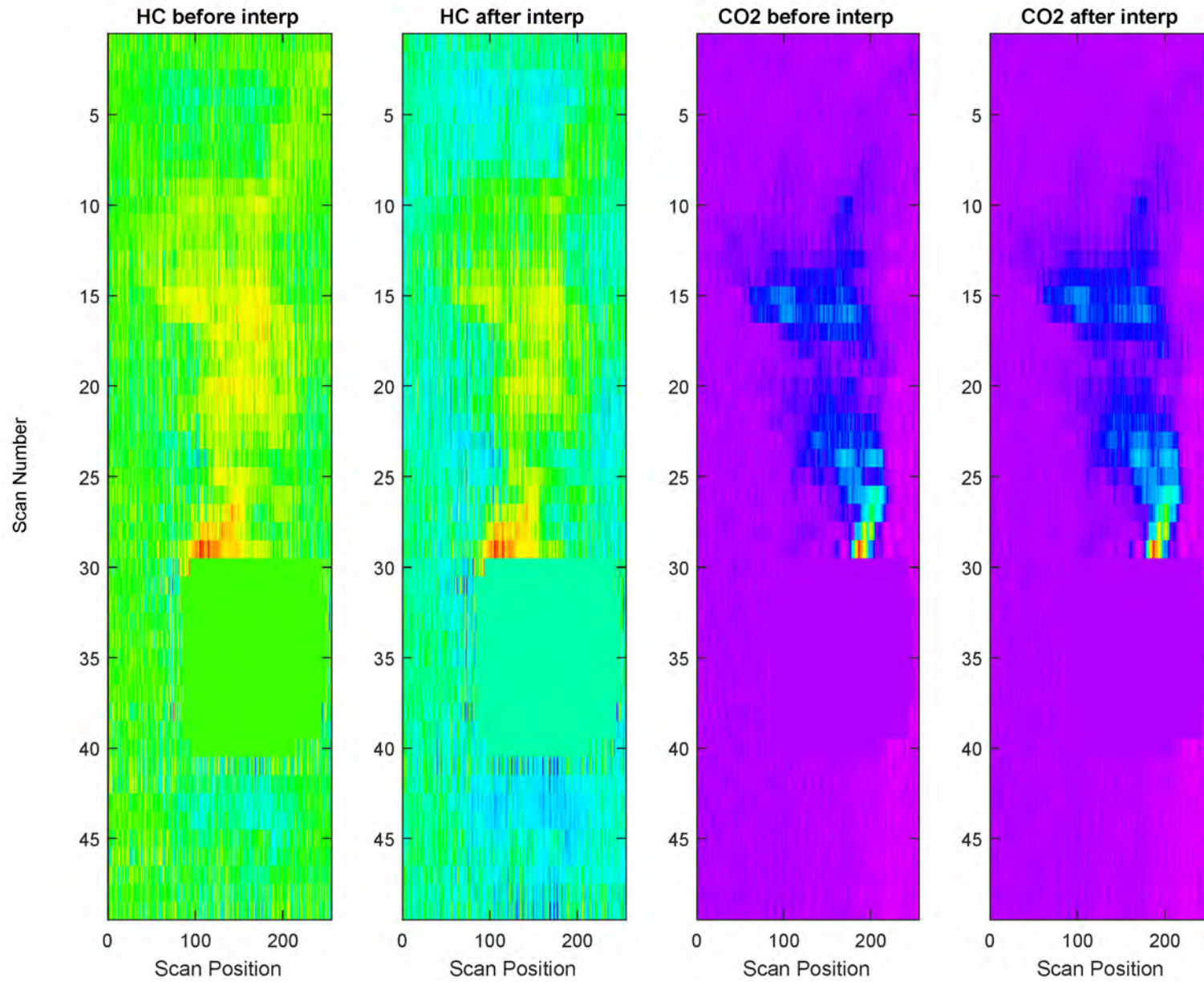
Figure C-41. ZigZag Interpolation Example: EV-1, High EvapHC from HOOD

7 20191022 000509 car 002092
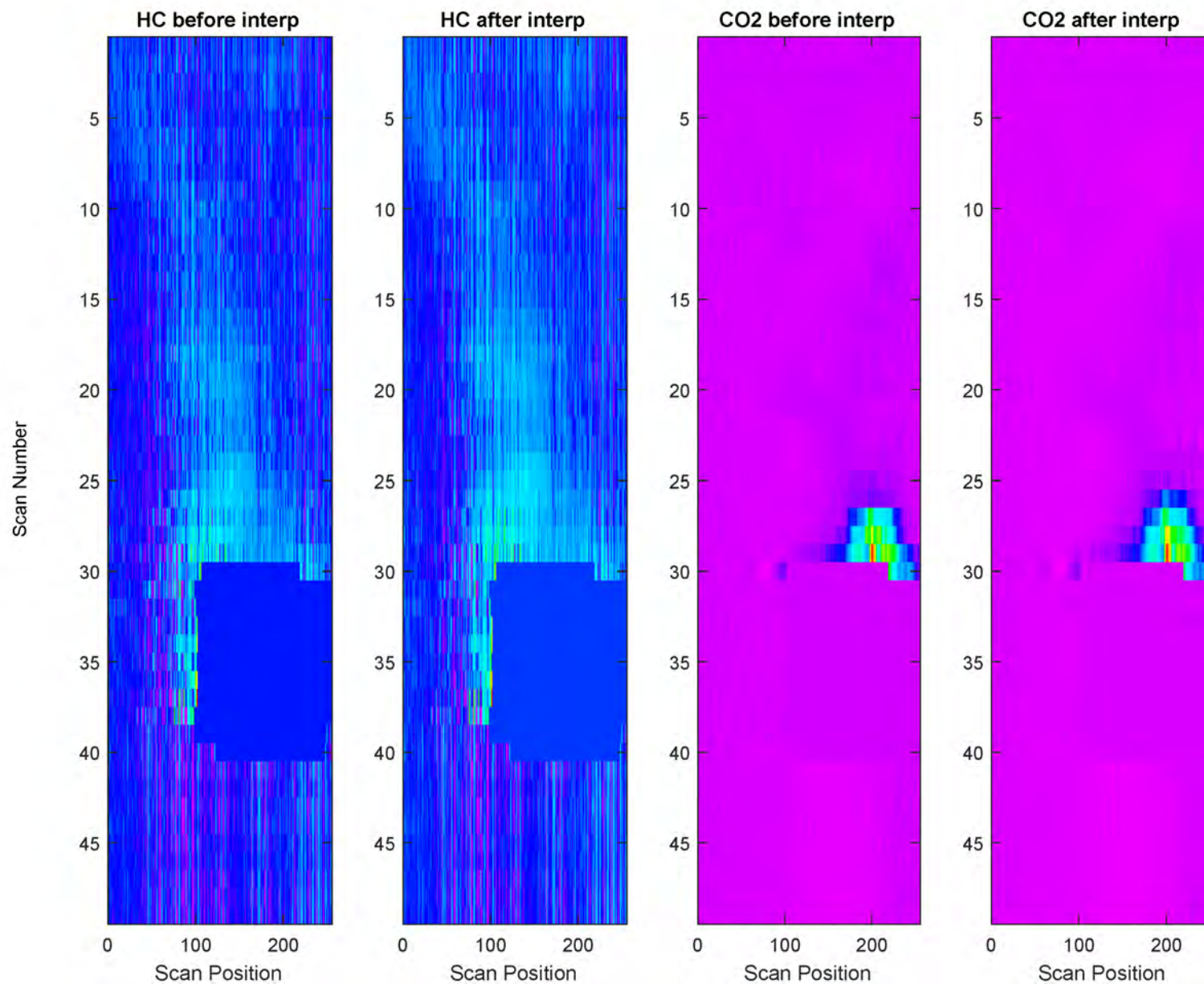
Figure C-42. ZigZag Interpolation Example: EV-1, Low EvapHC from DOOR

7 20191020 000506 car 000108
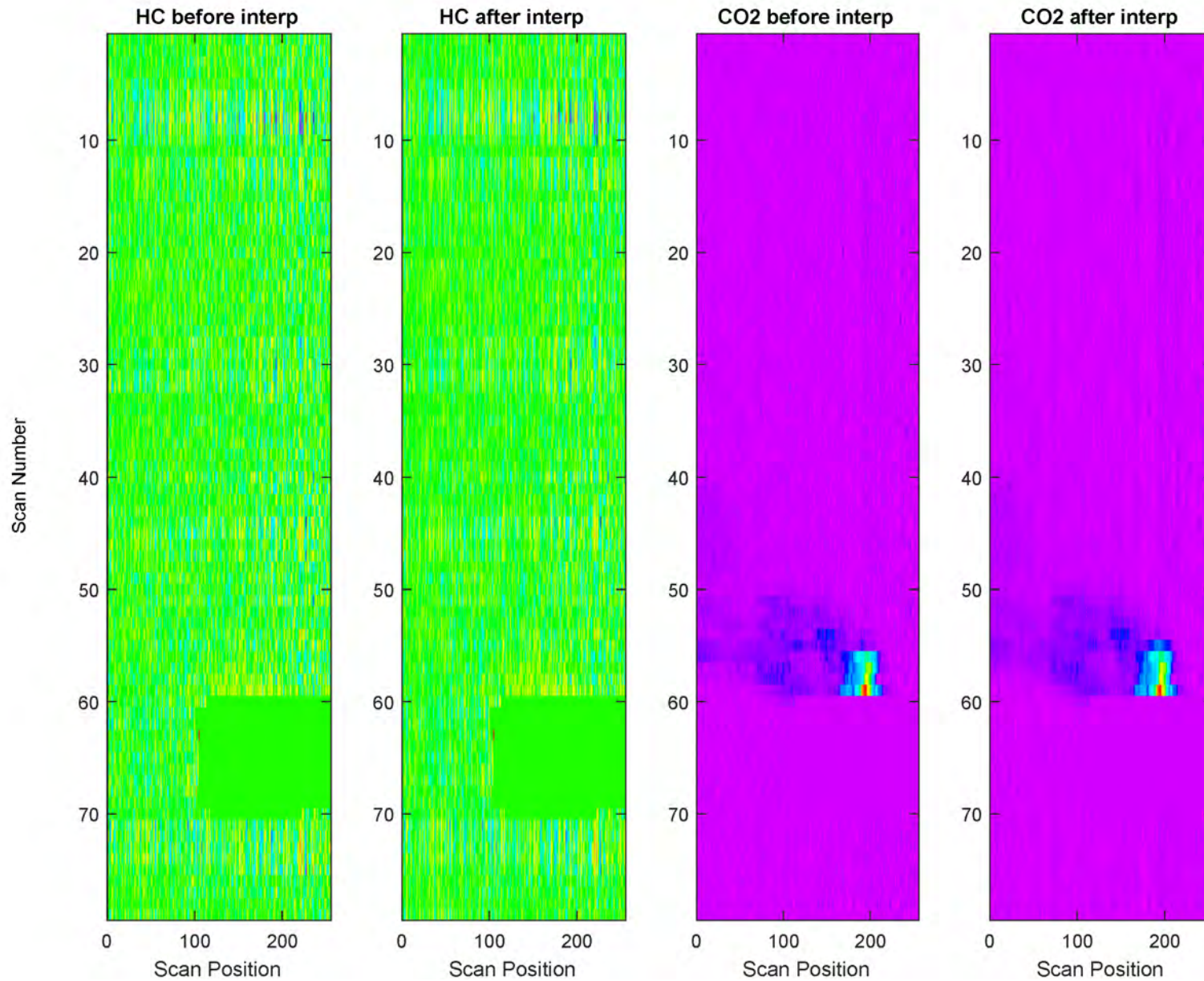
Figure C-43. ZigZag Interpolation Example: EV-1, Low EvapHC from TANK

7 20191021 000507 car 002354
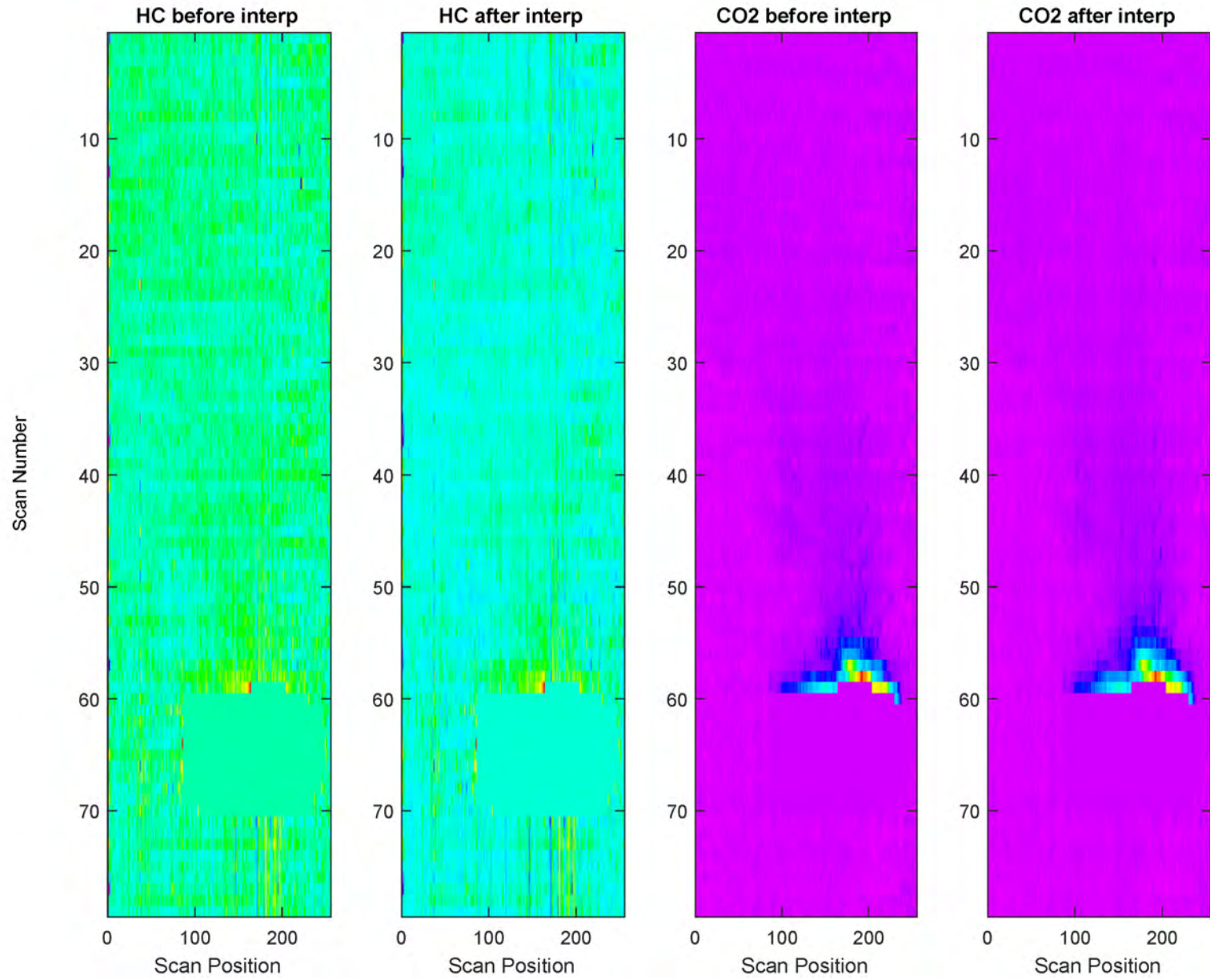
Figure C-44. ZigZag Interpolation Example: EV-1, Low EvapHC from HOOD

7 20191020 000505 car 002864
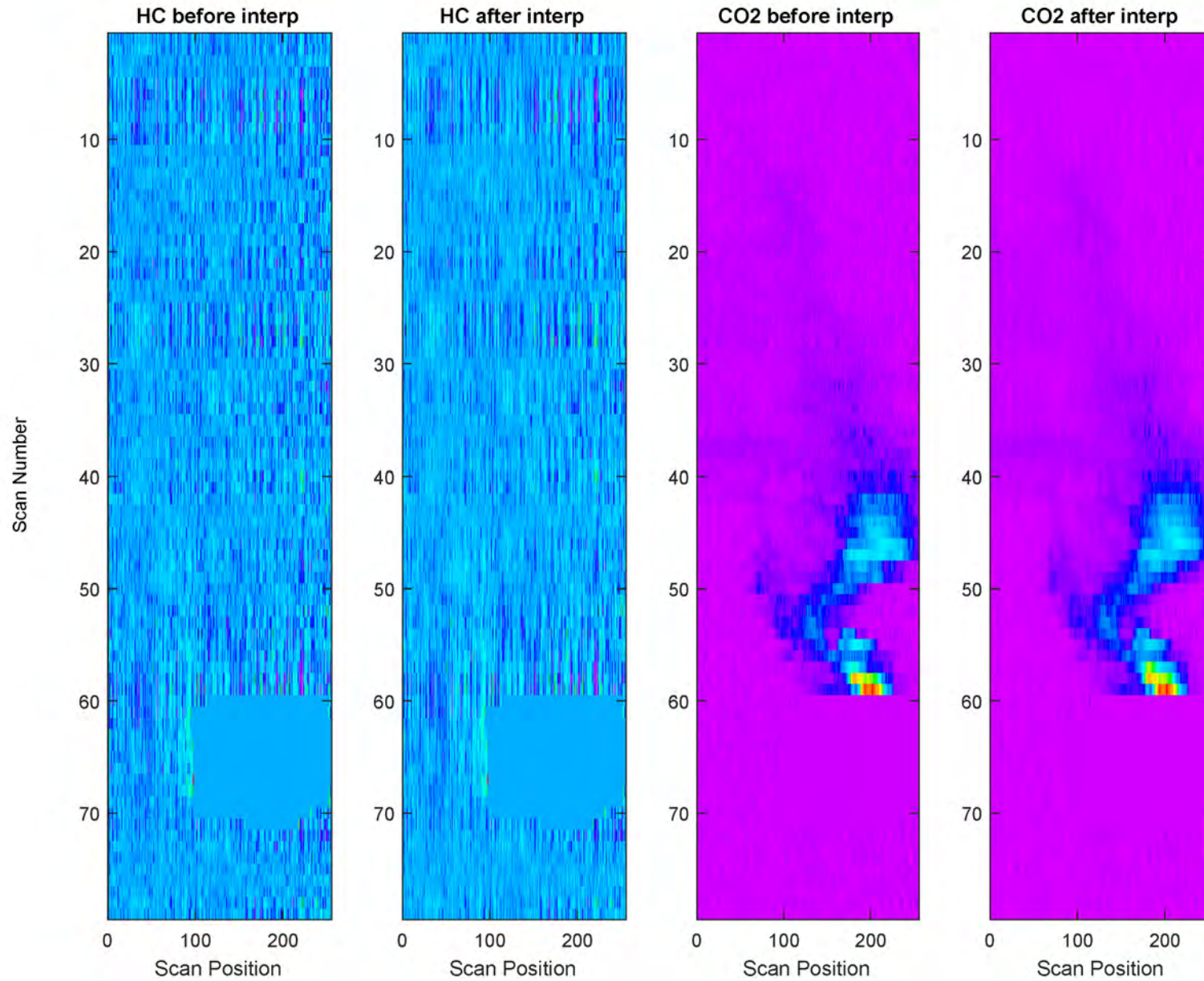
Appendix D:
Examples of Blind Source Separation
using Standard ICA

Figure D-1. BSS Example: EV-1, no EvapHC, Low Speed, no Exh

7 20191023 000513 car 000225

1-EV1 0mg n/a 22mph N
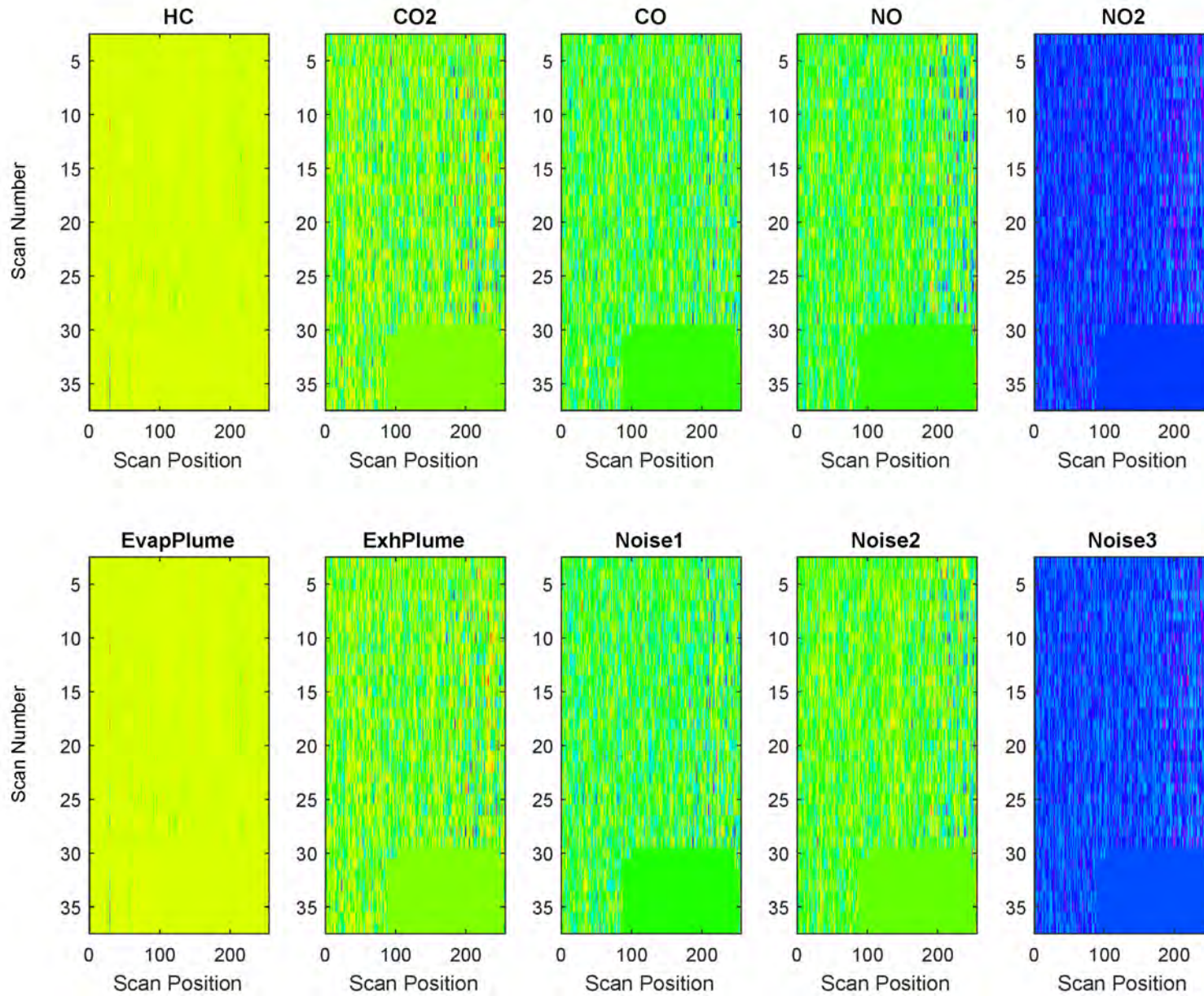
Figure D-2. BSS Example: EV-1, no EvapHC, Low Speed, CO2 Exh

7 20191020 000505 car 001287   1-EV1 0mg n/a 22mph Y
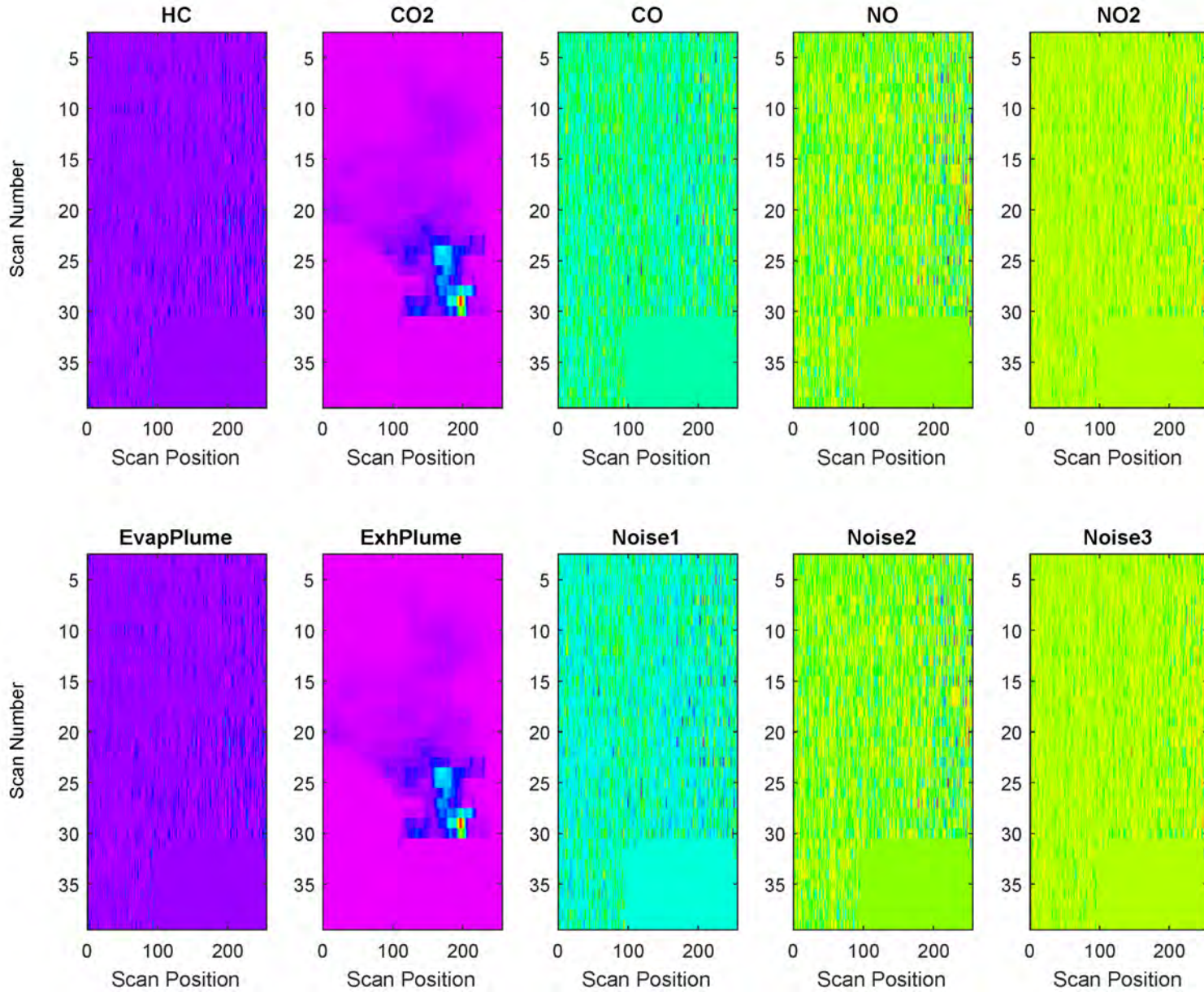
Figure D-3. BSS Example: EV-1, High EvapHC from DOOR, Low Speed, CO2 Exh

D-3
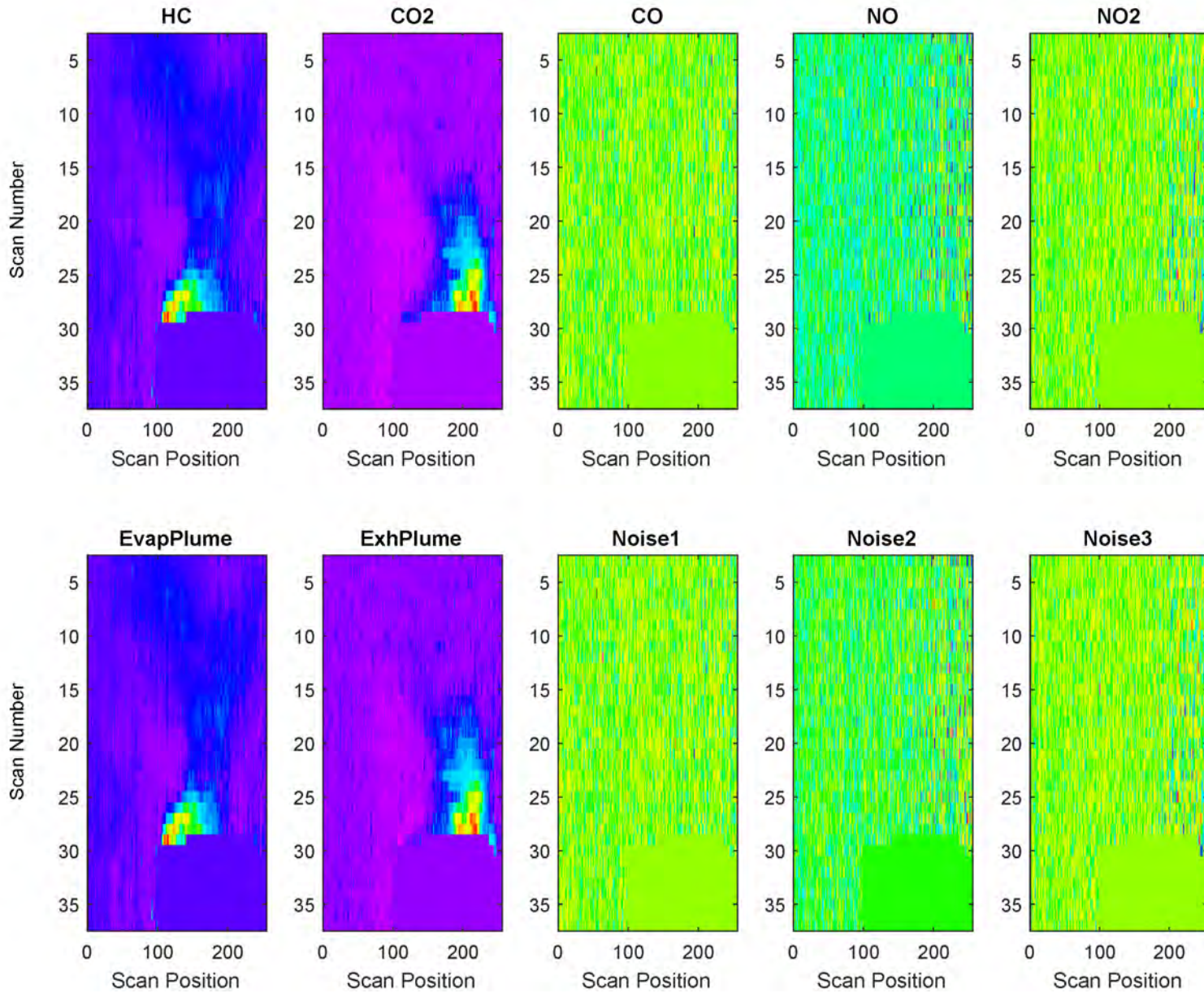
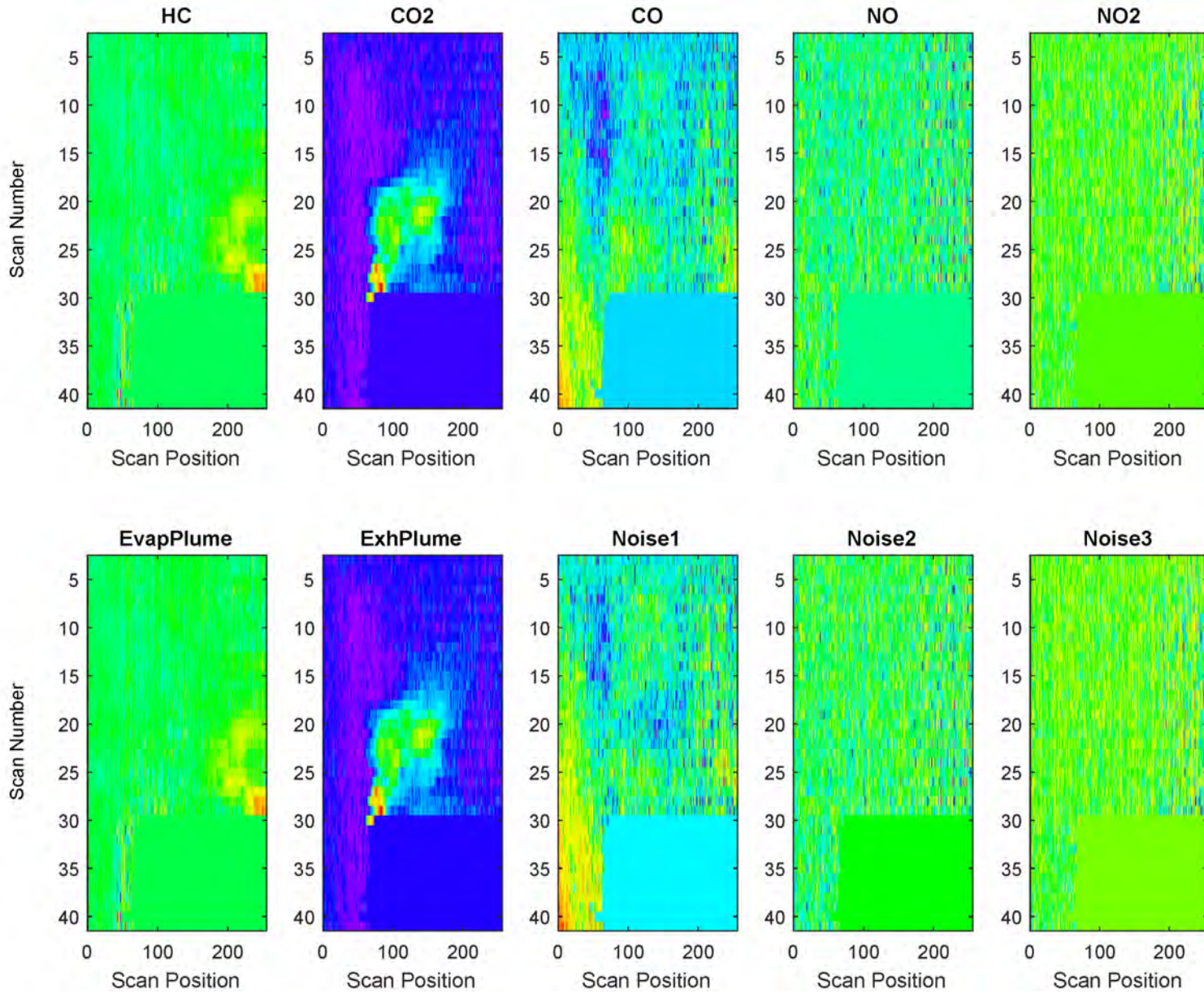# Figure D-4. BSS Example: EV-1, Medium EvapHC from DOOR, Low Speed, CO2 Exh

Figure D-5. BSS Example: EV-1, Low EvapHC from DOOR, Low Speed, CO2 Exh

7 20191022 000509 car 003372   1-EV1 200mg Door 22mph Y
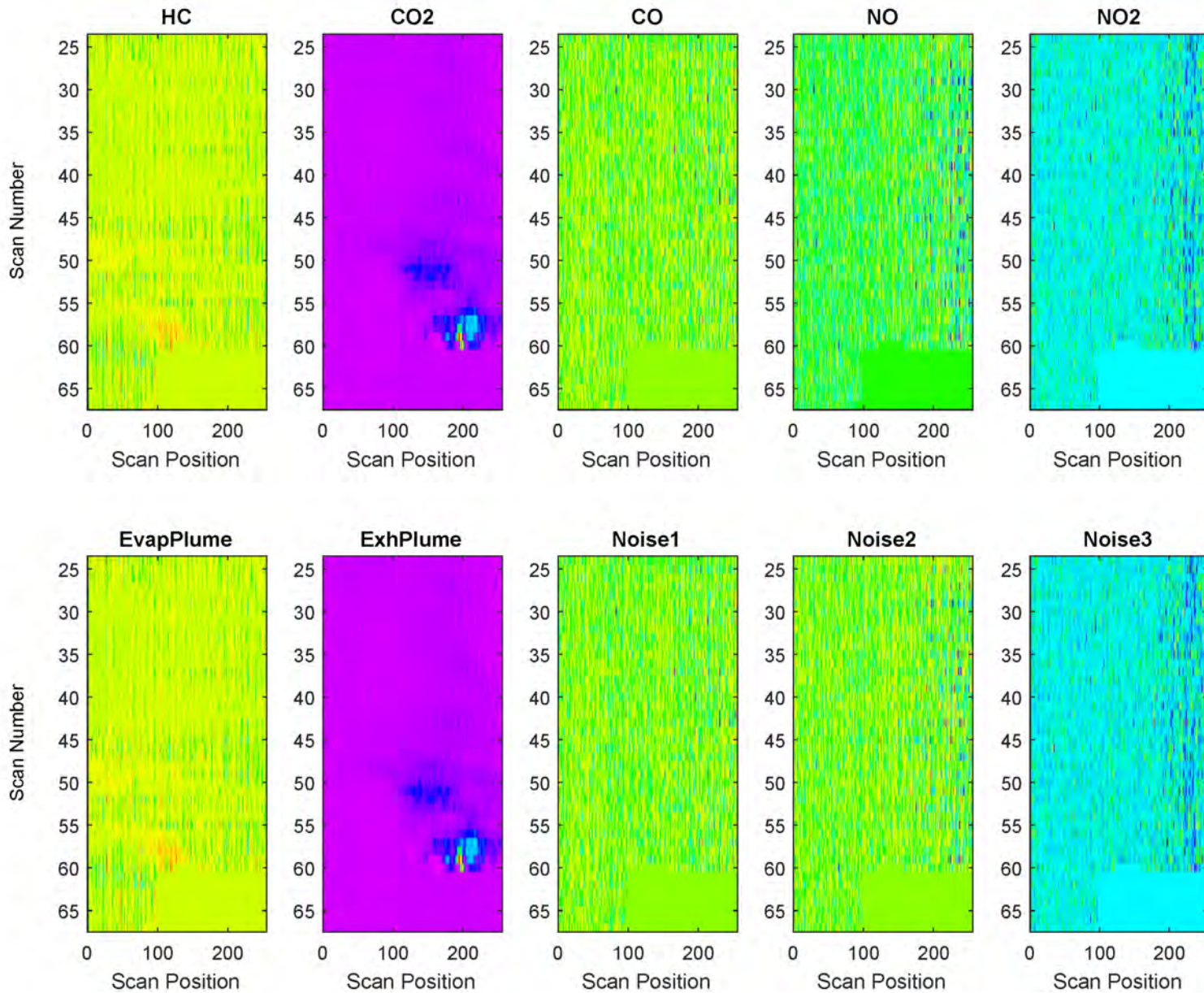
Figure D-6. BSS Example: EV-1, Medium EvapHC from DOOR, High Speed, CO2 Exh

7 20191021 000507 car 001454   1-EV1 800mg Door 45mph Y
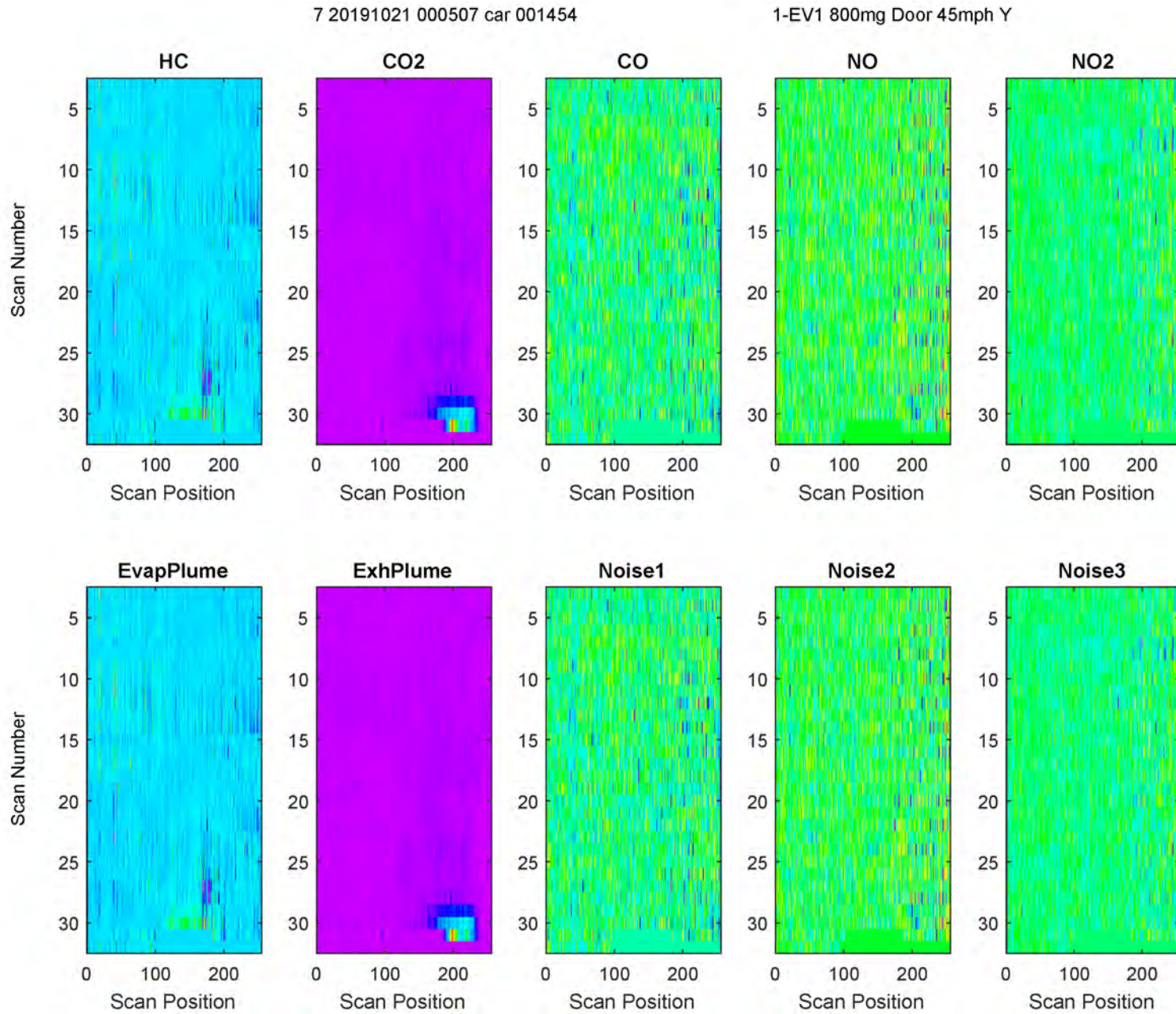
Figure D-7. BSS Example: EV-1, High EvapHC from TANK, Low Speed, CO2 Exh

7 20191024 000514 car 001634   1-EV1 6400mg Tank 22mph Y
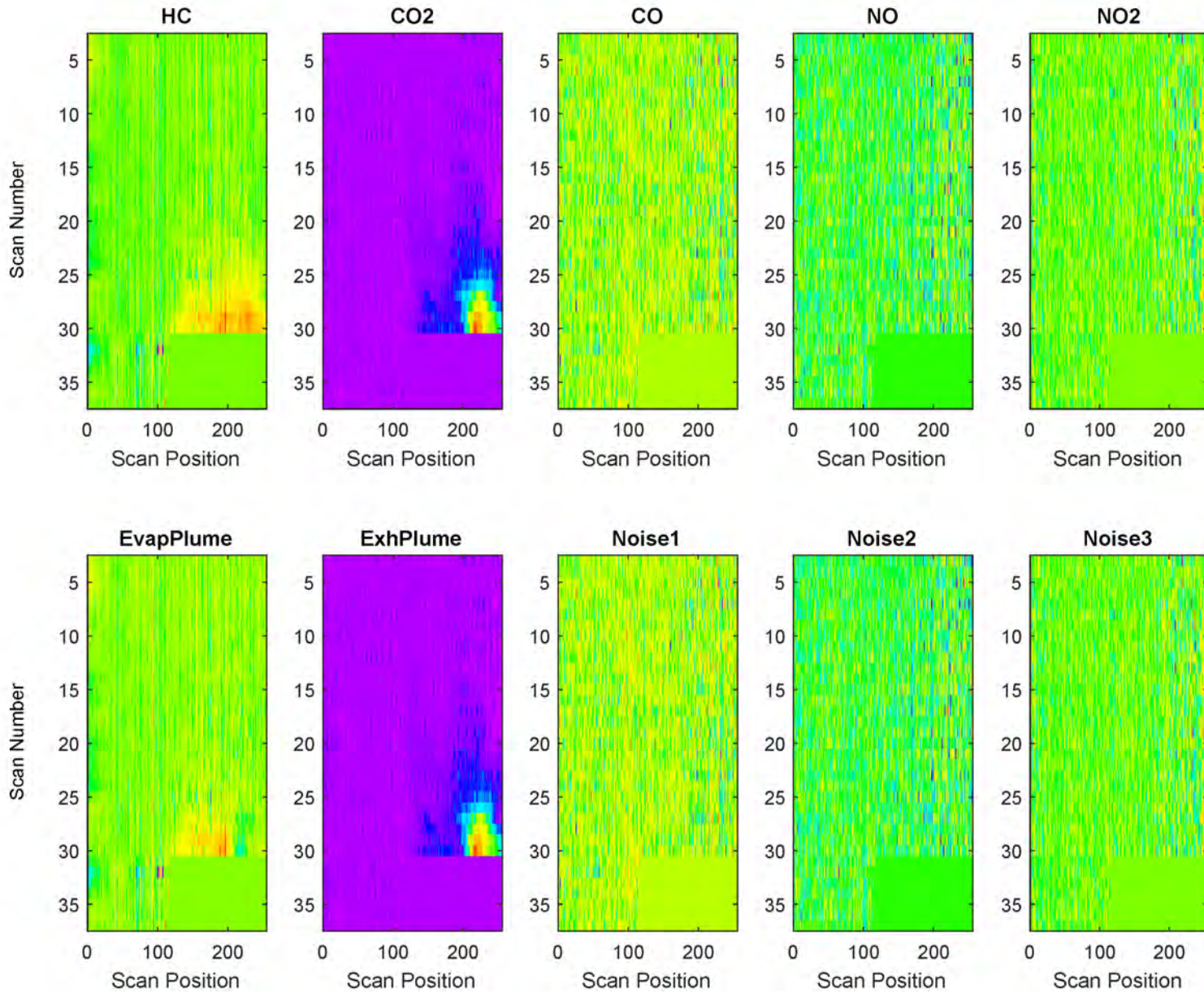
Figure D-8. BSS Example: EV-1, Medium EvapHC from TANK, Low Speed, CO2 Exh
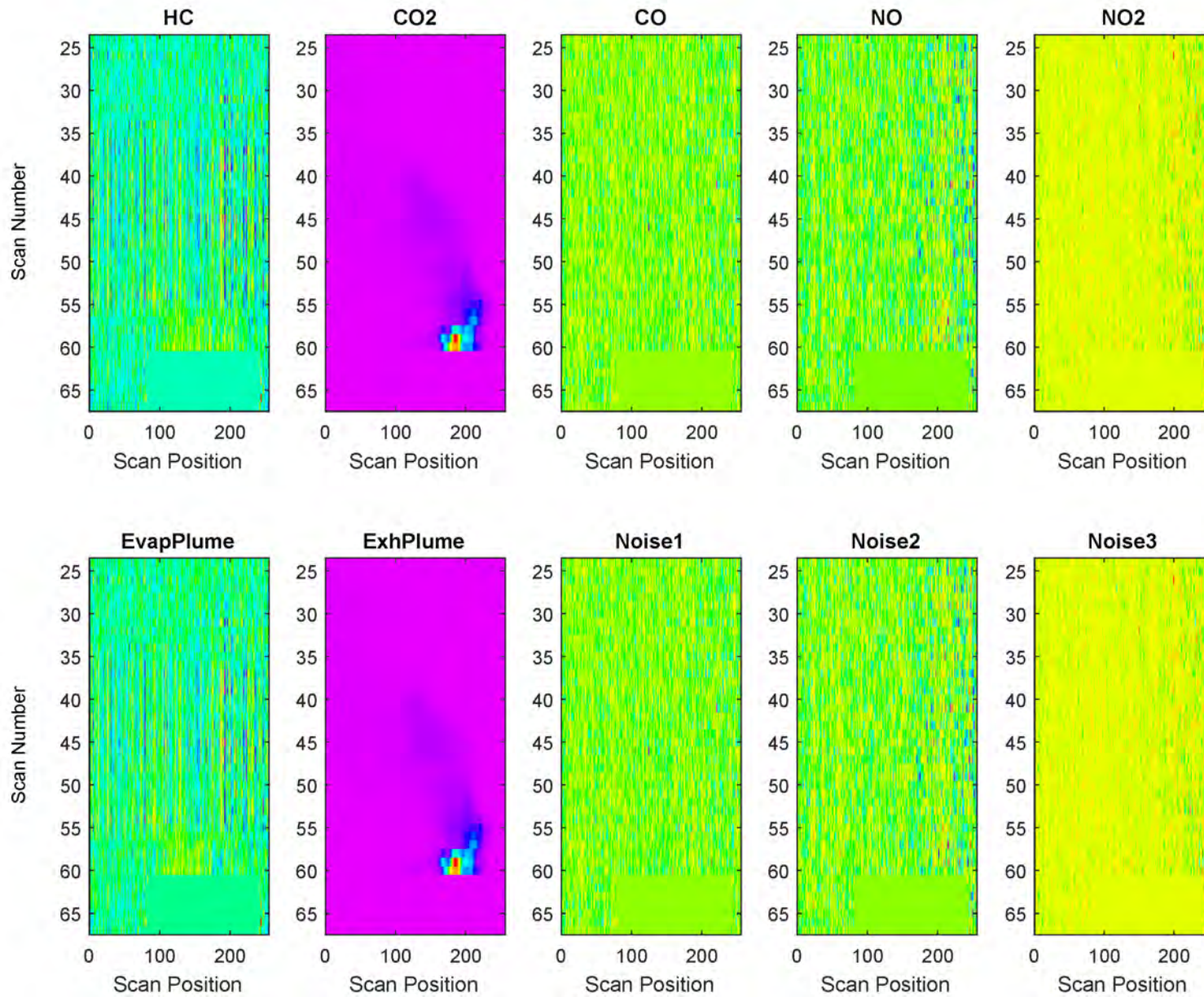
Figure D-9. BSS Example: EV-1, Low EvapHC from TANK, Low Speed, CO2 Exh
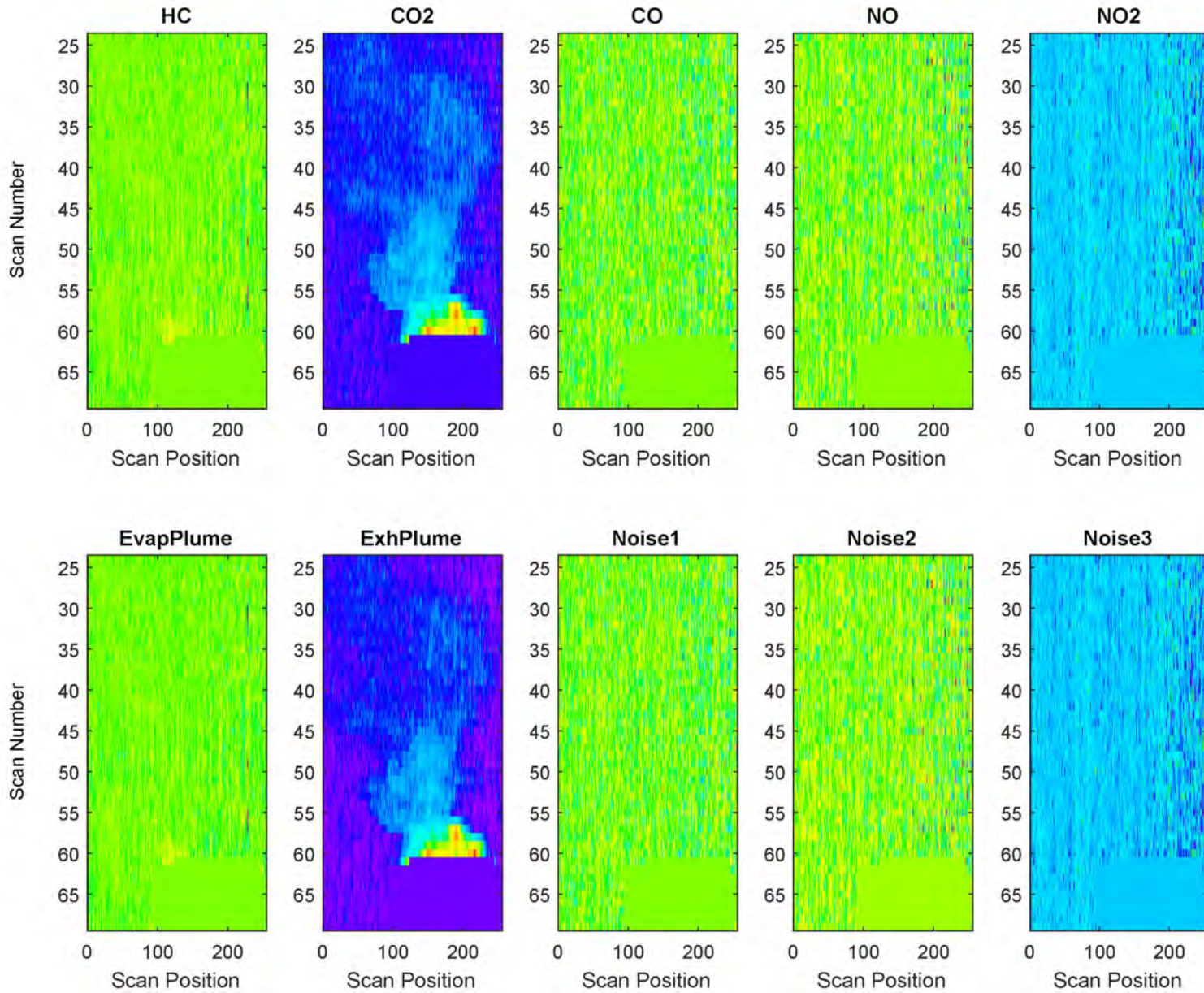
Figure D-10. BSS Example: EV-1, Medium EvapHC from TANK, High Speed, CO2 Exh

7 20191020 000505 car 001347   1-EV1 800mg Tank 45mph Y
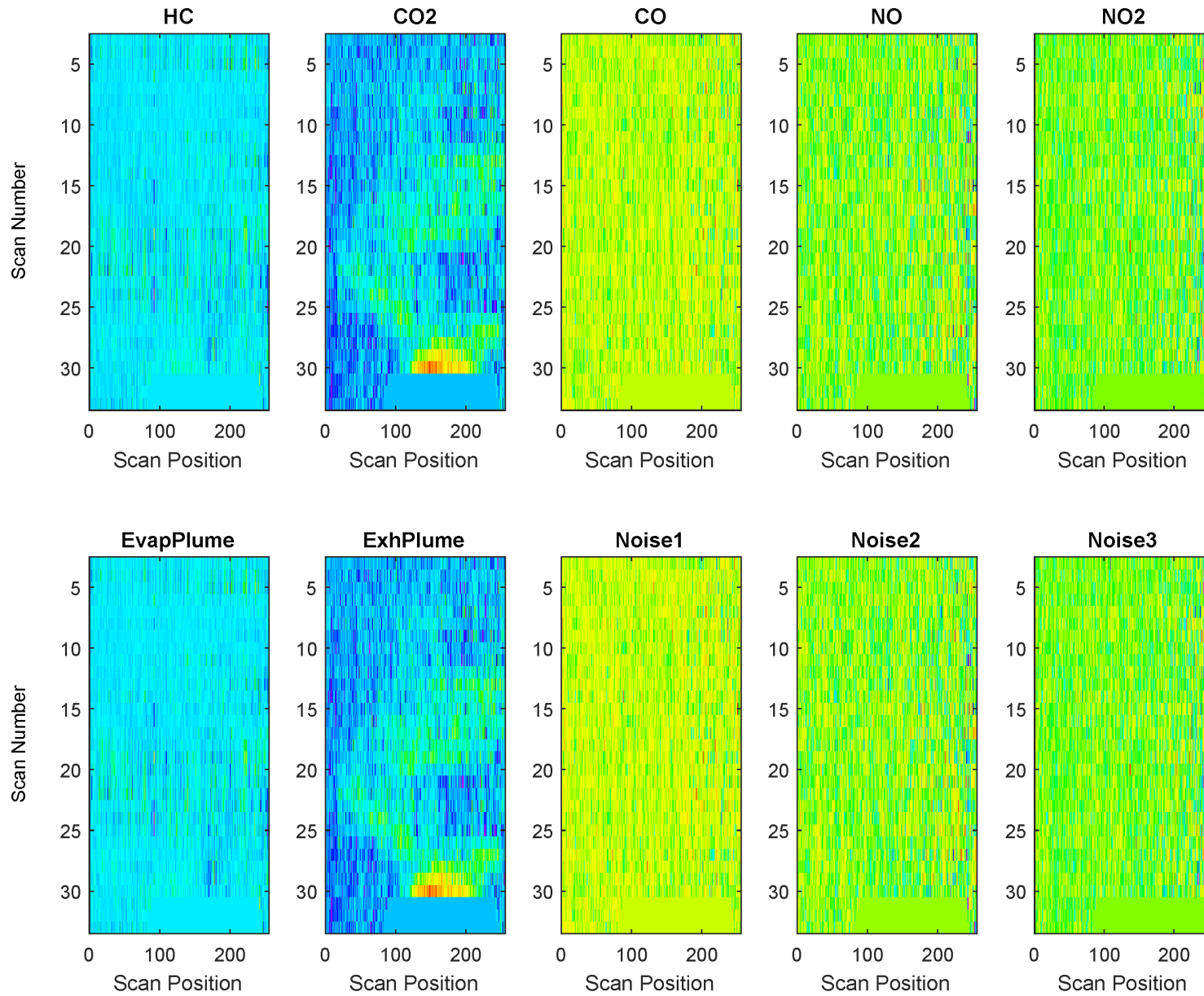
Figure D-11. BSS Example: EV-1, High EvapHC from HOOD, Low Speed, CO2 Exh

7 20191020 000505 car 001812   1-EV1 6400mg Hood 22mph Y
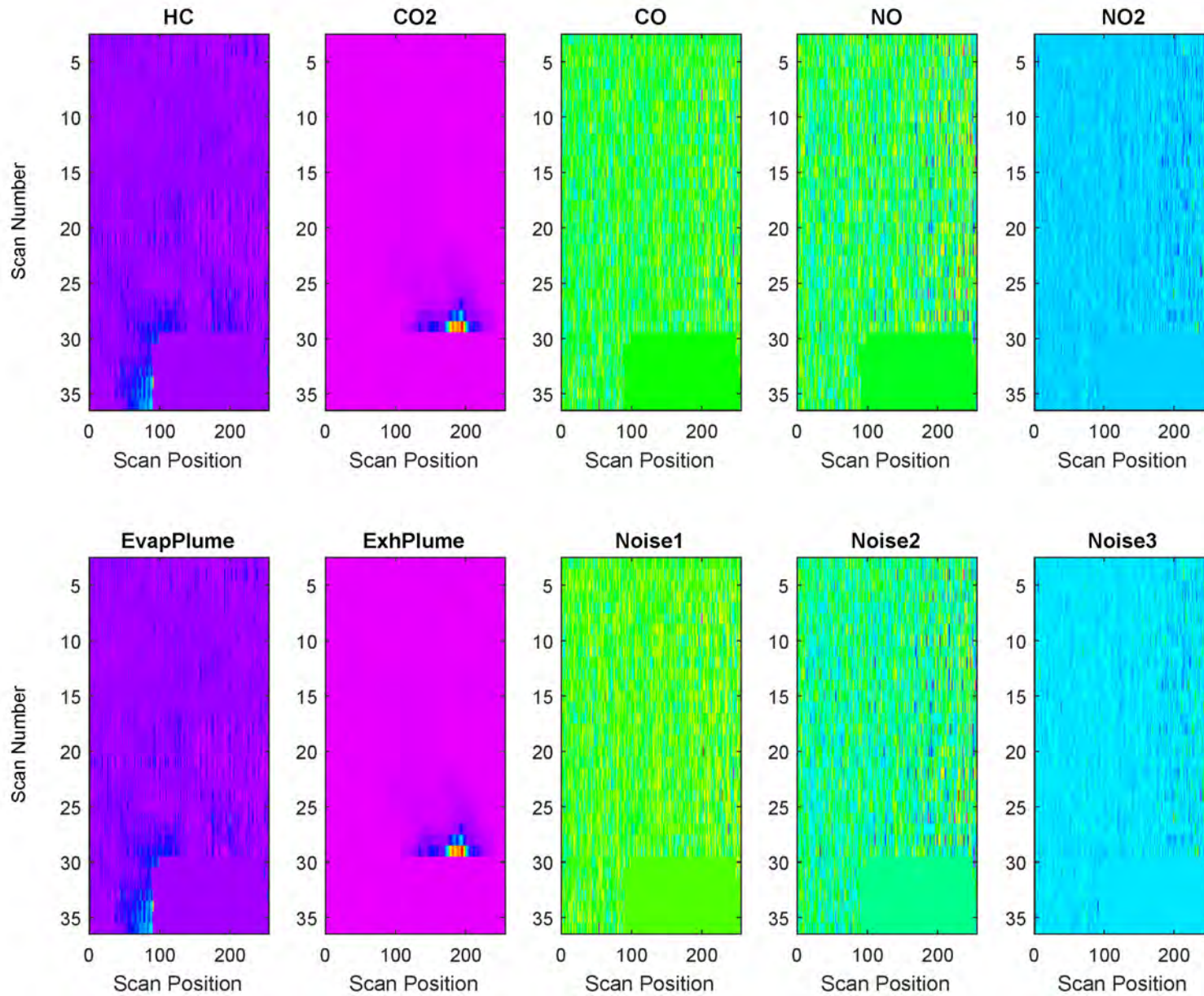
Figure D-12. BSS Example: EV-1, Medium EvapHC from HOOD, Low Speed, CO2 Exh

7 20191021 000507 car 002554   1-EV1 800mg Hood 22mph Y
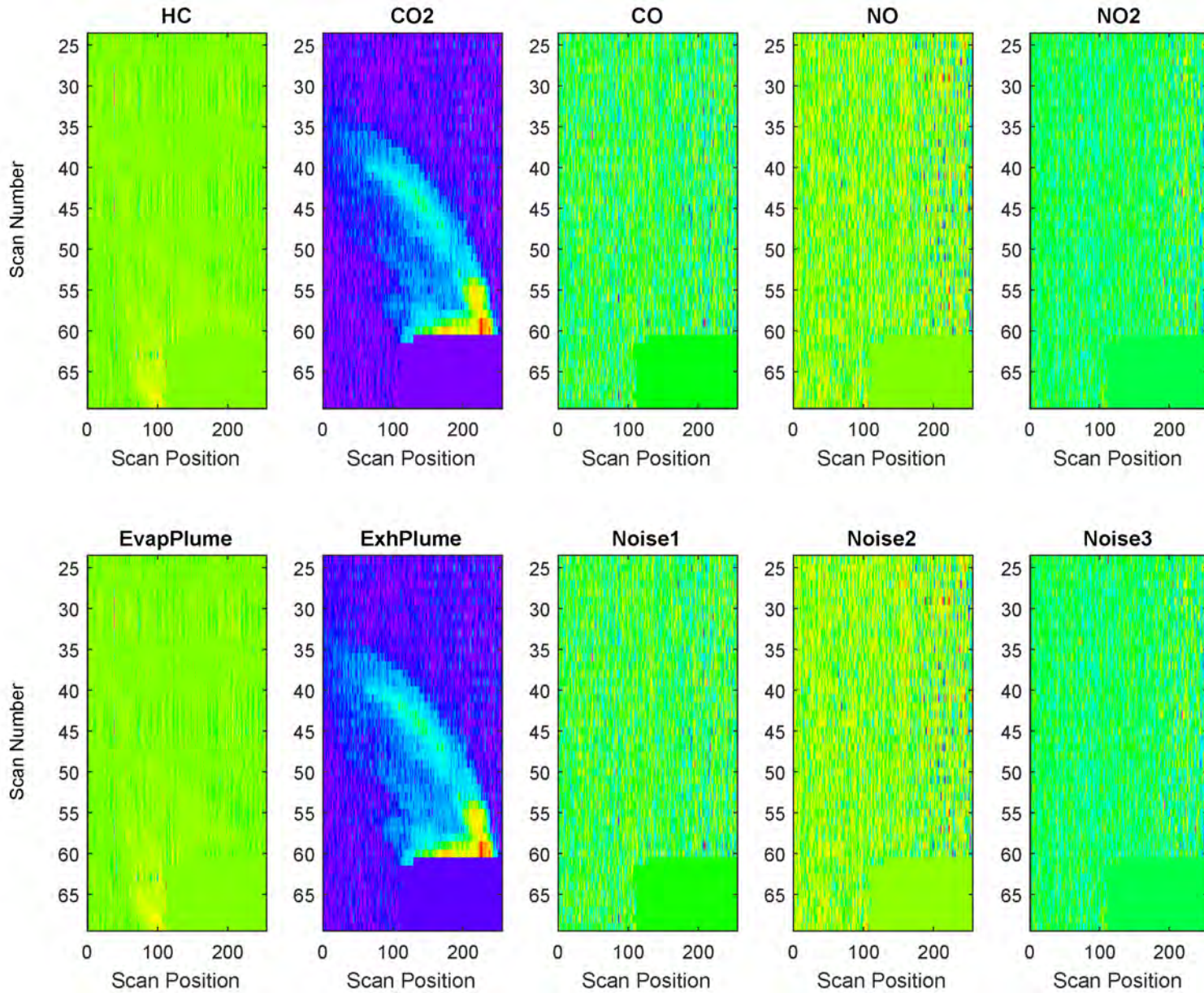
Figure D-13. BSS Example: EV-1, Low EvapHC from HOOD, Low Speed, CO2 Exh

7 20191022 000509 car 003188   1-EV1 200mg Hood 22mph Y
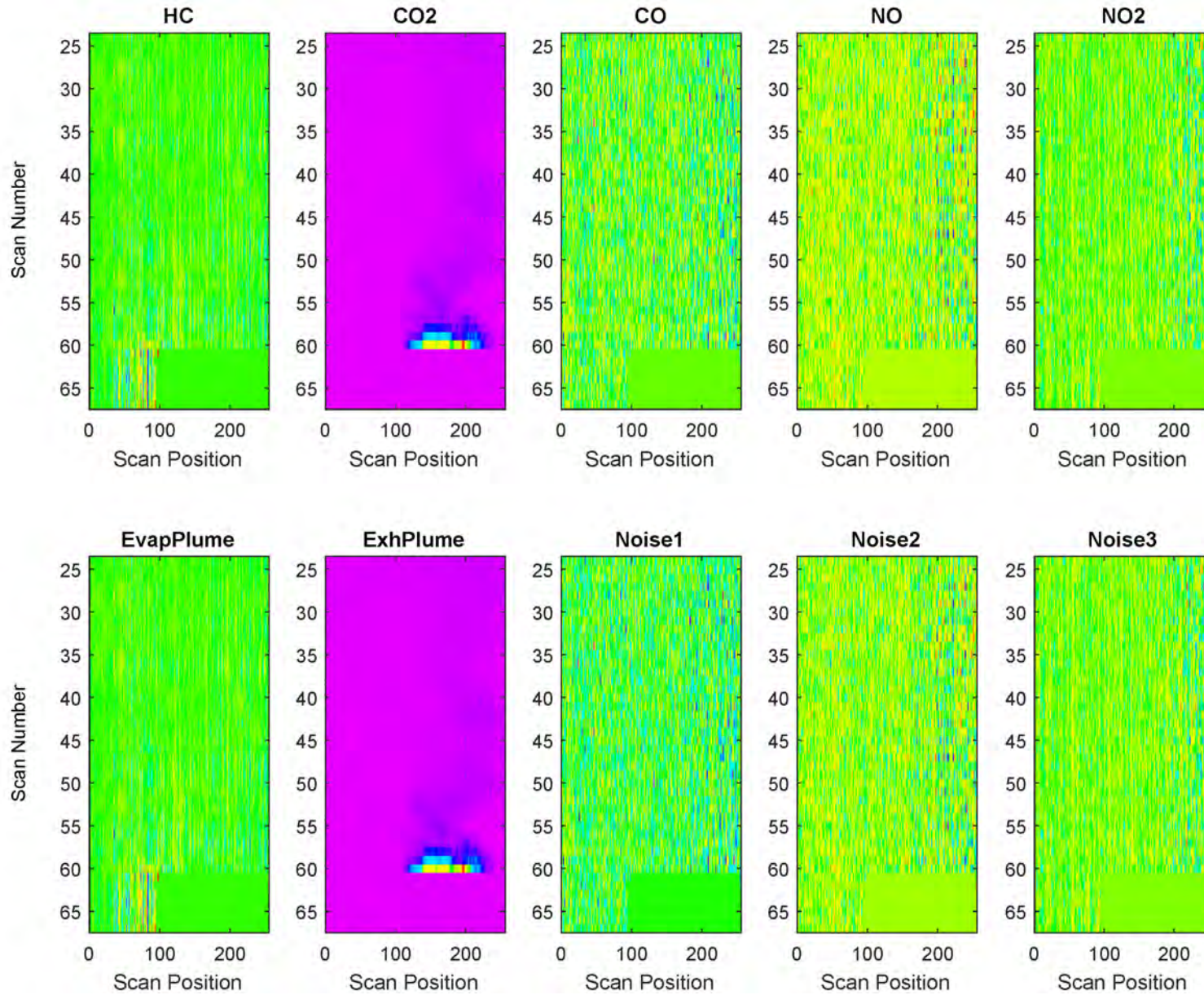
Figure D-14. BSS Example: EV-1, Medium EvapHC from HOOD, High Speed, CO2 Exh

7 20191022 000509 car 002243

1-EV1 800mg Hood 45mph Y
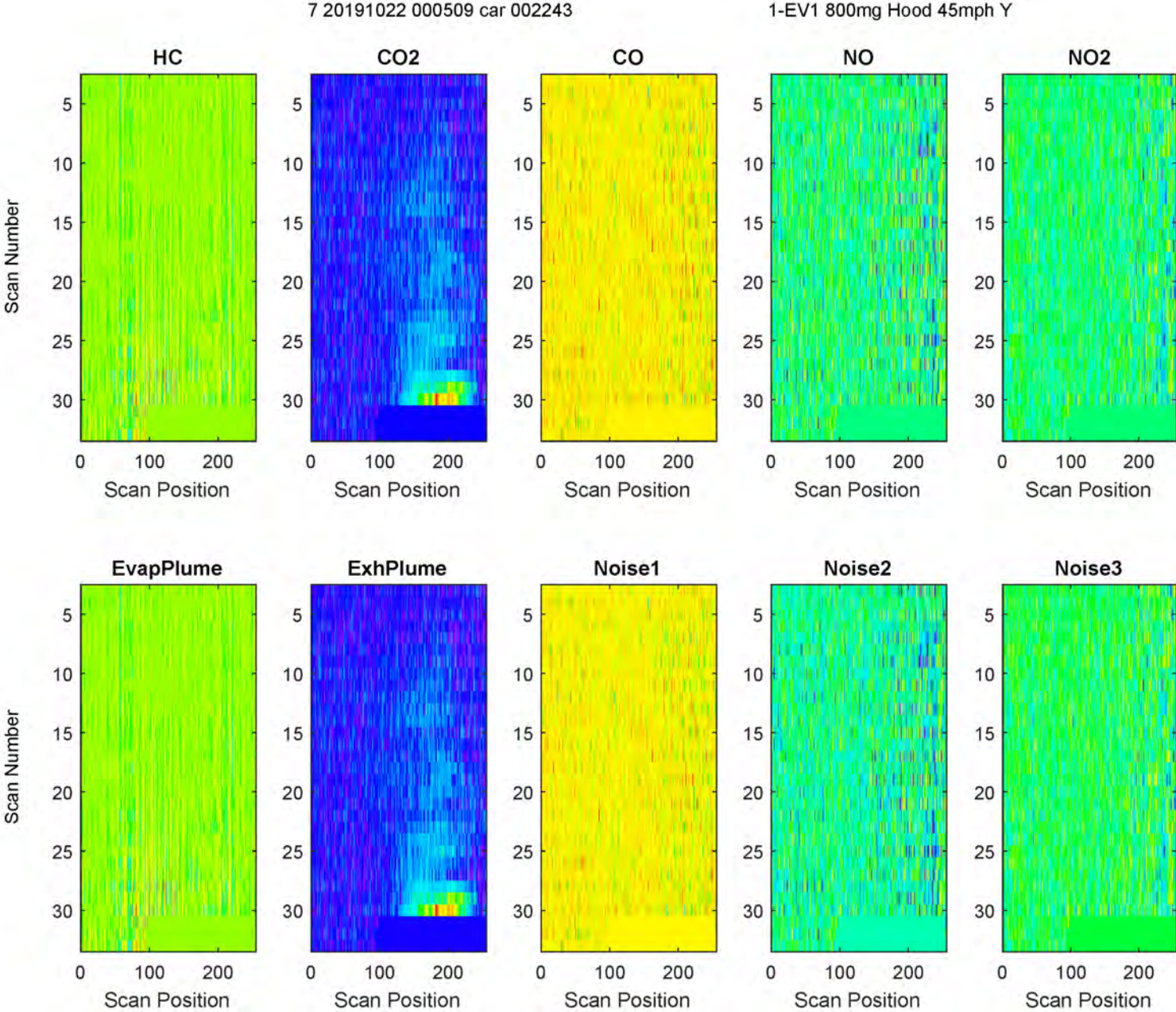
Figure D-15. BSS Example: EV-2, no EvapHC, Low Speed, no Exh

7 20191021 000507 car 001619   2-EV2 0mg n/a 22mph N
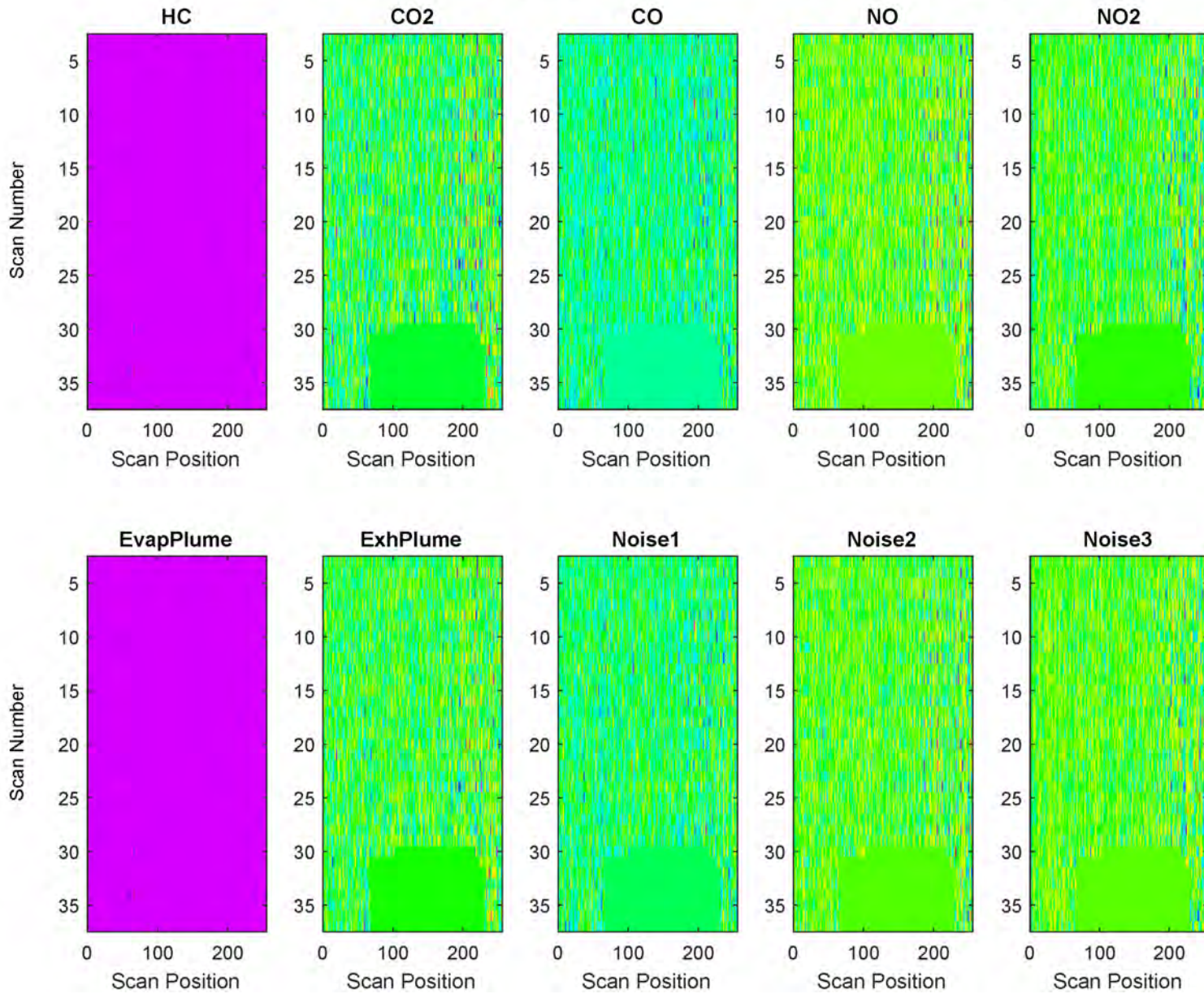
Figure D-16. BSS Example: EV-2, no EvapHC, Low Speed, HC/CO2/CO/NO Exh

7 20191021 000507 car 001430   2-EV2 0mg n/a 22mph Y
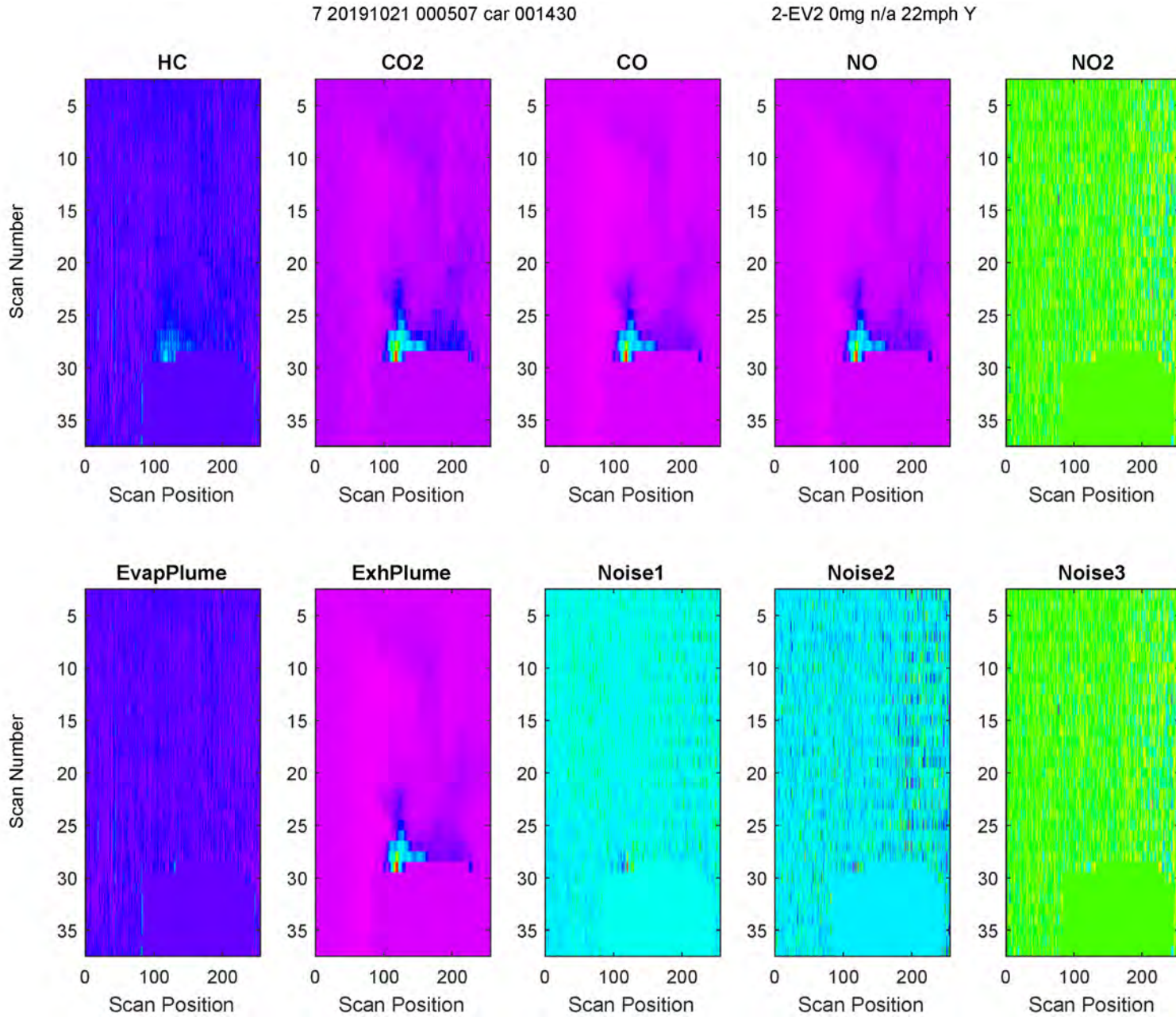
Figure D-17. BSS Example: EV-2, High EvapHC from DOOR, Low Speed, HC/CO2/CO/NO Exh
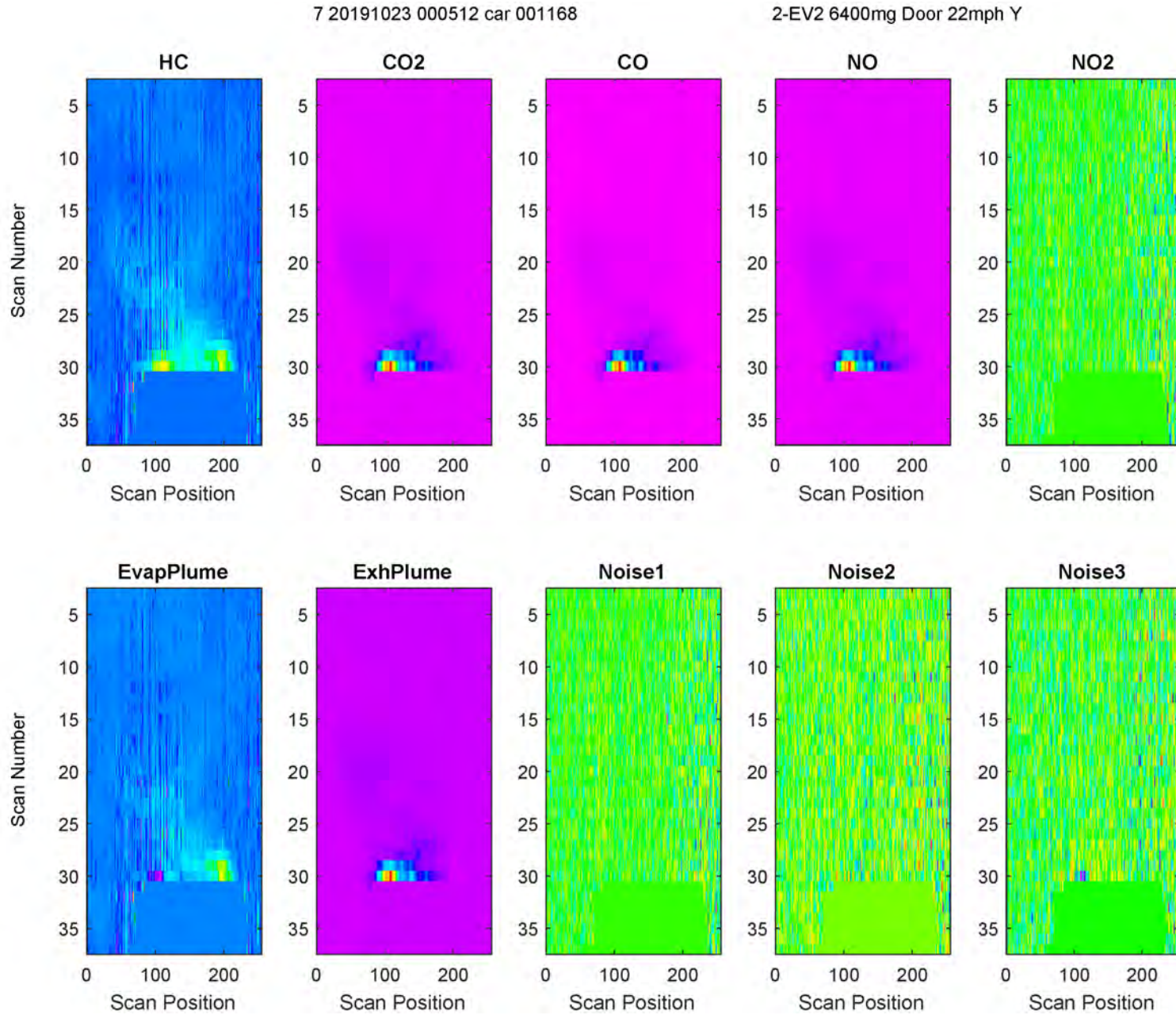
Figure D-18. BSS Example: EV-2, Medium EvapHC from DOOR, Low Speed, HC/CO2/CO/NO Exh

7 20191024 000514 car 000795   2-EV2 800mg Door 22mph Y
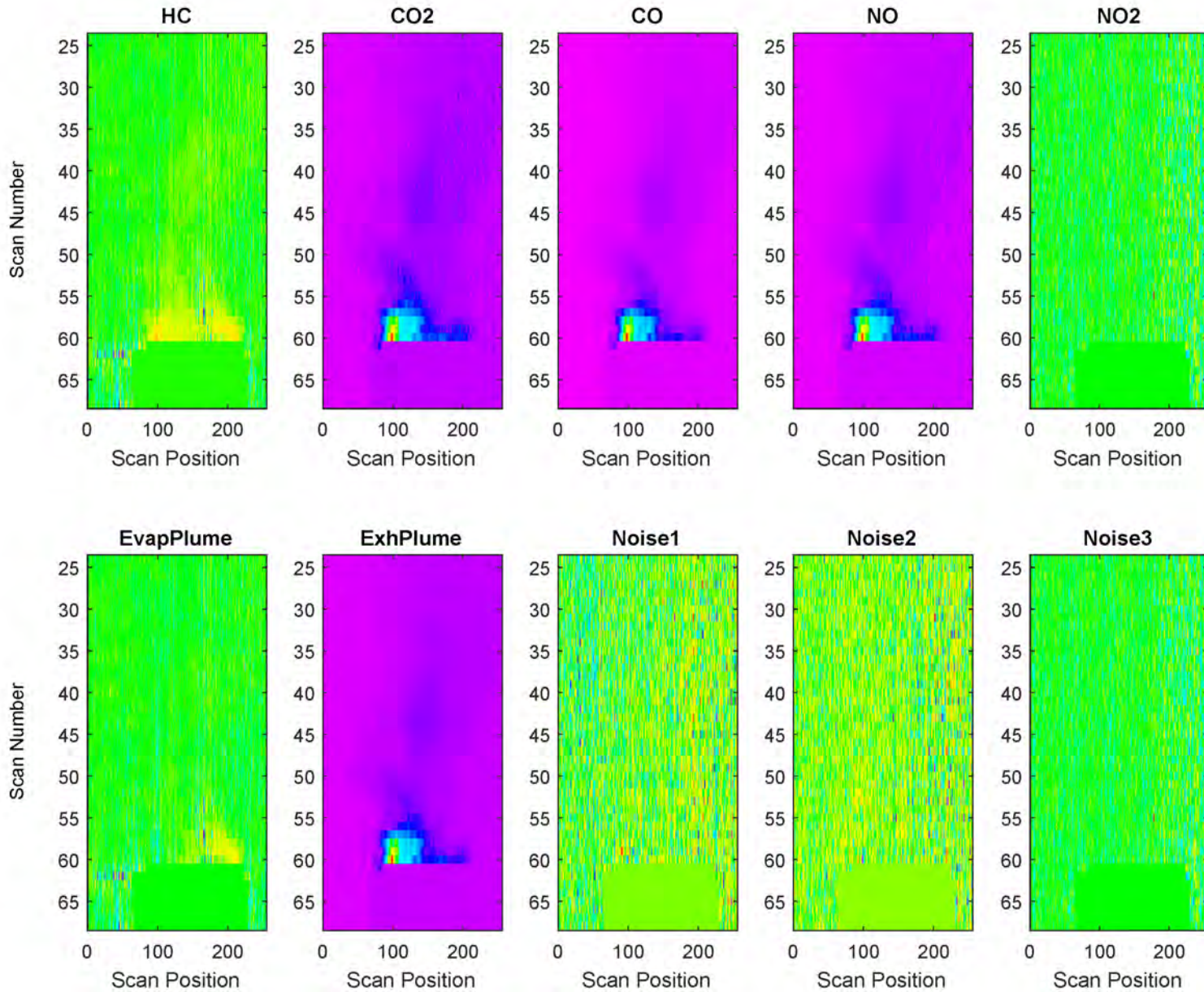
Figure D-19. BSS Example: EV-2, Low EvapHC from DOOR, Low Speed, HC/CO2/CO/NO Exh

7 20191024 000514 car 001202   2-EV2 200mg Door 22mph Y
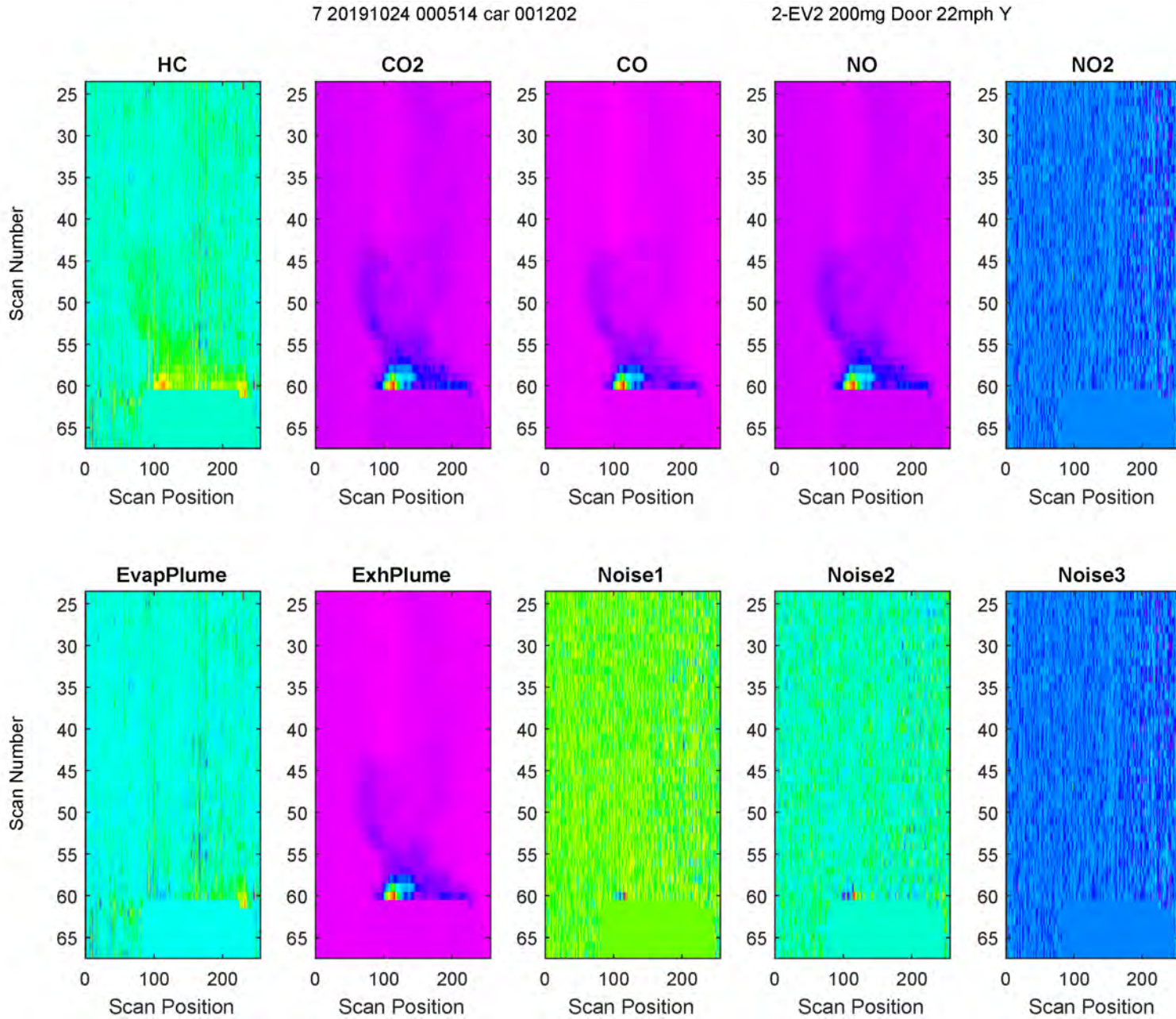
Figure D-20. BSS Example: EV-2, Medium EvapHC from DOOR, High Speed, HC/CO2/CO/NO Exh
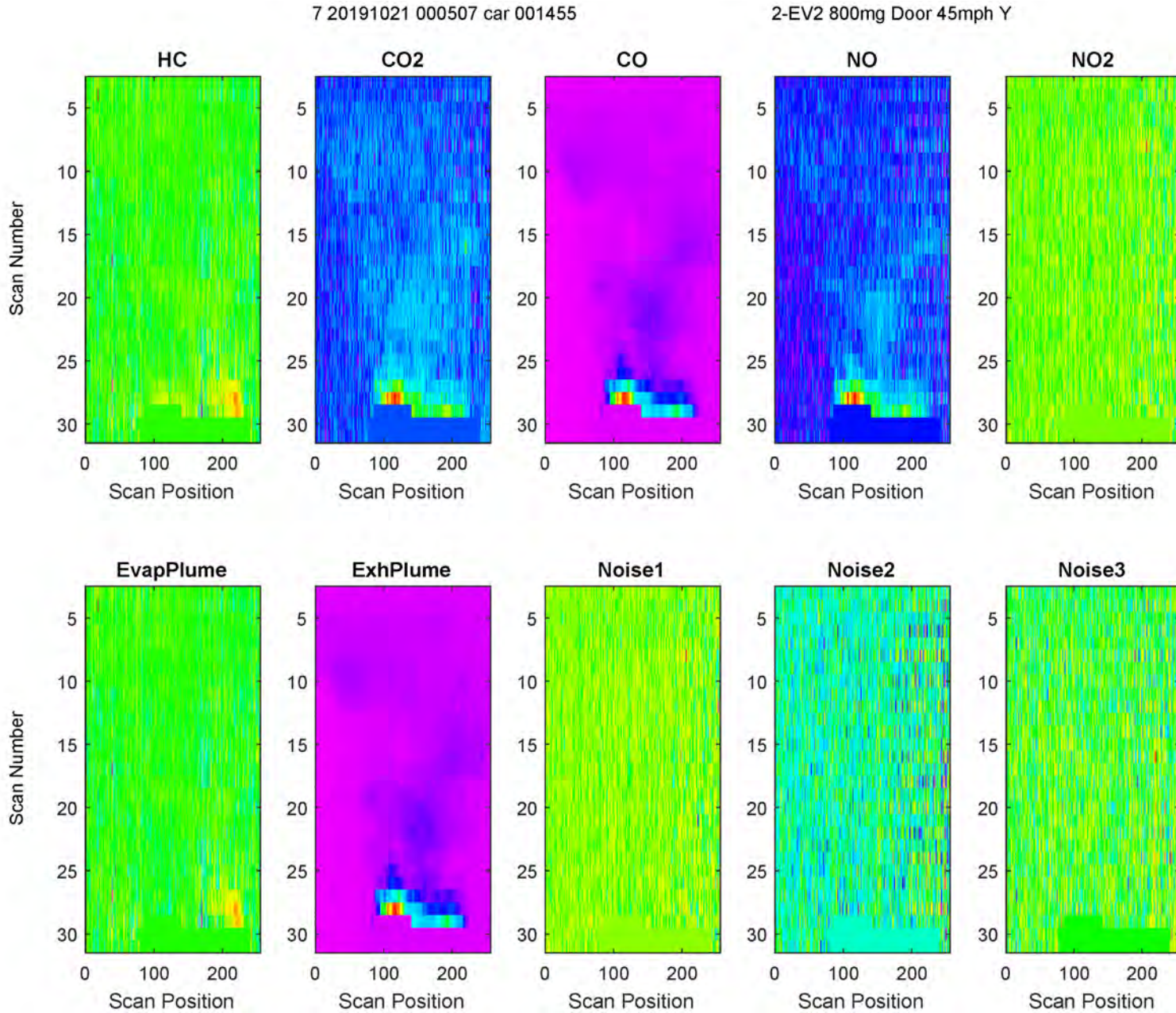
Figure D-21. BSS Example: EV-2, High EvapHC from TANK, Low Speed, HC/CO2/CO/NO Exh

7 20191024 000514 car 001635   2-EV2 6400mg Tank 22mph Y
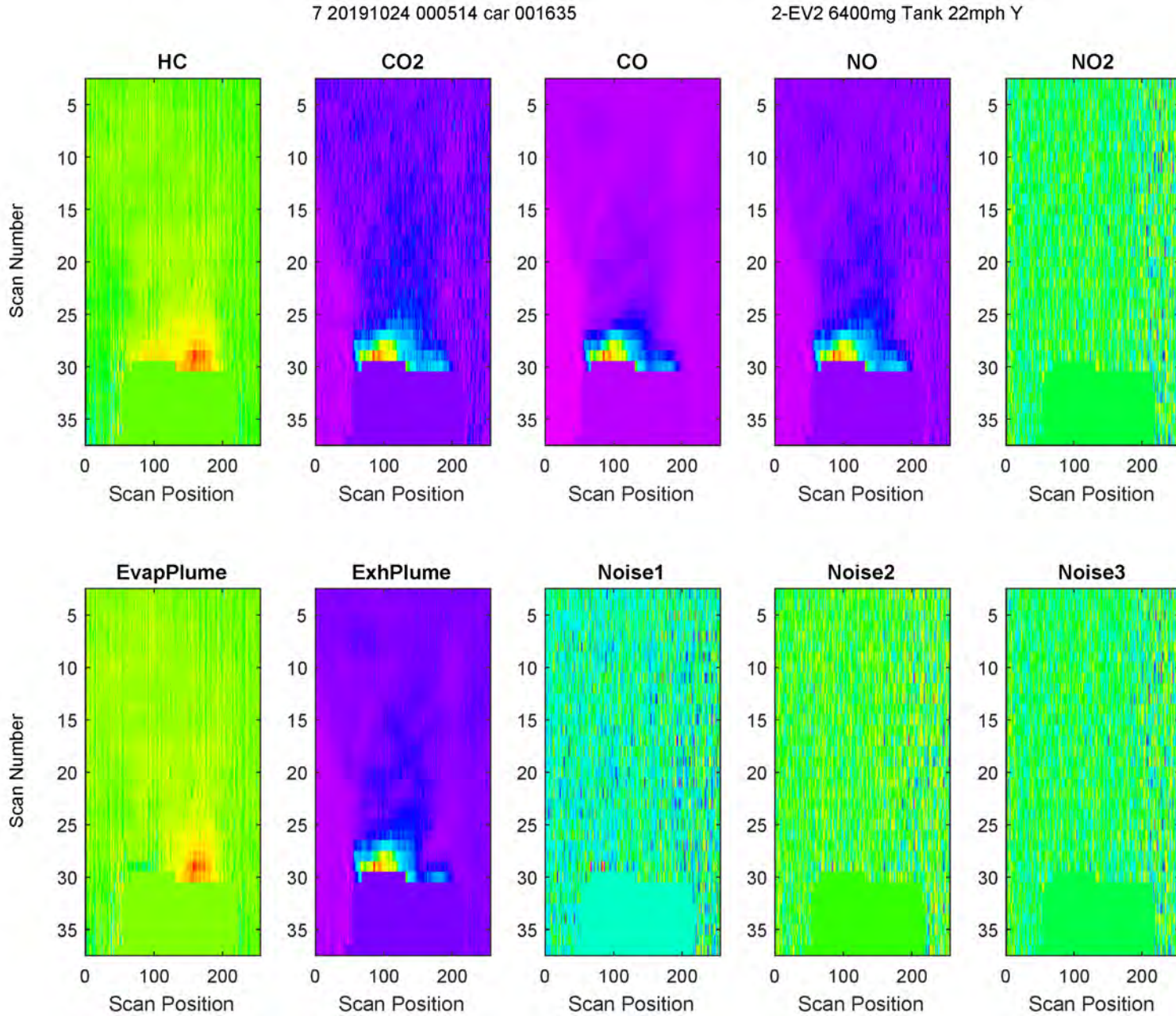
Figure D-22. BSS Example: EV-2, Medium EvapHC from TANK, Low Speed, HC/CO2/CO/NO Exh

7 20191024 000514 car 000917   2-EV2 800mg Tank 22mph Y
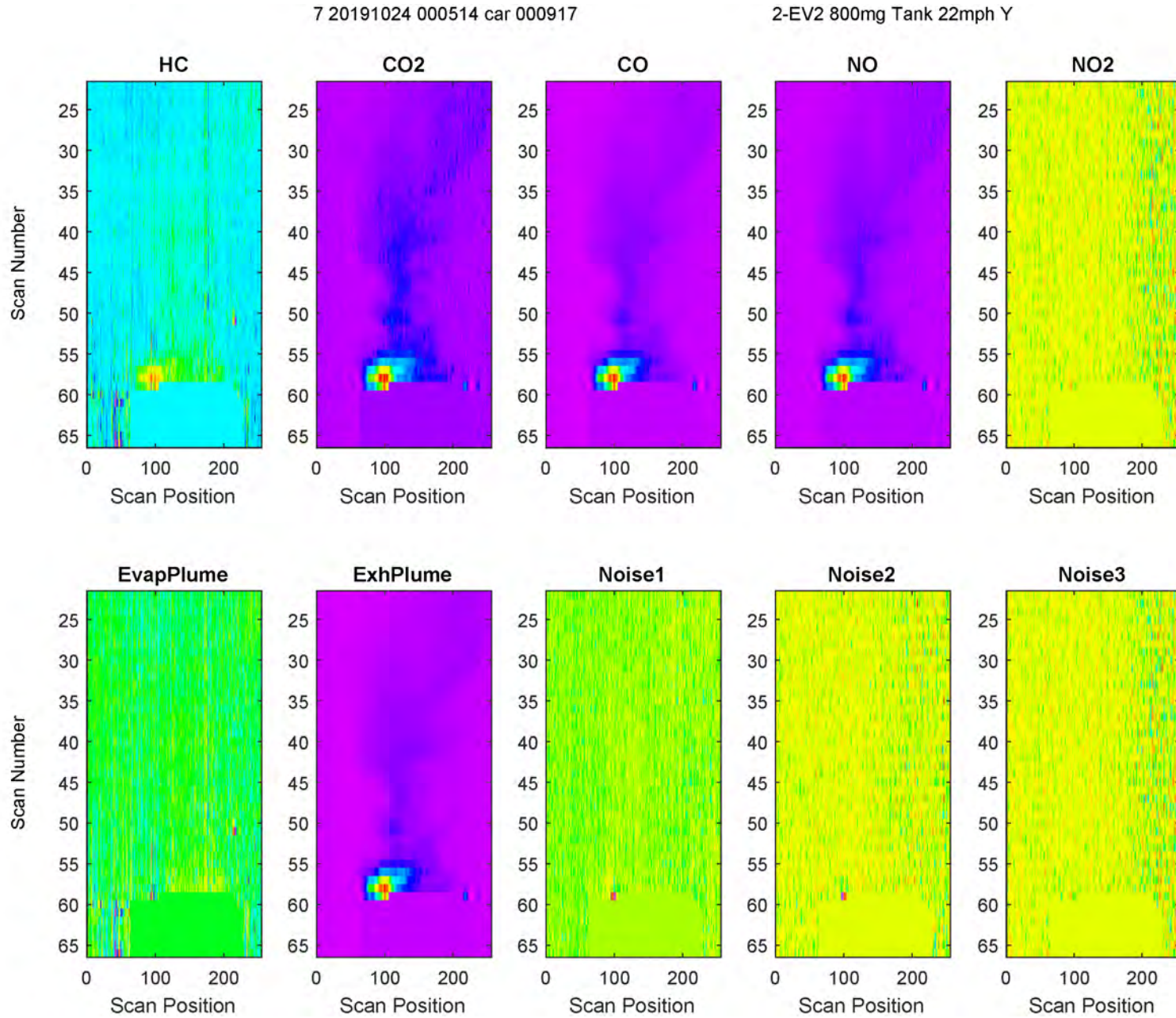
Figure D-23. BSS Example: EV-2, Low EvapHC from TANK, Low Speed, HC/CO2/CO/NO Exh

7 20191020 000506 car 000245

2-EV2 200mg Tank 22mph Y
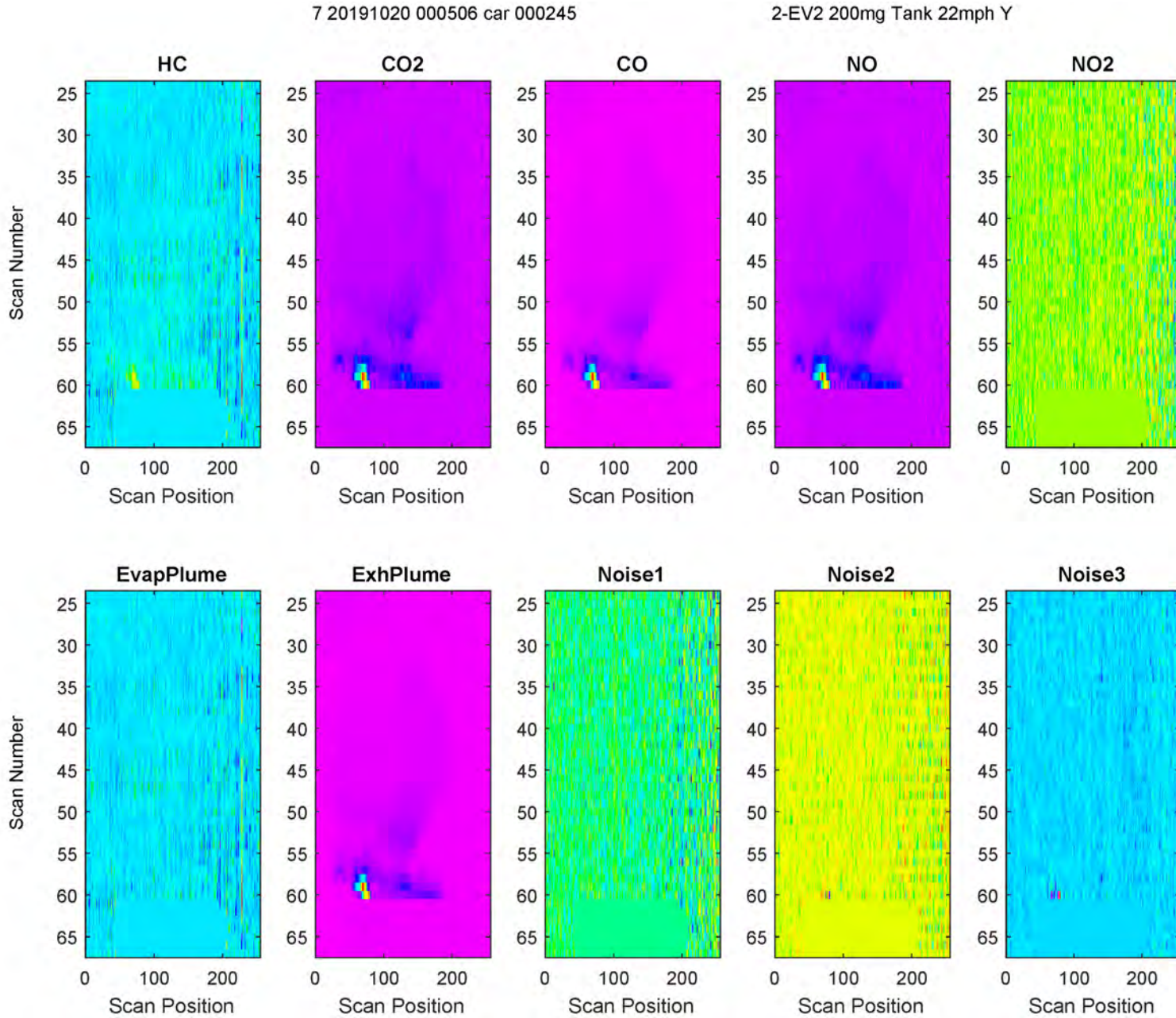
Figure D-24. BSS Example: EV-2, Medium EvapHC from TANK, High Speed, HC/CO2/CO/NO Exh
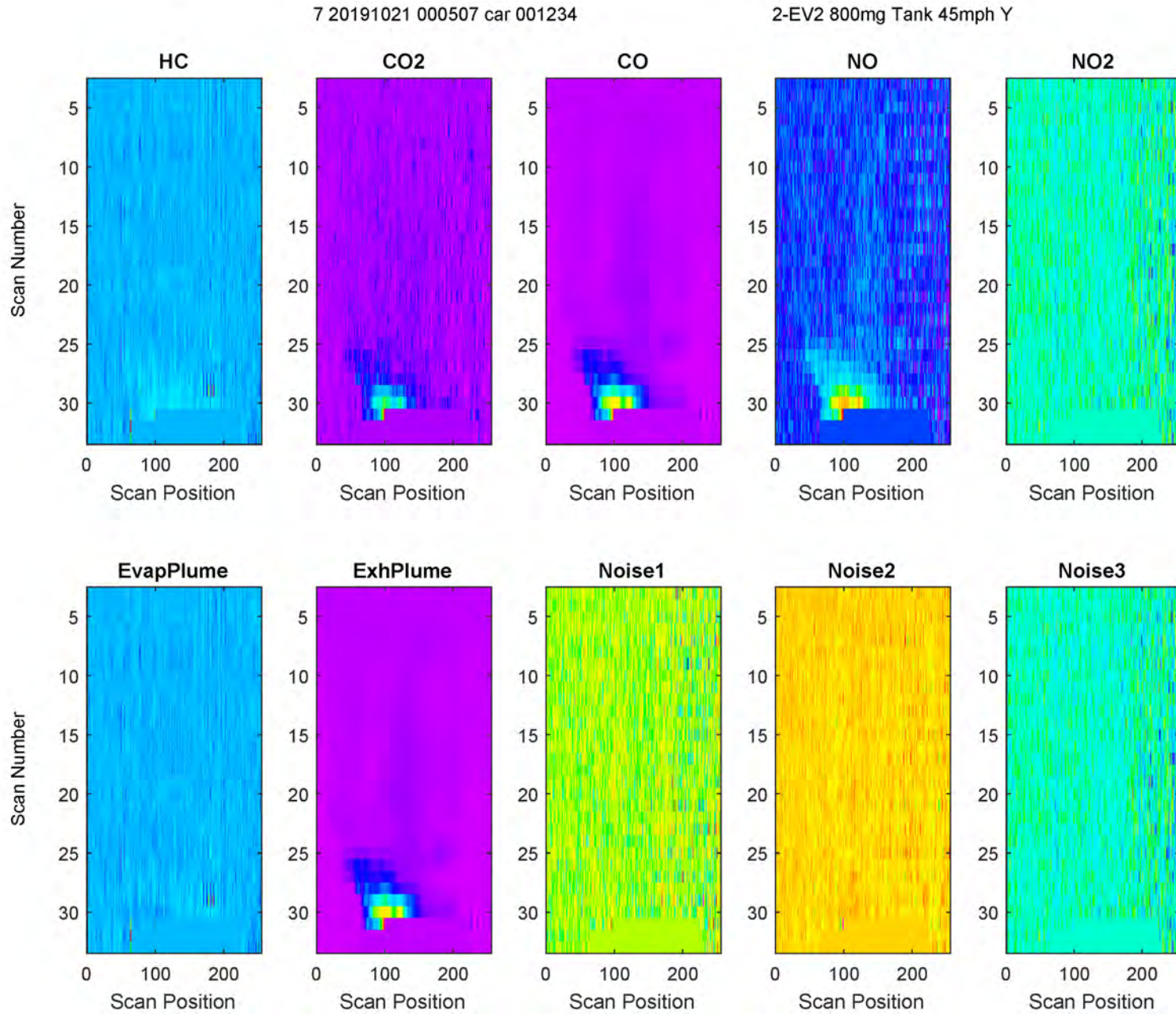
Figure D-25. BSS Example: EV-2, High EvapHC from HOOD, Low Speed, HC/CO2/CO/NO Exh
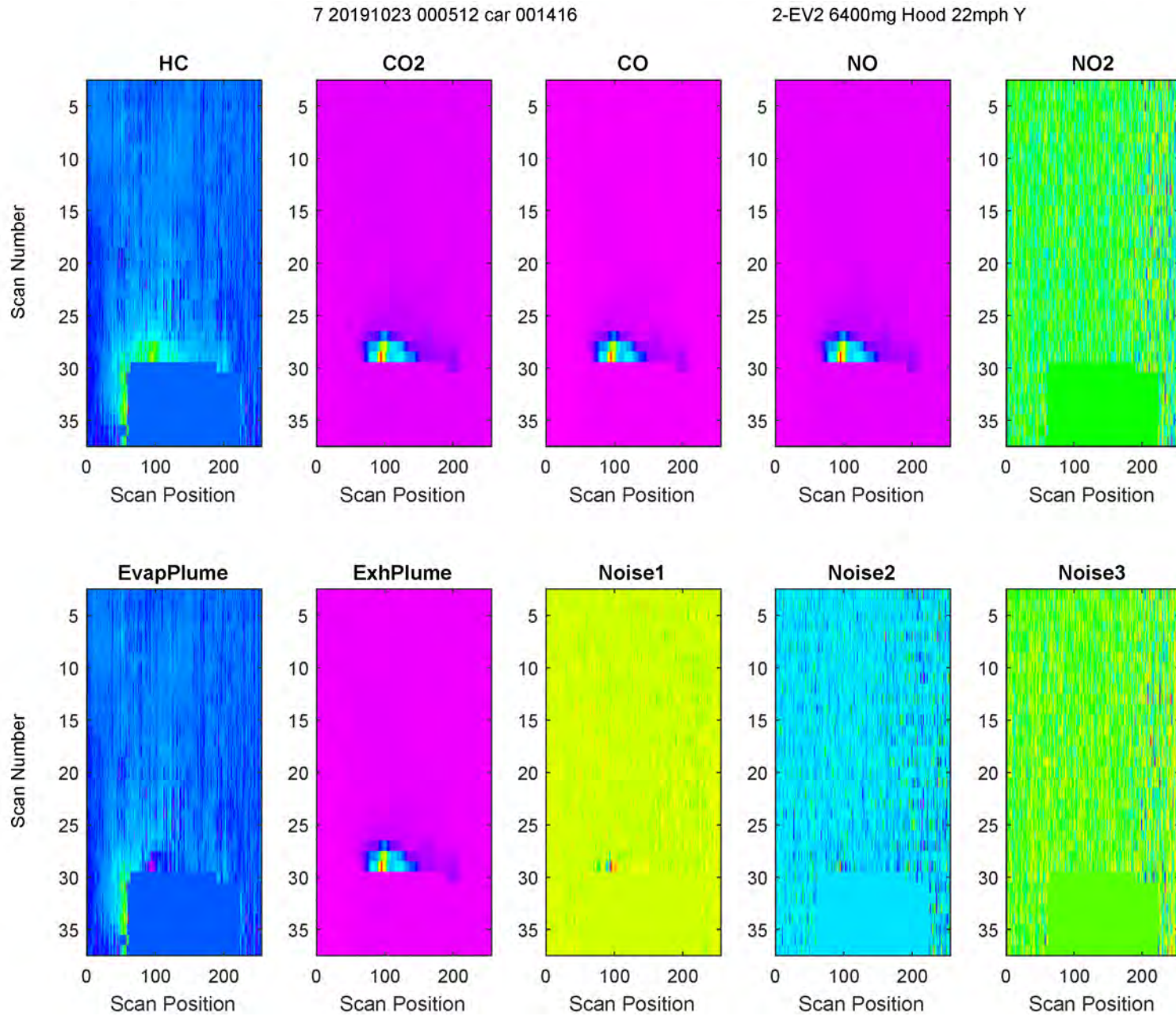
Figure D-26. BSS Example: EV-2, Medium EvapHC from HOOD, Low Speed, HC/CO2/CO/NO Exh

7 20191022 000509 car 002751   2-EV2 800mg Hood 22mph Y
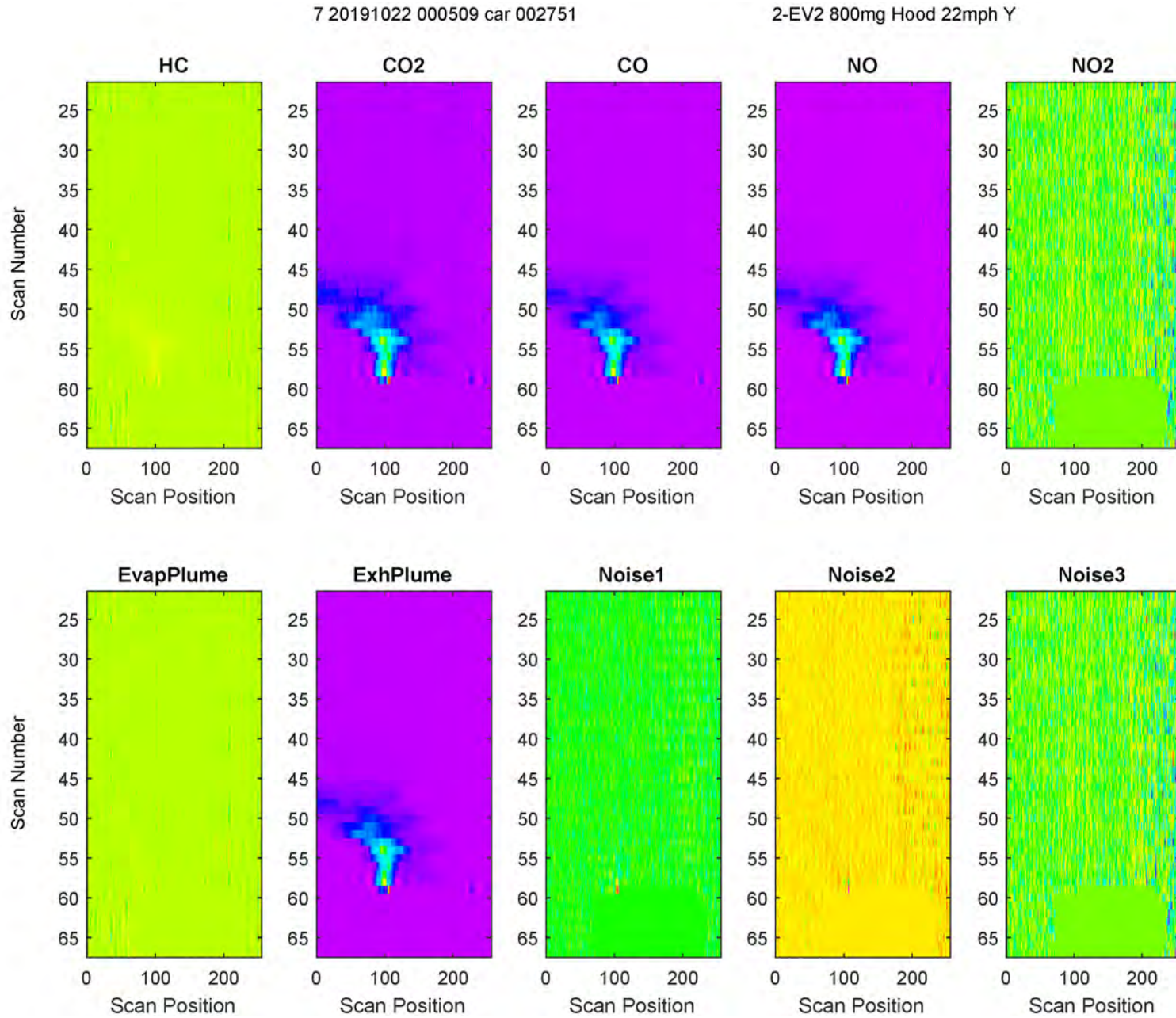
Figure D-27. BSS Example: EV-2, Low EvapHC from HOOD, Low Speed, HC/CO2/CO/NO Exh

7 20191020 000505 car 002865   2-EV2 200mg Hood 22mph Y
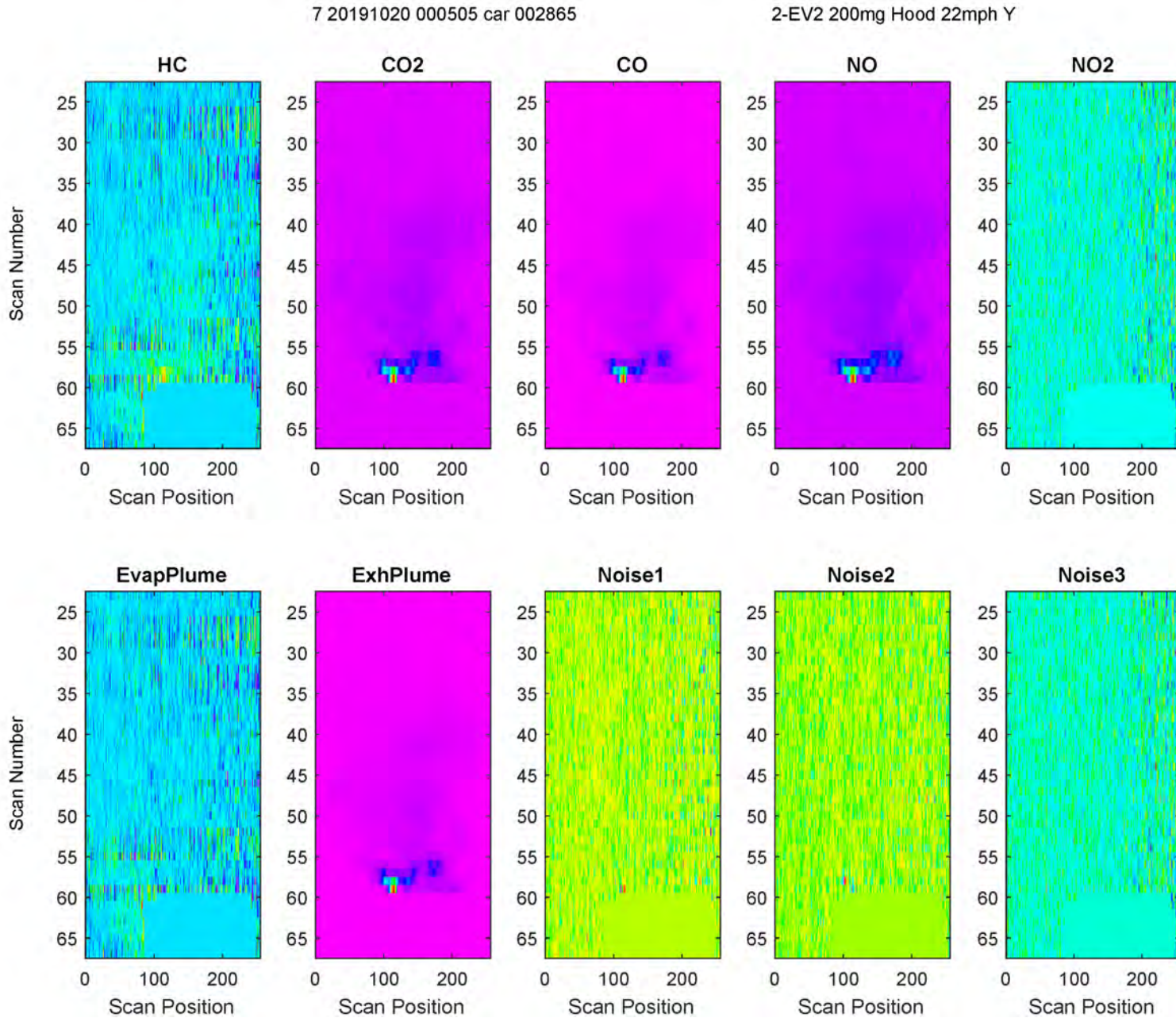
Figure D-28. BSS Example: EV-2, Medium EvapHC from HOOD, High Speed, HC/CO2/CO/NO Exh

7 20191021 000507 car 001815   2-EV2 800mg Hood 45mph Y
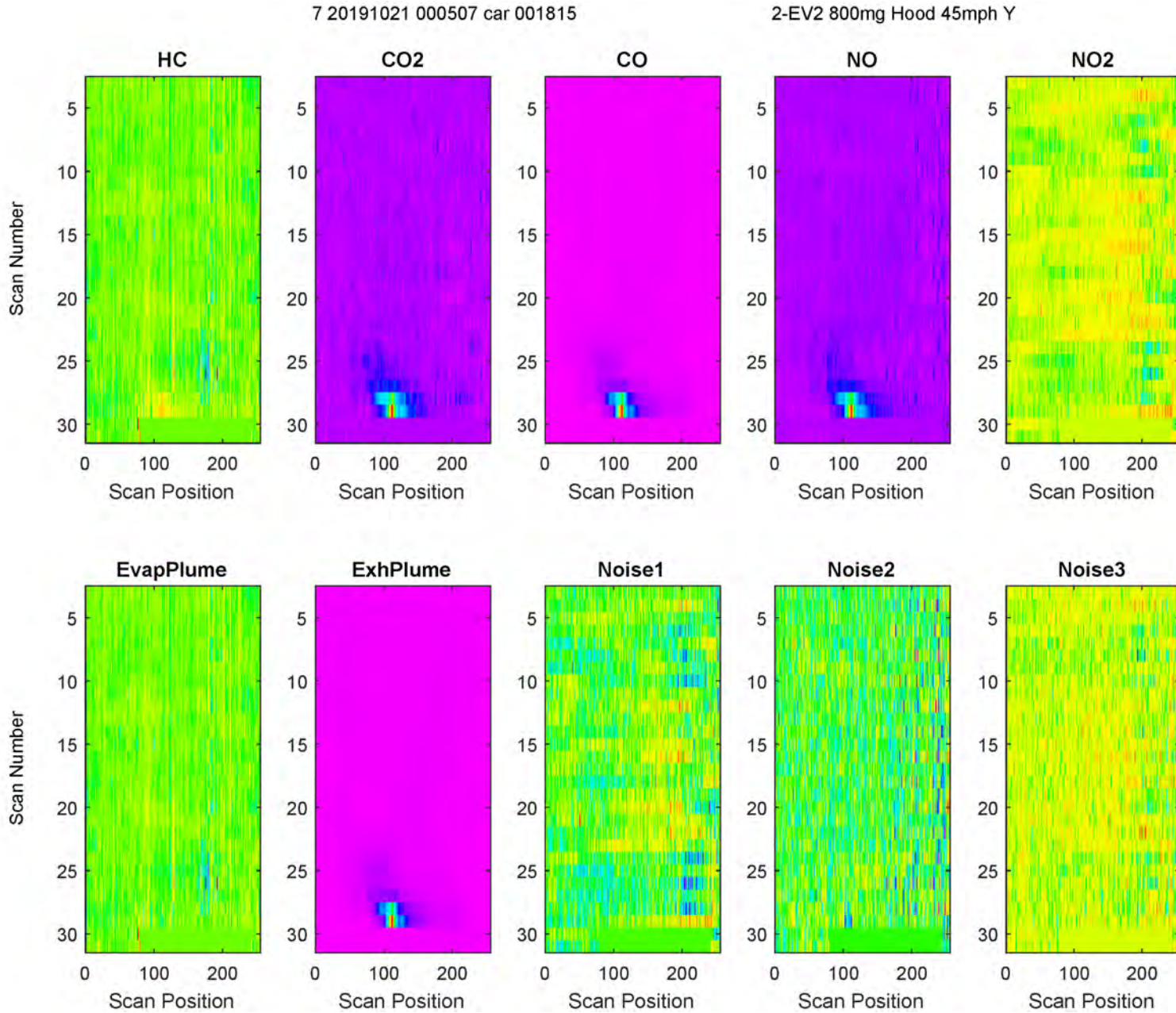
Figure D-29. BSS Example: Subaru, High EvapHC from DOOR, Low Speed, natural Exh

7 20191020 000505 car 001495   3-Subaru 6400mg Door 22mph Y
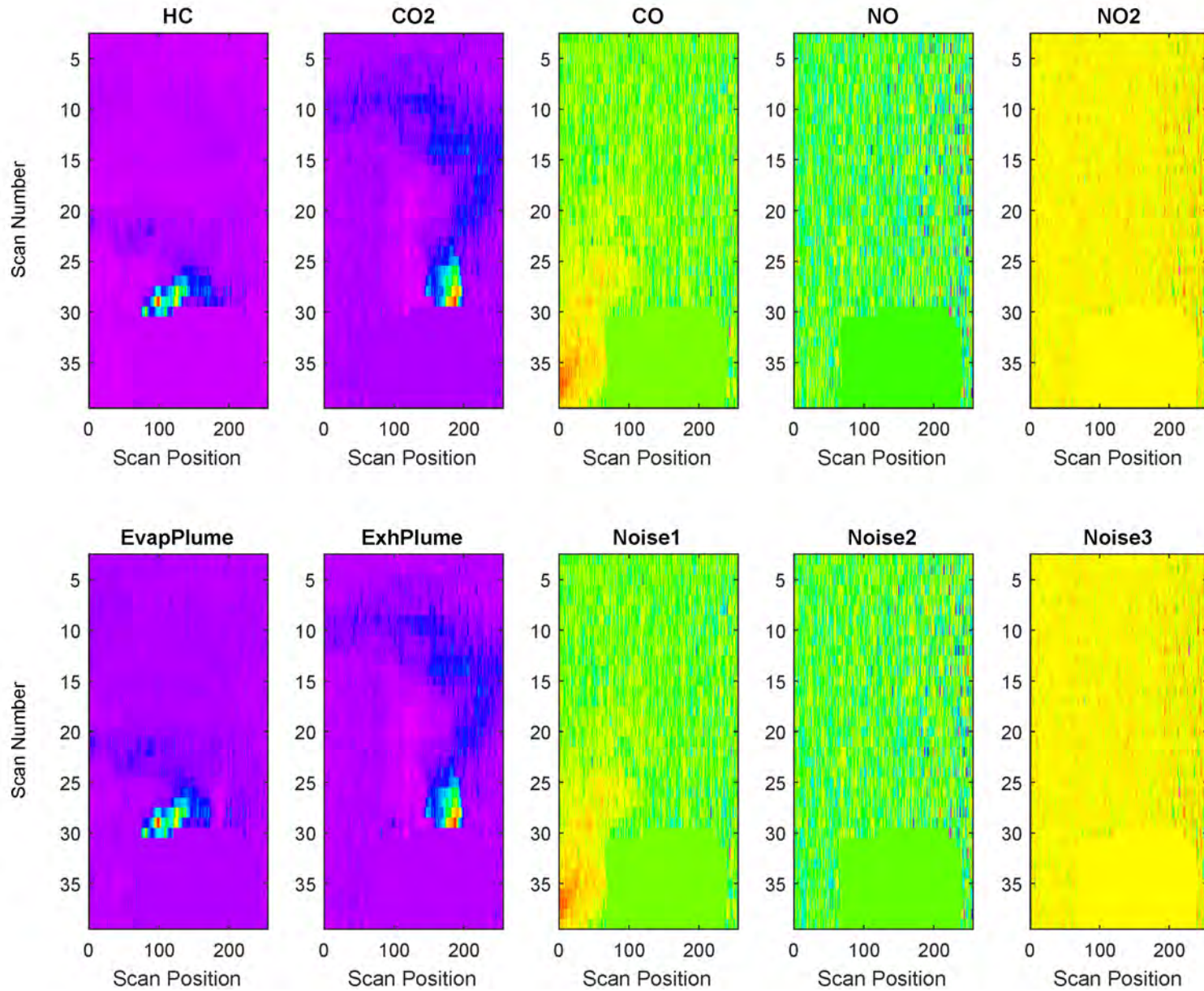
Figure D-30. BSS Example: Subaru, Medium EvapHC from DOOR, Low Speed, natural Exh
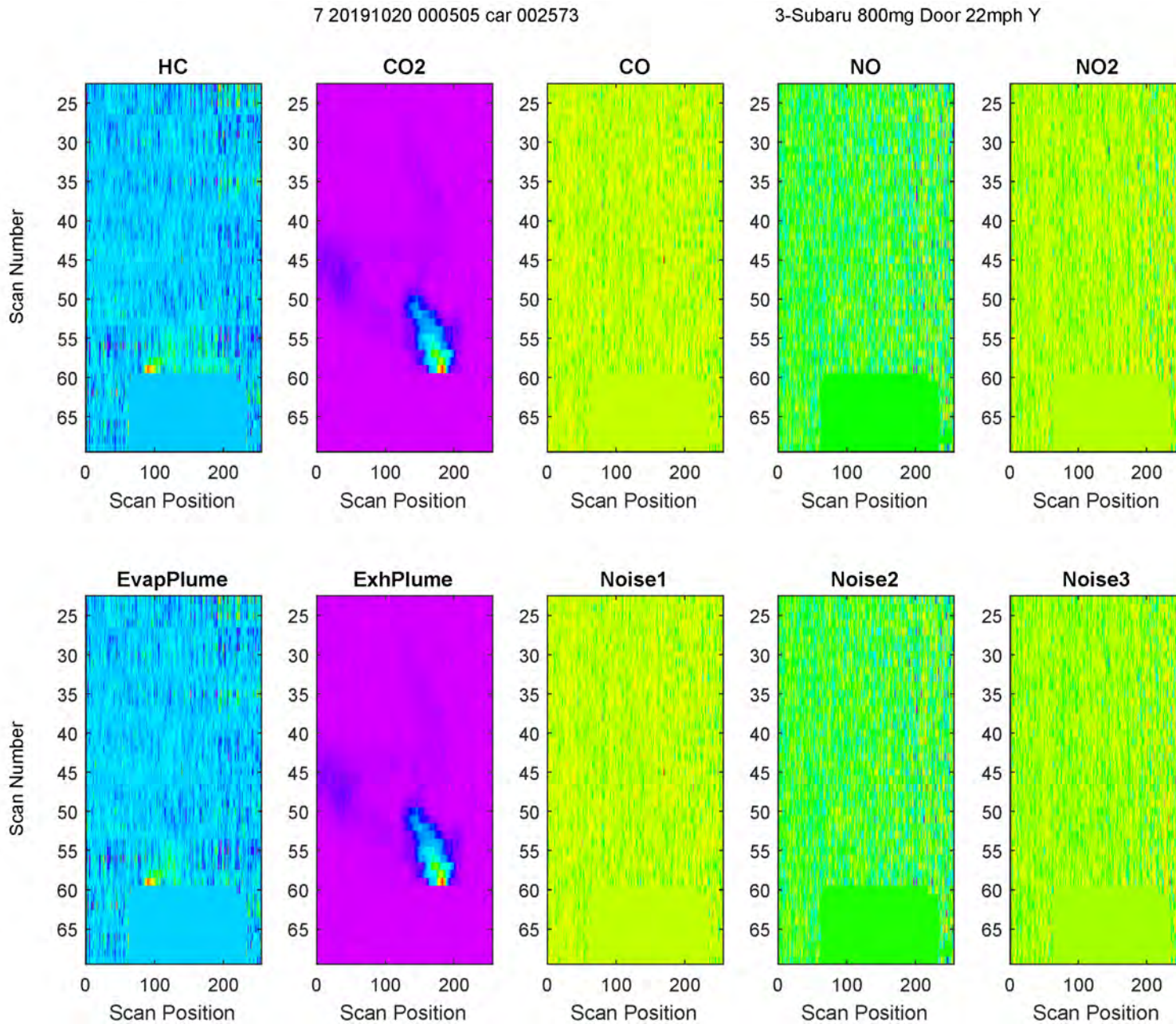
Figure D-31. BSS Example: Subaru, Low EvapHC from DOOR, Low Speed, natural Exh

7 20191021 000507 car 002191   3-Subaru 200mg Door 22mph Y
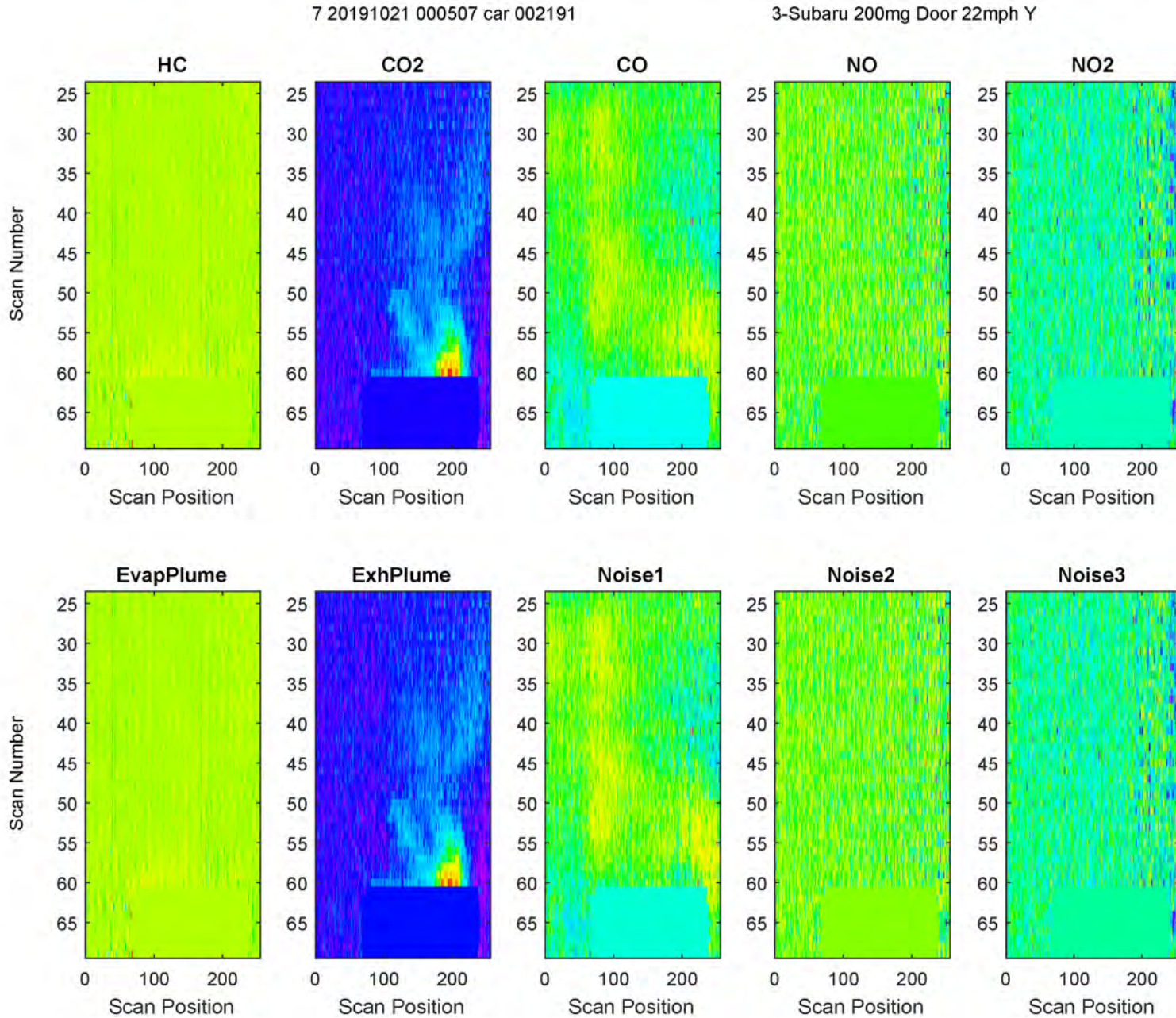
Figure D-32. BSS Example: Subaru, Medium EvapHC from DOOR, High Speed, natural Exh

7 20191020 000505 car 001682   3-Subaru 800mg Door 45mph Y
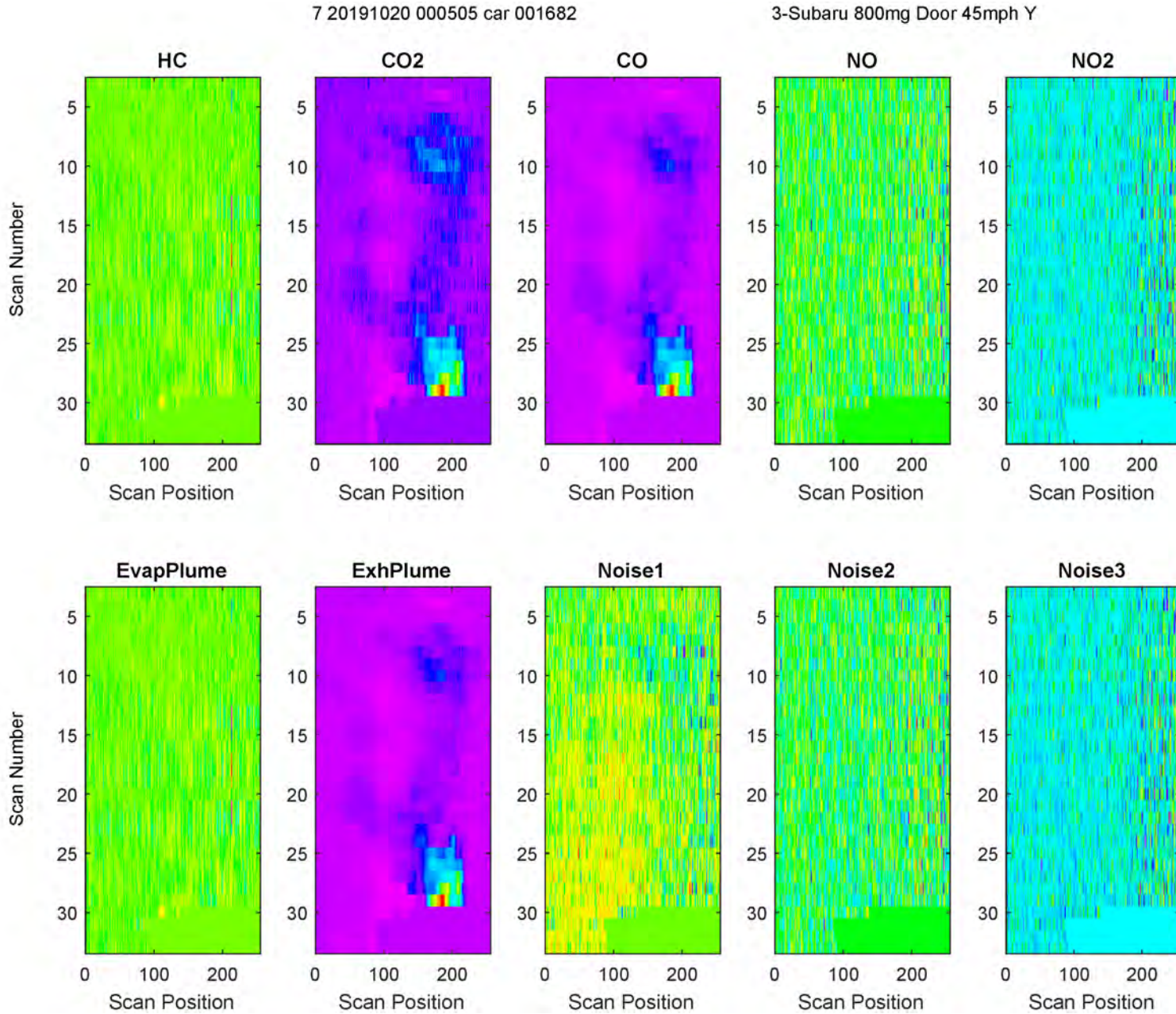
Figure D-33. BSS Example: Subaru, High EvapHC from TANK, Low Speed, natural Exh
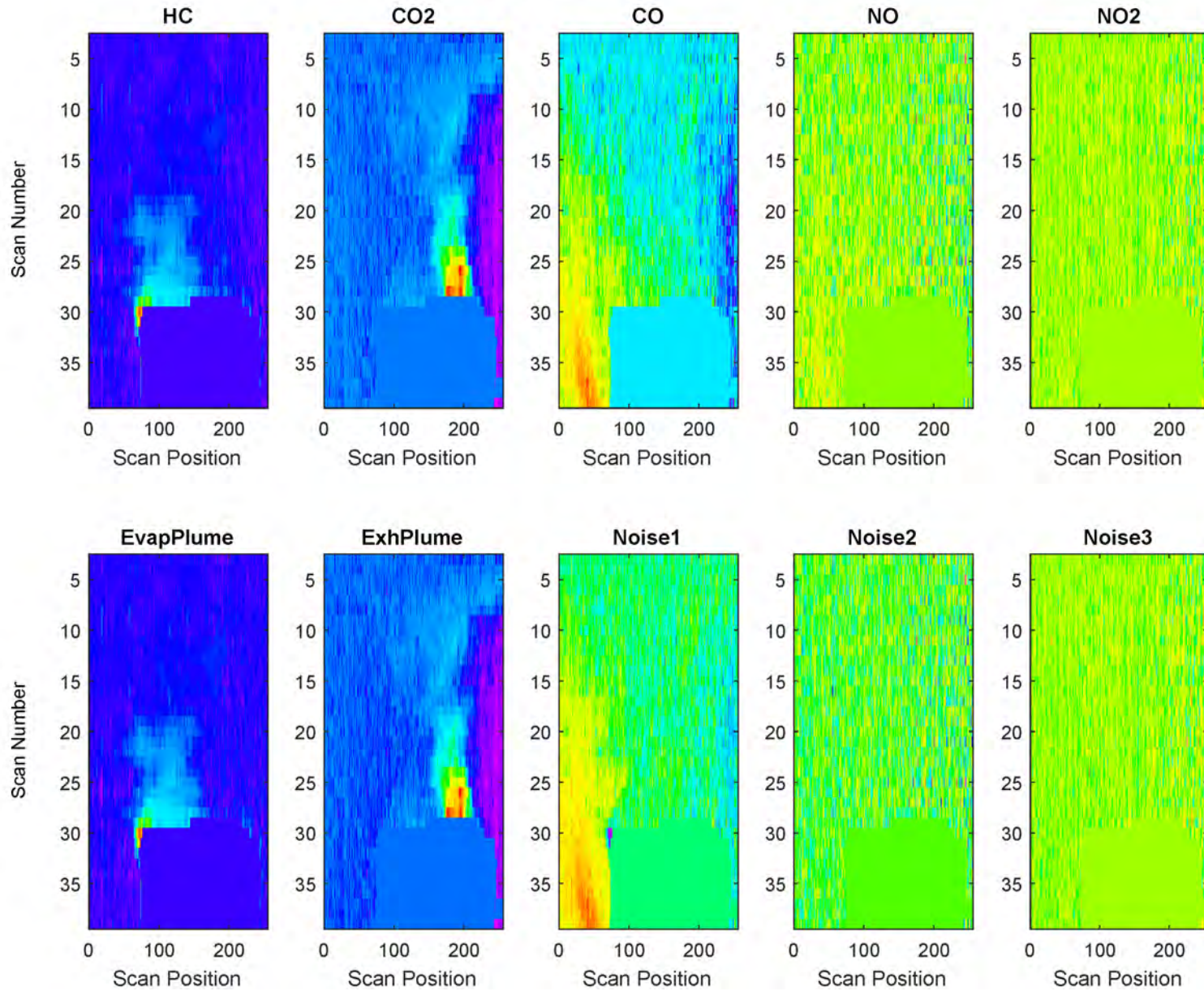
Figure D-34. BSS Example: Subaru, Medium EvapHC from TANK, Low Speed, natural Exh

7 20191021 000507 car 002807   3-Subaru 800mg Tank 22mph Y
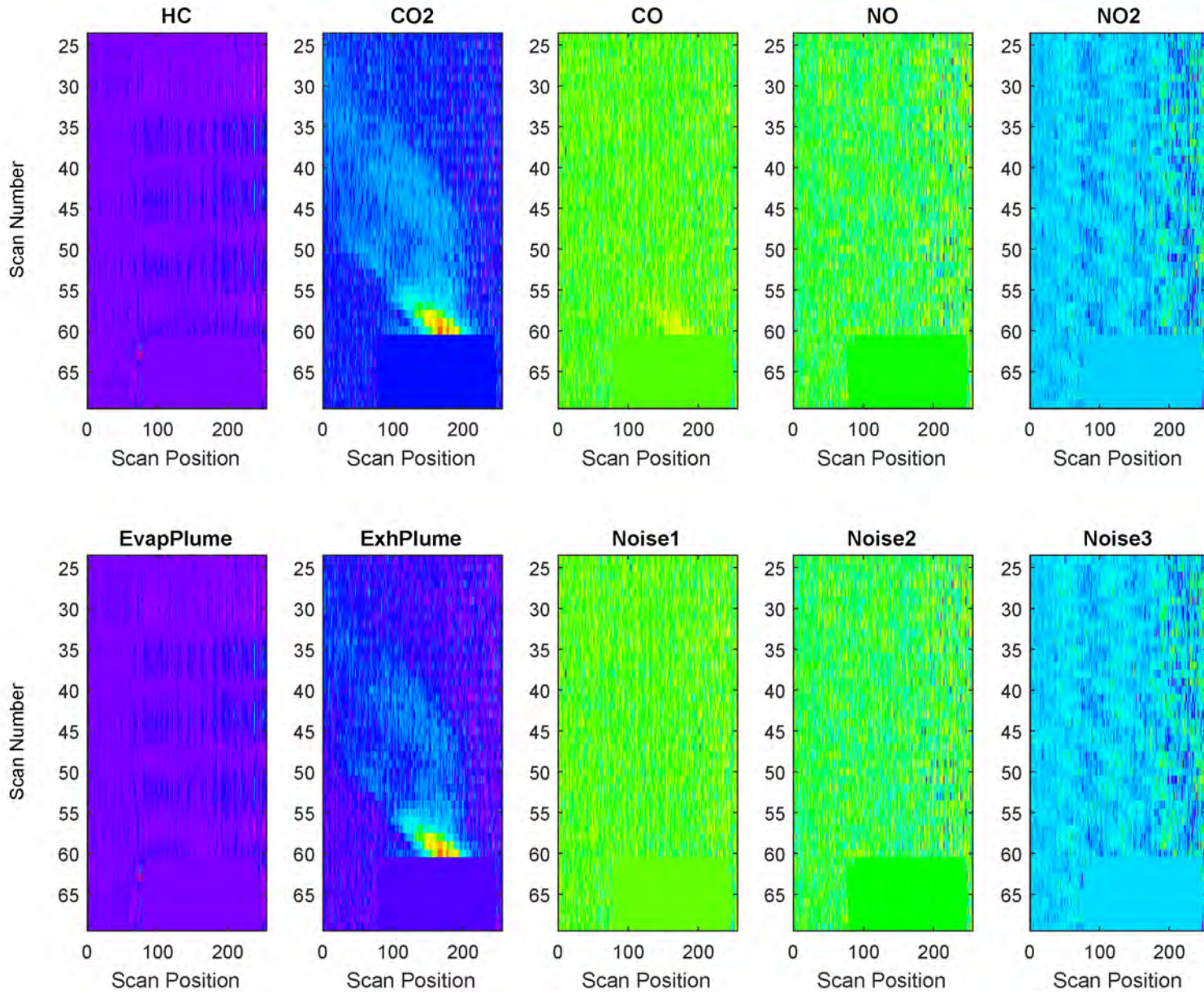
Figure D-35. BSS Example: Subaru, Low EvapHC from TANK, Low Speed, natural Exh
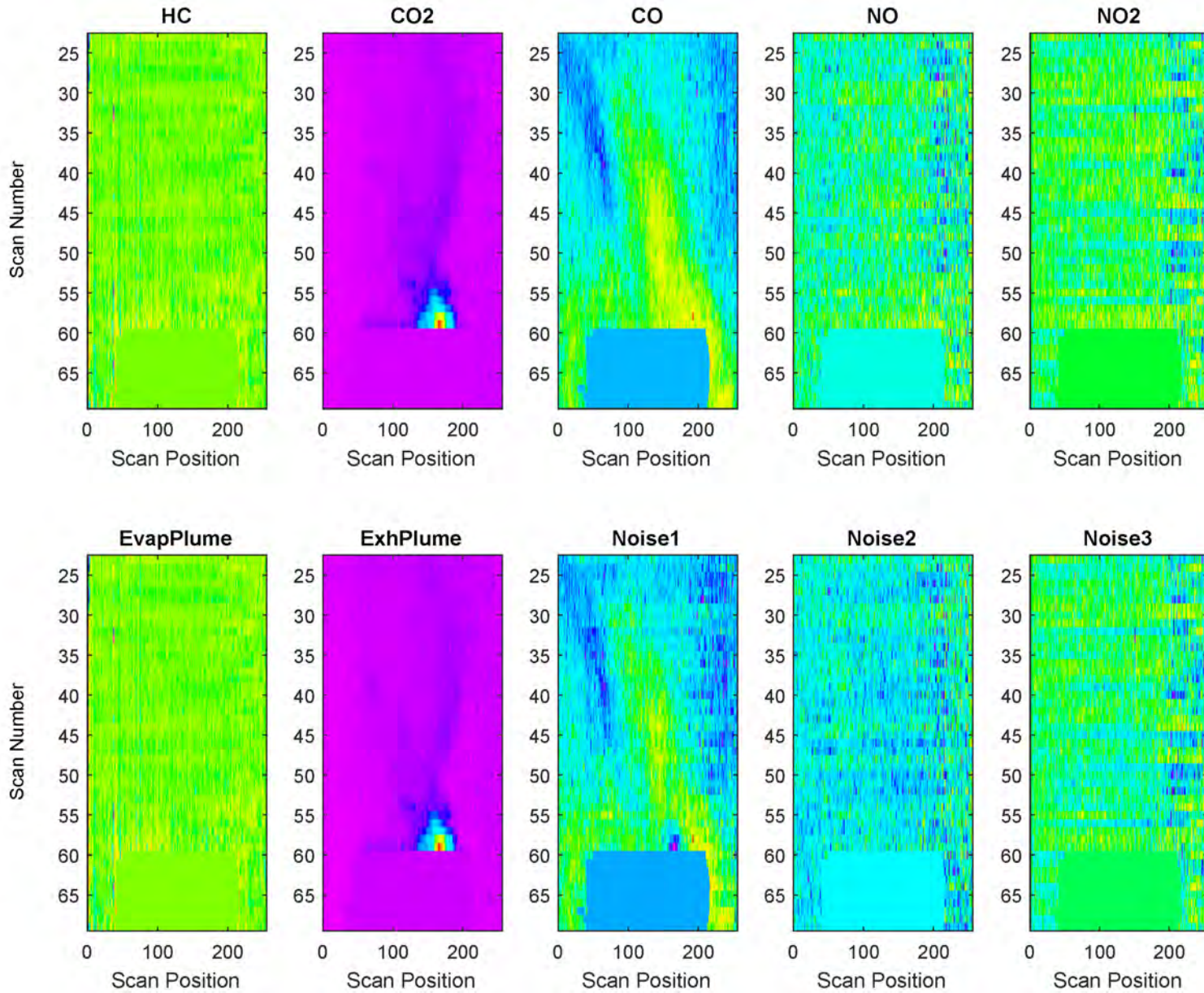
Figure D-36. BSS Example: Subaru, Medium EvapHC from TANK, High Speed, natural Exh

7 20191021 000507 car 001235   3-Subaru 800mg Tank 45mph Y
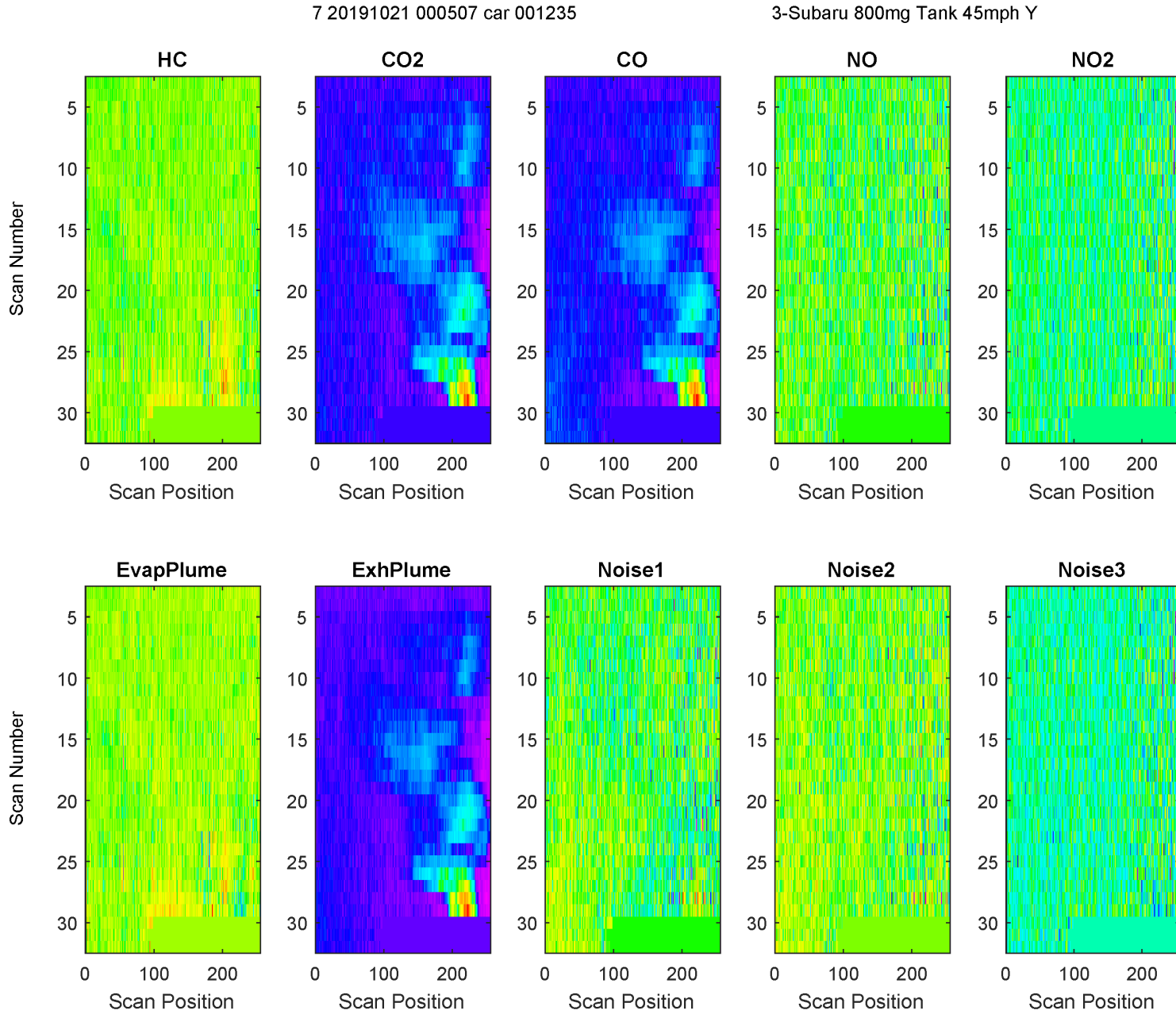
Figure D-37. BSS Example: Subaru, High EvapHC from HOOD, Low Speed, natural Exh

7 20191020 000505 car 001814   3-Subaru 6400mg Hood 22mph Y
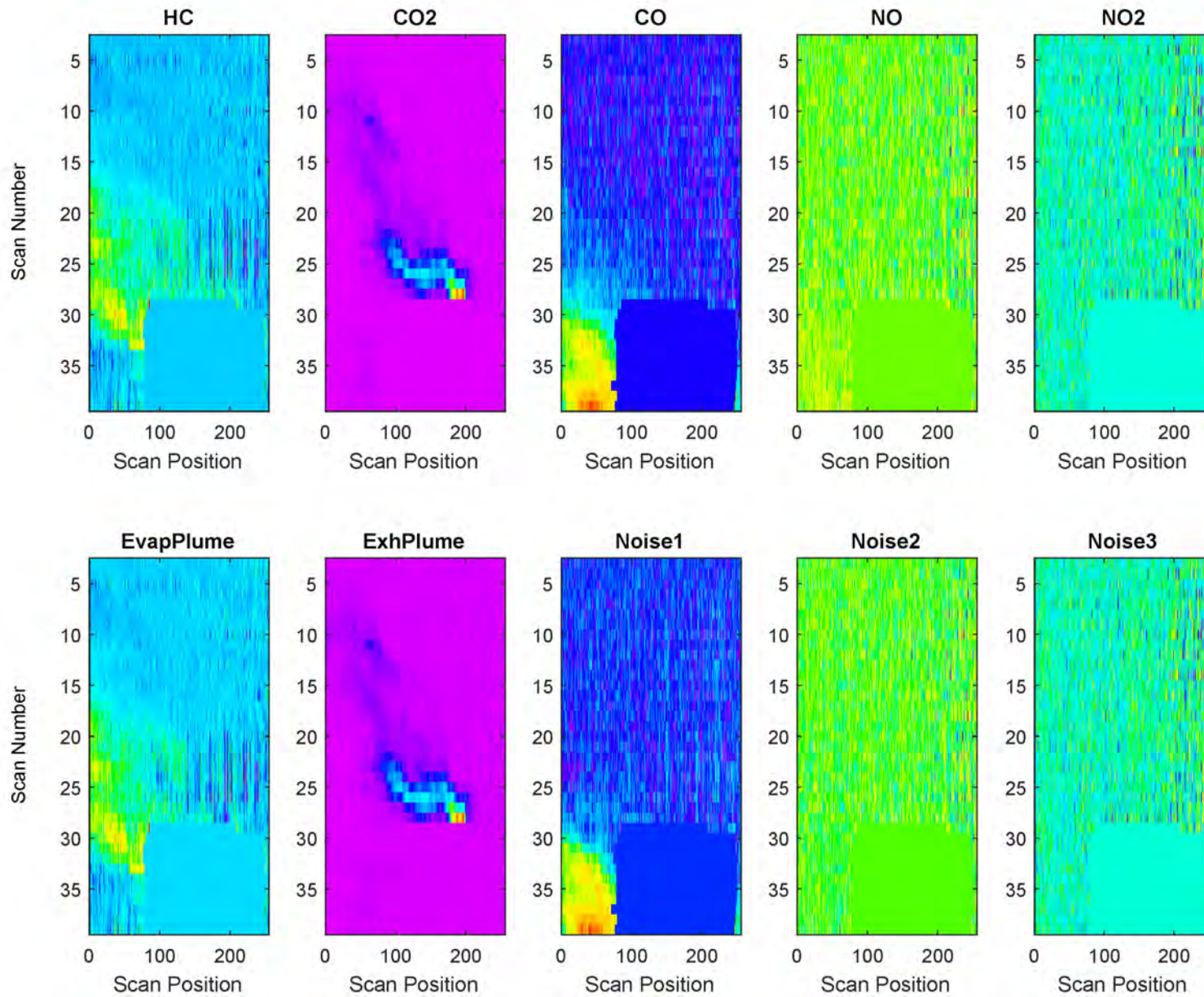
Figure D-38. BSS Example: Subaru, Medium EvapHC from HOOD, Low Speed, natural Exh

7 20191020 000505 car 002430   3-Subaru 800mg Hood 22mph Y

HC   CO2   CO   NO   NO2

EvapPlume   ExhPlume   Noise1   Noise2   Noise3
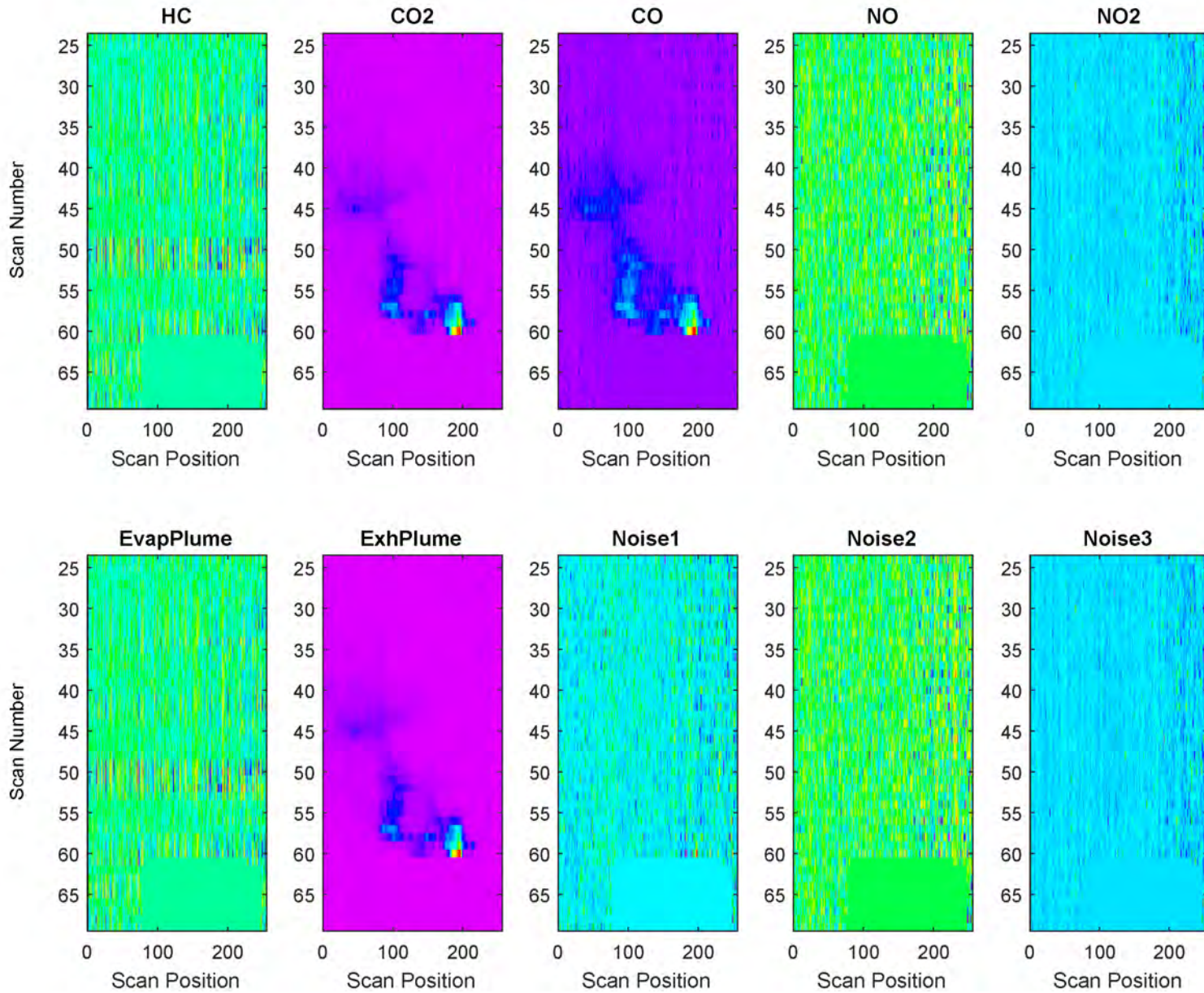
Figure D-39. BSS Example: Subaru, Low EvapHC from HOOD, Low Speed, natural Exh
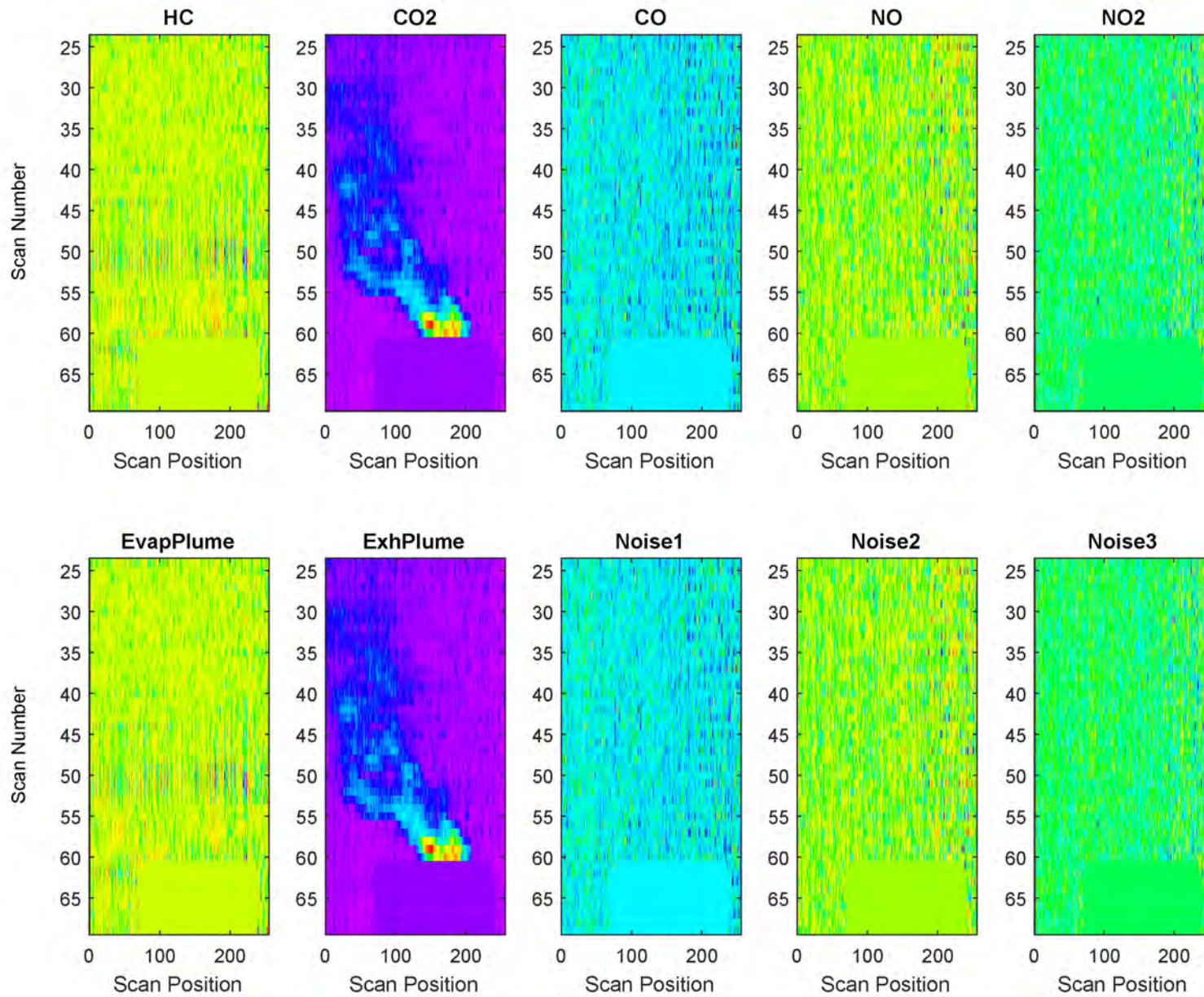
Figure D-40. BSS Example: Subaru, Medium EvapHC from HOOD, High Speed, natural Exh

7 20191021 000507 car 001816   3-Subaru 800mg Hood 45mph Y
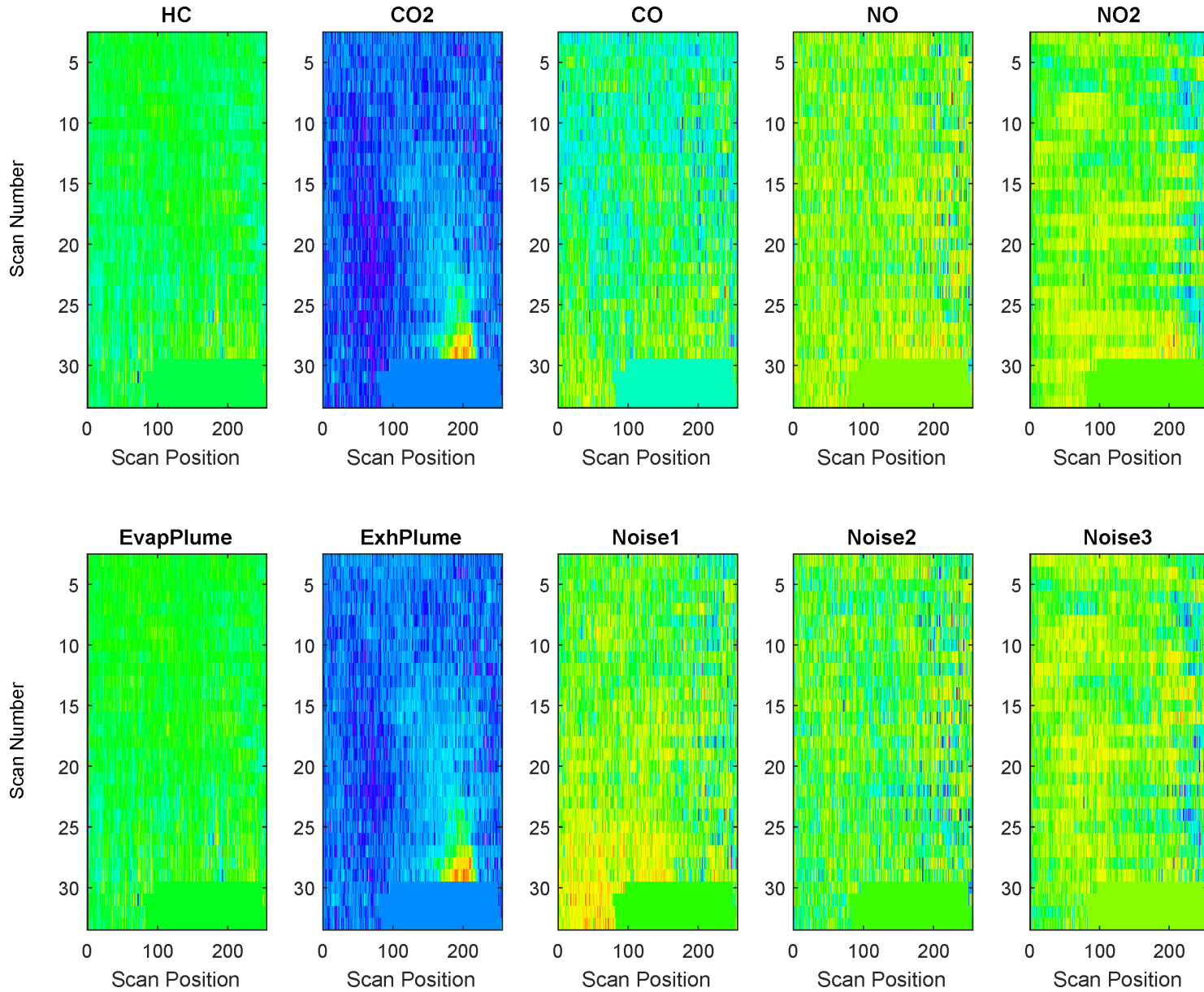
Figure D-41. BSS Example: F-150, High EvapHC from DOOR, Low Speed, natural Exh

Figure D-42. BSS Example: F-150, Medium EvapHC from DOOR, Low Speed, natural Exh

7 20191023 000512 car 002587   3-F150 800mg Door 22mph Y
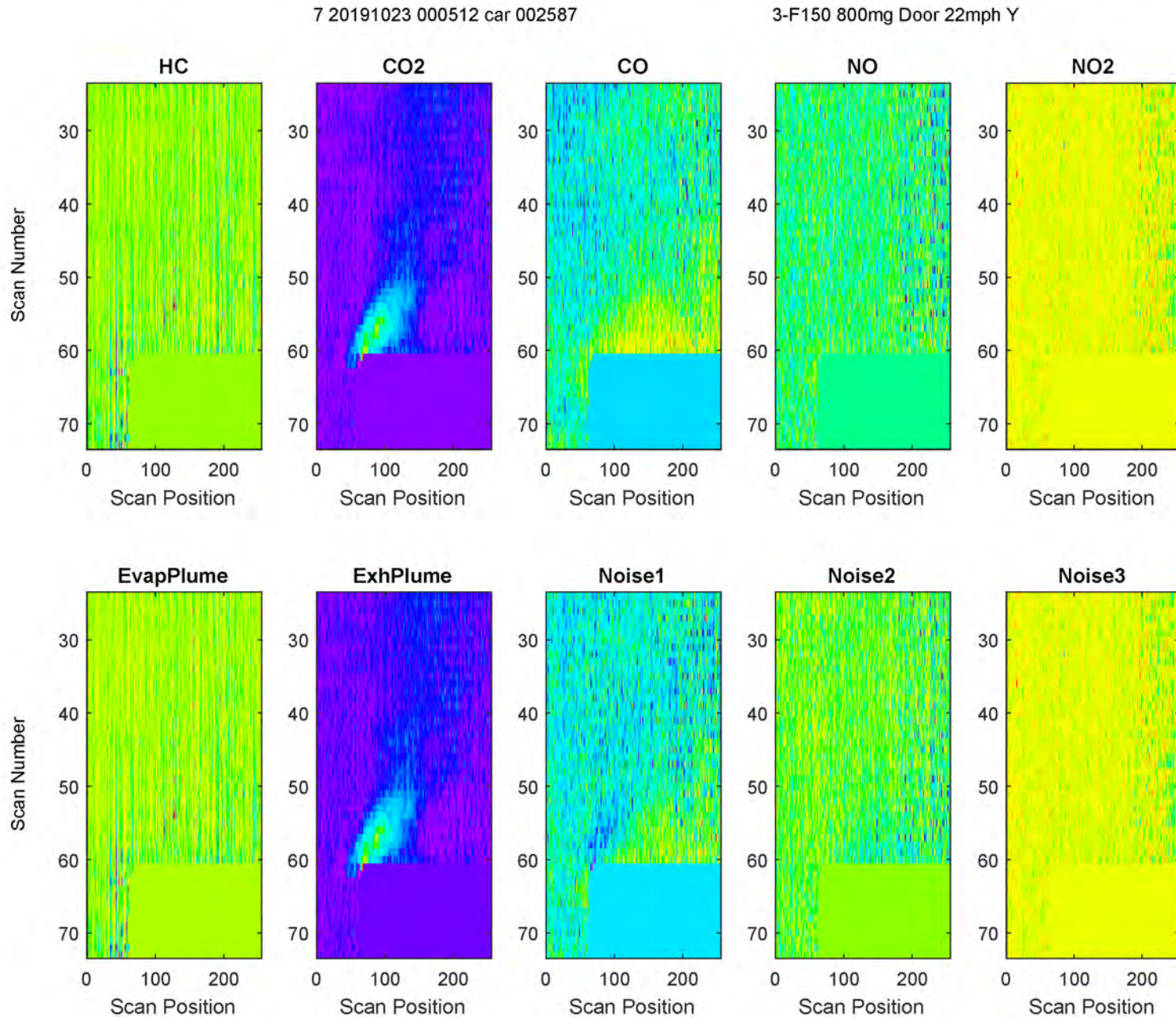
Figure D-43. BSS Example: F-150, Low EvapHC from DOOR, Low Speed, natural Exh

7 20191023 000512 car 001956   3-F150 200mg Door 22mph Y
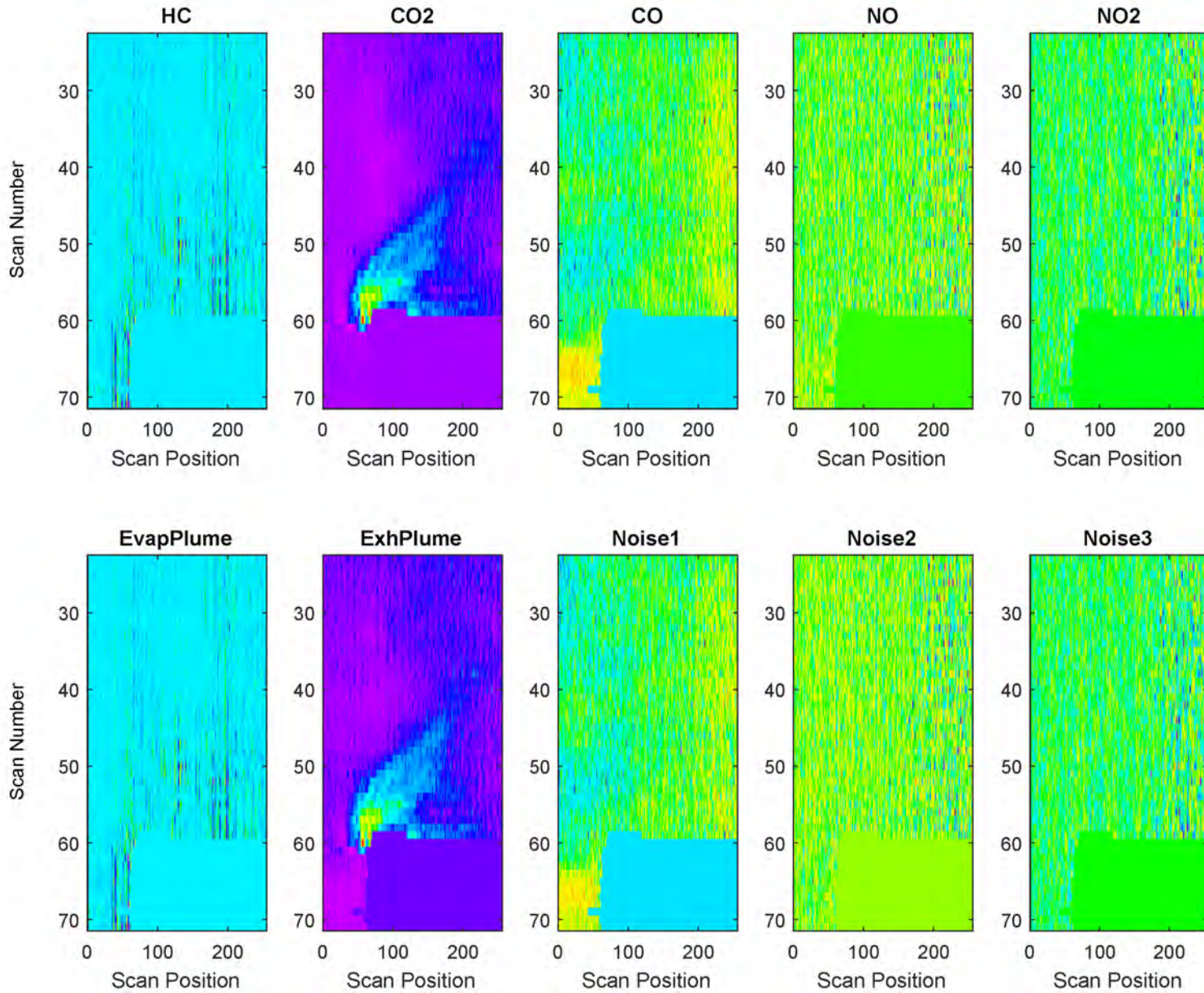
Figure D-44. BSS Example: F-150, Medium EvapHC from DOOR, High Speed, natural Exh

7 20191023 000513 car 000044   3-F150 800mg Door 45mph Y
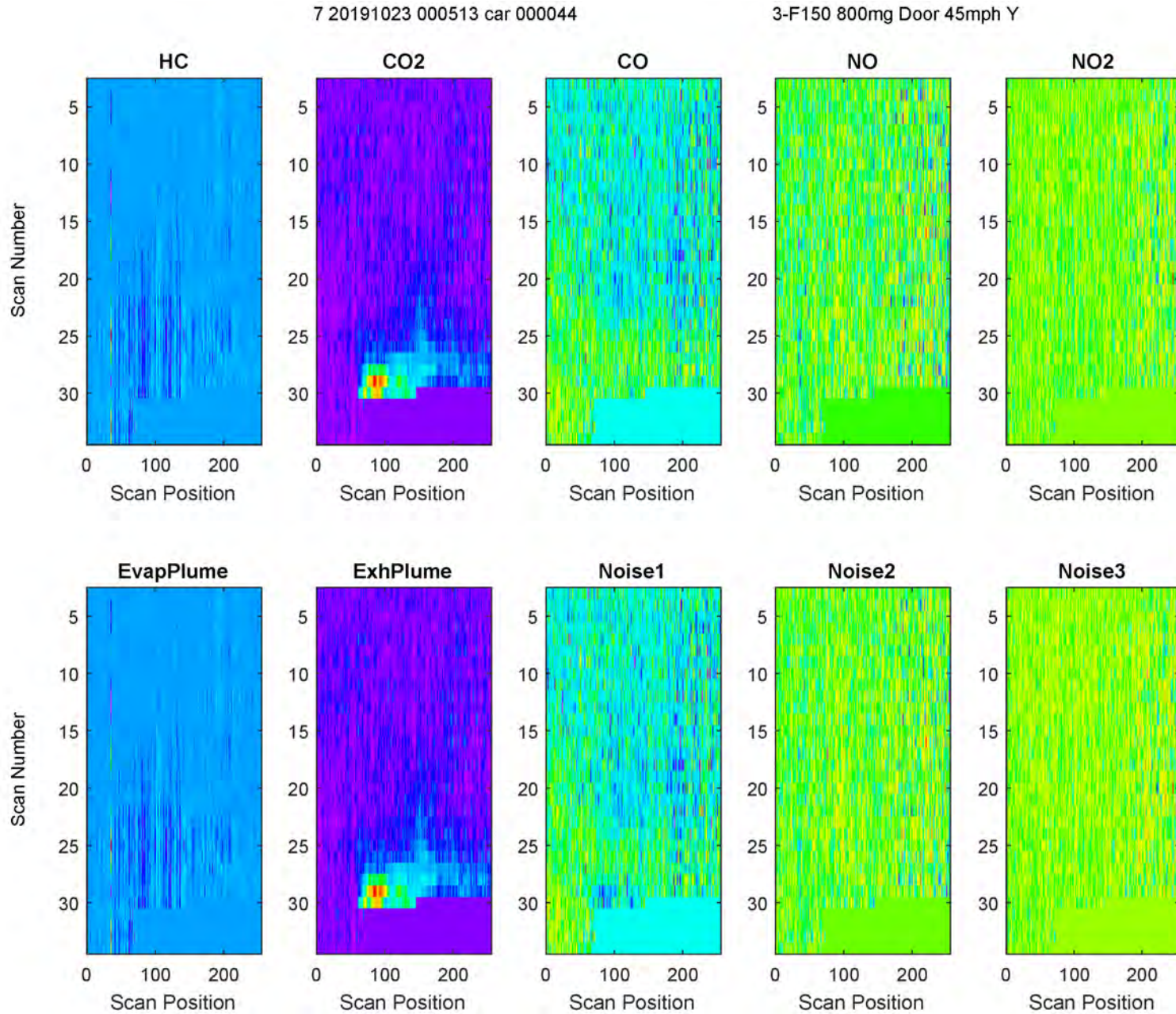
Figure D-45. BSS Example: F-150, High EvapHC from TANK, Low Speed, natural Exh

7 20191023 000512 car 000927   3-F150 6400mg Tank 22mph Y
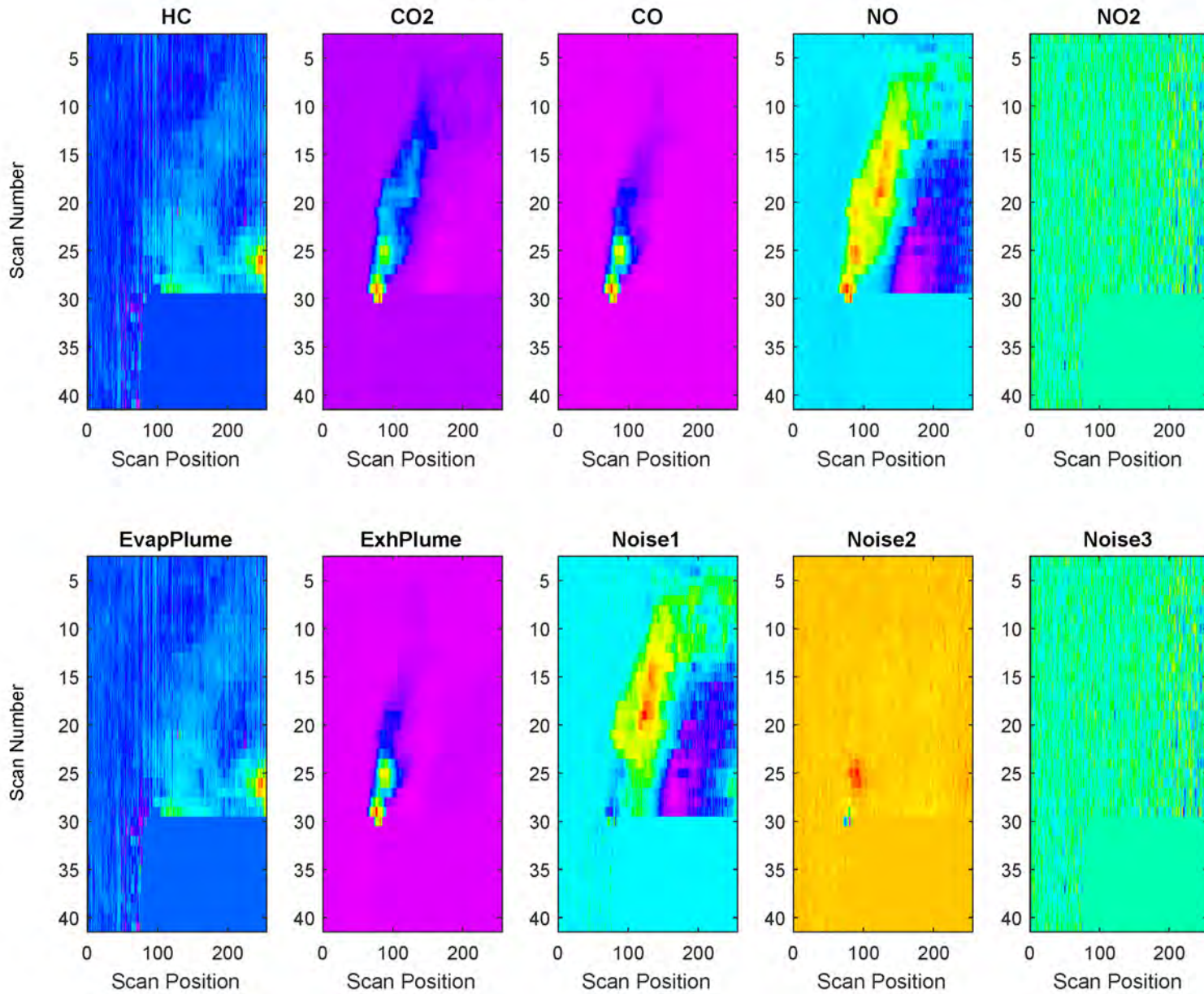
Figure D-46. BSS Example: F-150, Medium EvapHC from TANK, Low Speed, natural Exh

7 20191023 000512 car 002719   3-F150 800mg Tank 22mph Y
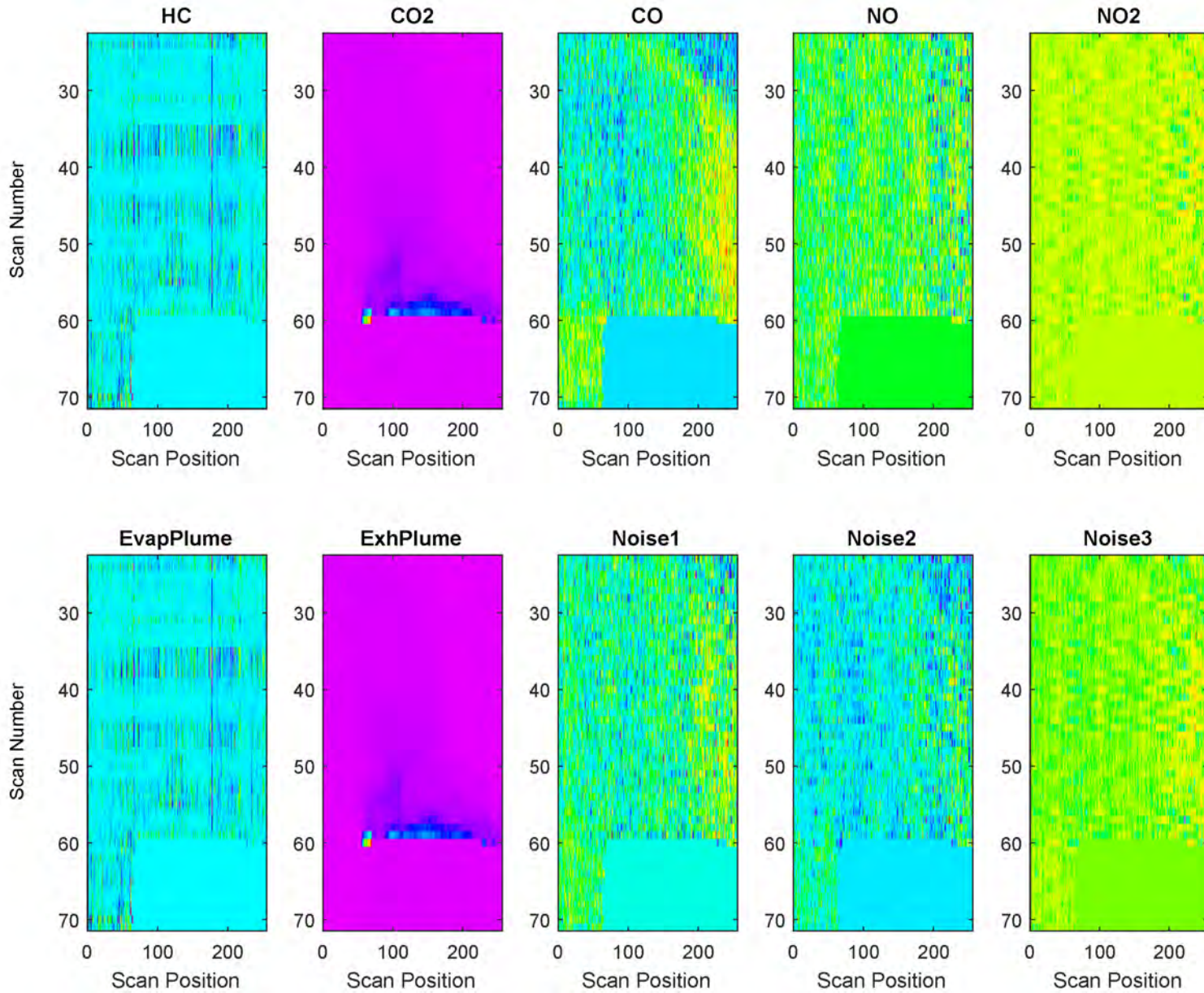
Figure D-47. BSS Example: F-150, Low EvapHC from TANK, Low Speed, natural Exh

7 20191023 000512 car 002207   3-F150 200mg Tank 22mph Y
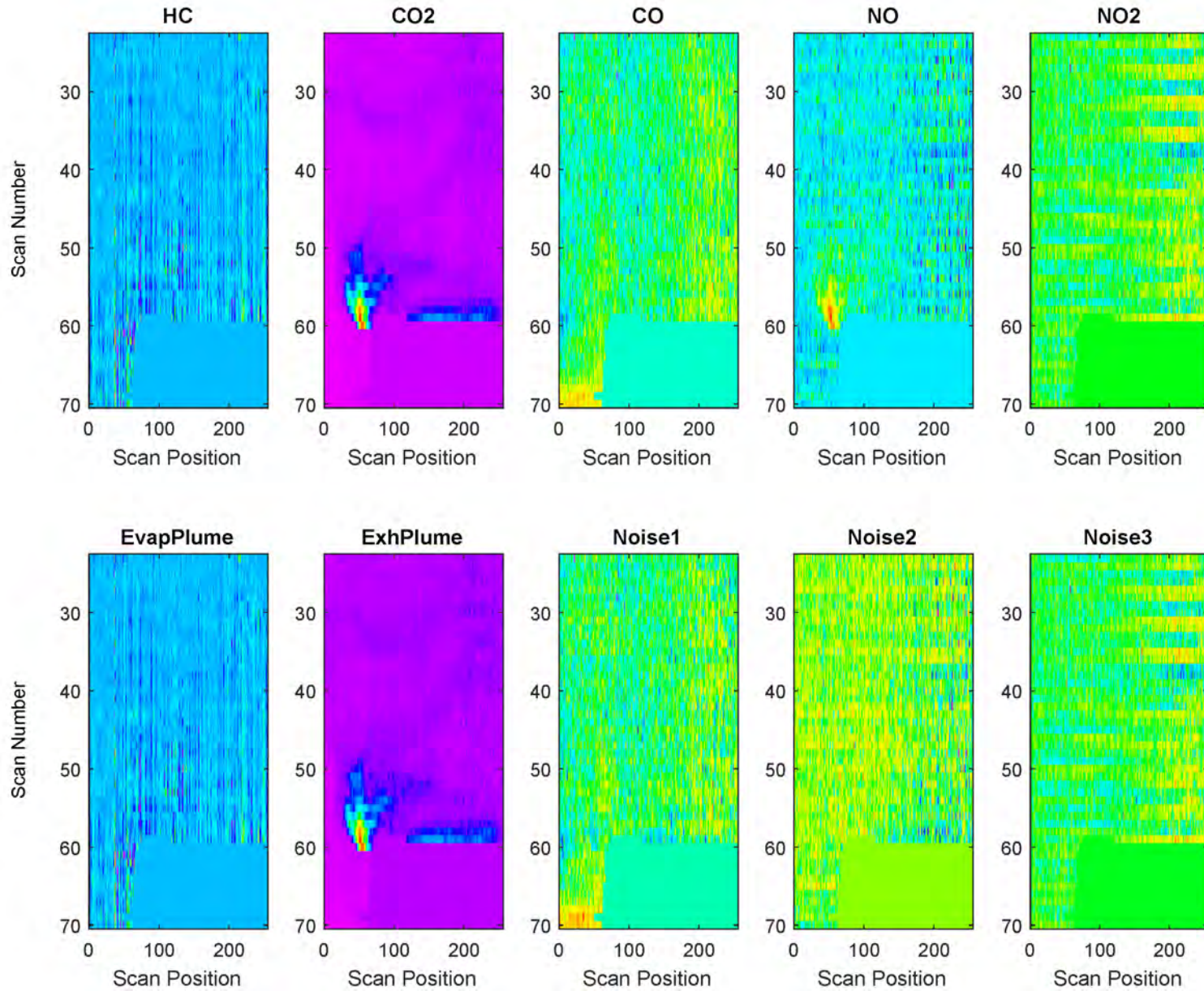
Figure D-48. BSS Example: F-150, Medium EvapHC from TANK, High Speed, natural Exh

7 20191023 000512 car 002998   3-F150 800mg Tank 45mph Y
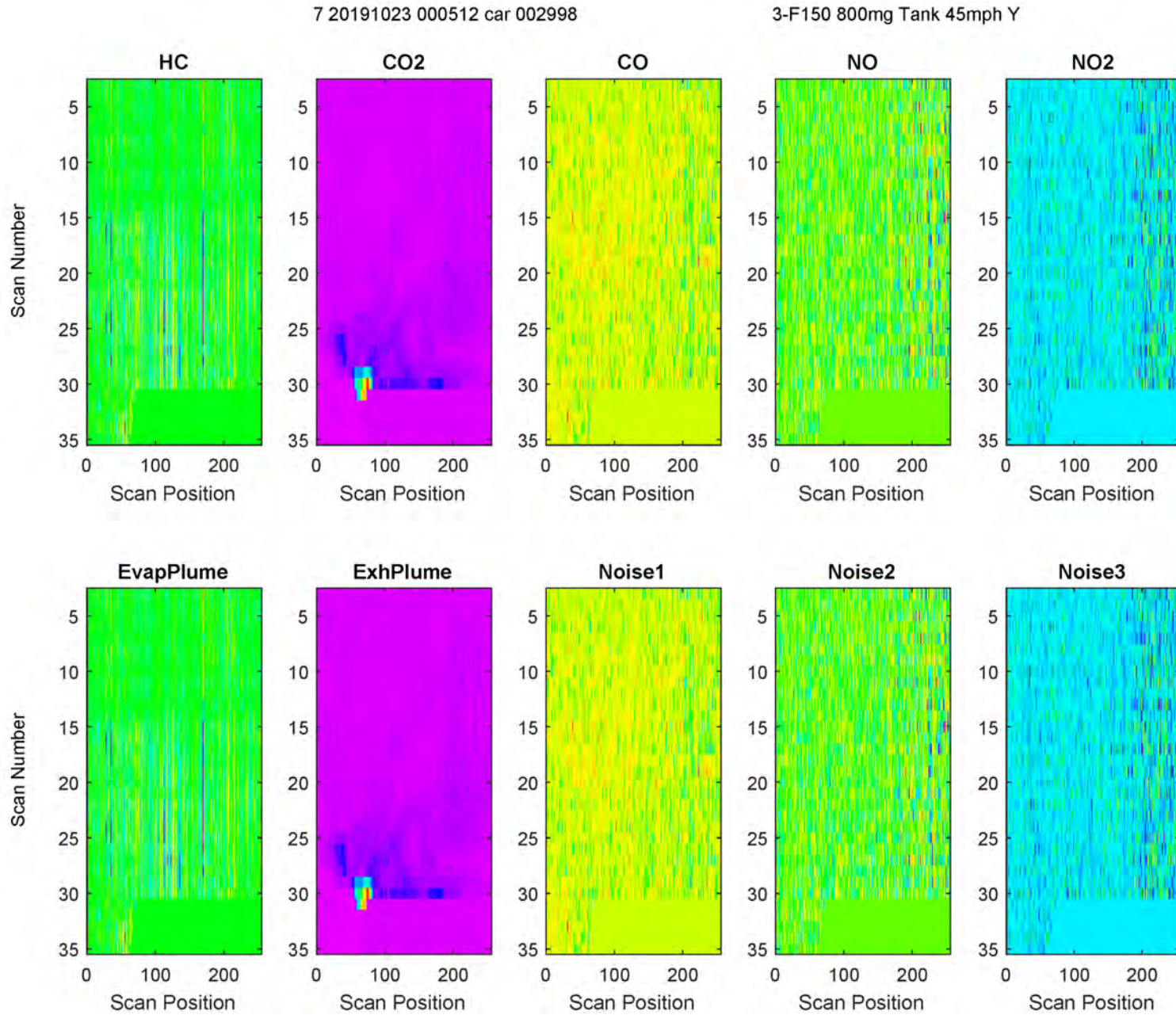
Figure D-49. BSS Example: F-150, High EvapHC from HOOD, Low Speed, natural Exh

7 20191023 000513 car 000272

3-F150 6400mg Hood 22mph Y
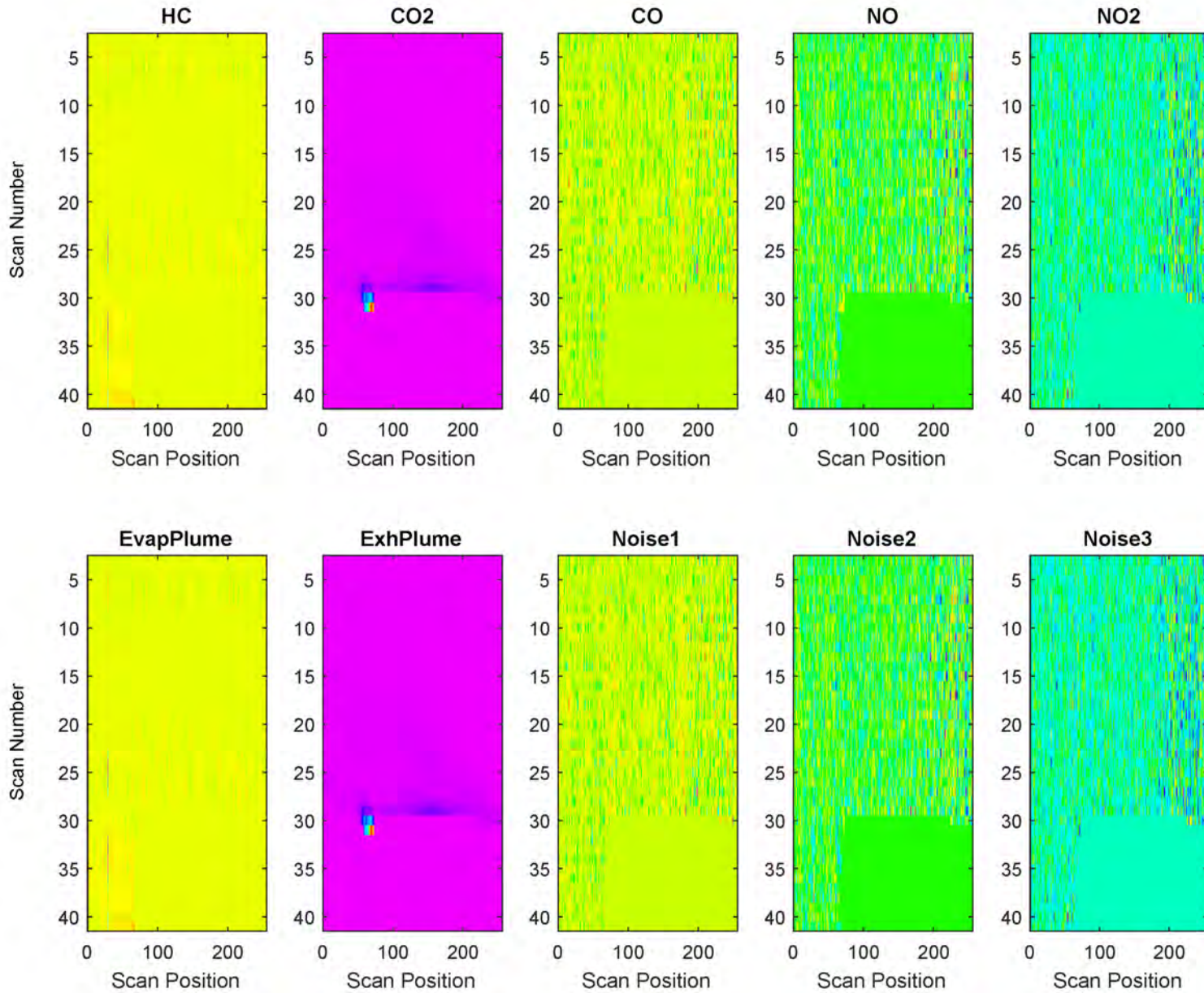
Figure D-50. BSS Example: F-150, Medium EvapHC from HOOD, Low Speed, natural Exh
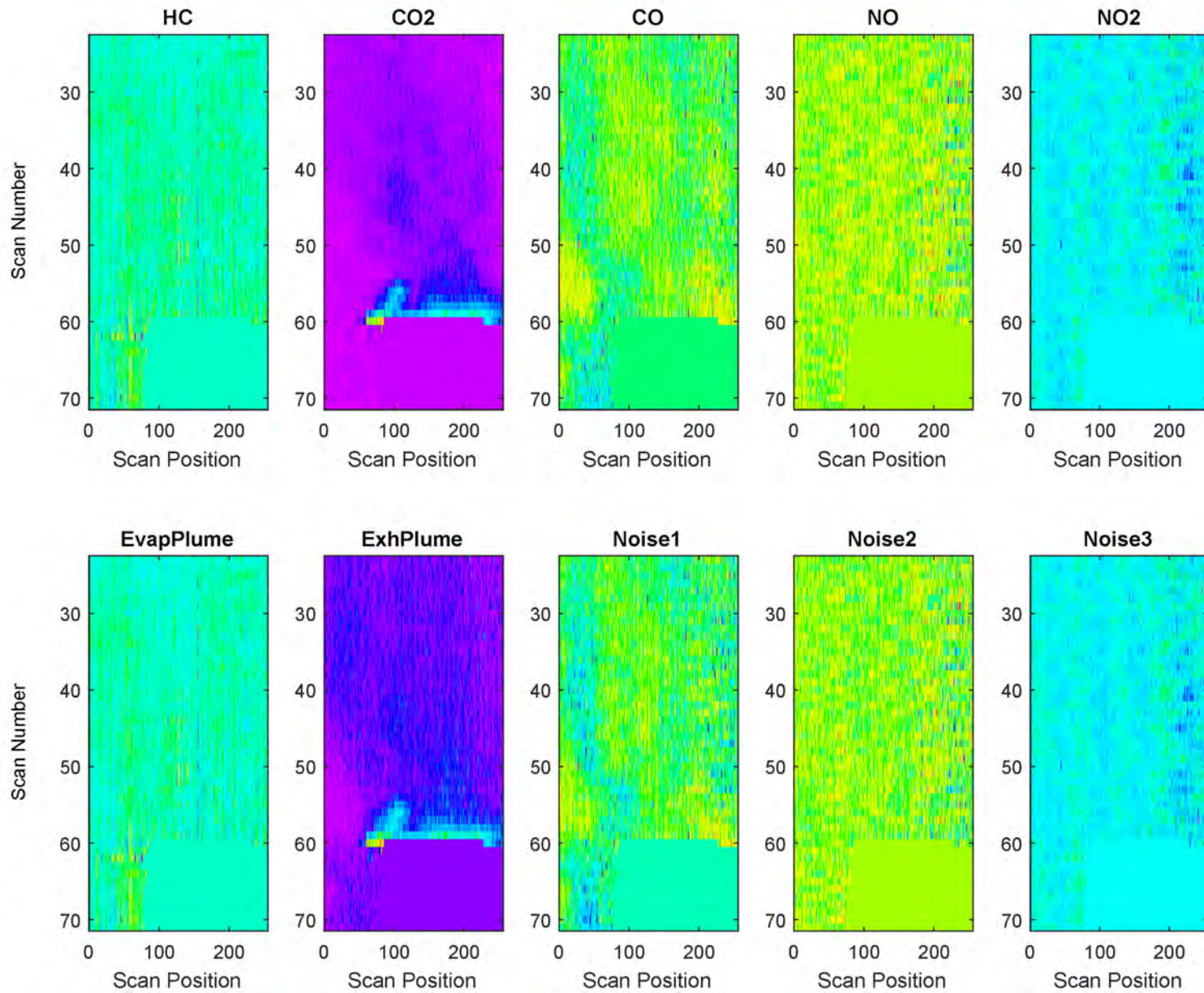
Figure D-51. BSS Example: F-150, Low EvapHC from HOOD, Low Speed, natural Exh

7 20191023 000512 car 001835   3-F150 200mg Hood 22mph Y
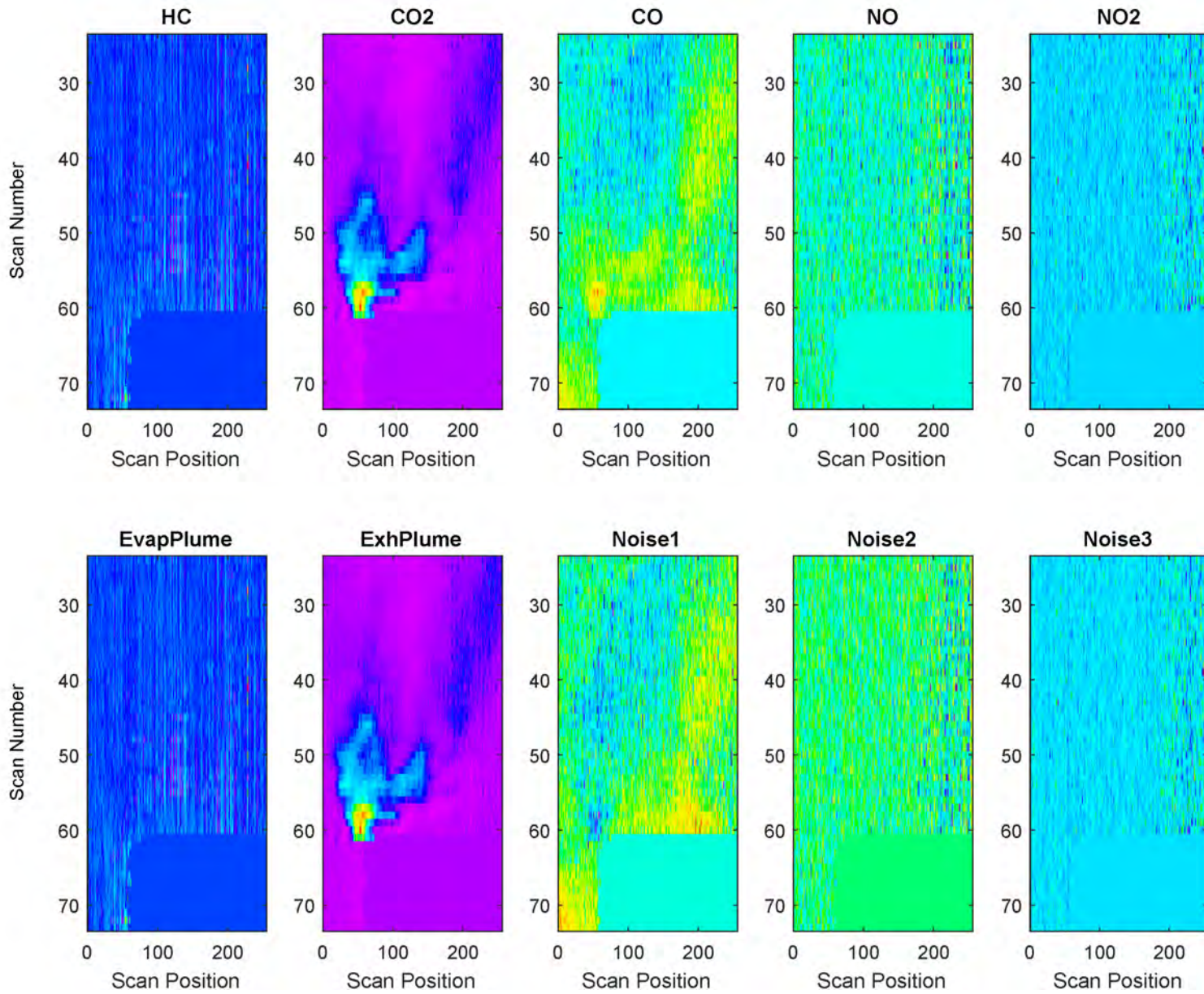
Figure D-52. BSS Example: F-150, Medium EvapHC from HOOD, High Speed, natural Exh

7 20191023 000513 car 000556   3-F150 800mg Hood 45mph Y
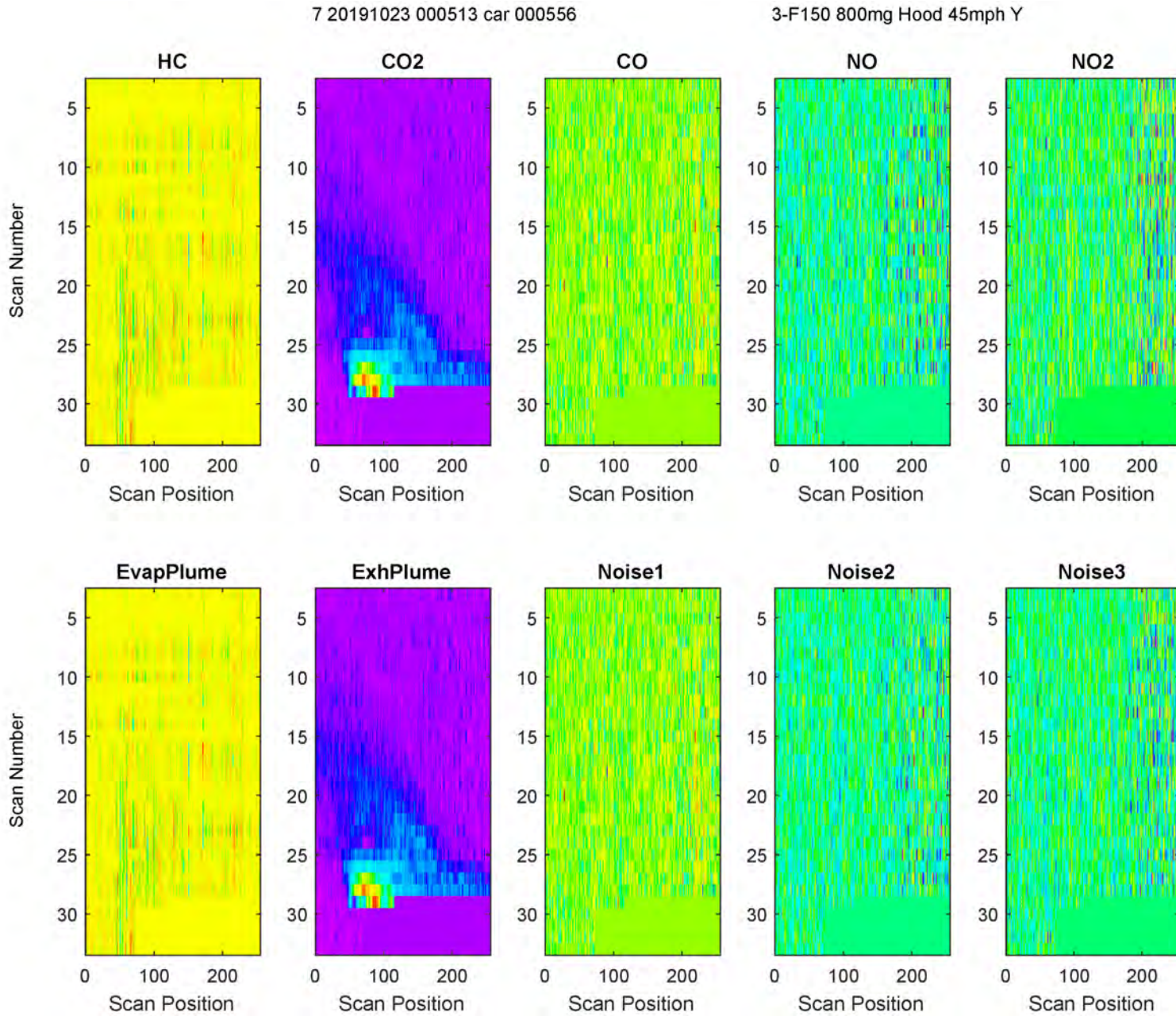
Appendix E:
Examples of Blind Source Separation
with Correlation Constraints (BSScov)

Figure E-1. BSS ICA Separation (ρ=0) of Example: EV-1, High EvapHC from TANK

7 20191020 000505 car 001188   1-EV1 6400mg Tank 22mph Y
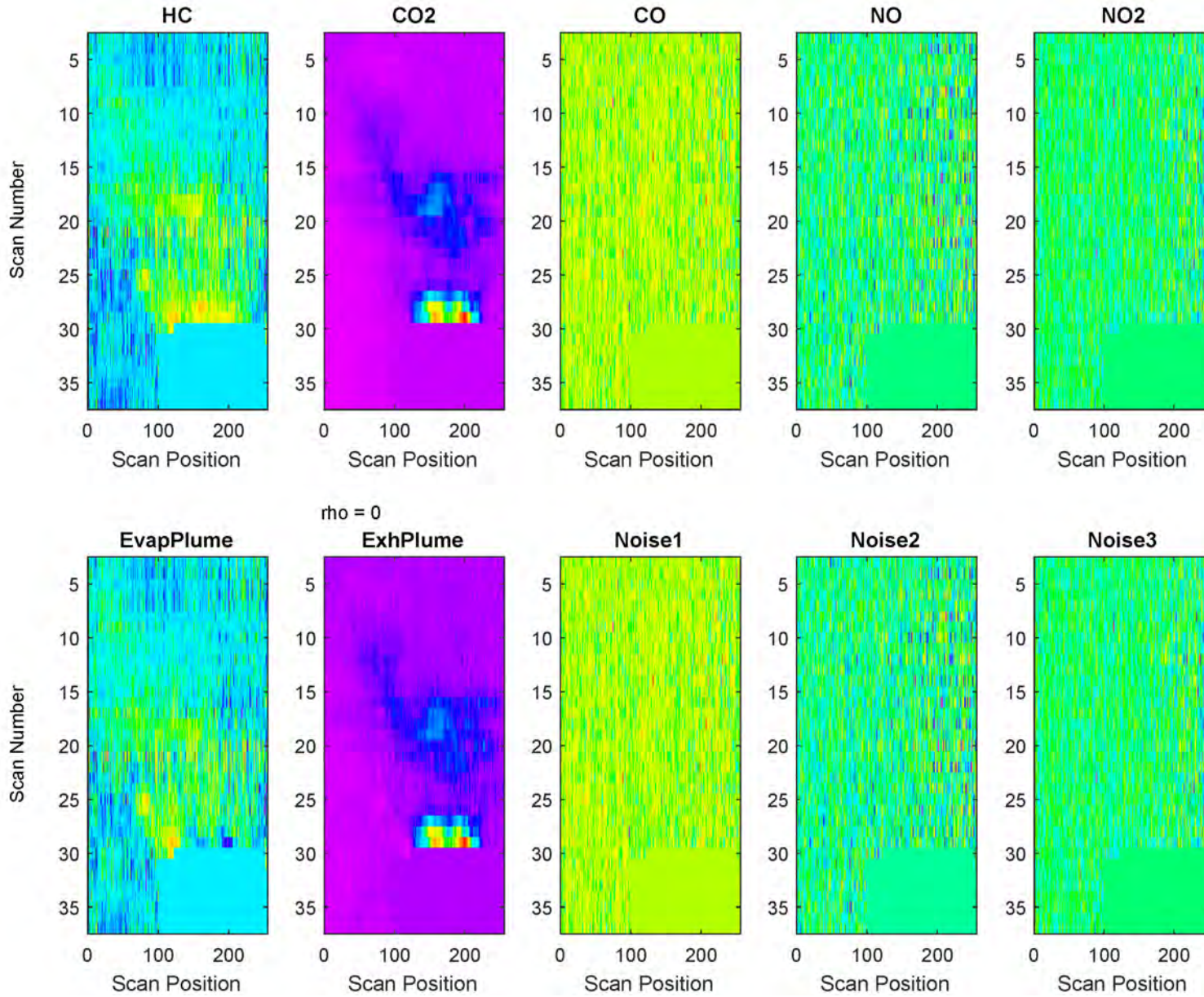
Figure E-2. BSScov Separation (ρ=0.1) of Example: EV-1, High EvapHC from TANK

7 20191020 000505 car 001188   1-EV1 6400mg Tank 22mph Y
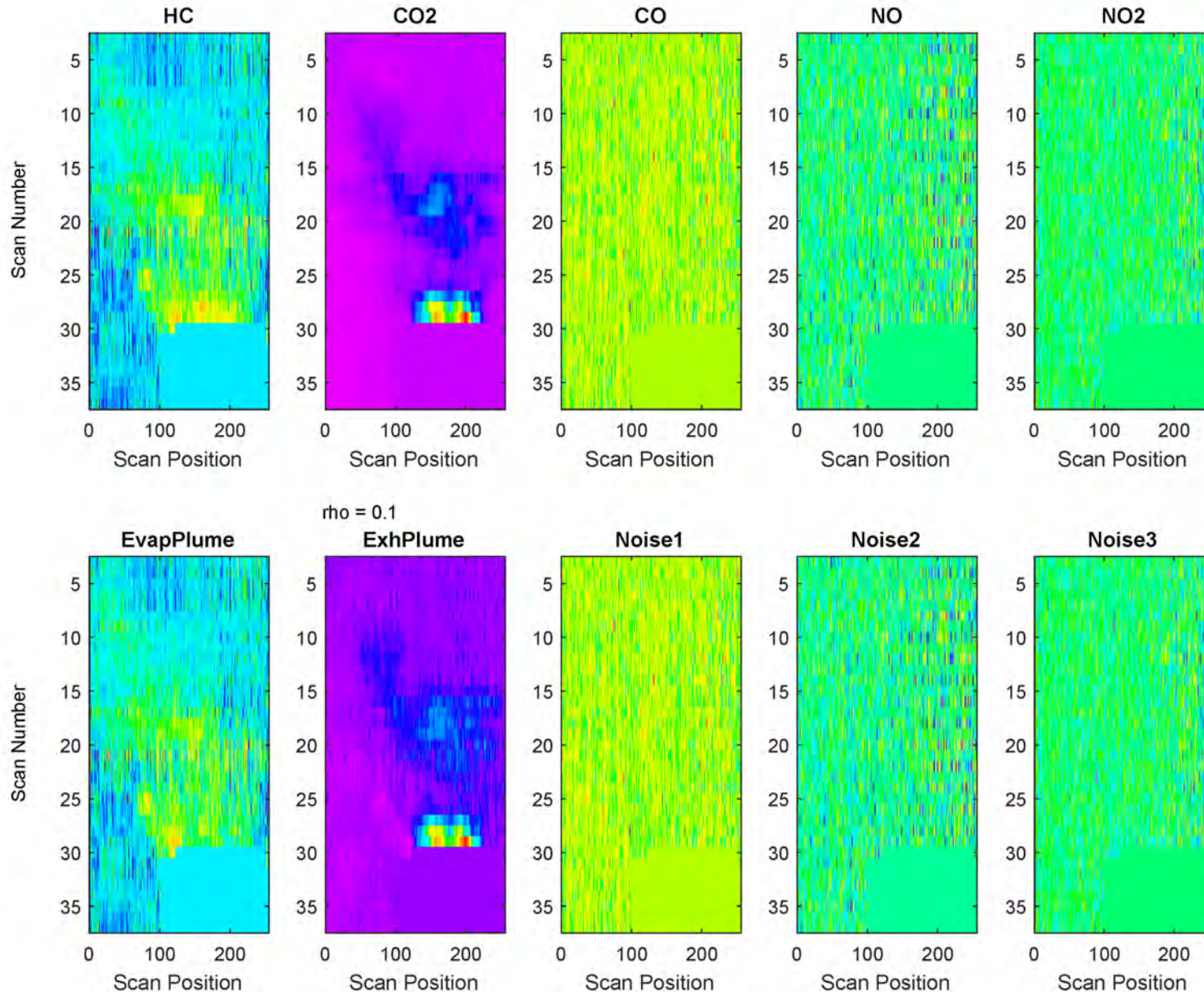
Figure E-3. Evaluation of Plume Outputs while Varying ρ for Example: EV-1, High EvapHC from TANK
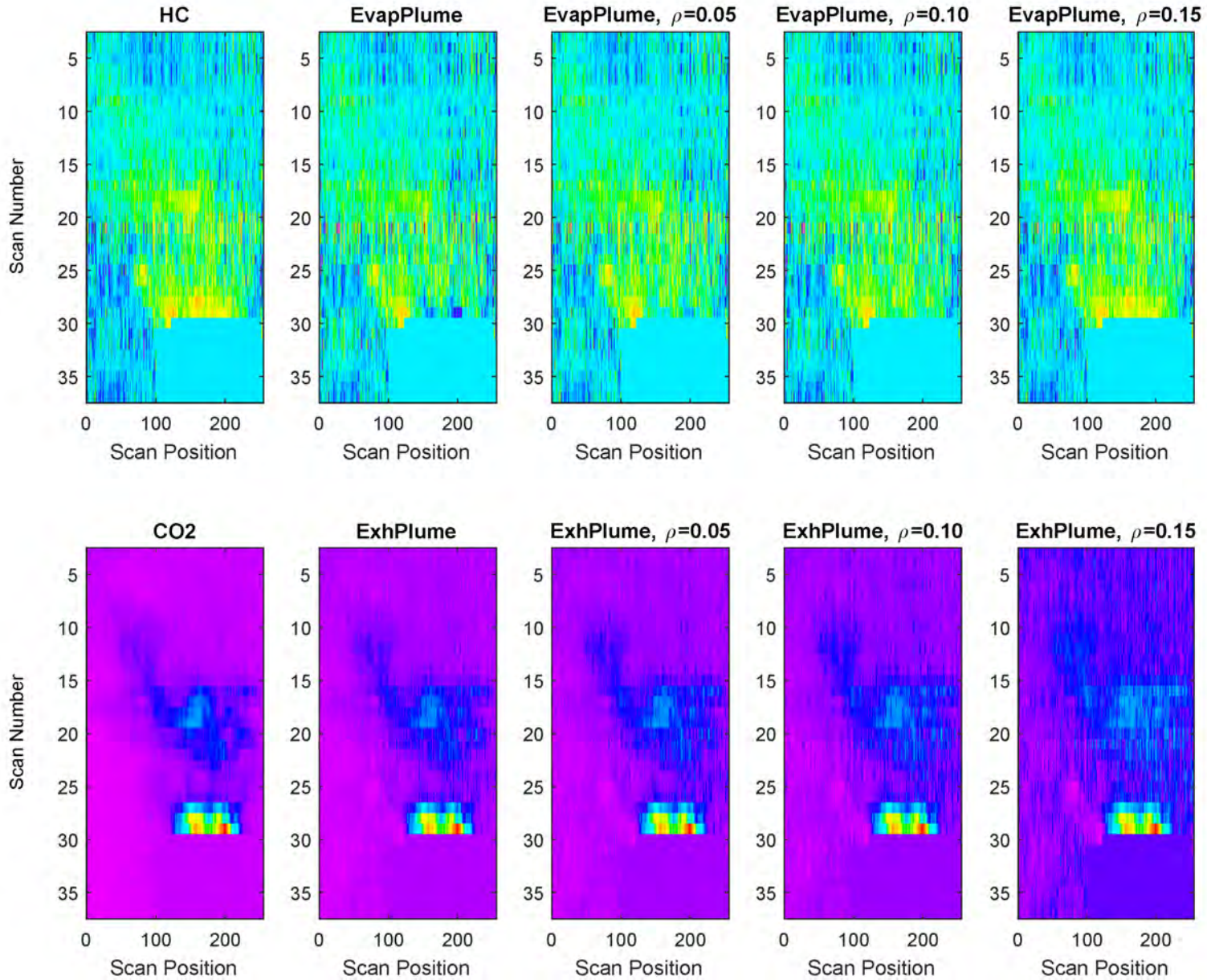
Figure E-4. BSS ICA Separation (ρ=0) of Example: EV-2, High EvapHC from DOOR

7 20191023 000512 car 001168   2-EV2 6400mg Door 22mph Y
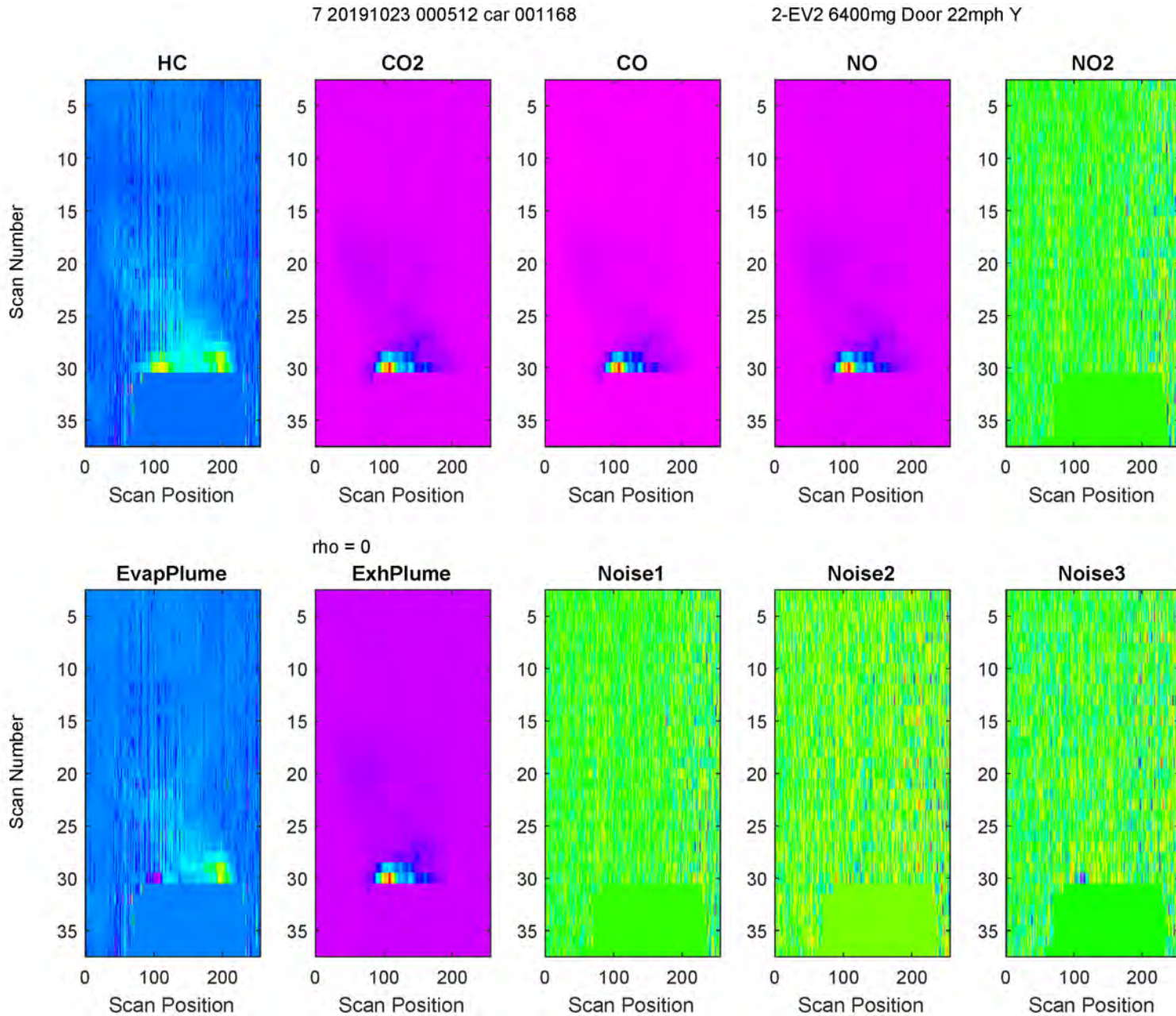
Figure E-5. BSScov Separation (ρ=0.1) of Example: EV-2, High EvapHC from DOOR

7 20191023 000512 car 001168   2-EV2 6400mg Door 22mph Y
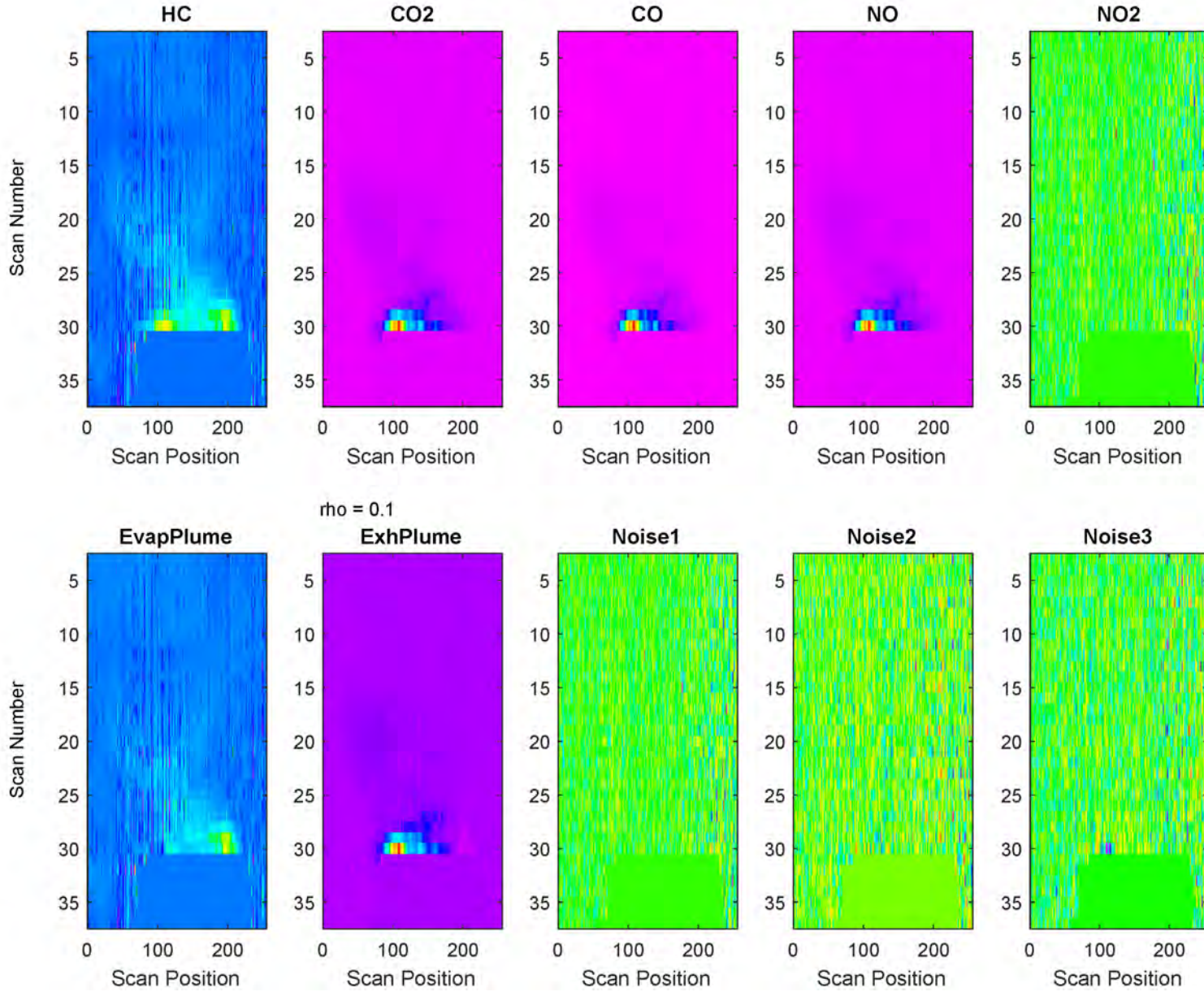
Figure E-6. Evaluation of Plume Outputs while Varying ρ for Example: EV-2, High EvapHC from DOOR

7 20191023 000512 car 001168   2-EV2 6400mg Door 22mph Y
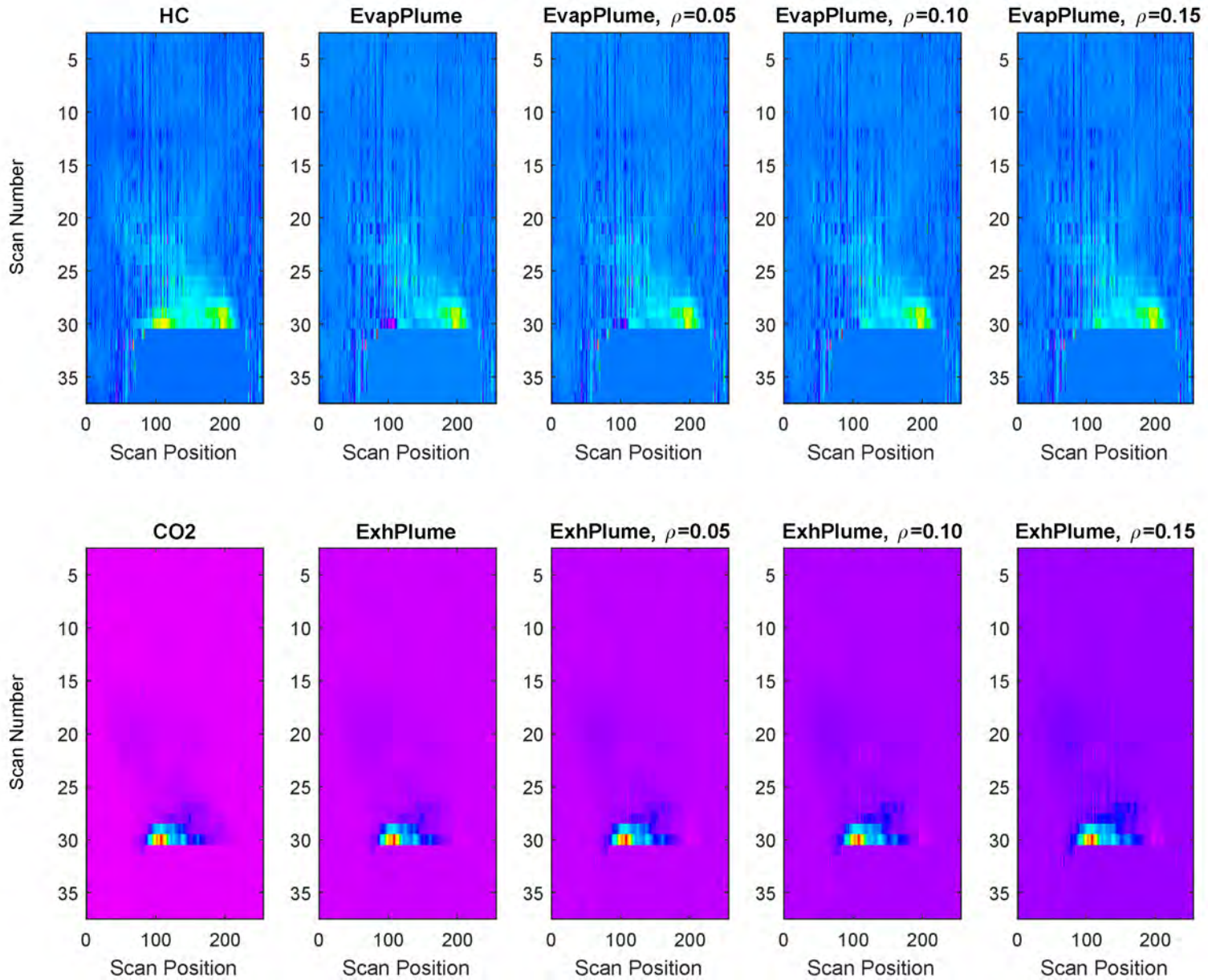
Figure E-7. BSS ICA Separation (ρ=0) of Example: EV-2, High EvapHC from TANK
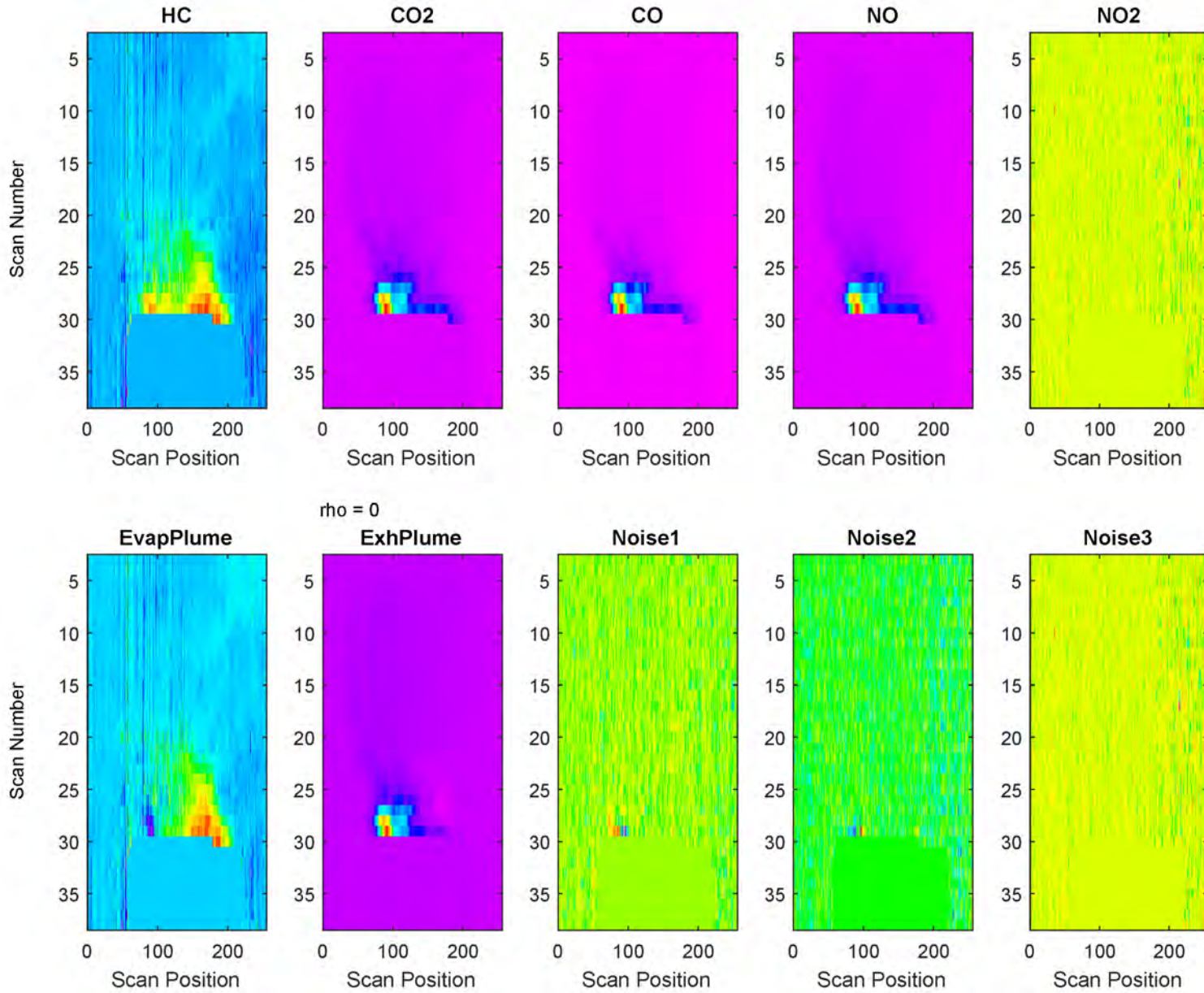
Figure E-8. BSScov Separation (ρ=0.15) of Example: EV-2, High EvapHC from TANK

7 20191023 000512 car 000926   2-EV2 6400mg Tank 22mph Y
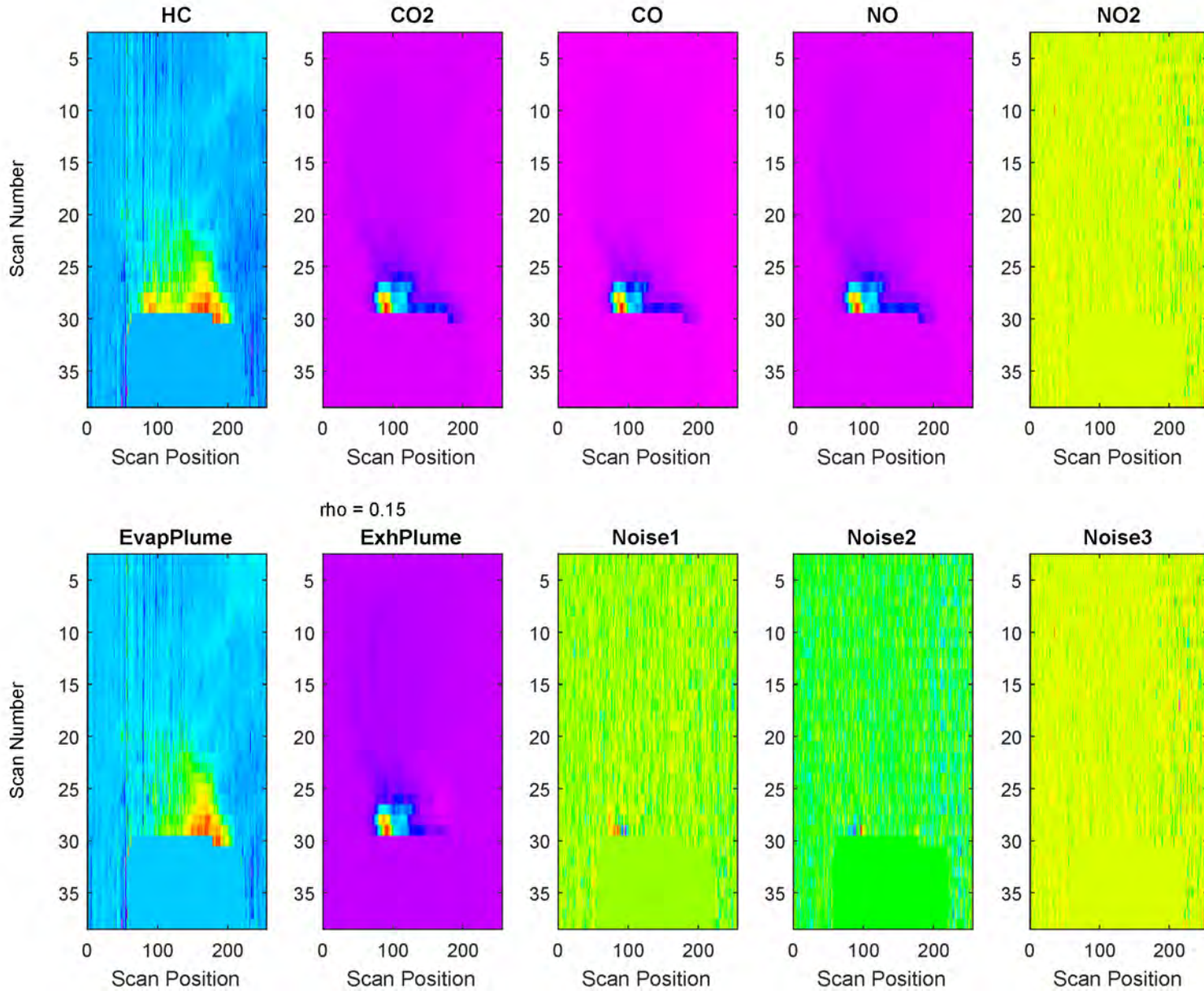
Figure E-9. Evaluation of Plume Outputs while Varying ρ for Example: EV-2, High EvapHC from TANK

7 20191023 000512 car 000926   2-EV2 6400mg Tank 22mph Y
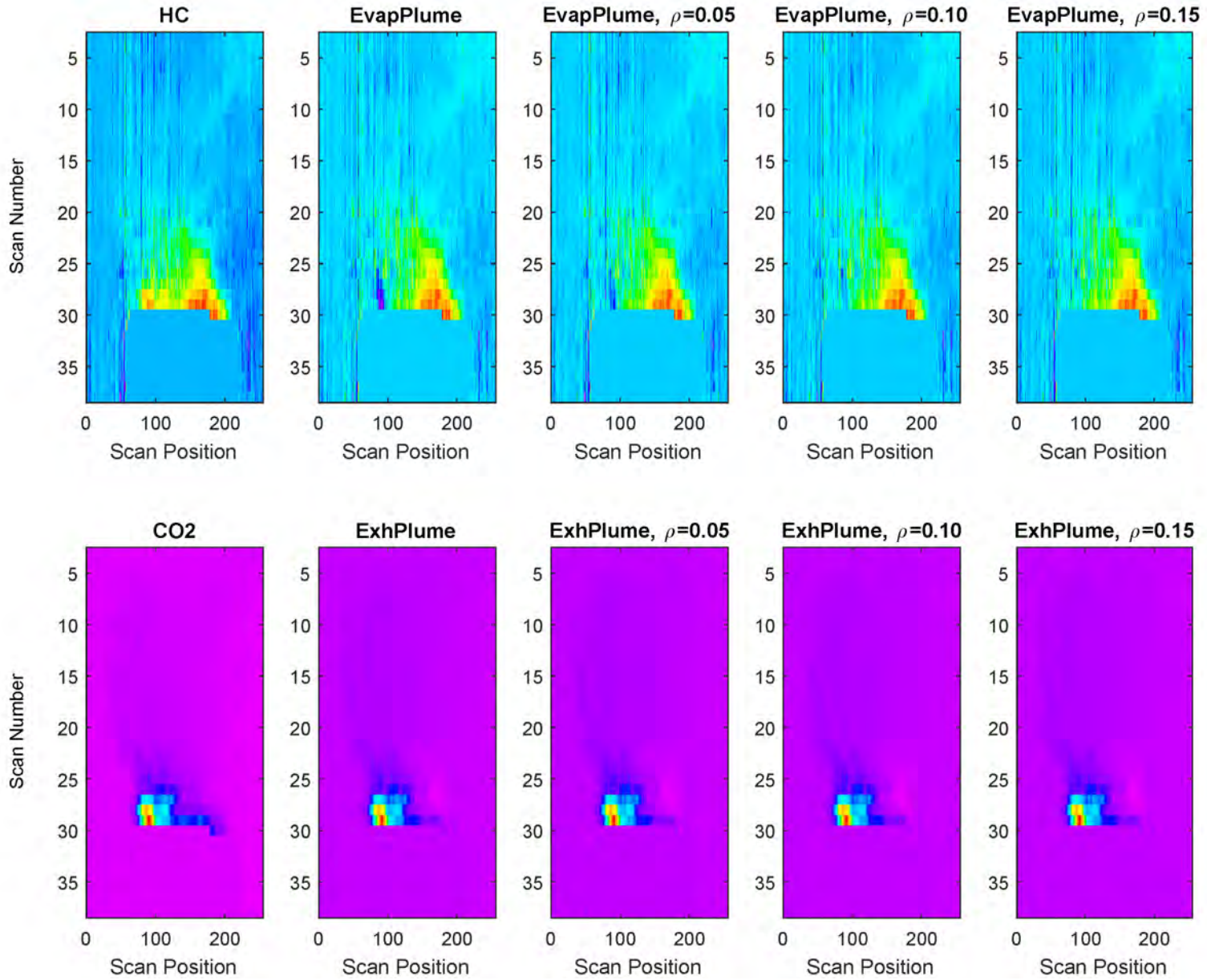
Figure E-10. BSS ICA Separation (ρ=0) of Example: EV-2, High EvapHC from HOOD

Figure E-11. BSScov Separation (ρ=0.1) of Example: EV-2, High EvapHC from HOOD

Figure E-12. Evaluation of Plume Outputs while Varying ρ for Example: EV-2, High EvapHC from HOOD

7 20191023 000512 car 001416   2-EV2 6400mg Hood 22mph Y
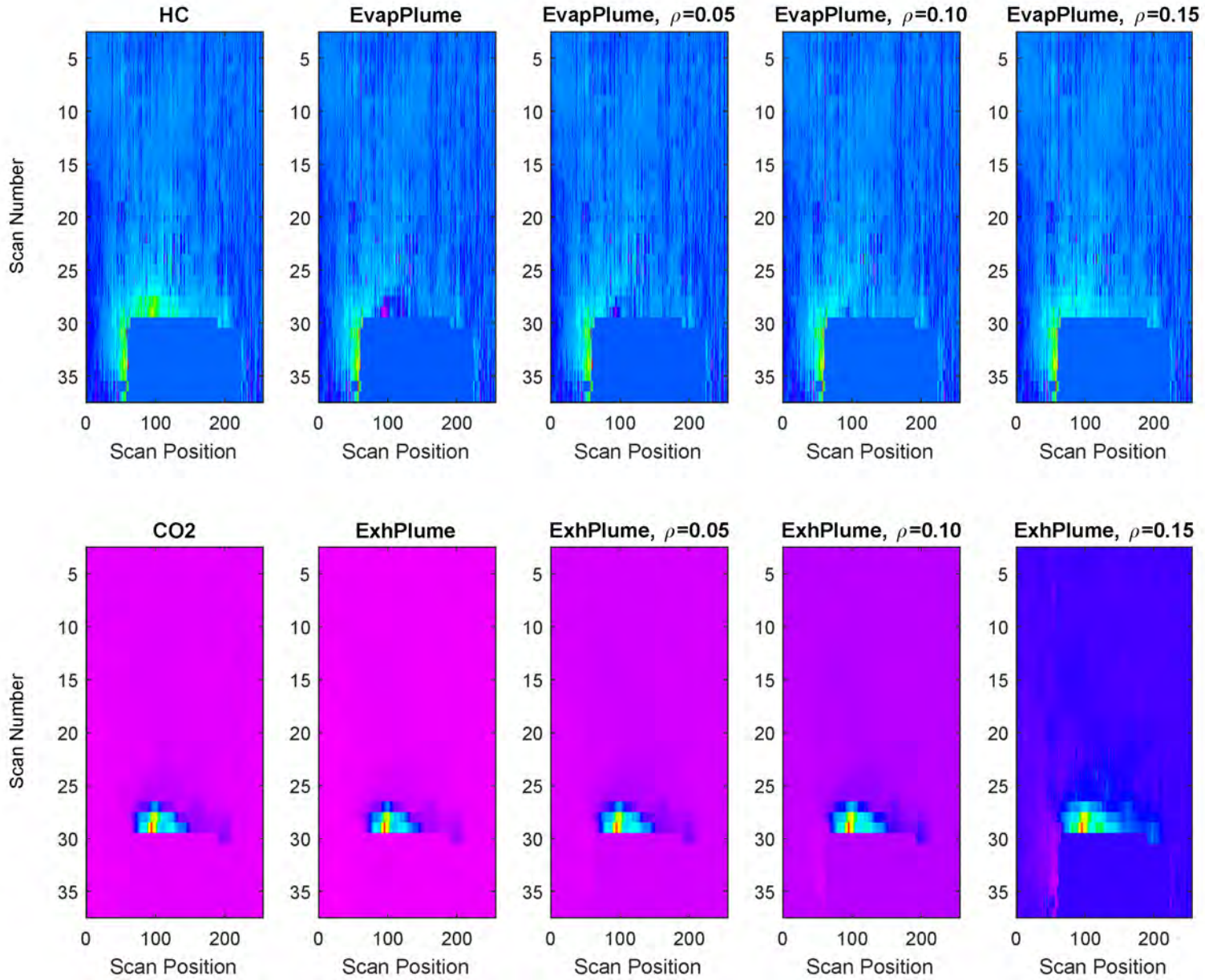
Appendix F:
Comparing Westminster and MOVES Release Rates
by Class and Age Group

Figure F-1. Comparison of Release Rates for 0-to-3-Year-Old LDTs in 2019
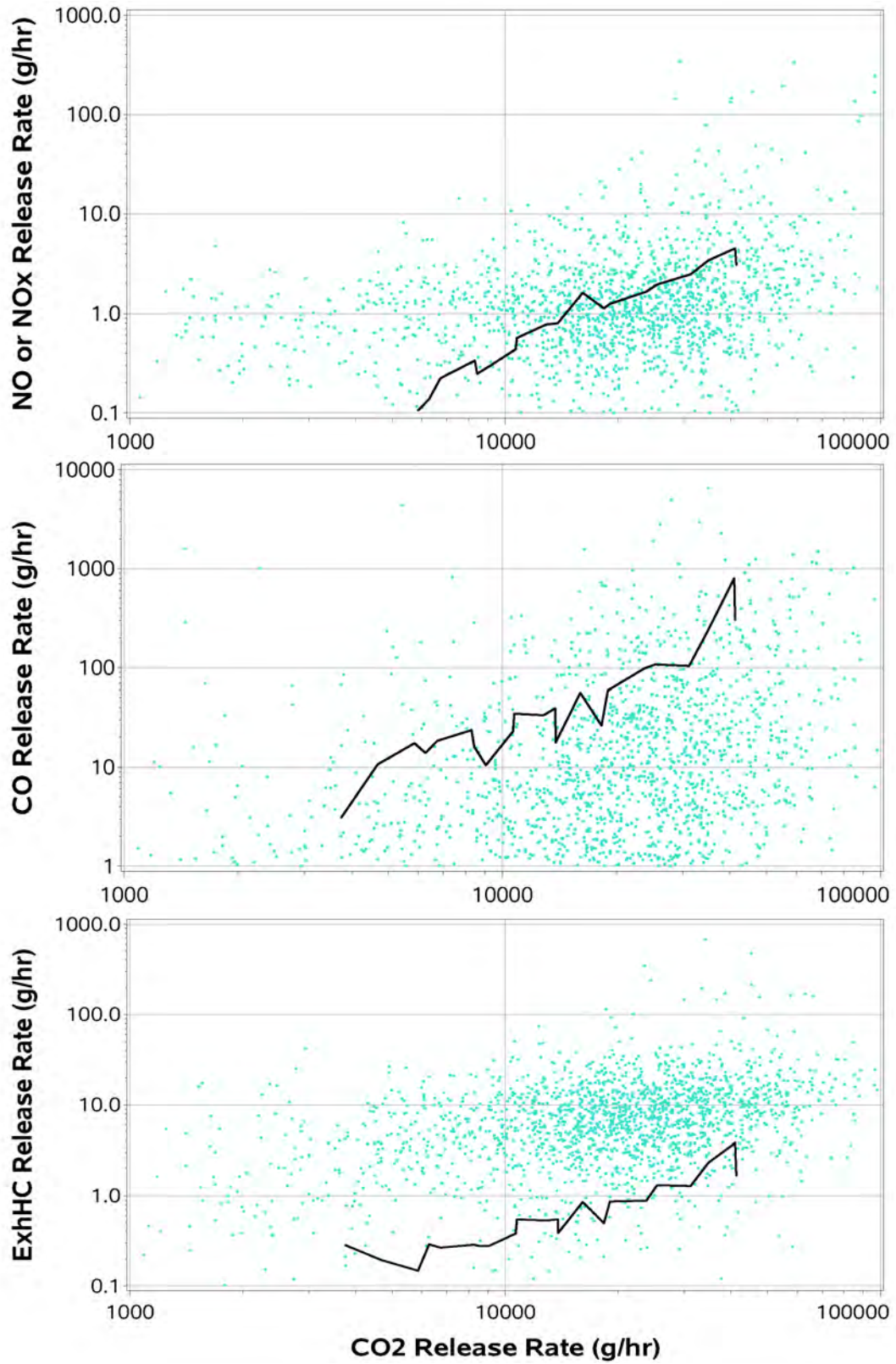
Source: • • • Westminster Vehicle RSD Transits　——— MOVES Average for Calendar 2019

/proj1/EDARinDenver-OCT2019/Analysis_MLout/220113/Anal_MLout/OCT19_VSPbins_4_CP.sas 02MAR23 13:09
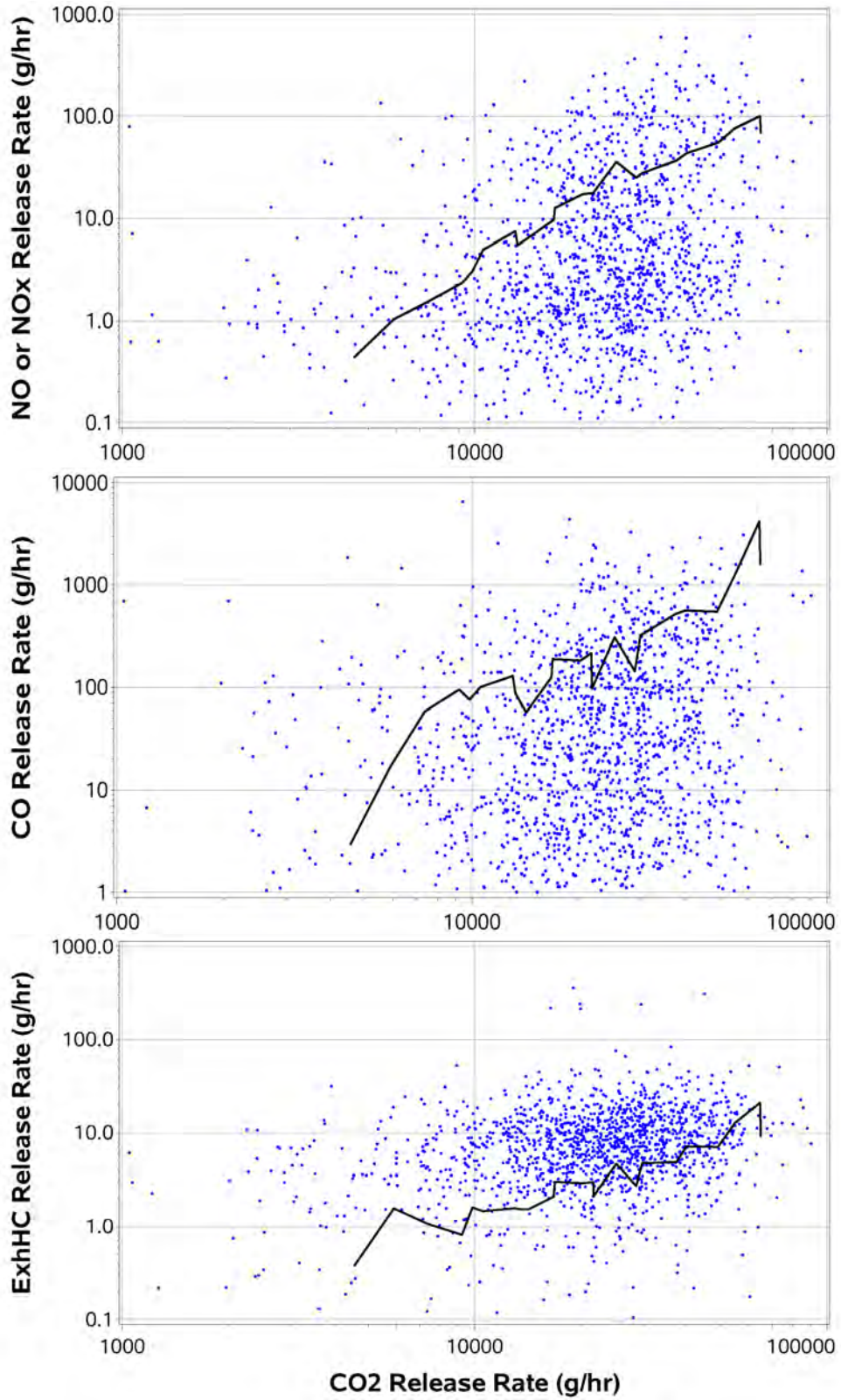
Figure F-2. Comparison of Release Rates for 4-to-5-Year-Old LDTs in 2019
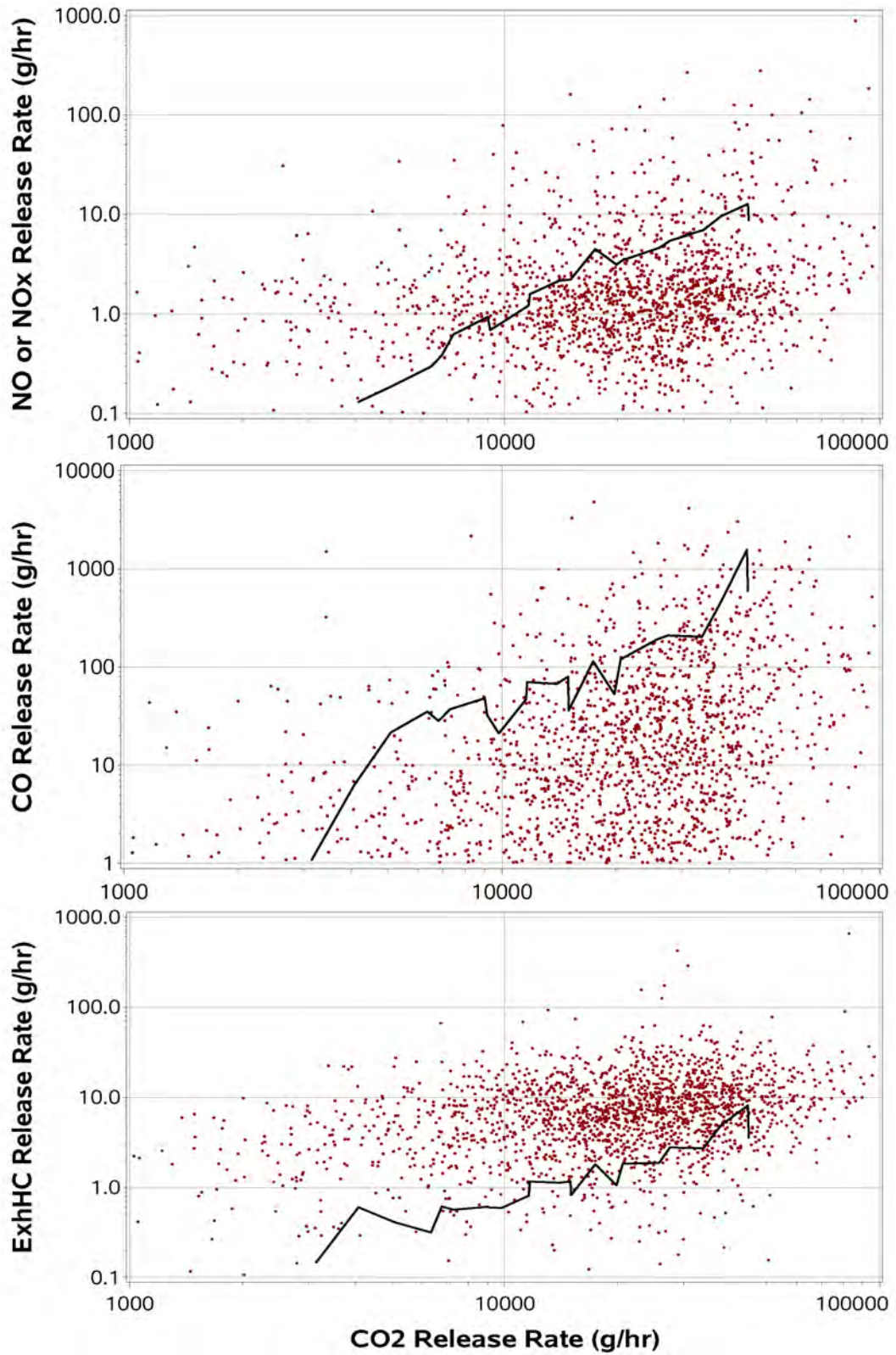
Source: • • • Westminster Vehicle RSD Transits   —— MOVES Average for Calendar 2019

/proj1/EDARinDenver-OCT2019/Analysis_MLout/220113/Anal_MLout/OCT19_VSPbins_4_CP.sas 02MAR23 13:09
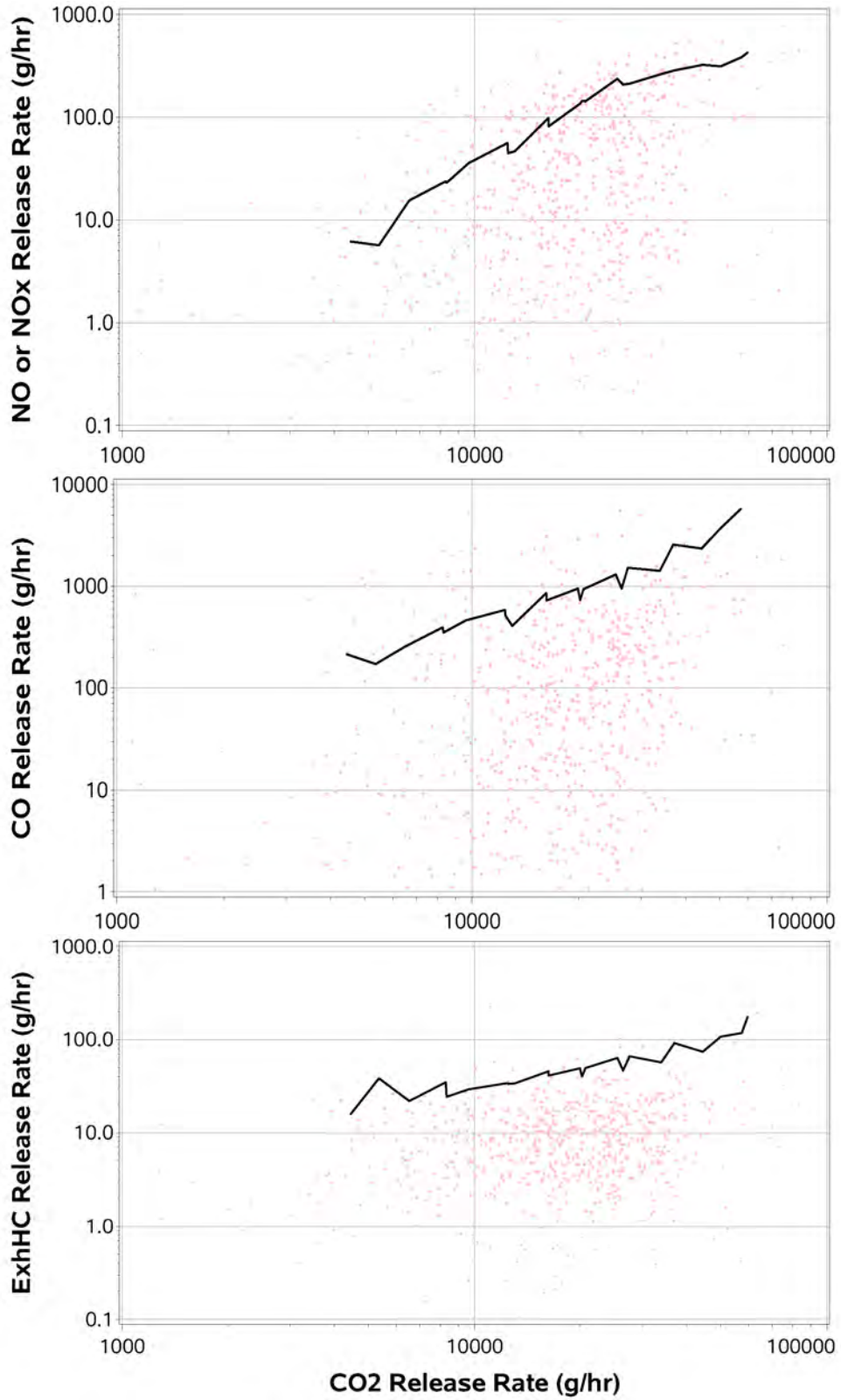
Figure F-3. Comparison of Release Rates for 6-to-7-Year-Old LDTs in 2019
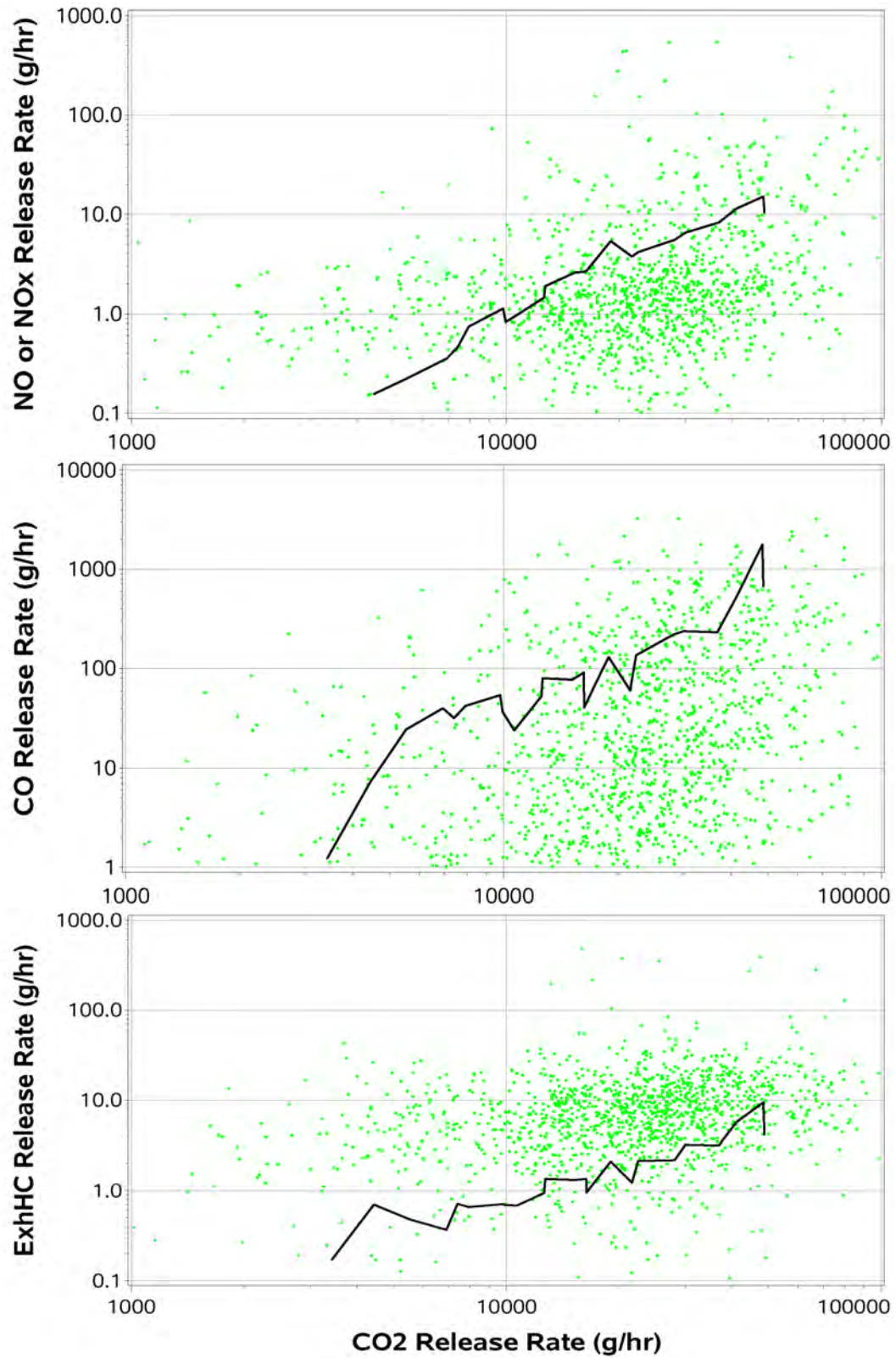
Source: • • • Westminster Vehicle RSD Transits —— MOVES Average for Calendar 2019

/proj1/EDARinDenver-OCT2019/Analysis_MLout/220113/Anal_MLout/OCT19_VSPbins_4_CP.sas 02MAR23 13:09
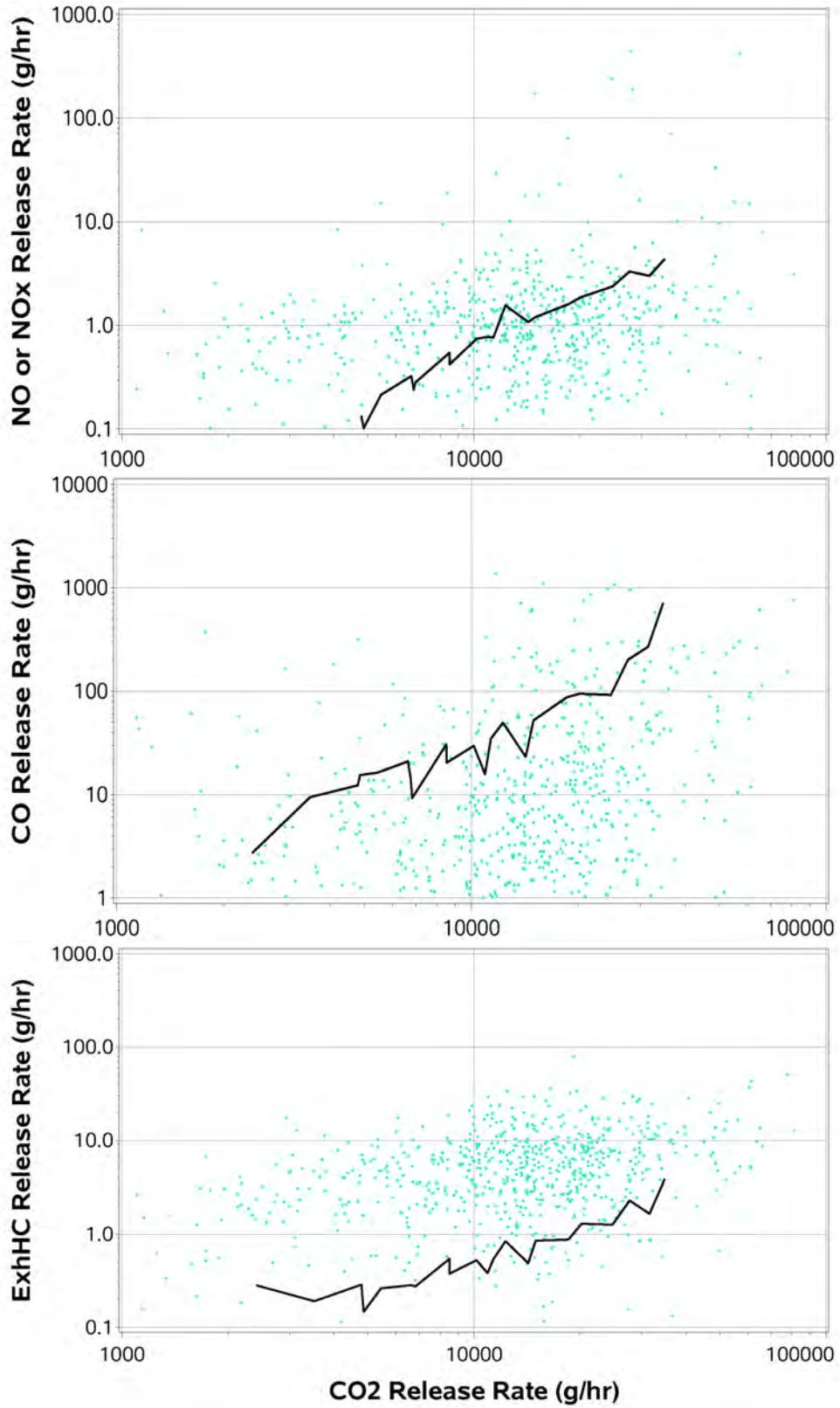
Figure F-4. Comparison of Release Rates for 8-to-9-Year-Old LDTs in 2019
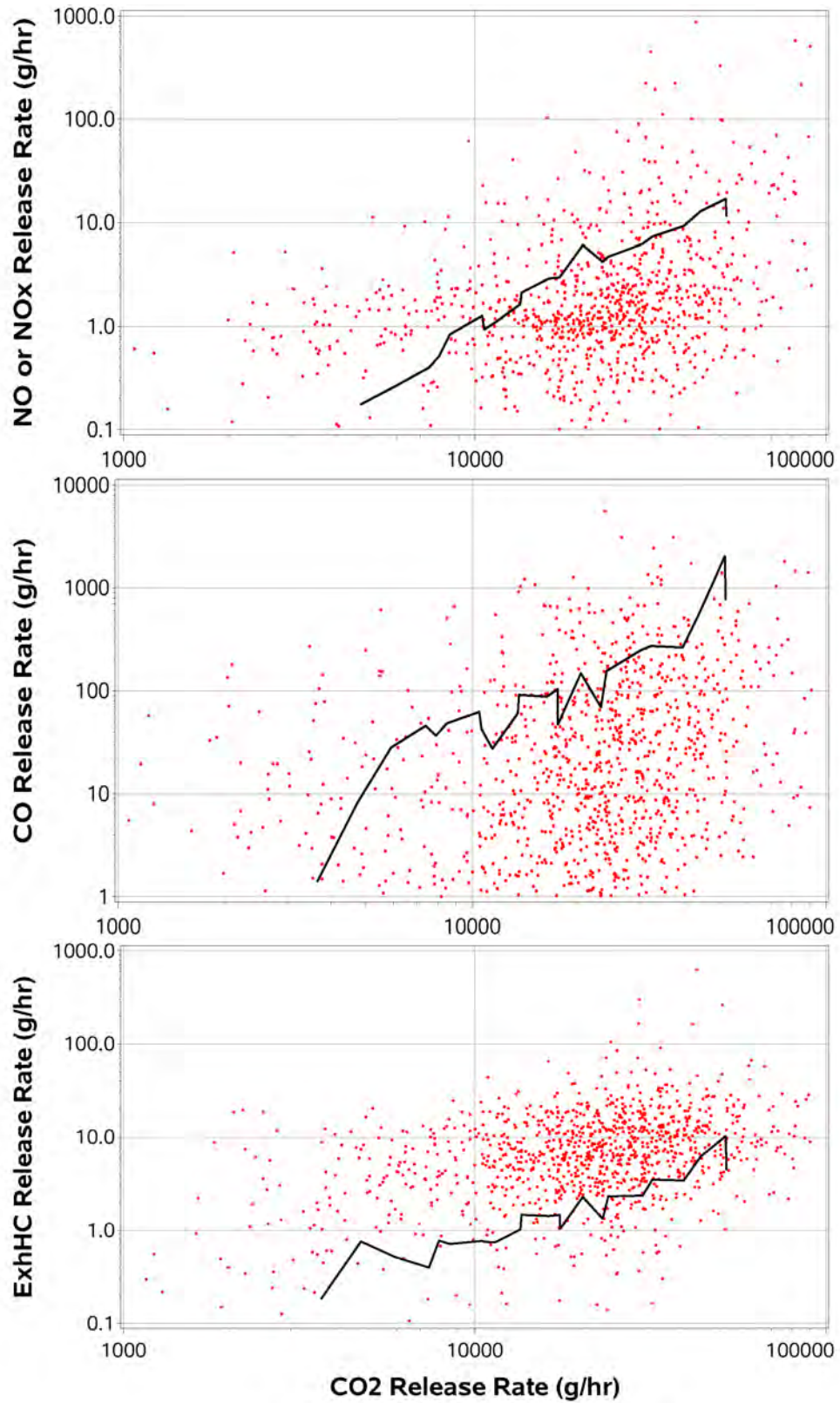
Source: • • • Westminster Vehicle RSD Transits   —— MOVES Average for Calendar 2019

/proj1/EDARinDenver-OCT2019/Analysis_MLout/220113/Anal_MLout/OCT19_VSPbins_4_CP.sas 02MAR23 13:09

Figure F-5. Comparison of Release Rates for 10-to-14-Year-Old LDTs in 2019
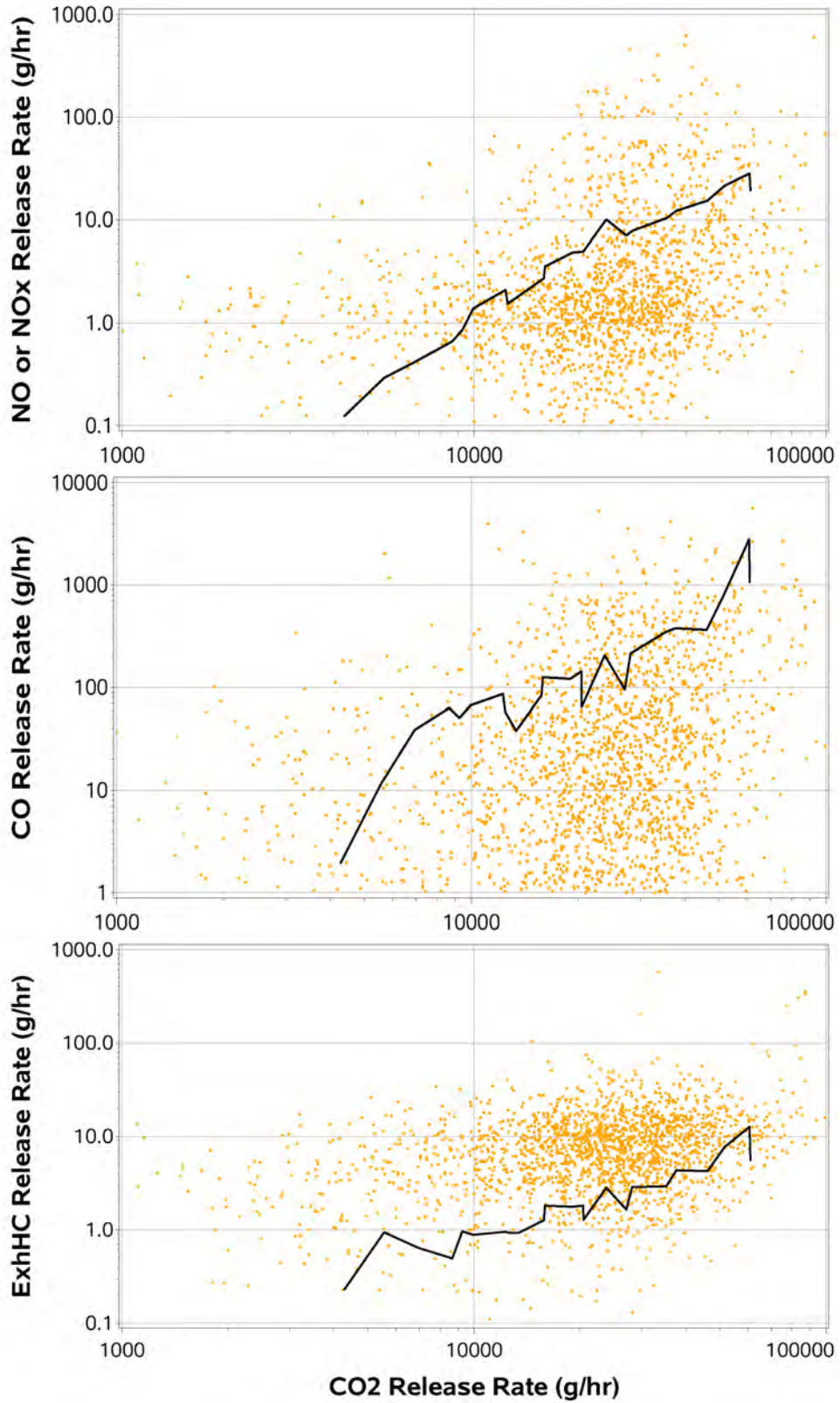
Source: • • • Westminster Vehicle RSD Transits   —— MOVES Average for Calendar 2019

/proj1/EDARinDenver-OCT2019/Analysis_MLout/220113/Anal_MLout/OCT19_VSPbins_4_CP.sas 02MAR23 13:09
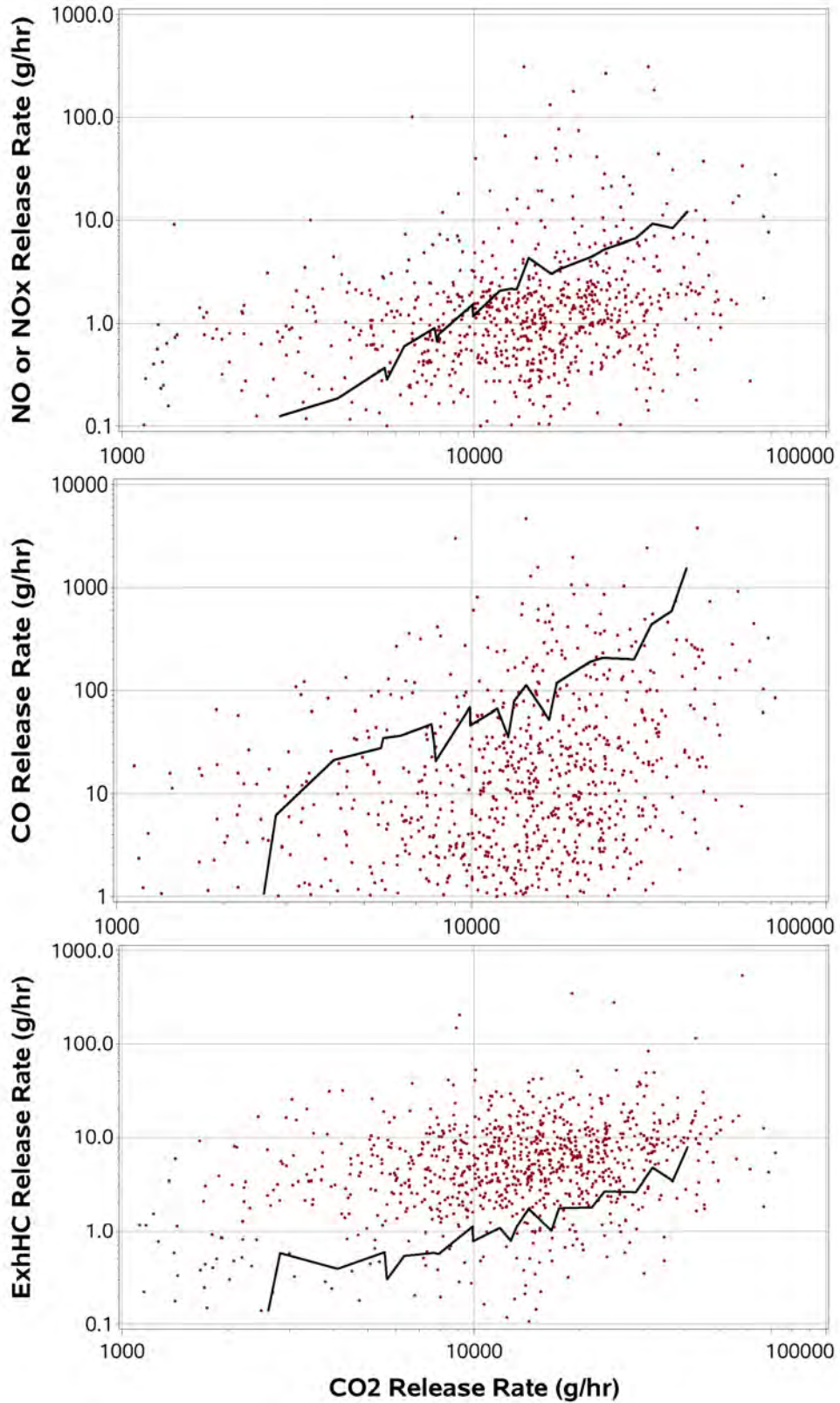
Figure F-6. Comparison of Release Rates for 15-to-19-Year-Old LDTs in 2019

Source: • • • Westminster Vehicle RSD Transits   —— MOVES Average for Calendar 2019

/proj1/EDARinDenver-OCT2019/Analysis_MLout/220113/Anal_MLout/OCT19_VSPbins_4_CP.sas 02MAR23 13:09
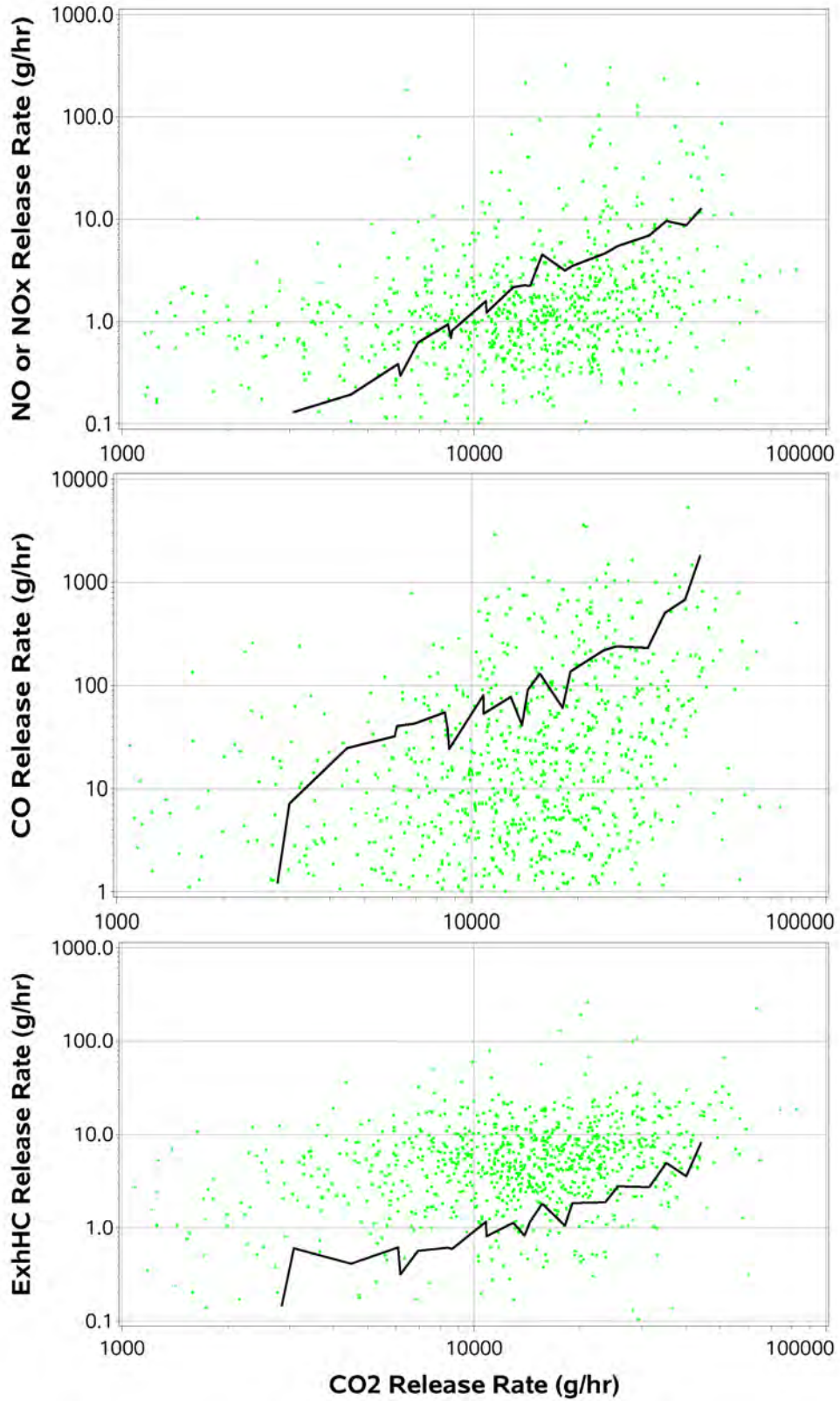
Figure F-7. Comparison of Release Rates for 20-to-99-Year-Old LDTs in 2019

Source: • • • Westminster Vehicle RSD Transits   —— MOVES Average for Calendar 2019

/proj1/EDARinDenver-OCT2019/Analysis_MLout/220113/Anal_MLout/OCT19_VSPbins_4_CP.sas 02MAR23 13:09

Figure F-8. Comparison of Release Rates for 0-to-3-Year-Old LDVs in 2019

Source: • • • Westminster Vehicle RSD Transits — MOVES Average for Calendar 2019

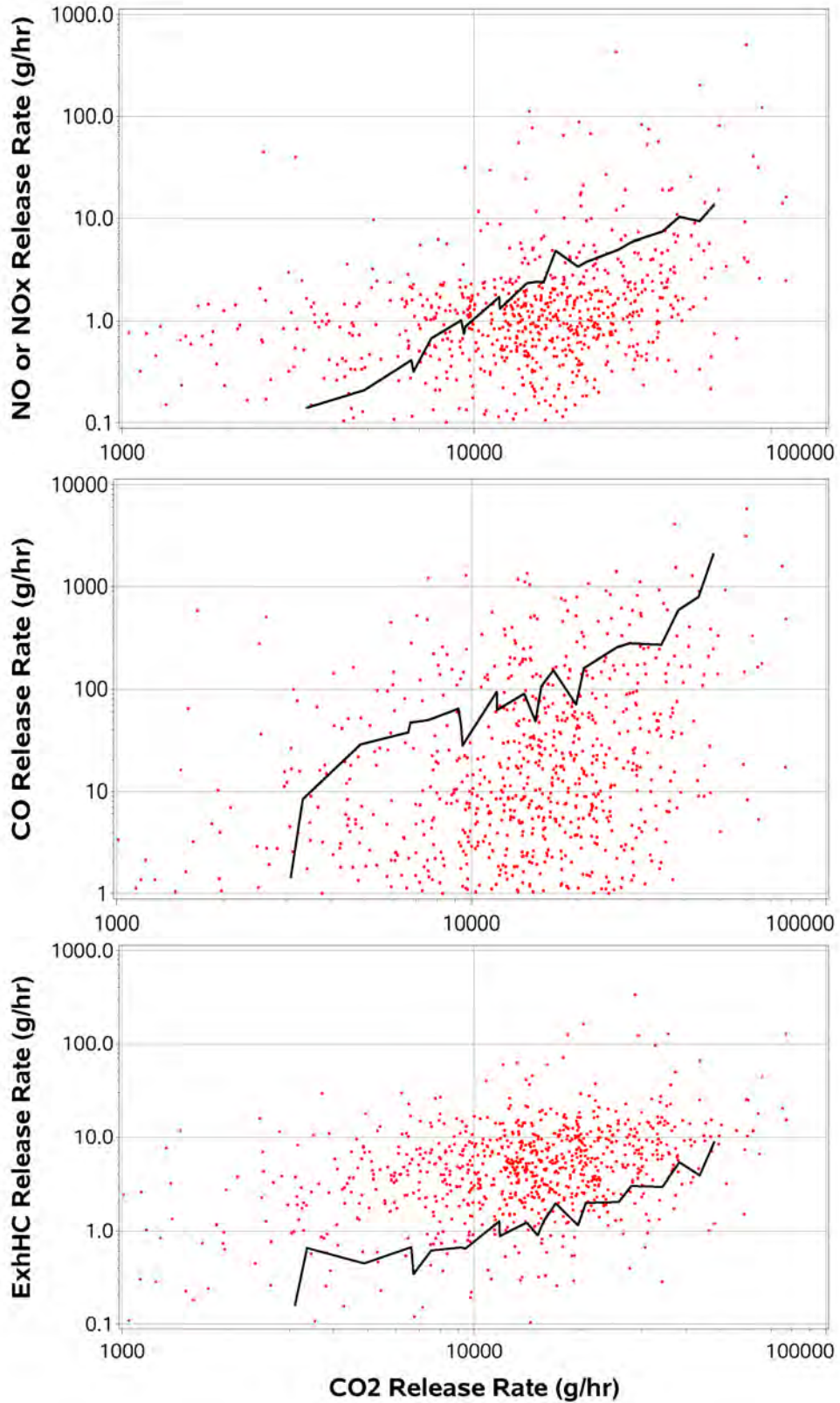/proj1/EDARinDenver-OCT2019/Analysis_MLout/220113/Anal_MLout/OCT19_VSPbins_4_CP.sas 02MAR23 13:09

F-8

Figure F-9. Comparison of Release Rates for 4-to-5-Year-Old LDVs in 2019

Source:　•••Westminster Vehicle RSD Transits　——MOVES Average for Calendar 2019

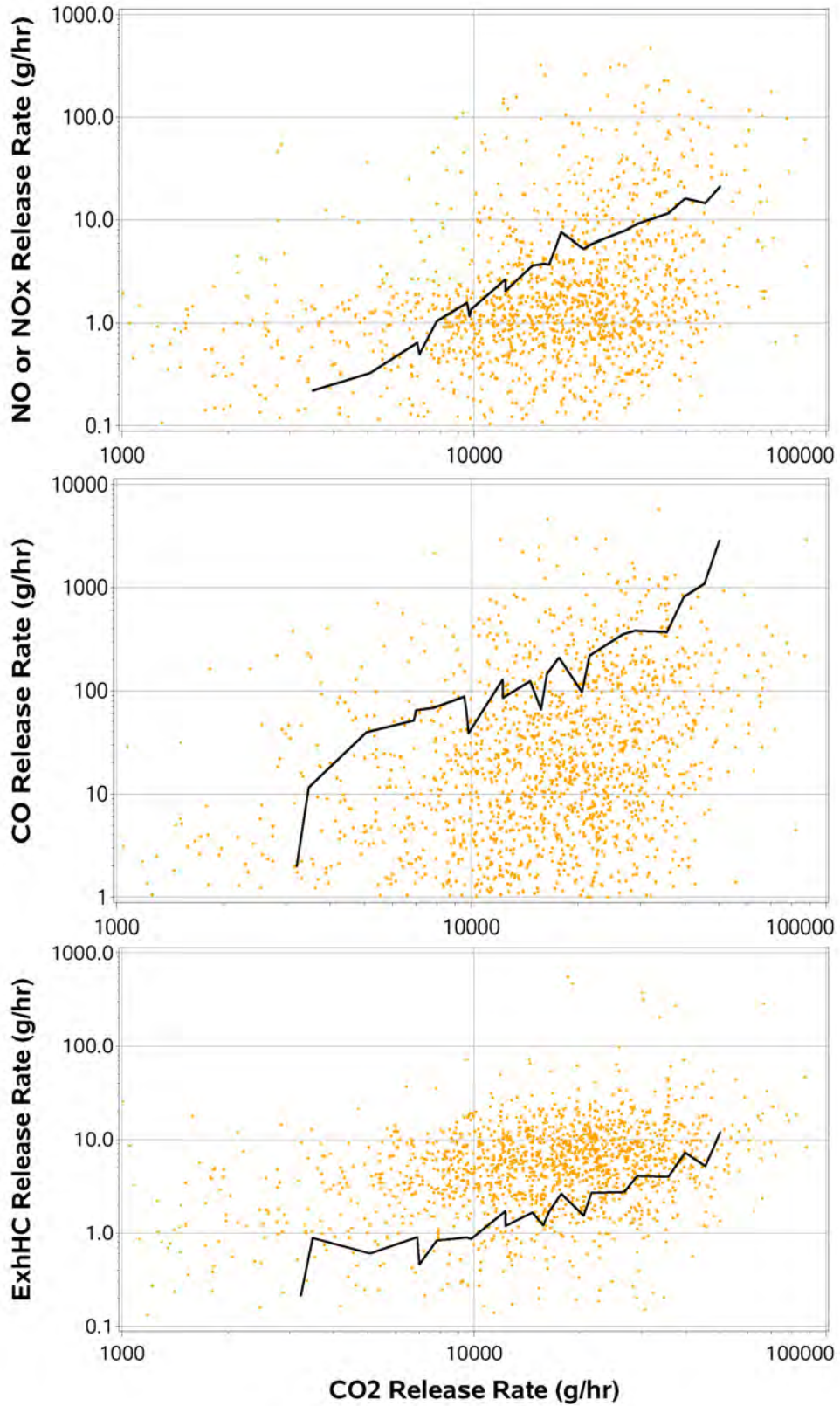/proj1/EDARinDenver-OCT2019/Analysis_MLout/220113/Anal_MLout/OCT19_VSPbins_4_CP.sas 02MAR23 13:09

Figure F-10. Comparison of Release Rates for 6-to-7-Year-Old LDVs in 2019

Source: • • • Westminster Vehicle RSD Transits   —— MOVES Average for Calendar 2019

/proj1/EDARinDenver-OCT2019/Analysis_MLout/220113/Anal_MLout/OCT19_VSPbins_4_CP.sas 02MAR23 13:09

Figure F-11. Comparison of Release Rates for 8-to-9-Year-Old LDVs in 2019

Source: • • • Westminster Vehicle RSD Transits   —— MOVES Average for Calendar 2019

/proj1/EDARinDenver-OCT2019/Analysis_MLout/220113/Anal_MLout/OCT19_VSPbins_4_CP.sas 02MAR23 13:09
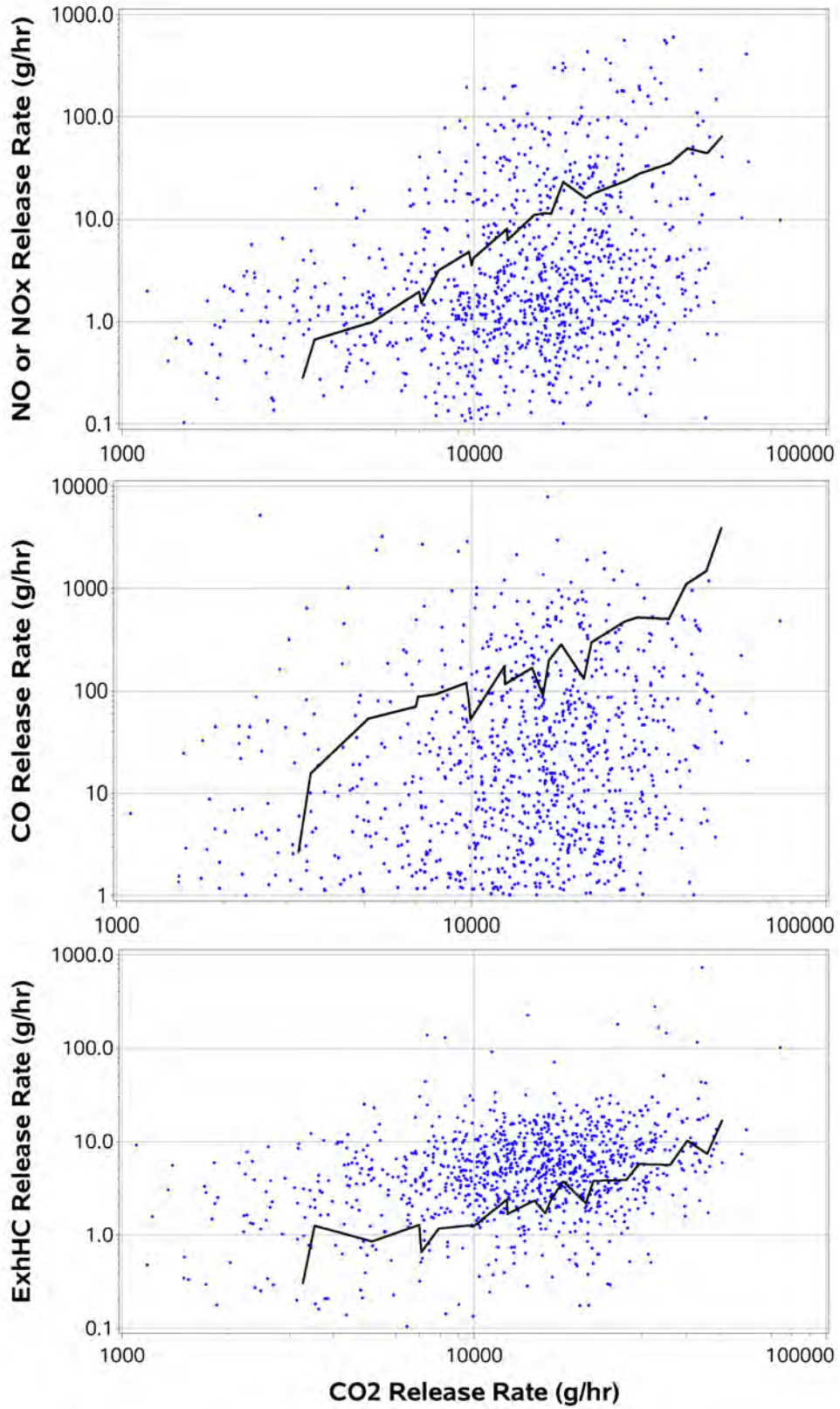
Figure F-12. Comparison of Release Rates for 10-to-14-Year-Old LDVs in 2019

Source: ••• Westminster Vehicle RSD Transits   —— MOVES Average for Calendar 2019

/proj1/EDARinDenver-OCT2019/Analysis_MLout/220113/Anal_MLout/OCT19_VSPbins_4_CP.sas 02MAR23 13:09
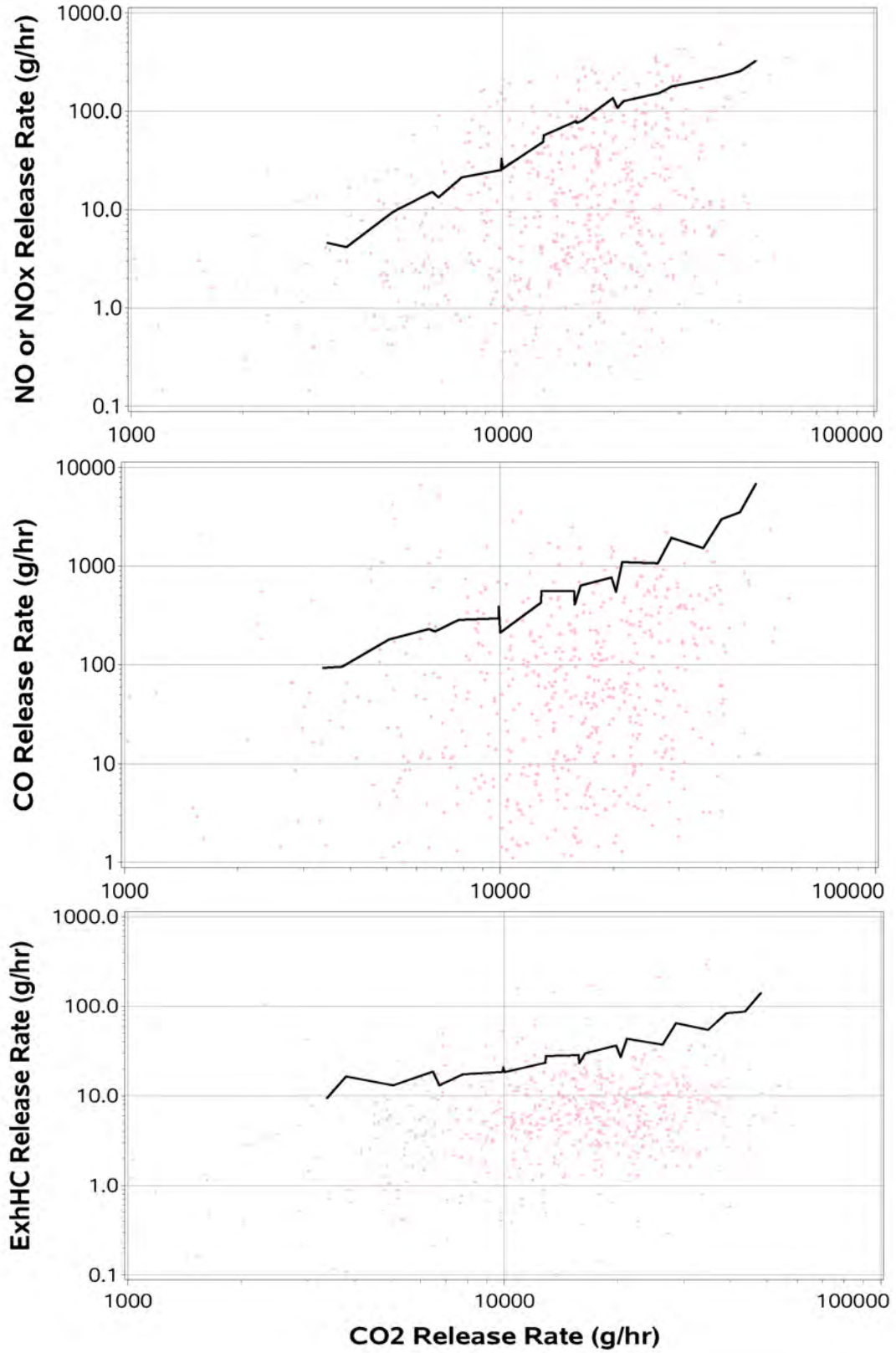
Figure F-13. Comparison of Release Rates for 15-to-19-Year-Old LDVs in 2019

Source: • • • Westminster Vehicle RSD Transits   —— MOVES Average for Calendar 2019

/proj1/EDARinDenver-OCT2019/Analysis_MLout/220113/Anal_MLout/OCT19_VSPbins_4_CP.sas 02MAR23 13:09

Figure F-14. Comparison of Release Rates for 20-to-99-Year-Old LDVs in 2019

Source: • • • Westminster Vehicle RSD Transits   —— MOVES Average for Calendar 2019

/proj1/EDARinDenver-OCT2019/Analysis_MLout/220113/Anal_MLout/OCT19_VSPbins_4_CP.sas 02MAR23 13:09